Ali Reza Ashrafi
Mircea V. Diudea   *Editors*

Distance, Symmetry, and Topology in Carbon Nanomaterials

Springer

Carbon Materials: Chemistry and Physics

Volume 9

Series Editors
Franco Cataldo
Soc. Lupi Chemical Research Institute Dipto. Ricerca e Sviluppo
Roma
Italy

Paolo Milani
Università Milano-Bicocca Dipto. Fisica
Milano
Italy

Carbon Materials: Chemistry and Physics aims to be a comprehensive book series with complete coverage of carbon materials and carbon-rich molecules. From elemental carbon dust in the interstellar medium, to the most specialized industrial applications of the elemental carbon and derivatives. With great emphasis on the most advanced and promising applications ranging from electronics to medicinal chemistry.

The aim is to offer the reader a book series which not only should be made of self-sufficient reference works, but should stimulate further research and enthusiasm.

More information about this series at http://www.springer.com/series/7825

Ali Reza Ashrafi • Mircea V. Diudea
Editors

Distance, Symmetry, and Topology in Carbon Nanomaterials

Editors
Ali Reza Ashrafi
Department of Nanocomputing,
   Institute of Nanoscience
   and Nanotechnology
University of Kashan
Kashan, Iran

Department of Pure Mathematics,
   Faculty of Mathematical Sciences
University of Kashan
Kashan, Iran

Mircea V. Diudea
Department of Chemistry, Faculty of Chemistry
   and Chemical Engineering
Babes-Bolyai University
Cluj-Napoca, Romania

Preface

In 1872, Felix Klein published his pioneering paper on the importance of symmetry, which was later named "Erlanger Programm" for his professorship at the University of Erlangen, Germany. He wrote: "we can say that geometry studies those and only those properties of the figure F which are shared by F and all the figures which are equal to F". He continued that the most essential idea required in the study of symmetry is that of a group of space transformations. Topology is the mathematical study of shapes. *Distance, Symmetry and Topology in Carbon Nanomaterials* gathers the contributions of some leading experts in a new branch of science that is recently named "Mathematical Nanoscience".

This volume continues and expands upon the previously published titles *The Mathematics and Topology of Fullerenes* (Carbon Materials: Chemistry and Physics series, Vol. 4, Springer 2011) and *Topological Modelling of Nanostructures and Extended Systems* (Carbon Materials: Chemistry and Physics series, Vol. 7, Springer 2013) by presenting the latest research on this topic. It introduces a new attractive field of research like the symmetry-based topological indices, multi-shell clusters, dodecahedron nano-assemblies and generalized fullerenes, which allow the reader to obtain a better understanding of the physico-chemical properties of nanomaterials.

Topology and symmetry of nanomaterials like fullerenes, generalized fullerenes, multi-shell clusters, graphene derivatives, carbon nanocones, corsu lattices, diamonds, dendrimers, tetrahedral nanoclusters and cyclic carbon polyynes give some important information about the geometry of these new materials that can be used for correlating some of their physico-chemical or biological properties.

We would like to thank to all the authors for their work and support, also to Springer for giving us the opportunity to publish this edited book and finally to Springer people who allowed all our efforts to make this an interesting book.

Kashan, Iran   Ali Reza Ashrafi
Cluj-Napoca, Romania   Mircea V. Diudea

Contents

Contributors

Ali Reza Ashrafi Department of Nanocomputing, Institute of Nanoscience and Nanotechnology, University of Kashan, Kashan, Iran

Department of Pure Mathematics, Faculty of Mathematical Sciences, University of Kashan, Kashan, Iran

Mahdieh Azari Department of Mathematics, Kazerun Branch, Islamic Azad University, Kazerun, Iran

Sorana D. Bolboacă University of Agricultural Science and Veterinary Medicine Cluj-Napoca, Cluj-Napoca, Romania

Department of Medical Informatics and Biostatistics, Iuliu Haţieganu University of Medicine and Pharmacy, Cluj-Napoca, Romania

Mircea V. Diudea Department of Chemistry, Faculty of Chemistry and Chemical Engineering, Babes-Bolyai University, Cluj-Napoca Romania

Tomislav Došlić Faculty of Civil Engineering, University of Zagreb, Zagreb, Croatia

Morteza Faghani Department of Mathematics, Payam-e Noor University, Tehran, Iran

G. H. Fath-Tabar Department of Pure Mathematics, Faculty of Mathematical Sciences, University of Kashan, Kashan, Iran

Farzaneh Gholaminezhad Department of Pure Mathematics, Faculty of Mathematical Sciences, University of Kashan, Kashan, Iran

Modjtaba Ghorbani Department of Mathematics, Faculty of Science, Shahid Rajaee Teacher Training University, Tehran, Iran

A. Graovac The Rugjer Boskovic Institute, NMR Center, Zagreb, Croatia

Asma Hamzeh Department of Mathematics, Faculty of Mathematical Sciences, Tarbiat Modares University, Tehran, Iran

Mohammad Ali Hosseinzadeh Department of Mathematics, Faculty of Mathematical Sciences, Tarbiat Modares University, Tehran, Iran

Samaneh Hossein-Zadeh Department of Mathematics, Faculty of Mathematical Sciences, Tarbiat Modares University, Tehran, Iran

Ali Iranmanesh Department of Pure Mathematics, Faculty of Mathematical Sciences, Tarbiat Modares University, Tehran, Iran

Lorentz Jäntschi Department of Physics and Chemistry, Technical University of Cluj-Napoca, Cluj-Napoca, Romania

Institute for Doctoral Studies, Babeş-Bolyai University, Cluj-Napoca, Romania

University of Agricultural Science and Veterinary Medicine Cluj-Napoca, Cluj-Napoca, Romania

Department of Chemistry, University of Oradea, Oradea, Romania

Dusanka Janezic Natural Sciences and Information Technologies, Faculty of Mathematics, University of Primorska, Koper, Slovenia

M. Javarsineh Department of Pure Mathematics, Faculty of Mathematical Sciences, University of Kashan, Kashan, Iran

N. Kahkeshani Department of Mathematics, Faculty of Sciences, University of Qom, Qom, Iran

Gyula Y. Katona Department of Computer Science and Information Theory, Budapest University of Technology and Economics, Budapest, Hungary

MTA-ELTE Numerical Analysis and Large Networks, Research Group, Budapest, Hungary

Z. Khalaj Department of Physics, Shahr-e-Qods Branch, Islamic Azad University, Tehran, Iran

Fatemeh Koorepazan-Moftakhar Department of Nanocomputing, Institute of Nanoscience and Nanotechnology, University of Kashan, Kashan, Iran

Department of Pure Mathematics, Faculty of Mathematical Sciences, University of Kashan, Kashan, Iran

István László Department of Theoretical Physics, Institute of Physics, Budapest University of Technology and Economics, Budapest, Hungary

Z. Mehranian Department of Mathematics, University of Qom, Qom, Iran

Mojgan Mogharrab Department of Mathematics, Faculty of Sciences, Persian Gulf University, Bushehr, Iran

Majid Monemzadeh Department of Particle Physics and Gravity, Faculty of Physics, University of Kashan, Kashan, Iran

Csaba L. Nagy Department of Chemistry, Faculty of Chemistry and Chemical Engineering, University of Babes-Bolyai, Cluj-Napoca, Romania

Katalin Nagy Department of Chemistry, Faculty of Chemistry and Chemical Engineering, University of Babes-Bolyai, Cluj-Napoca, Romania

Salman Abarghouei Nejad Department of Particle Physics and Gravity, Faculty of Physics, University of Kashan, Kashan, Iran

Ottorino Ori Actinium Chemical Research, Rome, Italy

Laboratory of Computational and Structural Physical-Chemistry for Nanosciences and QSAR, Department of Biology-Chemistry, Faculty of Chemistry, Biology, Geography, West University of Timişoara, Timişoara, Romania

Atena Parvan-Moldovan Department of Chemistry, Faculty of Chemistry and Chemical Engineering, Babes-Bolyai University, Cluj-Napoca, Romania

Raluca Pop Faculty of Pharmacy, University of Medicine and Pharmacy "Victor Babes" Timişoara, Timişoara, Romania

Mihai V. Putz Laboratory of Computational and Structural Physical-Chemistry for Nanosciences and QSAR, Department of Biology-Chemistry, Faculty of Chemistry, Biology, Geography, West University of Timişoara, Timişoara, Romania

Laboratory of Renewable Energies-Photovoltaics, R&D National Institute for Electrochemistry and Condensed Matter, Timişoara, Romania

Ali Asghar Rezaei Department of Pure Mathematics, Faculty of Mathematical Sciences, University of Kashan, Kashan, Iran

Mahboubeh Saheli Department of Pure Mathematics, University of Kashan, Kashan, Iran

Reza Sharafdini Department of Mathematics, Faculty of Basic Sciences, Persian Gulf University, Bushehr, Iran

G. H. Shirdel Department of Mathematics, Faculty of Sciences, University of Qom, Qom, Iran

Mahin Songhori Department of Mathematics, Faculty of Science, Shahid Rajaee Teacher Training University, Tehran, Iran

Beata Szefler Department of Physical Chemistry, Faculty of Pharmacy, Collegium Medicum, Nicolaus Copernicus University, Bydgoszcz, Poland

F. Taghvaee Department of Pure Mathematics, Faculty of Mathematical Sciences, University of Kashan, Kashan, Iran

Zahra Yarahmadi Department of Mathematics, Faculty of Sciences, Khorramabad Branch, Islamic Azad University, Khorramabad, Iran

G. V. Zhizhin Member of "Skolkovo" OOO "Adamant", Saint-Petersburg, Russia

Ibolya Zsoldos Faculty of Technology Sciences, Széchenyi István University, Győr, Hungary

Chapter 1
Molecular Dynamics Simulation of Carbon Nanostructures: The Nanotubes

István László and Ibolya Zsoldos

Abstract Molecular dynamics calculations can reveal the physical and chemical properties of various carbon nanostructures or can help to devise the possible formation pathways. In our days the most well-known carbon nanostructures are the fullerenes, the nanotubes, and the graphene. The fullerenes and nanotubes can be thought of as being formed from graphene sheets, i.e., single layers of carbon atoms arranged in a honeycomb lattice. Usually the nature does not follow the mathematical constructions. Although the first time the C_{60} and the C_{70} were produced by laser-irradiated graphite, the fullerene formation theories are based on various fragments of carbon chains and networks of pentagonal and hexagonal rings. In the present article, using initial structures cut out from graphene will be presented in various formation pathways for the armchair (5,5) and zigzag (9,0) nanotubes. The interatomic forces in our molecular dynamics simulations will be calculated using tight-binding Hamiltonian.

1.1 Introduction

The fullerenes, nanotubes, and graphene are three allotrope families of carbon, and their production in the last 27 years has triggered intensive researches in the field of carbon structures (Fowler and Manolopulos 1995, Dresselhaus et al. 1996). Each of them marks a breakthrough in the history of science. The fullerenes, the multi-walled carbon nanotubes, the single-walled carbon nanotubes, and the graphene jumped into the center of interest in 1985, 1991, 1993, and in 2004 in order (Kroto et al. 1985; Iijima 1991; Iijima and Ichihashi

---

I. László (✉)
Department of Theoretical Physics, Institute of Physics, Budapest University of Technology and Economics, H-1521 Budapest, Hungary
e-mail: laszlo@eik.bme.hu

I. Zsoldos
Faculty of Technology Sciences, Széchenyi István University, H-9126 Győr, Hungary

1993; Bethune et al. 1993; Novoselov et al. 2004). All of these breakthroughs are good examples for the fact that a breakthrough can be realized only if the science has a certain level of maturity concerning the combination of a set of favorable conditions, as, for example, having the right materials available, as well as the related theory, investigation tools, and scientific minds (Monthioux and Kuznetsov 2006).

In 1965 Schultz studied the geometry of closed cage hydrocarbons and among them the truncated icosahedron $C_{60}H_{60}$ molecule (Schultz 1965). In 1966 Jones using the pseudonym Daedalus was speculating about graphite balloon formations in high-temperature graphite productions (Jones 1966). Osawa suggested the C_{60} molecule to be a very aromatic one in a paper written in Japanese language (Osawa 1970), and two Russian scientists wrote a paper in their native language about the electronic structure of the truncated icosahedron molecule (Bochvar and Galpern 1973). In the early 1980s, Orville Chapman wanted to develop synthetic routes to C_{60} (Kroto 1992; Baggott 1996). All of these theoretical and experimental studies were isolated. As we have mentioned, the breakthrough happened in 1985 (Kroto et al. 1985), but before that in the years 1982–1983, Krätschmer and Huffman have found some kind of "junk" in the ultraviolet spectrum of carbon soot produced in arc discharge experiment (Baggott 1996; Krätschmer 2011). After calculating the ultraviolet spectrum of the C_{60} molecule (László and Udvardi 1987; Larsson et al. 1987), they have realized that the "junk" was due to the C_{60} fullerene. Publishing their results they have supplied a new breakthrough in fullerene research as they have produced fullerenes in crystal structure (Krätschmer et al. 1990).

In the early studies of fullerenes, most of the people knew that they were studying the C_{60} molecule, but they could not produce it. The only exception was Krätschmer and Huffman, namely, they produced it without recognizing it. In the history of nanotubes, there are many people who produced multi-walled carbon nanotubes, but they, or the scientific community, did not realize its importance (Boehm 1997; Monthioux and Kuznetsov 2006). The first authors who presented electron transmission images of multi-walled carbon nanotubes were perhaps Radushkevich and Lukyanovich in a paper written in Russian language in 1952 (Radushkevich and Lukyanovich 1952). But as we have mentioned, it was a publication without breakthrough.

The story of graphene is also interesting. In 1935 and 1937, Peielrs (1935) and Landau (1937) theoretically showed that strictly two-dimensional crystals were thermodynamically unstable and could not exist. Thus the study of electronic structure of graphene seemed to be a theoretical exercise without any experimental application (Wallace 1947). It was also found that this nonexisting material is an excellent condensed-matter analogue of $(2 + 1)$-dimensional quantum electrodynamics (Semenoff 1984). In 2004 Novoselov et al. realized the breakthrough by experimental study producing the graphene (Novoselov et al. 2004). There was not any contradiction between the theory and experiment, because it turned out that the produced graphene was not ideally two-dimensional. It was by gentle crumpling in the third dimension.

Since the experimental production of graphene, many authors working on carbon nanostructures start their talks with a picture presenting a graphene sheet containing various cut out patterns which are turning into fullerenes and nanotubes (Geim and Novoselov 2007). These processes follow the textbook geometric construction of fullerenes and nanotubes and explain the fact that the graphene is the "mother of all graphitic forms" (Geim and Novoselov 2007). In our previous tight-binding molecular dynamics calculations, we have shown that such processes can be realized by starting the simulation with some graphene cut out patterns (László and Zsoldos 2012a). We have presented more details for the C_{60} formation in László and Zsoldos (2012b) and for the C_{70} formation in László and Zsoldos (2014). In the present work, we give details for the nanotube productions. In the next paragraph, we describe the initial structures used in our molecular dynamics simulation and give also the parameters of our calculations. Then we describe the results obtained for the formation processes of armchair (5,5) and zigzag (9,0) nanotubes.

This idea can be used for any chiral nanotube as well.

1.2 Method

1.2.1 Initial Patterns

We cut out special patterns from the graphene in order to use them as initial structures in molecular dynamics calculations. Depending on the initial structure, we obtain fullerenes and nanotubes in a self-organizing way. The information built in the initial structure determine precisely the structure of the fullerenes and nanotubes in study. Thus we cut out the initial patterns from the graphene in a way which has the following properties: (1) It contains only hexagons. (2) There are some fourth (or fifth) neighboring atoms on the perimeter which can approach each other during their heat motion by constructing new pentagonal (or hexagonal) faces. (3) After the formation of new faces, other carbon atoms will be in appropriate positions for producing pentagons and/or hexagons. Repeating steps 2 and 3, we obtain the structure selected by the initial pattern.

This construction of initial patterns is similar to Dürer's unfolding method (O'Rourke 2011) but it has some important differences as well. Albrecht Dürer, the famous painter, presented polyhedrons by drawing nets for them. The nets were obtained by unfolding of the surfaces to a planar layout which contained each of the polygons. Our layout does not contain all of the polygons but it contains all of the vertices. It must contain all of the vertices (atoms) which are arranged in a special way for supplying the driving forces for the upfolding.

In Fig. 1.1a, b, we present initial structures applied for the formation of C_{60} and C_{70} nanotubes. Other structures can be found in references (László and Zsoldos
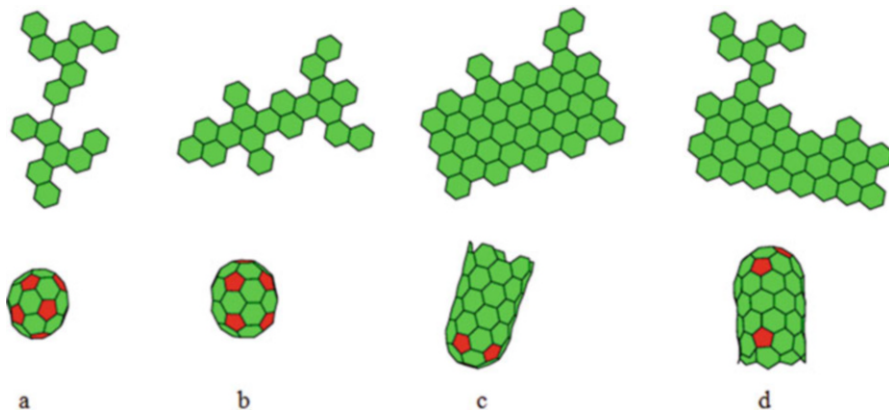
Fig. 1.1 Initial and final structures for the formation of (**a**) fullerene C_{60}, (**b**) fullerene C_{70}, (**c**) armchair nanotube (5,5), and (**d**) zigzag nanotube (9,0). The upper structures are the initial structures and the lower structures are the final ones

2012a, b, 2014). In the formation of fullerenes, the driving force comes from the pentagon constructions. Only the pentagons can form curved surfaces. Before forming a new bond, the system must cross an energy barrier. In order to have a one-way process, the potential energy must decrease after crossing the energy barriers of the potential landscape. The system works like a molecular motor. Mathematically the nanotubes are constructed by rolling up a parallelogram cut out from a hexagonal network of carbon atoms. These constructions do not have pentagons and the curved surface cannot be produced in a self-organizing way. This is why we are using half of a fullerene as a molecular motor. This molecular motor will roll up the parallelogram and the final structure will be a half capped nanotube. Figure 1.1c, d show the initial structures for (5,5) armchair and (9,0) zigzag carbon nanotube. The initial pattern of armchair nanotube contains half of a C_{70} fullerene and the molecular motor of the zigzag nanotube is half of a C_{60} fullerene.

1.2.2   The Molecular Dynamics Simulation

We calculated the interatomic carbon-carbon interaction with the help of a quantum chemical tight-binding method based on parameters adjusted to ab initio density functional calculations (Porezag et al. 1995). Verlet algorithm (Verlet 1967) supplied the solution of the equations of motion. The applied time step was 0.7 fs. As we have remarked it before, during the formation process, the system goes to lower and lower potential energy states. Namely, the decreasing potential energy can guarantee the progress of the process to the desired structure. From the conservation of the energy follows that the kinetic energy will increase, if we

decrease the potential energy. This increased kinetic energy can destroy other already formed bonds of the structure and yielding a fragmentized structure instead of the desired one. In order to avoid this unfavorable situation, we performed the simulations with constant environmental temperature T_{env}. In the present calculation, the environmental temperature was controlled with the help of Nosé-Hoover thermostat (Nosé 1984; Hoover 1985; Allen and Tildesley 1996; Frenkel and Smit 1996; László 1998). The Nosé-Hoover thermostat made it possible to make distinction between the temperature of the environment and the instantaneous temperature of the carbon structure. The temperature of the environment T_{env} was given by a parameter in the algorithm and the temperature of the carbon atoms was calculated from the kinetic energy of the atoms. This latter temperature usually made oscillations around the value of the environmental temperature.

As the initial velocity of the atoms in the pattern was not known, we determined randomly the initial velocities corresponding to an initial temperature T_{init}. When the number of atoms was N, we generated 3 N random numbers uniform in the range (0,1). After shifting these random numbers by −0.5, we added them to the atomic coordinates of the atoms. The desired initial temperature was obtained by scaling of this displacement vector. In our simulation the interaction between the Nosé-Hoover thermostat and the carbon atoms was so strong that the final structure did not depend strongly on the initial temperature in the range of $0 \text{ K} < T_{init} < 2000 \text{ K}$. This is why we used the initial temperature $T_{init} = 1200 \text{ K}$ practically in all of the simulations.

1.3 Results

1.3.1 The Armchair Nanotube

The initial structure of the (5,5) armchair nanotube can be seen on Fig. 1.1c. It contains half of the initial structure of the fullerene C_{70} (Fig. 1.1b). First we have made a constant energy molecular dynamics simulation. Here we supposed that the initial temperature was 0 K. The parameters of this run can be seen in Table 1.1 in the line of run 1. The final structure after a simulation of 146 ps is shown in Fig. 1.2a. The fragmentation process has already started and we obtained four pentagons and one heptagon. The formation of the pentagon and the starting of fragmentation show that the information built into the initial pattern has already been lost. This is why we made the calculations at constant temperatures. The results of various runs are in Table 1.1 and Fig. 1.2.

In run 2 the initial temperature of the carbon atoms was 1200 K and the environmental temperature was 500 K. Figure 1.2b shows that during the simulation time of 15.1 ps, two pentagons were formed, but the structure looked to be frozen. That is, we did not hope further structure changing during a

Table 1.1 Simulation processes performed for the formation of a (5,5) armchair nanotube using the initial structure of Fig. 1.1c

Run	Random number	T_{init}	T_{env}	Time of simulation	Final structure
1	−1	0		146.0	a
2	1	1200	(0)500	15.1	b
3	1	1200	(0)800	3.9	c
4	1	1200	(0)1000	81.6	d
5	1	1200	(0)1000,(28.7–28.91)1300	37.5	e
6	2	1200	(0)1000	12.3	f
7	2	1200	(0)1500	4.9	g
8	3	1200	(0)1300	4.7	h
9	3	1200	(0)1000	4.4	i
10	3	1200	(0)1000	24.3	j
11	3	1200	(0)500	46.0	k
12	3	1200	(0)500(46,2–46.41)800	84.62	l
13	3	1200	(0)500(46,2–46.41)800 (46,41–46.62)500	58.66	m
			(0)500(46,2–46.41)800 (46,41–46.62)500		
14	3	1200	(58.1–58.31)800(58.31–58.52) 500	70.38	n
			(0)500(46,2–46.41)800 (46,41–46.62)500		
			{(58.1–58.31)800(58.31–58.52) 500}		
			{ } repeated in each 3.5 ps		
15	3	1200	(0)500(46,2–46.41)800 (46,41–46.62)500	103.11	o
			{(58.1–58.31)800(58.31–58.52) 500}		
			{ } repeated in each 2.1 ps		
			(0)500(46,2–46.41)800 (46,41–46.62)500		
			{(58.1–58.31)1000 (58.31–58.52)500}		
16	3	1200	{ } repeated in each 2.1 ps	90.18	p
			(0)500(46,2–46.41)800 (46,41–46.62)500		
			(57.75–58.03)100		
			{(58.1–58.45)600(58.31–58.52) 100}		
			{ } repeated in each 2.1 ps		

Table 1.1 (continued)

Run	Random number	T_{init}	T_{env}	Time of simulation	Final structure
17	3	1200	(0)500(46,2–46.41)800 (46,41–46.62)500	76.31	q
			(57.75–58.03)100		
			(58.1–58.45)600(58.31–58.52) 100		
18*	3	1200		78.02	r
19	3	1200		162.45	s

The Tinit and Tenv initial and environmental temperatures are given in K and the time of simulation is given in ps. Under the notation (t1–t2)T in Tenv, we mean increasing the temperature during the time interval (t1–t2) to the temperature T. The letters in the column of final structure are shown in Fig. 1.2. The parameters for the successful nanotube formation are marked by (*) in the run number. Random number is the serial number of random number generator used generating the corresponding Tinit

possible simulation time in a computer. If the structure was frozen in the time scale of a simulation, it did not mean that it was frozen also in a realistic time scale as well. In the various steps of the simulation, we tried to mimic some imagined structure – environment interaction or an experimental intervention. Increasing and decreasing the environmental temperature correspond to the random interaction with an environmental particle or it corresponds to an appropriate laser impulse or electron beam (Chuvilin et al. 2010; Terrones et al. 2002).

In run 3 we increased the environmental temperature to 800 K but the final structure was very similar to that of run 2. Thus in run 4, the environmental temperature was 1000 K, and Fig. 1.2d shows that the system developed further, but it was also frozen in another structure. In run 5 we wanted to avoid this frozen structure by continuous increasing of the initial environmental temperature of 1000 K to 1300 K in the time range from 28.7 ps to 28.91 ps. As fragmentation process was starting, we changed the random number generator, and we obtained a promising structure in run 11 at the environmental temperature of 500 K (Fig. 1.2k and Table 1.1). Run 12 was the same as run 11 only the temperature was raised from 500 K to 800 K from 46,2 ps to 46.41 ps (Fig. 1.2l and Table 1.2). In run 13 we increased the initial environmental temperature of 500 K to 800 K as before, but after we decreased it to 500 K in the time range from 46.41 ps to 46.62 ps. We call such kind of increasing and decreasing the environmental temperature sawtooth changing. The final structure is in Fig. 1.2m. In runs from 14 to 19, we put such kind of sawtooth changing of the environmental temper-ature at various point of times and we obtained the desired nanotube in run 18 (Fig. 1.2r and Table 1.1).In this successful run, the changing of the environ-mental temperature was the following. The simulation started at 500 K. This environmental temperature was raised to 800 K and decreased to 500 K with a sawtooth changing from 46.2 ps to 46.62 ps. From 57.75 ps to 58.03 ps, we decreased the environmental temperature to 100 K. From 58.1 ps to 58.52 ps, we
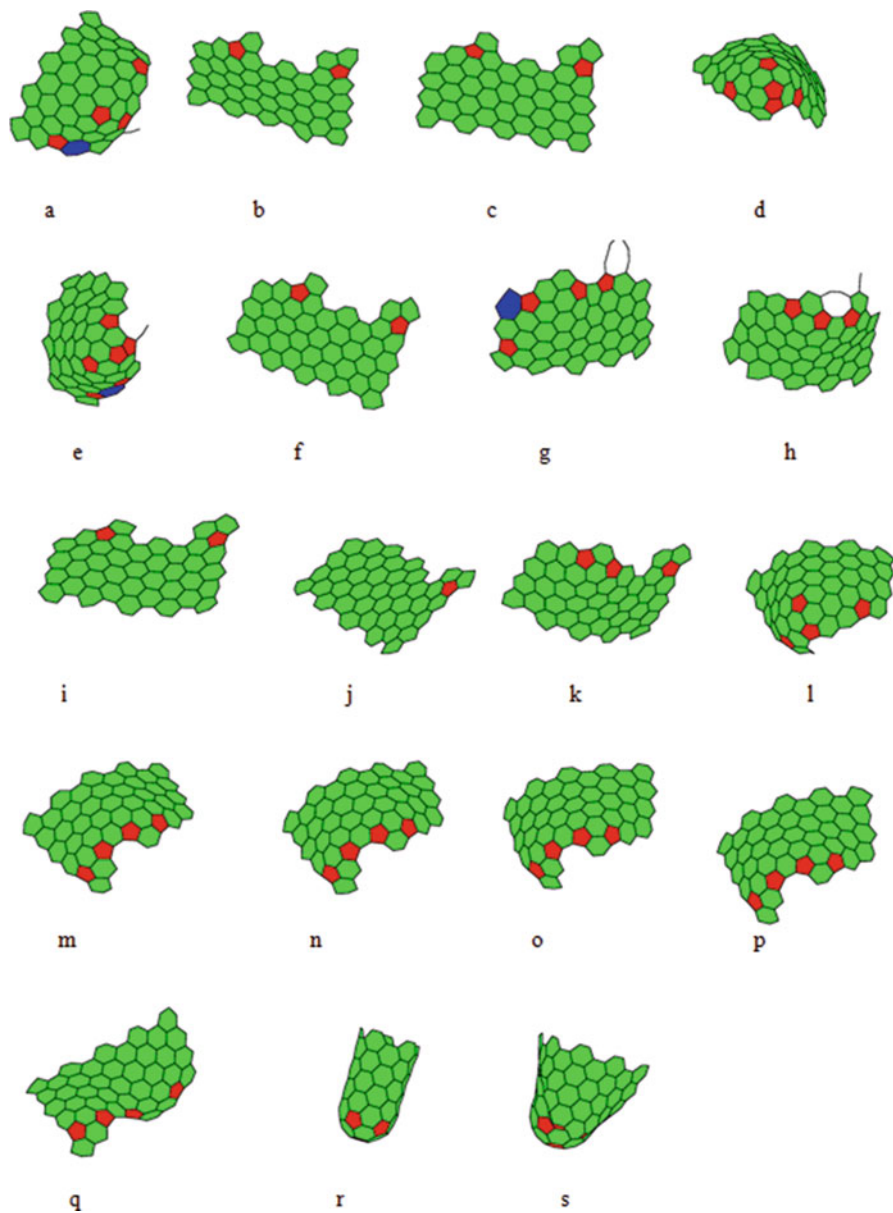
Fig. 1.2 The final structures of the processes in Table 1.1. To the Figures **a–s** correspond the Final structures of Table 1.1

Table 1.2 Simulation processes performed for the formation of a (9,0) zigzag nanotube using the initial structure of Fig. 1.1d

Run	Random number	T_{init}	T_{env}	Time of simulation	Final structure
1	–	0	(0)500		a
2	1	1200	(0)100	12.48	b
3	1	1200	(0)200	6.86	c
4	1	1200	(0)200(14.7–14.91)500	19.04	d
5	1	1200	(0)200(14.7–15.26)1000	20.86	e
6	1	1200	(0)500	23.47	f
7	2	1200	(0)1000	12.9	g
8	2	1200	(0)8000	6.45	h
9	3	1200	(0)500	2.49	i
10	3	1200	(0)100	19.35	j
11	3	1200	(0)100	2.7	k
12	4	1200	(0)100(28.7–28.91)400 (28.91–29.12)100	28.93	l
13	4	1200	(0)100	34.55	m
14*	3	1200	{(28.7–28.91)400(28.91–29.12) 100} {} repeated in each 3.5 ps	40.49	n

The T_{init} and T_{env} initial and environmental temperatures are given in K and the time of simulation is given in ps. Under the notation $(t_1–t_2)T$ in T_{env}, we mean increasing the temperature during the time interval $(t_1–t_2)$ to the temperature T. The letters in the column of final structure are shown in Fig. 1.3. The parameters for the successful nanotube formation are marked by (*) in the run number. Random number is the serial number of random number generator used generating the corresponding T_{init}

increased this temperature to 600 K and decreased it to 100 K. We repeated this sawtooth changing in each 2.1 ps and we obtained the armchair nanotube at the time of 70.21 ps. We continued such kind of variation of environmental temperature until 78.02 ps but the obtained nanotube was not destroyed. This shows the stability of the obtained nanotube.

1.3.2   The Zigzag Nanotube

The initial structure of the (9,0) zigzag nanotube is shown on Fig. 1.1d. It contains half of the initial structure of the fullerene C_{60} (Fig. 1.1a). The final structure of the constant energy calculation is in Fig. 1.3a with the parameters of run 1 in Table 1.2. Our strategy of simulation was the same as that of the armchair nanotube. The parameters of various runs are in Table 1.2 and the final structures are in Fig. 1.3. We changed the random distribution of the initial velocities and made calculations with various environmental temperatures.
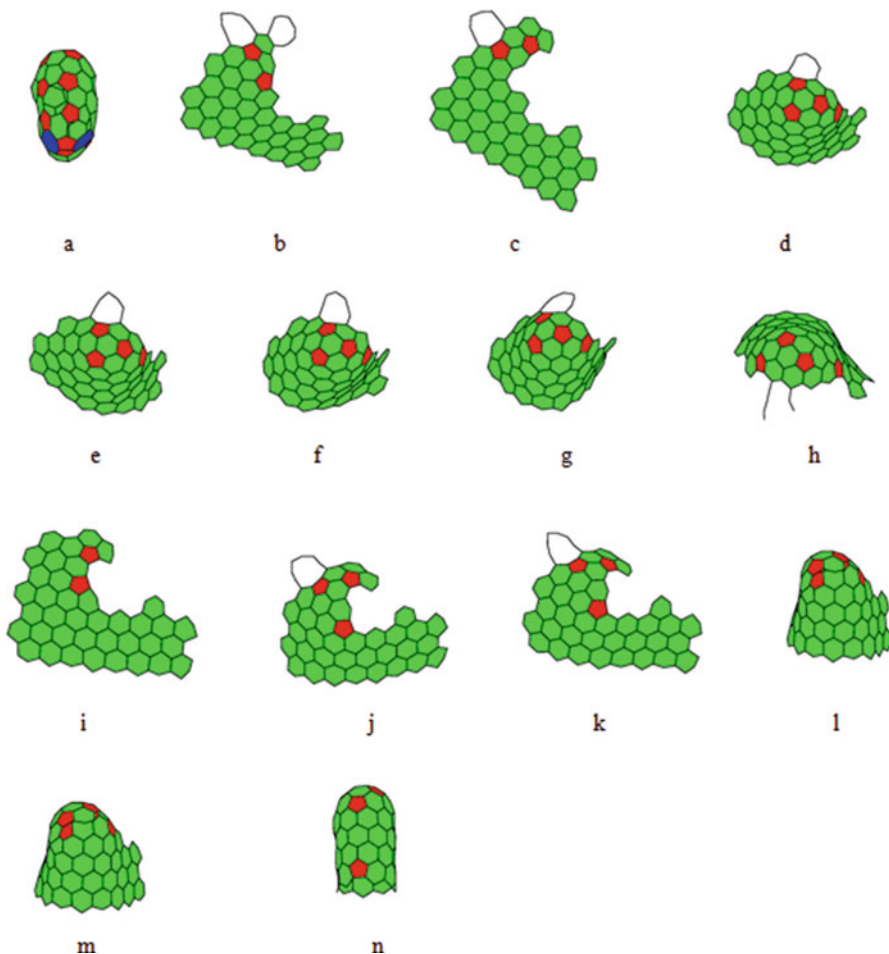
Fig. 1.3 The final structures of the processes in Table 1.2. To the Figures **a–n** correspond the Final structurers of Fig. 1.3

We obtained the zigzag nanotube in run 14 after the simulation time of 37.57 ps (Fig. 1.3n Table 1.2). Here we started the simulation at 100 K, producing a sawtooth changing from 28.7 ps to 29.12 ps, and we increased and decreased the environmental temperature from 100 K to 400 K and back to 100 K. We repeated this changing in each 3.5 ps. As we can see, the final structure obtained at 37.57 ps contains a pentagon at the open side of the nanotube. This pentagon can be eliminated by an extra hexagon in the initial structure of Fig. 1.1d (László and Zsoldos 2012a).

1.4   Conclusions

We have shown that using appropriate environmental temperatures, one can control the chirality-dependent formation of carbon nanotubes. In two examples we presented results for an armchair and a zigzag nanotube. The same idea can be used for nanotubes of any chirality. The final structure is coded in the initial pattern and it can be produced in a deterministic way. According to our experiences, the beginning of the formation process is the most critical. If the structure survives the first tens of picoseconds, the final desired structure can be formed. In the cases when the structure was frozen in the time scale of computer simulations, we increased or decreased the environmental temperature for simulating the stronger interaction with the environment. Our days of patterning graphene are not yet at atomic precision. There are however promising experiments in electron-beam lithography (Chuvilin et al. 2010; Chen et al. 2007; Han et al. 2007), scanning tunneling microscope lithography (Tapasztó et al. 2008), or the rational chemical synthesis by polycyclic aromatic hydrocarbons (Boorum et al. 2001; Scott et al. 2002). Until the experimental realization of the initial pattern of our simulation, our results not only give new insight into the formation processes of fullerenes and nanotubes but they give ideas for experimental selective production of known and not yet known carbon materials.

References

Allen MP, Tildesley DJ (1996) PC computer simulation of liquids. Clarendon Press, Oxford

Baggott J (1996) Perfect symmetry. The accidental discovery of buckminsterfullerene. Oxford University Press, Oxford/New York/Tokyo

Bethune DS, Kiang CH, De Vries MS, Gorman G, Savoy R, Vazquez J, Beyers R (1993) Cobalt catalysed growth of carbon nanotubes with single-atomic-layer walls. Nature 363:605–607

Bochvar DA, Galpern EG (1973) Hypothetical systems: carbododecahedron, s-icosahedron and carbo-s-icosahedron. Dokl Acad Nauk SSSR 209:610–612 (In Russian)

Boehm HP (1997) The first observation of carbon nanotubes. Carbon 35:581–584

Boorum MM, Vasil'ev YV, Drewello T, Scott LT (2001) Groundwork for rational synthesis of C_{60}: cyclodehydrogenation of a $C_{60}H_{30}$ polyarene. Science 294:828–831

Chen Z, Lin Y, Rooks MJ, Avouris P (2007) Graphene nanoribbon electronics. Phys E 40:228–232

Chuvilin A, Kaiser U, Bichoutskaia E, Besley NA, Khlobystov AN (2010) Direct transformation of graphene to fullerene. Nat Chem 2:450–453

Dresselhaus MS, Dresselhaus G, Eklund PC (1996) Science of fullerenes and carbon nanotubes: their properties and applications. Academic Press, New York/London

Fowler PW, Manolopulos DE (1995) An atlas of fullerenes. Clarendon Press, Oxford

Frenkel S, Smit B (1996) Understanding molecular simulation. Academic Press, San Diego

Geim AK, Novoselov KS (2007) The rise of graphene. Nature Mat 6:183–191

Han MY, Ozylmaz B, Zhang YB, Kim P (2007) Energy band-gap engineering of band gap nanoribbons. Phys Rev Lett 98:206805

Hoover WG (1985) Canonical dynamics: equilibrium phase-space distributions. Phys Rev A31:1965–1967

Iijima S (1991) Helical microtubules of graphite carbon. Nature 354:56–58

Iijima S, Ichihashi T (1993) Single-shell carbon nanotubes of 1nm diameter. Nature 363:603–605

Jones DEH (1966) Ariadne. New Scientist 32: 245–245.

Krätschmer W (2011) The story of making fullerenes. Nanoscale 3:2485–2489

Krätschmer W, Lamb LD, Fostiropoulos K, Huffman DR (1990) Solid C_{60}. A new form of carbon. Nature 347:354–358

Kroto HW (1992) C-60-Buckminsterfullerene, the celestial sphere that fell to earth. Angew Chem Int Ed 31:111–129

Kroto HK, Heath JR, O'Brien SC, Curl RF, Smalley RE (1985) C_{60}: buckminsterfullerene. Nature 318:162–163

Landau LD (1937) Zur Theorie der Phasenumwandlungen II. Phys Z Sowjetunion 11:26–35

Larsson S, Volosov A, Rosen A (1987) Optical spectrum of the icosahedral C_{60} – "follene-60". Chem Phys Lett 137:501–504

László I (1998) Formation of cage-like C_{60} clusters in molecular-dynamics simulations. Europhys Lett 44:741–746

László I, Udvardi L (1987) On the geometrical structure and UV spectrum of the truncated icosahedron molecule. Chem Phys Lett 136:418–422

László I, Zsoldos I (2012a) Graphene-based molecular dynamics nanolithography of fullerenes, nanotubes and other carbon structures. Europhys Lett 99:63001p1–63001p5

László I, Zsoldos I (2012b) Molecular dynamics simulation of carbon nanostructures: the C_{60} buckminsterfullerene. Phys Stat Solidi B 249:2616–2619

László I, Zsoldos I (2014) Molecular dynamics simulation of carbon nanostructures: the D_{5h} C_{70} fullerene. Phys E 56:422–426

Monthioux M, Kuznetsov VL (2006) Who should be given the credit for the discovery of carbon nanotubes? Carbon 44:1621–1623

Nosé S (1984) Molecular dynamics method for simulations in the canonical ensemble. Mol Phys 52:255–268

Novoselov KS, Geim AK, Morozov SV, jiang D, Zhang Y, Dubonos SV, Grigorieva IV, Firsov AA (2004) Electric field effect in atomically thin carbon films. Science 306:666–669

O'Rourke J (2011) How to fold it science of fullerenes and carbon nanotubes: their properties and applications. Cambridge University Press, Cambridge

Osawa E (1970) Superaromaticity. Kagaku 25:854–863 (In Japanese)

Peierls RE (1935) Quelques propriétés typiques des corps solides. Ann I H Poincaré 5:177–222

Porezag D, Frauenheim T, Köhler T, Seifert G, Kaschner R (1995) Construction of tight-binding potentials on the basis of density-functional theory – Application to carbon. Phys Rev B 51:12947–12957

Radushkevich LV, Lukyanovich VM (1952) About the structure of carbon formed by thermal decomposition of carbon monoxide on iron substrate. Zurn Fisic Chim 26:88–95 (in Russian)

Schultz HP (1965) Topological organic chemistry. Polyhedranes and prismanes. J Org Chem 30:1361–1364

Scott LT, Boorum MM, McMahon BJ, Hagen S, Mack J, Blank J, Wegner H, Meijere A (2002) A rational chemical synthesis of C_{60}. Science 295:1500–1503

Semenoff GW (1984) Condensed-matter simulation of a three-dimensional anomaly. Phys Rev Lett 53:2449–2452

Tapasztó L, Dobrik G, Lambin P, Bíró L (2008) Tailoring the atomic structure of graphene nanoribbons by scanning tunneling microscope lithography. Nat Nanotechnol 3:397–401

Terrones M, Banhart F, Grobert N, Charlier J-C, Terrones H, Ajayan PM (2002) Molecular junctions by joining single-walled carbon nanotubes. Phys Rev Lett 89:075505

Verlet L (1967) Computer "experiments" on classical fluids. I. Thermodynamical properties of Lennard-Jones molecules. Pys Rev B 159:98–103

Wallace PR (1947) The band theory of graphite. Phys Rev 71:622–634

Chapter 2
Omega Polynomial in Nanostructures

Mircea V. Diudea and Beata Szefler

Abstract Omega polynomial, developed in 2006 in Cluj, Romania, counts the number of topologically parallel edges in all the opposite edge stripes of a connected graph. Definitions and relations with other polynomials and well-known topological indices are given. Within this chapter, omega polynomial is computed in several 3D nanostructures and crystal networks, and analytical formulas as well as examples are given. This polynomial is viewed as an alternative to the crystallographic description.

2.1 Definitions

2.1.1 Relation co

In a connected graph $G = (V(G), E(G))$, with the vertex set $V(G)$ and edge set $E(G)$, two edges $e = (u,v)$ and $f = (x,y)$ of G are called *co-distant*, *e co f* (John et al. 2007a, b; Diudea and Klavžar 2010), if

$$e \ \ co \ f \Leftrightarrow d(v,x) = d(v,y) + 1 = d(u,x) + 1 = d(u,y) \qquad (2.1)$$

where d is the shortest-path distance function. Relation *co* is reflexive, that is, *e co e* for any edge e of G, and it is also symmetric: if *e co f* then also *f co e*. In general, *co* is not transitive; a small example in this respect is the complete bipartite graph $K_{2,3}$. A graph is called a *co*-graph if the relation *co* is also transitive and relation *co* is an equivalence relation.

M.V. Diudea (✉)
Department of Chemistry, Faculty of Chemistry and Chemical Engineering, Babes-Bolyai University, Arany Janos Street 11, Cluj-Napoca RO-400028, Romania
e-mail: diudea@chem.ubbcluj.ro

B. Szefler
Department of Physical Chemistry, Faculty of Pharmacy, Collegium Medicum, Nicolaus Copernicus University, Kurpińskiego 5, 85-950 Bydgoszcz, Poland

13

For an edge $e \in E(G)$, let $c(e) := \{f \in E(G); \ f \ co \ e\}$ be the set of edges co-distant to e in G; the set $c(e)$ is called an *orthogonal cut* of G, with respect to e. If G is a *co*-graph then its orthogonal cuts $C(G) = c_1, \ c_2, .., c_k$ form a partition: $E(G) = c_1 \cup c_2 \cup \ldots \cup c_k, \ c_i \cap c_j = \varnothing, \ i \neq j$.

A subgraph $H \subseteq G$ is called *isometric* with G if $d_H(u, v) = d_G(u, v)$, for any $(u, v) \in H$; it is *convex* if any shortest path in G between vertices of H belongs to H. The n-cube Q_n is the graph whose vertices are all binary strings of length n, two strings being adjacent if they differ in exactly one position (Harary 1969). The distance function in the n-cube is just the Hamming distance: the distance between two vertices of Q_n equals the number of positions in which they differ. A graph G is called a *partial cube* if there exists an integer n such that G is an isometric subgraph of Q_n.

For any edge $e = (u,v)$ of a connected graph G, let n_{uv} denote the set of vertices lying closer to u than to v: $n_{uv} = \{w \in V(G) | d(w, u) < d(w, v)\}$. By definition, $n_{uv} = \{w \in V(G) | d(w, v) = d(w, u) + 1\}$. The sets (and subgraphs) induced by these vertices, n_{uv} and n_{vu}, are called *semicubes* of G; these semicubes are *opposite* and disjoint (Diudea and Klavžar 2010; Diudea et al. 2008; Diudea 2010a, b, c).

A graph G is *bipartite* if and only if, for any edge of G, the opposite semicubes define a partition of G: $n_{uv} + n_{vu} = v = |V(G)|$. The relation *co* is related to the $\sim$ (Djoković 1973) and Θ (Winkler 1984) relations (Klavžar 2008a, b):

$$e \ \Theta \ f \Leftrightarrow d(u, x) + d(v, y) \neq d(u, y) + d(v, x) \tag{2.2}$$

In a connected graph, two edges of G are in the Djoković relation $e \sim f$ if f joins a vertex in n_{uv} with a vertex in n_{vu}. For more information about the relation $\sim$, see refs (Wilkeit 1990; Brešar 2001).

Lemma 2.1.1 In any connected graph, $co = \sim$.

Proof Let $e = (uv)$ and $f = (xy)$ be two edges of a connected graph G. Suppose first $e \ co \ f$, that is, $d(v, x) = d(v, y) + 1 = d(u, x) + 1 = d(u, y)$. Since $d(x, u) < d(x, v)$, $x \in n_{uv}$, and since $d(y, v) < d(y, u)$, $y \in n_{vu}$, thus, $e \sim f$. Suppose $e \sim f$, with $x \in n_{uv}$ and $y \in n_{vu}$. It follows that $d(v, x) = d(v, u) + d(u, x) = d(u, x) + 1$ and $d(u, y) = d(u, v) + d(v, y) = 1 + d(v, y)$.

Since $d(u, x) = d(v, y)$, we conclude that $e \ co \ f$, q.e.d.

In general graphs $\sim \subseteq \Theta$ and in bipartite graphs $\sim = \Theta$. From this and the above lemma, it follows (Diudea and Klavžar 2010).

Theorem 2.1.2 In a bipartite graph, the following statements are equivalent: (Diudea and Klavžar 2010)

(i) G is a *co*-graph; (ii) G is a partial cube; (iii) all semicubes of G are convex; (iv) relation Θ is transitive.

Equivalence between (i) and (ii) was observed in Klavžar (2008a, b), equivalence between (ii) and (iii) is due to Djoković (1973), while the equivalence between (ii) and (iv) was proven by Winkler (1984).

2.1.2 *Relation* op

Two edges e and f of a plane graph G are in relation *opposite*, e op f, if they are opposite edges of an inner face of G. Then e co f holds by assuming the faces are isometric. Note that relation co involves distances in the whole graph, while op is defined only locally (it relates face-opposite edges). A partial cube is also a co-graph but the reciprocal is not always true. There are co-graphs which are non-bipartite (Diudea 2010a, b, c), thus being non-partial cubes (see examples below).

Using the relation op, we can partition the edge set of G into *opposite* edge *strips* *ops*: any two subsequent edges of an *ops* are in op-relation and any three subsequent edges of such a strip belong to adjacent faces. Also note that John et al. (2007a, b) implicitly used the "op" relation in defining the Cluj-Ilmenau index CI.

Lemma 2.1.3 If G is a co-graph, then its opposite edge strips *ops* $\{s_k\}$ superimpose over the orthogonal cuts *ocs* $\{c_k\}$.

Proof Let us remind the co-relation is defined on parallel equidistant edge relation (2.1). The same is true for the op-relation, with the only difference (2.1) limited to a single face. Suppose e_1, e_2 are two consecutive edges of *ops*; by definition, they are topologically parallel and also co-distant (*i.e.*, belong to *ocs*). By induction, any newly added edge of *ops* will be parallel to the previous one and also co-distant. Because, in co-graphs, co-relation is transitive, all the edges of *ops* will be co-distant, and thus *ops* and *ocs* will coincide, *q.e.d.*

Corollary In a co-graph, all the edges belonging to an *ops* are topologically parallel.

Observe the relation co is a particular case of the edge *equidistant eqd* relation. The equidistance of two edges $e = (uv)$ and $f = (xy)$ of a connected graph G includes conditions for both (i) topologically parallel edges (relation (2.1)) and (ii) topologically perpendicular edges (in the tetrahedron and its extensions – relation (2.3)) (Diudea et al. 2008; Ashrafi et al. 2008a, b):

$$e \ eqd \ f(ii) \Leftrightarrow d(u,x) = d(u,y) = d(v,x) = d(v,y) \tag{2.3}$$

Recall that a graph is *planar* if it allows an embedding into the plane such that no two edges cross. A planar graph together with its fixed embedding into the plane is called a *plane* graph. In chemistry, not only the structure of a chemical graph but also its geometry is important. Most of the chemical graphs are by their nature planar.

The *op*-strips can be either cycles (if they start/end in the edges e_{even} of the same even face f_{even}) or paths (if they start/end in the edges e_{odd} of the same or different odd faces f_{odd}) (Diudea and Ilić 2009). In a planar bipartite graph, representing a polyhedron, all *op*-strips are cycles.

The *ops* is maximum possible, irrespective of the starting edge. The choice is about the maximum size of face/ring searched, and mode of face/ring counting, which will decide the length of the strip.

2.2 Omega and Related Polynomials

2.2.1 Definitions and Relations

Let s_1, s_2, .., s_k be the *op*-strips in a connected graph G; the *ops* form a partition of $E(G)$. Define the Omega polynomial $\Omega(x)$ as (Diudea 2006)

$$\Omega(x) = \sum_{i=1}^{k} x^{|s_i|} \tag{2.4}$$

Now consider the set of edges *co*-distant to edge e in G, $c(e)$. A polynomial counting the edges equidistant to every edge e is named Theta (Diudea et al. 2008) polynomial $\Theta(x)$ and is written as

$$\Theta(x) = \sum_{e \in E(G)} x^{|c(e)|} \tag{2.5}$$

Suppose now G is a *co*-graph, when $|c_k| = |s_k|$, then

$$\Theta(x) = \sum_{e \in E(G)} x^{|c(e)|} = \sum_{i=1}^{k}\sum_{e \in S_i} x^{|c(e)|} = \sum_{e} |c(e)| x^{|c(e)|} = \sum_{i=1}^{k} |s_i| x^{|s_i|} \tag{2.6}$$

If the polynomial counts the edges non-equidistant to the reference edges e, it is called the Π-polynomial (Diudea et al. 2008) $\Pi(x)$ and is defined as

$$\Pi(x) = \sum_{e \in E(G)} x^{|E(G)| - |c(e)|} = \sum_{i=1}^{k} |s_i| x^{|E(G)| - |s_i|} \tag{2.7}$$

A fourth polynomial, also related to the ops in G but counting the non-opposite edges, is the *Sadhana Sd* polynomial (Ashrafi et al. 2008a, b), defined as

$$Sd(x) = \sum_{i=1}^{k} x^{|E(G)| - |s_i|} \tag{2.8}$$

The first derivative (computed at $x = 1$) $P'(G,1)$ of these counting polynomials gives information on the counted topological property (Diudea 2010a, b, c):

$$\Omega'(G, 1) \;=\; \sum_{i=1}^{k} |s_i| = |E(G)| \tag{2.9}$$

$$\Theta'(G, 1) \;=\; \sum_{i=1}^{k} (|s_i|)^2 = \theta(G) \tag{2.10}$$

$$\Pi'(G, 1) \;=\; \sum_{i=1}^{k} |s_i| \big(|E(G)| - |s_i| \big) = \Pi(G) \tag{2.11}$$

$$Sd'(G, 1) \;=\; \sum_{i=1}^{k} \big(|E(G)| - |s_i| \big) = Sd(G) \tag{2.12}$$

An index, called Cluj-Ilmenau (John et al. 2007a, b) $CI(G)$, is defined on $\Omega(x)$

$$CI(G) = \left\{ \left[\Omega'(G, 1) \right]^2 - \left[\Omega'(G, 1) + \Omega''(G, 1) \right] \right\} \tag{2.13}$$

The sum of $P'(G,1)$ of the polynomials counting equidistant and non-equidistant edges in G equals the square of the number of edges in G:

$$\Theta'(G, 1) + \Pi'(G, 1) \;=\; \Big(\Omega'(G, 1) \Big)^2 = (|E(G)|)^2 \tag{2.14}$$

while the value of these polynomials in $x = 1$ $P(G,1)$ is

$$\Theta(G, 1) = \Pi(G, 1) \;=\; \Omega'(G, 1) = |E(G)| \tag{2.15}$$

There are graphs with single *ops*, of length $s = e = |E(G)|$, which is precisely a *cycle* (Diudea and Ilić 2009). Also, there are graphs with $s = 1$, namely, graphs with either odd rings or with no rings, i.e., tree graphs. For such graphs, minimal and maximal value, respectively, of CI is calculated (Diudea 2010a, b, c):

$$\Omega(x)_{CI_{\min}} = 1 \cdot x^e; \;\; CI_{\min} = e^2 - (e + e(e-1)) = 0 \tag{2.16}$$

$$\Omega(x)_{CI_{\max}} = e \cdot x^1; \;\; CI_{\max} = e^2 - (e + 0) = e(e-1) \tag{2.17}$$

Among the graphs on v vertices, $CI_{\min}$ is provided by the complete bipartite graphs $K_{2,v-2}$ (with $e = 2(v-2)$), while $CI_{\max}$ is given by the complete graphs K_v (with $e = v(v-1)/2$):

$$CI_{\min} = CI(K_{2, v-2}) = 0 \tag{2.18}$$

$$CI_{\max} = CI(K_v) = (1/4)v(v-1)(v^2 - v - 2) \qquad (2.19)$$

The first derivative (in $x = 1$) of Sadhana polynomial equals the Sadhana index (Khadikar et al. 2002) and is a multiple of $|E(G)|$:

$$
\begin{aligned}
Sd'(G,1) &= \sum_{i=1}^{k}\big(|E(G)| - |s_i|\big) = |E(G)|Sd(G,1) - |E(G)| \\
&= |E(G)|\big(|ops(G)| - 1\big)
\end{aligned}
\qquad (2.20)
$$

Since $|ops(G)| = \Omega(G,1) = Sd(G,1)$, and considering (2.9), the relation of Sadhana index with the omega polynomial, out of the basic definition, is (Diudea et al. 2010a, b):

$$Sd'(G,1) = \Omega'(G,1)(\Omega(G,1) - 1) \qquad (2.21)$$

In words, the first derivative of Sadhana polynomial (in $x = 1$) is the product of the number of edges $e = |E(G)|$ and the number of strips $\Omega(1)$ less one. In co-graphs, there is the equality (Diudea and Klavžar 2010; Diudea 2010a, b, c; Djoković 1973)

$CI(G) = \Pi(G)$. It comes out from their definitions:

$$
\begin{aligned}
CI(G) &= \left(\sum_{i=1}^{k}|s_i|\right)^2 - \left(\sum_{i=1}^{k}|s_i| + \sum_{i=1}^{k}|s_i|\big(|s_i| - 1\big)\right) \\
&= |E(G)|^2 - \sum_{i=1}^{k}(|s_i|)^2 = \Pi'(G,1) = \Pi(G)
\end{aligned}
\qquad (2.22)
$$

Relation (2.22) is valid only assuming $|c_k| = |s_k|$, $k = 1,2,..$ (see relations (2.6) and (2.7)), which provides the same value for the exponents of Omega and Theta polynomials; this is precisely achieved in co-graphs. In general graphs, however, $|s_i| \neq |c_k|$, and as a consequence, $CI(G) \neq \Pi(G)$.

The above equality between the two indices can be considered as a necessary condition for the co-graph/partial cube status. This is, however, not sufficient, and finally, the transitivity of ocs/ops must be proven.

Now consider relations (2.9, 2.10, and 2.11) in reformulating (2.22) as

$$\Pi(G) = |E(G)|^2 - \sum_{i=1}^{k}(|s_i|)^2 = \left\{\left[\Omega'(G,1)\right]^2 - \Theta'(G,1)\right\} \qquad (2.23)$$

Relation (2.23) is just the formula proposed by John et al. (2007a, b) to calculate the Khadikar's PI index 2 (Khadikar 2000). Ashrafi defined the equidistance of edges by considering the distance from a vertex z to the edge $e = uv$ as the minimum

distance between the given point and the two end points of that edge (Ashrafi et al. 2006, 2008a, b):

$$d(z,e) = \min\{d(z,u), d(z,v)\} \qquad (2.24)$$

Then, for two edges $e = (uv)$ and $f = (xy)$ of G,

$$e \ eqd \ f(iii) \Leftrightarrow d(x,e) = d(y,e) \ \text{ and } \ d(u,f) = d(v,f) \qquad (2.25)$$

In bipartite graphs, relations (2.1) and (2.3) superimpose over relations (2.24) and (2.25); in such graphs, the following equality holds $\Pi(G) = PI_e(G)$. In general graphs, this is, however, not true.

The problem of equidistance of vertices was firstly put by Gutman when defining the Szeged index (Gutman 1994) $Sz(G)$ of which calculation leaves out the equidistant vertices. Similarly, the index $PI_e(G)$ does not account for the equidistant edges. According to Ashrafi's notations (Ashrafi et al. 2006), it can be written as

$$PI_e(G) = PI_e^{'}(1) = \sum_{e \in E(G)} [n(e,u) + n(e,v)] - m(u,v) \qquad (2.26)$$

where $n(e, u)$ is the number of edges lying closer to the vertex u than to the v vertex and $m(u, v)$ is the number of equidistant edges from u and v. This index can be calculated as the first derivative, in $x = 1$, of the polynomial defined by Ashrafi as

$$PI_e(x) = \sum_{e \in E(G)} x^{n(e,u)+n(e,v)} \qquad (2.27)$$

In partial cubes, since they are also bipartite, the previous equality can be expanded to the triple one:

$$CI(G) = \Pi(G) = PI_e(G) \qquad (2.28)$$

a relation which is not obeyed in all co-graphs. In general graphs, the above triple equality turns to the corresponding inequality:

$$CI(G) \neq \Pi(G) \neq PI_e(G) \qquad (2.29)$$

The question about a simple and rapid criterion/condition to be used in order to decide if a given bipartite graph is a partial cube (or a co-graph) is still open (Diudea and Klavžar 2010). Unfortunately, no such a condition is known (see refs. Aurenhammer and Hagauer 1995; Imrich and Klavžar 1993; Eppstein 2008; Brešar et al. 2003).

The number of structures investigated for transitivity can be reduced by using an orthogonal edge-cutting procedure (see below).

2.2.2 Omega Polynomial by Edge-Cutting Procedures

In bipartite graphs, an orthogonal edge-cutting procedure (Diudea 2010a, b, c; Diudea et al. 2010a, b; Gutman and Klavžar 1995; Klavžar 2008a, b) can be used to generate the *ops*. In performing a cut, take a straight line segment, orthogonal to the edge e, and intersect e and all its parallel edges (in a polygonal plane graph). The set of these intersections is called an *orthogonal cut*, with respect to e (Fig. 2.1). To any orthogonal cut c_k, two numbers are here associated: (i) the number of intersected edges e_k (or the cutting cardinality $|c_k|$) and (ii) the number of points v_k, lying to the left hand with respect to c_k (in round brackets, in Fig. 2.1). In *co-graphs*, the exponents in Omega and Theta polynomials are identical, while in $\Pi(x)$, they result as the difference between $e = |E(G)|$ and the Omega s_k exponents. Since the polyhexes are bipartite graphs (and partial cubes), the triple equality $CI(G) = \Pi(G) = PI_e(G)$ holds (Diudea 2010a, b, c).

2.2.3 When $CI(G) = \Pi(G)$?

The answer to the above question is not immediate, as can be seen from the following examples.

$$= 6x^3 + 6x^6 + 15x^8$$

$$CI(G) = 29046$$

$$\Theta(x) = 3 \cdot 6x^3 + 6 \cdot 6x^6 + 8 \cdot 15x^8$$

$$\Theta'(1) = 1230$$

$$\Pi(x) = 3 \cdot 6x^{174-3} + 6 \cdot 6x^{174-6} + 8 \cdot 15x^{174-8}$$

$$\Pi'(1) = 29046$$

Labels on figure: C3(5), C6(16), C81(31), C82(47), C83(63), C82(47), C81(31), C6(16), C3(5)
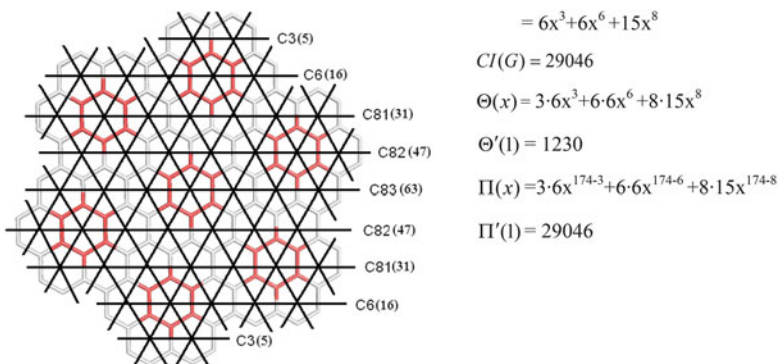
Fig. 2.1 Cutting procedure in the calculation of several topological descriptors; the graph is *co-graph*, *partial cube*, and also bipartite and $CI(G) = \Pi(G) = PI_e(G)$

2.2.3.1   Tree Graphs

Tree graphs are bipartite and partial cubes but non-*co*-graphs; Omega polynomial simply counts the non-equidistant edges or self-equidistant ones, being included in the term of exponent $s = 1$. In such graphs, $CI(G) = \Pi(G) = (v - 1)(v - 2)$ (a result known from Khadikar) (Diudea et al. 2006) and the Omega and Theta polynomials show the same expression.

2.2.3.2   Planar Polyhexes

All the planar polyhexes are bipartite, *co*-graphs, and also partial cubes and for which $CI(G) = \Pi(G)$ is true. This is the case of acenes and phenacenes (Tables 2.1 and 2.2) (Diudea 2010a, b, c).

2.2.3.3   Nanocones

Conical nanostructures, represented by graphs symbolized $C(a, n)$, with $a = $ apex polygon size and $n = $ number of hexagon rows around apex, show $CI(G) = \Pi(G)$, excepting the case $a = 3$. According to the net parameter parity, nanocones are (Diudea 2010a, b, c):

(a) $a = 4$; $n = $ odd; bipartite, *co*-graphs but non-partial cubes
(b) $a = 4$; $n = $ even; bipartite; non-*co*-graphs and non-partial cubes
(c) $a > 4$; $a = $ odd; n-all; non-bipartite, non-partial cubes but *co*-graphs
(d) $a > 4$; $a = $ even; n-all; bipartite, partial cubes and *co*-graphs

Table 2.1   Acenes

Acenes A_h; $h = $ no. of hexagons in molecule

$\Omega(A_h, x) = 2h \cdot x^2 + x^{(h+1)}$; $\Omega'(A_h, 1) = \|E(G)\| = e = 5h + 1$
$CI(A_h) = \left(\Omega'(A_h)\right)^2 - \left(\Omega'(A_h) + \Omega''(A_h)\right) = (5h+1)^2 - (5h+1+h(h+5)) = 24h^2$
$\|\Omega(A_h, 1)\| = \|V(G)\|/2 = v/2 = 2h + 1$
$\Pi(A_h, x) = 4h \cdot x^{5h-1} + (h+1) \cdot x^{4h}$; $\Pi'(A_h, 1) = 24h^2$
$\Theta(A_h, x) = 4h \times x^2 + (h+1) \times x^{h+1}$; $\Theta'(A_h, 1) = h^2 + 10h + 1$

Examples

h	$\Omega(A_h, x)$	$CI(G)$	$\Theta(A_h, x)$	$\theta(G)$	$\Pi(A_h, x)$	$\Pi(G)$
3	$6x^2 + x^4$	216	$12x^2 + 4x^4$	40	$4x^{12} + 12x^{14}$	216
4	$8x^2 + x^5$	384	$16x^2 + 5x^5$	57	$5x^{16} + 16x^{19}$	384

Table 2.2 Phenacenes

Phenacenes Ph_h; $h =$ no. of hexagons in molecule

$\Omega(Ph_h, x) = (h+2) \cdot x^2 + (h-1) \cdot x^3$; $\Omega'(Ph_h, 1) = |E(G)| = e = 5h + 1$
$CI(Ph_h) = (5h+1)^2 - (5h+1+8h-2) = 25h^2 - 3h + 2$
$\Omega(Ph_h, 1)| = |V(G)|/2 = v/2 = 2h + 1$
$\Pi(Ph_h, x) = 2(h+2) \cdot x^{5h-1} + 3(h-1) \cdot x^{5h-2}$; $\Pi'(Ph_h, 1) = 25h^2 - 3h + 2$
$\Theta(Ph_h, x) = 2(h+2) \cdot x^2 + 3(h-1) \cdot x^3$; $\Theta'(Ph_h, 1) = 13h - 1$

Examples

h	$\Omega(Ph_h, x)$	$CI(G)$	$\Theta(Ph_h, x)$	$\theta(G)$	$\Pi(Ph_h, x)$	$\Pi(G)$
3	$5x^2 + 2x^3$	218	$10x^2 + 6x^3$	38	$6x^{13} + 10x^{14}$	218
4	$6x^2 + 3x^3$	390	$12x^2 + 9x^3$	51	$9x^{18} + 12x^{19}$	390

2.2.3.4 Toroidal Graphs

There are distinct (4,4) tori (Table 2.3), which show both degenerate $\Omega(x)$ polynomial and index $CI(G)$ (rows 1 and 2, in italics), for which $\Pi(x)$ and $\Theta(x)$ are distinct (Diudea et al. 2008; Diudea 2010a, b, c). Next, there are (4,4) tori which show degenerate $\Pi(G)$ and $\Theta(G)$ index values but distinct $\Pi(x)$ and $\Theta(x)$ polynomials (as the tori in Table 2.3, rows 1 and 3). The above tori all show $CI(G) \neq \Pi(G)$. Finally, there are excepted (4,4) tori which show $CI(G) = \Pi(G)$ (e.g., the torus T(4,4)[4,4] or that in the fourth row of Table 2.3; see below).

According to the parity of net parameters, non-twisted tori T(4,4)[c,n] are (Diudea 2010a, b, c):

(a) c,n-all odd; non-bipartite, non-co-graphs and non-partial cubes
(b) c-odd/even; n-even/odd; non-bipartite; non-partial cubes but co-graphs
(c) c,n-all even; bipartite, co-graphs and partial cubes

The only torus which shows $CI(G) = \Pi(G)$ is the simplest T(4,4)[4,4]: $\Omega(x) = 4x^8$; $CI(G) = 768$; $\Pi(x) = 32x^{24}$; $\Pi(G) = 768$; $\Theta(x) = 32x^8$; $\Theta(G) = 256$.

The example in Table 2.3, entry 4, is a twisted (4,4) torus (Fig. 2.2):

$\Omega(x) = 3x^{20} + 10x^6$; $\Omega'(1) = e = 120$; $CI = 12840 = \Pi'(1) = PI_e'(1)$;

$$\Theta(x) = 60x^{20} + 60x^6; \quad \Theta(G) = 1560$$

$$\Pi(x) = 60x^{114} + 60x^{100}; \quad \Pi'(1) = \Pi(G) = 12840$$

$PI_e(x) = 60x^{114} + 60x^{100}$; $PI_e(1) = e = 120$; $v = 60$; $PI_e'(1) = PI_e(G) = 12840$
$PI_v(x) = 120x^{54}$ (like in NBP graphs, $54 < 60 = v$); $PI_v'(1) = 6480$
$CJS(x) = 240x^{27}$ (a single term, like in BP tori); $CJ'S(1) = 6480$

Table 2.3 Polynomials in (4,4) tori: bipartite graphs for which $CI(G) \neq \Pi(G)$ (rows 1 to 3) and a non-bipartite graph showing $CI(G) = \Pi(G)$ (row 4); all tori are non-partial cubes

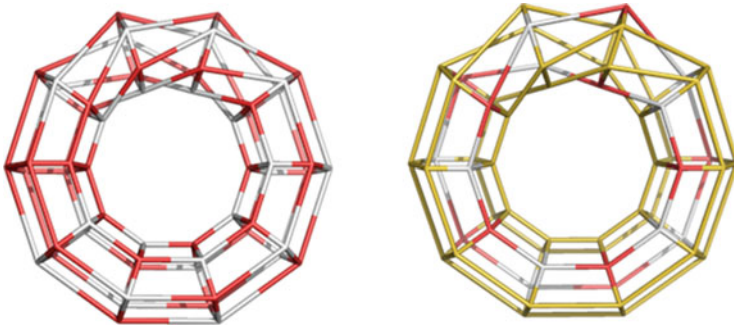|	Torus	$\Omega(x)$		$\Pi(x)$		$\Theta(x)$	
	(4,4)		$CI(G)$		$\Pi(G)$		$\Theta(G)$
1	TWH2D[6,10]	$6x^{10} + 2x^{30}$	12000	$60x^{96} + 60x^{102}$	11880	$60x^{18} + 60x^{24}$	2520
2	TWH6D[6,10]	$6x^{10} + 2x^{30}$	12000	$60x^{92} + 60x^{94}$	11160	$60x^{26} + 60x^{28}$	3240
3	TWV2D[6,10]	$10x^6 + 2x^{30}$	12240	$60x^{94} + 60x^{104}$	11880	$60x^{16} + 60x^{26}$	2520
4	**TWV3D[6,10]**	$\mathbf{10x^6 + 3x^{20}}$	**12840**	$\mathbf{60x^{100} + 60x^{114}}$	**12840**	$\mathbf{60x^6 + 60x^{20}}$	**1560**

Fig. 2.2 Twisted torus TWV3[6,10](4,4); non-bipartite (*left*) and as the union of 3 *co*-graphs, one of them being colored in alternating *white red* (*right*); *non-partial cube*

It is a 3D Möbius structure, which is a union of 3 *co*-graphs (for which the identity $\{s_k\} \equiv \{c_k\}$ is true) and the equality $CI(G) = \Pi(G)$ holds (Diudea 2010a, b, c). However, per global, it is a *non-bipartite* graph, which is shown in $PI_v(x) = 120x^{54}$, with the exponent lower than the number of vertices ($54 < 60$), the difference being equidistant vertices, nonexisting in bipartite graphs.

On the other hand, the Cluj polynomial shows a single term, as in bipartite tori. It is the only found non-bipartite graph which shows the equality $\Pi(G) = PI_e(G)$ (usually holding in bipartite graphs).

Tori of other tessellation ((6,3); ((4,8)3), ((5,7)3), etc.) all show $CI(G) \neq \Pi(G)$ and only exceptionally this relation becomes equality (see Table 2.4); all these tori are non-*co*-graphs and non-partial cubes.

The third torus in Fig. 2.3 and Table 2.4 is a non-bipartite torus, covered by odd faces, in a ((5,7)3) tessellation. It is included here to illustrate the triple inequality $CI(G) \neq \Pi(G) \neq PI_e(G)$ and an extreme case of $\Omega(x)$, with a single term, and of exponent 1 (see relation (2.17)) (Diudea 2010a, b, c).

2.2.3.5 Cubic Net and Corresponding Cage

The cubic net in Fig. 2.4 left is bipartite and for sure partial cube and *co*-graph; it shows the triple equality $CI(G) = \Pi(G) = PI_e(G)$. Its corresponding cage (Fig. 2.4, right) contains *non-isometric subgraphs* (see the red edges, which are non *co*-distant

Table 2.4 Polynomials in bipartite and non-bipartite tori in Figure 2.3

| T(6,3)H[8,12]; $v = 96$; $e = 144$; bipartite; non-co-graph; non-partial cube	
Polynomial	Index
$\Omega(x) = 12x^4 + 4x^{24}$	$CI(G) = 18240$
$Sd(x) = 4x^{120} + 12x^{140}$	$Sd(G) = 2160$
$\Theta(x) = 48x^8 + 96x^{22}$	$\Theta(G) = 2496$
$\Pi(x) = 96x^{122} + 48x^{136}$	$\Pi(G) = 18240$
$PI_e(x) = 96x^{122} + 48x^{136}$	$PI_e'(1) = 18240$
T((4,8),3)V[8,20]; $v = 160$; $e = 144$; bipartite; non-co-graph; non-partial cube	
Polynomial	Index
$\Omega(x) = 10x^8 + 8x^{10} + 2x^{40}$	$CI(G) = 52960$
$Sd(x) = 2x^{200} + 8x^{230} + 10x^{232}$	$Sd(G) = 4560$
$\Theta(x) = 80x^{16} + 80x^{20} + 80x^{22}$	$\Theta(G) = 4640$
$\Pi(x) = 80x^{218} + 80x^{220} + 80x^{224}$	$\Pi(G) = 52960$
$PI_e(x) = 80x^{218} + 80x^{220} + 80x^{224}$	$PI_e'(1) = 52960$
T((5,7),3)H[8,12]; $v = 96$; $e = 144$; non-bipartite; non-co-graph; non-partial cube	
Polynomial	Index
$\Omega(x) = 144x^1$	$CI(G) = 20592$
$Sd(x) = 144x^{143}$	$Sd(G) = 20592 = CI(G)$
$\Theta(x) = 48x^6 + 36x^8 + 36x^{10} + 24x^{11}$	$\Theta(G) = 1200$
$\Pi(x) = 24x^{133} + 36x^{134} + 36x^{136} + 48x^{138}$	$\Pi(G) = 19536$
$PI_e(x) = 24x^{75} + 12x^{102} + 24x^{103} + 12x^{108} + 12x^{130} + 36x^{132} + 24x^{134}$	$PI_e'(1) = 16320$

T(6,3)H[8,12]   T((4,8),3)V[8,20]   T((5,7),3)H[8,12]
v=96; e=144 v=160; e=144 v=96; e=144
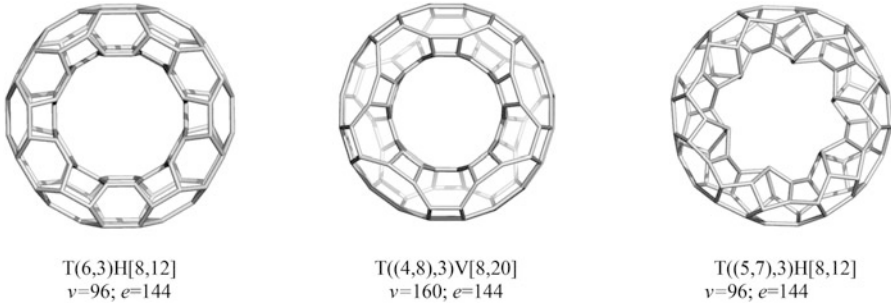
Fig. 2.3 Tori of different tessellation; all are non-*co*-graphs and *non-partial cubes*

$$\Omega(x) = 6x^9; \ \Omega(1) = 54 \ ; \ CI = 2430 \ ; \ (R[4])$$

$$\Theta(x) = 54x^9 \ ; \ \Theta'(1) = 486$$

$$\Pi(x) = 54x^{45} \ ; \ \Pi'(1) = 2430$$

$$Sd(x) = 6x^{54-9} = 6x^{45} \ ; \ Sd'(1) = 270$$

$$PI_e(x) = 54x^{45} \ ; \ PI_e(1) = 2430$$

$$\Omega(x) = 6x^8; \ \Omega'(1) = 48 \ ; \ CI = 1920 \ (f_4)$$

$$\Theta(x) = 24x^8 + 24x^{10} \ ; \ \Theta'(1) = 432$$

$$\Pi(x) = 24x^{38} + 24x^{40} \ ; \ \Pi'(1) = 1872$$

$$Sd(x) = 6x^{48-8} = 6x^{40} \ ; \ Sd'(1) = 240$$

$$PI_e(x) = 24x^{38} + 24x^{40} \ ; \ PI_e'(1) = 1872$$

non-isometric subgraph (see edges in red)

Fig. 2.4 Cubic net (*left*) and its corresponding cage (*right*)

to each other despite both belonging to the same *ops*); the graph is non-*co*-graph and non-partial cube and shows $CI(G) \neq \Pi(G)$ (Diudea 2010a, b, c, d).

Numerical data were computed by our software program Nano Studio (Nagy and Diudea 2009).

In conclusion, the only clear answer to the question "when $CI(G) = \Pi(G)$?" is when $|s_k| = |c_k|$, which can happen in any graph, irrespective if it is *co*-graph and/or partial cube. In plane, bipartite graphs, which are also *co*-graphs and partial cubes, the above condition is achieved immediately. In 3D structures, non-isometric subgraphs often appear, this turning the above equality into an inequality. Despite *co*-graph/partial cube properties being decisive in planar graphs, in 3D structures, they seem not so much involved. Symmetry plays an important role in achieving the above equality. Reformulating "which kind of graph shows the above equality?" will remain as an open question.

2.3 Omega Polynomial in Polybenzenes

2.3.1 Omega Polynomial in 3-Periodic Polybenzenes

O'Keeffe et al. (1992) have proposed, about 20 years ago, two 3D networks of benzene: the first one, called $6.8^2 D$ (also polybenzene, Fig. 2.5), is described to belong to the space group $Pn3m$ and having the topology of the diamond. The second structure (Fig. 2.6) was called $6.8^2 P$ and it belongs to the space group $Im3m$, corresponding to the P-type surface. In fact these networks represent embeddings of the hexagon patch in the two surfaces of negative curvature, D and P, respectively (Szefler and Diudea 2012).

Formulas to calculate Omega polynomial and CI index in three infinite networks, designed on the ground of BTA_48 and BCZ_48 units, are presented in Table 2.5. It was calculated at $R_{max}(8)$ and $R_{max}(12)$, respectively; formulas for the number of atoms, edges, and rings ($R(6)$, $R(8)$, and $R(12)$) are included in this table; examples are also given in view of an easy verification of the general formulas (Szefler and Diudea 2012).

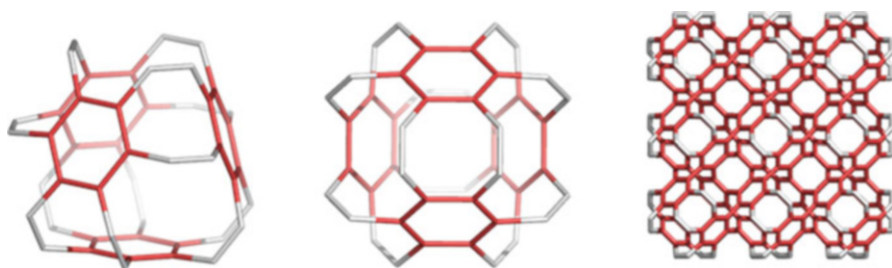**Fig. 2.5** Benzene rings embedded in the D-surface; BTA_48 = $6.8^2 D$ (left), the face-centered BTA_48 unit (*middle*) and the corresponding diamondoid BTA_*fcc*-network (in a (k,k,k)-domain, $k = 3$, *right*)
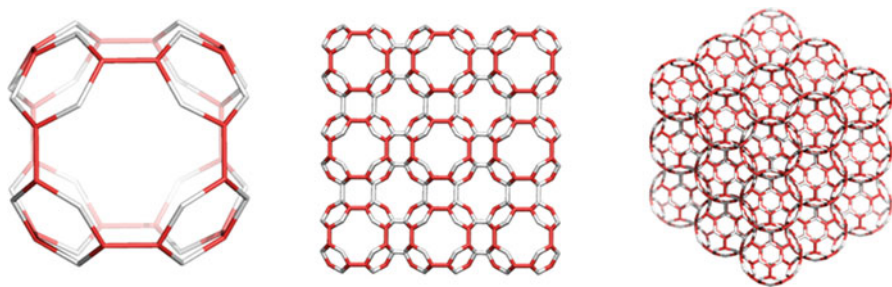

Fig. 2.6 Benzene rings embedded in the P-surface; BCZ_48 = $6.8^2 P$ (*left*), the corresponding networks in a cubic (k,k,k)-domain, $k = 3$ (*middle*), and the same network in the corner view (*right*)

Table 2.5 Omega polynomial and net parameters in 3-periodic polybenzene networks

Net unit	Omega polynomial
BTA_48	$R_{\max}(8)$
	$\Omega(BTA\_48) = 18k^2X^2 + 6k(k-1)X^{2k} + 6kX^{4k} + \sum_{s=1}^{k-1} 12kX^{4s}$
	$\Omega'(1) = 12k^2(3k+2) = e = |E(G)|$
	$CI(G) = 8k^2(162k^4 + 216k^3 + 61k^2 + 3k - 13)$
	$v = |V(G)| = 24k^2(k+1)$
	$R(6) = 4k^3;\ R(8) = 6k^3 - 3k^2 + 3k$
	$R_{\max}(12)$
	$\Omega(BT\_48) = 6X^{2k(2k+1)} + 3X^{4k^2(k+1)} + \sum_{s=1}^{k-1} 12X^{2s(2k+1)}$
	$\Omega'(1) = 12k^2(3k+2) = e = |E(G)|$
	$CI(G) = 8k(6k^2 + 2k - 1)(26k^3 + 24k^2 + 6k + 1)$
	$R(12) = 4k^3$
Examples	$R_{\max}(8)$
	$k=5;\ \Omega(G) = 450X^2 + 60X^4 + 60X^8 + 120X^{10} + 60X^{12} + 60X^{16} + 30X^{20}$
	$CI = 25955400;\ v = 3600;\ e = 5100;\ R(6) = 500;\ R(8) = 690$
	$k=6;\ \Omega(G) = 648X^2 + 72X^4 + 72X^8 + 252X^{12} + 72X^{16} + 72X^{20} + 36X^{24}$
	$CI = 74536992;\ v = 6048;\ e = 8640;\ R(6) = 864;\ R(8) = 1206$
	$R_{\max}(12)$
	$k=5;\ 12X^{22} + 12X^{44} + 12X^{66} + 12X^{88} + 6X^{110} + 3X^{600}$
	$CI = 24683160;\ R(12) = 500$
	$k=6;\ 12X^{26} + 12X^{52} + 12X^{78} + 12X^{104} + 12X^{130} + 6X^{156} + 3X^{1008}$
	$CI = 71009232;\ R(12) = 864$
BCZ_48	$R_{\max}(8)$
	$\Omega(BCZ\_48) = 12kX + 12k(k+1)X^2 + 3k(k-1)(2k-1)X^4 + \sum_{s=1}^{k-1} 24kX^{(2+4s)}$
	$\Omega'(1) = 12k^2(6k-1) = e = |E(G)|$
	$CI(G) = 4k(1296k^5 - 432k^4 + 4k^3 - 24k^2 + 32k - 3)$
	$v = |V(G)| = 48k^3$
	$R(6) = (2k)^3;\ R(8) = 12k^2(k-1)$
	$R_{\max}(12)$
	$\Omega(BC\_48) = (6k-3)X^{(2k)^2} + 6X^{(2k)^3}$
	$\Omega'(1) = 12k^2(6k-1) = |E(G)| = e$
	$CI(G) = 96k^4(50k^2 - 19k + 2)$
	$R(12) = 6k(2k^2 - 2k + 1)$

<div align="right">(continued)</div>

Table 2.5 (continued)

Net unit	Omega polynomial
Examples	$R_{\max}(8)$
	$k = 5$; $60X + 360X^2 + 540X^4 + 120X^6 + 120X^{10} + 120X^{14} + 120X^{18}$
	$CI = 75601140$; $v = 6000$; $e = 8700$; $R(6) = 1000$; $R(8) = 1200$
	$k = 6$; $72X + 504X^2 + 990X^4 + 144X^6 + 144X^{10} + 144X^{14} + 144X^{18} + 144X^{22}$
	$CI = 228432312$; $v = 10368$; $e = 15120$; $R(6) = 1728$; $R(8) = 2160$
	$R_{\max}(12)$
	$k = 5$; $27X^{100} + 6X^{1000}$; $CI = 69420000$; $R(12) = 1230$
	$k = 6$; $33X^{144} + 6X^{1728}$; $CI = 210014208$; $R(12) = 2196$
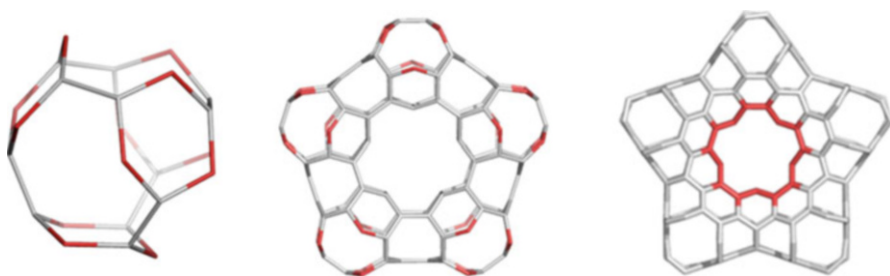
Fig. 2.7 BTZ_24 unit (*left*) and its hyper-pentagons $BTZ_{Cy}5\_120$ (*middle*); hyper-pentagons $BTA_{Cy}5\_210$ (*right*)

2.3.2 Omega Polynomial in 1-Periodic Polybenzenes

The units BTA_48 (Fig. 2.5, left) and BTZ_24 (Fig. 2.7, left) can form "eclipsed" dimers that next provide hyper-pentagons (Fig. 2.7) and further multi-tori **BT**X20 (Fig. 2.8, left column) (Diudea and Szefler 2012).

Multi-tori are complex structures consisting of more than one single torus (Diudea and Nagy 2007; Diudea 2005; Diudea and Petitjean 2008). They can appear as self-assembly products of some repeating units/monomers (formed eventually by spanning of cages/fullerenes), as in spongy carbon or in natural zeolites. Multi-tori can grow by a linear periodicity (Fig. 2.8, right column) or by forming spherical arrays (Diudea and Szefler 2012).

Formulas for calculating Omega polynomial and CI index in the two infinite networks BTA20_k and BTZ20_k are presented in Table 2.6. Formulas were derived from the numerical data calculated on rods consisting of k units BTX20. Omega polynomial was calculated at $R_{\max} = R(8)$; formulas for the number of atoms, edges, and rings (R_6, R_8, and R_{15}, the last one being the simple ring of the hyper-ring $BTX_{Cy}5$) are included in Table 2.6 (Diudea and Szefler 2012).
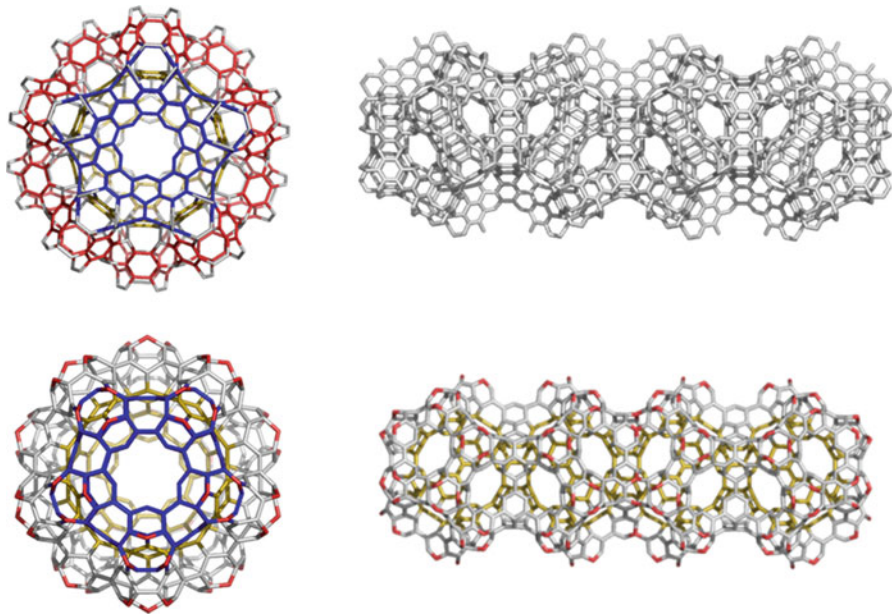
Fig. 2.8 Top row: multi-torus **BT**A20_1_780 (*left*) and its 1-periodic net (BTA20_4_2490, *right*).
Bottom row: multi-torus **BT**Z20_1_480 (*left*) and its 1-periodic net (BTZ20_4_1560, *right*)

Table 2.6 Formulas for omega polynomial and net parameters in 1-periodic BTX20_k network

BTA20_k	$R_{\max}(8)$
	$\Omega(BTA20\_k\_R_8) = 10(k+2)X^3 + 5(k-1)X^4 + (11k+1)X^5 + 20(k+3)X^8 + 10(k-1)X^{10} + 15(k-1)X^{12} + (11k+1)X^{20} + 10X^{2(3k+1)}$
	$\Omega'(1) = 825k + 285 = \left|E(G)\right| = e;$
	$CI(G) = 15\left(45351k^2 + 30715k + 5332\right);$
	$v = \left|V(G)\right| = 10(57k+21);$
	$R_6 = 5(27k+7); \;\; R_8 = 30(3k+1); \;\; R_{15} = 11k+1$
Examples	$k=5$
	$CI = 19390230; \; v = 3060; \; e = 4410; \; R_6 = 710; \; R_8 = 480; \; R_{15} = 56$
	$K=6$
	$CI = 27333870; \; v = 3630; \; e = 5235; \; R_6 = 845; \; R_8 = 570; \; R_{15} = 67$
BTZ20_k	$R_{\max}(8)$
	$\Omega(BTZ20\_k\_R_8) = 10(k+2)X^2 + 30kX^3 + (11k+1)X^5 + 10(k+5)X^6 + 10(k-1)X^8 + 10(k-1)X^{10} + 6kX^{20}$
	$\Omega'(1) = 525k + 165 = \left|E(G)\right| = e$
	$CI(G) = 5\left(55125k^2 + 33653k + 5392\right)$
	atoms $= 120(3k+1) = \left|V(G)\right| = 24u_{24} = 6R_6 \; v = \left|V(G)\right| = 120(3k+1)$
	$R_6 = 20(3k+1) = \left|V(G)\right|/6; \; R_8 = 15(5k+1); \; R_{15} = 11k+1$
Examples	$k=5; \; 70X^2 + 150X^3 + 56X^5 + 100X^6 + 40X^8 + 40X^{10} + 30X^{20}$
	$CI = 7758910; \; v = 1920; \; e = 2790; \; R_6 = 320; \; R_8 = 390; \; R_{15} = 56$
	$K=6; \; 80X^2 + 180X^3 + 67X^5 + 110X^6 + 50X^8 + 50X^{10} + 36X^{20}$
	$CI = 10959050; \; v = 2280; \; e = 3315; \; R_6 = 380; \; R_8 = 465; \; R_{15} = 67$

2.4 Conclusions

Omega polynomial counts the number of topologically parallel edges in all the opposite edge stripes of a connected graph. Definitions and relations with other polynomials and well-known topological indices were given. Omega polynomial was computed in several 3D nanostructures and crystal networks and analytical formulas as well as examples were given. This polynomial is viewed as an alternative to the crystallographic description.

References

Ashrafi AR, Ghorbani M, Jalali M (2008a) Computing sadhana polynomial of V-phenylenic nanotubes and nanotori. Indian J Chem 47A:535–537

Ashrafi AR, Jalali M, Ghorbani M, Diudea MV (2008b) Computing PI and omega polynomials of an infinite family of fullerenes. MATCH Commun Math Comput Chem 60:905–916

Ashrafi AR, Manoochehrian B, Yousefi-Azari H (2006) On the PI polynomial of a graph. Util Math 71:97–108

Aurenhammer F, Hagauer J (1995) Recognizing binary Hamming graphs in O(n2logn) time. Math Syst Theory 28:387–396

Brešar B (2001) Partial Hamming graphs and expansion procedures. Discret Math 237:13–27

Brešar B, Imrich W, Klavžar S (2003) Fast recognition algorithms for classes of partial cubes. Discret Appl Math 131:51–61

Diudea MV (2005) Nanostructures novel architecture. Nova, New York

Diudea MV (2006) Omega polynomial. Carpath J Math 22:43–47

Diudea MV (2010a) Counting polynomials and related indices by edge cutting procedures. MATCH Commun Math Comput Chem 64(3):569–590

Diudea MV (2010b) Counting polynomials in partial cubes. In: Gutman I, Furtula B (eds) Novel molecular structure descriptors – theory and applications II. University of Kragujevac, Kragujevac, pp 191–215

Diudea MV (2010c) Nanomolecules and nanostructures – polynomials and indices. MCM Ser. 10. University of Kragujevac, Kragujevac

Diudea MV, Klavžar S (2010) Omega polynomial revisited. Acta Chem Sloven 57:565–570

Diudea MV, Cigher S, John PE (2008) Omega and related counting polynomials. MATCH Commun Math Comput Chem 60:237–250

Diudea MV, Dorosti N, Iranmanesh A (2010a) Cluj CJ polynomial and indices in a dendritic molecular graph. Studia UBB Chemia LV 4:247–253

Diudea MV, Vizitiu AE, Mirzargar M, Ashrafi AR (2010b) Sadhana polynomial in nano-dendrimers. Carpath J Math 26:59–66

Diudea MV, Florescu MS, Khadikar PV (2006) Molecular topology and its applications. EFICON, Bucharest

Diudea MV, Ilić A (2009) Note on omega polynomial. Carpath J Math 25(2):177–185

Diudea MV, Nagy CL (2007) Periodic nanostructures. Springer, Dordrecht

Diudea MV, Petitjean M (2008) Symmetry in multi tori. Symmetry Culture Sci 19(4):285–305

Diudea MV, Szefler B (2012) Omega polynomial in polybenzene multitori. Iran J Math Sci Info 7:67–74

Djoković DŽ (1973) Distance preserving subgraphs of hypercubes. J Combin Theory Ser B 14:263–267

Eppstein D (2008) Recognizing partial cubes in quadratic time. 19th ACM-SIAM Symp. Discrete Algorithms, San Francisco, 1258–1266

Gutman I (1994) A formula for the Wiener number of trees and its extension to graphs containing cycles. Graph Theory Notes of New York 27:9–15

Gutman I, Klavžar S (1995) An algorithm for the calculation of the szeged index of benzenoid hydrocarbons. J Chem Inf Comput Sci 35:1011–1014

Harary F (1969) Graph theory. Addison-Wesley, Reading

Imrich W, Klavžar S (1993) A simple O(mn) algorithm for recognizing Hamming graphs. Bull Inst Comb Appl 9:45–56

John PE, Khadikar PV, Singh J (2007a) A method of computing the PI index of benzenoid hydrocarbons using orthogonal cuts. J Math Chem 42:37–45

John PE, Vizitiu AE, Cigher S, Diudea MV (2007b) CI index in tubular nanostructures. MATCH Commun Math Comput Chem 57:479–484

Khadikar PV (2000) On a novel structural descriptor PI. Nat Acad Sci Lett 23:113–118

Khadikar PV, Agrawal VK, Karmarkar S (2002) Prediction of lipophilicity of polyacenes using quantitative structure-activity relationships. Bioorg Med Chem 10:3499–3507

Klavžar S (2008a) A bird's eye view of the cut method and a survey of its applications in chemical graph theory. MATCH Commun Math Comput Chem 60:255–274

Klavžar S (2008b) Some comments on co graphs and CI index. MATCH Commun Math Comput Chem 59:217–222

Nagy CsL, Diudea MV (2009) Nano Studio software, "Babes-Bolyai" University, Cluj

O'Keeffe M, Adams GB, Sankey OF (1992) Predicted new low energy forms of carbon. Phys Rev Lett 68:2325–2328

Szefler B, Diudea MV (2012) Polybenzene revisited. Acta Chim Slov 59:795–802

Wilkeit E (1990) Isometric embeddings in Hamming graphs. J Combin Theory Ser B 50:179–197

Winkler PM (1984) Isometric embedding in products of complete graphs. Discret Appl Math 8:209–212

Chapter 3
An Algebraic Modification of Wiener and Hyper–Wiener Indices and Their Calculations for Fullerenes

Fatemeh Koorepazan-Moftakhar, Ali Reza Ashrafi, Ottorino Ori, and Mihai V. Putz

Abstract A molecular graph is a graph in which vertices are atoms and edges are chemical bonds. A graph is called 3-connected, if there does not exist two vertices whose removal disconnects the graph. A fullerene graph is a cubic, planar, and 3-connected whose faces are all pentagons or hexagons. A fullerene is a molecule, that is, its molecular graph is a fullerene graph. In 1991, Graovac and Pisanski (1991) proposed an algebraic modification of the Wiener index of a graph by considering its automorphism group. In this chapter, an algebraic modification for the hyper–Wiener index is presented. These quantities will be computed for some classes of fullerenes.

F. Koorepazan-Moftakhar • A.R. Ashrafi (✉)
Department of Nanocomputing, Institute of Nanoscience and Nanotechnology, University of Kashan, Kashan 87317-53153, Iran

Department of Pure Mathematics, Faculty of Mathematical Sciences, University of Kashan, Kashan 87317-53153, Iran
e-mail: ashrafi@kashanu.ac.ir

O. Ori
Actinium Chemical Research, Via Casilina 1626/A, 00133 Rome, Italy

Laboratory of Computational and Structural Physical-Chemistry for Nanosciences and QSAR, Department of Biology-Chemistry, Faculty of Chemistry, Biology, Geography, West University of Timişoara, Pestalozzi Str. No. 16, 300115 Timişoara, Romania

M.V. Putz
Laboratory of Computational and Structural Physical-Chemistry for Nanosciences and QSAR, Department of Biology-Chemistry, Faculty of Chemistry, Biology, Geography, West University of Timişoara, Pestalozzi Str. No. 16, RO-300115 Timişoara, Romania

Laboratory of Renewable Energies-Photovoltaics, R&D National Institute for Electrochemistry and Condensed Matter, Dr. A. Paunescu Podeanu Str. No. 144, RO-300569 Timişoara, Romania

3.1 Introduction

A *graph* is a pair $G = (V, E)$ of sets such that V is nonempty and E is a subset of the set of all 2-element subsets of V. The elements of V and E are called *vertices* and *edges*, respectively. The graph G is called *connected*, if we cannot partition the vertex set V into two subsets A and B such that there is no edge with an end point in A and another in B. Suppose v is a vertex of G. The *degree* of v, $\deg_G(v)$, in G is the number of edges incident to the v. The graph G is said to be a *molecular graph*, if all vertex degrees are ≤ 4. A *cubic graph* is a molecular graph in which all vertex degrees are equal to 3.

A graph G is called *3-connected*, if there do not exist two vertices whose removal disconnects the graph. A *fullerene graph* is cubic, planar, and 3-connected whose faces are all pentagons or hexagons. A *fullerene* is a molecule, that is, its molecular graph is a fullerene graph. After discovering buckminsterfullerene C_{60} by Kroto and his team (Kroto et al. 1985), the study of fullerenes started as a new topic in nanochemistry, and some mathematicians devoted their time to obtain the mathematical properties of these new materials.

Suppose G is a graph and $\beta: V(G) \rightarrow V(G)$ is a function. β is called an *automorphism* if and only if β and β^{-1} preserve adjacency relation in G. The set of all such mapping is denoted by $\text{Aut}(G)$, the *automorphism group* of G. This group is called also the *topological symmetry* group of G. If G is a molecular graph, then $\text{Aut}(G)$ is the largest group which can occur as the symmetry group of the molecule under consideration. It is well known that the symmetry and topological symmetry of fullerenes are the same. For mathematical properties of fullerene graphs, we refer to the famous book of Fowler and Manolopoulos (1995). The books (Cataldo et al. 2011; Ashrafi et al. 2013) also contain recent literature reviews on theory and experiment of fullerenes. Graver (2005) published a complete catalog of fullerenes with ten or more symmetries (Ori et al. 2010), and the authors presented a measure for evaluation of sphericality in fullerenes. This gives correct numbers of NMR resonance peaks and relative intensities. We recommend the interested readers to consult Myrvold et al. (2007) and Schwerdtfeger et al. (2013) for two important packages for working by fullerenes.

The *distance* between two vertices u and v in a graph G, $d(u, v)$, is defined as the number of edges in the shortest path connecting them. The *Wiener index* of G, $W(G)$, is defined as the sum of distances between all pairs of vertices in G (Wiener 1947). This graph invariant has remarkable applications in chemistry and also in computer science. We refer to Gutman and Šoltés (1991) for application of this number in chemistry.

A connected graph G without cycles is said to be an *acyclic graph*. The hyper–Wiener index of acyclic graphs was introduced by Milan Randić, as a generalization of the Wiener index. Then Klein et al. (1995) extended this graph invariant for arbitrary graphs. It is defined as

$$WW(G) = 1/2W(G) + 1/2\sum\nolimits_{\{x,y\}} d(x,y)^2.$$

The mathematical properties and chemical meaning of this topological index are reported in Khalifeh et al. (2008) and Gutman et al. (1997). It is merit to mention here that there is a matrix version of the hyper–Wiener index introduced by M.V. Diudea (1996a, b, 1997; Diudea et al. 1997). To explain, we have to introduce some algebraic concepts. Suppose G is a connected graph. The distance matrix $D = D(G)$ is an $n \times n$ matrix in which the ijth entry is the length of the shortest path connecting the ith and jth vertices of the graph under consideration. The Wiener matrix $W = W(G)$ is another $n \times n$ matrix such that its ijth entry is defined as the number of paths containing the (i,j) path. These matrices are basis for calculating W, whereas distance path and Wiener path are basis for the calculation of hyper–Wiener index. We encourage the interested readers to consult the mentioned papers by Diudea and references therein for more information on this topic.

Graovac and Pisanski (1991) in their seminal paper combine distance and symmetry to propose a generalization of the classical Wiener index. To explain, we assume that G is a graph with automorphism group $\Gamma = \text{Aut}(G)$. The modified Wiener index of G is defined as

$$\hat{W}(G) = \frac{|V(G)|}{2|\Gamma|} \sum\nolimits_{x \in V(G)} \sum\nolimits_{\alpha \in \Gamma} d(x, \alpha(x)) \ .$$

Firouzian et al. (2014) introduced in a similar way the modified hyper–Wiener index of a graph G as follows:

$$\overset{\wedge}{WW}(G) = \frac{1}{2} \hat{W}(G) + \frac{|V(G)|}{4|\Gamma|} \sum\nolimits_{u \in V(G), \ \alpha \in \Gamma} d(u, \alpha(u))^2.$$

The aim of this chapter is to compute the modified Wiener and modified hyper–Wiener indices of some classes of fullerene graphs. To compute these graph invariants, we use the symmetry groups of these fullerenes reported in Djafari et al. (2013), Koorepazan-Moftakhar and Ashrafi (2013, 2014), and Koorepazan-Moftakhar et al. (2014). In our calculations, we first draw the molecular graphs of the fullerenes under consideration by HyperChem (HyperChem package Release 7.5 for Windows 2002). Then the distance matrix will be computed by TopoCluj (Diudea et al. 2002). Finally, we apply some GAP (The GAP Team 1995) and MAGMA (Bosma et al. 1997) codes to calculate the automorphism group and modified Wiener and modified hyper–Wiener indices of four classes of fullerenes. We refer the interested readers to consult papers (Ashrafi et al. 2008, 2009; Ashrafi and Sabaghian-Bidgoli 2009) and references therein for more information on topological properties of fullerenes.

3.2   Wiener and Hyper–Wiener Indices of a Fullerene Under Its Symmetry

Suppose Γ is a finite group and $a, b \in \Gamma$. The elements a and b are said to be *conjugate* if and only if there exists $x \in \Gamma$ such that $b = x^{-1}ax$. The set of all conjugates of the element a is denoted by $Cl_{\Gamma}(a)$. A function from a group Γ into the complex numbers is called a class function if the images of Γ under conjugate elements are the same. We now assume that G is a graph and $\Gamma = \text{Aut}(G)$. It is easy to see that the function $\delta : \Gamma \to C$ given by

$$\delta(g) = \frac{1}{|V(G)|} \sum_{x \in V(G)} d(x, g(x))$$

is a class function and the modified hyper $-$ Wiener index of G can be computed by the following formula:

$$\hat{W}(G) = \frac{|V(G)|^2}{2|\Gamma|} \sum_{g \in \Gamma} \delta(g)$$

Suppose G and H are finite groups. A mapping $f: G \to H$ is called a *homomorphism*, if for each $x, y \in G$, $f(xy) = f(x)f(y)$. If f is also invertible, then it is called an *isomorphism*. The isomorphism is an equivalence relation on groups. Since an isomorphism preserves all group properties, mathematicians usually consider two isomorphic groups to be the same. The Cartesian product $G \times H$ is a group in which for all (a,b), $(x,y) \in G \times H$, $(a,b)(x,y) = (ax,by)$.

A homomorphism $f: G \to GL(n,C)$ is called a *representation* of G, where $GL(n,C)$ denotes the set of all $n \times n$ invertible matrices over the complex field C. The mapping $\chi: G \to C$ given by $\chi(g) = Trf(g)$ is called a *character* afforded by f. Suppose χ and ψ are characters of G. The inner product $\langle \chi, \psi \rangle$ is defined as

$$\langle \chi, \psi \rangle = \frac{1}{|G|} \sum_{g \in G} \chi(g) \, \psi(g).$$

The character χ is called *irreducible*, if $\langle \chi, \chi \rangle = 1$. It is well known that the number of irreducible characters is the same as the number of conjugacy classes in G.

One of the main applications of group theory in science is studying *symmetry of molecules*. This is important in understanding *vibrational spectra*. It can help to analyze and predict vibrational spectra and response to this question in which vibration is IR or Raman active, but it cannot help to predict positions of the bands. The concept of *group action* that will be explained later is the basic tool of such applications.

Suppose X is a set. The set of all permutations of X is a group under composition denoted by S_X. If $X = \{1,2, \ldots, n\}$, then it is convenient to write S_n as S_X. It is well

known that $|S_n| = n!$ and S_n has a unique subgroup of order $n!/2$. This group is called the alternating group on n symbols and denoted by A_n. The set of all rotation and reflection of an n-gon is a finite group of order $2n$. This group is called the dihedral group, denoted by D_{2n}.

In this chapter four infinite classes $A[n]$, $B[n]$, $C[n]$, and $D[n]$ of fullerene graphs are considered into account. In Koorepazan-Moftakhar and Ashrafi (2014), the symmetry and topology of these fullerenes are investigated in details. We use this information to compute the modified Wiener and hyper–Wiener indices of these fullerenes.

3.2.1 The Fullerene Series A[n] and B[n]

In a recent paper (Ashrafi and Koorepazan-Moftakhar 2014), the authors calculated generator sets for the fullerene series $A[n]$ and $B[n]$ in general. The general term of the fullerene series $A[n]$ (Fig. 3.1) has exactly $50 + 10n$, $n \geq 2$, carbon atoms, and the general term of the fullerene series $B[n]$ (Figs. 3.2 and 3.3) has exactly $60 + 12n$, $n \geq 1$. In Koorepazan-Moftakhar and Ashrafi (2015), the authors conjectured that for each graph G, the class function δ is a rational combination of the trivial character χ_1 and at most two other irreducible characters of $\mathrm{Aut}(G)$. In this section some counterexamples for this conjecture are supplied. For the first counterexample, we use the generator set of the symmetry group of $A[n]$ which is presented in Ashrafi and Koorepazan-Moftakhar (2014) as follows:

$A_1 :=$ (2, 5)(3, 4)(7, 10)(8, 9)(11, 20)(12, 19)(13, 18)(14, 17)(15, 16)...(10n + 31, 10n + 40) (10n + 32, 10n + 39) (10n + 33, 10n + 38) (10n + 34, 10n + 37) (10n + 35, 10n + 36)(10n + 42, 10n + 45) (10n + 43, 10n + 44)(10n + 47, 10n + 50)(10n + 48, 10n + 49).

$A_2 :=$ (1,2,3,4,5)(6,7,8,9,10)(11,13,15,17,19)(12,14,16,18,20)...(10n + 31,10n + 33, 10n + 35,10n + 37, 10n + 39) (10n + 32, 10n + 34, 10n + 36, 10n + 38,
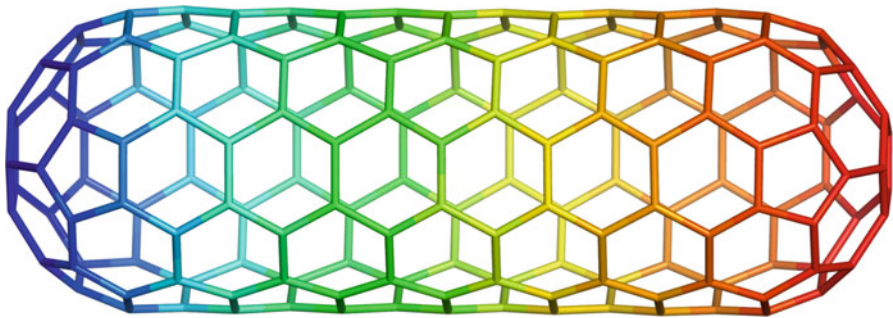

Fig. 3.1 The fullerene $A[12]$
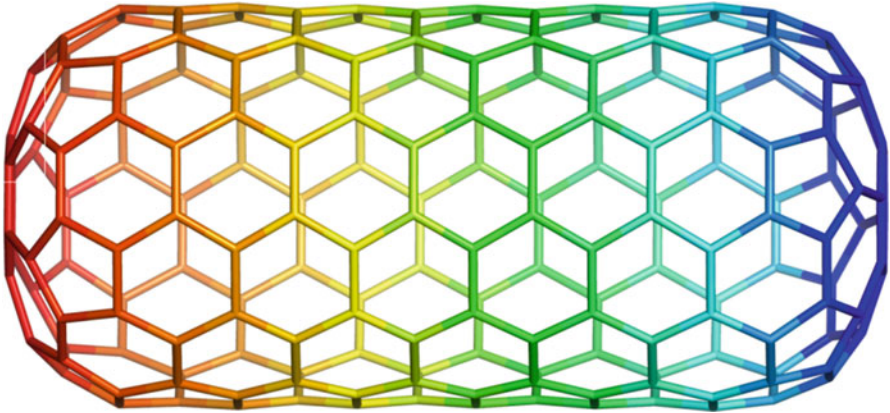
Fig. 3.2 The fullerene graph $B[11]$
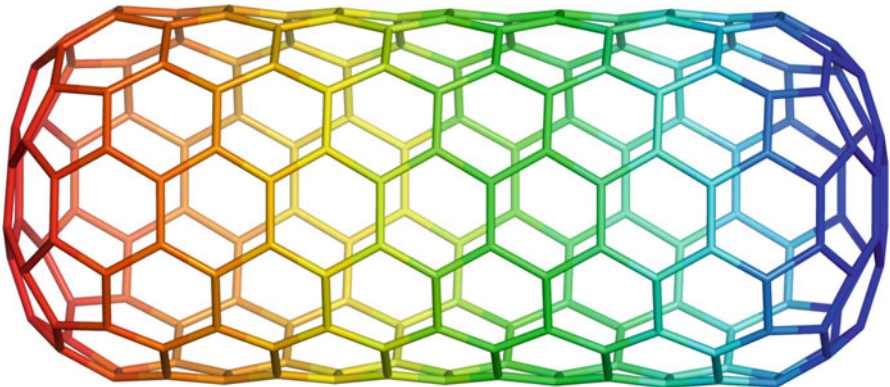
Fig. 3.3 The fullerene $B[12]$

$10n + 40$) ($10n + 41, 10n + 42, 10n + 43, 10n + 44, 10n + 45$) ($10n + 46, 10n + 47,$
$10n + 48, 10n + 49, 10n + 50$).

A_3:= (1, $10n + 46$) (2, $10n + 47$) (3, $10n + 48$) (4, $10n + 49$) (5, $10n + 50$)
(6, $10n + 41$) (7, $10n + 42$) (8, $10n + 43$) (9, $10n + 44$) (10, $10n + 45$)
(11, $10n + 31$) (12, $10n + 32$) (13, $10n + 33$) (14, $10n + 34$) (15, $10n + 35$)
(16, $10n + 36$) (17, $10n + 37$) (18, $10n + 38$) (19, $10n + 39$) (20, $10n + 40$)
(21, $10n + 21$) ... (30, $10n + 30$) ... ($5n + 11, 5n + 31$) ($5n + 12, 5n + 32$)
($5n + 13, 5n + 33$) ($5n + 14, 5n + 34$) ($5n + 15, 5n + 35$) ($5n + 16, 5n + 36$)
($5n + 17, 5n + 37$) ($5n + 18, 5n + 38$) ($5n + 19, 5n + 39$) ($5n + 20, 5n + 40$).

It is easy to see that A_1, A_2, and A_3 have orders 2, 5 and 2, respectively. On the other hand, $(A_2A_1)^2 = e$, $A_2A_3A_2^{-1}A_3^{-1} = e$ and $A_1A_3A_1^{-1}A_3^{-1} = e$. Therefore, Aut $(A[n]) = \langle A_1, A_2, A_3 \rangle$ is isomorphic to a dihedral group of order 20, D_{20}.

Result 3.2.1.1 (Koorepazan-Moftakhar and Ashrafi 2015, Example 8) The modified Wiener and modified hyper–Wiener indices of these fullerenes can be computed by the following formulas:

$$\hat{W}(A[n]) = \begin{cases} \dfrac{25}{2}n^3 + \dfrac{745}{2}n^2 + \dfrac{5285}{2}n + \dfrac{10925}{2} & n \text{ is odd} \\\\ \dfrac{25}{2}n^3 + \dfrac{745}{2}n^2 + 2640n + 5450 & n \text{ is even} \end{cases}.$$

Result 3.2.1.2 (Firouzian et al. 2014, p. 169)

$$WW \wedge (A[n]) = \begin{cases} \dfrac{25}{6}n^4 + \dfrac{725}{6}n^3 + \dfrac{5320}{3}n^2 + \dfrac{60745}{6}n + \dfrac{37575}{2} & n \text{ is odd} \\\\ \dfrac{25}{6}n^4 + \dfrac{725}{6}n^3 + \dfrac{5350}{3}n^2 + \dfrac{30335}{3}n + 18475 & n \text{ is even} \end{cases}.$$

In Koorepazan-Moftakhar and Ashrafi (2015), the authors settled a conjecture about the class function δ. They announced that their calculations show that the class function δ can be decomposed into linear combination of three irreducible characters $\psi_1 = 1$, ψ_2, and ψ_3 with rational coefficients.

In what follows, we present a counterexample for this conjecture. Choose the fullerene $G = A[12]$. It is easy to see that $\Gamma = \text{Aut}(G) \cong D_{20}$. The character table of this group is as follows:

Table 3.1 The character table of $\text{Aut}(A[12]) \cong D_{20}$ and the class function δ_1

	1a	2a	5a	5b	2b	10a	10b	2c
χ_1	1	1	1	1	1	1	1	1
χ_2	1	−1	1	1	−1	1	1	1
χ_3	1	−1	1	1	1	−1	−1	−1
χ_4	1	1	1	1	−1	−1	−1	−1
χ_5	2	0	$\frac{-1-\sqrt{5}}{2}$	$\frac{-1+\sqrt{5}}{2}$	0	$\frac{1+\sqrt{5}}{2}$	$\frac{1-\sqrt{5}}{2}$	−2
χ_6	2	0	$\frac{-1+\sqrt{5}}{2}$	$\frac{-1-\sqrt{5}}{2}$	0	$\frac{1-\sqrt{5}}{2}$	$\frac{1+\sqrt{5}}{2}$	−2
χ_7	2	0	$\frac{-1-\sqrt{5}}{2}$	$\frac{-1+\sqrt{5}}{2}$	0	$\frac{-1-\sqrt{5}}{2}$	$\frac{-1+\sqrt{5}}{2}$	2
χ_8	2	0	$\frac{-1+\sqrt{5}}{2}$	$\frac{-1-\sqrt{5}}{2}$	0	$\frac{-1+\sqrt{5}}{2}$	$\frac{-1-\sqrt{5}}{2}$	2
δ_1	0	$\frac{377}{85}$	$\frac{62}{17}$	$\frac{120}{17}$	$\frac{959}{85}$	$\frac{180}{17}$	$\frac{219}{17}$	$\frac{146}{17}$

Using calculations given in Table 3.1, one can see that

$$\delta_1 = \frac{661}{85}\chi_1 - \frac{7}{85}\chi_2 + \frac{1}{170}\chi_3 - \frac{581}{170}\chi_4 + \left(\frac{-75+19\sqrt{5}}{340}\right)\chi_5$$
$$+ \left(\frac{-75-19\sqrt{5}}{340}\right)\chi_6 + \left(\frac{-289+97\sqrt{5}}{340}\right)\chi_7 + \left(\frac{-289-97\sqrt{5}}{340}\right)\chi_8.$$

We now present other counterexamples for the mentioned conjecture in our fullerene series. Start by the fullerene series $B[n]$. We first assume that n is odd. Then, the following two permutations generate $\mathrm{Aut}(B[n])$ (Ashrafi and Koorepazan-Moftakhar 2014):

$B_1 :=$ (1, $12n+55$) (2, $12n+60$) (3, $12n+59$) ... (7, $12n+49$) (8, $12n+54$) (9, $12n+53$) .... (12, $12n+50$) (13,$12n+37$) (14,$12n+48$) ... (24,$12n+38$) (25, $12n+25$) (26, $12n+36$) ... (36,$12n+26$) (37,$12n+13$) (38,$12n+24$)... ($6n+19, 6n+31$) ($6n+20, 6n+42$) ($6n+21,6n+41$) ... ($6n+30, 6n+32$).

$B_2 :=$ (2,6)(3,5) (8,12) (9,11) (13,24) (14,23) (15,22) (16,21) (17,20) (18,19)... ($12n+37,12n+48$) ($12n+38,12n+47$)($12n+39,12n+46$)($12n+40,12n+45$) ($12n+41$, $12n+44$)($12n+42$, $12n+43$) ($12n+49,12n+54$) ($12n+50$, $12n+53$)($12n+51,12n+52$) ($12n+55$, $12n+60$) ($12n+56$, $12n+59$) ($12n+57, 12n+58$).

Since B_1 and $B_1 B_2$ have orders 2 and 12, respectively, the symmetry groups of these fullerenes are isomorphic to the dihedral group of order 24.

It is possible to find a formula for the class function of the fullerene series $A[n]$ in general. We encourage the interested readers to consult Koorepazan-Moftakhar and Ashrafi (2015, Example 8) for calculations given in Table 3.2.

Again by Ashrafi and Koorepazan-Moftakhar (2014), the following three permutations, when n is even, generate $B[n]$:

$B_3 :=$ (2,6) (3,5) (8,12) (9,11) (13,24) (14,23) (15,22) (16,21) (17,20) (18, 19) ... ($12n+37,12n+48$) ($12n+38,12n+47$) ($12n+39,12n+46$) ($12n+40,12n+45$) ($12n+41,12n+44$) ($12n+42,12n+43$) ($12n+50, 12n+53$)($12n+51, 12n+52$) ($12n+56, 12n+60$)($12n+57, 12n+59$).

Table 3.2 The class functions $\delta'(g) = |V(G)|\delta(g)$ on each conjugacy class

n is Even			
Conjugacy Classes	1a	2a	5a	5b
$\delta(g)$	0	$50n+154$	$40n+140$	$80n+240$
Conjugacy Classes	2b	2c	10a	10b
$\delta(g)$	$5n^2+50n+140$	$5n^2+76n+286$	$5n^2+70n+240$	$5n^2+90n+390$
n is Odd			
Conjugacy Classes	1a	2a	5a	5b
$\delta(g)$	0	$50n+154$	$40n+140$	$80n+240$
Conjugacy Classes	10a	2b	10b	2c
$\delta(g)$	$5n^2+60n+175$	$5n^2+74n+281$	$5n^2+80n+305$	$5n^2+100n+475$

$B_4 :=$ (1,12n + 55) (2, 12n + 56) (3,12n + 57)(4, 12n + 58)(5, 12n + 59) (6, 12n + 60)(7, 12n + 49) (8, 12n + 50) (9, 12n + 51) (10,12n + 52) (11,12n + 53)(12, 12n + 54)(13, 12n + 37) (14, 12n + 38) (15,12n + 39) (16,12n + 40) (17, 12n + 41) (18,12n + 42) (19, 12n + 43)(20, 12n + 44) (21, 12n + 45) (22, 12n + 46) (23, 12n + 47) (24,12n + 48) . . . (6n + 13,6n + 37) (6n + 14, 6n + 38) (6n + 15, 6n + 39) (6n + 16, 6n + 40) (6n + 17, 6n + 41) (6n + 18, 6n + 42) (6n + 19, 6n + 43) (6n + 20, 6n + 44) (6n + 21, 6n + 45) (6n + 22, 6n + 46) (6n + 23, 6n + 47, 6n + 24, 6n + 48).

$B_5 :=$ (1, 2, 3, 4, 5, 6) (7, 8, 9, 10, 11, 12) (13, 15, 17, 19, 21, 23) (14, 16, 18, 20, 22, 24) . . . (12n + 37, 12n + 39, 12n + 41, 12n + 43, 12n + 45, 12n + 47) (12n + 38,12n + 40,12n + 42,12n + 44,12n + 46, 12n + 48) (12n + 49,12n + 50, 12n + 51,12n + 52,12n + 53,12n + 54)(12n + 55,12n + 56,12n + 57,12n + 58, 12n + 59, 12n + 60).

It is easy to see that B_3 and B_4 have order 2; B_5 is a symmetry element of order 6 and $B_5 B_3$, $B_5 B_4 B_5^{-1} B_4^{-1}$ and $B_3 B_4 B_3^{-1} B_4^{-1}$ are symmetry elements of order 2, 2, and 6, respectively. Therefore, the symmetry group of $B[n]$ is isomorphic to $Z_2 \times Z_2 \times S_3$.

By calculation given in Table 3.3, the class function δ_2 can be computed as follows:

$$\delta_2 = \frac{1741}{204}\chi_1 - \frac{1}{204}\chi_2 - \frac{1}{204}\chi_3 - \frac{7}{204}\chi_4 - \frac{37}{204}\chi_5 - \frac{55}{204}\chi_6$$
$$- \frac{3}{68}\chi_7 - \frac{671}{204}\chi_8 - \frac{1}{68}\chi_9 - \frac{7}{68}\chi_{10} - \frac{73}{204}\chi_{11} - \frac{383}{204}\chi_{12}.$$

So, our third counterexample for conjecture 5 in Koorepazan-Moftakhar and Ashrafi (2015) is $B[11]$. The character table of $\mathrm{Aut}(B[11])$ is recorded in Table 3.4. Apply this table to compute the class function δ_3 as follows:

Table 3.3 The character table of $\mathrm{Aut}(B[12]) \cong Z_2 \times Z_2 \times S_3$ and the class function δ_2

	1a	2a	2b	6a	3a	2c	2d	6b	6c	2e	2f	2g
χ_1	1	1	1	1	1	1	1	1	1	1	1	1
χ_2	1	−1	−1	1	1	1	−1	1	1	−1	1	1
χ_3	1	−1	−1	1	1	1	1	−1	−1	1	−1	−1
χ_4	1	−1	1	−1	1	−1	−1	1	−1	1	−1	1
χ_5	1	−1	1	−1	1	−1	1	−1	1	−1	1	−1
χ_6	1	1	−1	−1	1	−1	−1	−1	1	1	1	−1
χ_7	1	1	−1	−1	1	−1	1	1	−1	−1	−1	1
χ_8	1	1	1	1	1	1	−1	−1	−1	−1	−1	−1
χ_9	2	0	0	−1	−1	2	0	−1	−1	0	2	2
χ_{10}	2	0	0	−1	−1	2	0	1	1	0	−2	−2
χ_{11}	2	0	0	1	−1	−2	0	−1	1	0	−2	2
χ_{12}	2	0	0	1	−1	−2	0	1	−1	0	2	−2
δ_2	0	$\frac{263}{51}$	$\frac{91}{17}$	$\frac{62}{17}$	$\frac{120}{17}$	10	$\frac{607}{51}$	$\frac{180}{17}$	$\frac{219}{17}$	$\frac{599}{51}$	$\frac{146}{17}$	$\frac{262}{17}$

Table 3.4 The character table of $\mathrm{Aut}(B[11]) \cong D_{24}$ and the class function δ_3

	1a	2a	6a	3a	2b	12a	2c	4a	12b
χ_1	1	1	1	1	1	1	1	1	1
χ_2	1	-1	1	1	1	-1	1	-1	-1
χ_3	1	-1	1	1	1	1	-1	1	1
χ_4	1	1	1	1	1	-1	-1	-1	-1
χ_5	2	0	-2	2	-2	0	0	0	0
χ_6	2	0	-1	-1	2	-1	0	2	-1
χ_7	2	0	-1	-1	2	1	0	-2	1
χ_8	2	0	1	-1	-2	$\sqrt{3}$	0	0	$-\sqrt{3}$
χ_9	2	0	1	-1	-2	$-\sqrt{3}$	0	0	$\sqrt{3}$
δ_3	0	$\frac{125}{24}$	$\frac{29}{8}$	7	$\frac{79}{8}$	9	$\frac{541}{48}$	$\frac{179}{16}$	$\frac{109}{8}$

$$\delta_3 = \frac{527}{64}\chi_1 - \frac{1}{192}\chi_2 - \frac{1}{192}\chi_3 - \frac{583}{192}\chi_4 - \frac{25}{96}\chi_5 - \frac{1}{12}\chi_6 - \frac{1}{24}\chi_7$$
$$- \left(\frac{106 + 37\sqrt{3}}{96}\right)\chi_8 + \left(\frac{-106 + 37\sqrt{3}}{96}\right)\chi_9.$$

Using these calculations, we have

Result 3.2.1.2 The modified Wiener and modified hyper–Wiener indices of the fullerene series $B[n]$ can be computed as follows:

- $\hat{W}(B[1]) = 13500$ and $\hat{W}(B[2]) = 20034$.
- $\hat{W}(B[n]) = \begin{cases} 18n^3 + 594n^2 + 4284n + 8820 & n \text{ is odd} \\ 18n^3 + 594n^2 + 4326n + 9030 & n \text{ is even} \end{cases}$.
- $\overset{\wedge}{WW}(B[n]) = \begin{cases} 6n^4 + 183n^3 + 3069n^2 + 18075n + 32775 & n \text{ is odd} \\ 6n^4 + 183n^3 + 3093n^2 + 18606n + 34830 & n \text{ is even} \end{cases}$.

3.2.2 The Fullerene Series C[n] and D[n]

The fullerene series $C[n]$ (Figs. 3.4 and 3.5) has exactly $10n$ carbon atoms. We first calculate the permutation symmetry of these fullerenes. In the case of $n = 2$, the following permutations generated the automorphism group of $C[2]$.

$C_1 := (2, 5)(3, 4)(7, 10)(8, 9)(11, 12)(13, 15)(16, 17)(18, 20)$
$C_2 := (1, 2, 3, 4, 5)(6, 7, 8, 9, 10)(11, 12, 13, 14, 15)(16, 17, 18, 19, 20)$
$C_3 := (3, 7)(4, 12)(5, 6)(8, 13)(9, 17)(10, 11)(14, 18)(15, 16)$
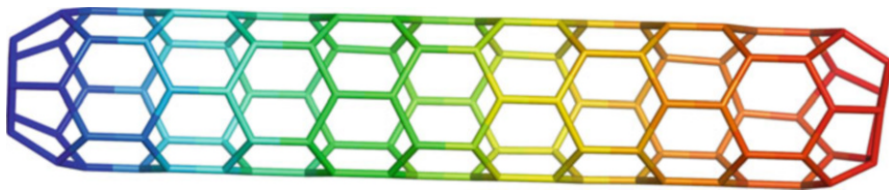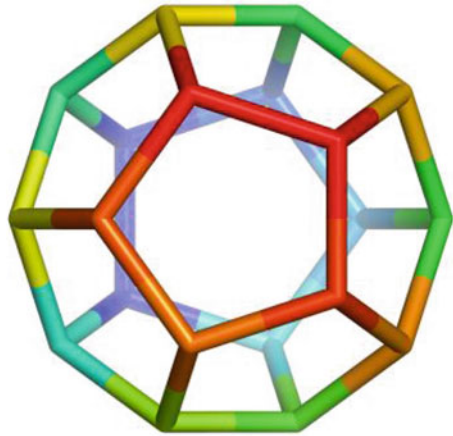
Fig. 3.4 The fullerene $C[2]$

Fig. 3.5 The fullerene $C[11]$

It is easy to apply computer algebra system GAP to show that the group generated by C_1, C_2, and C_3 is isomorphic to $Z_2 \times A_5$ (Djafari et al. 2013). Notice that this group is isomorphic to the I_h point group symmetry. If $n \geq 2$, then the automorphism group of $C[n]$ is isomorphic to D_{20}. In what follows, a generator set for the automorphism group of $C[11]$ is computed.

$C_4 := $ (1, 2, 3, 4, 5)(6, 7, 8, 9, 10)(11, 12, 13, 14, 15)(16, 17, 18, 19, 20)(21, 22, 23,24,25)(26,27,28,29, 30) (31, 32, 33, 34, 35) (36, 40, 39, 38, 37) (41, 45, 44, 43, 42) (46, 50, 49, 48, 47) (51, 55, 54, 53, 52) (56,57,58,59,60) (61,62,63,64,65)(66,70,69,68,67)(71,75,74,73,72) (76,80, 79, 78, 77) (81, 85, 84, 83, 82) (86,90,89,88,87)(91,95,94,93,92)(96,100, 99, 98, 97) (101, 105, 104, 103, 102) (106, 110, 109, 108, 107).

$C_5 := $ (2, 5)(3, 4)(7, 10)(8, 9) (11, 12) (13, 15) (16, 17) (18, 20) (21, 23) (24, 25) (27, 30) (28, 29) (31, 32) (33, 35) (36, 37) (38, 40)(41, 43)(44, 45)(46, 48) (49, 50)(51, 54)(52, 53)(56, 60) (57, 59) (62, 65)(63, 64) (67, 70)(68, 69) (71, 72) (73, 75) (76, 77) (78, 80)(81, 83)(84, 85)(86, 88)(89, 90) (91, 94)(92, 93)(96, 97) (98, 100)(101, 103) (104, 105) (106, 108)(109, 110).

$C_6 := $ (1,106,3,109,5,107,2,110,4,108) (6,101,8,104,10,102,7,105,9,103) (11,96,13,99, 15,97,12,100,14,98) (16,92,18,95,20,93,17,91,19,94) (21,87,23,90,25,88, 22, 86, 24, 89) (26, 81, 28, 84, 30, 82, 27, 85, 29, 83) (31,76,33,79,35,77,32,80,34,78)

Table 3.5 The character table of $\mathrm{Aut}(C[2]) \cong Z_2 \times A_5$ and the class function δ_4

	1a	2a	3a	2b	5a	10a	5b	6a	10b	2c
χ_1	1	1	1	1	1	1	1	1	1	1
χ_2	1	-1	1	1	1	-1	1	-1	-1	-1
χ_3	3	-1	0	-1	$\frac{1-\sqrt5}{2}$	$\frac{1+\sqrt5}{2}$	$\frac{1+\sqrt5}{2}$	0	$\frac{1-\sqrt5}{2}$	3
χ_4	3	-1	0	-1	$\frac{1+\sqrt5}{2}$	$\frac{1-\sqrt5}{2}$	$\frac{1-\sqrt5}{2}$	0	$\frac{1+\sqrt5}{2}$	3
χ_5	3	1	0	-1	$\frac{1-\sqrt5}{2}$	$\frac{-1-\sqrt5}{2}$	$\frac{1+\sqrt5}{2}$	0	$\frac{-1+\sqrt5}{2}$	-3
χ_6	3	1	0	-1	$\frac{1+\sqrt5}{2}$	$\frac{-1+\sqrt5}{2}$	$\frac{1-\sqrt5}{2}$	0	$\frac{-1-\sqrt5}{2}$	-3
χ_7	4	0	1	0	-1	-1	-1	1	-1	4
χ_8	4	0	1	0	-1	1	-1	-1	1	-4
χ_9	5	1	-1	1	0	0	0	-1	0	5
χ_{10}	5	-1	-1	1	0	0	0	1	0	-5
δ_4	0	$\frac{9}{5}$	$\frac{12}{5}$	$\frac{16}{5}$	$\frac{3}{2}$	2	3	$\frac{13}{5}$	$\frac{7}{2}$	5

Table 3.6 The character table of $\mathrm{Aut}(C[11]) \cong D_{20}$ and the class function δ_5

	1a	2a	5a	5b	2b	10a	2c	10b
χ_1	1	1	1	1	1	1	1	1
χ_2	1	-1	1	1	-1	1	1	1
χ_3	1	-1	1	1	1	-1	-1	-1
χ_4	1	1	1	1	-1	-1	-1	-1
χ_5	2	0	$\frac{-1-\sqrt5}{2}$	$\frac{-1+\sqrt5}{2}$	0	$\frac{1+\sqrt5}{2}$	-2	$\frac{1-\sqrt5}{2}$
χ_6	2	0	$\frac{-1+\sqrt5}{2}$	$\frac{-1-\sqrt5}{2}$	0	$\frac{1-\sqrt5}{2}$	-2	$\frac{1+\sqrt5}{2}$
χ_7	2	0	$\frac{-1-\sqrt5}{2}$	$\frac{-1+\sqrt5}{2}$	0	$\frac{-1-\sqrt5}{2}$	2	$\frac{-1+\sqrt5}{2}$
χ_8	2	0	$\frac{-1+\sqrt5}{2}$	$\frac{-1-\sqrt5}{2}$	0	$\frac{-1+\sqrt5}{2}$	2	$\frac{-1-\sqrt5}{2}$
δ_5	0	$\frac{126}{55}$	$\frac{21}{11}$	$\frac{37}{3}$	$\frac{125}{11}$	$\frac{112}{9}$	11	$\frac{129}{11}$

(36,75,39,73,37,71,40,74,38,72) (41,69,44,67, 42, 70, 45, 68, 43, 66) (46, 63, 49, 65, 47, 62, 50, 64, 48, 61) (51, 58, 54, 60, 52, 57, 55, 59, 53, 56).

Using Table 3.5, the class function δ_4 can be computed by the following formula:

$$\delta_4 = \frac{5}{2}\chi_1 + \left(\frac{-7+3\sqrt5}{20}\right)\chi_5 - \left(\frac{7+3\sqrt5}{20}\right)\chi_6 - \frac{1}{10}\chi_8.$$

Again, we can see that the class function δ lack the mentioned conjecture.

By applying calculations given in Table 3.6, one can easily compute the class function δ_5 as follows:

$$\delta_5 = \frac{751}{110}\chi_1 - \frac{499}{110}\chi_4 - \left(\frac{243 + 175\sqrt{5}}{220}\right)\chi_5 - \left(\frac{53 + 15\sqrt{5}}{220}\right)\chi_6$$
$$+ \left(\frac{-73 + 27\sqrt{5}}{220}\right)\chi_7 - \left(\frac{73 + 27\sqrt{5}}{220}\right)\chi_8.$$

We are now ready to calculate the modified Wiener and hyper–Wiener indices of the fullerene series $C[n]$ based on our calculations given above and some results in Djafari et al. (2013).

Result 3.2.2.1 The modified Wiener and modified hyper–Wiener indices of the fullerene series $C[n]$ is computed as follows:

- $\hat{W}(C[2]) = 500$, $\hat{W}(C[3]) = 1395$ and $\hat{W}(C[4]) = 2820$.
- $\hat{W}(C[n]) = 25n^3 + 60n^2 + 70n (n \geq 5)$.
- $\overset{\wedge}{WW}(C[2]) = 1020$, $\overset{\wedge}{WW}(C[3]) = 3570$, $\overset{\wedge}{WW}(C[4]) = 8420$.
- $\overset{\wedge}{WW}(C[n]) = \begin{cases} \frac{50}{3}n^4 + \frac{25}{2}n^3 + \frac{755}{6}n^2 + 320n & n \text{ is odd} \\ \frac{50}{3}n^4 + \frac{25}{2}n^3 + \frac{755}{6}n^2 + 380n & n \text{ is even} \end{cases}$

The fullerene series $D[n]$ (Figs 3.6 and 3.7) has exactly $12n$ carbon atoms. We first calculate the permutation symmetry of these fullerenes in two cases that $n = 11$ and $n = 12$.

$D_1 :=$ (1, 2, 3, 4,5,6) (7,8,9, 10, 11, 12) (13,14,15, 16, 17, 18) (19,20,21, 22, 23, 24) (25,26,27, 28, 29, 30) (31,32,34,36,38,40) (33,35,37,39,41,42) (43,45,46,48,50,52) (44,47,49,51, 53, 54) (55, 56, 58, 60, 62, 64) (57,59,61,63,65,66) (67,71,68,69,73,75) (70,74,76,77,78,72) (79,81,88, 80, 85, 83)(82, 90, 89, 87, 86, 84) (91,92,100,98,96,94) (93,102,101,99,97,95) (103, 110, 106, 105, 104, 107) (108, 109, 111, 112, 113, 114) (115, 124, 122, 118, 117, 116) (119, 126, 125, 123, 121, 120)(127, 132, 131, 130, 129, 128).

$D_2 :=$ (2,6)(3,5)(8,12)(9,11)(13, 18)(14, 17)(15, 16)(19, 22)(20, 21)(23, 24)(25, 29) (26, 28)(31, 34)(33, 35) (36, 40) (37, 42) (39, 41) (43, 52) (44, 53) (45, 50) (46, 48)(47, 51)(56, 64)(57, 66)(58, 62)(59, 65)(61, 63) (67,69)(68,71) (70,78) (73,75) (74,77) (79,85) (80, 81) (82, 87) (84, 86) (89, 90) (91, 94) (92, 96) (93, 97) (98, 100)(99, 102) (103, 106) (105, 107)(108, 114)(109, 113)(111, 112) (115, 116)(117, 124)(118, 122) (120, 126)(121, 125) (127, 129) (130, 132).

$D_3 :=$ (1, 128)(2, 127)(3, 132)(4, 131)(5, 130)(6, 129)(7, 119)(8, 126)(9, 125) (10, 123)(11, 121) (12, 120) (13, 115) (14, 124) (15, 122) (16, 118) (17, 117) (18, 116)(19, 109)(20, 111)(21, 112)(22, 113) (23, 114) (24, 108)(25, 107) (26, 103) (27, 110)(28, 106)(29, 105)(30, 104)(31, 97)(32, 95) (33, 94)(34, 93) (35, 91) (36,102)(37,92)(38,101) (39, 100)(40, 99)(41, 98)(42, 96)(43, 84) (44, 79) (45, 82)(46, 90)(47, 81)(48, 89) (49, 88)(50, 87)(51, 80)(52, 86)
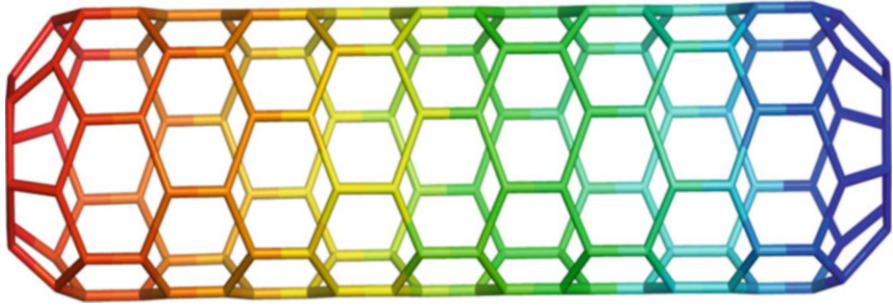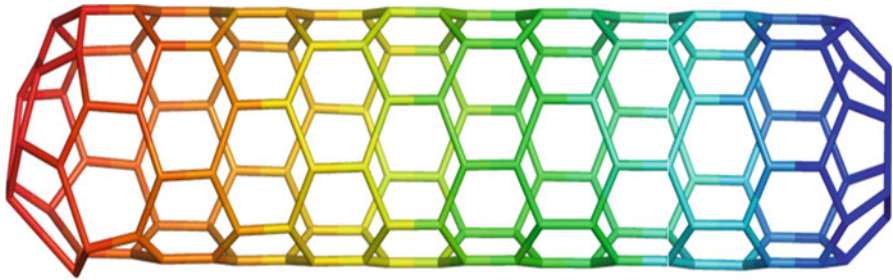
Fig. 3.6 The fullerene $D[11]$

Fig. 3.7 The fullerene $D[12]$

(53, 85)(54, 83)(55, 72)(56, 70) (57, 68)(58, 74)(59, 69)(60, 76)(61, 73) (62, 77) (63, 75)(64, 78)(65, 67)(66, 71).

D_4:= (1,2,3,4,5,6) (7,8,9,10,11,12) (13, 14, 15, 16, 17, 18) (19, 20, 21, 22, 23, 24) (25, 26, 27, 28, 29, 30) (31,32,34,36,38,40) (33,35,37,39,41,42) (43,45,46,48,50,52) (44,47,49, 51, 53, 54)(55, 56, 58, 60, 62, 64) (57,59,61,63,65,66) (67,71,68,69,73,75) (70,74,76,77,78,72) (79,81,88, 80, 85, 83)(82, 90, 89, 87, 86, 84) (91,92,100,98,96,94) (93,102,101,99,97,95) (103, 110, 106, 105, 104, 107) (108, 109, 111, 112, 113, 114) (115, 124, 122, 118, 117, 116) (119, 126, 125, 123, 121, 120) (127, 136, 130, 129, 128, 131) (132, 138, 137, 135,134,133) (139,144,143,142, 141, 140).

D_5:= (1, 141)(2, 142)(3, 143)(4, 144)(5, 139)(6, 140)(7, 133)(8, 134)(9, 135) (10, 137)(11, 138) (12, 132) (13, 128) (14, 129)(15, 130)(16, 136)(17, 127) (18, 131)(19, 121)(20, 123)(21, 125) (22, 126) (23, 119) (24, 120) (25, 117) (26, 118) (27, 122)(28, 124)(29, 115)(30, 116)(31, 108)(32, 114) (33, 104) (34, 113) (35, 105) (36, 112) (37, 106) (38, 111)(39, 110)(40, 109)(41, 103) (42, 107) (43, 97) (44, 96)(45, 99) (46, 101) (47, 98)(48, 102)(49, 100) (50, 93) (51, 92) (52, 95) (53, 91) (54, 94) (55, 86) (56, 87) (57, 85) (58, 89) (59, 80) (60, 90) (61, 88) (62, 82) (63, 81) (64, 84) (65, 79) (66, 83) (67, 70) (68, 78) (69, 77)(71, 72)(73, 76)(74, 75).

D_6:= (2, 6) (3, 5) (8, 12) (9, 11) (13, 18) (14, 17) (15, 16)(19, 22)(20, 21)(23, 24) (25, 29)(26, 28)(31, 34) (33, 35) (36, 40) (37, 42) (39, 41) (43, 52) (44, 53)

(45, 50) (46, 48) (47, 51) (56, 64) (57, 66) (58, 62) (59, 65) (61, 63) (67, 69)
(68, 71) (70, 78) (73, 75) (74, 77) (79, 85) (80, 81) (82, 87) (84, 86) (89, 90)
(91, 94) (92, 96)(93, 97)(98, 100) (99, 102) (103, 106) (105, 107) (108, 114)
(109, 113) (111, 112) (115, 116) (117, 124) (118, 122) (120, 126) (121, 125)
(127, 128) (129, 136) (132, 133) (134, 138) (135, 137) (139, 142)(140, 141)
(143, 144).

Notice that the automorphism group of the fullerene series $D[n]$ is isomorphic to the dihedral group of order 24, when n is even and $Z_2 \times Z_2 \times S_3$, otherwise.

Using above arguments and Tables 3.7 and 3.8, we have

$$\delta_6 = \frac{238}{33}\chi_1 - \frac{1}{33}\chi_4 - \frac{4}{33}\chi_5 - \frac{5}{66}\chi_6 - \frac{5}{66}\chi_7 - \frac{48}{11}\chi_8 + \frac{7}{132}\chi_9 - \frac{3}{44}\chi_{10}$$

$$- \frac{59}{132}\chi_{11} - \frac{107}{132}\chi_{12},$$

$$\delta_7 = \frac{551}{72}\chi_1 - \frac{115}{24}\chi_4 - \frac{11}{72}\chi_5 + \frac{1}{48}\chi_6 - \frac{5}{144}\chi_7 - \left(\frac{91 + 12\sqrt{3}}{144}\right)\chi_8$$

$$+ \left(\frac{-91 + 12\sqrt{3}}{144}\right)\chi_9.$$

The modified Wiener and hyper–Wiener indices of $D[n]$ is a direct consequence of calculations given above. We have:

Result 3.2.2.2 The modified Wiener and modified hyper–Wiener indices of the fullerene series $D[n]$ is computed as follows:

Table 3.7 The character table of $Aut(D[11]) \cong Z_2 \times Z_2 \times S_3$ and the class function δ_6

	1a	2a	2b	6a	3a	2c	2d	6b	2e	2f	6c	2g
χ_1	1	1	1	1	1	1	1	1	1	1	1	1
χ_2	1	−1	−1	1	1	1	−1	1	1	−1	1	1
χ_3	1	−1	−1	1	1	1	1	−1	−1	1	−1	−1
χ_4	1	−1	1	−1	1	−1	−1	1	−1	1	−1	1
χ_5	1	−1	1	−1	1	−1	1	−1	1	−1	1	−1
χ_6	1	1	−1	−1	1	−1	−1	−1	1	1	1	−1
χ_7	1	1	−1	−1	1	−1	1	1	−1	−1	−1	1
χ_8	1	1	1	1	1	1	−1	−1	−1	−1	−1	−1
χ_9	2	0	0	−1	−1	2	0	−1	2	0	−1	2
χ_{10}	2	0	0	−1	−1	2	0	1	−2	0	1	−2
χ_{11}	2	0	0	1	−1	−2	0	−1	−2	0	1	2
χ_{12}	2	0	0	1	−1	−2	0	1	2	0	−1	−2
δ_6	0	$\frac{94}{33}$	$\frac{94}{33}$	$\frac{21}{11}$	$\frac{42}{11}$	$\frac{62}{11}$	$\frac{379}{33}$	$\frac{123}{11}$	11	$\frac{35}{3}$	$\frac{129}{11}$	$\frac{139}{11}$

Table 3.8 The character table of $\mathrm{Aut}(D[12]) \cong D_{24}$ and the class function δ_7

	1a	2a	6a	3a	2b	2c	4a	12a	12b
χ_1	1	1	1	1	1	1	1	1	1
χ_2	1	-1	1	1	1	-1	1	1	1
χ_3	1	-1	1	1	1	1	-1	-1	-1
χ_4	1	1	1	1	1	-1	-1	-1	-1
χ_5	2	0	-2	2	-2	0	0	0	0
χ_6	2	0	-1	-1	2	0	-2	1	1
χ_7	2	0	-1	-1	2	0	2	-1	-1
χ_8	2	0	1	-1	-2	0	0	$\sqrt{3}$	$-\sqrt{3}$
χ_9	2	0	1	-1	-2	0	0	$-\sqrt{3}$	$\sqrt{3}$
δ_7	0	$\frac{103}{36}$	$\frac{23}{12}$	$\frac{23}{6}$	$\frac{17}{3}$	$\frac{112}{9}$	$\frac{37}{3}$	12	13

$$\hat{W}(D[2]) = 816, \ \hat{W}(D[3]) = 2304, \ \hat{W}(D[4]) = 4512, \ \hat{W}(D[5]) = 8010.$$

$$\hat{W}(D[n]) = \begin{cases} 36n^3 + 108n^2 + 132n & n \text{ is even } \& \ n \geq 6 \\ 36n^3 + 108n^2 + 168n & n \text{ is odd } \& \ n \geq 7 \end{cases}.$$

$$W\hat{W}(D[2]) = 1932, \ W\hat{W}(D[3]) = 6552, \ W\hat{W}(D[4]) = 14184, \ W\hat{W}(D[5]) = 28620.$$

$$W\hat{W}(D[n]) = \begin{cases} 24n^4 + 18n^3 + 276n^2 + 726n & n \text{ is even } \& \ n \geq 6 \\ 24n^4 + 18n^3 + 276n^2 + 960n & n \text{ is odd } \& \ n \geq 7 \end{cases}.$$

3.3   Conclusions

In this chapter a general formula for the class function δ for four sequences of fullerenes is reported. By applying this formula, the Wiener and hyper–Wiener indices of these fullerene series under their symmetry groups are computed. Some counterexamples for a recent open question on this topic are also presented; see Koorepazan-Moftakhar and Ashrafi (2015). We end this chapter with the following open question.

Open Question   Find a general formula for the class functions of fullerenes.

References

Ashrafi AR, Koorepazan-Moftakhar F (2014) Fullerenes and capped nanotubes: applications and geometry. In: Aliofkhazraei M (ed) Handbook of functional nanomaterials, volume 3, application and development. Nova Science Publisher, Inc, New York, pp 225–237

Ashrafi AR, Sabaghian-Bidgoli H (2009) A numerical method for computing PI index of fullerene molecules containing carbon atoms. J Comput Theor Nanosci 6:1706–1708

Ashrafi AR, Ghorbani M, Jalali M (2008) The vertex PI and Szeged indices of an infinite family of fullerenes. J Theor Comput Chem 7:221–231

Ashrafi AR, Ghorbani M, Jalali M (2009) Study of IPR fullerenes by counting polynomials. J Theor Comput Chem 8:451–457

Ashrafi AR, Cataldo F, Iranmanesh A, Ori O (eds) (2013) Topological modelling of nanostructures and extended systems, carbon materials: chemistry and physics, vol 7. Springer Science + Business Media, Dordrecht

Bosma W, Cannon J, Playoust C (1997) The magma algebra system. I. The user language. J Symb Comput 24:235–265

Cataldo F, Graovac A, Ori O (eds) (2011) The mathematics and topology of fullerenes. Carbon materials: chemistry and physics, vol 4. Springer Science + Business Media B.V, Dordrecht

Diudea MV (1996a) Walk numbers $^{e}W_{M}$: Wiener numbers of higher rank. J Chem Inf Comput Sci 36:535–540

Diudea MV (1996b) Wiener and hyper–Wiener numbers in a single matrix. J Chem Inf Comput Sci 36:833–836

Diudea MV (1997) Cluj matrix invariants. J Chem Inf Comput Sci 37:300–305

Diudea MV, Katona G, Pârv B (1997) Delta number, Dde, of dendrimers. Croat Chem Acta 70:509–517

Diudea MV, Ursu O, Nagy LCS (2002) TOPOCLUJ. Babes − Bolyai University, Cluj

Djafari S, Koorepazan-Moftakhar F, Ashrafi AR (2013) Eccentric sequences of two infinite classes of fullerenes. J Comput Theor Nanosci 10:2636–2638

Firouzian S, Faghani M, Koorepazan-Moftakhar F, Ashrafi AR (2014) The hyper-Wiener and modified hyper-Wiener indices of graphs with an application on fullerenes. Studia Universitatis Babes − Bolyai Chemia 59:163–170

Fowler PW, Manolopoulos DE (1995) An atlas of fullerenes. Oxford University Press, Oxford

Graovac A, Pisanski T (1991) On the Wiener index of a graph. J Math Chem 8:53–62

Graver JE (2005) Catalog of all fullerenes with ten or more symmetries, graphs and discovery, DIMACS ser. discrete math theoret comput sci, 69. American Mathematical Society, Providence, pp 167–188

Gutman I, Šoltés L (1991) The range of the Wiener index and its mean isomer degeneracy. Z Naturforsch 46a:865–868

Gutman I, Linert W, Lukovits I, Dobrynin AA (1997) Trees with extremal hyper–Wiener index: mathematical basis and chemical applications. J Chem Inf Comput Sci 37:349–354

HyperChem package Release 7.5 for Windows (2002) Hypercube Inc., Florida, USA

Khalifeh MH, Yousefi–Azari H, Ashrafi AR (2008) The hyper-Wiener index of graph operations. Comput Math Appl 56:1402–1407

Klein DJ, Lukovits I, Gutman I (1995) On the definition of the hyper–Wiener index for cycle–containing structures. J Chem Inf Comput Sci 35:50–52

Koorepazan-Moftakhar F, Ashrafi AR (2013) Symmetry and PI index of C_{60+12n} fullerenes. J Comput Theor Nanosci 10:2484–2486

Koorepazan-Moftakhar F, Ashrafi AR (2014) Fullerenes: topology and symmetry. In: Gutman I (ed) Topics in chemical graph theory. University of Kragujevac and Faculty of Science, Kragujevac, pp 163–176

Koorepazan-Moftakhar F, Ashrafi AR (2015) Distance under symmetry. MATCH Commun Math Comput Chem 74(2):259–272

Koorepazan-Moftakhar F, Ashrafi AR, Mehranian Z (2014) Symmetry and PI polynomials of C_{50+10n} fullerenes. MATCH Commun Math Comput Chem 71:425–436

Kroto HW, Heath JR, O'Brien SC, Curl RF, Smalley RE (1985) C_{60}: buckminsterfullerene. Nature 318:162–163

Myrvold W, Bultena B, Daugherty S, Debroni B, Girn S, Minchenko M, Woodcock J, Fowler PW (2007) FuiGui: a graphical user interface for investigating conjectures about fullerenes. MATCH Commun Math Comput Chem 58:403–422

Ori O, Cataldo F, Iglesias-Groth S, Graovac A (2010) Topological modeling of $C_{60}H_{36}$ hydrides. In: Cataldo F, Iglesias-Groth S (eds) Fulleranes: the hydrogenated fullerenes. Springer, Dordrecht/London, pp 251–272

Schwerdtfeger P, Wirz L, Avery J (2013) Program fullerene: a software package for constructing and analyzing structures of regular fullerenes. J Comput Chem 34:1508–1526

The GAP Team (1995) GAP, Groups, Algorithms and Programming. Lehrstuhl De für Mathematik. RWTH, Aachen

Wiener HJ (1947) Structural determination of paraffin boiling points. J Am Chem Soc 69:17–20

Chapter 4
Distance Under Symmetry: (3,6)-Fullerenes

Ali Reza Ashrafi, Fatemeh Koorepazan − Moftakhar, and Mircea V. Diudea

Abstract A (3,6)-fullerene is a planar 3-connected cubic graph whose faces are triangles and hexagons. In this chapter, the modified Wiener and hyper–Wiener indices of three infinite classes of (3,6)-fullerenes are considered into account. Some open questions are also presented.

4.1 Introduction

Throughout this paper all graphs are assumed to be simple. This means that our graphs don't have multiple edges and loops. A graph G is called *connected* if for each vertex x and y in G, there is path connecting them. The graph G is said to be *3-connected*, if G has more than three vertices and remains connected whenever fewer than three vertices are removed from G. A *chemical graph* is a graph in which the vertices are atoms and edges are the chemical bonds. The *distance* between two vertices of G is defined as the length of the shortest path connecting them. The *distance matrix* $D(G)$ of G is a square matrix of order $n = |V(G)|$, where (i, j) entry is the distance between the ith and jth vertices of G.

A group is a pair $(G, \bullet)$ such that $\bullet: G \times G \to G$ is a function and the following three axioms are satisfied:

A.R. Ashrafi (✉) • F. Koorepazan − Moftakhar

Department of Nanocomputing, Institute of Nanoscience and Nanotechnology, University of Kashan, Kashan 87317-53153, Iran

Department of Pure Mathematics, Faculty of Mathematical Sciences, University of Kashan, Kashan 87317-53153, Iran
e-mail: ashrafi@kashanu.ac.ir

M.V. Diudea
Department of Chemistry, Faculty of Chemistry and Chemical Engineering, Babes-Bolyai University, Arany Janos Street 11, Cluj-Napoca RO-400028, Romania

1. For each $x, y, z \in G$, $x \bullet (y \bullet z) = (x \bullet y) \bullet z$. This equation is called *associative law*.
2. There exists an element $e \in G$ such that for each $x \in G$, $x \bullet e = e \bullet x = x$. The element e is called the *identity* of G.
3. For each element $x \in G$, there exists an element $y \in G$ such that $x \bullet y = y \bullet x = e$. The element y is unique. It is called the *inverse* of x and denoted by x^{-1}.

The concept of group is very useful in explanation of the symmetry properties of molecules. A subgroup of G is a nonempty subset that is closed under taking group product and inverse. A group containing a finite set of elements is said to be finite. Fix an element $x \in G$ and define

$$\langle x \rangle = \left\{ x^n \,\middle|\, n \text{ is an integer} \right\}.$$

Then $\langle x \rangle$ is called a *cyclic subgroup* of G with *generator x*. G is said to be cyclic, if there exists an element $a \in G$ such that $G = \langle x \rangle$. A cyclic group of order k is denoted by Z_k.

Suppose $X = \{1, \ldots, n\}$ and S_n denote the set of all one to one and onto mapping from X onto X. Then it is easy to see that the set S_n has a group structure under composition of functions. This group is called the *symmetric group* on n symbols. Clearly, the symmetric group on n symbols has order $n!$. The elements of the symmetric group S_n is called a *permutation* on X, and a permutation α on X is said to be *even*, if α can be obtained from an even number of two-element swaps. The set of all even permutations of S_n constitutes a subgroup A_n of order $n!/2$. This subgroup is called the *alternating group* on n symbols. A *dihedral group* is the group of symmetries of a regular polygon containing rotations and reflections. This group can be considered as the rigid motions of the plane preserving a regular n-gon with respect to composition of symmetries. Obviously, this group has order $2n$ denoted by D_{2n}.

Suppose G is a graph and $\alpha: G \to G$ is a function. The mapping α is called an *automorphism*, if α has an inverse and α, α^{-1} preserve adjacency in G. The set of all such mappings is denoted by Aut(G). This set has a group structure under composition of functions and so it is named the *automorphism group* of G. If G is a chemical graph, then the automorphism group of G represents the maximum possible symmetry elements in the molecule under consideration. In some classes of molecules like fullerenes, this group and the symmetry group are the same.

4.2 Distance Under Symmetry for (3,6)-Fullerenes

A cubic graph is a graph in which all vertices have degree 3. A *(3,6)-fullerene graph* ((3,6)-fullerene or fullerene for short) is a planar 3-connected cubic graph whose faces are only triangles and hexagons. A pyramid is a (3,6)-fullerene with the minimum possible number of vertices. It is possible to define (4,6)- and (5,6)-fullerene graphs in a similar way, but by Euler's theorem, there is no $(k,6)$-fullerene graphs for other values of k. We encourage the interested readers to consult the famous book of Fowler and Manolopoulos (1995). The books (Cataldo et al. 2011; Ashrafi et al. 2013) also contain recent literature reviews on theory and experiment

of fullerenes. We refer also to two important computer packages FuiGui (Myrvold et al. 2007) and Program Fullerene (Schwerdtfeger et al. 2013) for investigating conjectures and constructing and analyzing structures of fullerenes. For the mathematical properties of (3,6)-fullerenes, the interested readers can consult Fowler et al. (2000), John and Sachs (2009), Devos et al. (2009), Yang and Zhang (2012), Ashrafi and Mehranian (2013), and Behmaram et al. (2013).

This chapter is mainly concerned with the symmetry and distance topology of (3,6)-fullerenes. In Ghorbani et al. (2015), it is proved that the order of the automorphism group of a (3,6)-fullerene divides 24. It is merit to state here that Deza et al. (2009) proved that there are five possible symmetry groups for a (3,6)-fullerene. These are $D_2 \cong Z_2 \times Z_2$, $D_{2h} \cong Z_2 \times Z_2 \times Z_2$, $D_{2d} \cong D_8$, $T \cong A_4$, and $T_d \cong S_4$. The 2D and 3D perceptions of (3,6)-fullerenes with these symmetry groups and minimum possible number of vertices are depicted in Figs. 4.1 and 4.2, respectively.

Aut(G)$\cong S_4 \cong T_d$	Aut(G)$\cong Z_2 \times Z_2 \cong D_2$
Aut(G)$\cong Z_2 \times Z_2 \times Z_2 \cong D_{2h}$	Aut(G)$\cong A_4 \cong T$
Aut(G)$\cong D_8 \cong D_{2d}$	
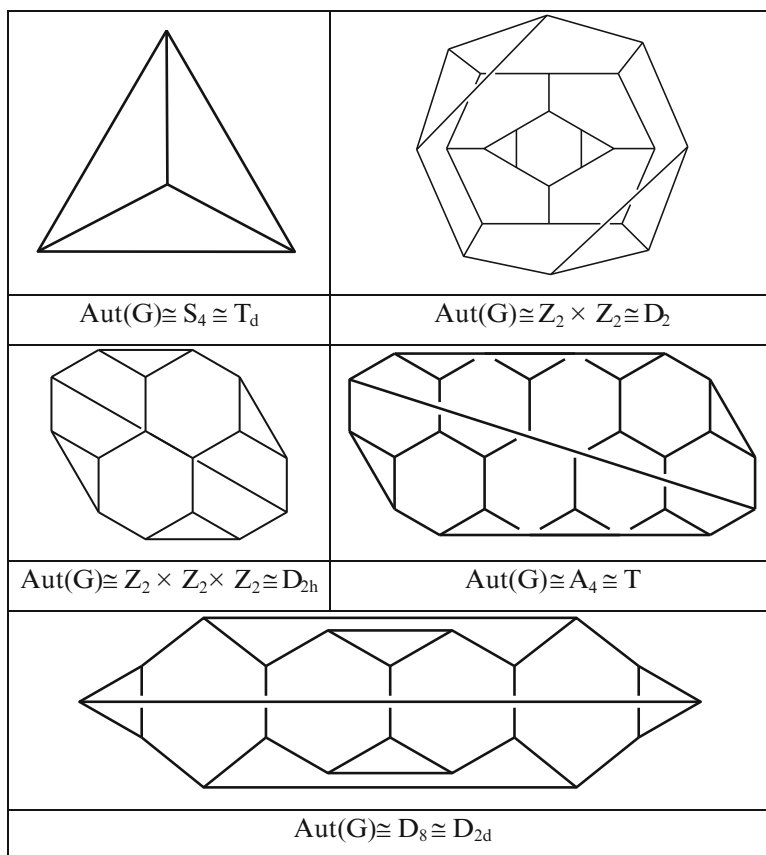
Fig. 4.1 2D perception of (3,6)-fullerenes with five different symmetry groups
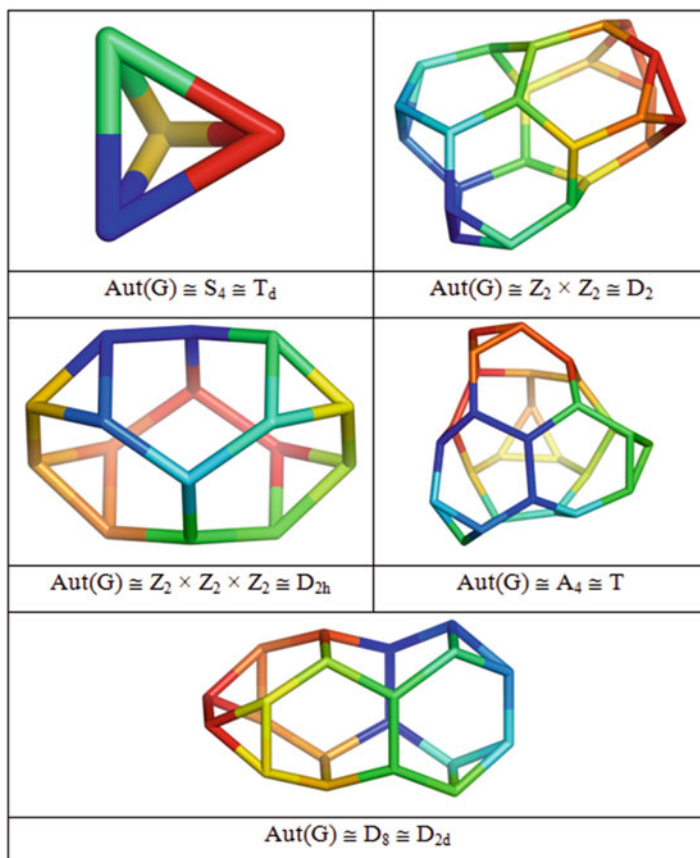
Fig. 4.2 3D perception of (3,6)-fullerenes with five different symmetry groups

The *Wiener index* of G, $W(G)$, is defined as the sum of distances between all pairs of vertices in G (Wiener 1947). This graph invariant has remarkable applications in chemistry and also in computer science. We refer to Gutman and Šoltés (1991) for application of this number in chemistry.

A connected graph G without cycles is said to be an *acyclic graph*. The hyper–Wiener index of acyclic graphs was introduced by Milan Randić, as a generalization of the Wiener index. Then Klein et al. (1995) extended this graph invariant for arbitrary graphs. It is defined as

$$WW(G) = \frac{1}{2}W(G) + \frac{1}{2}\sum_{\{x,y\}} d(x,y)^2.$$

The mathematical properties and chemical meaning of this topological index are reported in Khalifeh et al. (2008) and Gutman et al. (1997). It is merit to mention here that there is a matrix version of the hyper–Wiener index introduced by

M.V. Diudea (1996a, b, 1997, Diudea et al. 1997). To explain, we assume that G is a connected graph and $D = D(G)$ is its distance matrix. The Wiener matrix $W = W(G)$ is another $n \times n$ matrix such that its ijth entry is defined as the number of paths containing the (i, j) path. These matrices are basis for calculating W, whereas distance path and Wiener path are basis for the calculation of hyper–Wiener index. We encourage the interested readers to consult the mentioned papers by Diudea and references therein for more information on this topic.

Graovac and Pisanski (1991) in their seminal paper combine distance and symmetry to propose a generalization of the classical Wiener index. To explain, we assume that G is a graph with automorphism group $\Gamma = \mathrm{Aut}(G)$. The modified Wiener index of G is defined as

$$\hat{W}(G) = \frac{|V(G)|}{2|\Gamma|} \sum_{x \in V(G)} \sum_{\alpha \in \Gamma} d(x, \alpha(x)).$$

Firouzian et al. (2014) introduced in a similar way the modified hyper–Wiener index of a graph G as follows:

$$\overset{\wedge}{WW}(G) = \frac{1}{2} \hat{W}(G) + \frac{|V(G)|}{4|\Gamma|} \sum_{u \in V(G),\, \alpha \in \Gamma} d(u, \alpha(u))^2.$$

The aim of this chapter is to compute the modified Wiener and modified hyper–Wiener indices of three classes of fullerene graphs. To compute these graph invariants, we need their symmetry groups. The symmetry group of some classes of ordinary fullerenes ((5,6)-fullerenes) is reported in Djafari et al. (2013) and Koorepazan−Moftakhar and Ashrafi (2013). For symmetry of our three classes of (3,6)-fullerenes, we refer to Koorepazan−Moftakhar and Ashrafi (2014) and Koorepazan−Moftakhar et al. (2014a, b). In our calculations, we use the computer packages HyperChem (HyperChem Package Release 7.5 for Windows 2002), TopoCluj (Diudea et al. 2002), GAP (The GAP Team 1995), and MAGMA (Bosma et al. 1997). We refer the interested readers to consult papers (Ashrafi et al. 2008, 2009; Ashrafi and Sabaghian−Bidgoli 2009) and references therein for more information on topological properties of fullerenes.

We are now ready to construct the first (3,6)-fullerene series $B[n]$ of order $8n$, $n \geq 2$. The ninth term of the fullerene sequence $B[n]$ is depicted in Fig. 4.3. This sequence can be constructed by an inductive argument. To explain, we assume that
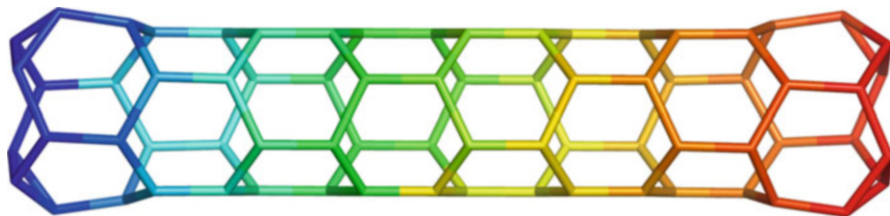
Fig. 4.3 The fullerene B[9]

the term $B[n]$ is constructed. To obtain $B[n+1]$, we add eight new vertices to the tube-shaped part of $B[n]$ and connect them to their corresponding vertices in B $[n]$. By a result in Koorepazan−Moftakhar et al. (2014a, b),

$$Aut(B[n]) = \begin{cases} S_4 & n = 2 \\ D_8 & n \geq 4 \text{ is even} \\ Z_2 \times Z_2 & n \geq 3 \text{ is odd} \end{cases}.$$

We first notice that $W(B[1]) = 294$ and $WW(B[2]) = 981$. The Wiener index of B $[n]$ is computed in general in Ashrafi and Mehranian (2013). In this paper, the authors proved that if $n \geq 3$, then

$$W(B[n]) = \frac{64}{3}n^3 + \frac{464}{3}n - 206.$$

Using a similar argument given the mentioned paper, it is possible to prove

$$WW(B[n]) = \frac{64}{3}n^4 + \frac{32}{3}n^3 - \frac{16}{3}n^2 + \frac{3112}{3}n - 1729.$$

In Koorepazan–Moftakhar and Ashrafi (2015), a representation theory method for computing the modified Wiener index of graphs is presented. Applying this method and the general form of the automorphism group of this fullerene series, we have:

Result 4.1 The modified Wiener and hyper–Wiener indices of $B[n]$ can be computed as follows:

$$\widehat{W}(B[n]) = \begin{cases} 16n^3 + 32n^2 + 20n & n \not\equiv 2 \,(\mathrm{mod}\,4) \\ 16n^3 + 32n^2 + 36n & n \equiv 2 \,(\mathrm{mod}\,4) \end{cases}.$$

$$\widehat{WW}(B[n]) = \begin{cases} \dfrac{32}{3}n^4 + 8n^3 + \dfrac{232}{3}n^2 + 64n & n \equiv 1, \, 3 \,(\mathrm{mod}\,4) \\[2mm] \dfrac{32}{3}n^4 + 8n^3 + \dfrac{208}{3}n^2 + 56n & n \equiv 4 \,(\mathrm{mod}\,4) \\[2mm] \dfrac{32}{3}n^4 + 8n^3 + \dfrac{208}{3}n^2 + 128n & n \equiv 2 \,(\mathrm{mod}\,4) \end{cases}.$$

We now continue our calculations to obtain the same invariant for another sequence of fullerenes, $C[n]$. The general term of this sequence is a fullerene with exactly $8n+4$ carbon atoms. Again, by a result in Koorepazan−Moftakhar et al. (2014a, b) (Fig. 4.4),

$$Aut(C[n]) = \begin{cases} S_4 & n = 1 \\ D_8 & n > 1 \end{cases}.$$
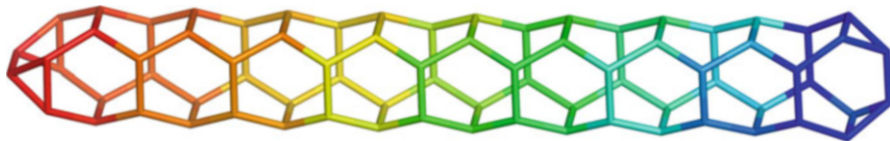
Fig. 4.4 The fullerene C[9]

In a similar way as $B[n]$, the general term of $C[n]$ can be constructed by an inductive argument. A result in Ashrafi and Mehranian (2013) states that *for $n \geq 1$*, we have

$$W(C[n]) = \frac{64}{3}n^3 + 64n^2 + \frac{152}{3}n + 2.$$

Again, we use calculations given this paper to show that

$$WW(C[n]) = \frac{64}{3}n^4 + 96n^3 + \frac{464}{3}n^2 + 148n - 21.$$

Result 4.2 The modified Wiener and hyper–Wiener indices of the fullerene sequence $C[n]$ can be computed as follows:

$$\hat{W}(C[1]) = 138 \text{ and } \hat{W}(C[n]) = 16n^3 + 72n^2 + 40n + 4(n \geq 2).$$
$$\hat{WW}(C[n]) = \frac{32}{3}n^4 + \frac{136}{3}n^3 + \frac{388}{3}n^2 + \frac{152}{3}n - 2(n \geq 1).$$

Our final fullerene sequence is $D[n]$ of order $16n + 48$. The general term of this fullerene series can be constructed inductively from $D[16]$. The automorphism groups of these fullerenes were reported in Koorepazan−Moftakhar et al. (2014a, b), and its Wiener index can be found in Ashrafi and Mehranian (2013) (Fig 4.5):

$$Aut(D[n]) = \begin{cases} Z_2 \times Z_2 & n \text{ is even} \\ Z_2 \times Z_2 \times Z_2 & n \text{ is odd} \end{cases}.$$

The reported Wiener index of this fullerene series is not correct. Its correct value is

$$W(D[n]) = \frac{256}{3}n^3 + 768n^2 + \frac{14912}{3}n + 3540 \ (n \geq 4).$$

In the exceptional cases that $n = 1, 2, 3$, we have $W(D[1]) = 9968$, $W(D[2]) = 17432$ and $W(D[3]) = 27714$. The hyper–Wiener index of D[n] in some special
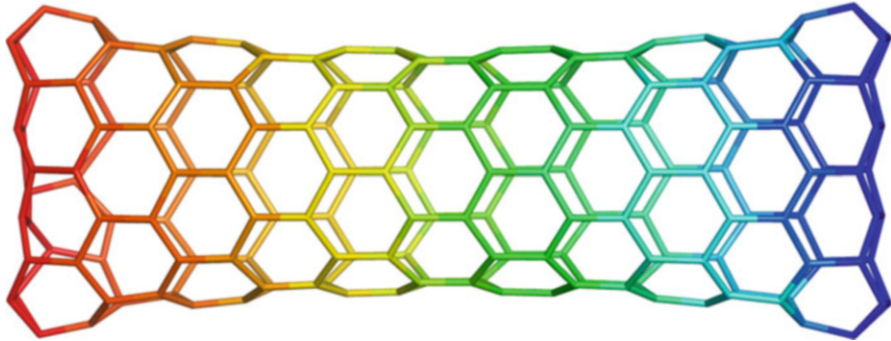
Fig. 4.5 The fullerene D[9]

cases can be computed as $WW(D[1]) = 62872$, $WW(D[2]) = 121392$, and $WW(D[3]) = 212167$. In general, if $n \geq 4$,

$$WW(D[n]) = \frac{256}{3}n^4 + \frac{3200}{3}n^3 + \frac{14912}{3}n^2 + \frac{131488}{3}n - 1022.$$

Our calculation shows that:

Result 4.3 The Wiener and hyper–Wiener indices of $D[n]$ can be computed as follows:

$$\hat{W}(D[1]) = 9728, \ \hat{W}(D[2]) = 16160, \ \hat{W}(D[3]) = 26400, \ \overset{\wedge}{WW}(D[2]) = 69080.$$

$$\hat{W}(D[n]) = \begin{cases} 64n^3 + 832n^2 + 3664n + 5232 & n \equiv 0, \ 2 \ (\text{mod } 4) \\ 49n^3 + 1237n^2 + 547n + 14871 & n \equiv 1 \ (\text{mod } 4) \\ 64n^3 + 832n^2 + 3888n + 5904 & n \equiv 3 \ (\text{mod } 4) \end{cases} \quad n \geq 4.$$

$$\overset{\wedge}{WW}(D[n]) = \frac{128}{3}n^4 + 544n^3 + \frac{11200}{3}n^2 + 14872n + 22248, \quad n \text{ is even}.$$

4.3   Conclusions

In this chapter, the modified Wiener and hyper–Wiener indices of three fullerene series are considered into account. In each case, exact formulas for computing these invariants are presented. Our calculations show that in computing the modified hyper–Wiener index of $D[n]$, when n is odd, there is no regularity. We end this chapter by the following open questions:

Open Question 4.4 Find a general formula for the modified hyper–Wiener of D [$16n + 48$] in odd case.

Open Question 4.5 Is it true that the modified Wiener and hyper–Wiener indices of (3,6)-fullerenes can be evaluated by polynomials of degrees 3 and 4, respectively?

References

Ashrafi AR, Mehranian Z (2013) Topological study of (3,6)– and (4,6)–fullerenes. In: Ashrafi AR, Cataldo F, Iranmanesh A, Ori O (eds) Topological modelling of nanostructures and extended systems, Carbon materials: chemistry and physics. Springer, Dordrecht/New York, pp 487–510

Ashrafi AR, Sabaghian – Bidgoli H (2009) A numerical method for computing PI index of fullerene molecules containing carbon atoms. J Comput Theor Nanosci 6:1706–1708

Ashrafi AR, Ghorbani M, Jalali M (2008) The vertex PI and Szeged indices of an infinite family of fullerenes. J Theor Comput Chem 7:221–231

Ashrafi AR, Ghorbani M, Jalali M (2009) Study of IPR fullerenes by counting polynomials. J Theor Comput Chem 8:451–457

Ashrafi AR, Cataldo F, Iranmanesh A, Ori O (eds) (2013) Topological modelling of nanostructures and extended systems, vol 7, Carbon materials: chemistry and physics. Springer Science + Business Media, Dordrecht

Behmaram A, Yousefi – Azari H, Ashrafi AR (2013) On the number of matchings and independent sets in (3,6) – fullerenes. MATCH Commun Math Comput Chem 70:525–532

Bosma W, Cannon J, Playoust C (1997) The magma algebra system. I. The user language. J Symb Comput 24:235–265

Cataldo F, Graovac A, Ori O (eds) (2011) The mathematics and topology of fullerenes, vol 4, Carbon materials: chemistry and physics. Springer Science + Business Media B.V, Dordrecht

Devos M, Goddyn L, Mohar B, Samal R (2009) Cayley sum graphs and eigenvalues of (3,6) – fullerenes. J Combin Theory Ser B99:358–369

Deza M, Dutour Sikiric M, Fowler PW (2009) The symmetries of cubic polyhedral graphs with face size no larger than 6. MATCH Commun Math Comput Chem 61:589–602

Diudea MV (1996a) Walk numbers W_M: Wiener numbers of higher rank. J Chem Inf Comput Sci 36:535–540

Diudea MV (1996b) Wiener and hyper–Wiener numbers in a single matrix. J Chem Inf Comput Sci 36:833–836

Diudea MV (1997) Cluj matrix invariants. J Chem Inf Comput Sci 37:300–305

Diudea MV, Katona G, Pârv B (1997) Delta number, D_{de}, of dendrimers. Croat Chem Acta 70:509–517

Diudea MV, Ursu O, Nagy LCs (2002) TOPOCLUJ. Babes – Bolyai University, Cluj

Djafari S, Koorepazan – Moftakhar F, Ashrafi AR (2013) Eccentric sequences of two infinite classes of fullerenes. J Comput Theor Nanosci 10:2636–2638

Firouzian S, Faghani M, Koorepazan – Moftakhar F, Ashrafi AR (2014) The hyper – Wiener and modified hyper – Wiener indices of graphs with an application on fullerenes. Studia Universitatis Babes – Bolyai Chemia 59:163–170

Fowler PW, Manolopoulos DE (1995) An atlas of fullerenes. Oxford University Press, Oxford

Fowler PW, John PE, Sachs H (2000) (3,6) – cages, hexagonal toroidal cages, and their spectra. DIMACS Ser Discrete Math Theoret Comput Sci 51:139–174

Ghorbani M, Songhori M, Ashrafi AR, Graovac A (2015) Symmetry group of (3,6)-fullerenes. Fullerenes, Nanotubes, Carbon Nanostruct 23(9):788–791

Graovac A, Pisanski T (1991) On the Wiener index of a graph. J Math Chem 8:53–62

Gutman I, Šoltés L (1991) The range of the Wiener index and its mean isomer degeneracy. Z Naturforsch 46a:865–868

Gutman I, Linert W, Lukovits I, Dobrynin AA (1997) Trees with extremal hyper–Wiener index: mathematical basis and chemical applications. J Chem Inf Comput Sci 37:349–354

HyperChem package Release 7.5 for Windows (2002) Hypercube Inc., Florida, USA

John PE, Sachs H (2009) Spectra of toroidal graphs. Discret Math 309:2663–2681

Khalifeh MH, Yousefi–Azari H, Ashrafi AR (2008) The hyper − Wiener index of graph operations. Comput Math Appl 56:1402–1407

Klein DJ, Lukovits I, Gutman I (1995) On the definition of the hyper–Wiener index for cycle–containing structures. J Chem Inf Comput Sci 35:50–52

Koorepazan − Moftakhar F, Ashrafi AR (2013) Symmetry and PI index of C_{60+12n} fullerenes. J Comput Theor Nanosci 10:2484–2486

Koorepazan − Moftakhar F, Ashrafi AR (2014) Fullerenes: topology and symmetry. In: Gutman I (ed) Topics in chemical graph theory. University of Kragujevac and Faculty of Science, Kragujevac, pp 163–176

Koorepazan − Moftakhar F, Ashrafi AR (2015) Distance under symmetry. MATCH Commun Math Comput Chem 74:259–272

Koorepazan − Moftakhar F, Ashrafi AR, Mehranian Z (2014a) Symmetry and PI polynomials of C_{50+10n} fullerenes. MATCH Commun Math Comput Chem 71:425–436

Koorepazan − Moftakhar F, Ashrafi AR, Mehranian Z, Ghorbani M (2014b) Automorphism group and fixing number of (3,6)– and (4, 6)–fullerene graphs. Elec Notes Disc Math 45:113–120

Myrvold W, Bultena B, Daugherty S, Debroni B, Girn S, Minchenko M, Woodcock J, Fowler PW (2007) FuiGui: a graphical user interface for investigating conjectures about fullerenes. MATCH Commun Math Comput Chem 58:403–422

Schwerdtfeger P, Wirz L, Avery J (2013) Program fullerene: a software package for constructing and analyzing structures of regular fullerenes. J Comput Chem 34:1508–1526

The GAP Team (1995) GAP, groups, algorithms and programming. Lehrstuhl De für Mathematik. RWTH, Aachen

Wiener HJ (1947) Structural determination of paraffin boiling points. J Am Chem Soc 69:17–20

Yang R, Zhang H (2012) Hexagonal resonance of (3,6) − fullerenes. J Math Chem 50:261–273

Chapter 5
Topological Symmetry of Multi-shell Clusters

**Mircea V. Diudea, Atena Parvan-Moldovan,
Fatemeh Koorepazan-Moftakhar, and Ali Reza Ashrafi**

Abstract Symmetry is an intrinsic property of the organized matter. Topological symmetry is referred to the maximum possible symmetry achievable by a given molecular structure; it can be performed either by permutations on the adjacency matrix of its associate graph or by calculating the values of some topological indices. The equivalence classes of substructures of some multi-shell clusters, with icosahedral and octahedral symmetry, designed by the aid of operations on maps, were solved by using a topological index of centrality, computed on the layer matrix of rings surrounding the vertices in the molecular graph, and compared with the results of matrix permutation. A centrality order of vertices in multi-shell clusters is given. The design of multi-shell clusters was performed by our original CVNET and NanoStudio software programs.

5.1 Introduction

Polytopes Complexity of a chemical increases with the dimensionality of its associate graph. Going up from a polygon (2D) or a polyhedron (3D) to n-dimensions, the higher dimensional objects are called polytopes. By using the Schlüfli

M.V. Diudea (✉) • A. Parvan-Moldovan

Department of Chemistry, Faculty of Chemistry and Chemical Engineering, Babes-Bolyai University, Arany Janos Street 11, Cluj-Napoca RO-400028, Romania
e-mail: diudea@chem.ubbcluj.ro

F. Koorepazan-Moftakhar • A.R. Ashrafi

Department of Nanocomputing, Institute of Nanoscience and Nanotechnology, University of Kashan, Kashan 87317-53153, Iran

Department of Pure Mathematics, Faculty of Mathematical Sciences, University of Kashan, Kashan 87317-53153, Iran

(1901) symbols, one can write the platonic solids tetrahedron T, octahedron Oct, cube C, dodecahedron Do, and icosahedron Ico as {3,3}, {3,4}, {4,3},{5,3}, and {3,5}, respectively. Within {*p,q,r*} symbol,{*p,q*}is the cell type, while {*q,r*} represents the vertex figures: *p* is the polygon size, *q* is the number of edges incident in a vertex (of the isolated cell), and *r* is the number of cells incident on an edge.

A 3D polytope is convex if any of its edges shares no more than two polygons; next, a 4D polytope is convex if any polygon shares no more than two cells. Each convex 4D polytope is bounded by a set of 3D cells. If its cells are all platonic solids of the same type and size, the 4-polytope is called regular. There are six regular 4D polytopes, also called polychora: 5-cell {3,3,3}, 8-cell {4,3,3}, 16-cell {3,3,4}, 24-cell {3,4,3}, 120-cell {5,3,3}, and 600-cell {3,3,5}. Five of them can be associated to the platonic solids, but the sixth, the 24-cell, has no close 3D equivalent. Among them, 5-cell and 24-cell are self-cage dual, while the others are pairs: 8-cell and 16-cell and 120-cell and 600-cell.

To investigate *n*-dimensional polytopes, a generalization of Euler's formula, also due to Schlüfli (1901), is used:

$$\sum_{i=0}^{n-1} (-1)^i f_i = 1 - (-1)^n$$

In the above formula, f_i are elements of the *f*-vector $(f_0, f_1, \ldots, f_{n-1})$ of a convex polytope. In case $n = 4$, f_i are identified to vertices, edges, rings, and cells, respectively, while the above sum of figures becomes

$$Sum(f_i) = f_0 - f_1 + f_2 - f_3 = 0$$

This formula is also obeyed by 3D polytopes if embedded in 4D: the bounded faces are shared to the infinite cell, i.e., the envelope, and this one has to be added to the number of f_i. In case $n = 3$, the above is the well-known Euler-Poincaré formula (Euler 1758). These formulas are useful to check the consistency of the attributed structures.

Topological Symmetry Molecular structures show various types of geometrical symmetry (Diudea and Nagy 2007, 2013; Diudea 2013; Ashrafi et al. 2013); it is reflected in several molecular properties, dependent on the spatial structure of molecules. Molecular topology reveals a *topological symmetry* (i.e., constitutional symmetry), defined in terms of *connectivity*; it expresses equivalence relationships among elements of the graph: vertices, bonds, faces, or larger subgraphs.

Using notions of the group action (Hungerford 1980), in which every element of the group acts like a one-to-one mapping, the group G is said to act on a set X if there is a function ϕ such that $\phi{:}G \times X \to X$, and for any element $x \in X$, there exists the relation $\phi(g,\phi(h,x)) = \phi(gh,x)$, for all $g,h \in G$, with $\phi(e,x) = x$, e being the identity element of G. The mapping ϕ is called a group action, while the set $\{\phi(gx) \mid g \in G\}$ is called the *orbit* of x. For a permutation σ on n objects, the

permutation matrix is an $n \times n$ matrix P_σ, with elements $x_{ij} = 1$ if $i = \sigma(j)$ and 0 otherwise. For any permutation σ and τ on n objects, $P_\sigma P_\tau = P_{\sigma\tau}$, while the set of all permutation matrices is a group isomorphic to the symmetry group S_n on n symbols. A permutation σ of the vertices of a graph $H(V,E)$ (V being the set of vertices and E the set of edges in H) belongs to an automorphism group G if one satisfies the relation $P_\sigma{}^t A P_\sigma = A$, where A is the adjacency matrix of the graph H. Given $Aut(H) = \{\sigma_1, \ldots, \sigma_m\}$, the matrix $S_G = [s_{ij}]$, where $s_{ij} = \sigma_i(j)$, is called a solution matrix for H, and its calculation will provide the automorphism group of H.

Given a graph $H(V,E)$ and the automorphism group $Aut(H)$, two vertices, $i, j \in V$, are called *equivalent* if $\{\phi(ij) \mid i, j \in Aut(H)\}$; in other words, they belong to the same orbit of automorphisms. Suppose $v_1, v_2, \ldots, v_m$ are m disjoint *automorphic partitions* of the set of vertices $V(H)$, then $V = V_{v1} \cup V_{v2} \cup \ldots \cup V_{vm}$ and $V_{v_i} \cap V_{v_j} = \varnothing$.

Let us now consider a vertex invariant, $In = In_1, In_2, \ldots, In_m$, which assigns a value In_i to the vertex i. Two vertices i and j of a molecular graph (with vertices meaning the atoms and edges the bonds in the molecule) belong to the same *invariant class* if $In_i = In_j$. The partitioning in *classes* of vertices/atoms leads to m classes, with $v_1, v_2, \ldots, v_m$ atoms in each class; such a partitioning may differ from the *orbits of automorphism*, i.e., *classes of equivalence*, since no vertex invariant is known so far to always discriminate two nonequivalent vertices in any graph. The classes of vertices are eventually *ordered* according to some rules. It is worthy to mention that topological symmetry equals the maximum geometrical symmetry a molecular graph can have.

Centrality A layer matrix (Diudea 1994; Diudea and Ursu 2003) is built up on a layer partition of a vertex i in the graph $H(V,E)$:

$$H(i) = \left\{ H(i)_j, j \in [0, ecc_i] \text{ and } v \in H(i)_j \Leftrightarrow d_{iv} = j \right\}$$

where ecc_i is the eccentricity of i (i.e., the largest distance from i to the other vertices of H). The entries in a layer matrix, LM, collect the vertex property p_v (a topological, chemical, or physical property) for all the vertices v belonging to the layer $H(i)_j$:

$$[\mathrm{LM}]_{ij} = \sum_{v \in G(i)_j} p_v,$$

located at distance j from vertex i. The matrix LM is defined as

$$LM(H) = \left\{ [LM]_{ij}; \ i \in V(H); \ j \in [0, d(H)] \right\}$$

where $d(H)$ is the diameter of the graph. The dimensions of the matrix are $N \times (d(H) + 1)$; the zero-distance column is just the column of vertex properties. The most

simple and essential layer matrix is the *counting* property (i.e., the existence of a vertex in a given position at a given distance is counted by 1 and zero otherwise). In the following, as a property, the count of rings R around each vertex is considered, the layer matrix being LR.

Layer matrices are used to derive the indices of *centrality* $c(LM)$ that quantify the centrality of vertices (and finally the global centrality of the graph):

$$c_i(\text{LM}) = \left[\sum_{k=1}^{ecc_i} \left([\text{LM}]_{ik}^{2k} \right)^{1/(ecc_i)^2} \right]^{-1}$$

where ecc_i is the eccentricity of i.

The global centrality (seen as a mean vertex centrality) can be evaluated by the formula

$$C(G) = (1/vk) \sum_{i=1}^{k} (c_i/c_{\max}) v_i$$

where $v = |V(G)|$ is the cardinality of vertices in the graph G, k is the number of vertex equivalence classes, c_i is the centrality index of the class i, and $c_{\max}$ is the maximum of vertex centrality among all the equivalence classes of G.

5.2   Design of Clusters

The clusters herein discussed represent 3D tessellations, recently developed by Diudea (2010, 2013); they are achieved by map operations (Pisanski and Randić 2000; Diudea 2003, 2005; Diudea et al. 2006), as implemented by our original software programs CVNET (Stefu and Diudea 2005) and NanoStudio (Nagy and Diudea 2009). The map operations were applied on the platonic solids (Fig. 5.1): tetrahedron (T), cube (C), octahedron (Oct), dodecahedron (Do), and icosahedron (Ico). A map M is a discretized surface domain, while the operations on maps are

Tetrahedron   Cube   Octahedron   Dodecahedron   Icosahedron

Fig. 5.1   The five platonic polyhedra

topological modifications of a parent map. The parent (named by a subscript zero) and transformed map parameters refer to regular maps (i.e., having all vertices and faces of the same valence/size). The symmetry of parents is preserved by running these operations.

Several operations on maps are known and are currently used to decorate a surface domain. The reader is invited to consult some recent publications in this respect. In the following, only the most important operations are described.

Dual (Du)   put a point in the center of each face of the map; next, join two such points if their corresponding faces share a common edge. It is the (Poincaré) dual $Du(M)$. The vertices of $Du(M)$ represent faces in M and vice versa. In the transformed map, the following relations exist: $Du(M)$, $v = f_0$, $e = e_0$, and $f = v_0$. Dual of the dual returns the original map: $Du(Du(M)) = M$. Tetrahedron is self-dual, while the other platonic polyhedra form pairs: $Du(cube) = octahedron$ and $Du(dodecahedron) = icosahedron$. It is also known as the Petrie dual. Also, a cage dual is known: in the center of a cage, put a point and join two such points if the corresponding cages share a face. If the dual does not account for the infinite face/cage, the dual is called inner dual.

Medial (Med)   put new vertices in the middle of the original edges, and join two vertices if the edges span an angle (and are consecutive). Medial is a 4-valent graph and $Med(M) = Med(Du(M))$. The transformed map parameters are $Med(M)$, $v = e_0$, $e = 2e_0$, and $f = f_0 + v_0$. The medial operation rotates parent s-gonal faces by π/s. Points in the medial represent original edges; thus, this property can be used in topological analysis of edges in the parent polyhedron. Similarly, the points in dual give information on the parent faces.

Truncation (Tr)   cut off the neighborhood of each vertex by a plane close to the vertex, such that it intersects each edge meeting the vertex. Truncation is similar to the medial, the transformed map parameters being $Tr(M)$, $v = 2e_0 = d_0v_0, e = 3e_0$, and $f = f_0 + v_0$. This was the main operation used by Archimedes in building its well-known 13 solids.

Stellation (St)   add a new vertex in the center of each face and connect the central point with the vertices on the face boundary. Thus, the parent face is covered by triangles. The transformed map parameters are $St(M)$, $v = v_0 + f_0$, $e = 3e_0$, and $f = s_0f_0$. The symmetry of the parent graphs is preserved by these operations.

5.3 Icosahedral Clusters

Clusters herein studied represent 3D tessellations, recently developed by Diudea (2013), achieved by map operations, as implemented by the original software CVNET (Stefu and Diudea 2005).

In building the cluster C_{750}, a sequence of operations was used: TRS(P4(C60)) 330, S2(C60)420, and TRS(P4(C60))@S2(C60)750 (Fig. 5.2).

The structure TRS(P4(C60))@S2(C60)750 = C60((C20)$_{60}$)750 is a "spongy" one, with the central hollow of exact topology of TRS(P4(C60))330. It has a C_{20} tessellation: formally, every point in the graph of C60(I_h) is changed by a cage C20; notation C60((C20)$_{60}$) means $60 \times$ (C20) within the topology of C60(I_h). The joining of the two halves was made by our original software NanoStudio (Nagy and Diudea 2009).

C60((C20)$_{60}$)750

TRS(P4(C60))@(S2(C60)420)750

C60   TRS(P4(C60))330   S2(C60)420
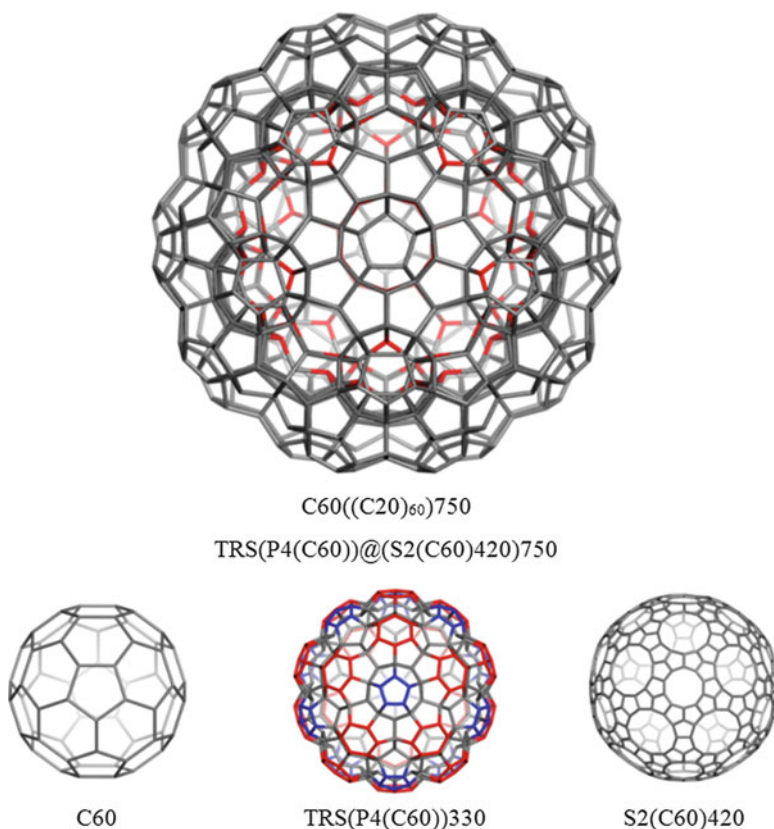
Fig. 5.2 C750 and its substructures

C60@C60(Do60)810

C60@((C20)12;(C24)20)@Do60.810

C24   C60(@((C20)12;(C24)20)390   C60(Do60)750
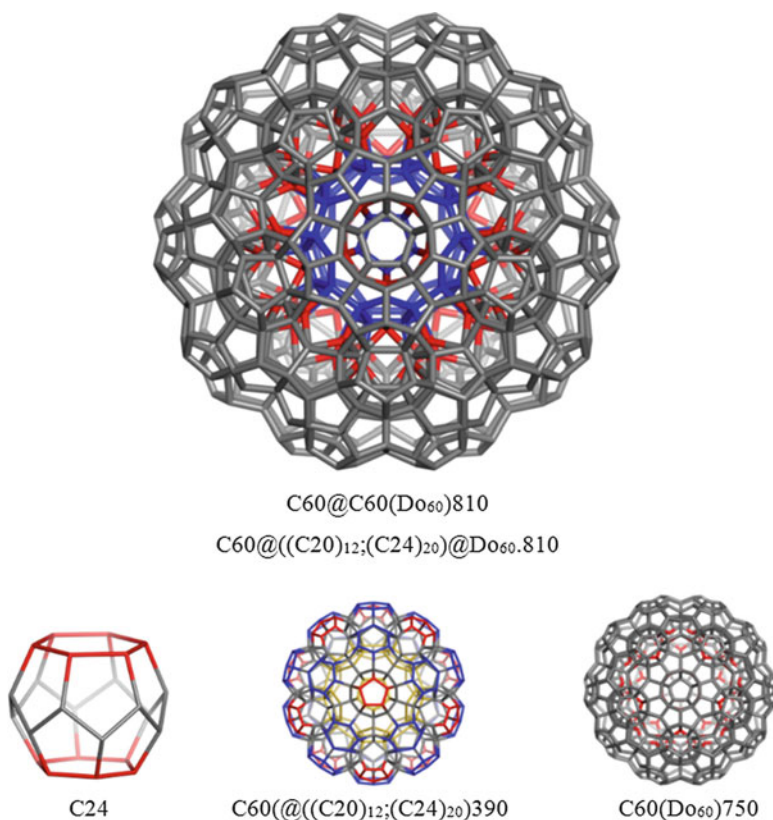
Fig. 5.3 C810 and its components

C810 (Fig. 5.3) has the same structure as C750, with the difference that it has a C60 fullerene inside C750, so we can write C810 as C60@C750. When merged to the hollow of C750 (i.e., TRS(P4(C60))330), C60 provides C20 and C24 cells, as shown in the structure C60(@((C20)12;(C24)20)390. The involved substructures are illustrated at the bottom of figures.

In the idea of 4D icosahedral {3,3,5} polytope, consisting of 600 tetrahedral cells, with five tetrahedra joined around each line, a structure C_{84} having the topology of dodecahedron in which the points are replaced by truncated tetrahedra, TT, was designed by truncating the centered icosahedron IcoP13. More detailed, it is Ico@(TT20;(Py5)12)84, an icosahedron surrounded by 20 truncated tetrahedra and 12 pentagonal pyramids Py5 (Fig. 5.4, bottom). An experimental realization of this structure was brought by Breza et al. (2004), as a beautiful icosahedral diamond crystal. Next, a cluster of general formula $M@M_{12}$, namely,

C84@(C84)$_{12}$.408

(Ico@(TT$_{20}$)@(Ico$_{12}$;TT$_{20}$;TT$_{30}$)@(Py5@TT$_5$)$_{12}$.408

Tr(Diu45)408

IcoP13   Tr(IcoP)84   Diu$_{45}$=IcoP@(IcoP)$_{12}$.45
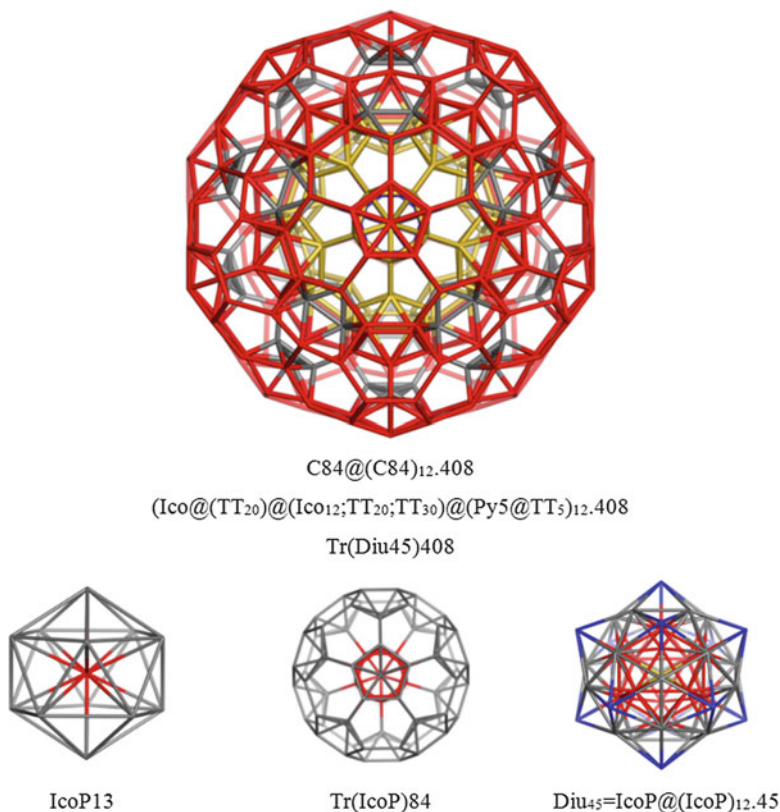
Fig. 5.4 C408 and its substructures

C408 = C84@(C84)$_{12}$.408 = Tr(Diu45)408 (Parvan-Moldovan et al. 2014 – Fig. 5.4), was made by truncation of Diudea's cluster Diu45 = IcoP@(IcoP)$_{12}$.45 (in general Diu$_k$, with k being the number of atoms). It is the intersection of 12 × C84, the core being the 13^{ne}C84 (Fig. 5.4). Recall C84 is related to Samson's (1968) cluster C104, made by putting a point/atom in the center of each TT.

At the end of this section, a complex structure, made by truncation of Diu125 = St(C60@(Du(C60)P$^{\wedge 32}$)125 cluster (Fig. 5.5), is presented; it is detailed as C1208 = Tr(Diu125)1208 = (Du(C60))@(C84)$_{12}$;C100)$_{20}$)1208. One can recognize the topology of C60 fullerene, with C$_{100}$ being the hexagon analogue of the pentagon analogue C84. The core of C1208 is Du(C60), a triangulation with 32 trigonal faces.

In another view, C1208 is the intersection of 12 × C84 and 20 × C100 with C244 (Fig. 5.6), the last one being Tr(Diu33)244 = (Du(C60))@(TT$_{12}$;TT$_{20}$)@C180(I_h)244.

Du(C60)@(C84)₁₂;C100)₂₀)1208

TR(Diu125)1208

TR(IcoP)84   TR(St(Ap6)P)100   St(C60@(Du(C60)P^³²)125
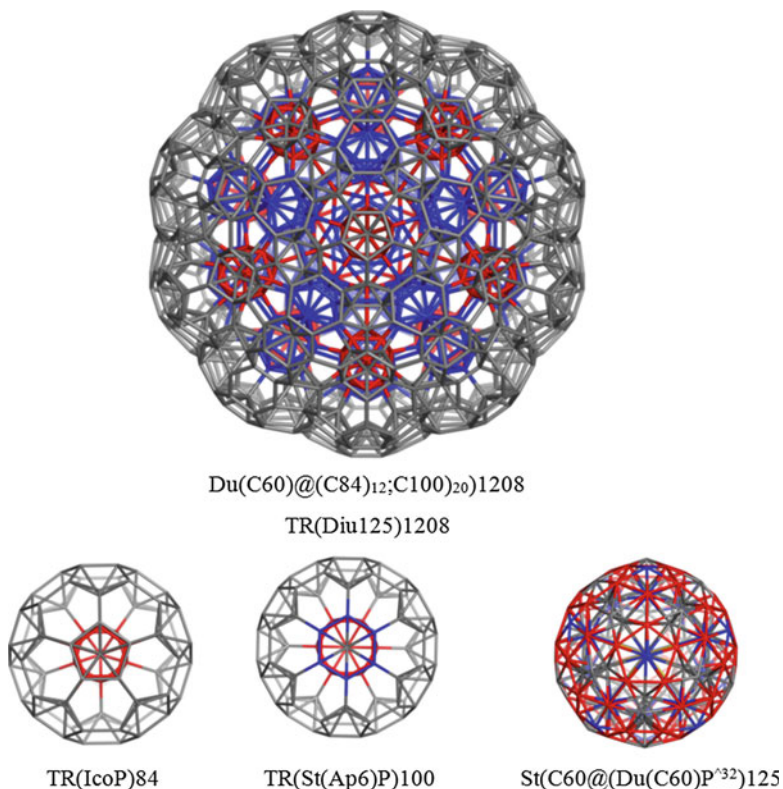
Fig. 5.5 C1208 and its substructures

Observe the missing pyramidal external shapes in the name of these structures, while the envelope of C244 is C180(I_h) (i.e., the leapfrog transform of C60, *Le* (C60)). A last comment Diu33 = St(Do)P^32.33 = Du(C60)P^32.33 (Fig. 5.6) is a 4D polytope(a 32(T)-cell), as it is also IcoP13 (a 20(T)-cell) (Fig. 5.4, bottom).

Figure counting for some of the icosahedral clusters herein discussed is shown in Table 5.1. One can see, in column *M*, # = 1 is for the true 4D structures, while # = 2 is for the clusters embedded by their "molecular envelope" in the 4D space; M_k refers to different types of shapes.

Topological symmetry and centrality index for the icosahedral clusters herein discussed are shown in Tables 5.2, 5.3, 5.4, 5.5, 5.6, and 5.7 (Parvan-Moldovan et al. 2014). The equivalence classes of atoms are given in the descending order of their centrality (cf. LR matrix). The automorphism group is calculated (cf. GAP permutations) (The GAP Team 2014).

C244= Tr(Diu33)244

(Du(C60))@(TT$_{12}$;TT$_{20}$)@C180(I_h)244

TT12   Do20   Diu33=St(Do)P$^{\wedge 32}$.33
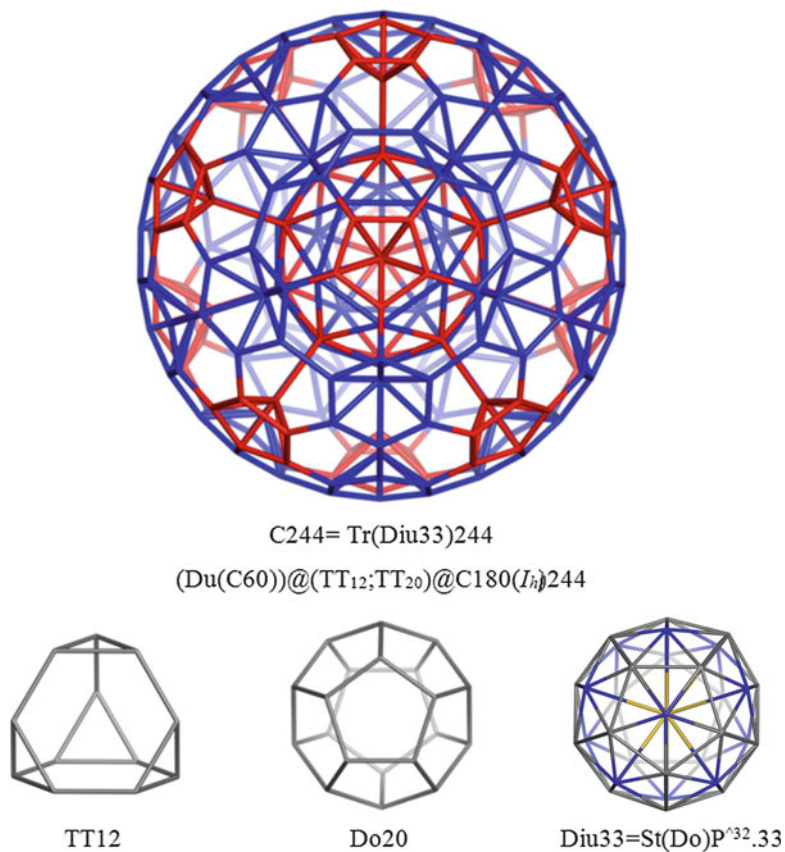
Fig. 5.6 C244 and its substructures

Table 5.1 Figure counting in some icosahedral clusters

Cluster	V	e	f_3	f_5	f_6	f	M_1	M_2	M_3	M	Cells	Sum$f$
IcoP13	13	42	50	0	0	50	20	0	0	1	21	0
Diu33	33	122	150	0	0	150	60	0	0	1	61	0
Diu45	45	204	290	0	0	290	130	0	0	1	131	0
Diu125	125	604	870	0	0	870	390	0	0	1	391	0
Tr(Icop)84	84	192	80	0	62	142	20	12	0	2	34	0
Tr(Diu$_{33}$)244	244	572	240	12	170	422	60	12	20	2	94	0
Tr(Diu$_{45}$)408	408	1074	520	12	290	822	130	12	12	2	156	0

Table 5.2 Symmetry of C750: automorphism group $= C_2 \times A_5 = I_h$; $|I_h| = 120$

Class	Centrality signature LF 56	No. of elements	Vertex degree	Atom type
1	0.0425537487829127	60	4	5^5
2	0.0425405656366799	30	4	5^5
3	0.0408741428983785	60	3	5^3
4	0.0403249632533878	60	4	5^6
5	0.0403215210989583	60	4	5^5.6
6	0.0403184110690464	60	4	5^5.6
7	0.0380980964599947	60	4	5^5
8	0.0380776127196794	60	4	5^5
9	0.0380525586272046	60	4	5^5
10	0.0363966020960237	60	3	5^3
11	0.0363899446618803	60	3	5^3
12	0.0363398403991418	120	3	5^3
C(G)	0.0760383561			

Table 5.3 Symmetry of C810: automorphism group $= C_2 \times A_5 = I_h$

Class	Centrality signature LF 56	No. of elements	Vertex degree	Atom type
1	0.0583077074930839	60	4	5^4.6^2
2	0.0535677234743963	60	4	5^6
3	0.0527954841138494	60	4	5^6
4	0.0527665144390053	30	4	5^6
5	0.0487543466004813	60	4	5^5.6
6	0.0487490577203367	60	4	5^6
7	0.0487323390119923	60	4	5^5.6
8	0.0451984025518483	60	4	5^5
9	0.0451950801970316	60	4	5^5
10	0.0451790710273149	60	4	5^5
11	0.0424285737796061	60	3	5^3
12	0.0423731722780051	120	3	5^3
13	0.0398282805799518	60	3	5^3
C(G)	0.0515968044			

Table 5.4 Symmetry of C408: automorphism group $= C_2 \times A_5 = I_h$; $|I_h| = 120$

Class	Centrality signature LF 36	No. of elements	Vertex degree	Atom type
1	0.0825432266953615	12	6	3^5.5^5.6^5
2	0.0723127280340924	12	6	3^5.5^5.6^5
3	0.064639289864084	60	6	3^5.5^5.6^5
4	0.05803576223073222	60	6	3^5.5^5.6^5
5	0.0572358681133143	12	6	3^5.5^5.6^5
6	0.0564467194639707	60	6	3^5.5^2.6^5
7	0.0552836553218085	60	5	3^3.5^2.6^4
8	0.0512081941907237	12	6	3^5.6^5
9	0.0505895569851173	60	4	3^2.5.6^3
10	0.0467456474901417	60	4	3^2.5.6^3
C(G)	0.0684847290			

Table 5.5 Symmetry of Diu45: automorphism group $= C_2 \times A_5$

Class	Centrality signature LF 33	No. of elements	Vertex degree	Atom type
1	0.147759191901086	1	12	3^30
2	0.0765155719593704	12	12	3^30
3	0.0466230965152783	20	9	3^18
4	0.0404089478576394	12	6	3^10
C(G)	0.1442821876			

Table 5.6 Symmetry of C244: automorphism group $= C_2 \times A_5$

Class	Centrality signature LF 36	No. of elements	Vertex degree	Atom type
1	0.0837441494075746	12	6	3^5.6^10
2	0.0832240289226498	20	7	3^6.5^3.6^9
3	0.0679636030600054	12	6	3^5.6^5
4	0.0675306046381466	20	7	3^6.6^6
5	0.0560796687460724	60	4	3^2.5.6^3
6	0.0557098367436541	60	4	3^2.6^4
7	0.0557092598622740	60	4	3^2.6^4
C(G)	0.1040690102			

Table 5.7 Symmetry of C1208: automorphism group $= C_2 \times A_5$

Class	Centrality signature	No. of elements	Vertex degree	Atom type
1	0.0692967724225917	12	6	3^5.6^10
2	0.0691365154423208	20	7	3^6.5^3.6^9
3	0.0619497820844220	12	6	3^5.5^5.6^5
4	0.0618024674066362	20	7	3^6.5^6.6^6
5	0.0557957706506803	60	6	3^5.5^5.6^5
6	0.0556613506327981	60	6	3^5.5^4.6^6
7	0.0556608929712865	60	6	3^5.5^4.6^6
8	0.0505563870936009	60	6	3^5.5^5.6^5
9	0.0504284365686111	120	6	3^5.5^4.6^6
10	0.0460693873679426	12	6	3^5.5^5.6^5
11	0.0460485352602655	60	6	3^5.5^2.6^5
12	0.0459536270202304	20	7	3^6.5^6.6^6
13	0.0459430688968205	120	6	3^5.5^2.6^5
14	0.0451843719178823	60	5	3^3.5^2.6^4
15	0.0451485654894074	120	5	3^3.5^2.6^4
16	0.0421607708595767	12	6	3^5.6^5
17	0.0421402682758050	60	4	3^2.5.6^3
18	0.0420471142414957	20	7	3^6.6^6
19	0.0420415003258929	120	4	3^2.5.6^3
20	0.0387298595614090	60	4	3^2.5.6^3
21	0.0386382508751928	120	4	3^2.6^4
C(G)	0.0324605914			

5.4 Octahedral Clusters

5.4.1 Octahedral 3D Clusters

In this section we present multi-shell structures, of octahedral symmetry, designed by map operations on some Diudea's small multi-shell clusters Diu$k$, consisting of tetrahedra or octahedra (see below).

The first cluster is C424 = C88@(C88)$_6$.424, of general formula M@M$_6$, made by truncation of Diu57 cluster (see the second name, Tr(Diu57)424, to remind the way of its design, Fig. 5.7) which consists of six cages C88 joined on the cube faces (see the third name for this cluster: C@(C$_{88}$)$_6$.424) or intersected with a seventh C88, the last being the core (Kooperazan-Moftakhar et al. 2015). This kind of repetition was encountered in the icosahedral cluster C408 (Sect. 5.3), but, here, the

C88@(C88)6.424

C@(C88)6.424

Tr(Diu57)424

C8

C88=C@TO6.88

Tr(St(C)P^815)88

Diu57=(St(C)P^815)@(St(C)P^815)6.57
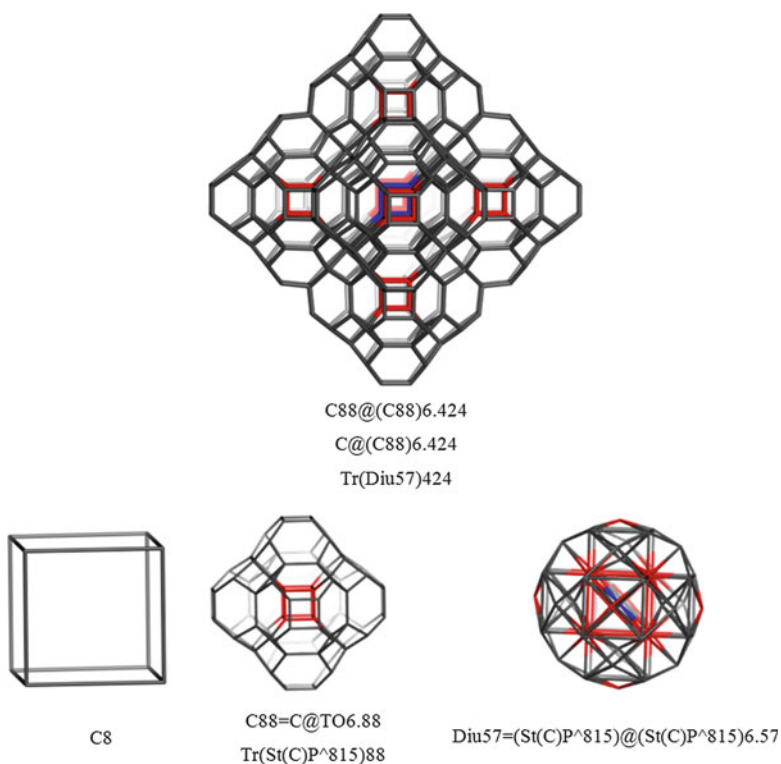
Fig. 5.7 Cluster C424 and its substructures

C88.222.538
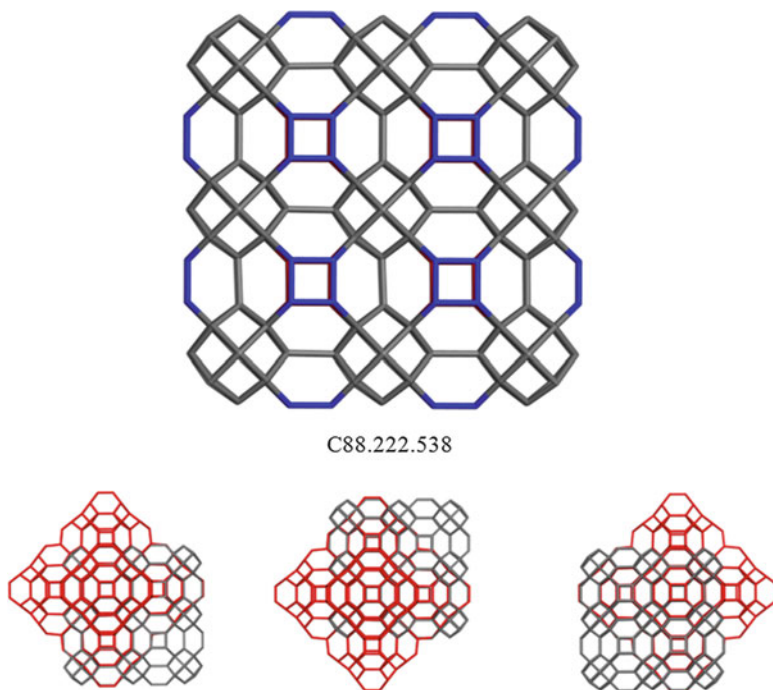
Fig. 5.8 The triple-periodic network of C88 and its superposition with C424 cluster

octahedral symmetry enables the unit translation along the three coordinates and 3-periodicity, as in the crystal state. In this case, the repeating unit is $C88 = C@TO_6.88$ (i.e., a cube surrounded by six truncated octahedra, TO), while the superposition of the cluster over the triple-periodic network is clearly shown in Fig. 5.8, bottom.

The second cluster herein introduced is $C212 = C44@(C44)_6.212$, of general formula $M@M_6$, also named $C@(C44)_6.212$ and even $Med(Diu57)212$ (Fig. 5.9); its repeating unit is $C44 = C@CO_6.44$, also named $Med(St(C)P^{\wedge 8}15)88$, to remind the map operation used for its design and its origin, the small cluster $St(C)P^{\wedge 8}15$ (see below, Fig. 5.10). This is also translatable over the three coordinate axes, as shown above, for C88.

The cluster Diu57 (Fig. 5.10), the source for C424 and C212, consists of 36 octahedra, arranged in six $P^{\wedge 8}@Oct_6.15$ in octahedral disposition; it was designed by capping/stellating, St, of the cluster $Diu51 = Med(St(C)P^{\wedge 14}.15)P^{\wedge 8}.51$ (Fig. 5.11). The cluster $St(C)P^{\wedge 14}.15 = P^{\wedge 14}@T_{24}.15$ (consisting of 24 tetrahedra, Fig. 5.11, bottom) is the cage-dual $CD(Med(Oct@Oct_8.18)60)15$ (Fig. 5.12) of Med

C44@(C44)₆.212

C@(C44)₆.212

Med(Diu57).212

C8

C44=C@CO₆.44

Med(St(C)P^$15)44

Diu57=St(C)P^$15)@

(St(C)P^$15)₆.57
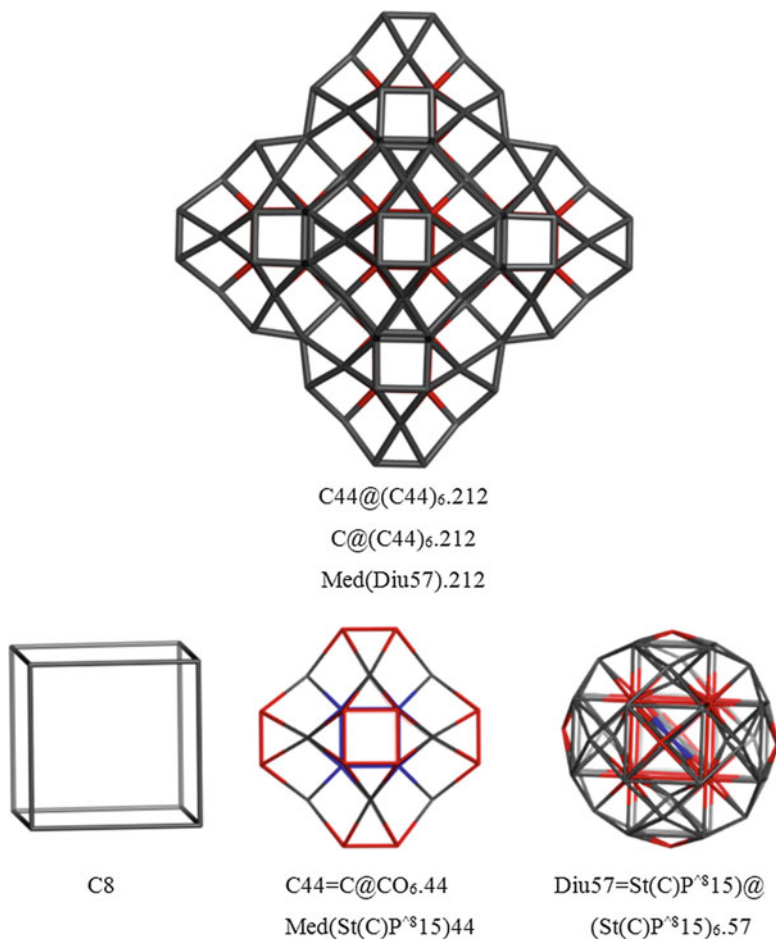
Fig. 5.9 Cluster C212 and its substructures

(Oct@Oct₈.18)60 (Fig. 5.12, bottom), and it represents a 4D object. Table 5.8 shows the figure count for some octahedral clusters. As in Sect. 5.4.3, in column "M," $\# = 2$ is for the clusters embedded by their "molecular envelope" in the 4D space, while $\# = 1$ is for the true 4D structures.

The name of multi-shell structures can be written at least in three ways, as shown above, which one is to be used varies by needs. In the name of these structures, the (subscript) P_k means a prism of size k, while the (superscript) P^k represents a
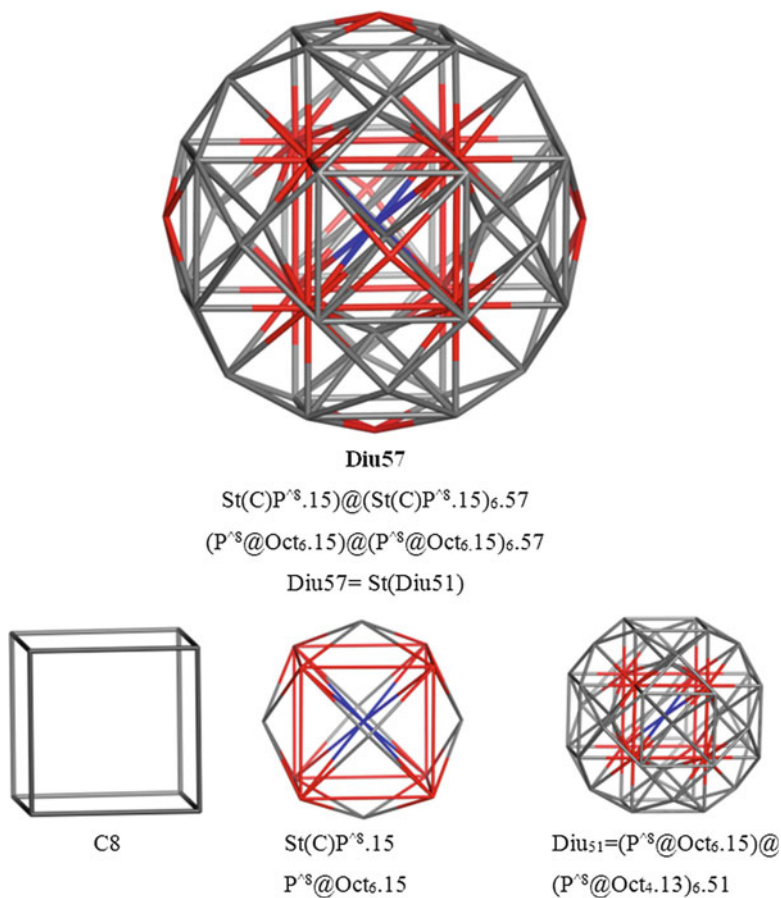
Fig. 5.10 Cluster Diu57 and its substructures

k-connected point-centered cage; the last number is the number of atoms in the structure.

Topological symmetry for the octahedral clusters herein discussed is given in Tables 5.9 and 5.10.

Note that point-centered cages MP represent inner cage duals for families of structures, e.g., $IcoP13 = IcoP^{\wedge 12}.13$ is the inner cage dual of $C20@(C20)_{12}.130$.

Figures and the centrality of vertex equivalence classes have been performed by NanoStudio program (Nagy and Diudea 2009).

Diu51

$(P^{\wedge 8}@Oct_6.15)@(P^{\wedge 8}@Oct_4.13)_6.51$

$Med(St(C)P^{\wedge 14}.15)P^{\wedge 8}.51$

Oct6

$St(C)P^{\wedge 14}.15$

$P^{\wedge 14}@T_{24}.15$

$CD(Med(Oct@Oct_8.18)60)15$

$(P^{\wedge 8}@Oct_6.15)@$

$(P^{\wedge 8}@Oct_6.15)_6.57$
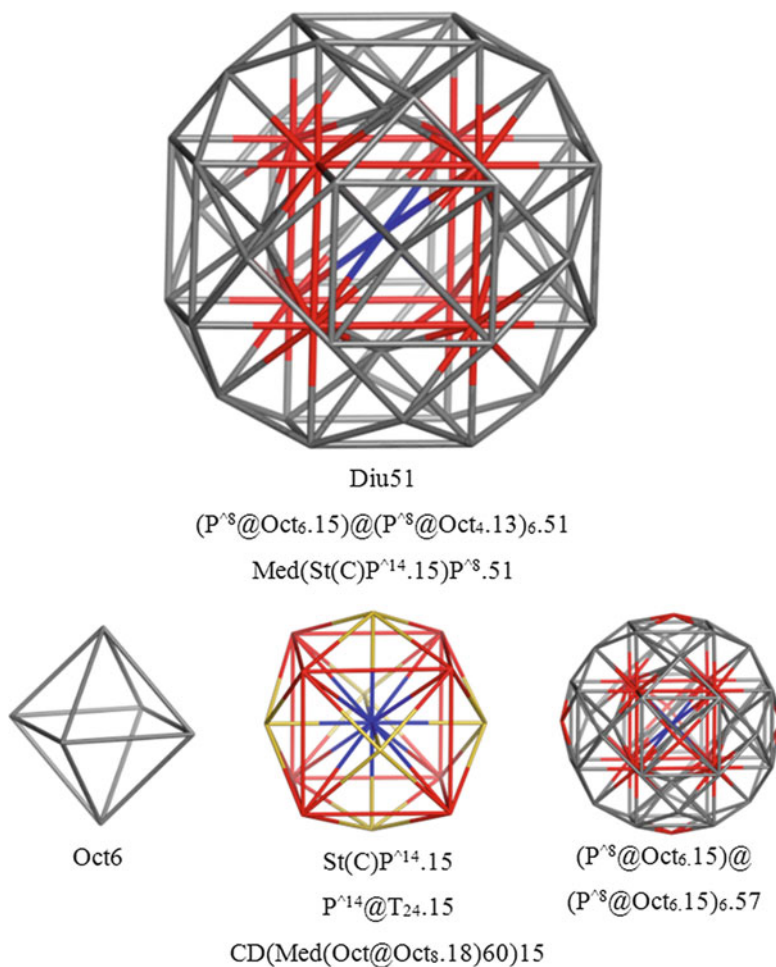
Fig. 5.11 Cluster Diu51 and its substructures

5.4.2   Octahedral 4D Clusters

The object 24-cell24 (CP (23) – Fig. 5.13, top left) was built up starting from the point-centered cube CP9 meeting six octahedra Oct in that point and in the corresponding six faces of the cube. If the pattern is let to curl up into the fourth dimension, one gets the projection into 3D space of a 4D regular polytope, the 24-cell, having 24 octahedral cells, 6 meeting at each vertex. Also known as the

$(St(C)P^{\wedge 14}.15)@ (CO@((CO)_8;(C)_6)60)$

CO12   Oct@Oct$_s$.18   CO@((CO)$_s$;(C)$_6$)60

Oct@(Oct$_s$;(Py$_4$)$_6$)@(CO)18   Med((Oct@(Oct$_s$)18)60
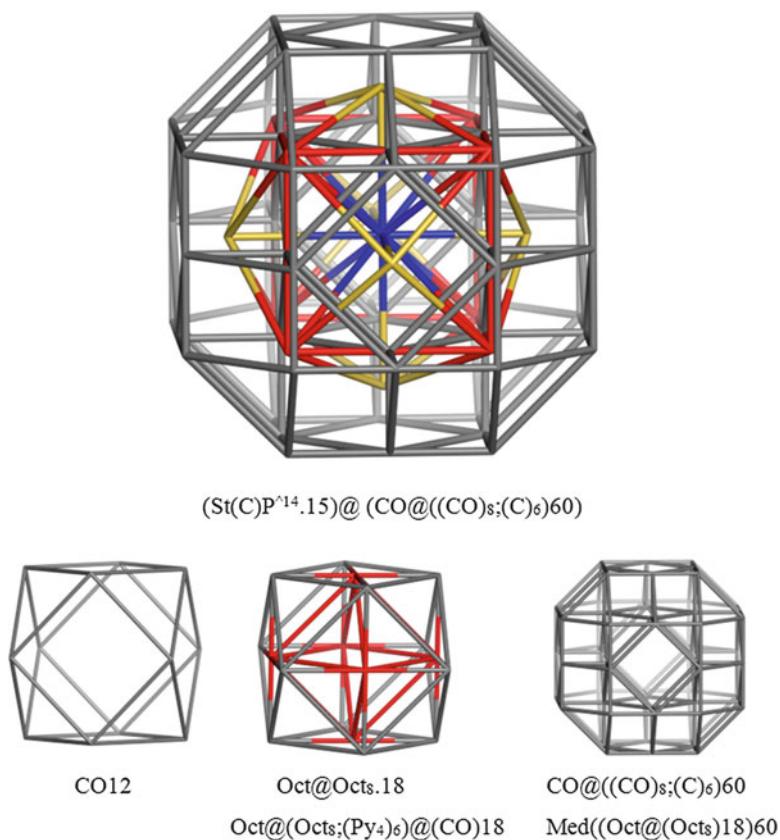
Fig. 5.12 Cuboctahedron of cuboctahedra (CO@((CO)$_8$;(C)$_6$)60), its cage-dual (St(C)P$^{\wedge 14}$.15), and related substructures

Table 5.8 Figure count in octahedral clusters

Cluster	v	e	f_3	f_4	f_6	f	M_1	M_2	M_3	M	Cells	Sum$f$
C_{424}	424	788	0	216	200	416	6	36	8	2	52	0
C_{212}	212	576	192	216	0	408	6	36	0	2	44	0
C_{88}	88	152	0	36	36	72	0	6	0	2	8	0
C_{44}	44	108	36	36	0	72	0	6	0	2	8	0
Oct@Oct$_8$.18	18	60	52	6	0	58	8	6	0	2	16	0
Diu$_{57}$	57	212	192	0	0	192	36	0	0	1	37	0
Diu$_{51}$	51	188	168	6	0	174	30	6	0	1	37	0
St(C)P$^{\wedge 8}$.15	15	44	36	0	0	36	0	6	0	1	7	0
St(C)P$^{\wedge 14}$.15	15	50	60	6	0	66	24	6	0	1	31	0

Table 5.9 Symmetry of C212: automorphism group $= C_2 \times S_4 = O_h$; $|O_h| = 48$

Class	Centrality signature	No. of elements	Vertex degree	Atom type
1	0.1193393940030620	8	6	3^3.4^6.6^6
2	0.0991794357360293	12	8	3^4.4^8.6^8
3	0.0857941451388779	24	6	3^3.4^6.6^6
4	0.0830428609565858	24	6	3^3.4^4.6^5
5	0.0727345452596509	24	6	3^3.4^6.6^6
6	0.0727327140609193	24	6	3^3.4^4.6^5
7	0.0714664787850572	48	4	3^2.4^2.6^2
8	0.0626805298098102	24	6	3^3.4^4.6^4
9	0.0546571449698314	24	4	3^2.4^2.6^2
C(G)	0.0699810999			

Table 5.10 Symmetry of C424: automorphism group $= C_2 \times S_4 = O_h$; $|O_h| = 48$

Class	Centrality signature	No. of elements	Vertex degree	Atom type
1	0.0727569230162741	8	4	4^3.6^3
2	0.0666680578969843	8	4	4^3.6^3
3	0.0616230071445152	24	5	4^4.6^4
4	0.0574675860576482	24	4	4^3.6^3
5	0.0568998116993004	24	4	4^2.6^4
6	0.0536201441861738	24	4	4^3.6^3
7	0.0532955870173036	24	4	4^2.6^4
8	0.0528085158641600	24	4	4^2.6^3
9	0.0499140490133102	24	4	4^3.6^3
10	0.0496180786008872	24	4	4^2.6^3
11	0.0491734820171032	48	3	4.6^2
12	0.0466528853100227	24	4	4^3.6^3
13	0.0464203441687386	48	3	4.6^2
14	0.0437573286882863	48	4	4^2.6^3
15	0.0411646928023433	24	3	4.6^2
16	0.0388393029516746	24	3	4.6^2
C(G)	0.0065819621			

hyperdiamond or octaplex, it is self-dual and has no analogue among the five platonic solids of 3D space. This projection shows only 23 distinct points/vertices from all 24 vertices (indicated in round parentheses). The symmetry group of this polychoron is a Coxeter group (Coxeter 1934).

Keeping in mind that 24-cell has only octahedral cells and that, by operations on maps, the octahedron Oct can be obtained from the cube by the dual operation Du (C) while from the tetrahedron T by the medial operation Med(T), we performed this 4D object starting from 8-cell, [4,3,3] and 16-cell, [3,3,4], respectively, as
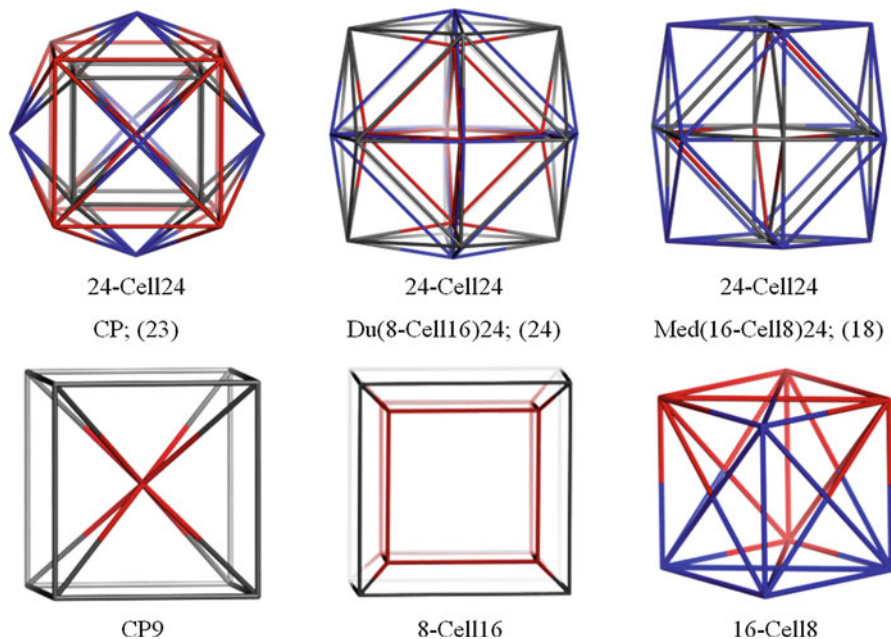
Fig. 5.13 The octaplex or 24-cell and some related structures
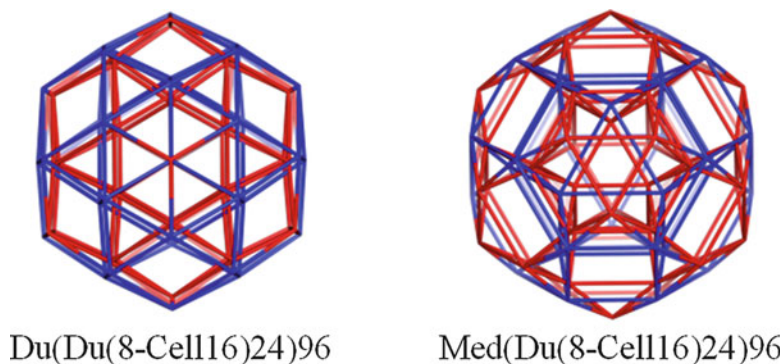
Fig. 5.14 Two different projections of 24-Cell built up by dual Du and medial Med operations, respectively

follows (Diudea 2015): Du(8-cell)24 (with all 24 distinct vertices) and Med (16-cell)24 (with only 18 distinct points – Fig. 5.13).

In view of demonstrating the topological symmetry (i.e., the equivalence orbits of figures) of 24-cell, we performed Du(24-cell) = {C@(C_8;CO_6)52 &(C@(CO_6) 44}96 for faces and Med(24-cell) = {CO@(C_6;CO_8)60&(CO@(C_6;$(J_3)_8$)@TO.36} 96 for edges (Fig. 5.14). Being a self-dual 4D structure, the cage classes will be the

Table 5.11 Figure count for some 4D clusters

Cluster	V	e	f_3	f_4	f	c	Sum(f)	Class
24-cell24	24	96	96	0	96	24	0	1{24}
Med(16-cell)24	24	96	96	0	96	24	0	1{24}
Du(8-cell)24	24	96	96	0	96	24	0	1{24}
Med(24-cell)96	96	288	96	144	240	48	0	1{96}
Du(24-cell)96	96	288	96	144	240	48	0	1{96}
16-cell8	8	24	32	0	32	16	0	1{8}
8-cell16	16	32	0	24	24	8	0	1{16}
5-cell5	5	10	10	0	10	5	0	1{5}

same as the vertex classes in the original cluster. Data are listed in Table 5.11; since there is only one orbit for all the four figures of 24-cell, it means it is 4-transitive and really a regular 4D polytope. Due to the high symmetry of 24-cell, its transforms Du(24-cell)96 and Med(24-cell)96 represent one and the same structure, in two different projections.

5.5 Computational Details

The multi-shell clusters have been designed by using CVNET (Stefu and Diudea 2005) software program and their topology analyzed by NanoStudio software (Nagy and Diudea 2009). The automorphism data were provided by the GAP (The GAP Team 2014).

5.6 Conclusions

The classes of equivalence of figures (vertices/atoms, edges/bonds, faces, and cages) in some icosahedral and octahedral multi-shell clusters have been solved by using the centrality topological index, computed on the layer matrix of all rings around atoms, and confirmed by the results of matrix permutation. The classes for edges, faces, and cages could be calculated as for the vertices, in the transformed graphs operated by medial, dual, and cage dual, respectively. The centrality index can provide an image of molecular/global centrality, when normalized to account for all atoms and their equivalence classes in the molecular graph.

References

Ashrafi AR, Kooperazan-Moftakhar F, Diudea MV, Stefu M (2013) In: Diudea MV, Nagy CL (eds) Diamond and related nanostructures. Springer, Dordrecht/Heidelberg/New York/London, pp 321–333

Breza J, Kadlečikova M, Vojs M, Michalka M, Vesely M, Danis T (2004) Diamond icosahedron on a TiN-coated steel substrate. Microelectron J 35:709–712

Coxeter HSM (1934) Discrete groups generated by reflections. Ann of Math (2) 35(3):588–621

Diudea MV (1994) Layer matrices in molecular graphs. J Chem Inf Comput Sci 34:1064–1071

Diudea MV (2003) Capra-a leapfrog related operation on maps. StudiaUniv"Babes-Bolyai" Chemia 48(2):3–7

Diudea MV (2005) Nanoporous carbon allotropes by septupling map operations. J Chem Inf Model 45:1002–1009

Diudea MV (2010) Nanomolecules and Nanostructures – Polynomials and Indices. MCM No 10, University of Kragujevac, Serbia

Diudea MV (2013) Quasicrystals, between spongy and full space filling. In: Diudea MV, Nagy CL (eds) Diamond and related nanostructures. Springer, Dordrecht/Heidelberg/New York/London, pp 333–383

Diudea MV (2015) 4D-Octahedral structures. Int J Chem Model (accepted)

Diudea MV, Nagy CL (2007) Periodic nanostructures. Springer, Dordrecht

Diudea MV, Nagy CL (2013) Diamond and related nanostructures. Springer, Dordrecht

Diudea MV, Ursu O (2003) Layer matrices and distance property descriptors. Indian J Chem 42A:1283–1294

Diudea MV, Stefu M, John PE, Graovac A (2006) Generalized operations on maps. Croat Chem Acta 79:355–362

Euler L (1758) Elementa doctrinae solidorum. Novi Comm Acad Scient Imp Petrop 4:109–160

Hungerford TW (1980) Algebra, graduate texts in mathematics. Reprint of the 1974 original, vol 73. Springer, New York/Berlin

Koorepazan-Moftakhar F, Pîrvan-Moldovan A, Diudea MV (2015) Topological symmetry of multi-shell clusters with octahedral symmetry. Int J Chem Model 6:231–239

Nagy CL, Diudea MV (2009) Nano-studio software. Babes-Bolyai University, Cluj

Parvan-Moldovan A, Kooperazan-Moftakhar F, Diudea MV (2014) Topological symmetry of multi-shell icosahedral clusters. Studia Univ "Babes-Bolyai" Chemia 59(3):103–108

Pisanski T, Randić M (2000) Bridges between geometry and graph theory. Geometry at work. MAA Notes 53:174–194

Samson S (1968) Structural chemistry and molecular biology. In: Rich A, Davidson N (eds) Structural chemistry and molecular biology. Freeman, San Francisco, pp 68–717

Schläfli L (1901) Theorie der vielfachen Kontinuität Zürcher und Furrer, Zürich (Reprinted in: Schläfli Ludwig, 1814–1895, Gesammelte Mathematische Abhandlungen, Band 1:167–387, Birkhäuser Verlag, Basel, 1950 (in German)

Stefu M, Diudea MV (2005) CageVersatile_CVNET software program. Babes-Bolyai Univ, Cluj

The GAP Team (2014) GAP – Groups, Algorithms, Programming – a system for computational discrete algebra, **GAP** 4.7.5 release. http://www.gap-system.org

Chapter 6
Further Results on Two Families of Nanostructures

Zahra Yarahmadi and Mircea V. Diudea

Abstract A topological index is a numeric quantity derived from the structure of a graph which is invariant under automorphisms of the graph under consideration. In this chapter, the Wiener, Szeged, and Cluj-Ilmenau indices and one-alpha descriptor will be calculated for an infinite family of nanocones, $CNC_4[n]$, and eccentric connectivity; augmented eccentric connectivity; and Wiener, Szeged, PI, vertex PI, and the first and second Zagreb indices of N-branched phenylacetylenes nanostar dendrimers will be obtained. For obtaining Wiener and Szeged indices, we use a powerful method given by Klavžar.

6.1 Introduction

In the past years, nanostructures involving carbon have been the focus of an intense research activity which is driven to a large extent by the request for new materials with specific applications. Throughout this section, G is a simple connected graph with the vertex and edge sets $V(G)$ and $E(G)$, respectively. Usually, the distance between the vertices u and v of a connected graph G is denoted by $d_G(u,v)$, and it is defined as the number of edges in a minimal path connecting the vertices u and v. A topological index is a numeric quantity, derived from the structure of a graph, which is invariant under automorphisms of the graph under consideration. One of the most famous topological indices is the Wiener index, introduced by Harold Wiener, see (Wiener 1947). The Wiener index of G is the sum of distances between all unordered pairs of vertices of G,

Z. Yarahmadi (✉)
Department of Mathematics, Faculty of Sciences, Khorramabad Branch, Islamic Azad University, Khorramabad, Iran
e-mail: Z.yarahmadi@khoiau.ac.ir; Z.yarahmadi@gmail.com

M.V. Diudea
Department of Chemistry, Faculty of Chemistry and Chemical Engineering, Babes-Bolyai University, Arany Janos Street 11, Cluj-Napoca RO-400028, Romania

$$W(G) = \sum_{\{u,v\} \subseteq V(G)} d_G(u,v).$$

The Szeged index is another topological index which is defined by Ivan Gutman (Gutman 1994) as $Sz(G) = \sum_{e=uv \in E(G)} n_u(e)n_v(e)$, where $n_u(e)$ is the number of vertices of G lying closer to u than to v and $n_v(e)$ is the number of vertices of G lying closer to v than to u. If in the definition of Szeged index, we consider the sum of contributions, then we obtain a recently defined topological index, named vertex PI index. In mathematical language, the vertex PI index of G is defined as $PI_v(G)$ $= \sum_{e=uv \in E(G)} [n_u(e) + n_v(e)]$ (see Ashrafi et al. 2008; Ashrafi and Rezaei 2007).

Let $G(V, E)$ be a connected bipartite graph, with the vertex set $V(G)$ and edge set $E(G)$. Two edges $e = (x,y)$ and $f = (u,v)$ of G are called codistant (briefly: e co f) if

$$d(x,v) = d(x,u) + 1 = d(y,v) + 1 = d(y,u).$$

Let $C(e) := \{f \in E(G); f \ co \ e\}$ denote the set of edges in G, codistant to the edge $e \in E(G)$. If relation co is an equivalence relation, then G is called a co-graph. The set $C(e)$ is called an orthogonal cut (oc for short) of G, with respect to edge e. If G is a co-graph, then its orthogonal cuts $C_1, C_2, \ldots, C_k$ form a partition of $E(G)$: $E(G) = C_1 \cup C_2 \cup \ldots \cup C_k$, $C_i \cap C_j = \phi$, $i \neq j$. Observe co is a Θ relation (Djoković-Winkler) (Djoković 1973).

We say that edges e and f of a plane graph G are in relation opposite, e op f, if they are opposite edges of an inner face of G. Note that the relation co is defined in the whole graph, while op is defined only in faces. Using the relation op, we can partition the edge set of G into opposite edge strips, ops. An ops is a quasi-orthogonal cut qoc, since ops is not transitive.

Let G be a connected graph and $S_1, S_2, \ldots, S_k$ be the ops strips of G. Then the ops strips form a partition of $E(G)$. The length of ops is taken as maximum. It depends on the size of the maximum fold face/ring Fmax/Rmax considered, so that any result on Omega polynomial will have this specification.

Denote by $m(G,s)$ the number of ops of length s, and define the Omega polynomial as: $\Omega(G,x) = \sum_s m(G,s)x^s$ (see Diudea et al. 2008). Its first derivative (in $x = 1$) equals the number of edges in the graph: $\Omega'(G,1) = \sum_s m(G,s).s = e = |E(G)|$.

On Omega polynomial, the Cluj-Ilmenau index (see John et al. 2007), $CI = CI$ (G), was defined:

$$CI(G) = \left\{ \left[\Omega'(G,1) \right]^2 - \left[\Omega'(G,1) + \Omega''(G,1) \right] \right\}.$$

The formulas for calculating CI index are established on cones of various apex rings and various extensions of the cone shirt.

Recently, one-two descriptor has been defined, and it has been shown that it is a good predictor of the heat capacity at P constant (CP) and of the total surface area

(TSA). In this chapter, we analyze its generalizations by replacing the value 2 by arbitrary positive-value α. The molecular descriptor is the final result of a logical and mathematical procedure which transforms chemical information encoded within a symbolic representation of a molecule into a useful number or the result of some standardized experiment (Todeschini and Consonni 2000). Molecular descriptors have been shown to be useful in modeling many physicochemical properties in numerous QSAR and QSPR studies (Trinajstić 1992), (Devillers and Balaban 1999; Karelson 2000).

One-alpha descriptor is defined as the sum of the vertex contributions in such a way that each pendant vertex contributes 1, each vertex of degree two adjacent to pendant vertex contributes α, and also each vertex of degree higher than two also contributes α. If we take $\alpha = 2$, we get one-two descriptor. In Vukičević et al. 2010, this is the definition for 3-ethyl-hexane by Fig. 6.1:

One-alpha descriptor of graph G will be denoted by $OA(G)$. For instance, if G is 3-ethyl-hexane, then $OA(G) = 3 + 4\alpha$.

The Padmakar-Ivan (*PI*) index of the graph G is defined as $PI(G) = \sum_{e=uv \in E(G)} [m_u(e) + m_v(e)]$, where $m_u(e)$ is the number of edges of G lying closer to u than to v and $m_v(e)$ is the number of edges of G lying closer to v than to u (see Khadikar 2000; Khadikar and Karmarkar 2001). Finally, the first and second Zagreb indices of the graph G are defined as $Zg_1(G) = \sum_{u \in V(G)} \deg_G^2 u$ and $Zg_2(G) = \sum_{e=uv \in E(G)} \deg_G u \deg_G v$, respectively (see Gutman and Das 2004; Gutman and Trinajstic 1972; Khalifeh et al. 2009) for mathematical properties and chemical applications.

For a given vertex u of $V(G)$, its eccentricity $\varepsilon(u)$ is the largest distance between u and any other vertex v of G. The maximum eccentricity over all vertices of G is called the diameter of G and denoted by $d(G)$, and the minimum eccentricity among the vertices of G is called radius of G and denoted by $r(G)$. Also, u is a central vertex if $\varepsilon(u) = r(G)$. The center of G, $C(G)$ is defined as $C(G) = \{u \in V(G) | \varepsilon(u) = r(G)\}$. The eccentric connectivity index is a topological index that has been much used in the study of various properties of many classes of chemical compounds. This index is defined as

$$\xi(G) = \sum_{u \in V(G)} \deg(u)\,\varepsilon(u)$$

Fig. 6.1 Vertex contributions of 3-ethyl-hexane
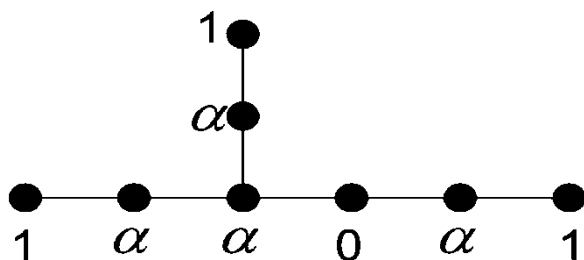
where deg (u) denotes the degree of vertex u in G and $\varepsilon(u)$ is its eccentricity. It used in a series of papers concerned with QSAR/QSPR studies. Its mathematical properties started to be studied only recently (see Ashrafi et al. 2011; Ilić and Gutman 2011 for details). The investigation of its mathematical properties started only recently, and so far, results in determining the extremal values of the invariant and the extremal graphs where those values are achieved are also in a number of explicit formulas for the eccentric connectivity index of several classes of graphs (see Fischermann et al. 2002; Gupta et al. 2002; Kumar et al. 2004; Sardana and Madan 2001; Sharma et al. 1997).

Another topological index that we attended in this paper is augmented eccentric connectivity index. This is defined as the summation of the quotients of the product of adjacent vertex degrees and eccentricity of the concerned vertex, for all vertices in the hydrogen-suppressed molecular graph. It is expressed as

$$\xi(G) = \sum_{u \in V(G)} \frac{M(u)}{\varepsilon(u)},$$

where $M(u)$ denotes the product of degrees of all neighbors of vertex u (see Dureja and Madan 2007).

A chemical graph is a graph such that each vertex represents an atom of the molecule and covalent bonds between atoms are represented by edge between the corresponding vertices.

The nanocone is an important type of nanostructure involving carbon. In recent years, some researchers considered the mathematical properties of such nanostructures (Alipour and Ashrafi 2009a, b). One type of nanocones is the C_4 nanocone, which is symbolized by $CNC_4[n]$ (Fig. 6.2).

Fig. 6.2 The nanocone $CNC_4[3]$
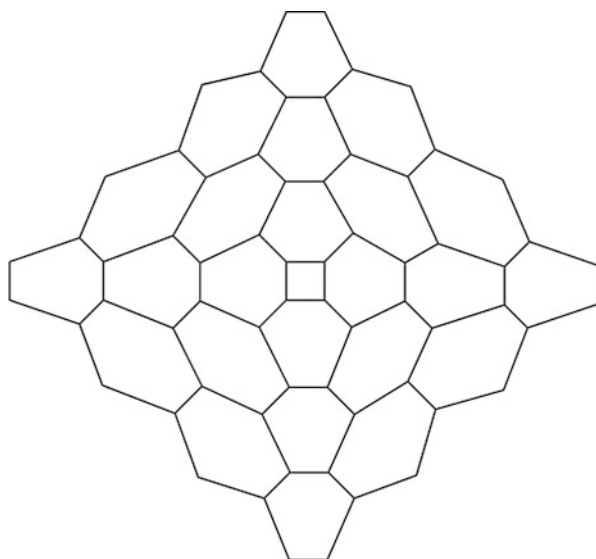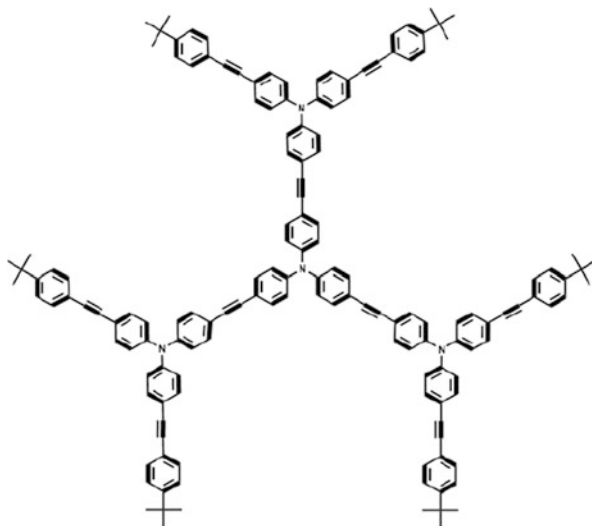
Nanostar dendrimer is a kind of nanostructure. One type of nanostar dendrimer is N-branched phenylacetylenes, and it is shown that by *NSB*[*n*], some topological indices were obtained in Yarahmadi (2010) (Yarahmadi and Fath-Tabar 2011). In Fig. 6.3, the molecular graph of *NSB*[1] and in Fig. 6.4 the molecular graph of *NSB* [2] are shown.

In this chapter, at first we compute the Wiener and Szeged and Cluj-Ilmenau indices of a family of cones, denoted $CNC_4[n]$. Moreover, we present explicit formula for Wiener, Szeged, *PI*, vertex *PI*, the first and second Zagreb eccentric connectivity, and augmented eccentric connectivity indices of N-branched phenylacetylenes nanostar dendrimer. For terms and concepts not defined here, we refer the reader to any of several standard monographs, such as Cameron (1994) and Trinajstić (1992).

6.2 The Wiener, Szeged, and Cluj-Ilmenau Indices of $CNC_4[n]$ Nanocones

In this section, we study on some graph invariant of $CNC_4[n]$. In order to compute some topological indices of $CNC_4[n]$, firstly the number of vertices of this nanostructure is computed.

Lemma 6.2.1 The number of vertices of $CNC_4[n]$ is computed by the formula:

$$\left|V\left(CNC_4[n]\right)\right| = 4(n+1)^2.$$
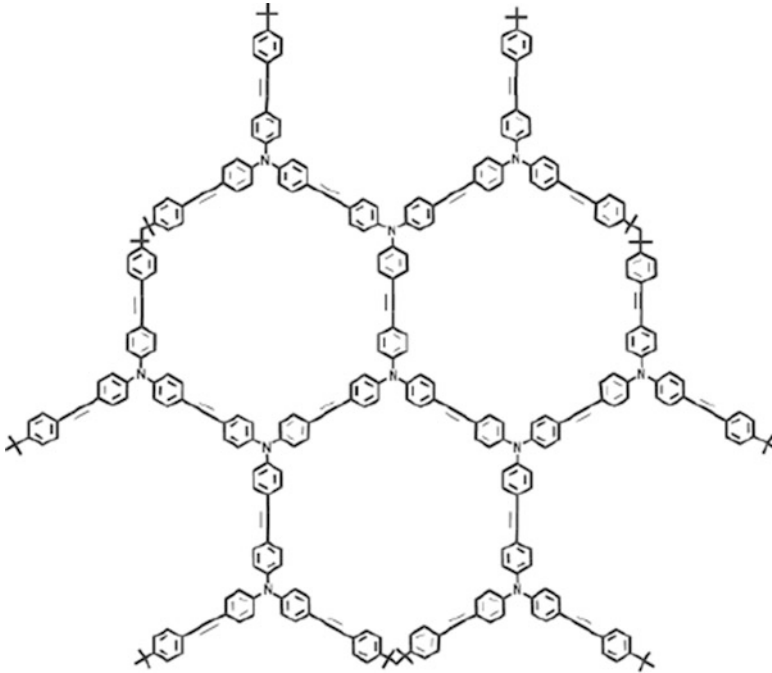
Fig. 6.4 The molecular graph of *NSB*[2]

For computing the Wiener index of $CNC_4[n]$, the method of Klavžar (2008) is used. In what follows, we recall some useful concepts.

Let G be a connected graph. Then edges $e = xy$ and $f = uv$ of G are in the Djoković-Winkler relation Θ (Djoković 1973; Winkler 1984), if

$$d(x, u) + d(y, v) \neq d(x, v) + d(y, u).$$

The relation Θ is always reflexive and symmetric. Let Θ^* be the transitive closure of Θ. Then Θ^* is an equivalence relation on $E(G)$ for any connected graph, and it partitions the edge set of G into Θ^*-classes. For computing Θ^*-classes, it is useful to know the following facts. Since two adjacent edges of G are in relation Θ if and only if they belong to a common triangle, all the edges of a given complete subgraph of G will be in the same Θ^*-class. Also, since an edge e of an isometric cycle C of G is in relation Θ with its antipodal edge(s) on C, all the edges of an odd cycle will be in the same Θ^*-class.

In what follows a powerful method, given by Klavžar (see Klavžar 2006, 2008), enabling to compute the Wiener index of a graph is presented. The canonical metric representation α of a connected graph G is defined as:

- Let G be connected graph and $F_1, F_2, \ldots, F_k$ its Θ^*-classes.

- Define quotient graph G/F_i, $i = 1, \ldots, k$, as follows. Its vertices are the connected components of $G\text{-}F_i$, two vertices C and C' being adjacent if there exist vertices $x \in C$ and $y \in C'$ such that $xy \in F_i$.

- Define $\alpha : G \to \prod_{i=1}^{k} G/F_i$ with $\alpha\colon u \to (\alpha_1(u), .., \alpha_k(u))$,

where $\alpha i(u)$ is a connected component of $G\text{-}Fi$ that contains u. Let G be an arbitrary connected graph and

$$\alpha : G \to \prod_{i=1}^{k} G/F_i$$

the canonical metric representation of G. Let $(G/F_i, w_i)$ be natural weighted graphs; the weight of G/F_i is the number of vertices in the corresponding connected component of $G\text{-}F_i$.

Theorem   6.2.2 (Klavžar   2008)   For   any   connected   graph G,
$W(G) = \sum_{i=1}^{k} W(G/F_i, w_i)$.

Theorem 6.2.3 The Wiener index of $CNC_4[n]$ is computed as follows:

$$W(CNC_4[n]) = \frac{1}{2}|V|\sum_{k=1}^{n}\left(k\,\alpha_n + k(k-1)\right)\left(|V| - k\alpha_n - k(k-1)\right),$$

where $|V| = |V(CNC_4[n]|$ and $\alpha_n = 2n + 3$.

In the following theorems, Szeged and Cluj-Ilmenau indices for $CNC_4[n]$ are computed.

Theorem 6.2.4 The Szeged index of $CNC_4[n]$ is computed as follows:

$$\begin{aligned}
Sz(CNC_4[n]) = {} & (n+1)|V|^2 \\
& + \sum_{k=1}^{n}(n+k+1)(k\alpha_n - k(k-1))\left(|V|(k\alpha_n - k(k-1)),\right.
\end{aligned}$$

by notation of pervious theorem.

Theorem 6.2.5 The Cluj-Ilmenau index of $CNC_4[n]$ is computed by:

$$\begin{aligned}
CI\left(CNC_{p(\text{even})}[n]\right) = {} & (1/12)p(n+1) \\
& \times (27pn^3 - 28n^2 + 63pn^2 - 50n + 48pn + 12p - 24), \\
CI\left(CNC_{p(\text{odd})}[n]\right) = {} & CI\left(CNC_{p(\text{even})}[n]\right) + p(n+1)^2.
\end{aligned}$$

Theorem 6.2.6 One-alpha descriptor of $CNC_4[n]$ is computed as follows:

$$OA\big(CNC_4[n] = 4\alpha\big(n^2 + n + 1\big).$$

6.3 Topological Indices of N-Branched Phenylacetylene Nanostar Dendrimer

The nanostar dendrimer is a part of a new group of macromolecules that seem photon funnels just like artificial antennas, and also, it is a great resistant of photo bleaching. Experimental and theoretical insight is needed in order to understand the energy transfer mechanism. In recent years, some people investigated the mathematical properties of these nanostructures (Ashrafi and Mirzargar 2008; Dorosti et al. 2009; Iranamanesh and Gholami 2009; Mirzargar 2009; Yousefi-Azari et al. 2008). One type of nanostar dendrimers is N-branched phenylacetylenes (see Bharathi et al. 1995). It is shown by $NSB[\underline{n}]$ (see Fig. 6.1). In order to compute some topological indices of the nanostar dendrimer $NSB[n]$, we first compute the number of vertices and edges of this nanostructure.

Lemma 6.3.1 The numbers of vertices and edges of dendrimer $NSB[n]$ are given as:

$$|V(NSB[n])| = 87 \times 2^n - 38,$$
$$|E(NSB[n])| = 99 \times 2^n - 45.$$

Also for computing the Wiener index of $NSB[n]$, we use the method of Theorem 6.2.2 (see Klavžar 2008).

Theorem 6.3.2 The Wiener index of $NSB[n]$ is given as follows:

$$W(NSB[n]) = 27\sum_{k=0}^{n} 2^{n-k}\big(\alpha_k|V| - {\alpha_k}^2 - 14\big) + 9 \times 2^n(87 \times 2^n - 39),$$

where $\alpha_n = 29 \times 2^n - 19$, $|V| = |V(NSB[n])|$.

Theorem 6.3.3 With notation of Theorem 6.3.2, the Szeged index of $NSB[n]$ is given by:

$$S_Z(NSB[n]) = 5 \times 3^2\sum_{k=0}^{n} 2^{n-k}\big(\alpha_k|V| - \alpha_k^2 - 14\big) + 9 \times 2^n(87 \times 2^n - 39).$$

Theorem 6.3.4 The *PI* index of the dendrimer *NSB*[*n*] is obtained by:

$$PI(NSB[n]) = 9801 \times 2^{2n} - 9081 \times 2^n + 2106.$$

Theorem 6.3.5 The vertex *PI* index of the dendrimer *NSB*[*n*] is obtained as follows:

$$PI_V(NSB[n]) = 8613 \times 2^{2n} - 7677 \times 2^n + 1710.$$

Theorem 6.3.6 The first and second Zagreb indices of *NBS*[*n*] are computed as follows:

$$Z_{g1}(NSB[n]) = 492 \times 2^n - 222, \ Z_{g2}(NSB[n]) = 591 \times 2^n - 273.$$

In the following lemma, the eccentricity of each vertex of *NSB*[*n*] is obtained, by using the eccentricity of the central vertex.

Lemma 6.3.7 Let v_0 be the central vertex and u is a vertex of *NSB*[*n*], such that $d(u, v_0) = k$. Then

$$\varepsilon(v_0) = 9n + 10,$$
$$\varepsilon(u) = 9n + k + 10.$$

By Lemma 6.3.1 and 6.3.7, we can compute the eccentric connectivity index of N-branched phenylacetylenes.

Theorem 6.3.8 The eccentric connectivity index of *NSB*[*n*] is computed as follows:

$$\xi(NSB[n]) = \left(945n + \frac{3015}{2}\right)2^{n+1} - 810n - 1359 + 837\sum_{i=1}^{n} i2^i.$$

Finally, in the following theorem, we obtained the augmented eccentric connectivity index of *NSB*[*n*].

Theorem 6.3.9 The augmented eccentric connectivity index of *NSB*[*n*] is given by the following formula:

$$^A\xi(NSB[n]) = 3^2.2^2\sum_{i=0}^{n}\sum_{j=2}^{9}\frac{2^i}{9(n-i)+10+j}$$
$$+ 3^4\sum_{i=0}^{n-1}\frac{1}{9(n+i)+19} \qquad + \frac{3^2.2^n}{18n+19} + \frac{3^2.2^{n+1}+3^3}{9n+10}.$$

References

Alipour MA, Ashrafi AR (2009a) A numerical method for computing the Wiener index of one-heptagonal carbon nanocone. J Comput Theor Nanosci 6:1204–1207

Alipour MA, Ashrafi AR (2009b) Computer calculation of the Wiener index of one-pentagonal carbon nanocone. Dig J Nanomater Biostruct 4:1–6

Ashrafi AR, Mirzargar M (2008) PI, Szeged and edge Szeged indices of an infinite family of nanostar dendrimers. Indian J Chem 47A:538–541

Ashrafi AR, Rezaei F (2007) PI index of polyhex nanotori. MATCH Commun Math Comput Chem 57:243–250

Ashrafi AR, Ghorbani M, Jalali M (2008) The vertex PI and Szeged polynomials of an infinite family of fullerenes. J Theor Comput Chem 7:221–231

Ashrafi AR, Došlić T, Saheli M (2011) The eccentric connectivity index of $TUC_4C_8(R)$ nanotubes. MATCH Commun Math Comput Chem 65:221–230

Bharathi P, Patel U, Kawaguchi T, Pesak DJ, Moore JS (1995) Improvements in the synthesis of phenylacetylene monodendrons including a solid-phase convergent method. Macromolecules 28:5955–5963

Cameron PJ (1994) Combinatorics: topics, techniques, algorithms. Cambridge University Press, Cambridge

Devillers J, Balaban AT (1999) Topological indices and related descriptors in QSAR and QSPR. Gordon and Breach, Amsterdam

Diudea MV, Cigher S, John PE (2008) Omega and related counting polynomials. MATCH Commun Math Comput Chem 60:237–250

Djoković D (1973) Distance preserving subgraphs of hypercubes. J Combin Theory Ser B 14:263–267

Dorosti N, Iranmanesh I, Diudea MV (2009) Computing the Cluj index of dendrimer nanostars. MATCH Commun Math Comput Chem 62:389–395

Dureja H, Madan AK (2007) Superaugmented eccentric connectivity indices: new-generation highly discriminating topological descriptors for QSAR/QSPR modeling. Med Chem Res 16:331–341

Fischermann M, Homann A, Rautenbach D, Szekely LA, Volkmann L (2002) Wiener index versus maximum degree in trees. Discret Appl Math 122:127–137

Gupta S, Singh M, Madan AK (2002) Application of graph theory: relationship of eccentric connectivity index and Wiener's index with anti-inflammatory activity. J Math Anal Appl 266:259–268

Gutman I (1994) A formula for the Wiener number of trees and its extension to graphs containing cycles. Graph Theory Notes N Y 27:9–15

Gutman I, Das KC (2004) The first Zagreb index 30 years after. MATCH Commun Math Comput Chem 50:83–92

Gutman I, Trinajstic N (1972) Graph theory and molecular orbitals, total π- electron energy of alternant hydrocarbons. Chem Phys Lett 17:535–538

Ilić A, Gutman I (2011) Eccentric connectivity index of chemical trees. MATCH Commun Math Comput Chem 65:731–744

Iranamanesh I, Gholami NA (2009) Computing the Szeged index of Styrylbenzene dendrimer and Triarylamine dendrimer of generation 1–3. MATCH Commun Math Comput Chem 62:371–379

John PE, Vizitiu AE, Cigher S, Diudea MV (2007) CI index in tubular nanostructures. MATCH Commun Math Comput Chem 57:479–484

Karelson M (2000) Molecular descriptors in QSAR/QSPR. Wiley-Interscience, New York

Khadikar PV (2000) Fabrication of indium bumps for hybrid infrared focal plane array applications. Natl Acad Sci Lett 23:113–118

Khadikar PV, Karmarkar S (2001) A novel PI index and its applications to QSPR/QSAR studies. J Chem Inf Comput Sci 41:934–949

Khalifeh MH, Yousefi-Azari H, Ashrafi AR (2009) The first and second Zagreb indices of some graph operations. Discret Appl Math 157:804–811

Klavžar S (2006) On the canonical metric representation, average distance, and partial Hamming graphs. Eur J Comb 27:68–73

Klavžar S (2008) A bird's eye view of the cut method and a survey of its applications in chemical graph theory. MATCH Commun Math Compu Chem 60:255–274

Kumar V, Sardana S, Madan AK (2004) Predicting anti–HIV activity of 2,3–diary l–1,3–thiazolidin–4–ones:computational approaches using reformed eccentric connectivity index. J Mol Model 10:399–407

Mirzargar M (2009) PI, Szeged and edge Szeged polynomials of a dendrimer nanostar. MATCH Commun Math Comput Chem 62:363–370

Sardana S, Madan AK (2001) Application of graph theory: relationship of molecular connectivity index, Wiener's index and eccentric connectivity index with diuretic activity. MATCH Commun Math Comput Chem 43:85–98

Sharma V, Goswami R, Madan AK (1997) Eccentric connectivity index: a novel highly discriminating topological descriptor for structure property and structure activity studies. J Chem Inf Comput Sci 37:273–282

Todeschini R, Consonni V (2000) Handbook of molecular descriptors. Wiley-VCH, Weinheim

Trinajstić N (1992) Chemical graph theory. CRC Press, Boca Raton

Vukičević D, Bralo M, Klarić A, Markovina A, Spahija D, Tadić A, Žilić A (2010) One-two descriptor. J Math Chem 48:395–400

Wiener H (1947) Structural determination of paraffin boiling points. J Am Chem Soc 69:17–20

Winkler P (1984) Isometric embeddings in products of complete graphs. Discret Appl Math 7:221–225

Yarahmadi Z (2010) Eccentric connectivity and augmented eccentric connectivity indices of N-branched Phenylacetylenes nanostar dendrimers. Iranian J Math Chem 1(2):105–110

Yarahmadi Z, Fath-Tabar GH (2011) The Wiener, Szeged, PI, vertex PI, the first and second Zagreb indices of N-branched Phenylacetylenes dendrimers. MATCH Commun Math Comput Chem 65:201–208

Yousefi-Azari H, Ashrafi AR, Bahrami A, Yazdani J (2008) Computing topological indices of some types of benzenoid systems and nanostars. Asian J Chem 20:15–20

Chapter 7
Augmented Eccentric Connectivity Index of Grid Graphs

Tomislav Došlić and Mojgan Mogharrab

Abstract We present explicit formulas for augmented eccentric connectivity indices of several classes of grid graphs that arise via Cartesian product. We also explore their asymptotic behavior and compute the compression ratios for considered graphs.

7.1 Introduction

The augmented eccentric connectivity index is one of several modifications of the eccentric connectivity index, a topological invariant much used recently in the quantitative structure-activity relationship (QSAR) and quantitative structure-property relationship (QSPR) studies. Like the original invariant, it soon gained popularity in the QSAR/QSPR community. Its basic mathematical properties have been explored in a recent paper (Došlić and Saheli 2011), where the authors also presented a number of explicit formulas for some classes of graphs. Here we continue that line of research by exploring how this invariant behaves under Cartesian product.

7.2 Definitions and Preliminaries

All graphs in this paper are finite, simple, and connected. For terms and concepts not defined here, we refer the reader to any of several standard monographs such as Harary (1969) and West (1996).

T. Došlić (✉)
Faculty of Civil Engineering, University of Zagreb, Kačićeva 26, 10000 Zagreb, Croatia
e-mail: doslic@math.hr

M. Mogharrab
Department of Mathematics, Faculty of Science, Persian Gulf University, Bushehr 75169, Iran

Let G be a graph on n vertices. We denote the vertex and the edge set of G by $V(G)$ and $E(G)$, respectively. For two vertices u and v of $V(G)$, we define their distance $d(u, v)$ as the length of any shortest path connecting u and v in G. For a given vertex u of $V(G)$, its *eccentricity* $\varepsilon(u)$ is the largest distance between u and any other vertex v of G. Hence, $\varepsilon(u) = \max_{v \in V(G)} d(u,v)$. The maximum eccentricity over all vertices of G is called the *diameter* of G and denoted by $D(G)$; the minimum eccentricity among the vertices of G is called the *radius* of G and denoted by $R(G)$. The set of all vertices of minimum eccentricity is called the *center* of G.

The *eccentric connectivity index* $\xi(G)$ of a graph G is defined as

$$\xi(G) = \sum \delta_u\, \varepsilon(u),$$

where δ_u denotes the degree of vertex u, i. e., the number of its neighbors in G. The eccentric connectivity index was introduced by Madan et al. and used in a series of papers concerned with QSAR/QSPR studies (Gupta et al 2002; Sardana and Madan 2001; Sharma et al 1997).

The *augmented eccentric connectivity index* $^A\xi(G)$ of a graph G is defined as

$$^A\xi(G) = \sum_{u \in V(G)} \frac{M(u)}{\varepsilon(u)}\ ,$$

where $M(u)$ denotes the product of degrees of all neighbors of vertex u. It was introduced in another paper by the abovementioned group of authors (Dureja and Madan 2007). We can see that the vertex contributions are both nonlocal (the degrees are taken over the neighborhoods and then multiplied) and nonlinear in $\varepsilon(u)$. The combination of those two properties makes the augmented eccentric connectivity index rather unyielding to the standard approach to distance-based invariants, resulting in a number of difficulties arising when one tries to obtain explicit formulas or find the extremal graphs and values.

A graph G is *vertex − transitive* if its automorphism group is transitive. A vertex-transitive graph is necessarily regular, and its center contains all its vertices. Hence, we have a particularly simple expression for the augmented eccentric connectivity index of a vertex-transitive graph.

Proposition 7.1 Let G be a vertex-transitive graph on n vertices of degree δ. Then,

$$^A\xi(G) = \frac{n\delta^\delta}{R(G)}\ .$$

As a consequence, we obtain explicit formulas for the eccentric connectivity indices of several familiar classes of graphs.

Corollary 7.1

1.
$$^A\xi(K_n) = n(n-1)^{n-1}.$$

2.
$$^A\xi(C_n) = \frac{4n}{\lfloor \frac{n}{2} \rfloor} = \begin{cases} 8, & n \quad \text{even} \\ \dfrac{8n}{n-1}, & n \quad \text{odd} \end{cases}.$$

3.
$$^A\xi(\Pi_m) = \frac{54m}{\lfloor \frac{m}{2} \rfloor + 1} = \begin{cases} \dfrac{108m}{m+2}, & m \quad \text{even} \\ \dfrac{108m}{m+1}, & m \quad \text{odd} \end{cases}.$$

Here, K_n, C_n, and $\prod_m$ denote the complete graph on n vertices, the cycle on n vertices, and the m-sided prism, respectively.

The situation is a bit more complicated for paths. The explicit formula for $^A\xi(P_n)$ was obtained in Došlić and Saheli (2011).

Proposition 7.2 Let P_n be a path of length $n \geq 3$. Then, $^A\xi(P_n) = 8\left(H_n - H_{\lfloor \frac{n}{2} \rfloor}\right)$ $-R_n$, where

$$R_n = \begin{cases} \dfrac{4}{n(n-1)}, & n \quad \text{even} \\ \dfrac{8n-4}{n(n-1)}, & n \quad \text{odd} \end{cases}.$$

Here, H_n denotes the nth harmonic number, defined as the nth partial sum of the harmonic series, $H_n = \sum_{i=1}^{n} \frac{1}{i}$. Since the eccentricities of vertices of a path increase by one from $\lceil n/2 \rceil$ to n, and the products of degrees of their neighborhoods are fairly constant, the above formula can be easily verified by a direct computation.

It is intuitively clear that a typical distance-based graph invariant (such as the eccentric connectivity index or the Wiener index) of an open linear polymer should exceed the value of the same invariant for a closed polymer of the same size and type. That idea has been quantified by introducing the concept of compression ratio in Došlić et al. (2011), where it was shown that the eccentric connectivity index reduces by a factor of 2/3 when an open polymer is closed by joining its end units, for a large enough number of units. Let G_n^o be an open linear polymer built from n identical units joined in a certain way and G_n^c be a closed linear polymer obtained from G_n^o by identifying the free parts of its end units. For a graph invariant $i(G)$, its compression ratio is the limit of the quotient $i(G_n^c)/i(G_n^o)$ when $n \to \infty$. For example, it can be easily verified that the compression ratio for the Wiener numbers of paths and cycles is 3/4.

It was shown in Došlić and Saheli (2011) that the augmented eccentric connectivity index behaves in the opposite way, since its values for open polymers tend to be smaller than for their closed analogues, yielding "compression ratios" larger than one.

It is well known that the harmonic numbers asymptotically behave as $H_n \approx \ln n + \gamma$, where γ is the Euler-Mascheroni constant. Hence, $^A\xi(P_n)$ is asymptotically equal to 8 ln 2. As a corollary, we obtain the compression ratio of the augmented eccentric connectivity index for paths and cycles.

Corollary 7.2

$$\lim_{n\to\infty} \frac{^A\xi(C_n)}{^A\xi(P_n)} = \frac{1}{\ln 2}.$$

7.3   Main Results

In this section we compute the augmented eccentric connectivity index for Cartesian products of paths and cycles. We start with the case of two paths.

7.3.1   Grid Graphs

We consider only the case when both paths are of odd lengths, say $2m+1$ and $2n+1$. Then, each of them has an even number of vertices, and the total number of vertices in $P_{2m+1}\Box P_{2n+1}$ is divisible by four. Because of the symmetry obvious from Fig. 7.1, it suffices to compute the contributions of vertices for just one quarter of the graph, say from the northeast quadrant of the graph shown in the figure.

To each vertex from the northeast quadrant, we assign a pair of coordinates (i,j) in the way shown in Fig. 7.1.

The eccentricities of all vertices from the considered region are achieved at the leftmost vertex in the bottom row that gives us a simple formula:

$$\varepsilon(i,j) = m+n+i+j.$$

We start by partitioning all vertices in the northeast quadrant into four classes, according to the product of degrees of their neighbors. The most numerous class is formed by the vertices with all four neighbors of degree 4.

We denote this class by *I*. There are $(m-1)(n-1)$ vertices in class I; their coordinates vary from (1,1) to (n-1,m-1). Let us compute their contribution to $^A\xi(P_{2m+1}\Box P_{2n+1})$. We first add the reciprocal values of their eccentricities and then multiply the result by 256. Starting from $\varepsilon(i;j) = m+n+i+j$, we obtain
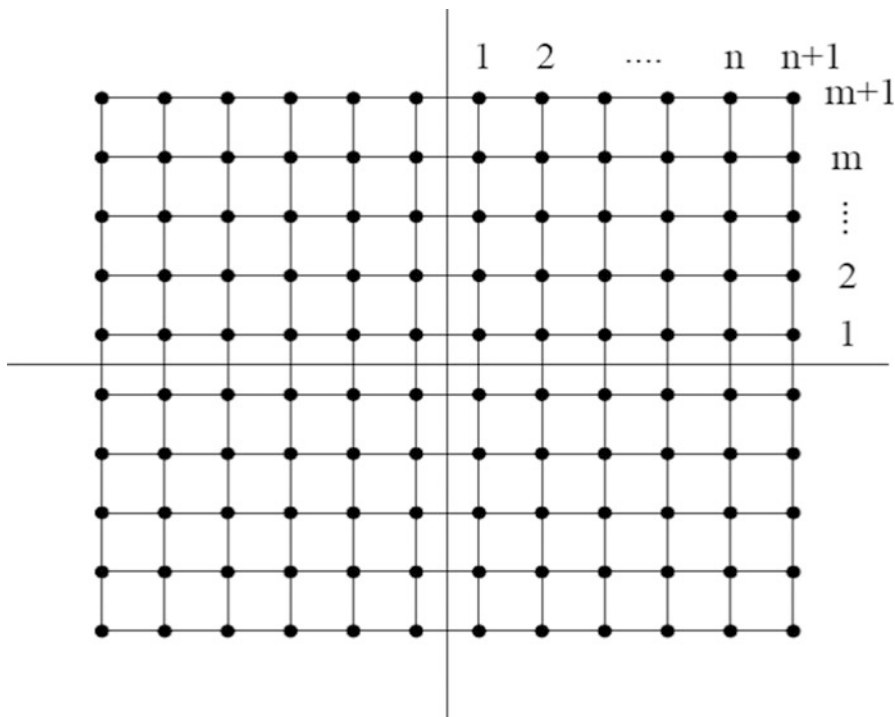
Fig. 7.1 Coordinates of vertices in grid graph $P_{2m+1} \square P_{2n+1}$

$$\sum_{i=1}^{m-1} \sum_{j=1}^{n-1} \frac{1}{m+n+i+j} = \sum_{i=1}^{m-1} [H_{2n+m+i-1} - H_{m+n+i}]$$

$$= (2m + 2n - 1)H_{2m+2n-1} + (m + n + 1)H_{m+n-1}$$

$$- (2m + n)H_{2m+n-1} - (m + 2n)H_{m+2n-1} + \frac{1}{m+n}.$$

Now the total contribution of all vertices from class I is obtained by multiplying the above expression by 256.

The class II consists of vertices with coordinates (k,m), where $k = 1,\ldots,n-1$, and (n, k), where $k = 1,\ldots,m-1$. The eccentricities of vertices in class II run from $2m+n+1$ to $2m+2n-1$ for vertices in row m and from $m+2n+1$ to $2m+2n-1$ for vertices in column n. The sum of their reciprocal values is given by

$$\sum_{i=1}^{m-1} \frac{1}{m+2n+i} + \sum_{j=1}^{n-1} \frac{1}{2m+n+j} = 2H_{2m+2n-1} - H_{m+2n} - H_{2m+n},$$

and the total contribution of class II is obtained by multiplying this by 192.

In a similar way, we obtain the contribution of vertices of class III. They lie in the uppermost row, where their first coordinate runs from 1 to $n-1$, and in the

rightmost column, with the second coordinate varying from 1 to $m-1$. Their collective contribution is equal to $36\ (2H_{2m+2n}-H_{m+2n+1}-H_{2m+n+1})$. Finally, the contribution of the four vertices in the upper right corner is given by $\left(\frac{9}{2m+2n+2}+\frac{48}{2m+2n+1}+\frac{72}{m+n}\right)$. The explicit formula for $^A\xi(P_{2m+1}\square P_{2n+1})$ is now easily obtained by adding the contributions of all four classes and multiplying the resulting expression by 4.

Theorem 7.1

$$
\begin{aligned}
^A\xi(P2m+1\square P2n+1) =\ &1024\big[(2m+2n-1)H_{2m+2n-1}+(m+n+1)H_{m+n-1}\\
&-(2m+n)H_{2m+n-1}-(m+2n)H_{m+2n-1}\big]\\
&+768[2H_{2m+2n-1}-H_{2m+n}-H_{m+2n}]\\
&+144[2H_{2m+2n}-H_{2m+n+1}-H_{m+2n+1}]\\
&+4\left(\frac{9}{2m+2n+2}+\frac{48}{2m+2n+1}+\frac{72}{m+n}\right).
\end{aligned}
$$

The above expression cannot be made much simpler in general case. However, if we keep one dimension fixed, we can derive the asymptotic behavior.

Corollary 7.3 Let m be fixed. Then,

$$
^A\xi(P_{2m+1}\square P_{2n+1}) \sim (1024m-112)\ln2
$$

for large values of n.

Another simplification is possible for $m=n$. By direct computations, one can verify that $^A\xi(P_{2m+1}\square P_{2m+1})$ diverges, but it scales linearly with m.

Corollary 7.4

$$
\lim_{m\to\infty}\ \left(A\xi(P_{2m+1}\square P_{2m+1})/m\right) = 2048\ln\frac{32}{27}\ \cdot m.
$$

For paths of even lengths, the formula of the above theorem is slightly different, but all other results remain essentially the same. Hence, we omit the details.

7.3.2   Cylinders

Now we use the results for grid graphs to derive explicit formulas for the augmented eccentric connectivity index of cylinders. We start from the grid graph $P_{2m+1}\square P_{2n+1}$ and connect by an edge the vertices in the first and $(2n+2)$-nd column of each row. In that way we obtain the cylinder $P_{2m+1}\square C_{2n+2}$. Now the eccentricities of all vertices are modified so that they do not depend on their position in the cycle, only on the cycle length. Hence, all vertices from the ith row have the same eccentricity, $m+n+i+1$. Again, we make use of the underlying symmetry and consider only the values of $i=1,\dots,m+1$. For all i between (and including) 1 and m-1, the contribution of ith row is given by

$$256 \cdot 2 (n+1) \sum_{i=1}^{m-1} \frac{1}{m+n+i+1} = 512 (n+1) [H_{2m+n} - H_{m+n+1}].$$

The contribution of the mth row is given by $\frac{384(n+1)}{2m+n+1}$ and of the uppermost row by $\frac{72(n+1)}{2m+n+2}$. As the lower half of the cylinder contributes the same amount, we have the following result.

Theorem 7.2
$$^A\xi(P_{2m+1}\square C_{2n+2}) = (n+1) \left[1024 (H_{2m+n} - H_{m+n+1}) + \frac{768 (n+1)}{2m+n+1} + \frac{144 (n+1)}{2m+n+2} \right].$$

For the fixed circumference $2n+2$ (hence for the fixed n) and for large values of m, the above quantity is linear in n:

$$^A\xi(P_{2m+1}\square C_{2n+2}) \sim 1024\ln 2 \cdot (n+1).$$

On the other hand, by fixing m we obtain

$$^A\xi(P_{2m+1}\square C_{2n+2}) \sim 1024m - 112.$$

By combining this with Corollary 7.3, we obtain the compression ratio for a ribbon of width m.

Corollary 7.5 Let m be fixed. Then the compression ratio for $P_{2m+1}\square P_{2n+1}$ is equal to $\frac{1}{\ln 2}$.

It is the same type of behavior observed for paths and other linear polymers in Došlić and Saheli (2011).

Again, the results are essentially the same for cylinders with lengths and circumferences of other parities.

7.3.3 Tori

Finally, by adding the edges between the uppermost and the lowermost vertex in each column of $P_{2m+1}\square C_{2n+2}$, we obtain the torus $C_{2m+2}\square C_{2n+2}$. It is a vertex-transitive graph on $4(m+1)(n+1)$ vertices, each of them of the eccentricity $m+n+2$ and degree 4. Its augmented eccentric connectivity index is now easily computed from Proposition 7.1.

Theorem 7.3

$$^A\xi(C_{2m+2}\square C_{2n+2}) = \frac{1024 (m+1) (n+1)}{m+n+2}.$$

For a fixed m, that quantity behaves as $1024(m + 1)$ for large values of n. Combining this with the behavior of $^A\xi(P_{2m+1} \square C_{2n+2})$ for fixed m and large n, we obtain the compression ratio for cylinders again as $1/_{\ln 2}$.

7.4 Concluding Remarks

In this paper, we have presented some explicit formulas for the augmented eccentric connectivity index of Cartesian products of paths and cycles, i.e., for the rectangular grid graphs, cylinders, and tori. Our results could be extended also to some other types of lattices that appear in chemistry. Some progress in that direction has already been made for the case of hexagonal grids, cylinders, and tori, but most of other cases remain unexplored.

References

Došlić T, Graovac A, Ori O (2011) Eccentric connectivity indices of hexagonal belts and chains. MATCH Commun Math Comput Chem 65:745–752

Došlić T, Saheli M (2011) Augmented eccentric connectivity index. Miskolc Math Notes 12:149–157

Dureja H, Madan AK (2007) Superaugmented eccentric connectivity indices: new − generation highly discriminating topological descriptors for QSAR/QSPR modeling. Med Chem Res 16:331–341

Harary F (1969) Graph theory. Addison − Wesley, Reading

Gupta S, Singh M, Madan AK (2002) Application of graph theory: relationship of eccentric connectivity index and Wiener's index with anti − inflammatory activity. J Math Anal Appl 266:259–268

Sardana S, Madan AK (2001) Application of graph theory: relationship of molecular connectivity index, Wiener's index and eccentric connectivity index with diuretic activity. MATCH Commun Math Comput Chem 43:85–98

Sharma V, Goswami R, Madan AK (1997) Eccentric connectivity index: a novel highly discriminating topological descriptor for structure − property and structure − activity studies. J Chem Inf Comput Sci 37:273–282

West DB (1996) Introduction to graph theory. Prentice Hall, Upper Saddle River

Chapter 8
Cluj Polynomial in Nanostructures

Mircea V. Diudea and Mahboubeh Saheli

Abstract Cluj polynomial, developed in 2009–2010 in Cluj, Romania, counts the vertex proximities in a connected graph. Definitions and relations with other polynomials and topological indices are given. Within this chapter, Cluj and related polynomials are computed in several 3D nanostructures and crystal networks and analytical formulas as well as examples are given.

8.1 Introduction

Cluj matrices and indices have been proposed by Diudea on the ground of fragments/subgraphs (Diudea 1997a, b, 1999; Diudea et al. 1997) $CJ_{i,j,p}$ that collects vertices v lying closer to i than to j, the endpoints of a path $p(i,j)$. Such fragments represent vertex proximities of i against any vertex j, joined by the path p, with the distances measured in the subgraph $D_{(G-p)}$, as shown in relation:

$$CJ_{i,j,p} = \left\{ v \middle| v \in V(G); \ D_{(G-p)}(i,v) < D_{(G-p)}(j,v) \right\} \qquad (8.1)$$

In graphs containing rings, more than one path could join the pair (i, j), thus resulting more than one fragment related to i (with respect to j and a given path p); the entries in the Cluj matrix are taken, by definition, as the maximum cardinality among all such fragments:

$$[\mathbf{UCJ}]_{i,j} = \max_p \left| CJ_{i,j,p} \right| \qquad (8.2)$$

M.V. Diudea (✉)
Department of Chemistry, Faculty of Chemistry and Chemical Engineering, Babes-Bolyai University, Arany Janos Street 11, Cluj-Napoca RO-400028, Romania
e-mail: diudea@chem.ubbcluj.ro

M. Saheli
Department of Pure Mathematics, University of Kashan, Kashan 87317-53153, Iran

In trees, the fragments $CJ_{i,j,p}$ are unique and represent the set of paths going to j through i. Thus, the path $p(i,j)$ is characterized by a single endpoint, which is sufficient to calculate the nonsymmetric matrix UCJ. The path p can belong to either the set of distances $DI(G)$ or to the set of detours $DE(G)$, thus providing different Cluj matrices and indices (eventually labeled with DI/DE as suffix).

Cluj polynomials are developed on the nonsymmetric matrices $UCJDI$ calculated on path $UCJDI_p$ or on edges $UCJDI_e$ (which can be obtained by the Hadamard multiplication: $UCJ_e = \mathbf{A} \cdot \mathbf{UCJ_p}$, A being the adjacency matrix, with entries 1 if two vertices are adjacent and zero otherwise).

The general form of Cluj polynomials is (Diudea 2009; Diudea et al. 2007, 2010a, b)

$$CJ(x) = \sum_k m(k) \cdot x^k \qquad (8.3)$$

They count the vertex proximity of the vertex i with respect to any vertex j in G, joined to i by an edge (the Cluj-edge polynomials $CJDI_e(x)$) or by a path (the Cluj-path polynomials $CJDI_p(x)$). In (8.3), the coefficients $m(k)$ can be calculated from the entries of $UCJDI$ matrices by the TOPOCLUJ software program (Ursu and Diudea 2005). The summation runs overall $k = |\{p\}|$ in G. The *matrix method* to calculate the Cluj polynomials is exemplified on the molecular graph of diphenylene DPH (Fig. 8.1).

$UCJDI_p$(DPH); *SCJDI*e

	1	2	3	4	5	6	7	8	9	10	11	12	RS
1	0	6	8	8	8	**9**	7	7	6	7	5	6	77
2	6	0	**9**	8	8	8	7	6	7	7	6	5	77
3	2	3	0	9	5	5	5	5	4	5	3	4	50
4	2	2	3	0	6	2	4	4	4	4	3	3	37
5	2	2	2	6	0	3	4	4	4	4	3	3	37
6	3	2	5	5	**9**	0	5	4	5	5	4	3	50
7	3	4	5	5	4	5	0	**9**	5	5	2	3	50
8	3	3	4	4	4	4	3	0	6	2	2	2	37
9	3	3	4	4	4	4	2	6	0	3	2	2	37
10	4	3	5	4	5	5	5	5	**9**	0	3	2	50
11	5	6	7	7	6	7	8	8	8	**9**	0	6	77
12	6	5	7	6	7	7	**9**	8	8	8	6	0	77
CS	39	39	59	66	66	59	59	66	66	59	39	39	656

$CJDI_p(x) = 16x^2 + 20x^3 + 24x^4 + 24x^5 + 16x^6 + 12x^7 + 12x^8 + 8x^9$; $D1|_{x=1} = 656$
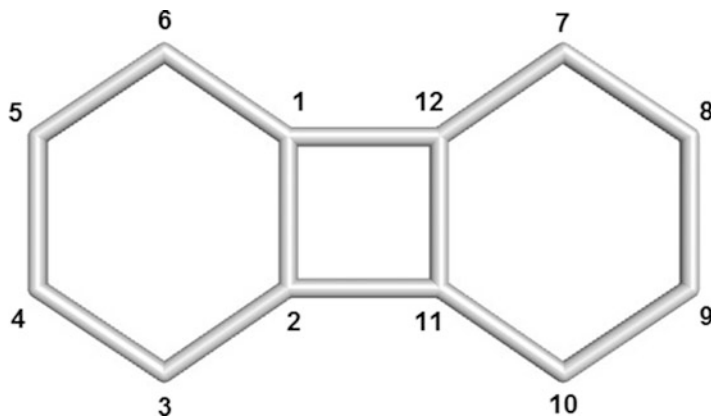
Fig. 8.1 Diphenylene DPH and its numbering

$UCJDI_e(DPH)$

	1	2	3	4	5	6	7	8	9	10	11	12	RS
1	0	6	0	0	0	**9**	0	0	0	0	0	6	21
2	6	0	**9**	0	0	0	0	0	0	0	6	0	21
3	0	**3**	0	9	0	0	0	0	0	0	0	0	12
4	0	0	**3**	0	6	0	0	0	0	0	0	0	9
5	0	0	0	6	0	**3**	0	0	0	0	0	0	9
6	**3**	0	0	0	9	0	0	0	0	0	0	0	12
7	0	0	0	0	0	0	0	9	0	0	0	3	12
8	0	0	0	0	0	0	**3**	0	6	0	0	0	9
9	0	0	0	0	0	0	0	6	0	**3**	0	0	9
10	0	0	0	0	0	0	0	0	9	0	**3**	0	12
11	0	6	0	0	0	0	0	0	0	**9**	0	6	21
12	6	0	0	0	0	0	**9**	0	0	0	6	0	21
CS	15	15	12	15	15	12	12	15	15	12	15	15	168

$$CJDI_e(x) = 8x^3 + 12x^6 + 8x^9; \; Pl\,|_{x=1} = 28 = 2e; \; Dl\,|_{x=1} = v \times e = 168$$

When the subscript e/p is omitted, it is by default e.

8.2 Cluj and Related Polynomials

In bipartite graphs, the coefficients of *CJ* polynomial can be calculated by an orthogonal edge-cut procedure (Diudea et al. 2010a, b; Gutman and Klavžar 1995; Diudea 2010b). For this, a theoretical background is needed.

A graph *G* is a *partial cube* if it is embeddable in the *n*-cube Q_n, which is the regular graph whose vertices are all binary strings of length *n*, two strings being

adjacent if they differ in exactly one position (Harary 1969). The distance function in the $n-$ cube is the Hamming distance. A hypercube can also be expressed as the Cartesian product: $Q_n = \square_{i=1}^n K_2$.

For any edge $e = (u,v)$ of a connected graph G, let n_{uv} denote the set of vertices lying closer to u than to v: $n_{uv} = \{w \in V(G)|d(w,u) < d(w,v)\}$. It follows that $n_{uv} = \{w \in V(G)|d(w,v) = d(w,u) + 1\}$. The sets (and subgraphs) induced by these vertices, n_{uv} and n_{vu}, are called *semicubes* of G; the semicubes are called *opposite semicubes* and are disjoint (Diudea et al. 2008; Diudea and Klavžar 2010). A graph G is bipartite if and only if, for any edge of G, the opposite semicubes define a partition of G: $n_{uv} + n_{vu} = v = |V(G)|$. These semicubes are just the vertex proximities (see above) of (the endpoints of) edge $e = (u,v)$, which CJ_e polynomial counts. In partial cubes, the semicubes can be estimated by an orthogonal edge-cutting procedure. The orthogonal cuts form a partition of the edges in G: $E(G) = c_1 \cup c_2 \cup \ldots \cup c_k, \quad c_i \cap c_j = \varnothing, \quad i \neq j$.

To perform an orthogonal edge-cut, take a straight line segment, orthogonal to the edge e, and intersect e and all its parallel edges (in a plane graph). The set of these intersections is called an *orthogonal cut* $c_k(e)$, $k = 1,2,..,k_{max}$. An example is given in Fig. 8.2.

To any orthogonal cut c_k, two numbers are associated: the first one represents the *number of edges* e_k intersected (or the cutting cardinality $|c_k|$), while the second (in round brackets, in Fig. 8.2) is v_k or the number of points lying to the left hand with respect to c_k. Because in bipartite graphs the opposite semicubes define a partition of vertices, it is easy to identify the two semicubes: $n_{uv} = v_k$ and $n_{vu} = v\text{-}v_k$ or vice versa. By this cutting procedure, four polynomials can be counted, differing only in the mathematical operation used to recompose the local contributions to the global graph property (Diudea 2010b; Klavžar 2008):
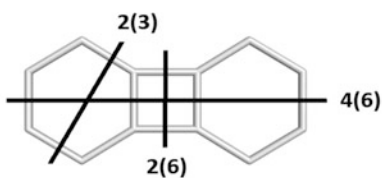
$$CJS(x) = 4(x^6+x^{(12-6)})+2(x^6+x^{(12-6)})+4\times2(x^3+x^{(12-3)})= 8x^9+12x^6+8x^3; \quad CJS`(1)=168=$$
$$v\times e=Sum(\mathbf{UCJDI_e})_{i,j}$$

$$CJP(x) = 4(x^{6(12-6)})+2(x^{6(12-6)})+4\times2(x^{3(12-3)})= 6x^{36}+8x^{27} \quad CJP`(1)=432=864/2=(1/2)Sum(\mathbf{SCJDI_e})_{i,j}$$

$$\Omega(x) = x^4+5x^2; \quad \Omega`(1)=14; \quad CI=160$$

Fig. 8.2 Calculating Cluj and related descriptors by the cutting procedure
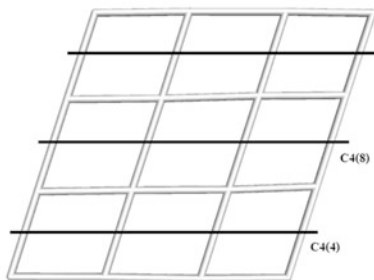
$$CJS(x) = 2 \cdot 2 \cdot 4(x^4 + x^{12}) + 2 \cdot 1 \cdot 4(x^8 + x^8)$$
$$= 16x^4 + 16x^8 + 16x^{12}$$
$$CJS'(1) = 384$$

$$PI_v(x) = 2 \cdot 2 \cdot 4(x^{4+12}) + 2 \cdot 1 \cdot 4(x^{8+8})$$
$$= 16x^{16} + 8x^{16} = 24x^{16}$$
$$PI_v'(1) = 384$$

$$CJP(x) = 2 \cdot 2 \cdot 4(x^{4 \cdot 12}) + \cdot 1 \cdot 4(x^{8 \cdot 8})$$
$$= 16x^{48} + 8x^{64} = SZ_v(x)$$
$$CJP'(1) = 1280 = SZ_v'(1)$$

$$W(x) = 2 \cdot 2(x^{4 \times 12}) + 2 \cdot 1(x^{8 \times 8})$$
$$= 4x^{48} + 2x^{64}$$
$$W'(1) = 320 = W(G)$$

1. *Summation*—the polynomial is called *Cluj-Sum* and is symbolized *CJS* by Diudea et al. (Diudea 2009; Diudea et al. 2007; 2010a, b; Vizitiu and Diudea 2009)

$$CJS(x) = \sum_e (x^{v_k} + x^{v - v_k}) \tag{8.4}$$

2. *Pairwise summation*—the polynomial is called PI_v (vertex Padmakar−Ivan (Khadikar 2000)) − Ashrafi et al. (Khalifeh et al. 2008a, b; Ashrafi et al. 2008; Mansour and Schork 2009):

$$PI_v(x) = \sum_e x^{v_k + (v - v_k)} \tag{8.5}$$

3. *Pairwise product*—the polynomial is called *Cluj-Product* (and symbolized *CJP*) (Diudea 1997a, b, 1999, 2010a, b; Diudea et al. 1997, 2010a, b) or also *Szeged* (and symbolized *SZ*) (Khalifeh et al. 2008b; Ashrafi et al. 2008; Mansour and Schork 2009):

$$CJP(x) = SZ(x) = \sum_e x^{v_k(v - v_k)} \tag{8.6}$$

4. *Single edge pairwise product*—the polynomial is called *Wiener* and symbolized *W* (Diudea 2010b):

$$W(x) = \sum_k x^{v_k \cdot (v - v_k)} \tag{8.7}$$

The first derivative (in $x = 1$) of a counting polynomial provides single numbers, often called topological indices. The coefficients of polynomial terms are calculated (except $W(x) -$; see the right-hand column of Fig. 8.2) as the product of three numbers: $\text{sym}(G) \times \text{freq}(c_k) \times e_k$.

Comments One can see that the first derivative (in $x = 1$) of the first two polynomials gives one and the same value; however, their second derivative is different and the following relations hold in any graph (Diudea et al. 2010a, b; Diudea 2010b):

$$CJS'(1) = PI_v'(1); \quad CJS''(1) \neq PI_v''(1) \tag{8.8}$$

In bipartite graphs, the first derivative (in $x = 1$) of $PI_v(x)$ takes the maximal value:

$$PI_v'(1) = e \cdot v = |E(G)| \cdot |V(G)| \tag{8.9}$$

Keeping in mind the definition of the corresponding index, one can see that (Ilić 2010)

$$PI_v(G) = PI_v'(1) = \sum_{e=uv} n_{u,v} + n_{v,u} = |V| \cdot |E| - \sum_{e=uv} m_{u,v} \tag{8.10}$$

where $n_{u,v}$, $n_{v,u}$ count the non-equidistant vertices with respect to the endpoints of the edge $e = (u,v)$, while $m(u,v)$ is the number of equidistant vertices vs. u and v. However, it is known that, in bipartite graphs, there are no equidistant vertices, so that the last term in (8.10) is missing. The value of $PI_v(G)$ is thus maximal in bipartite graphs, among all graphs on the same number of vertices; the result of (8.9) can be used as a criterion for the "bipartivity" of a graph (Diudea et al. 2007).

The third polynomial, $CJP(x)$, uses the pairwise product; it is precisely the (vertex) Szeged polynomial $SZ_v(x)$, defined by Ashrafi et al. (Khalifeh et al. 2008b; Ashrafi et al. 2008; Mansour and Schork 2009). This comes out from the relations between the Cluj (Diudea (Diudea 1997b, 1999; Diudea et al. 2002)) and Szeged (Gutman (Diudea et al. 2002; Gutman 1994)) descriptors:

$$CJP'(1) = (1/2)Sum(SCJDI_e) = SZ(G) = SZ_v'(1) \tag{8.11}$$

All the three above polynomials (and their derived indices) do not count the equidistant vertices, an idea introduced in chemical graph theory by Gutman (Gutman 1994). We call these *polynomials of vertex proximity*.

The last polynomial, $W(x)$, we call Wiener, because it is calculated as Wiener performed the index $W(G)$ in tree graphs: multiply the number of vertices lying to the left and to the right of each edge (actually read orthogonal cut c_k):

$$W(G) = W'(1) = \sum_k v_k \cdot (v - v_k) \tag{8.12}$$

where v_k and $v-v_k$ are the disjoint semicubes forming a partition with respect to each edge in c_k taken as a "single edge" (as in trees). In partial cubes, the exponents of $W(x)$ are identical to those in $CJP(x)$ and $SZ(x)$, while the coefficients are those in the above polynomials, divided by e_k. When subscript letter is missing, $SZ(x)$ is $SZ_v(x)$.

8.3   More Examples

In the following, more details are given about the edge-cut procedures in defining and counting $CJS(x)$ and $PI_v(x)$.

8.3.1   Bipartite Graph

Table 8.1 shows that in diphenylene DPH graph, the edge contributions to the global propriety are summed separately for $CJS(x)$, as given by (8.4), while for $PI_v(x)$ they are pairwise summed, as shown in (8.5). The global polynomial $CJS(x)$ is the sum of two partial polynomials: $CJ(x; i < j)$ and $CJ(x; i > j)$, which can be identical or not (see below), depending on the graph symmetry (Diudea 2009, Diudea 2010b; Diudea et al. 2007, 2010a, b). The v_k-values are given at the two ends of cutting segments.

The case of path-defined polynomial $CJ_pS(x)$ is much more complicated, and it can be calculated by the matrix procedure. Since DPH is a bipartite graph, the formula for $PI_v(x)$ is very simple, the sum of semicubes giving (cf. (8.5)), for any edge, the number of vertices in the graph ($e = |E(G)|$ and $v = |V(G)|$):

$$PI_v(x) = e \cdot x^v \tag{8.13}$$

A particular case of bipartite graphs is that of tree graphs (Diudea et al. 2007, 2010a; Diudea 2010a). In trees, we have the following (Diudea 2009; Diudea et al. 2007):

Theorem 8.3.1 *The sum of all path-counted vertex proximities in G is twice the sum of all distances in G or twice the Wiener index W: $p_p = CJ_pS'(1) = 2W$.*

Proof The column sums in the **UCJDI**$_p$ matrix equal the column sums in the matrix of distances, while the row sums in this matrix are identical to those in the Wiener matrix (Diudea et al. 2002, 2006; Diudea and Ursu 2003). Half of the sum of entries in these matrices equals the sum of all distances in a tree graph or the Wiener index (Wiener 1947). Since the first derivative of $CJ_pS(x)$ is just the sum of all entries in **UCJDI**$_p$ matrix, the theorem is thus demonstrated.

Table 8.2 illustrates the cutting procedure in trees. As it can be seen, the terms of CJ polynomial represent (connected) fragments of k vertices: figures illustrate the

Table 8.1 Edge-cutting procedure in calculating CJ and PI_v polynomials in diphenylene DPH bipartite graph
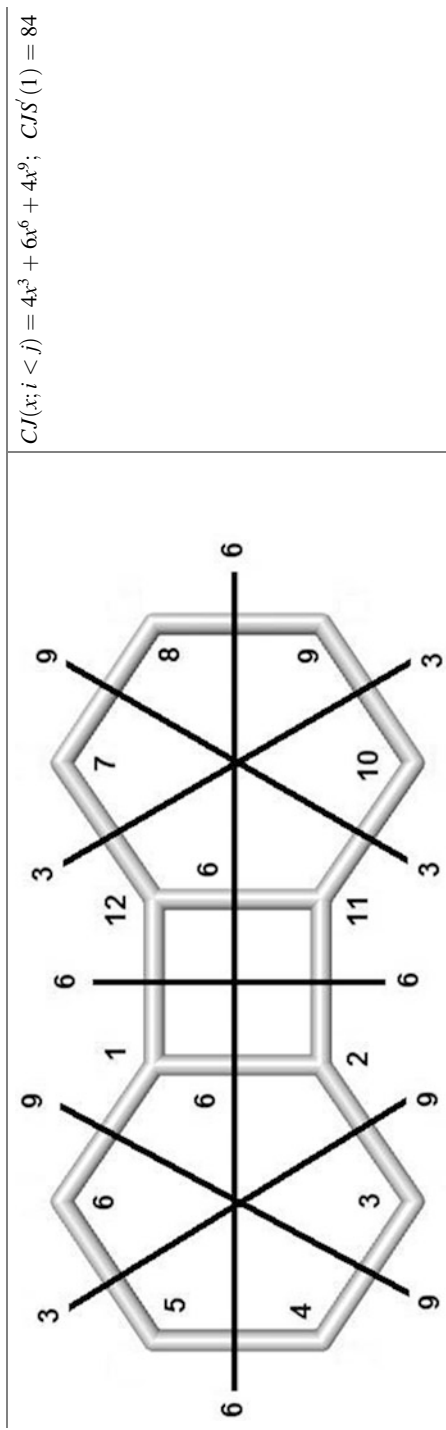
$CJ(x; i < j) = 4x^3 + 6x^6 + 4x^9$; $CJS'(1) = 84$
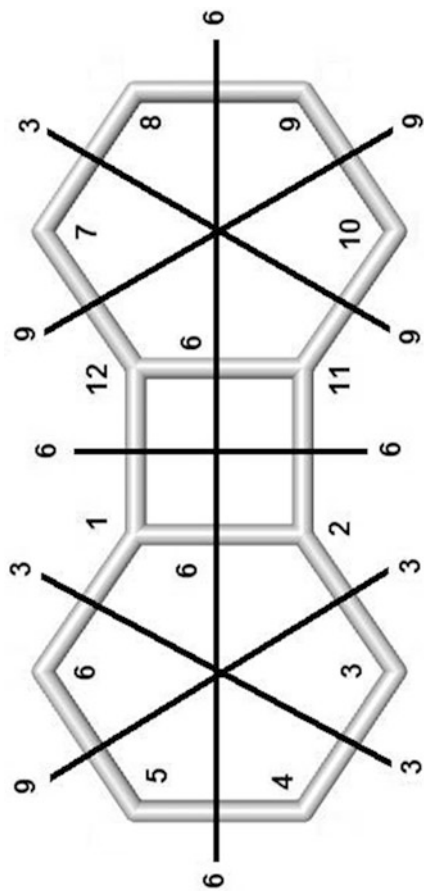
$CJ(x; i > j) = 4x^3 + 6x^6 + 4x^9$; $CJS'(1) = 84$

Global polynomial: $CJS(x) = CJ(x; i < j) + CJ(x; i > j)$

$CJS(x) = 8x^3 + 12x^6 + 8x^9$; $CJS(1) = 28 = 2e$; $CJS'(1) = 168 = v \times e$

$CJ_pS(x) = 16x^2 + 20x^3 + 24x^4 + 24x^5 + 16x^6 + 12x^7 + 12x^8 + 8x^9$; $CJ_pS'(1) = 656$

$PI_v(x) = 14x^{12}$; $PI_v(1) = 14 = e$; $PI_v'(1) = 168 = v \times e$

Table 8.2 Cluj polynomial $CJS(x)$ in trees (bipartite graphs)
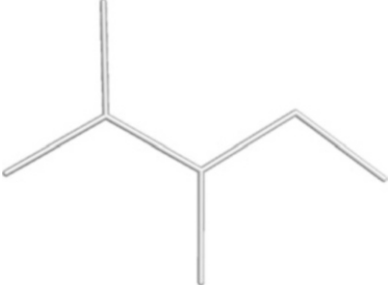
	$CJS(x) = 4(x^1 + x^6) + (x^2 + x^5) + (x^3 + x^4)$
	$CJS(1) = 2e = 2|E(G)| = 12; \ v = |V(G)| = 7$
	$CJS'(1) = 42 = ev$
	$CJS''(1) = 160$
	$4(x^1 + x^6)$
	$(x^3 + x^4)$
	$(x^2 + x^5)$
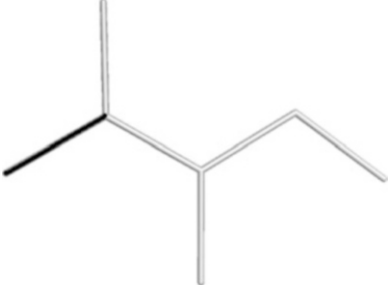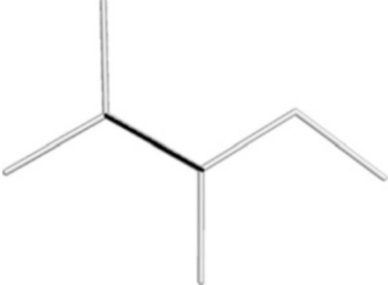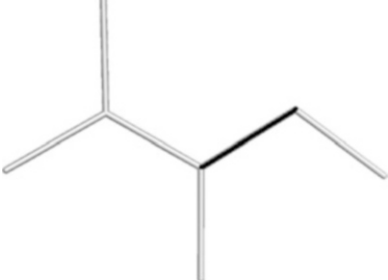
twin fragments, at the ends of each edge type (left-hand column) and the corresponding associate terms in polynomial (right-hand column).

Formulas to calculate Cluj polynomial in several classes of planar bipartite graphs are given in Tables 8.3 and 8.4 (Diudea 2009; Diudea et al. 2007).

Table 8.3 Acenes

Acenes A_h; $h =$ no. of hexagons in molecule

$$CJS(A_{h-even}, x) = 8 \cdot \sum_{k=1}^{h/2} x^{(4k-1)} + 2(h+1) \cdot x^{(2h+1)} + 8 \cdot \sum_{k=(h+2)/2}^{h} x^{(4k-1)};$$

$$CJS'(A_{h-even}, 1) = 2(2h+1)(5h+1) = |V(G)| \cdot |E(G)| = v \cdot e$$

$$CJS(A_{h-odd}, x) = 8 \cdot \sum_{k=1}^{(h-1)/2} x^{(4k-1)} + (2(h-3)+16) \cdot x^{(2h+1)} + 8 \cdot \sum_{k=(h+3)/2}^{h} x^{(4k-1)};$$

$$CJS'(A_{h-odd}, 1) = |V(G)| \cdot |E(G)| = v \cdot e$$

$$CJDE(A_{h-even}, x) = (8h+4) \cdot x + 4 \cdot \sum_{k=2}^{h/2} x^{(2k-1)} + 2 \cdot x^{(h+1)};$$

$$CJDE'(A_{h-even}, 1) = h^2 + 10h + 2$$

$$CJDE(A_{h-odd}, x) = (8h+4) \cdot x + 4 \cdot \sum_{k=2}^{(h+1)/2} x^{(2k-1)};$$

$$CJDE'(A_{h-odd}, 1) = h^2 + 10h + 1$$

Table 8.4 Phenacenes

Phenacenes Ph_h; $h =$ no. of hexagons in molecule

$$CJS\big(Ph_{h-even/odd}, x\big) = 8 \cdot x^3 + 4 \cdot \sum_{k=2}^{h-1} x^{(4k-1)} + 6 \cdot \sum_{k=1}^{h-1} x^{(4k+1)} + 8 \cdot x^{4h-1};$$

$$CJS'\big(Ph_{h-even/odd}, 1\big) = |V(G)| \cdot |E(G)| = v \cdot e$$

$$CJDE(Ph_{h-even}, x) = (8h+4) \cdot x + h \cdot x^3 + 2 \cdot \sum_{k=2}^{h/2} x^{(4k-1)};$$

$$CJDE'(Ph_{h-even}, 1) = h^2 + 12h - 2$$

$$CJDE(Ph_{h-odd}, x) = (8h+4) \cdot x + (h+1) \cdot x^3 + 2 \cdot \sum_{k=2}^{(h-1)/2} x^{(4k-1)};$$

$$CJDE'(Ph_{h-odd}, 1) = h^2 + 10h + 1$$

8.4   Cluj Polynomials in Nanostructures

In the following, we apply the cutting procedure or the numerical analysis to several classes of nanostructures. Numerical examples are given.
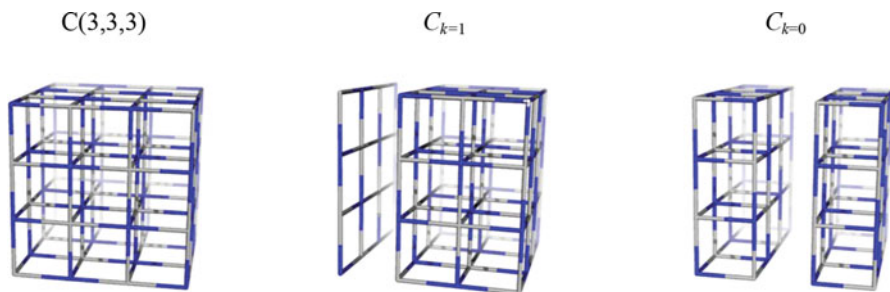
Fig. 8.3 Cutting procedure in *pcu* cubic net

8.4.1 Cluj Polynomials in pcu Cubic Net

We apply the orthogonal cutting procedure in the pcu cubic network, appearing in crystal structures (Fig. 8.3); among various orthogonal cuts, ocs, the central one is denoted by k = 0. The formulas for the net parameters and topological descriptors are given in Table 8.5.

8.4.2 Cluj Polynomials in Nanocones

Conical nanostructures have been reported in Nanoscience since 1968 (Krishnan et al. 1997; Ebbesen 1998) before the discovery of fullerenes. If a graphite sheet is divided into six sectors, each with an angle of 60°, and if m of these sectors (with $m = 1$ to 3) are deleted sequentially, the dangling bonds being fused together, three classes of graphs, associated to single-walled nanocones, are obtained; their apex polygon will be a pentagon ($a = 5$), a square ($a = 4$), or a triangle ($a = 3$), respectively. One can extend the construction principle and accept in the family of "topological cone" structures having the apex polygon $a \geq 6$; of course, that "cone" with $a = 6$ is just the plane graphite sheet, while those having larger polygons will show a saddle shape. In the recent years, several researchers have considered the mathematical properties of such nanostructures (Vizitiu and Diudea 2006, 2008; Alipour and Ashrafi 2009). Figure 8.4 gives two examples of such "topological cones," with application of the cutting procedures in view of deriving some important topological descriptors.

In the case of bipartite cones, namely, those with $a > 4$, the orthogonal edge-cutting procedure is applied normally (Fig. 8.4, the central structure). Formulas, referring to net parameters and descriptors, are given in the Table 8.6.

In the case of cones with $a = 4$, values $v_k > v/2$ appear, which indicate non-convex, non-isometric subgraphs, and thus the whole graphs are not partial cubes (Diudea 2010a, b). In consequence, the edge-cutting procedure was modified as presented in Fig. 8.4 (left-hand structure) and Table 8.7; numerical examples are given in Table 8.8.

Table 8.5 Net parameters and topological descriptors in *pcu* cubic lattice

Type	Formulas
$v(C(a))$	$v(C(a)) = \|V(C(a))\| = (a+1)^3$
$e(C(a))$	$e(C(a)) = \|E(G)\| = 3a(a+1)^2$
v_k	$v_k(C(a)) = k(a+1)^2$
v_0	$v_0(C(a)) = (a+1)^3/2$
$e_k = s_k$	$e_k(C(a)) = (a+1)^2$
Cluj polynomial	$CJS(C(a,odd),x) = 6e_k \cdot \left[x^{v/2} + \sum\limits_{k=1}^{(a-1)/2} (x^{v_k} + x^{v-v_k}) \right]$
	$CJS(C(a,odd),x) = 6(a+1)^2 \cdot \left[x^{(a+1)^3/2} + \sum\limits_{k=1}^{(a-1)/2} \left(x^{k(a+1)^2} + x^{\left[(a+1)^3 - k(a+1)^2 \right]} \right) \right]$
	$CJS(C(a,even),x) = 6e_k \sum\limits_{k=1}^{a/2} \left(x^{v_k} + x^{v-v_k} \right)$
	$CJS(C(a,even),x) = 6(a+1)^2 \sum\limits_{k=1}^{a/2} \left(x^{k(a+1)^2} + x^{\left[(a+1)^3 - k(a+1)^2 \right]} \right)$
	$CJS(C(a),x) = 6e_k \cdot \sum\limits_{k=1}^{a} x^{v_k}$
	$CJS(C(a),x) = 6(a+1)^2 \cdot \sum\limits_{k=1}^{a} x^{k(a+1)^2}$
	$CJS'(C(a),1) = e \cdot v = 3a(a+1)^2 \cdot (a+1)^3 = 3a(a+1)^5$
	$CJS''(C(a),1) = a(a+1)^5(2a^3 + 5a^2 + 4a - 2)$
Examples:	$a = 4;\ CJS(x) = 150x^{100} + 150x^{75} + 150x^{50} + 150x^{25}$
	$CJS'(1) = 37{,}500;\ CJS''(1) = 2{,}775{,}000$
	$a = 5;\ CJS(x) = 216x^{180} + 216x^{144} + 216x^{108} + 216x^{72} + 216x^{36}$
	$CJS'(1) = 116{,}640;\ CJS''(1) = 15{,}279{,}840$
PI_v	$PI_v(C(a),x) = ex^v = 3a(a+1)^2 x^{(a+1)^3}$
	$PI_v'(C(a),1) = e \cdot v = 3a(a+1)^2(a+1)^3 = CJS'(C(a),1)$
	$PI_v''(C(a),1) = e \cdot v \cdot (v-1) = 3a^2(a^2 + 3a + 3)(a+1)^5$
Examples:	$a = 4;\ PI_v(x) = 300x^{125}$
	$PI_v'(1) = 37{,}500;\ PI_v''(1) = 4{,}650{,}000$
	$a = 5;\ PI_v(x) = 540x^{216}$
	$PI_v'(1) = 116{,}640;\ PI_v''(1) = 25{,}077{,}600$
Szeged	$SZ(C(a),x) = e_k(C(a)) \cdot W(C(a),x) = (a+1)^2 \cdot W(C(a),x)$
$SZ = CJP$	
Cluj	$W(C(a,odd),x) = 3x^{\left((v/2)^2 \right)} + 6 \sum\limits_{k=1}^{(a-1)/2} x^{v_k \cdot (v-v_k)}$
	$W(C(a,even),x) = 6 \sum\limits_{k=1}^{a/2} x^{v_k \cdot (v-v_k)}$
	$W'(C(a),1) = (1/2)a(a+2)(a+1)^5$
Examples:	$SZ'(1) = (a+1)^2 \cdot W'(C(a),1) = (1/2)a(a+2)(a+1)^7$
	$a = 4;\ SZ(x) = 150x^{2500} + 150x^{3750};\ SZ'(1) = 937{,}500$
	$a = 5;\ SZ(x) = 216x^{6480} + 216x^{10368} + 108x^{11664};\ SZ'(1) = 4{,}898{,}880$
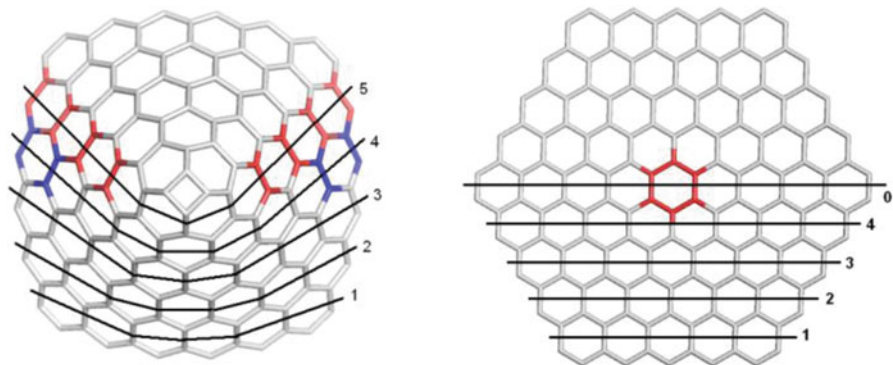
Fig. 8.4 Cutting procedure in nanocones of apex $a = 4;6$

Table 8.6 Net parameters and topological descriptors in bipartite (partial cubes) nanocones

Type	Formulas for cones C(a,n); $a =$ even; $a > 4$
$v(a,n)$	$v(a,n) = a(n+1)^2$
$e(a,n)$	$e(a,n) = (a/2)(3n^2 + 5n + 2)$
h_k	$h_k = n + k$
h_0	$h_0 = 2n + 1$
v_k	$v_k = \sum_{i=1}^{k} (2n + 2i + 1) = k(2n + k + 2)$
$e_k = s_k$	$e_k = n + k + 1$
e_0	$e_0 = 2(n + 1)$
$CJS(x)$	$CJS(x) = CJS_0(x) + CJS_k(x)$
	$CJS_0(x) = [(a/2)(h_0 + 1) + (a - 6)(n + 1)] \cdot \left(x^{v/2} + x^{v/2}\right)$
	$CJS_0(x) = (a/2)e_0 \cdot \left(x^{v/2} + x^{v/2}\right)$
	$CJS_k(x) = a \sum_{k=1}^{n} (h_k + 1) \cdot \left(x^{v_k} + x^{v - v_k}\right)$
	$CJS_k(x) = a \sum_{k=1}^{n} e_k \cdot \left(x^{v_k} + x^{v - v_k}\right)$
	$CJS(x) = (a/2)e_0 \cdot \left(x^{v/2} + x^{v/2}\right) + a \sum_{k=1}^{n} e_k \cdot \left(x^{v_k} + x^{v - v_k}\right)$
	$CJS'(1) = e \cdot v = (a/2)(3n^2 + 5n + 2) \times a(n+1)^2 = (a^2/2)(n+1)^3(3n+2)$
$PI_v(x)$	$PI_v(x) = e \cdot x^v = (a/2)(3n^2 + 5n + 2) \cdot x^{a(n+1)^2}$
	$PI_v'(1) = CJS'(1) = e \cdot v = (a^2/2)(n+1)^3(3n+2)$
$CJP(x) = SZ$ (x)	$CJP(x) = (a/2)e_0 \cdot \left(x^{(v/2)^2}\right) + a \sum_{k=1}^{n} e_k \cdot x^{v_k \left(v - v_k\right)}$
	$CJP'(1) = (a/4)(n+1)^2\big(-18n^4 + 9an^4 - 36n^3 + a^2n^3 + 24an^3 + 21an^2 - 19n^2 + 3a^2n^2 + 3a^2n - 2n + 6an + a^2\big)$
	$CJP(x) = s_k \cdot W(x)$

Table 8.7 Net parameters and topological descriptors in bipartite (non-partial cubes) nanocones

Type	Formulas for cones $C(4,n)$	
$v(4,n)$	$v(4,n) = 4(n+1)^2$	
$e(4,n)$	$e(4,n) = 2(3n^2 + 5n + 2)$	
$e_k = s_k$	$e_k = n + k + 1$	
v_k	$v_k = k(2n + k + 2)$	
	$n = $ odd:	$n = $ even:
Last normal cut	$k_0 = (n+1)/2$	$k_0 = n/2$
Corrected cut	$k_c = k_0 + 1 = (n+3)/2$	$k_c = k_0 + 1 = (n+2)/2$
Correction	$c_k = 2(k - k_c) + 2 = 2k - n - 1$	$c_k = 2(k - k_c) + 2 = 2k - n - 1$
$CJS(x)$	$$CJS(C(4,n),x) = 4(n+1)\left(x^{v/2} + x^{v/2}\right) + 4\sum_{k=1}^{k_c-1} e_k \cdot \left(x^{v_k} + x^{v-v_k}\right) + \\ 4\sum_{k=k_c}^{n}(e_k - 2c_k) \cdot \left(x^{v_k} + x^{v-v_k}\right) + 4\sum_{k=k_c}^{n} 2c_k \cdot \left(x^{v_k-(c_k)^2} + x^{v-v_k+(c_k)^2}\right)$$	
	$$CJS'(C(4,n),1) = e \cdot v = 2(3n^2 + 5n + 2) \cdot 4(n+1)^2 = 8(3n+2)(n+1)^3$$	
$CJP(x)$	$$CJP(C(4,n),x) = 4(n+1) \cdot x^{(v/2)^2} + 4\sum_{k=1}^{k_c-1} e_k \cdot x^{v_k(v-v_k)} + \\ 4\sum_{k=k_c}^{n}(e_k - 2c_k) \cdot x^{v_k(v-v_k)} + 4\sum_{k=k_c}^{n} 2c_k \cdot x^{\left(v_k-(c_k)^2\right)\left(v-v_k+(c_k)^2\right)}$$	
	$$CJP'(C(4,n_{even}),1) = 16 + (538/5)n + (4129/15)n^2 + 370n^3 + \\ (1669/6)n^4 + (557/5)n^5 + (557/30)n^6$$	
	$$CJP'(C(4,n_{odd}),1) = (31/2) + (523/5)n + (8213/30)n^2 + 370n^3 + \\ (1669/6)n^4 + (557/5)n^5 + (557/30)n^6$$	

Table 8.8 Examples of topological descriptors in nanocones

a	n	Polynomial	Index
4	3	$CJS(x) = 20x^{55} + 24x^{44} + 16x^{35} + 12x^{33} + 32x^{32} + 12x^{31} + 16x^{29} + 24x^{20} + 20x^9$	$CJS'(1) = 5632$
		$PI_v(x) = 88x^{64}$	$PI_v'(1) = 5632$
		$SZ(x) = 20x^{495} + 24x^{880} + 16x^{1015} + 12x^{1023} + 16x^{1024}$	$SZ'(1) = 75,920$
4	4	$CJS(x) = 24x^{89} + 28x^{76} + 8x^{62} + 24x^{61} + 12x^{56} + 24x^{53} + 40x^{50} + 24x^{47} + 12x^{44} + 24x^{39} + 8x^{38} + 28x^{24} + 24x^{11}$	$CJS'(1) = 14,000$
		$PI_v(x) = 140x^{100}$	$PI_v'(1) = 14,000$
		$SZ(x) = 24x^{979} + 28x^{1824} + 8x^{2356} + 24x^{2379} + 12x^{2464} + 24x^{2491} + 20x^{2500}$	$SZ'(1) = 289,864$
6	3	$CJS(x) = 30x^{87} + 36x^{76} + 42x^{63} + 48x^{48} + 42x^{33} + 36x^{20} + 30x^9$	$CJS'(1) = 12,672$
		$PI_v(x) = 132x^{96}$	$PI_v'(1) = 12,672$
		$SZ(x) = 30x^{783} + 36x^{1520} + 42x^{2079} + 24x^{2304}$	$SZ'(1) = 220,824$
6	4	$CJS(x) = 36x^{139} + 42x^{126} + 48x^{111} + 54x^{94} + 60x^{75} + 54x^{56} + 48x^{39} + 42x^{24} + 36x^{11}$	$CJS'(1) = 31,500$
		$PI_v(x) = 210x^{150}$	$PI_v'(1) = 31,500$
		$SZ(x) = 36x^{1529} + 42x^{3024} + 48x^{4329} + 54x^{5264} + 30x^{5625}$	$SZ'(1) = 842,850$

(continued)

Table 8.8 (continued)

a	n	Polynomial	Index
8	3	$CJS(x) = 40x^{119} + 48x^{108} + 56x^{95} + 64x^{64} + 56x^{33} + 48x^{20} + 40x^9$	$CJS'(1) = 22{,}528$
		$PI_v(x) = 176x^{128}$	$PI_v'(1) = 22{,}528$
		$SZ(x) = 40x^{1071} + 48x^{2160} + 56x^{3135} + 32x^{4096}$	$SZ'(1) = 453{,}152$
8	4	$CJS(x) = 48x^{189} + 56x^{176} + 64x^{161} + 72x^{144} + 80x^{100} + 72x^{56} +$ $64x^{39} + 56x^{24} + 48x^{11}$	$CJS'(1) = 56{,}000$
		$PI_v(x) = 280x^{200}$	$PI_v'(1) = 56{,}000$
		$SZ(x) = 48x^{2079} + 56x^{4224} + 64x^{6279} + 72x^{8064} + 40x^{10000}$	$SZ'(1) = 1{,}718{,}800$
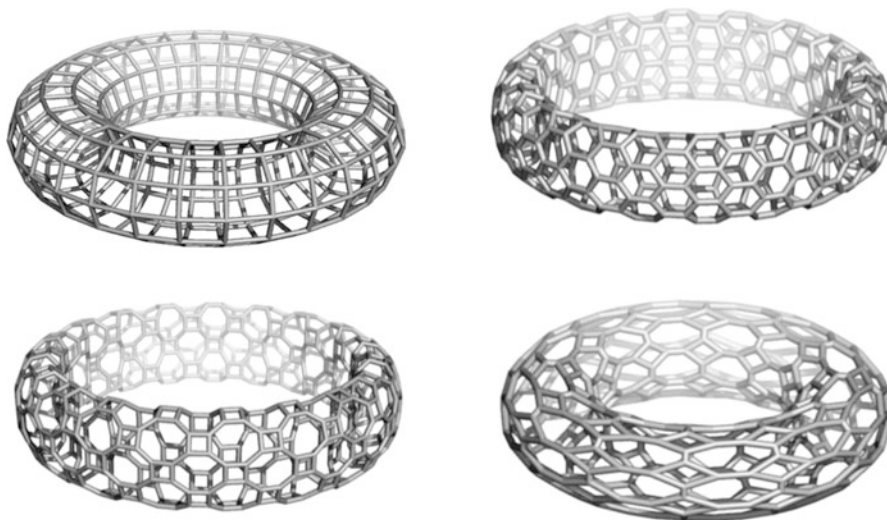
Fig. 8.5 Tori: (4,4); (6,3) (*top row*) and ((4,8)3)S; ((4,8)3)R (*bottom row*)

Numerical calculation was done by our original software programs TOPOCLUJ (Ursu and Diudea 2005).

8.4.3 Cluj Polynomials in Bipartite Tori

In bipartite (all even [*c*,*n*] net parameters) tori of (4,4), (6,3), and ((4,8)3) tessellations (Diudea 2005; Diudea and Nagy 2007) (Fig. 8.5), the Cluj and related polynomials (i.e., the polynomials of vertex proximity) and their derived indices show very simple formulas (Table 8.9), which can be obtained by the cutting procedure. These tori are neither partial cubes nor *co*-graphs. The case of non-bipartite (4,4) tori will be presented in the next section.

Table 8.9 Cluj and related polynomials in bipartite tori

$CJS(x) = e(x^{v/2} + x^{v/2})$					$CJP(x) = SZ(x) = e(x^{v/2 \cdot v/2})$		
$CJS'(1) = e(v/2 + v/2) = e \cdot v = 2(cn)^2$					$CJP'(1) = e(v/2 \cdot v/2) = e(v/2)^2$		
					$\quad = (1/2)v^3 = (1/2)(cn)^3$		
$PI_v(x) = e(x^{v/2+v/2}) = e \cdot x^v$					$v = cn;\ e = (d/2)v$		
$PI_v{}'(1) = e \cdot v = CJ_eS'(1)$							
c,n	v	e	$PI_v(x)$	$CJS(x)$		$CJS'(1)$	$SZ'(1)$
(4,4); d = 4							
10,10	100	200	$200x^{100}$	$400x^{50}$		20,000	500,000
12,14	168	336	$336x^{168}$	$672x^{84}$		56,448	2,370,816
10,20	200	400	$400x^{200}$	$800x^{100}$		80,000	4,000,000
10,50	500	1000	$1000x^{500}$	$2000x^{250}$		500,000	62,500,000
(6,3); d = 3							
H 8,8	64	96	$96x^{64}$	$192x^{32}$		6144	98,304
H 8,10	80	120	$120x^{80}$	$240x^{40}$		9600	192,000
V 8,26	208	312	$312x^{208}$	$624x^{104}$		64,896	3,374,592
V 8,32	256	384	$384x^{256}$	$768x^{128}$		98,304	6,291,456
((4,8)3)S; d = 3							
20,20 (m = 1)	400	600	$600x^{400}$	$1200x^{200}$		240,000	24,000,000
28,42 (m = 1)	1176	1764	$1764x^{1176}$	$3528x^{588}$		2,074,464	609,892,416
5, 10 (m = 8)	400	600	$600x^{400}$	$1200x^{200}$		240,000	24,000,000
7, 21 (m = 8)	1176	1764	$1764x^{1176}$	$3528x^{588}$		2,074,464	609,892,416
((4,8)3)R; d = 3							
10,10 (m = 4)	400	600	$600x^{400}$	$1200x^{200}$		240,000	24,000,000
10,20 (m = 4)	800	1200	$1200x^{800}$	$2400x^{400}$		960,000	192,000,000
14,21 (m = 4)[a]	1176	1764	$294x^{1176} + 1176x^{1162}$ $+ 294x^{1148}$	$1764x^{588}$ $+ 1764x^{574}$		2,049,768	595,428,792

[a] In the case c,n = odd, the graph is non-bipartite

8.4.4   Cluj Polynomials in Tori (4,4)

8.4.4.1   Square-Tiled Tori

The cutting procedure will be applied on square-tiled tori T(4,4)S[c,n]. It can be seen (Fig. 8.6) that there are only two cutting types: circular "cir"(around the large hollow) and across "acr" the tube. Accordingly, the proximities are easily calculable from the net parameters c (the number of atoms/points across the tube) and n (the number of cross sections around the torus large hollow). Formulas are given in Table 8.10, along with some examples.
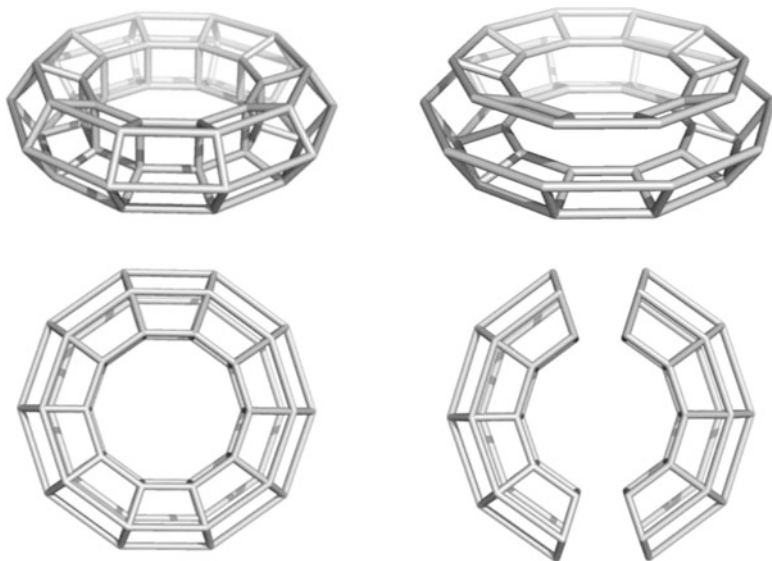
Fig. 8.6 Cutting procedure in *square-tiled* tori T(4,4)S[c,n]: circular (*top*) and across (*bottom*) cuttings

Table 8.10 Cluj and related polynomials in T(4,4)S[c,n] tori

	Formulas
1	$CJS(x) = cn \left[x^{c(n-p_n)/2} + x^{c(n-p_n)/2} \right]_{acr} + cn \left[x^{n(c-p_c)/2} + x^{n(c-p_c)/2} \right]_{cir}$
	$CJS(x) = cn \cdot 2x^{cn/2} + cn \cdot 2x^{cn/2}; \quad c, n - even$
	$CJS'(1) = cn(2cn - c - n); \quad c, n - odd$
	$CJS'(1) = 2c^2n^2; \quad c, n - even$
	$CJS'(1) = cn^2(2c - 1); \quad c - odd; n - even$
	$CJS'(1) = c^2n(2n - 1); \quad c - even; n - odd$
Examples	T(4,4)S[7,35]; $CJS(x) = 490x^{119} + 490x^{105}$; $CJS'(1) = 109{,}760$
	T(4,4)S[8,40]; $CJS(x) = 1280x^{160}$; $CJS'(1) = 204{,}800$
	T(4,4)S[7,20]; $CJS(x) = 280x^{70} + 280x^{60}$; $CJS'(1) = 36{,}400$
	T(4,4)S[8,35]; $CJS(x) = 560x^{140} + 560x^{136}$; $CJS'(1) = 154{,}560$
2	$CJP(x) = cn \cdot x^{[c(n-p_n)/2]^2} + cn \cdot x^{[n(c-p_c)/2]^2}$
	$CJP(x) = cn \cdot x^{(cn/2)^2} + cn \cdot x^{(cn/2)^2}; \quad c, n - even$
	$CJP'(1) = (cn/4)(2c^2n^2 - 2c^2n + c^2 - 2cn^2 + n^2); \quad c, n - odd$
	$CJP'(1) = cn(c^2n^2/4) + cn(c^2n^2/4); \quad c, n - even$
	$CJP'(1) = (cn^3/4)(2c^2 - 2c + 1); \quad c - odd, n - even$
	$CJP'(1) = (c^3n/4)(2n^2 - 2n + 1); \quad c - even, n - odd$
Examples	T(4,4)S[7,35]; $CJP(x) = 245x^{11025} + 245x^{14161}$; $CJP'(1) = 6{,}170{,}570$
	T(4,4)S[8,40]; $CJP(x) = 320x^{25600} + 320x^{25600}$; $CJP'(1) = 16{,}384{,}000$
	T(4,4)S[7,20]; $CJP(x) = 140x^{3600} + 140x^{4900}$; $CJP'(1) = 1{,}190{,}000$
	T(4,4)S[8,35]; $CJP(x) = 280x^{18496} + 280x^{19600}$; $CJP'(1) = 10{,}666{,}880$

(continued)

Table 8.10   (continued)

3	$PI_v(x) = cn \cdot x^{c(n-p_n)} + cn \cdot x^{n(c-p_c)}$
	$PI_v(x) = 2cn \cdot x^{cn}$; $c, n - even$
	$PI_v'(1) = cn(2cn - c - n)$; $c, n - odd$
	$PI_v'(1) = 2c^2n^2$; $c, n - even$
	$PI_v'(1) = cn^2(2c - 1)$; $c - odd, n - even$
	$PI_v'(1) = c^2n(2n - 1)$; $c - even, n - odd$
Examples	T(4,4)S[7,35]; $PI_v(x) = 245x^{238} + 245x^{210}$; $PI_v'(1) = 109{,}760$
	T(4,4)S[8,40]; $PI_v(x) = 640x^{320}$; $PI_v'(1) = 204{,}800$
	T(4,4)S[7,20]; $PI_v(x) = 140x^{140} + 140x^{120}$; $PI_v'(1) = 36{,}400$
	T(4,4)S[8,35]; $PI_v(x) = 280x^{280} + 280x^{272}$; $PI_v'(1) = 154{,}560$
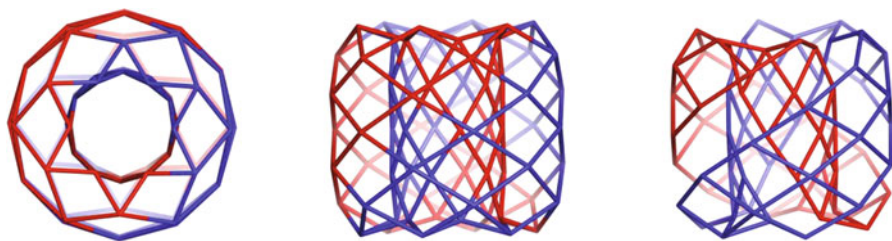
Fig. 8.7 Cutting procedure in *rhomb-tiled* tori: T(4,4)R[6,6]_72; the two halves are *red/blue* colored

8.4.4.2   Rhomb-Tiled Tori

The covering by squares (4,4)S, embedded in the torus, can be changed to the rhombic (4,4)R pattern by the Medial *Med* operation on maps:

$$Med(T(4,4)S[c, n]) \rightarrow (T(4,4)R[2c, n])$$

Since the *Med* operation will double the number of points in the original object (i.e., the vertex multiplicity $m = 2$), it is clear that the resulting graphs are bipartite.

The cutting procedure was applied in the case of rhomb-tiled tori T(4,4)R[c,n] (Fig. 8.7); the same formulas as for bipartite tori (Fig. 8.5 and Table 8.9) were found. Table 8.11 includes both formulas and some examples in this series.

8.4.5   *Cluj Polynomial in TiO₂ Networks*

After the discovery of carbon nanotubes, many researchers addressed the question about the possible existence of nanotubular forms of other elements, and they tried to obtain inorganic nanostructures (Tenne 2002; Rao and Nath 2003; Patzke

Table 8.11 Cluj and related polynomials in tori T(4,4)R[c,n]

Formulas	
$CJS(x) = e\left(x^{v/2} + x^{v/2}\right)$	$CJP(x) = SZ(x) = e\left(x^{v/2 \cdot v/2}\right)$
$CJS'(1) = e(v/2 + v/2) = e \cdot v = 2(cn)^2$	$CJP'(1) = e(v/2 \cdot v/2) = e(v/2)^2$
$PI_v(x) = e\left(x^{v/2+v/2}\right) = e \cdot x^v$	$= (1/2)v^3 = (1/2)(cn)^3$
$PI_v'(1) = e \cdot v = CJ_eS'(1)$	$v = cn;\ e = 2c \cdot 2n$
Examples	
Med(T(4,4)S[5,10]): $CJS(x) = 400x^{50}$; P'(1) = 20,000; $PI_v(x) = 200x^{100}$; P'(1) = 20,000	
Med(T(4,4)S[5,15]): $CJS(x) = 600x^{75}$; P'(1) = 45,000; $PI_v(x) = 300x^{150}$; P'(1) = 45,000	
Med(T(4,4)S[5,20]): $CJS(x) = 800x^{100}$; P'(1) = 80,000; $PI_v(x) = 400x^{200}$; P'(1) = 80,000	
Med(T(4,4)S[5,10]): $CJP(x) = 200x^{2500}$; P'(1) = 500,000; $v = 100$; $e = 200$	
Med(T(4,4)S[5,15]): $CJP(x) = 300x^{5625}$; P'(1) = 1,687,500; $v = 150$; $e = 300$	
Med(T(4,4)S[5,20]): $CJP(x) = 400x^{10000}$; P'(1) = 4,000,000; $v = 200$; $e = 400$	

et al. 2002). Among numerous oxide nanostructures, the titanium nanotubular materials are of high interest due to their chemical inertness, endurance, strong oxidizing power, large surface area, high photocatalytic activity, non-toxicity, and low production cost. The application of TiO_2 nanotubes to photocatalysis, in solar cells, as nanoscale materials for lithium-ion batteries and as gas-sensing material was discussed in the literature (Imai et al. 2002; Adachi et al. 2003; Zhou et al. 2003; Varghese et al. 2003a, b, c; Grimes et al. 2003; Mor et al. 2004). The nanotubes of TiO_2 were synthesized using various precursors (Kasuga et al. 1999; Zhang et al. 2000; Du et al. 2001; Seo et al. 2001; Lin et al. 2002; Yao et al. 2003; Wang et al. 2003), carbon nanotubes, porous alumina or polymer membranes as templates (Varghese et al. 2003b; Grimes et al. 2003; Mor et al. 2004; Kasuga et al. 1999; Zhang et al. 2000; Du et al. 2001; Seo et al. 2001; Lin et al. 2002; Yao et al. 2003; Wang et al. 2003; Sun et al. 2003; Hoyer 1996; Imai et al. 1999; Liu et al. 2002; Shi et al. 2002; Li et al. 2003; Peng et al. 2004), fabrication by anodic oxidation of Ti (Gong et al. 2001; Varghese et al. 2003a; Mor et al. 2003), sol-gel technique (Lakshmi et al. 1997; Kasuga et al. 1998; Kobayashi et al. 2000; Zhang et al. 2001; Wang et al. 2002), and sonochemical synthesis (Zhou et al. 2001). Models of possible growth mechanisms of titanium nanotubes are discussed (Yao et al. 2003; Wang et al. 2002, 2003), but the details of the atomic structure of the nanotube walls and their stacking mode are unknown.

TiO_2 NTs are semiconductors with a wide bandgap, and their stability increases with the increasing of their diameters. Theoretical studies on the stability and electronic characteristics of TiO_2 nanostructures were presented in ref. Ivanovskaya et al. (2003, 2004) and Enyashin and Seifert (2005). The titanium nanostructures presented below can be achieved by the map operations $Du[Med(G)]$, $m = 1.5$, applied on polyhex tori or tubes (Fig. 8.8).

Formulas for calculating Cluj and related polynomials, in toroidal TiO_2 structures, are given in Table 8.12.
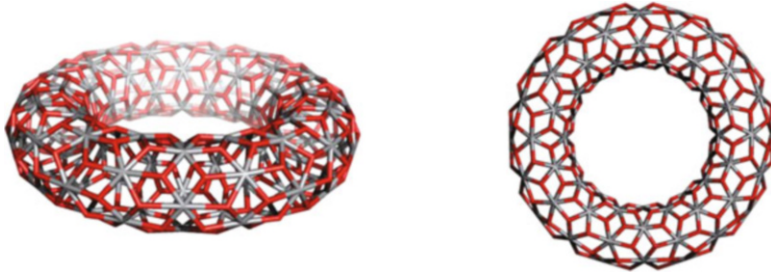
Fig. 8.8 TiO_2 covering embedded in the torus, designed by $Du(Med(H(6,3)[c,n]))$; multiplication factor $m = 1.5$

Table 8.12 Cluj counting polynomials and indices in non-twisted toroidal TiO_2 structures

$CJS(x) = e(x^{e_{ka}} + x^{e_{kb}})$	$v = (3/2)cn$
$CJS'(1) = e(e_{ka} + e_{kb}) = e \cdot v = (1/2)e^2$	$e = 3cn$
$PI_v(x) = e(x^{e_{ka}+e_{kb}}) = e \cdot x^v$	$e_{ka} = e_1 k + (k-1)(c/2)$
$PI_v'(1) = e(e_{ka} + e_{kb}) = e \cdot v = CJ_eS'(1)$	$e_{kb} = e_{ka} + c$
$CJP(x) = SZ(x) = e(x^{e_{ka} \cdot e_{kb}})$	$e_1 = c^2 - (c/2) \cdot (c/2 + 1)$
$CJP'(1) = e(e_{ka} \cdot e_{kb}) = e(c/4)^2(3n-2)(3n+2)$	$k = n/c$
	$m = 1.5$

Tori	$CJS(x)$	$CJS'(1)$	$CJP(x)$	$CJP'(1)$
H[10,10]	$300x^{70} + 300x^{80}$	45,000	$300x^{5600}$	1,680,000
H[10,20]	$600x^{145} + 600x^{155}$	180,000	$600x^{22475}$	13,485,000
H[10,30]	$900x^{220} + 900x^{230}$	405,000	$900x^{50600}$	45,540,000
H[12,14]	$504x^{120} + 504x^{132}$	127,008	$504x^{15840}$	7,983,360
V[8,10]	$240x^{56} + 240x^{64}$	28,800	$240x^{3584}$	860,160
V[10,20]	$600x^{145} + 600x^{155}$	180,000	$600x^{22475}$	13,485,000
V[10,30]	$900x^{220} + 900x^{230}$	405,000	$900x^{50600}$	45,540,000
V[10,50]	$1500x^{370} + 1500x^{380}$	1,125,000	$1500x^{140600}$	210,900,000

8.4.6   Cluj Polynomial in *flu* Crystal Network

The crystal network named ***flu*** belongs to the symmetry group Fm-$3m$ and is identified by point symbol for net: $(4^{12}.6^{12}.8^4)(4^6)2$; 4,8-c net with stoichiometry (4-c)2(8-c); 2-nodal net. It can be designed by map operation Du(Med(C)) next translation of the unit over the three directions of the Euclidean space (Fig. 8.9). Formulas for Cluj and related polynomials, also examples, are given in Table 8.13.

8.4.7   *Cluj Polynomial in Circumcoronenes*

Circumcoronenes are analogues of benzene, designed by adding hexagons around the central hexagon (of benzene); in Fig. 8.10, they are symbolized by Cor_n where
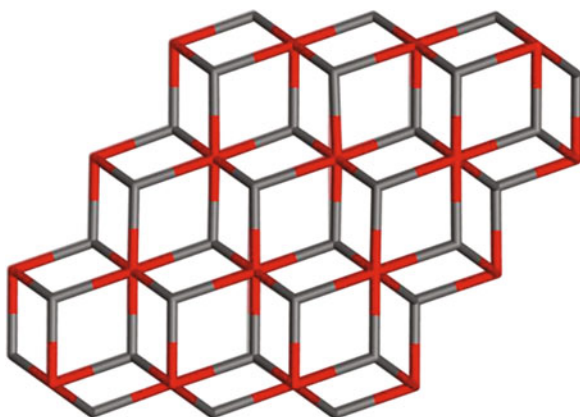
n represents the number of hexagon rows around the central one. Formulas for Cluj
and related polynomials, also examples, are given in Table 8.14.

8.5   Cluj Polynomials in Dendrimers

Cluj and related polynomials and their indices are calculated on a dendritic molec-
ular graph, a (bipartite) periodic structure with the repeat unit $v_0 = 8$ atoms, taken
here both as the root and branching nodes in the design of the dendron (Fig. 8.11,
see also (Dorosti et al. 2009; Hecht and Frechet 2001; Diudea and Katona 1999)).

Formulas collect the contributions of the *root*, the internal (*Int*), and external
(*Ext*) parts of the structure, but close formulas to calculate first derivative (in $x = 1$)
of polynomials were derived for the whole molecular graph. Formulas for calcu-
lating the number of vertices, in the whole wedge or in local ones, and the number
of edges are also given (Diudea et al. 2010b). Examples, at the bottom of
Tables 8.15 and 8.16, will help the reader to verify the presented formulas.

8.6   Conclusions

In this chapter, we presented the Cluj polynomial that counts the vertex proximities
in a connected graph. Definitions and relations with other polynomials and topo-
logical indices were given. The Cluj and related polynomials were computed in
several 3D nanostructures and crystal networks and analytical formulas as well as
examples were tabulated.

Table 8.13 Cluj polynomials in *flu* crystal network

Formulas	
1	$CJS(x) = \sum\limits_{i=1}^{\lfloor\frac{k}{2}\rfloor}(8k^2 + 16k)\,x^{(3k^3 + 7k^2 - 3k) - (3k^2 + 7k)(i-1)}$
	$\quad + \sum\limits_{i=1}^{\lfloor\frac{k}{2}\rfloor}(8k^2 + 16k)\,x^{(-6k^2 - 19k - 7) + (3k^2 + 7k)(i-1)}$
	$\quad + \sum\limits_{i=1}^{k-1}[(16k + 8) + (8k + 8)(i - 1)]\,x^{(3k^3 + 10k^2 - 4k - 2) - (8k+5)(i-1) - (3k+3)\frac{(i-1)(i-2)}{2}}$
	$\quad + \sum\limits_{i=1}^{k-1}[(16k + 8) + (8k + 8)(i - 1)]\,x^{(5k+2) + (8k+5)(i-1) + (3k+3)\frac{(i-1)(i-2)}{2}}$
	$\quad + \left[\left(3 - (-1)^k\right)\left(4k^2 + 8k\right)\right]x^{\frac{3}{2}k^3 + 5k^2 + \frac{1}{2}k}$
	$CJS'(1) = 24k^6 + 140k^5 + 196k^4 - 20k^3 - 4k^2$
2	$PI_v(x) = (8k^3 + 20k^2 - 4k)\,x^{3k^3 + 10k^2 + k}\quad PI_v'(1) = 24k^6 + 140k^5 + 196k^4 - 20k^3 - 4k^2 = CJ_eS'(1)$
3	$CJP(x) = SZ(x) = \sum\limits_{i=1}^{\lfloor\frac{k}{2}\rfloor}(8k^2 + 16k)\,x^{(k^2(3k^2 + 10k + 4 - 3ki - 7i)(-3 + 3ki + 7i))}$
	$\quad + \sum\limits_{i=1}^{k-1}[(16k + 8) + (8k + 8)(i - 1)]\,x^{\frac{(6k^3 + 20k^2 + 2k - 7ki - i - 3ki^2 - 3i^2)(7k + 1 + 3ki + 3i)i}{4}}$
	$\quad + \left[\left(3 - (-1)^k\right)\left(2k^2 + 4k\right)\right]x^{\left(\frac{3}{2}k^3 + 5k^2 + \frac{1}{2}k\right)^2}$
	$CJP'(1) = \frac{1}{15}\left(180k^9 + 1749k^8 + 5697k^7 + 6907k^6 + 2254k^5 + 621k^4 + 143k^3 + 83k^2 + 6k\right)$
4	$v = 3k^3 + 10k^2 + k \qquad e = 8k^3 + 20k^2 - 4k$

Examples

K	CJS(x)		CJS'(1)
1	$48x^7$		336

(continued)

Table 8.13 (continued)

2	$40x^{54} + 64x^{46} + 64x^{33} + 64x^{20} + 40x^{12}$	8976
3	$56x^{157} + 120x^{135} + 88x^{128} + 240x^{87} + 88x^{46} + 120x^{39} + 56x^{17}$	66,816
4	$72x^{334} + 112x^{297} + 192x^{292} + 152x^{245} + 192x^{216} + 192x^{178} + 192x^{140} + 152x^{111} + 192x^{64} + 112x^{59} + 72x^{22}$	290,496
5	$88x^{603} + 136x^{558} + 280x^{535} + 184x^{495} + 280x^{425} + 232x^{414} + 560x^{315} + 232x^{216} + 280x^{205} + 184x^{135} + 280x^{95} + 136x^{72} + 88x^{27}$	932,400

K	$CJP(x)$	$CJP'(1)$
1	$24x^{49}$	1176
2	$64x^{920} + 40x^{648} + 32x^{1089}$	119,648
3	$120x^{5265} + 56x^{2669} + 88x^{5888} + 120x^{7569}$	2,207,688
4	$192x^{18688} + 192x^{30240} + 72x^{7348} + 112x^{17523} + 152x^{27195} + 96x^{31684}$	19,061,112
5	$280x^{50825} + 280x^{87125} + 88x^{16281} + 136x^{40176} + 184x^{66825} + 232x^{89424} + 280x^{99225}$	106,347,832

K	$PI_v(x)$	$P'(1)$	v	e
1	$24x^{14}$	336	14	24
2	$136x^{66}$	8976	66	136
3	$384x^{174}$	66,816	174	384
4	$816x^{356}$	290,496	356	816
5	$180x^{630}$	932,400	630	1480

| Cor₁_24; k=2 | Cor₂_54; k=3 | Cor₃_96; k=4 |
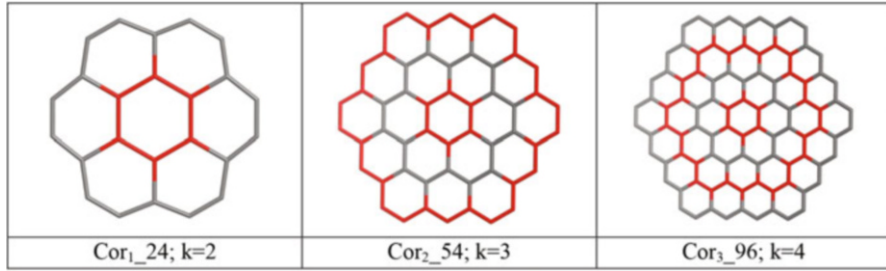
Fig. 8.10 Circumcoronenes: Cor_n $(k = n + 1)$

Table 8.14 Cluj polynomials in circumcoronenes

Formulas

$$CJS(x) = \sum_{i=1}^{k-1} 6(k+i)\left[x^{6k^2-2ki-i^2} + x^{2ki+i^2}\right] + 12kx^{3k^2}$$

$$CJS'(1) = 18k^3(3k-1)$$

$$PI_v(x) = 3k(3k-1)x^{6k^2}$$

$$PI_v'(1) = 18k^3(3k-1)$$

$$CJP(x) = SZ(x) = \sum_{i=1}^{k-1} 6(k+i)\, x^{\left(6k^2+2ki-i^2\right)\left(2ki+i^2\right)} + 6kx^{9k^4}$$

$$CJP'(1) = 54k^6 - \tfrac{3}{2}k^4 + \tfrac{3}{2}k^2$$

$$v = 6k^2 \qquad e = 3k(3k-1)$$

K	CJS(x)	CJS'(1)	PIᵥ(x)	P'(1)
1	$12x^3$	36	$6x^6$	36
2	$18x^{19} + 24x^{12} + 18x^5$	720	$30x^{24}$	720
3	$24x^{47} + 30x^{38} + 36x^{27} + 30x^{16} + 24x^7$	3888	$72x^{54}$	3888
4	$30x^{87} + 36x^{76} + 42x^{63} + 48x^{48} + 42x^{33} + 36x^{20} + 30x^9$	12,672	$132x^{96}$	12,672
5	$36x^{139} + 42x^{126} + 48x^{111} + 54x^{94} + 60x^{75} + 54x^{56} + 48x^{39}$ $+ 42x^{24} + 36x^{11}$	31,500	$210x^{150}$	31,500

K	CJP(x)	CJP'(1)	v	e
1	$6x^9$	1176	6	6
2	$18x^{95} + 12x^{144}$	119,648	24	30
3	$24x^{329} + 30x^{608} + 18x^{729}$	2,207,688	54	72
4	$30x^{783} + 36x^{1520} + 72x^{7348} + 42x^{2079} + 24x^{2304}$	19,061,112	96	132
5	$36x^{1529} + 42x^{3024} + 48x^{4329} + 54x^{5264} + 30x^{5625}$	106,347,832	150	210
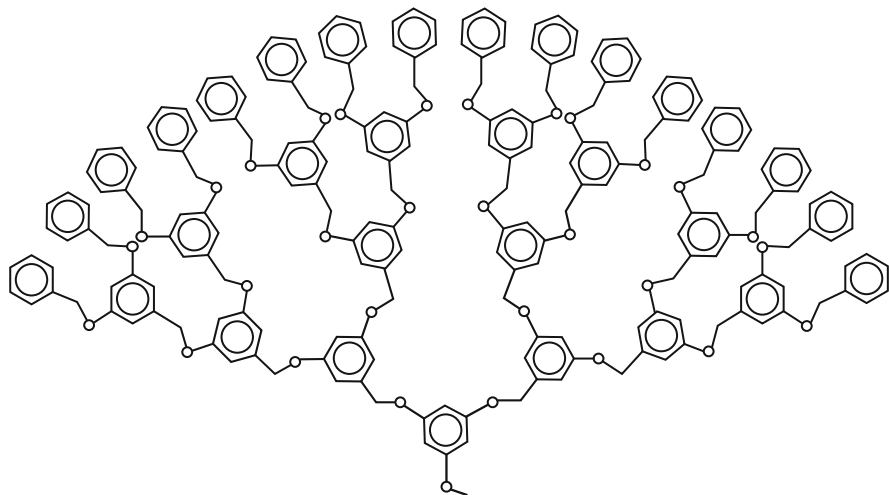
Fig. 8.11 A dendritic wedge, of generation $r = 4$; $v = 248$; $e = 278$

Table 8.15 Formulas to count CJS and PI_v polynomials in a dendritic D wedge graph

$CJS(D,x) = CJS(Root) + CJS(Int) + CJS(Ext)$
$CJS(Root) = (x^1 + x^{v-1}) + (x^2 + x^{v-2}) + 1 \cdot 2 \cdot (x^5 + x^{v-5}) + 2 \cdot 2 \cdot (x^{v/2-1} + x^{v/2+1})$
$CJS(Int) = \sum\limits_{d=1}^{r-1} \{ 2^{r-d} \cdot 2 \cdot 2 \cdot [x^{v_d+3} + x^{v-(v_d+3)}] + 2^{r-(d+1)} \cdot 2 \cdot 2 \cdot [x^{v_{d+1}-5} + x^{v-(v_{d+1}-5)}] +$ $2^{r-(d+1)} \cdot 2 \cdot 1 \cdot \{ [x^{v_{d+1}-2} + x^{v-(v_{d+1}-2)}] + [x^{v_{d+1}-1} + x^{v-(v_{d+1}-1)}] + [x^{v_{d+1}} + x^{v-v_{d+1}}] \} \}$
$CJS(Ext) = 2^r \cdot 3 \cdot 2 \cdot (x^3 + x^{v-3}) + 2^r \cdot 1 \cdot 1 \cdot \{ [x^{v_0-2} + x^{v-(v_0-2)}] +$ $[x^{v_0-1} + x^{v-(v_0-1)}] + [x^{v_0} + x^{v-v_0}] \}$
$CJ'S(1) = CJS(D) = v \cdot \left(8 + \sum\limits_{d=1}^{r-1} 18 \cdot 2^{r-(d+1)} + 9 \cdot 2^r \right) = v \cdot (18 \cdot 2^r - 10) = v \cdot e$
$v = v(D,r) = 2^3 (2^{r+1} - 1)$; $v_d = 2^3 (2^d - 1)$; $d = 1, 2, ..$
$e(D) = 18 \cdot 2^r - 10$
Example:
$v(r = 3) = 120$; $e(r = 3) = 134$; $v(r = 4) = 248$; $e(r = 4) = 278$
$PI_v(x) = e \cdot x^v = (18 \cdot 2^r - 10) \cdot x^{2^3(2^{r+1}-1)}$; $\quad PI_v'(1) = v \cdot e$
Example:
$CJS(x, r = 3) = (1x^1 + 1x^{119}) + (1x^2 + 1x^{118}) + (48x^3 + 48x^{117}) + (2x^5 + 2x^{115}) + (8x^6 + 8x^{114}) +$ $(8x^7 + 8x^{113}) + (8x^8 + 8x^{112}) + (16x^{11} + 16x^{109}) + (8x^{19} + 8x^{101}) + (4x^{22} + 4x^{98}) + (4x^{23} + 4x^{97})$ $+ (4x^{24} + 4x^{96}) + (8x^{27} + 8x^{93}) + (4x^{51} + 4x^{69}) + (2x^{54} + 2x^{66}) + (2x^{55} + 2x^{65}) + (2x^{56} + 2x^{64}) +$ $(4x^{59} + 4x^{61})$
$CJS'(1, r = 3) = 16{,}080$; $CJS'(1, r = 4) = 68{,}944$.

Table 8.16 Formulas to count *CJP* polynomial in a dendritic D wedge graph

$CJP(D,x) = CJP(Root) + CJP(Int) + CJP(Ext)$
$CJP(G) = \sum_e \left(x^{n_e(v-n_e)} \right)$
$CJP(Root) = x^{1(v-1)} + x^{2(v-2)} + 1 \cdot 2 \cdot \left[x^{5(v-5)} \right] + 2 \cdot 2 \cdot \left[x^{(v/2-1)(v/2+1)} \right]$
$CJP(Int) = \sum_{d=1}^{r-1} \left\{ 2^{r-d} \cdot 2 \cdot 2 \cdot \left[x^{(v_d+3)(v-(v_d+3))} \right] + 2^{r-(d+1)} \cdot 2 \cdot 2 \cdot \left[x^{(v_{d+1}-5)(v-(v_{d+1}-5))} \right] + \right.$ $\left. 2^{r-(d+1)} \cdot 2 \cdot 1 \cdot \left\{ \left[x^{(v_{d+1}-2)(v-(v_{d+1}-2))} \right] + \left[x^{(v_{d+1}-1)(v-(v_{d+1}-1))} \right] + \left[x^{(v_{d+1})(v-v_{d+1})} \right] \right\} \right\}$
$CJP(Ext) = 2^r \cdot 3 \cdot 2 \cdot \left(x^{3(v-3)} \right) + 2^r \cdot 1 \cdot 1 \cdot \left\{ \left[x^{(v_0-2)(v-(v_0-2))} \right] + \left[x^{(v_0-1)(v-(v_0-1))} \right] + \left[x^{v_0(v-v_0)} \right] \right\}$
$CJ'P(1) = CJP(D) = 3626 \cdot 2^r + 256 \cdot 2^{2r} - 3872 \cdot 4^r + 1792 \cdot 4^r \cdot r + 1120 \cdot 2^r \cdot r + 99$
Example:
$CJP(x, r = 3) = x^{119} + x^{236} + 48x^{351} + 2x^{575} + 8x^{684} + 8x^{791} + 8x^{896} + 16x^{1199} + 8x^{1919} + 4x^{2156} +$ $4x^{2231} + 4x^{2304} + 8x^{2511} + 4x^{3519} + 2x^{3564} + 2x^{3575} + 2x^{3584} + 4x^{3599}$
$CJP'(1, r = 3) = 168{,}627; \; CJP'(1, r = 4) = 1{,}039{,}107$

References

Adachi M, Murata Y, Okada I, Yoshikawa S (2003) Formation of Titania Nanotubes and Applications for Dye-Sensitized Solar Cells. J Electrochem Soc 150:488–493

Alipour MA, Ashrafi AR (2009) A numerical method for computing the Wiener index of one-heptagonal carbon nanocone. J Comput Theor Nanosci 6:1204–1207

Ashrafi AR, Ghorbani M, Jalali M (2008) The vertex PI and Szeged indices of an infinite family of fullerenes. J Theor Comput Chem 7:221–231

Diudea MV (1997a) Cluj matrix CJu: source of various graph descriptors. MATCH Commun Math Comput Chem 35:169–183

Diudea MV (1997b) Cluj matrix invariants. J Chem Inf Comput Sci 37:300–305

Diudea MV (1999) Valencies of property. Croat Chem Acta 72:835–851

Diudea MV (ed) (2005) Nanostructures, Novel Architecture. Nova, New York

Diudea MV (2009) Cluj polynomials. J Math Chem 45:295–308

Diudea MV (2010a) Counting polynomials in partial cubes. In: Gutman I, Furtula B (eds) Novel molecular structure descriptors-theory and applications I. Univ Kragujevac, Kragujevac, pp 191–215

Diudea MV (2010b) Counting polynomials and related indices by edge cutting procedures. In: Gutman I, Furtula B (eds) Novel molecular structure descriptors-theory and applications II. Univ Kragujevac, Kragujevac, pp 57–78

Diudea MV, Katona G (1999) Molecular topology of dendrimers, in: G A Newkome Ed. Adv Dendritic Macromol 4:135–201

Diudea MV, Klavžar S (2010) Omega polynomial revisited. Acta Chem Sloven 57:565–570

Diudea MV, Nagy CL (2007) Periodic Nanostructures. Springer, Dordrecht

Diudea MV, Ursu O (2003) Layer matrices and distance property descriptors. Indian J Chem 42A:1283–1294

Diudea MV, Parv B, Gutman I (1997) Detour-Cluj matrix and derived invariants. J Chem Inf Comput Sci 37:1101–1108

Diudea MV, Gutman I, Jäntschi L (2002) Molecular Topology. Nova, New York

Diudea MV, Florescu MS, Khadikar PV (2006) Molecular Topology and Its Applications. Eficon, Bucharest

Diudea MV, Vizitiu AE, Janežič D (2007) Cluj and related polynomials applied in correlating studies. J Chem Inf Model 47:864–874

Diudea MV, Cigher S, John PE (2008) Omega and related counting polynomials. MATCH Commun Math Comput Chem 60:237–250

Diudea MV, Ilić A, Ghorbani M, Ashrafi AR (2010a) Cluj and PIv polynomials. Croat Chem Acta 83:283–289

Diudea MV, Dorosti N, Iranmanesh A (2010b) Cluj CJ polynomial and indices in a dendritic molecular graph. Carpath J Math 4:247–253

Dorosti N, Iranmanesh A, Diudea MV (2009) Computing the Cluj index of dendrimer nanostars. MATCH Commun Math Comput Chem 62:389–395

Du GH, Chen Q, Che RC, Yuan ZY, Peng LM (2001) Preparation and Structure Analysis of Titanium Oxide Nanotubes. Appl Phys Lett 79:3702–3704

Ebbesen TW (1998) Cones and tubes: geometry in the chemistry of carbon. Acc Chem Res 31:558–566

Enyashin AN, Seifert G (2005) Structure stability and electronic properties of TiO2 nanostructures. Phys Stat Sol 242:1361–1370

Gong D, Grimes CA, Varghese OK, Hu W, Singh RS, Chen Z, Dickey EC (2001) Titanium oxide nanotube arrays prepared by anodic oxidation. J Mater Res 16:3331–3334

Grimes CA, Ong KG, Varghese OK, Yang X, Mor G, Paulose M, Dickey EC, Ruan C, Pishko MV, Kendig JW, Mason AJ (2003) A Sentinel Sensor Network for Hydrogen Sensing. Sensors 3:69–82

Gutman I (1994) A formula for the Wiener number of trees and its extension to graphs containing cycles. Graph Theory Notes NY 27:9–15

Gutman I, Klavžar S (1995) An algorithm for the calculation of the Szeged index of benzenoid hydrocarbons. J Chem Inf Comput Sci 35:1011–1014

Harary F (1969) Graph theory. Addison-Wesley, Reading

Hecht S, Frechet JMJ (2001) Dendritic encapsulation of function: applying nature's site isolation principle from biomimetics to materials science. Angew Chem Int Ed 40:74–91

Hoyer P (1996) Formation of a titanium dioxide nanotube array. Langmuir 12:1411–1413

Ilić A (2010) On the extremal graphs with respect to the vertex PI index. Appl Math Lett 23:1213–1217

Imai H, Takei Y, Shimizu K, Matsuda M, Hirashima H (1999) Direct preparation of anatase TiO_2 nanotubes in porous alumina membranes. J Mater Chem 9:2971–2972

Imai H, Matsuta M, Shimizu K, Hirashima N, Negishi N (2002) Morphology transcription with TiO_2 using chemical solution growth and its application for photocatalysts. Solid State Ion 151:183–187

Ivanovskaya VV, Enyashin AN, Ivanovskii AL (2003) Electronic structure of single-walled TiO_2 and VO_2 nanotubes. Mendeleev Comm 13:5–7

Ivanovskaya VV, Enyashin AN, Ivanovskii AL (2004) Nanotubes and fullerene-like molecules based on TiO_2 and ZrS_2: Electronic structure and chemical bond Russ. J Inorg Chem 49:244–251

Kasuga T, Hiramatsu M, Hoson A, Sekino T, Niihara K (1998) Formation of titanium oxide nanotube. Langmuir 14:3160–3163

Kasuga T, Hiramatsu M, Hoson A, Sekino T, Niihara K (1999) Titania nanotubes prepared by chemical processing. Adv Mater 11:1307–1311

Khadikar PV (2000) On a novel structural descriptor PI. Nat Acad Sci Lett 23:113–118

Khalifeh MH, Yousefi-Azari H, Ashrafi AR (2008a) Vertex and edge PI indices of Cartesian product graphs. Discret Appl Math 156:1780–1789

Khalifeh MH, Yousefi-Azari H, Ashrafi AR (2008b) A matrix method for computing Szeged and vertex PI indices of join and composition of graphs. Linear Algebra Appl 429:2702–2709

Klavžar S (2008) A brid's eye view of the cut method and a survey of its applications in chemical graph theory. MATCH Commun Math Comput Chem 60:255–274

Kobayashi S, Hanabusa K, Hamasaki N, Kimura M, Shirai H (2000) Preparation of TiO_2 hollow-fibers using supramolecular assemblies. Chem Mater 12:1523–1525

Krishnan A, Dujardin E, Treacy MMJ, Hugdahl J, Lynum S, Ebbesen TW (1997) Graphitic cones and the nucleation of curved carbon surfaces. Nature 388:451–454

Lakshmi BB, Dorhout PK, Martin CR (1997) Sol–gel template synthesis of semiconductor nanostructures. Chem Mater 9:857–872

Li XH, Liu WM, Li HL (2003) Template synthesis of well-aligned titanium dioxide nanotubes. Appl Phys A 80:317–320

Lin CH, Chien SH, Chao JH, Sheu CY, Cheng YC, Huang YJ, Tsai CH (2002) The synthesis of sulfated titanium oxide nanotubes. Catal Lett 80:153–159

Liu SM, Gan LM, Liu LH, Zhang WD, Zeng HC (2002) Synthesis of single-crystalline TiO_2 nanotubes. Chem Mater 14:1391–1397

Mansour T, Schork M (2009) The vertex PI index and Szeged index of bridge graphs. Discr Appl Math 157:1600–1606

Mor GK, Varghese OK, Paulose M, Mukherjee N, Grimes CA (2003) Fabrication of tapered, conical-shaped titania nanotubes. J Mater Res 18:2588–2593

Mor GK, Carvalho MA, Varghese OK, Pishko MV, Grimes CA (2004) A room − temperature TiO_2 − nanotube hydrogen sensor able to self-clean photoactively from environmental contamination. J Mater Res 19:628–634

Patzke GR, Krumeich F, Nesper R (2002) Oxidic nanotubes and nanorods − anisotropic modules for a future nanotechnology. Angew Chem Int Ed 41:2446–2461

Peng T, Yang H, Chang G, Dai K, Hirao K (2004) Synthesis of bamboo-shaped TiO_2 nanotubes in nanochannels of porous aluminum oxide membrane. Chem Lett 33:336–337

Rao CNR, Nath M (2003) Inorganic nanotubes. Dalton Trans 1:1–24

Seo DS, Lee JK, Kim H (2001) Preparation of nanotube − shaped TiO_2 powder. J Cryst Growth 229:428–432

Shi YL, Zhang XG, Li HL (2002) Liquid phase deposition templates synthesis of nanostructures of anatase titania. Mater Sci Engin A 333:239–242

Sun J, Gao L, Zhang Q (2003) TiO_2 tubes synthesized by using ammonium sulfate and carbon nanotubes as templates. J Mater Sci Lett 22:339–341

Tenne R (2002) Inorganic Nanotubes and Fullerene-Like Materials. Chem Eur J 8:5296–5304

Ursu O, Diudea MV (2005) TOPOCLUJ software program. Babes-Bolyai University, Cluj

Varghese OK, Gong D, Paulose M, Grimes CA, Dickey EC (2003a) Crystallization and high − temperature structural stability of titanium oxide nanotube arrays. J Mater Res 18:156–165

Varghese OK, Gong D, Paulose M, Ong KG, Dickey EC, Grimes CA (2003b) Extreme changes in the electrical resistance of titania nanotubes with hydrogen exposure. Adv Mater 15:624–627

Varghese OK, Gong D, Paulose M, Ong KG, Grimes CA (2003c) Hydrogen sensing using titania nanotubes. Sens Actuators B 93:338–344

Vizitiu AE, Diudea MV (2006) Conetori of high genera. Studia Univ Babes-Bolyai 51(1):39–48

Vizitiu AE, Diudea MV (2008) Omega and Theta polynomials in conical nanostructures. MATCH Commun Math Comput Chem 60:927–933

Vizitiu AE, Diudea MV (2009) Cluj polynomial description of TiO_2 nanostructures. Studia Univ Babes Bolyai 54(1):173–180

Wang YQ, Hu GQ, Duan XF, Sun HL, Xue QK (2002) Microstructure and formation mechanism of titanium dioxide nanotubes. Chem Phys Lett 365:427–431

Wang W, Varghese OK, Paulose M, Grimes CA (2003) Synthesis of CuO and Cu_2O crystalline nanowires using $Cu(OH)_2$ nanowire templates. J Mater Res 18:2756–2759

Wiener H (1947) Structural determination of paraffin boiling points. J Am Chem Soc 69:17–20

Yao BD, Chan YF, Zhang XY, Zhang WF, Yang ZY, Wang N (2003) Formation mechanism of TiO_2 nanotubes. Appl Phys Lett 82:281–283

Zhang S, Zhou J, Zhang Z, Du Z, Vorontsov AV, Jin Z (2000) Morphological structure and physicochemical properties of nanotube TiO_2. Chin Sci Bull 45:1533–1536

Zhang M, Bando Y, Wada K (2001) Sol–gel template preparation of TiO_2 nanotubes and nanorods. J Mater Sci Lett 20:167–170

Zhou Y, Li H, Koltypin Y, Hacohen YR, Gedanken A (2001) Sonochemical synthesis of titania whiskers and nanotubes. Chem Commun 24:2616–2617

Zhou Y, Cao L, Zhang F, He B, Li H (2003) Lithium insertion into TiO_2 nanotube prepared by the hydrothermal process. J Electrochem Soc 150A:1246–1249

Chapter 9
Graphene Derivatives: Carbon Nanocones and CorSu Lattice: A Topological Approach

Farzaneh Gholaminezhad and Mircea V. Diudea

Abstract Graphene is a graphite sheet with (6,3) covering and all sp^2 carbon atoms. In this chapter, two structural modifications of graphene are presented: the cones and CorSu (coronene-sumanene) tessellation. Topology of these modified graphenes is given in terms of several counting polynomials and corresponding topological indices. Analytical formulas were derived either by numerical analysis or by the cutting procedure. In the case of CorSu lattice, composition rules (with fragmental contributions) for the Omega polynomial were established.

9.1 Introduction

Graphene is a (6,3) graphite sheet consisting of only sp^2 carbon atoms disposed in hexagonal faces. Single-sheet or several-sheet graphenes can be exfoliated from the bulk graphite by forming graphene oxide (Okamoto and Miyamoto 2001; Tylianakis et al. 2010; Lee et al., 2009) or via chemical functionalization (Denis 2009; Paci et al. 2007; Ueta et al. 2010). Graphene has attracted considerable interest in the research community as a consequence of its outstanding properties.

Graphene is considered to be a zero-bandgap semiconductor material with the possibility of multiple applications in electronics, spintronics, hydrogen storage (Okamoto and Miyamoto 2001; Tylianakis et al. 2010), electrical batteries (Seger and Kamat 2009; Abouimrane et al. 2010), capacitors (Yu and Dai 2010; Wang et al. 2009a, b), etc. Interactions with oxygen, fluorine, sulfur, and other chemical

F. Gholaminezhad (✉)
Department of Pure Mathematics, Faculty of Mathematical Sciences, University of Kashan, Kashan 87317-53153, Iran
e-mail: farzane.gholaminezhad@gmail.com

M.V. Diudea
Department of Chemistry, Faculty of Chemistry and Chemical Engineering, Babes-Bolyai University, Arany Janos Street 11, Cluj-Napoca RO-400028, Romania
e-mail: diudea@chem.ubbcluj.ro

species permit various chemical modifications of the graphene (Lee et al. 2009; Denis 2009; Paci et al. 2007). Composites of graphene oxide and titanium oxide GO-TiO$_2$ exhibit improved photocatalytic activity toward mineralization of organic pollutants (Ng et al. 2010).

It is hoped that the future microprocessors could be fabricated by etching graphene wafers into desired device architectures (Geim and Novoselov 2007), while closely packed graphene sheets could be employed in applications such as transparent conductors (Watcharotone et al. 2007; Green and Hersam 2009), field emission displays (Eda et al. 2008; Novoselov et al. 2004), and various composite materials (Stankovich et al. 2006).

There are studies about the formation of carbon nanoscrolls (CNSs) from graphene. The scrolls can be prepared by ultrasonication of potassium-intercalated graphite (Viculis et al. 2003; Wang et al. 2009a, b) or by simply dipping the single-layer graphene deposited on a substrate in isopropyl alcohol (Xie et al. 2009). Because of the novel scroll topology, properties of CNSs differ from those of single-walled nanotubes (SWNTs) and multi-walled nanotubes (MWNTs). CNSs provide interlayer galleries that can be intercalated with donors and acceptors and may be valuable in energy storage, in super-capacitors, or in batteries.

Polymer composites of carbon nanotubes are known to exhibit high mechanical strength. Similar studies on graphene-polymer composites have shown promising mechanical properties. It has been shown that mechanical properties of polyvinyl alcohol and poly(methyl methacrylate) composites reinforced with small quantities of few-layer graphene (FG) lead to a significant increase in both elastic modulus and hardness (Das et al. 2009; Ilić et al. 2010).

Structural modifications of graphene can be performed by including ring defects, and such modified graphenes are no more planar. The aim of this chapter is to present some structurally modified graphenes and their topological characterization by means of topological polynomials and derived indices. The chapter is organized as follows. After an introduction to graphene science, the structural modifications of graphene are presented in the Sect. 9.2. Section 9.3 introduces to the ground topology of the modified graphenes herein discussed that is next completed in Sect. 9.4 with definitions of polynomials and topological indices computed on the above graphene derivatives. The main results of the chapter are presented in Sect. 9.5. The chapter is finished with conclusions and references.

9.2 Graphene Derivatives

9.2.1 Nanocones C(a,n)

Conical nanostructures (Krishnan et al. 1997; Ebbesen 1998) have been reported in Nanoscience since 1968, before the discovery of fullerenes. If a graphite sheet, i.e., graphene, is divided into six sectors, each with an angle of 60°, and if m of these sectors (with $m = 1$ to 3) is deleted sequentially, the dangling bonds being fused together, three classes of graphs, associated to single-walled nanocones, are
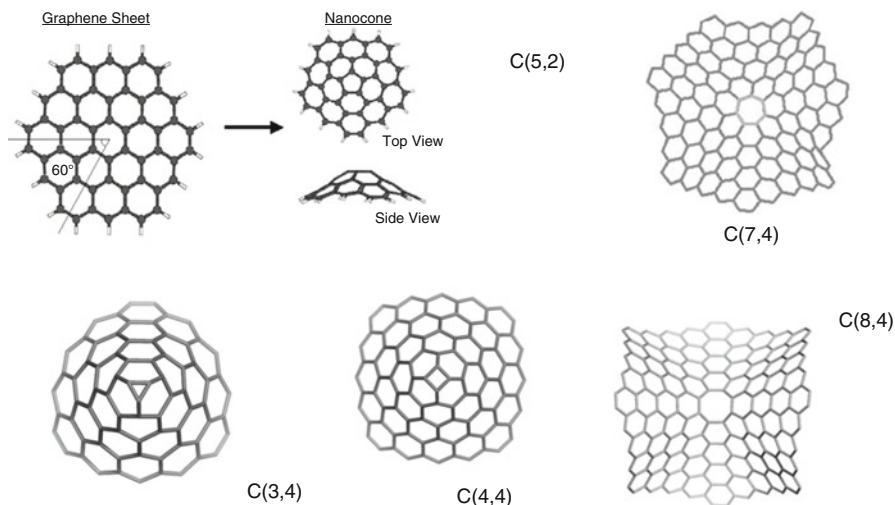
Fig. 9.1 Graphite modifications: C(*a*,*n*)

obtained; their apex polygon will be a pentagon ($a = 5$), a square ($a = 4$), or a triangle ($a = 3$), respectively. One can extend the construction principle and accept in the family of "topological cones" structures having the apex polygon $a \geq 6$; of course, that "cone" with $a = 6$ is just the plane graphite sheet, while those having larger polygons will show a saddle shape.

Pentagonal or heptagonal defects can be introduced into a graphene network to form nonplanar structures (Fig. 9.1). These two defects can be described as $+\pi/3$ and $-\pi/3$ disclinations, respectively. With these defects, a wide variety of carbon structures of different shapes can be formed.

9.2.2   Hourglasses CC(a,n,t)

Two conical units can be connected to form an hourglass (Fig. 9.2), symbolized CC (*a*,*n*,*t*) where *a* and *n* have the above meaning, while *t* is the number of polygon rows in the tube joining the two conical parts (Vizitiu and Diudea 2006).

To insert the tube, the apex polygon is taken out from the both cones (with $a_1 = a_2$ but n_1 and n_2 not necessarily equal). Next, the tube is linked to the conical units by means of polygons larger than six atoms (seven, in case of Fig. 9.2).

9.2.3   CorSu Lattice

This lattice was derived from the graphene sheet, of (6,3) tessellation, by decorating it with coronene-like flowers, having sumanene units as petals. The pattern, called
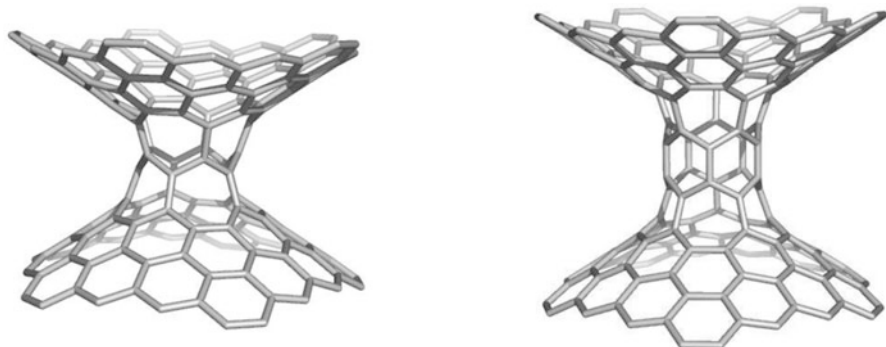
Fig. 9.2 Conical units joined to form an hourglass CC(*a,n,t*) (*a* = apex polygon; *n* = no. hexagon rows in the skirt (of parent *cone*); *t* = no. hexagon rows in the tube): CC(5,2,0)_160 (*left*) and CC (5,2,1)_170 (*right*), the last number counting the carbon atoms in the structure

CorSu, can be described as [6:(6:(5,6)3)6], with vertices/atoms of degree 3 (sp^2) and 4 (sp^3), as shown in Fig. 9.3. This idea is related to studies on aromaticity, in which circulene/flower units were proposed as extensions of the Clar theory of aromaticity (Clar 1964, 1972). Notice that coronene and sumanene are molecules synthesized in the labs. Additional support came from the synthesis of several bowl-shaped molecules, inspired from the architecture of fullerenes and, more recently, by the direct synthesis of fullerenes starting from open precursors. The design of various domains on the graphene sheet is nowadays a challenge study and practice.

The pentagonal rings, possibly entering as local bridges over the graphite sheet by reactions like oxidation, amination, or carbene action, will force the geometry of graphene to a bowl-shaped one (Fig. 9.3, the bottom row). The overall positive curvature depends on the bond length of the atoms involved in the bridges, it being as bowl-shaped as the atom covalent radius is smaller. The lattice appears, in the optimized geometry, as alternating positive (sumanene) and negative (coronene) curved domains (Diudea and Ilić 2009; Diudea 2010a, b).

9.3 Topological Background

Let *G* be a simple connected graph with the vertex and edge sets $V(G)$ and $E(G)$, respectively. The distance between the vertices *u* and *v* of a connected graph *G* is denoted by $d(u,v)$, and it counts the edges in a shortest path joining the vertices *u* and *v*. A topological index is a numeric quantity, derived from the structure of a graph, which is invariant under automorphisms of the given graph. The number of vertices in the cone $C(a,n)$ and in the *kth* semicube (numbering starting from the external row) is given by the formulas (Alipour and Ashrafi 2009):

$$v(C(a,n)) = a(n+1)^2; \quad v_k = \sum_{i=1}^{k}(2n+2i+1) = k(2n+k+2)$$

v=96

v=612

v= 1626
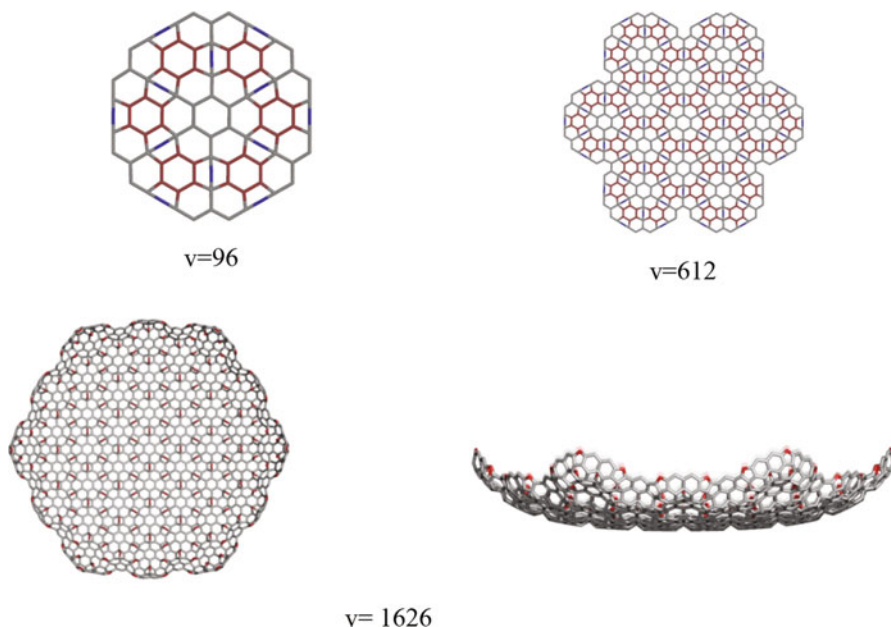
Fig. 9.3 Hexagonal domains in the CorSu graphene sheet: graphs (*top row*) associated to the hypothetical molecules (*bottom row*)

A simple counting of the hexagons leads to the formula of edges in the cone:

$$e(C(a,n)) = a\left[(n+1) + \sum_{k=1}^{n}(n+k+1)\right] = (a/2)(3n^2 + 5n + 2)$$

The number of hexagons in the actual cut is $h_k = n + k$, while in the core cut is $h_0 = 2n + 1$; the number of edges in the actual cut is $e_k = n + k + 1$, and it equals the length of opposite edge strips ops, $e_k = s_k$.

9.4   Topological Indices and Polynomials

One of the most famous topological indices is the Wiener index, introduced by Harold Wiener (Wiener 1947). It equals the sum of topological distances between all unordered pair vertices of G:

$$W(G) = \sum_{(u,v)\in V(G)} d_G(u,v)$$

The Szeged index is another topological index, defined by Ivan Gutman (1994) as

$$Sz(G) = \sum\nolimits_{(u,v) \in E(G)} n_u(e) \cdot n_v(e)$$

where $n_u(e)$ is the number of vertices of G lying closer to u than to v, and $n_v(e)$ is the number of vertices of G lying closer to v than to u.

To define the Cluj-Ilmenau *CI* index (John et al. 2007), some additional definitions are needed. Let G be a bipartite, plane graph; two edges $e = (x,y)$ and $f = (u,v)$ of G are called *co*-distant (briefly: *e co f*) if $d(x,u) = d(x,u) + 1 = d(y,v) + 1 = d(y,u)$.

Let $C(e) := \{f \in E(G); \ f \ co \ e\}$ denote the set of edges in G, co-distant to the edge $e \in E(G)$. If relation *co* is an equivalence relation, then G is called a *co-graph*. The set $C(e)$ is called an *orthogonal cut (oc* for short*)* of G, with respect to the edge e. If G is a co-graph then its orthogonal cuts $C(G) = C_1, C_2, \ldots, C_k$ form a partition of $E(G)$: $E(G) = C_1 \cup C_2 \cup \ldots \cup C_k, C_i \cap C_j = \varnothing, \ i \neq j$. In bipartite graphs, *co* is a Θ relation, *(Djoković-Winkler)* (Djoković 1973; Winkler 1984; Klavžar 2008a, b).

We say the edges e and f of a plane graph G are in relation *opposite, e op f*, if they are opposite edges of an inner face of G. Note that the relation *co* is defined in the whole graph, while *op* is defined only in faces. Using the relation *op*, we can partition the edge set of G into *opposite* edge *strips, ops*. An *ops* is a quasi-orthogonal cut *qoc*, since *ops* is, in general, not transitive.

Let G be a connected graph and $S(G) = s_1, s_2, \ldots, s_k$ be the set of *ops* of G. Then *ops* form a partition of $E(G)$. Denote by $m(s)$ the number of *ops* of length $s = /s_k/$, and define the Omega polynomial as (Diudea 2006)

$$\Omega(x) = \sum\nolimits_s m(s) \cdot x^s$$

In partial cubes, other two related polynomials (Diudea et al. 2008, 2009) can be calculated on *ops*:

$$\Theta(x) = \sum\nolimits_s ms \cdot x^s; \ \Pi(x) = \sum\nolimits_s ms \cdot x^{e-s}$$

$\Theta(x)$ counts equidistant edges while $\Pi(x)$ non-equidistant edges. Thus, Omega and its related polynomials count edges, not vertices. Their first derivative (in $x = 1$) provides single-number topological descriptors:

$$\begin{aligned} \Omega'(1) \ &= \sum\nolimits_s m \cdot s = e = |E(G)|; \ \Theta'(1) = \sum\nolimits_s m \cdot s^2 = \theta(G); \ \Pi'(1) \\ &= \sum\nolimits_s ms \cdot (e-s) = \Pi(G) \end{aligned}$$

On Omega polynomial, the Cluj-Ilmenau index, $CI = CI(G)$, was defined as

$$CI(G) = \left\{ \left[\Omega'(1)\right]^2 - \left[\Omega'(1) + \Omega''(1)\right] \right\}$$

A polynomial related to $\Pi(x)$ was defined by (Ashrafi et al. 2006) as

$$PI_e(x) = \sum_{e \in E(G)} x^{n(e,u)+n(e,v)}$$

where $n(e,u)$ is the number of edges lying closer to the vertex u than to the v vertex. Its first derivative (in $x = 1$) provides the $PI(G)$ index, proposed by (Khadikar 2000).

In co-graphs/partial cubes, the equality $CI(G) = \Pi(G)$ holds. By expanding definition of CI (see above), it is evident that

$$CI(G) = \left(\sum_s m \cdot s \right)^2 - \left[\sum_s m \cdot s + \sum_s m \cdot s \cdot (s-1) \right] = e^2 - \sum_s m \cdot s^2$$
$$= \Pi(G)$$

The above relation is valid only in the assumption $|c_k| = |s_k|$, which provides the same value for the exponent s, and this is precisely achieved in co-graphs/partial cubes. In bipartite graphs, there exists another equality $\Pi(G) = PI(G)$ (Diudea et al. 2008).

A related index, defined by Ashrafiet al. (Khalifeh et al. 2008), on vertices, is the vertex PI_v:

$$PI_v(G) = \sum_{e=uv} n_{u,v} + n_{v,u} = |V| \cdot |E| - \sum_{e=uv} m_{u,v}$$

where $n_{u,v}$ and $n_{v,u}$ count the non-equidistant vertices vs. the endpoints of $e = (u,v)$, while $m(u,v)$ is the number of vertices lying at equal distance from the vertices u and v.

9.5   Main Results

In cones with $a > 4$, $a = 2\,s$, the Wiener index can be obtained by using a cutting procedure (Klavžar 2008a, b; Diudea 2010a, b), which sums the products of the number of vertices lying to the left and to the right of each orthogonal line (Fig. 9.4).
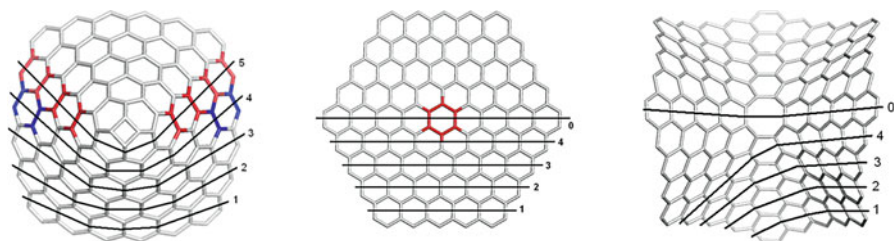
Fig. 9.4   Cones with various even apex values $a = 4$, 6, and 8; the cutting procedure

9.5.1   Topological Indices in Cones $C(a,n)$

Numerical analysis of the calculation and/or the cutting procedure (Diudea 2010a, b; Ashrafi and Gholaminezhad 2008, 2009) performed in cones enabled us to derive analytical formulas for several topological indices.

Case: a Is Even

$$W(C(2s,n)) = (1/15)s(n+1)\big(80sn^4 - 76n^4$$
$$- 169n^3 + 15s^2n^3 + 230sn^3 - 111n^2 + 45s^2n^2$$
$$+ 220sn^2 - 19n + 45s^2n + 70sn + 15s^2\big)$$

$$SZ_v(C(a_{\text{even}},n)) = (a/4)(n+1)^2\big(-18n^4 + 9an^4 - 36n^3 + a^2n^3 + 24an^3$$
$$+ 21an^2 - 19n^2 + 3a^2n^2 + 3a^2n - 2n + 6an + a^2\big);$$

$$W(C(4,n)) = 8 + (736/15)n + 108n^2 + (340/3)n^3 + 58n^4 + (58/5)n^5$$

$$SZ_v(C(4,n_{\text{even}})) = 16 + (538/5)n + (4129/15)n^2 + 370n^3 + (1669/6)n^4$$
$$+ (557/5)n^5 + (557/30)n^6$$

$$SZ_v(C(4,n_{\text{odd}})) = (31/2) + (523/5)n + (8213/30)n^2 + 370n^3 + (1669/6)n^4$$
$$+ (557/5)n^5 + (557/30)n^6$$

$$CI(C(a_{\text{even}},n)) = (1/12)a(n+1)\big(27an^3 - 28n^2 + 63an^2 + 48an + 12a - 50n - 24\big)$$

Case: a Is Odd

$$W(C(2s+1,n)) = \frac{1}{30}(n+1)(2s+1)$$
$$\times(16n - n^2 - 54n^3 - 36n^4 + 15s + 115ns + 265n^2s$$
$$+ 245n^3s + 80n^4s + 15s^2 + 45ns^2 + 45n^2s^2 + 15n^3s^2)$$

$$SZ_v(C(a_{\text{odd}},n))$$
$$= \frac{1}{4}\big((9a^2 - 18a)n^6 + (a^3 + 40a^2 - 71a)n^5 + (5a^3 + 68a^2 - 104a)n^4$$
$$+ (10a^3 + 52a^2 - 66a)n^3 + (10a^3 + 13a^2 - 13a)n^2$$
$$+ (5a^3 - 4a^2 + 3a)n + (a^3 - 2a^2 + a)\big)$$

$$CI(C(a_{\text{odd}},n)) = (1/12)a(n+1)(27an^3 - 28n^2 + 63an^2 + 48an + 12a - 38n - 12)$$
$$= CI(C(a_{\text{even}},n)) + a(n+1)^2$$

$$PI_v(C(a_{\text{odd}},n)) = (1/2)$$
$$\times(3a^2n^4 + (11a^2 - 2a)n^3 + (15a^2 - 6a)n^2 + (9a^2 - 6a)n + 2a^2 - 2a)$$

$$PI_e(C(a_{\text{odd}},n)) = (a/12)(n+1)\big(27an^3 + 63an^2 - 46n^2 - 56n + 48an + 12a - 12\big)$$

9.5.2 Polynomials in Cones C(a,n)

Case: *a* Is Even

$$SZ_v(C(4,n),x) = 4(n+1) \cdot x^{(v/2)^2} + 4\sum_{k=1}^{k_c-1} e_k \cdot x^{v_k(v-v_k)} + 4\sum_{k=k_c}^{n} (e_k - 2c_k) \cdot x^{v_k(v-v_k)}$$

$$+ 4\sum_{k=k_c}^{n} 2c_k \cdot x^{\left(v_k-(c_k)^2\right)\left(v-v_k+(c_k)^2\right)}$$

$$\Omega(C(a_{\text{even}},n),x) = (a/2) \cdot x^{2(n+1)} + \sum_{k=2}^{n+1} a \cdot x^{n+k}$$

$$\Omega'(C(a_{\text{even}},n),1) = (a/2)\left(3n^2 + 5n + 2\right)$$

$$\Theta(C(a_{\text{even}},n),x) = (a/2)\left(2(n+1) \cdot x^{2(n+1)} + \sum_{k=2}^{n+1} a(n+k) \cdot x^{n+k}\right)$$

$$\Theta'(C(a_{\text{even}},n),1) = (a/6)(n+1)\left(14n^2 + 25n + 12\right)$$

$$\Pi(C(a_{\text{even}},n),x) = (a/2)\left(2(n+1) \cdot x^{(a/2)\left(3n^2+5n+2\right)-2(n+1)}\right.$$

$$\left. + \sum_{k=2}^{n+1} a(n+k) \cdot x^{(a/2)\left(3n^2+5n+2\right)-(n+k)}\right.$$

$$\Pi'(C(a_{\text{even}},n),1) = CI(C(a_{\text{even}},n)) = PI_e'(C(a_{\text{even}},n),1)$$

Case: *a* Is Odd

$$\Omega(C(a_{\text{odd}},n),x) = \sum_{k=1}^{n+1} a \cdot x^{n+k}$$

$$\Omega'(C(a_{\text{odd}},n),1) = (a/2)\left(3n^2 + 5n + 2\right)$$

$$\Theta(C(a_{\text{odd}},n),x) = \sum_{k=1}^{n+1} a(n+k) \cdot x^{n+k}$$

$$\Theta'(C(a_{\text{odd}},n),1) = (a/6)(n+1)(2n+1)(7n+6)$$

$$\Pi(C(a_{\text{odd}},n),x) = \sum_{k=1}^{n+1} a(n+k) \cdot x^{(a/2)\left(3n^2+5n+2\right)-(n+k)}$$

$$\Pi'(C(a_{\text{odd}},n),1) = CI(C(a_{\text{odd}},n)) \neq PI_e'(C(a_{\text{odd}},n),1)$$

Table 9.1 Omega polynomial in hourglasses; $a = 4,5$

Omega polynomial	CI	V	E
$a = 4$; $n = 3$; $t = 0$	–	200	280
$16x + 24x^4 + 8x^6 + 8x^7 + 8x^8$	76,808		
$a = 4$; $n = 2$; $t = 2$		144	200
$8x + 32x^3 + 2x^4 + 8x^5 + 8x^6$	39,184	–	–
$a = 5$; $n = 4$; $t = 0$	–	360	510
$20x + 30x^5 + 10x^7 + 10x^8 + 10x^9 + 10x^{10}$	256,390	–	–
$a = 5$; $n = 4$; $t = 2$	–	380	540
$10x + 10x^3 + 32x^5 + 10x^7 + 10x^8 + 10x^9 + 10x^{10}$	287,760	–	–

9.5.3 Omega Polynomial in Hourglasses

Formulas to calculate Omega polynomial and derived topological descriptors, in hourglasses with $a = 4;5$ and various n and t, are given in Table 9.1, along with some examples:

$$\Omega(CC(a,n,t),x) = 2ax^1 + 6ax^{n+1} + tx^a + 2ax^{t+1} + 2a\sum_{k=1}^{n} x^{n+2+k}$$

$$\Omega'(CC(a,n,t),1) = a(3n^2 + 11n + 3t + 10)$$

$$\Omega''(CC(a,n,t),1) = 2a\big[(7/3)n^3 + 6n^2 + (11/3)n\big] + at(a-1) + 6an(n+1) + 2at(t+1)$$

$$\begin{aligned}CI(CC(a,n,t)) = {}& (a/3)\big(300a - 73n - 12t + 543an^2 \\ & + 198an^3 + 27an^4 + 27at^2 - 63n^2 \\ & - 14n^3 - 6t^2 + 660an + 177at + 198ant + 54an^2t \\ & - 30\big)\end{aligned}$$

9.6 Omega Polynomial in CorSu Lattice

The new graphene pattern, called CorSu, will be described, in the following, in terms of Omega polynomial. Composition rules for calculating the polynomial in various domains of the CorSu lattice were derived, and close formulas for regular hexagonal- and parallelogram-like domains were established.

The Omega polynomial of a graph G can be expressed by the contributions of the graph fragments F_i:

$$\Omega(G = \cup F_i) = \sum_i \Omega(F_i) + \sum_i \Omega(I(F_i))$$

where $I(F_i)$ represents the "interactions" manifested between (among) two (or more, depending of the connectivity of actual) fragments F_i, i.e., the ops strips which appear/disappear by the union of F_i. The union/composition of F_i to form the whole G can be achieved as follows:

1. The fragments F_i are united by "joining" of the involved vertices by appropriate edges; the composition is called "Jn." The reverse decomposition is allowed because the added edges represent "cut edges."
2. The fragments F_i are united by "identifying" of the actual polytopes (points, edges, faces, etc.); the composition is now symbolized by "Id." The reverse decomposition is not allowed because there are no "cut edges"; the fragments are not "real" ones but "precursors" of the target G.

Examples of union by identification are given in Fig. 9.5.

The edge- and vertex-type (of degree three) interactions are derived as shown in Table 9.2.

Now, we are ready to design composition rules for various domains defined on the *CorSu* lattice: any kind of domains can be described, but we will focus on the regular hexagonal h and parallelogram $p(a,a)$ ones, in view of finding some close formulas for the Omega polynomial. Table 9.3 provides some examples; herein, u refers to the repeating unit of *CorSu* lattice, while Su is just the sumanene associate graph. The prefix of fragment name gives the number of consisting units u, while the (subscript) suffix indicates the domain type. For the sake of simplicity, we can use only the suffixes, e.g., in the case of parallelogram-like domains.[29]
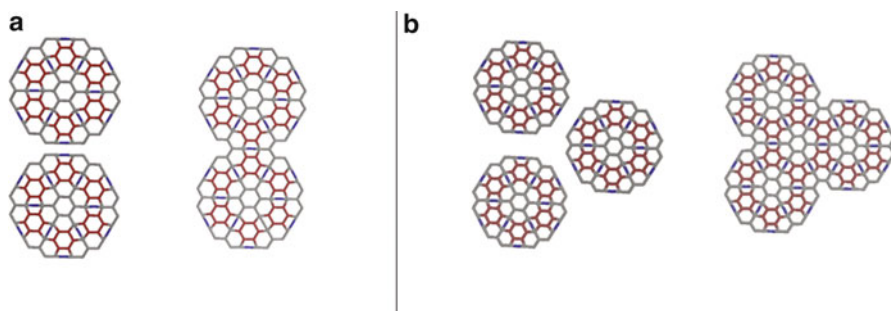
Fig. 9.5 Interactions in CorSu graphene: edge-type A (*left*) and vertex-type B (*right*)

Table 9.2 Edge- and vertex-type interactions A and B, respectively, in CorSu

G	Omega(G,x)	CI	Interaction
U	$24x + 12x^2 + 24x^3 + 3x^6$	18,648	–
$15u$	$298x + 56x^2 + 320x^3 + 96x^6$	3,780,058	–
$16u(1e)$	$320x + 64x^2 + 346x^3 + 99x^6$	4,319,146	1A
$16u(2e)$	$318x + 60x^2 + 342x^3 + 102x^6$	4,302,468	2A + B
$16u(3e)$	$316x + 56x^2 + 338x^3 + 105x^6$	4,285,822	3A + 2B

Table 9.3 Omega polynomial composition rules

Unit	Composition
$A = -2x - 4x^2 + 2x^3$	
$B = -6x^3 + 3x^6$	
$Su = 6x^1 + 6x^2 + 3x^3$	
$u = 24x^1 + 12x^2 + 24x^3 + 3x^6$	
$7CorSu_1 = 144x^1 + 36x^2 + 156x^3 + 39x^6$	$u = 6Su + 6A + B$
$19CorSu_2 = 372x^1 + 60x^2 + 396x^3 + 129x^6$	$7CorSu_1 = (u + 6u) + 12A + 6B$
$37CorSu_3 = 708x^1 + 84x^2 + 744x^3 + 273x^6$	$19CorSu_2 = (7CorSu_1 + 12u) + 30A + 18B$
	$37CorSu_3 = (19CorSu_2 + 18u) + 48A + 30B$
Examples (hexagonal domain), $CorSu_h$	$61CorSu_4 = (37CorSu_3 + 24u) + 66A + 42B$
	$9CorSu = 7CorSu_1 + 2u + 2B + 4A$
	$22CorSu = 19CorSu_2 + 3u + 4B + 7A$
Examples (parallelogram domain), $CorSu_{p(a,b)}$	$4CorSu_{p(2,2)} = 4u + 2B + 5A$
	$9CorSu_{p(3,3)} = 9u + 8B + 16A$
	$p(3,3) = p(3,2) + p(3,1) + 4B + 5A$

Table 9.4 Interaction of fragments in irregular domains of CorSu

G	$Omega(G,x)$	CI	Interaction
U	$24x + 12x^2 + 24x^3 + 3x^6$	18,648	–
$15u$	$298x + 56x^2 + 320x^3 + 96x^6$	3,780,058	–
$16u(1e)$	$320x + 64x^2 + 346x^3 + 99x^6$	4,319,146	1A
$16u(2e)$	$318x + 60x^2 + 342x^3 + 102x^6$	4,302,468	2A + B
$16u(3e)$	$316x + 56x^2 + 338x^3 + 105x^6$	4,285,822	3A + 2B

For the two domains of interest, we derived the formulas:

$$\Omega(M_{h,k}) = [\Omega(M_{h,k-1}) + 6k\Omega(M_{h,0})] + 6(3k-1)A + 6(2k-1)B$$

$$\Omega(M_{p(a,a)}) = a^2 \cdot u + (a-1)(3a-1)A + 2(a-1)^2 B$$

Note that $M_{h,0}$ is just the unit u, $k =1,2,3,\ldots$ while the other symbols are as above.

In the case of irregular domains, the polynomial does not depend on the position of fragment link but of the type of location of the newly added unit, as exemplified in Table 9.2. There are three possible locations, according of the number of (super-) edges involved, $(1e)$, $(2e)$, and $(3e)$, and the interactions are described in Table 9.4.

9.7   Conclusions

Two graphene structural modifications were presented in this chapter: the cones and CorSu (coronene-sumanene) lattice. Topology of these modified graphenes was given in terms of several counting polynomials: Omega, PI_v, PI_e, SZ_v, and

corresponding topological indices. Analytical formulas were derived either by numerical analysis or by following the cutting procedure. In the case of CorSu lattice and Omega polynomial, fragmental composition rules were established. Numerical examples were also given.

References

Abouimrane A, Compton OC, Amine K, Nguyen ST (2010) Non − annealed graphene paper as a binder − free anode for lithium − iron batteries. J Phys Chem C 114:12800–12804

Alipour MA, Ashrafi AR (2009) A numerical method for computing the Wiener index of one − heptagonal carbon nanocone. J Comput Theor Nanosci 6:1204–1207

Ashrafi AR, Gholaminezhad F (2008) The edge Szeged index of one − pentagonal carbon nanocones. Int J Nanosci Nanotechnol (IJNN) 4:135–138

Ashrafi AR, Gholaminezhad F (2009) The PI and edge Szeged indices of one − heptagonal carbon nanocones. Curr Nanosci 5:51–53

Ashrafi AR, Manoochehrian B, Yousefi − Azari H (2006) On the PI polynomial of a graph. Util Math 71:97–108

Clar E (1964) Polycyclic hydrocarbons. Academic, London

Clar E (1972) The aromatic sextet. Wiley, New York

Das B, Prasad KE, Ramamurty U, Rao CNR (2009) Nano − indentation studies on polymer matrix composites reinforced by few − layer graphene. Nanotechnology 20:25705

Denis PA (2009) Density functional investigation of thioepoxidated and thiolated graphene. J Phys Chem C 113:5612–5619

Diudea MV (2006) Omega polynomial. Carpath J Math 22:43–47

Diudea MV (2010a) Omega polynomial: composition rules in CorSu lattice. Int J Chem Model 2 (4):1–6

Diudea MV (2010b) Counting polynomials and related indices by edge cutting procedures. MATCH Commun Math Comput Chem 64:569–590

Diudea MV, Ilić A (2009) CorSu network − a new graphene design. Studia Univ "Babes − Bolyai" Chemia 54(4):171–177

Diudea MV, Cigher S, John PE (2008) Omega and related counting polynomials. MATCH Commun Math Comput Chem 60:237–250

Diudea MV, Cigher S, Vizitiu AE, Florescu MS, John PE (2009) Omega polynomial and its use in nanostructure description. J Math Chem 45:316–329

Djoković D (1973) Distance preserving subgraphs of hypercubes. J Combin Theory Ser B 14:263–267

Ebbesen TW (1998) Cones and tubes: geometry in the chemistry of carbon. Acc Chem Res 31:558–566

Eda G, Unalan HE, Rupesinghe N, Amaratunga GAJ, Chhowalla M (2008) Field emission from graphene based composite thin films. Appl Phys Lett 93:233–502

Geim AK, Novoselov KS (2007) The rise of graphene. Nat Mater 6:183–191

Green AA, Hersam MC (2009) Solution phase production of graphene with controlled thickness via density differentiation. Nano Lett 9:4031–4036

Gutman I (1994) A formula for the Wiener number of trees and its extension to graphs containing cycles. Graph Theory Notes N Y 27:9–15

Ilić A, Diudea MV, Gholami − Nezhaad F, Ashrafi AR (2010) Topological indices in nanocones. In: Gutman I, Furtula B (eds) Novel Molecular structure descriptors − theory and applications. Univ Kragujevac, Kragujevac, pp 217–226

John PE, Vizitiu AE, Cigher S, Diudea MV (2007) CI index in tubular nanostructures. MATCH Commun Math Comput Chem 57:479–484

Khadikar PV (2000) On a novel structural descriptor PI. Nat Acad Sci Lett 23:113–118

Khalifeh MH, Yousefi − Azari H, Ashrafi AR (2008) Vertex and edge PI indices of cartesian product graphs. Discret Appl Math 156:1780–1789

Klavžar S (2008a) Some comments on co graphs and CI index. MATCH Commun Math Comput Chem 59:217–222

Klavžar S (2008b) A bird's eye view of the cut method and a survey of its applications in chemical graph theory. MATCH Commun Math Comput Chem 60:255–274

Krishnan A, Dujardin E, Treacy MMJ, Hugdahl J, Lynum S, Ebbesen TW (1997) Graphitic cones and the nucleation of curved carbon surfaces. Nature 388:451–454

Lee G, Lee B, Kim J, Cho K (2009) Ozone adsorption on graphene: ab initio study and experimental validation. J Phys Chem C 113:14225–14229

Ng YH, Lightcap IV, Goodwin K, Matsumura M, Kamat PV (2010) To what extent do graphene scaffolds improve the photovoltaic and photocatalytic response of TiO_2 nanostructured films. J Phys Chem Lett 1:2222–2227

Novoselov KS, Geim AK, Morozov SV, Jiang D, Zhang Y, Dubonos SV, Grigorieva IV, Firsov AA (2004) Electric field effect in atomically thin carbon films. Science 306:666–669

Okamoto Y, Miyamoto Y (2001) Ab initio investigation of physisorption of molecular hydrogen on planar and curved graphenes. J Phys Chem B 105:3470–3474

Paci JT, Belytschko T, Schatz GC (2007) Computational studies of the structure, behavior upon heating, and mechanical properties of graphite oxide. J Phys Chem C 111:18099–18111

Seger B, Kamat PV (2009) Electrocatalytically active graphene − platinum nanocomposites. Role of 2 − D carbon support in PEM fuel cells. J Phys Chem C 113:7990–7995

Stankovich S, Dikin DA, Dommett GHB, Kohlhaas KM, Zimney EJ, Stach EA, Piner RD, Nguyen ST, Ruoff RS (2006) Graphene − based composite materials. Nature 442:282–286

Tylianakis E, Psofogiannakis GM, Froudakis GE (2010) Li − doped pillared graphene oxide: a graphene − based nanostructured material for hydrogen storage. J Phys Chem Lett 1:2459–2464

Ueta A, Tanimura Y, Prezhdo OV (2010) Distinct infrared spectral signatures of the 1,2 − and 1,4 − fluorinated single − walled carbon nanotubes: a molecular dynamics study. J Phys Chem Lett 1:1307–1311

Viculis LM, Mack JJ, Kaner RB (2003) A chemical route to carbon nanoscrolls. Science 299:1361

Vizitiu AE, Diudea MV (2006) Conetori of high genera. Studia Univ "Babes − Bolyai" Chemia 51:39

Wang Y, Shi ZQ, Huang Y, Ma YF, Wang CY, Chen MM, Chen YS (2009a) Supercapacitor devices based on graphene materials. J Phys Chem C 113:13103–13107

Wang S, Tang LA, Bao Q, Lin M, Deng S, Goh BM, Loh KP (2009b) Room − temperature synthesis of soluble carbon nanotubes by the sonication of graphene oxide nanosheets. J Am Chem Soc 131:16832–16837

Watcharotone S, Dikin DA, Stankovich S, Piner R, Jung I, Dommett GHB, Evmenenko G, Wu SE, Chen SF, Liu CP (2007) Graphene − silica composite thin films as transparent conductors. Nano Lett 7:1888–1892

Wiener H (1947) Structural determination of the paraffin boiling points. J Am Chem Soc 69:17–20

Winkler P (1984) Isometric embedding in products of complete graph. Discret Appl Math 7:221–225

Xie X, Ju L, Feng X, Sun Y, Zhou R, Liu K, Fan S, Li Q, Jiang K (2009) Controlled fabrication of high − quality carbon nanoscrolls from monolayer graphene. Nano Lett 9:2565–2570

Yu DS, Dai LM (2010) Self − assembled graphene/carbon nanotube hybrid films for supercapacitors. J Phys Chem Lett 1:467–470

Chapter 10
Hosoya Index of Splices, Bridges, and Necklaces

Tomislav Došlić and Reza Sharafdini

Abstract The Hosoya index $Z(G)$ of a graph G is the total number of matchings in G. We present explicit formulas for the Hosoya indices of several classes of graphs that arise from simpler graphs by repeating application of two simple operations.

10.1 Introduction

In this article we are concerned with simple graphs, that is, finite and undirected graphs without loops and multiple edges. We also assume that our graphs are connected, unless explicitly stated otherwise. Let G be such a graph, and let $V(G)$ and $E(G)$ be its vertex set and edge set, respectively. The edge of G connecting the vertices u and v will be denoted by uv.

A molecular graph is a simple graph, such that its vertices correspond to the atoms and its edges to the bonds of a given molecule (the hydrogen atoms are often omitted). A topological index of a molecular graph G is a numeric quantity related to G which is invariant under the symmetry properties of G.

Two edges of a graph G are said to be *independent* if they possess no vertex in common. Any subset of $E(G)$ containing no two mutually incident edges is called an *independent edge set* or a *matching*. The *Hosoya index* of a graph G is defined as the total number of matchings in G and denoted by $Z(G)$. Hence,

T. Došlić (✉)
Faculty of Civil Engineering, University of Zagreb, Kačićeva 26, 10000 Zagreb, Croatia
e-mail: doslic@grad.hr

R. Sharafdini
Department of Mathematics, Faculty of Basic Sciences, Persian Gulf University, Bushehr 75169, Iran
e-mail: sharafdini@pgu.ac.ir

$$Z(G) = \sum_{k \geq 0} m(G; k),$$

where $m(G; k)$ denotes the number of matchings of size k. Clearly, $m(G; 0) = 1$ and $m(G; 1) = |E(G)|$. The Hosoya index was introduced by Hosoya (Hosoya 1971) in 1971 and was investigated for correlations with boiling points, entropies, and calculated bond orders as well as for coding of chemical structures (Cyvin and Gutman 1988; Gutman et al. 1989; Turker 2003). For more information on topological indices and other molecular descriptors, we refer the reader to Todeschini and Consonni (2000).The citations for Cyvin et al. (1988), Gutman (1989) has been changed to Cyvin and Gutman (1988), Gutman et al. (1989) as per the reference list. Please check if okay.It is OK.

For a vertex v of a graph G, we denote by $N_G(v)$ the set of its neighbors in G, i.e., $N_G(v) = \{u \in V(G) | uv \in E(G)\}$. For $W \subseteq V(G)$, we denote by $G - W$ the subgraph of G obtained by deleting the vertices of W and the edges incident with them. Similarly, if $E_0 \subseteq E(G)$, we denote by $G - E_0$ the subgraph of G obtained by deleting the edges of E_0. When W or E_0 are singletons, we write simply $G - v$ and $G - uv$ instead of $G - \{v\}$ and $G - \{uv\}$, respectively.

Many graphs can be constructed from simpler graphs via certain operations called graph products. We will consider here two such classes of graphs.

Let G_1 and G_2 be two graphs with disjoint vertex sets. Following Došlić (2005), for given vertices $u \in V(G_1)$ and $v \in V(G_2)$, we define the *splice* of G_1 and G_2 by vertices u and v (denoted by $(G_1 \bullet G_2)(u, v)$) by identifying the vertices u and v in the union of G_1 and G_2.

There are several ways of extending the above definition to the case of more than two graphs. Some of them lead to the cactus graphs, but we do not consider them here. Instead, we restrict our attention to the case when in each G_i we chose a vertex v_i and then identify all v_i, for $i = 1, \ldots, n$. We denote so obtained graph by $\prod_{i=1}^{n} G_i(v_i)$ and call it the *bouquet* of $G_1, \ldots, G_n$. When $G_1 = \ldots = G_n$ and all v_i are the same, we say that $G^n(v) = \prod_{i=1}^{n} G(v_i)$ is the *n*-th *splice power* of G with respect to v. A splice of two graphs and the fourth splice power of a graph are shown in Fig. 10.1.
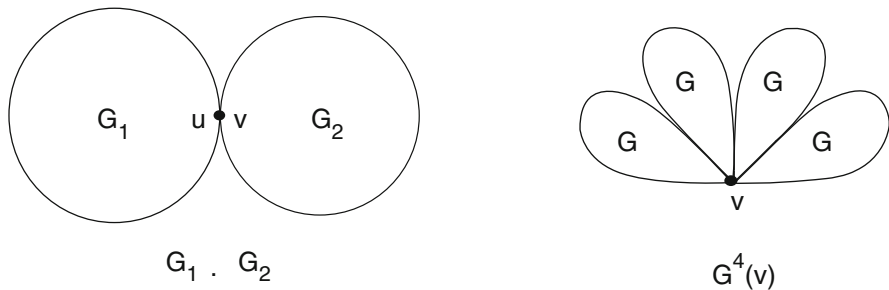
Fig. 10.1 The splice of two graphs and the fourth splice power of a graph
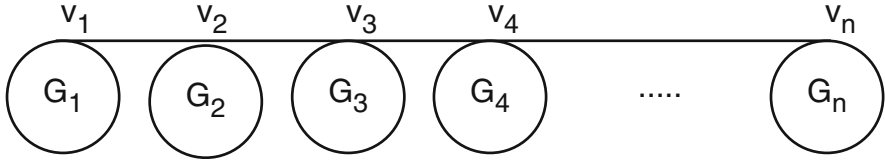
Fig. 10.2 The bridge graph

Let $\{G_i\}_{i=1}^n$ be a set of finite pairwise disjoint graphs with $v_i \in V(G_i)$. The *bridge graph*

$$B(G_1, G_2, \ldots, G_n; v_1, v_2, \ldots, v_n),$$

of $G_1, \ldots, G_n$ with respect to the vertices $\{v_i\}_{i=1}^n$ is the graph obtained from the graphs $G_1, \ldots, G_n$ by connecting the vertices v_i and v_{i+1} by an edge for all $i = 1, 2, \ldots, n-1$ (see Fig 10.2). In the case $n = 2$, we denote $B(G_1, G_2; v_1, v_2)$ by $(G_1 \sim G_2)(v_1, v_2)$ and call it the *link* of G_1 and G_2 (with respect to v_1 and v_2).

When $G_1 = \cdots = G_n = G$ and $v_1 = \cdots = v_n = v$, the graph $B(G, \ldots, G; v, \ldots, v)$ is the *rooted product* of P_n, the path on n vertices, and G with respect to v, since it can be obtained by identifying the vertex v in the i-th copy of G with the i-th vertex of P_n. We call such a graph an *open G-necklace* of length n. The *closed G-necklace* of the same length is obtained by adding the edge between the v-vertices in the first and the n-th copy of G; it is the rooted product of C_n and G with respect to v.

It is a well-known folklore result that the Hosoya index of the path P_n on n vertices is given by F_{n+1}, the $(n+1)$-st Fibonacci number. The Fibonacci numbers will appear repeatedly in subsequent sections; we refer the reader to the monograph (Koshy 2001) for more background.

For the cycle C_n, we have $Z(C_n) = L_n$, the n-th Lucas number, while $Z(K_{1,m}) = m + 1$. Some topological indices of bridge and splice graphs were computed in Ashrafi et al (2011), Mansour and Schork (2010), and Sharafdini and Gutman (2013). In this paper we aim to compute the Hosoya index for these graphs. We will need the following well-known results (see Gutman and Polansky (1986)):

Lemma 10.1 Let G be a graph with k components $G_1, G_2, \ldots, G_k$. Then

$$Z(G) = \prod_{i=1}^k Z(G_i).$$

Lemma 10.2 Let G be a graph, and let $uv \in E(G)$ and $u \in V(G)$. Then

(i) $Z(G) = Z(G - uv) + Z(G - \{u, v\})$;

(ii) $Z(G) = Z(G-u) + \sum_{w\in N_G(u)} Z(G-\{u,w\})$. In particular, when v is a pendent vertex of G and u is the unique vertex adjacent to v, we have

$$Z(G) = Z(G-v) + Z(G-\{u,v\}).$$

10.2 Main Results

In this section we establish explicit formulas for the Hosoya indices of splices, splice powers, links, bridges, and open and closed necklaces. We consider the splice operation first and then proceed to links, bridges, and necklaces.

10.2.1 Splices and Splice Powers

We begin by stating an auxiliary result for a splice of two graphs. As it follows directly from Lemma 10.1, we omit the proof.

Lemma 10.3 Let G_1 and G_2 be two graphs and $u\in V(G_1)$, $v\in V(G_2)$. Let $G = (G_1 \bullet G_2)(u,v)$ and $uw\in E(G)$. Then

$$Z(G-\{u,w\}) = Z(G_2-v)Z(G_1-\{u,w\})$$

if $w\in V(G_1)$, and

$$Z(G-\{u,w\}) = Z(G_1-u)Z(G_2-\{v,w\})$$

if $w\in V(G_2)$.

Now we can derive the formula for the Hosoya index of a splice of two graphs in terms of Hosoya indices of its components.

Theorem 10.4 Let G_1 and G_2 be two graphs with $u\in V(G_1)$ and $v\in V(G_2)$. Assuming that $G = (G_1 \bullet G_2)(u,v)$, we have

$$\begin{aligned} Z(G) = \quad &Z(G_1)Z(G_2-v) + Z(G_2)Z(G_1-u) \\ &-Z(G_1-u)Z(G_2-v). \end{aligned}$$

Proof It is clear that $G-u = (G_1-u)\cup(G_2-v)$, and so

$$Z(G-u) = Z(G_1-u)Z(G_2-v).$$

On the other hand, it follows from Lemma 10.3 that

$$\sum_{w \in N_G(u)} Z(G - \{u, w\}) = \sum_{w \in N_{G_2}(v)} Z(G_1 - u)Z(G_2 - \{v, w\})$$

$$+ \sum_{w \in N_{G_1}(u)} Z(G_2 - v)Z(G_1 - \{u, w\}).$$

Hence by Lemma 10.2,

$$Z(G) = Z(G - u) + \sum_{w \in N_G(u)} Z(G - \{u, w\}).$$

By substituting $Z(G - u)$ and $\sum_{w \in N_G(u)} Z(G - \{u, w\})$ in the above formula, we have

$$Z(G) = \ Z(G_2 - v)\left(Z(G_1 - u) + \sum_{w \in N_{G_1}(u)} Z(G_1 - \{u, w\})\right)$$

$$+ Z(G_1 - u)\left(Z(G_2 - v) + \sum_{w \in N_{G_2}(v)} Z(G_2 - \{v, w\})\right)$$

$$- Z(G_1 - u) \ Z(G_2 - v).$$

It follows from Lemma 10.2 (ii) that

$$Z(G) = Z(G_1)Z(G_2 - v) + Z(G_2)Z(G_1 - u) - Z(G_1 - u)Z(G_2 - v).$$

By an analogous reasoning, one could also derive formulas for the Hosoya index of a bouquet of several graphs. In order to keep the notation simple, we state just the result for the splice powers.

Theorem 10.5 Let $G^n(v)$ be the n-th splice power of G with respect to v. Then

$$Z(G^n(v)) = Z(G - v)^{n-1}\left[Z(G) + (n - 1)\sum_{w \in N_G(v)} Z(G - v - w)\right].$$

Proof All matchings that do not cover v are counted by $Z(G - v)^n$, while those that do cover v by an edge in, say, the first copy of G are counted by $Z(G - v)^n \sum_{w \in N_G(v)} Z(G - v - w)$. As all n copies of G enter $G^n(v)$ symmetrically, the total number of matchings that cover v is n times greater and is equal to $nZ(G - v)^n \sum_{w \in N_G(v)} Z(G - v - w)$. The claim now follows by adding the above quantities and factorizing the resulting expression.

If the vertex v is pendent in G, the above formula is simplified to

$$Z(G^n(v)) = Z(G - v)^{n-1}\Big[Z(G) + (n-1)^2 Z(G - v - w)\Big],$$

where w is the only neighbor of v in G. As an example, we consider the graph $P_m^n(v)$, where v is an end-vertex of a path P_m on m vertices. From the above theorem and the fact that $Z(P_m) = F_{m+1}$, we obtain the following result:

Corollary 10.6

$$Z\big(P_m^n(v)\big) = F_m^{n-1}\Big[F_{m+1} + (n-1)^2 F_{m-1}\Big].$$

For $n = 2$ we recover the well-known identity $F_{2m} = F_m(F_{m-1} + F_{m+1})$. Other identities for Fibonacci numbers can be established by concatenating (i.e., splicing by their end-vertices) two paths of different lengths.

10.2.2   Links, Bridges, and Necklaces

Again, we settle first the case of only two graphs.

Theorem 10.7 Let G_1 and G_2 be two graphs with $u \in E(G_1)$ and $v \in E(G_2)$. Then

$$Z((G_1 \sim G_2)(u,v)) = Z(G_1)Z(G_2) + Z(G_1 - u)Z(G_2 - v).$$

Assuming that $G := (G_1 \sim G_2)(u,v)$, it is obvious that $G - uv = G_1 \cup G_2$ and

$$G - \{u,v\} = (G_1 - u) \cup (G_2 - v).$$

Therefore, by Lemma 10.1 we have

$$Z(G - uv) = Z(G_1)Z(G_2)Z(G - \{u,v\}) = Z(G_1 - u)Z(G_2 - v).$$

Thus by Lemma 10.2, we have

$$\begin{aligned}Z(G) &= Z(G - uv) + Z(G - \{u,v\}) \\ &= Z(G_1)Z(G_2) + Z(G_1 - u)Z(G_2 - v).\end{aligned}$$

As an example, we take two paths, P_{m-1} and P_{n-m}, and link them by connecting an end-vertex of one path to an end-vertex of the other. Then the above theorem returns us another well-known identity for Fibonacci numbers,

$$F_n = F_m F_{n-m+1} + F_{m-1} F_{n-m}.$$

(e.g., see Koshy (2001), p.88). Additional identities for Fibonacci and Lucas numbers could be obtained by considering links of two cycles. Another way to

obtain interesting identities would be to link an end-vertex of one path to an internal vertex of another path or to a vertex of a cycle.

Let us now consider an open G-necklace of length n and denote it by G_n. We denote its Hosoya index by z_n, i.e., $z_n = Z(G_n)$. Now, consider the edge e connecting the n-th and the $(n-1)$-th copy of G in G_n. A matching in G_n either contains e or does not contain it. It is easy to see that there are exactly $Z(G-v)^2 z_{n-2}$ matchings that contain e and $Z(G)z_{n-1}$ matchings that do not contain it. That leads to the two-term recurrence for z_n:

$$z_n = \alpha z_{n-1} + \beta^2 z_{n-2},$$

where $\alpha = Z(G)$ and $\beta = Z(G-v)$. The initial conditions are $z_0 = 1$ and $z_1 = \alpha$. Hence the sequence $(z_n)_{n\geq0}$ is a Horadam sequence with parameters $(\alpha, \beta^2; \alpha, 1)$. We could, in principle, write down an explicit formula for z_n; however, the resulting expressions are neither very elegant nor very informative. Instead, we prefer to express the sequence (z_n) by its generating function. It can be derived in a standard way and we leave out the computational details.

Theorem 10.8 Let z_n be the Hosoya index of an open G-necklace of length n. Then its generating function $z(x)$ is given by

$$z(x) = \sum_{n\geq0} z_n x^n = \frac{1}{1 - \alpha x - \beta^2 x^2}.$$

From the generating function, we can deduce the asymptotic behavior of z_n for large n. It is given by $z_n \sim \xi^{-n}$, where ξ is the smallest positive solution of the equation $1 - \alpha x - \beta^2 x^2 = 0$.

Corollary 10.9

$$z_n \sim \left[\frac{\alpha}{2\beta^2} \left(\sqrt{1 + \left(\frac{2\beta}{\alpha}\right)^2} - 1 \right) \right]^{-n}.$$

An interesting special case is when the number of matchings in G is close to the number of matchings in $G - v$, i.e., when $\alpha \approx \beta$. In that case we obtain that $\xi \approx \varphi^{-\alpha}$, where $\varphi = \frac{\sqrt{5}+1}{2}$ is the golden section. Hence, for such graphs we have $z_n \sim (\varphi \cdot Z(G))^n$. The assumption $\alpha \approx \beta$ is not unrealistic. By taking $G = K_{1,m}$ with any pendent vertex as the root, we obtain $\frac{\beta}{\alpha} = \frac{m}{m+1}$, and that can be made arbitrarily close to 1 (see Fig. 10.3).

Fig. 10.3 A necklace with $\alpha \approx \beta$

Fig. 10.4 A necklace with $Z(G_n) = F_n(4)$

Another interesting case appears when $\beta = 1$. As each graph contains at least one matchings, the empty one, the above case can happen only when $G - v$ is a trivial graph, i.e., a graph without edges. That, in turn, means that $G = K_{1,m}$ for some $m \geq 0$ and that G_n is a necklace of stars with their central vertices as roots. Now z_n can be expressed as the sequence of values of Fibonacci polynomials at m. The *Fibonacci polynomials* $F(x)$ are defined recursively by $F_0(x) = 1$, $F_1(x) = x$, and $F_n(x) = xF_{n-1}(x) + F_{n-2}(x)$ for $n \geq 2$. The first few polynomials are $F_2(x) = x^2 + 1$, $F_3(x) = x^3 + 2x$, $F_4(x) = x^4 + 3x^2 + 1$, and, generally,

$$F_n(x) = \sum_{n/2}^{k=0} \binom{n-k}{k} x^{n-2k}.$$

One can easily see that $F_n(1) = F_{n+1}$. Again, we refer the reader to Koshy (2001) for more properties of Fibonacci polynomials. (Fig. 10.4)

Corollary 10.10 Let G_n be an open $K_{1,m}$-necklace of length n. Then $z_n = F_n(m + 1)$, where $F_n(x)$ is the n-th Fibonacci polynomial.

For $m = 0$ the $K_{1,0}$-necklace becomes the path P_n, and the above result reduces to $Z(P_n) = F_n(1) = F_{n+1}$. For $m = 1$ the necklace is known as the comb graph, and its Hosoya index is $F_n(2)$, the $(n + 1)$-st *Pell number*.

An obvious consequence of the above result is the following lower bound on the Hosoya index of any open G-necklace.

Corollary 10.11 Let G_n be an open G-necklace. Then $Z(G_n) \geq F_{n+1}$.

We invite the reader to obtain the analogous results for closed necklaces. The case of bridge graphs could be treated in a similar way, but the results are less elegant. The Hosoya indices of bridge graphs still satisfy two-term recurrences, but the coefficients are, generally, nonconstant. As an illustration, we consider the bridge graph formed by taking $G_i = K_{1,i-1}$ rooted at their central vertex. The recurrence for the Hosoya indices is $z_n = nz_{n-1} + z_{n-2}$, with the initial conditions $z_0 = z_1 = 1$. The first few terms are $1, 1, 3, 10, 43, 225, 1393, \ldots$. This sequence appears as entry A001040 in the *On-Line Encyclopedia of Integer Sequences* (OEIS); there we can learn that z_n can be expressed in terms of combinations of values of modified Bessel functions and that its asymptotic behavior is given by $z_n \sim I_0(2)n!$. Hence, its Hosoya index has factorial growth (see Fig. 10.5). However, if we modify our bridge by rooting G_is at their pendent vertices, the sequence satisfying the resulting recurrence $z_n = nz_{n-1} + (n-1)(n-2)z_{n-2}$ cannot be found in OEIS.
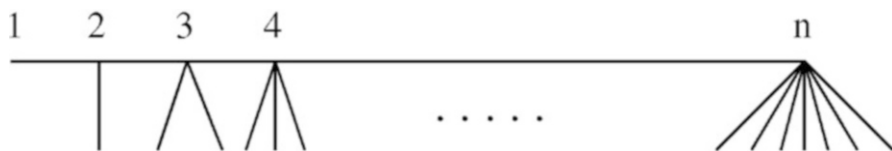
Fig. 10.5 A bridge graph with factorial growth of the Hosoya index

10.3   Concluding Remarks

In this paper we have considered two classes of graphs that arise via two simple operations. In spite of their simplicity, both of them could serve as useful models for many interesting structures. The techniques we used here could be applied also to some other classes of composite graphs. For example, the results for necklaces can be generalized to the rooted products of more general graphs. Another possible direction of research could be to first compute the Hosoya index for the suspension of a graph (i.e., for the join of G and K_1), and then use our results for rooted products to obtain formulas for the Hosoya indices of the corona product of two graphs.

Let G be a graph such that $V(G) = \{v_1, \ldots, v_n\}$. Let us denote the join of G and K_1 by G^*. It follows from Lemma 10.2 that

$$Z(G^*) = Z(G) + \sum_{i=1}^{n} Z(G - \{v_1, \ldots, v_i\}).$$

Applying this formula to a wheel graph W_n of n vertices, we obtain a formula for $Z(W_n)$ as follows:

$$Z(W_n) = L_{n-1} + (n-1)F_n.$$

It would be also interesting to have some information on the Hosoya indices of the Cartesian product of two or more graphs, as well as for some other products described in Imrich and Klavžar (2000).

References

Ashrafi AR, Hamzeh A, Hossein-Zadeh S (2011) Calculation of some topological indices of splices and links of graphs. J Appl Math Inform 29:327–335

Cyvin SJ, Gutman I (1988) Hosoya index of fused molecules. MATCH Commun Math Comput Chem 23:89–94

Došlić T (2005) Splices, links and their degree-weighted Wiener polynomials. Graph Theory Notes NY 48:47–55

Gutman I, Polansky OE (1986) Mathematical concepts in organic chemistry. Springer, Berlin

Gutman I, Kolaković N, Cyvin SJ (1989) Hosoya index of some polymers. MATCH Commun Math Comput Chem 24:105–117

Hosoya H (1971) Topological index, a newly proposed quantity characterizing the topological nature of structural isomers of saturated hydrocarbons. Bull Chem Soc Jpn 44:2332–2339

Imrich W, Klavžar S (2000) Product graphs: structure and recognition. Wiley, New York

Koshy T (2001) Fibonacci and Lucas numbers with applications. Wiley, New York

Mansour T, Schork M (2010) Wiener, hyper-Wiener, detour and hyper-detour indices of bridge and chain graphs. J Math Chem 47:72–98

Sharafdini R, Gutman I (2013) Splice graphs and their topological indices. Kragujevac J Sci 35:89–98

The Online Encyclopedia of Integer Sequences, OEIS Foundation. http://oeis.org

Todeschini R, Consonni V (2000) Handbook of molecular descriptors. Wiley, Weinheim

Turker L (2003) Contemplation on the Hosoya indices. J Mol Struct (THEOCHEM) 623:75–77

Chapter 11
The Spectral Moments of a Fullerene Graph and Their Applications

G.H. Fath-Tabar, F. Taghvaee, M. Javarsineh, and A. Graovac

Abstract A $(k,6)$-fullerene graph is a planar *3*-regular graph with *k*-polygon faces. In this chapter, we are going to obtain spectral moments of $(k,6)$-fullerene graph for $k = 3,4,5$ and use them for calculating the Estrada index of these graphs.

11.1 Introduction and Definitions

A simple *planar graph* is the graph that can be drawn in the plane such that edges do not cross. A *fullerene graph* is a planar *3*-regular graph with only pentagonal and hexagonal faces. The fullerenes are known as *(5,6)*-fullerene too. An *IPR fullerene* is a fullerene in which no two pentagons share an edge. Since the discovery of the fullerenes (Kroto et al. 1985, 1993), the fullerenes have been the object of interest of scientists all over the world. A *(3,6)-fullerene*, F_n, (Fig. 11.1), is a planar *3*-regular graph with only triangle and hexagonal faces. From Euler's theorem, it is straightforward to show that a *(3,6)*-fullerene molecule with *n* carbon atoms, C_n, has exactly 4 triangles and $n/2-2$ hexagons. A *(4,6)-fullerene* graph is a planar *3*-regular graph with only C_4 and C_6 faces, and similar to *(3,6)*-fullerene, it is easy to see that a *(4,6)*-fullerene molecule with *n* atoms, G_n, has exactly 6 squares and $n/2-4$ hexagons. An *ISR (4,6)-fullerene* is one for which no two squares share an edge (*ISR*: isolated square rule) (for more information about fullerene, see Fowler and Manolopoulos 1995; Myrvold et al. 2007; Balasubramanian 1994; Fath-Tabar et al. 2012). In this chapter, we are going to calculate the spectral moments of fullerenes and find an upper and lower bound for their Estrada index.

G.H. Fath-Tabar (✉) • F. Taghvaee • M. Javarsineh
Department of Pure Mathematics, Faculty of Mathematical Sciences, University of Kashan, Kashan 87317-51167, Iran
e-mail: fathtabar@kashanu.ac.ir

A. Graovac
The Rugjer Boskovic Institute, NMR Center, HR-10002 Zagreb, 180, Croatia

Let G be a simple graph and $\{v_1,\ldots,v_n\}$ be the set of all vertices of G. The adjacency matrix $A(G)$ of G is a (*0–1*) matrix $A(G) = [a_{ij}]_{n \times n}$, where a_{ij} is the number of edges connecting v_i and v_j. A *walk* in a simple graph is a sequence of vertices and edges $v_0 e_1 v_1 e_2 v_3 \ldots$ such that any two consecutive vertices are adjacent and $e_i = v_{i-1} v_i$. A *closed walk* is a walk in which the first and the last vertex are the same. The *spectrum of the graph G* is the set of eigenvalues of $A(G)$, together with their multiplicities (Cvetković et al. 1995; Cvetković and Stevanković 2004). An n-vertex graph has exactly n real eigenvalues $\lambda_1 \leq \lambda_2 \ldots \leq \lambda_n$. The *spectral moments* $Sm(G,k)$ and $k \geq 1$ are defined as $\sum_{i=1}^{n} \lambda_i^k$ and $Sm(G,0) = n$. The *Estrada index EE(G)* of the graph G is defined as the summation of e^{λ_i}, $1 \leq i \leq n$. By Taylor's theorem and definition, it can also be represented in terms of a series of spectral moments $EE(G) = \sum_{k \geq 0} \frac{Sm(G,k)}{k!}$. In the last 10 years, the Estrada index has found applications in measuring the degree of protein folding (Estrada 2000, 2002, 2004); the centrality of complex networks (Estrada 2007) such as social, metabolic, neural, protein−protein interaction networks; and the World Wide Web, and it was also proposed as a measure of molecular branching, accounting for the effects of all atoms in the molecule, giving higher weight to the nearest neighbors (Estrada et al. 2006). Within groups of isomers, *EE* was found to increase with the increasing extent of branching of the carbon atom skeleton (Gutman et al. 2007a, b, c). Some mathematical properties of the Estrada index and its basic computational techniques were reported in Aleksić et al. 2007; Fath−Tabar et al. 2008, 2009; Fath−Tabar and Ashrafi 2010; De La Pena et al. 2007; Gutman and Radenković 2007a, b; and Ashrafi and Fath−Tabar 2011).

11.2   The Spectral Moments of (3,6)-Fullerene and Its Applications

Suppose F_n is an arbitrary (3,6)-fullerene graph with n vertices. In this section, we find some formulas for the spectral moments $S_m(F_n,k)$. For the sake of completeness, we mention here a well-known theorem in graph theory:

Theorem 11.2.1 Suppose G is a graph with m edges, $A(G) = [a_{ij}]$ and $A^k(G) = [b_{ij}]$. The number of walks from u to v in G with length k is equal to b_{uv}. Moreover, $Tr(A) = 0$ and $Tr(A^2) = 2m$.

By Theorem 11.2.1, the number of closed walks of length k in G is then equal to $Tr(A^k) = Sm(G,k)$. Let A_n be adjacency matrix of F_n and let $\lambda_1, \lambda_2,\ldots,\lambda_n$ be the eigenvalues of A_n. Since a (3,6)-fullerene contains 4 triangles, $Tr(A_n^3) = 24$ and $Tr(A_n^2) = 3n$. Therefore, $Sm(F_n, 2) = 3n$ and $Sm(F_n,3) = 24$.

Theorem 11.2.2 $Sm(F_n, 3) = 24$ and $Sm(F_n,5) = 240$.

Proof The number of closed walks with length 3 is 24; thus, $Sm(F_n, 3) = 24$. For the second equality, by Table 11.1 Figures in F_n and associated closed walks with length 5 in first type (triangle form) is $4 \times 30 = 120$ and second type is $12 \times 10 = 120$. Therefore, the number of closed walks with length 5 is $120 + 120 = 240$.

Theorem 11.2.3 $Sm(F_n, 4) = 15n$.

Proof By Fath−Tabar and Ashrafi 2011, the number of closed walks with length 4 is $15n$.

Theorem 11.2.4 If F_n is an *ITR* (3,6)-fullerene, then $Sm(F_n, 6) = 93n$ and $Sm(F_n, 7) = 2184$.

Proof The closed walks of F_n form an edge in 1, 2, 3, 4, 5 in Table 11.2. Figures in F_n and associated closed walks with length 6 with form an edge is $3n$. Therefore, by Table 11.2, $Sm(F_n,6) = 3n + 12(n/2-2) + 4 \times 24 + 12 \times 3n + 6 (6n-12) + 12n = 93n$. The second part is similar to $Sm(F_n,5)$.

The *triangle distance* of a (3,6)-fullerene is defined as the minimum distance between all pairs of triangles in (3,6)-fullerene (Fig. 11.2).

Theorem 11.2.5 If F_n is an *ITR* (3,6)-fullerene with triangle distance at least 2, then $Sm(F_n, 8) = 578n +448$, and $Sm(F_n, 9) = 13,128$.

Table 11.1 Figures in F_n and associated closed walks

Row	Figures	The number of figures in F_n	The number of closed walks with length 5
1		4	30
2		12	10

Table 11.2 Figures in F_n and associated closed walks

Row	Figure	The number of figures in F_n	The number of closed walks with length 6
1		$n/2-2$	12
2		4	24
3		$3n$	12
4		$6n-12$	6
5		N	12
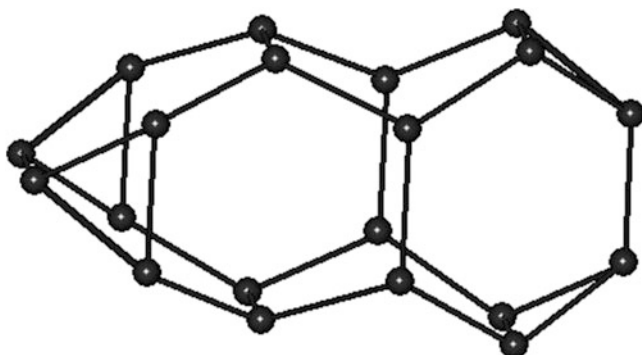
Fig. 11.2 A (*3,6*)-fullerene with triangle distance 1

Proof The proof of this theorem is similar to Theorems 11.2.2, 11.2.3, and 11.2.4.

In this part, we apply the theorems in section 1 and obtain some new estimation of Estrada index on (*3,6*)-fullerenes.

Theorem 11.2.6 There are real constants c_i, $EE(F_n) = 6 + \frac{25}{8}n + \sum_{i=1}^{n} \frac{\lambda_i^6 e^{c_i}}{6!}$.

Proof By Theorems 11.2.2, 11.2.3, and Taylor's theorem, there are real constant c_i,

$$EE(F_n)^n = n + \frac{3}{2}n + \frac{24}{6} + \frac{15}{24}n + \frac{240}{120} + \sum_{i=1}^{n} \frac{\lambda_i^6 e^{c_i}}{6!}. \text{ Thus, } EE(F_n) = 6 + \frac{25}{8}n + \sum_{i=1}^{n} \frac{\lambda_i^6 e^{c_i}}{6!}.$$

Theorem 11.2.7 If F_n is an *ITR* (*3,6*)-fullerene, then there are real numbers c_1, c_2, ..., c_n, $-3 < c_i \leq 3$, such that the Estrada index of any n-vertex (*3,6*)-fullerene can be written as:

$$EE(F_n) = \frac{291}{40}n + \frac{737}{30} + \sum_{i=1}^{n} \frac{\lambda_i^8 e^{c_i}}{8!}.$$

Proof By Theorems 11.2.1, 11.2.2, 11.2.3, 11.2.4, and a similar argument as Theorem 11.2.6, the proof is straightforward.

Theorem 11.2.8 If F_n is an *ITR* (*3,6*)-fullerene with triangle distance at least 2, then there are real numbers $c_1, c_2, \ldots, c_n$, $-3 < c_i \le 3$, such that the Estrada index of any n-vertex (*3,6*)-fullerene can be written as $EE(F_n) = \frac{9311}{1260}n + \frac{25181}{1008} + \sum_{i=1}^{n} \frac{\lambda_i^8 e^{c_i}}{8!}.$

Proof The proof is a similar argument as Theorem 11.2.7.

11.3 The Spectral Moments of (*4,6*)-Fullerene and Its Applications

A well-known theorem in linear algebra states that $Tr(A^k) = \sum_{i=1}^{n} \lambda_i^k =$ the number of closed walks in G. From now on, E_n denotes an n-vertex (*4,6*)-fullerene graph with adjacency matrix A_n. We also assume that $\lambda_1, \lambda_2, \ldots, \lambda_n$ are eigenvalues of A_n. Since a (*4,6*)-fullerene graph does not have triangles, $Tr(A_n) = Tr(A_n^3) = 0$ and $Tr(A_n^2) = 3n$. Therefore, $\sum_{i=1}^{n} \lambda_i = \sum_{i=1}^{n} \lambda_i^3 = 0$ and $\sum_{i=1}^{n} \lambda_i^2 = 3n$.

Lemma 11.3.1 $\sum_{i=1}^{n} \lambda_i^{2k-1} = 0, k \ge 1.$

Proof There is no closed walk with length $2k-1$. Thus, $\sum_{i=1}^{n} \lambda_i^{2k-1} = 0$.

Lemma 11.3.2 $\sum_{i=1}^{n} \lambda_i^4 = 15n + 48.$

Proof Every closed walk of length 4 in a (*4,6*)-fullerene with n atoms constructed from one edge, a path of length 2 or a square. Therefore, we must count the following kinds of sequences:

(a) $v_1 v_2 v_1 v_2 v_1$
(b) $v_1 v_2 v_3 v_2 v_1$
(c) $v_2 v_1 v_2 v_3 v_2$
(d) $v_1 v_2 v_3 v_4 v_1$

There are *3n* sequences of type (a), *6n* sequences of type (b), and *6n* sequences of type (c). On the other hand, a *(4,6)*-fullerene has exactly six squares. So, for counting the walks of length 4, it is enough to count sequences of the form $v_1v_2v_3v_4v_1$ where these closed walks are 48 in number. Therefore,

$$\sum_{i=1}^{n} \lambda_i^4 = 15n + 48.$$

Lemma 11.3.3 If G_n is *ISR*, then $\sum_{i=1}^{n} \lambda_i^6 = 93n + 720$ and $\sum_{i=1}^{n} \lambda_i^8 = 639n + 5040$.

Proof We apply an argument similar to that of Lemma 11.3.2 to count the number of closed walks of length 6 in G_n. Such walks are constructed from an edge, a path of length 2, a path of length 3, a star S_4, a hexagon, a square, or a square with an edge. If the v_1s are distinct vertices of the *(4,6)*-fullerene G_n, then we must count the sequences given in Table 11.3. In Table 11.3, we also give the number of walks in each case. From this table, one can see that $\sum_{i=1}^{n} \lambda_i^6 = 93n + 720$. The second part is deduced by a similar argument.

We are now ready to state the main result of our work, as follows:

Theorem 11.3.4 There are real numbers $c_1, c_2, \ldots, c_n$, $-3 < c_i \leq 3$, such that the Estrada index of vertex *ISR* *(4,6)*-fullerene G_n is computed as follows:
$EE(G_n) = \frac{91527}{8!}n + \frac{61973}{20160} + \sum_{i=1}^{n} \frac{\lambda_i^{10}e^{c_i}}{10!}$.

Corollary 11.3.5 If G_n is *ISR*, then

$$\frac{91527}{8!}n + \frac{61973}{20160} + \frac{e^{-3}(639n + 5040)}{8!} < EE(G_n) < \frac{91527}{8!}n + \frac{61973}{20160} + n\frac{e^3 3^{10}}{10!}.$$

Behmaram (Behmaram 2013) extended the notion of fullerene to *m*-generalized fullerene. By his definition, a *3*-connected cubic planar graph G is called *m*-generalized fullerene if its faces are two *m*-gons and all other pentagons and hexagons. The concepts of *m*-generalized *(3,6)*-fullerene can be defined in a similar way (Mehranian et al. 2014). From Euler's theorem, it is straightforward to show that a *(3,5,6)*-fullerene molecule with *n* atoms has exactly 2 triangles, 6 pentagons, and *n/2-6* hexagons. Let B_n be a *(3,5,6)*-fullerene molecule with *n* vertices. Then, we have the following theorem.

Theorem 11.3.6 The spectral moments of B_n, $Sm(B_n,k)$, and $3 \leq k \leq 8$ can be computed by the following formulas:

Table 11.3 The walks of length 6

Type	Sequence	No
A	$v1v2v1v2v1v2v1$	$3n$
B	$v1v2v3v2v3v3v2v1$	$18n$
C	$v2v1v2v3v2v3v2$	$18n$
D	$v1v2v3v4v3v2v1$	$12n$
E	$v2v1v2v3v4v3v2$	$12n$
F	$v1v2v3v2v4v2v1$	$12n$
G	$v2v3v2v4v2v1v2$	$12n$
H	$v1v2v3v4v5v6v1$	$6n{-}48$
K	The sequences traverse a square and one of its edges repeatedly	432
L	The sequences traverse a square with a pendent edge	288

$$Sm(B_n, 3) = 12, \ Sm(B_n, 4) = 15n, \ Sm(B_n, 5) = 180, \ Sm(B_n, 6) = 93n - 60,$$
$$Sm(B_n, 7) = 1932, \ Sm(B_n, 8) = 639n - 960.$$

Proof The proof of this theorem is obtained by (Taghvaee and Ashrafi 2016).

11.4 Estrada Index of C_n and Its Applications

The numbers of closed walks in fullerenes of lengths $4 \leq k \leq 11$ are given in the following table:

In this section, by use of Table 11.4, we are going to calculate the Estrada index of C_n and some interesting result about it.

Theorem 11.4.1 There are real numbers $c_1, c_2, \ldots, c_n, \ -3 < c_i \leq 3$, such that the Estrada index of any n-vertex fullerene can be written as $EE(C_n) = \frac{781}{240}n + \frac{7}{6} + \sum_{i=1}^{n} \frac{\lambda_i^8 e^{c_i}}{8!}$. Moreover,

$$\left(\frac{639}{8!e^3} + \frac{781}{240}\right)n + \frac{7}{6} < EE(C_n) < \left(\frac{e^3 3^4}{8!} + \frac{781}{240}\right)n + \frac{7}{6}.$$

Proof Let $F(\lambda_1, \lambda_2, \ldots, \lambda_n) = \sum_{i=1}^{n} \lambda_i^{2k}$. By Lagrange's multiplier method, the maximum of F under the boundary condition $\sum_{i=1}^{n} \lambda_i^2 = 3n$ is $n3^k$. Since $\sum_{i=1}^{n} \lambda_i^2 = 3n$,

Table 11.4 The numbers of closed walks in fullerenes of lengths $4 \leq k \leq 11$

K	Number of closed walks	k	Number of closed walks
4	15n	5	120
6	93n−120	7	1680
8	639n−1920	9	18,360
10	4653n−22,680	11	184,800

Table 11.5 The Estrada index of some fullerenes and their upper bounds

n	$EE(F_n)$	EE^*
20	66.60832800	67.05700818
24	79.69092739	80.23507649
28	93.11432441	93.41314478
30	98.77943780	100.0021789
36	118.9420270	119.7692814
40	132.0276836	132.9473497

$\sum_{i=1}^{n} \lambda_i^{2k} \leq n3^k$. The proof now follows from the last inequality, formulas for the numbers of closed walks in fullerenes for $k \leq 7$ and Taylor's theorem.

From above, $3.2549557n < EE(C_n) - 7/6 < 3.2945171n$ holds for any n-vertex fullerene, i.e., the value of $EE(C_n)$ belongs to an interval of length $0.0395614n$.

Balasubramanian computed the Laplacian eigenvalues of some small fullerenes. In Table 11.1, we use these calculations to compute the Estrada index of one member of each isomer classes of C_{20}, C_{24}, C_{26}, C_{30}, C_{36}, and C_{40} fullerenes. We notice that in real fullerenes, the number of carbon atoms will be at most 500, and our bounds for such fullerenes are reasonable. In Table 11.5, the values of column EE^* are related to our upper bounds for the Estrada index.

Theorem 11.4.2 There are real numbers $c_1, c_2, \ldots, c_n$, $-3 < c_i \leq 3$, such that the Estrada index of any n-vertex IPR fullerene can be written as

$$EE(C_n) = \frac{19012851119}{5811886080} n + \frac{2545157411}{2179457280} + \sum_{i=1}^{n} \frac{\lambda_i^{12} e^{c_i}}{12!}. \text{ Moreover,}$$

$$\left(\frac{35169}{12!e^3} + \frac{19012851119}{5811886080} \right) n$$

$$+ \frac{2545157411}{2179457280} < EE(C_n) < \left(\frac{e^3 3^6}{12!} + \frac{19012851119}{5811886080} \right) n + \frac{2545157411}{2179457280}.$$

From above, $3.2713773n < EE(C_n) - 1.1677941 < 3.2714043n$ holds for any n-vertex IPR fullerene, i.e., the value of $EE(C_n)$ belongs to an interval of length $0.0000270n$, which is remarkably strong approximation.

Following Cvetković and Stevanković, if C_n has isolated pentagons, then the distance of the vertex j to the nearest pentagons is called the penta-distance of j. Let P_s be the set of vertices at the distance s from the nearest pentagon and t be the

largest penta-distance of a vertex. The vertex set is then partitioned into subsets P_0, $P_1, \ldots, P_t$. Since the pentagons are disjoint, $|P_0| = 60$. The largest k for which $|P_k| = 60 \left\lceil \frac{k}{2} \right\rceil + 60$ is called the width of the fullerene under consideration. For *IPR* fullerenes with larger widths, the above bounds may be further improved.

Theorem 11.4.3 Suppose C_n is an *IPR* fullerene with width w.

(a) If $w \geq 4$, then

$$EE(C_n) = \frac{19012851119}{5811886080} n + \frac{2545157411}{2179457280} + \sum_{i=1}^{n} \frac{\lambda_i^{16} e^{c_i}}{16!}.$$

Moreover,

$$\left(\frac{2157759}{16!e^3} + \frac{19012851119}{5811886080} \right) n + \frac{2545157411}{2179457280} < EE(C_n)$$
$$< \left(\frac{e^3 3^8}{16!} + \frac{19012851119}{5811886080} \right) n + \frac{2545157411}{2179457280}.$$

(b) If $w \geq 5$, then

$$EE(C_n) = \frac{7605140687351}{2324754432000} n + \frac{101806237513}{87178291200} + \sum_{i=1}^{n} \frac{\lambda_i^{18} e^{c_i}}{18!}.$$

Moreover,

$$\left(\frac{17319837}{18!e^3} + \frac{7605140687351}{2324754432000} \right) n + \frac{101806237513}{87178291200} < EE(C_n)$$
$$< \left(\frac{e^3 3^9}{18!} + \frac{7605140687351}{2324754432000} \right) n + \frac{101806237513}{87178291200}.$$

(c) If $w \geq 6$, then

$$EE(C_n) = \frac{6981519156761497}{213412456857600} n + \frac{1479510240}{19!} + \sum_{i=1}^{n} \frac{\lambda_i^{20} e^{c_i}}{20!}.$$

Moreover,

$$\left(\frac{140668065}{20!e^3} + \frac{6981519156761497}{213412456857600} \right) n + \frac{1479510240}{19!} < EE(C_n)$$
$$< \left(\frac{e^3 3^{10}}{20!e^3} + \frac{6981519156761497}{213412456857600} \right) n + \frac{1479510240}{19!}.$$

References

Aleksić T, Gutman I, Petrović M (2007) Estrada index of iterated line graphs. Bull Academie Serbe des Sci et des Arts (Cl Math Natur) 134:33–41

Ashrafi AR, Fath−Tabar GH (2011) Bounds on the Estrada index of ISR $(4,6)$ − fullerenes. Appl Math Lett 24:337–339

Balasubramanian K (1994) Laplacian polynomials of fullerenes $(C20 − C40)$. Chem Phys Lett 224:325–332

Behmaram A (2013) Matching in fullerene and molecular graphs. Ph.D. thesis, University of Tehran

Cvetković D, Stevanković D (2004) Spectral moments of fullerene graphs. MATCH Commun Math Comput Chem 50:62–72

Cvetković D, Doob M, Sachs H (1995) Spectra of graphs − theory and application, 3rd edn. Johann Ambrosius Barth Verlag, Heidelberg/Leipzig

De La Pena JA, Gutman I, Rada J (2007) Estimating the Estrada index. Linear Algebra Appl 427:70–76

Estrada E (2000) Characterization of 3D molecular structure. Chem Phys Lett 319:713–718

Estrada E (2002) Characterization of the folding degree of proteins. Bioinformatics 18:697–704

Estrada E (2004) Characterization of the amino acid contribution to the folding degree of proteins. Proteins 54:727–737

Estrada E (2007) Topological structural classes of complex networks. Phys Rev 75:016103

Estrada E, Rodriguez − Valazquez JA, Randić M (2006) Atomic branching in molecules. Int J Quantum Chem 106:823–832

Fath−Tabar GH, Ashrafi AR (2010) Some remarks on Laplacian eigenvalues and Laplacian energy of graphs. Math Commun 15:443–451

Fath−Tabar GH, Ashrafi AR (2011) New upper bounds for Estrada index of bipartite graphs. Linear Algebra Appl 435:2607–2611

Fath−Tabar GH, Ashrafi AR, Gutman I (2008) Note on Laplacian energy of graphs. Bulletin de l'Academie Serbe des Sciences et des Arts 137:1–10

Fath−Tabar GH, Ashrafi AR, Gutman I (2009) Note on Estrada and L − Estrada indices of graphs. Bulletin del Academie Serbe des Sciences et des Arts 139:1–16

Fath-Tabar GH, Ashrafi AR, Stevanovic D (2012) Spectral properties of fullerenes. J Comput Theor Nanosci 9:1–3

Fowler PW, Manolopoulos DE (1995) An atlas of fullerenes. Oxford University Press, New York

Gutman I, Radenković S (2007a) A lower bound for the Estrada index of bipartite molecular graphs. Kragujevac J Sci 29:67–72

Gutman I, Radenković S (2007b) Estrada index of benzenoid hydrocarbons. Z Naturforschung 62a:254–258

Gutman I, Furtula B, Marković V, Glišić B (2007a) Alkanes with greatest Estrada index. ZNaturforsch 62a:495–498

Gutman I, Radenković S, Furtula B, Mansour T, Schork M (2007b) Relating Estrada index with spectral radius. J Serb Chem Soc 72:1321–1327

Gutman I, Furtula B, Glišic B, Marković V, Vesel A (2007c) Estrada index of acyclic molecules. Indian J Chem 46a:723–728

Kroto HW, Heath JR, O'Brien SC, Curl RF, Smalley RE (1985) C_{60} Buckminster fullerene. Nature 318:162–163

Kroto HW, Fichier JE, Cox DE (1993) The fullerene. Pergamon Press, New York

Mehranian Z, Gholami A, Ashrafi AR (2014) Experimental results on the symmetry and topology of 3− and 4 − generalized fullerenes. J Comput Theor Nanosci 11:2283–2288

Myrvold W, Bultena B, Daugherty S, Debroni B, Girn S, Minchenko M, Woodcock J, Fowler PW (2007) A graphical user interface for investigating conjectures about fullerenes. MATCH Commun Math Comput Chem 58:403–422

Taghvaee F, Ashrafi AR (2016) Comparing fullerenes by spectral moments. J Nanosci Nanotechnol 16:3132–3135

Chapter 12
Geometrical and Topological Dimensions of the Diamond

G.V. Zhizhin, Z. Khalaj, and M.V. Diudea

Abstract The question of possible existence of molecules in spaces of higher dimensions, as a consequence of special distribution of matter, is addressed. The geometrical features of the adamantane molecule are examined in detail. It is shown that the adamantane molecule has the dimension 4. The connection ways of the adamantane molecules are investigated on the basis of their geometric properties. Topological properties of the diamond, a 3-periodic net of adamantane, and of a hyperdiamond, called diamond D_5, are given in terms of Omega and Cluj polynomials.

12.1 Introduction

Carbon is one of the most important natural elements in the periodic table, in a variety of millions of compounds and forms. There are four valance electrons in the carbon atom, two in the 2s orbital and two in the 2p orbitals. When combine, these orbitals lead to three types of hybrid orbitals: sp, sp^2, and sp^3 ones. The electronic and atomic arrangements enable carbon to exist in different allotropes such as diamond, diamond-like carbon, graphite, fullerenes, nanotubes, nanowalls, etc. Some of these allotropes are shown in Fig. 12.1 (Khalaj et al. 2012; Khalaj and Ghoranneviss 2012).

Diamond D_6, the classical diamond, is an all-hexagonal ring network, of sp^3 hybridized carbon atoms with adamantane and diamantane the repeating units, as

G.V. Zhizhin
Member of "Skolkovo" OOO "Adamant", Saint-Petersburg, Russia

Z. Khalaj
Department of Physics, Shahr-e-Qods Branch, Islamic Azad University, Tehran, Iran

M.V. Diudea (✉)
Department of Chemistry, Faculty of Chemistry and Chemical Engineering, Babes-Bolyai University, Arany Janos Street 11, Cluj-Napoca RO-400028, Romania
e-mail: diudea@chem.ubbcluj.ro
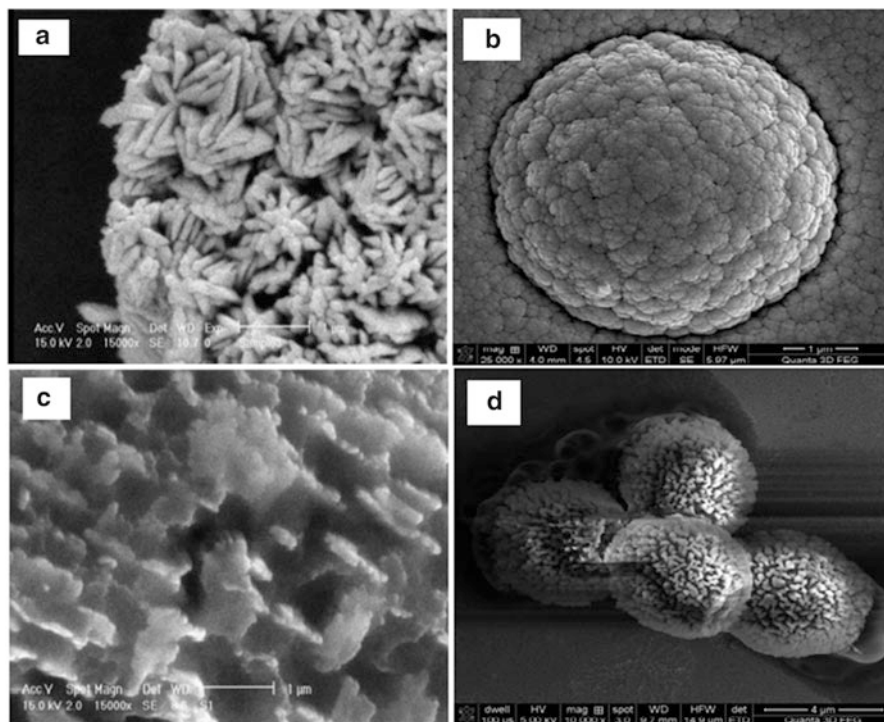
Fig. 12.1 Some of the carbon allotropes synthesized using different CVD systems: (**a**) self-assembled cone-like carbon, (**b**) cauliflower diamond-like carbon, (**c**) carbon nanowalls, (**d**) carbon microspheres

shown in Fig. 12.2; it is crystallized in a face-centered cubic *fcc* network (space group *Fd3m*).

Diamond has kept its highest importance among the carbon allotropes, in spite of many "nano" varieties appeared in the last years (Decarli and Jamieson 1961; Osawa 2007, 2008; Williams et al. 2007; Dubrovinskaia et al. 2006). Its physical characteristics: high thermal conductivity, large band gap, excellent hardness, high electrical resistivity, and low friction coefficient (Takano et al. 2005; Yamazaki et al. 2008), led to outstanding applications in electronics, optics, mechanics, etc. (Sharda et al. 2001). Composites including diamonds may overpass the resistance of steel or metal alloys. Synthetic diamonds can be produced by a variety of methods, including high pressure-high temperature HPHT, static or detonating procedures, chemical vapor deposition CVD (Lorentz 1995), ultrasound cavitation (Khachatryan et al. 2008), or mechanosynthesis (Merkle and Freitas 2003; Sourina and Korolev 2005; Tarasov et al. 2011).

Hyperdiamonds are covalently bonded carbon phases, more or less related to the diamond network, having a significant amount of sp^3 carbon atoms. Their physical properties are close to that of the classical diamond, sometimes with exceeding
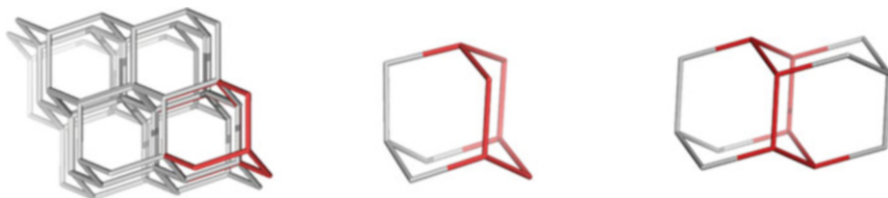
Fig. 12.2 Diamond D_6 (*left*), adamantane D_6_10 (*left*), diamantane D_6_14 (*middle*), and diamond D_6_52 (a 222 Net – *right*)

hardness and/or endurance. In this respect, the hyperdiamond D_5 will be presented in Sect. 12.5.

The chapter is structured as follows. After the introductory part, the main hypotheses of the space and matter will be introduced in Sect. 12.2. Next, the dimension of adamantane molecule is investigated in detail in Sect. 12.3, while its connecting ways evaluated in Sect. 12.4. Section 12.5 introduces the hyperdiamond D_5, while Sects. 12.6 and 12.7 deal with the topology of diamonds D_6 and D_5 in terms of Omega and Cluj polynomials, respectively. Conclusions and references will close the chapter.

12.2 Space and Matter

The space in mathematics is a logically conceivable form (or structure) that serves as a medium in which there are other forms or structures (Mathematical encyclopedia 1984). In this definition, it is essential that the space is a logically conceivable form. Visual image of any object on the retina of the human eye is two dimensional. By this reason, any object is perceived initially as a two-dimensional one. Similarly, we only touch the surface of objects, that is, again the palpable image of objects has the dimensionality two. The representation as three-dimensional forms only comes out as a result of the comparison of the mismatched images in the right and left eye, this difference being stronger observed in motion; the comparison is a result of thinking, of the rational. Although many people traditionally consider the world around us as three dimensional, it is only an abstract submission. It should be kept in mind that the geometrical axioms are neither synthetic a priori judgments nor experimental facts.

There are only contingent provisions: when choosing among all possible provisions, we are guided by experimental facts, but the choice is free and limited only by the need to avoid any controversy (Poincare' 1902).

Historically, there were two main concepts of space. In their frames, there are a set of modifications and corresponding geometries. The first idea, associated with the names of Aristotle and Leibniz, is that the real space is a property of the material provision of the objects. As a result, it is linked inextricably with the matter. The development of this idea led to the known position of the philosophy that *there is no space without matter* just as there is no matter without space. The space is a form of

existence of the matter. The second of these ideas, associated with the names of Democritus and Newton, is that the space is the repository of all material objects, which do not have any influence on the space (Einstein 1930). It was the defining idea for many centuries and the philosophical basis of Euclidean geometry (Euclid 2012). In accordance with it, the geometric space is continuous, endless, three dimensional, homogeneous (all points in space are identical to each other), and isotropic (all lines passing through one point are identical to each other). N. I. Lobachevsky (and independently, Bolyai) suggested a non-Euclidean geometry (Lobachevsky 1835). In accordance with this, there can be more than one parallel line through a point outside the line in the plane. This new geometry connected with physics, space, and matter. B. Riemann (1868) extended the geometry of Lobachevsky. He developed the idea of nonhomogeneous spaces, while their connection with the matter follows to the formation of space structure. Here Riemann idea merges with the concept of Leibniz, according to which the space is a property of the position of material objects. Riemannian nonhomogeneous spaces were realized in Einstein's physical theory of general relativity, which provided scientific proof of natural relationship of space and matter. It is believed that the issues of space heterogeneity and the emergence of high-dimensional spaces are important only for large-scale objects such as our universe and larger. The modern theory on the universal nature of the world (superstring theory) easily uses the concept of the nine-dimensional space (Atwood et al. 2008; Burgess and Quevedo 2008; Green 2011; Zwiebach 2011). However, in the near-to-us space, as the biosphere, we can find higher-dimension space objects with a specific distribution of atoms.

Modern researches show that the three-dimensional model of our world often leads to contradictions. For example, the three-dimensional space model could not certainly describe the experimental electron diffraction patterns of quasi crystals (intermetallic compounds) (Janssen et al. 2007). Only four-dimensional space model explains it (Shevchenko et al. 2013a, b; Zhizhin 2014a, b). Experimental studies of phase transitions of the second kind can be explained only by assuming the four-dimensional space (Landau 1937; Kadanoff 1966; Wilson 1971a, b; Fischer and Pfeuty 1972). Such phase transitions in solids occur not only in labs but also in the nature, for example, in the formation of rocks.

Clathrate compounds (i.e., inclusion compounds) are widely occurring in the nature. They are formed by inclusion of some molecules in the cavities of crystal lattices of molecules of another type (lattice clathrates), or in the cavities of another type of molecules (molecular clathrates). An important example of the lattice clathrate is the methane hydrate. In it, the methane molecules are enclosed in thevoids of the crystal lattice of ice. Reserves of methane on the ocean floor in this form are probably much higher than the gas reserves in a free state. Studies on clathrates with silicon and germanium atoms indicate a possible four-dimensional of these compounds (Adams et al. 1994; Nagy and Diudea 2013; Ashrafi et al. 2013). Many natural minerals exist in the nature in the form of fused different geometric shapes passing through each other. It also could be the formation of higher-dimensional geometric shapes. As it is known, the diamond unit cell could be identified through various polyhedra, such as tetrahedron, octahedron, and others (Shafranovsky 1964).

12.3 Dimension of Adamantane Molecule

In this section, the question of the dimensionality of a molecule is considered in detail in the case of adamantane. As a chemical compound, adamantane was discovered in 1933 (Landa and Machacek 1933). Adamantane molecule consists of 10 carbon atoms, a repeating unit of carbon atoms in the crystal lattice of diamond, and 16 hydrogen atoms. The hydrogen atoms are connected to carbon atoms on the unsaturated valences of the carbon atoms. Derivatives of adamantane (e.g., amantadine, memantine, rimantadine, tromantadine) have found practical applications in medicine (as antiviral, antispasmodics, anti-Parkinson drugs, etc.). Among the inorganic and organometallic compounds, there is a number of structural analogs of adamantane, such as phosphorus oxide, urotropine, and others. In 2005, a silicon analogue of adamantane has been synthesized (Fischer et al. 2005). The adamantane structure is a common one in the literature (Bauschlicher et al. 2007; Dahl et al. 2003 – see Fig. 12.2, middle).

Spicing about the adamantane molecule, we often keep in mind exactly ten carbon atoms of the molecule adamantane, although, strictly speaking, it is only a part of the adamantane molecule. However, this figure is a little informative and does not reflect the main features of the spatial arrangement of atoms.

Theorem (Zhizhin 2014c) The adamantane molecule is a convex polytope in the 4D space.

Proof We shall build an adamantane cell in the 3D Euclidean space by imposing the condition: six atoms from ten carbon atoms of adamantane be located in the center of planar faces of the cube.

Each of the remaining four carbon atoms inside the cube is equidistant to the three centers of the nearest flat faces of the cube (Fig. 12.3). In Fig. 12.3 one can see thin solid lines delineating the regular tetrahedron inscribed in the cube. Its edges are the diagonals of the cube faces. The solid thick lines correspond to the covalent bonds between carbon atoms. We suppose that the carbon atoms, in the vertices of the cube, are arranged as in the diamond structure. Other substance possible arrangement of carbon atoms in the vertices of a cube will not influence the analysis on the geometry of adamantane. The dotted line passing through the points α_2, α_6, α_3, α_4, α_8, and α_9 delineate a regular octahedron with its vertices located in the center of the cube faces and sharing some vertices with the adamantane. Barcode dotted lines delineate the regular tetrahedron whose vertices coincide with the carbon atoms of adamantane, located inside the cube α_1, α_5, α_7, and α_{10}. By construction, the formed segments connecting the vertices of adamantane split into ten families of parallel lines, each family of three parallel segments: (1) $\alpha_1\alpha_2$, $\alpha_7\alpha_6$, $\alpha_{10}\alpha_9$; (2) $\alpha_3\alpha_1$, $\alpha_8\alpha_{10}$, $\alpha_5\alpha_6$; (3) $\alpha_3\alpha_2$, $\alpha_7\alpha_5$, $\alpha_8\alpha_9$; (4) $\alpha_1\alpha_4$, $\alpha_7\alpha_8$, $\alpha_5\alpha_9$; (5) $\alpha_4\alpha_2$, $\alpha_8\alpha_6$, $\alpha_{10}\alpha_5$; (6) $\alpha_9\alpha_2$, $\alpha_3\alpha_8$, $\alpha_{10}\alpha_1$; (7) $\alpha_4\alpha_3$, $\alpha_7\alpha_{10}$, $\alpha_6\alpha_9$; (8) $\alpha_5\alpha_2$, $\alpha_7\alpha_3$, $\alpha_{10}\alpha_4$; (9) $\alpha_1\alpha_5$, $\alpha_3\alpha_6$, $\alpha_4\alpha_9$; and (10) $\alpha_6\alpha_2$, $\alpha_7\alpha_1$, $\alpha_4\alpha_8$. Consequently, the total number of segments, each of which is an edge of a polyhedron, is equal to 30. The length of the segments is determined by the length of the cube
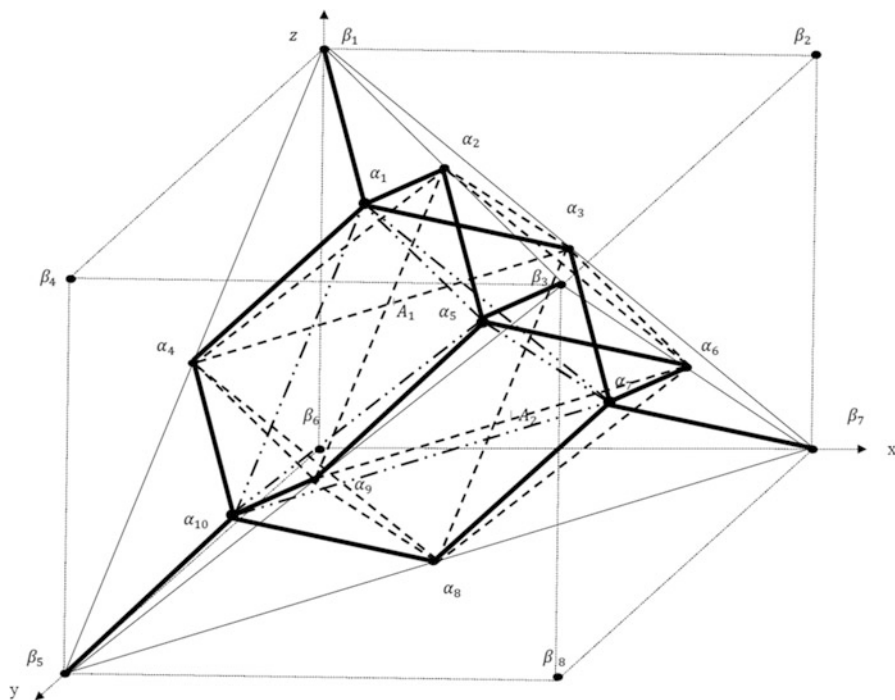
Fig. 12.3 Structure of adamantane

edges. Put the length of cube edge equal to 1 (to go to the specific dimensions of the bond length must enter a scale factor). Then a regular tetrahedron with the bases on the faces of the octahedron and the vertices in the vertices of the cube (e.g., a tetrahedron $\beta_1\alpha_2\alpha_3\alpha_4$) will have the length $a = 1/\sqrt{2}$ and the radius of the circle around the tetrahedron $b = \sqrt{3} / 4$ (the points α_2; α_6, α_3; and α_4 ,α_8 , α_9 are in the centers of the cube faces). Therefore, segments 2, 5, 6, 7, 9, and 10 have the length a, while the segments 1, 3, 4, and 8 have the length b. Thus, the two-dimensional geometric elements involved in adamantane are the lengths of sides a and b.

One can define (Fig. 12.3) a set of two-dimensional faces belonging to the adamantane, forming a regular triangle with sides a, an isosceles triangle with the base a and two sides b, squares with sides a, and a rectangle with sides a and b. Among the regular triangles, there are 4 triangles located at the outer edge of adamantane ($\alpha_2\alpha_3\alpha_6$, $\alpha_2\alpha_4\alpha_9$, $\alpha_4\alpha_3\alpha_8$, $\alpha_9\alpha_8\alpha_6$) and 8 triangles located in the inner part of adamantane ($\alpha_1\alpha_5\alpha_{10}$, $\alpha_1\alpha_7\alpha_{10}$, $\alpha_1\alpha_7\alpha_5$, $\alpha_2\alpha_9\alpha_6$, $\alpha_2\alpha_3\alpha_4$, $\alpha_8\alpha_3\alpha_6$, $\alpha_4\alpha_9\alpha_8$, $\alpha_5\alpha_{10}\alpha_7$). Among the irregular triangles, there are 12 triangles located at the outer edge of adamantane ($\alpha_2\alpha_3\alpha_1$, $\alpha_2\alpha_1\alpha_4$, $\alpha_1\alpha_3\alpha_4$, $\alpha_2\alpha_5\alpha_9$, $\alpha_2\alpha_5\alpha_6$, $\alpha_3\alpha_7\alpha_8$, $\alpha_3\alpha_7\alpha_6$, $\alpha_4\alpha_{10}\alpha_9$, $\alpha_4\alpha_{10}\alpha_8$, $\alpha_5\alpha_9\alpha_6$,$\alpha_7\alpha_8\alpha_6$, $\alpha_8\alpha_9\alpha_{10}$) and 6 triangles located in the inner part of adamantane ($\alpha_1\alpha_4\alpha_{10}$, $\alpha_2\alpha_5\alpha_1$,$\alpha_5\alpha_6\alpha_7$, $\alpha_1\alpha_7\alpha_3$, $\alpha_{10}\alpha_5\alpha_9$, $\alpha_7\alpha_8\alpha_{10}$). Thus, there is a total of 30 triangles in adamantane. In the inner part of adamantane, there are three squares of side a, as the three sections of the octahedron

$(\alpha_2\alpha_6\alpha_8\alpha_4, \alpha_2\alpha_3\alpha_8\alpha_9, \alpha_3\alpha_6\alpha_9\alpha_4)$, and 12 parallelograms (Fig. 12.3) with sides a and b $(\alpha_1\alpha_3\alpha_8\alpha_{10}, \quad \alpha_1\alpha_2\alpha_9\alpha_{10}, \quad \alpha_1\alpha_5\alpha_9\alpha_4, \quad \alpha_1\alpha_7\alpha_8\alpha_4, \alpha_1\alpha_3\alpha_5\alpha_6, \alpha_1\alpha_7\alpha_6\alpha_2, \alpha_2\alpha_4\alpha_5\alpha_{10},$ $\alpha_7\alpha_3\alpha_2\alpha_5, \alpha_7\alpha_3\alpha_4\alpha_{10}, \alpha_5\alpha_6\alpha_8\alpha_{10}, \alpha_5\alpha_7\alpha_8\alpha_9$, $\alpha_6\alpha_7\alpha_9\alpha_{10})$.

These parallelograms are rectangles, as one can prove that wrong plane triangles, based on the specified side of the squares, are perpendicular to the plane of these squares. Indeed, one may cut up the adamantane by a plane passing, for example (see Fig. 12.3), through the top $\alpha_2$and the edges $\alpha_1\alpha_2$, and α_2 α_5 (due to the symmetry of the octahedron and tetrahedron built on its edges, these edges lie in the same plane). This plane cuts up irregular triangles $\alpha_1\alpha_3\alpha_4$, $\alpha_5\alpha_9\alpha_6$ and regular triangles $\alpha_2\alpha_3\alpha_4$, $\alpha_6\alpha_8\alpha_9$on their height, passing through the middle of the edges $\alpha_3\alpha_4$ and $\alpha_6\alpha_9$ (respectively, the points A_1, A_2 in Fig. 12.3) and vertex α_8. Intersection plane is presented in Fig. 12.4. We prove that the segments $\alpha_1A_1$and α_3A_2 are perpendicular on the line A_1A_2. This will prove the wrong triangle perpendicular to the plane of the square plane $\alpha_6\alpha_3\alpha_9\alpha_4$. Let us consider the triangle $\alpha_2\alpha_3$ A_2; in it $A_1A_2 = a$ and $\alpha_2A_2 = b = \frac{\sqrt{6}}{4}a$, $A_2\alpha_3 = \frac{a}{2\sqrt{2}}$.

Therefore, $\cos \angle \alpha_2A_2\alpha_3 = \sqrt{\frac{2}{3}}$ and $\sin \angle \alpha_2A_2\alpha_3 = \frac{1}{\sqrt{3}}$. From the triangle $A_1A_2\alpha_2$, one can see that $\cos \angle \alpha_2A_2A_1 = \frac{1}{\sqrt{3}}$, $\sin \angle \alpha_2A_2A_1 = \sqrt{\frac{2}{3}}$. Consequently, $\cos \left(\angle \alpha_2A_2\alpha_3 + \angle \alpha_2A_2A_1 \right) = 0$. Then, $\alpha_3A_2 \perp A_1A_2$. This also implies that $\alpha_1\alpha_3 \perp \alpha_3\alpha_6$ and $\alpha_5\alpha_6 \perp \alpha_3\alpha_6$; in other words the parallelogram $\alpha_3\alpha_6\alpha_1\alpha_5$ is a rectangle. One can prove that the remaining parallelograms are also rectangles. Thus, the number of squares and rectangles is 15, and the total number of geometric elements of dimension 2 consisting of adamantane is 45.

These 2D geometric elements form in adamantane 25 of 3D polyhedron (Fig. 12.3):

Five tetrahedron $(\alpha_4\alpha_3\alpha_1\alpha_2, \alpha_{10}\alpha_7\alpha_1\alpha_5, \alpha_4\alpha_{10}\alpha_9\alpha_8, \alpha_3\alpha_6\alpha_7\alpha_8, \alpha_2\alpha_6\alpha_9\alpha_5)$

Six prisms $(\alpha_3\alpha_2\alpha_1\alpha_8 \quad \alpha_9\alpha_{10}, \quad \alpha_6\alpha_2\alpha_1\alpha_7 \quad \alpha_9\alpha_{10}, \quad \alpha_3\alpha_2\alpha_5\alpha_8 \quad \alpha_9\alpha_7,$ $\alpha_3\alpha_5\alpha_1\alpha_8$ $\alpha_6\alpha_1\alpha_{10}$, $\alpha_5\alpha_2\alpha_6\alpha_8$ $\alpha_4\alpha_4\alpha_{10}$, $\alpha_5\alpha_4\alpha_1\alpha_8$ $\alpha_9\alpha_7)$

Fourteen pyramids $(\alpha_4\alpha_2\alpha_1\alpha_9\alpha_{11}, \alpha_5\alpha_2\alpha_1\alpha_9\alpha_{10}, \alpha_4\alpha_3\alpha_1\alpha_8\alpha_{10}, \alpha_7\alpha_3\alpha_1\alpha_8\alpha_{10},$ $\alpha_4\alpha_2\alpha_3\alpha_9\alpha_8, \quad \alpha_3\alpha_2\alpha_6\alpha_9\alpha_8, \quad \alpha_3\alpha_2\alpha_1\alpha_5\alpha_6, \quad \alpha_5\alpha_3\alpha_1\alpha_6\alpha_7, \quad \alpha_4\alpha_3\alpha_6\alpha_9\alpha_8, \quad \alpha_4\alpha_2\alpha_3\alpha_9\alpha_6,$ $\alpha_4\alpha_3\alpha_1\alpha_7\alpha_{10}, \alpha_4\alpha_3\alpha_7\alpha_8\alpha_{10}$, $\alpha_4\alpha_5\alpha_1\alpha_9\alpha_{10}, \alpha_4\alpha_2\alpha_1\alpha_9\alpha_5)$

Calculation of 3D octahedron, as consisting from two pyramids, was not considered, because the square section of the octahedron is involved in the formation of other 3D shapes. We now calculate Euler's formula for the polytope P of dimension n (Poincare 1895; Grunbaum 1967) by substituting the number of figures/shapes of various dimensions included in adamantane: $\sum_{j=0}^{n-1} (-1)^j f_j(P) = 1 + (-1)^{n-1}$, $f_j(P)$ being the number of figures of dimension j in the polytope P.

As shown above, in this case we have $f_0(P) = 10$, $f_1(P) = 30$, $f_2(P) = 45$, $f_3(P) = 25$. All the elements of dimension 3 are convex (including 3D boundary of the points set), and no elements of dimension greater than 3 exists within the adamantane. Substituting the values obtained for the number of figures of different dimension in Euler's formula, for $n = 4$, we have $10–30 + 45–25 = 0$. This proves the theorem.

Fig. 12.4 Section of
adamantane
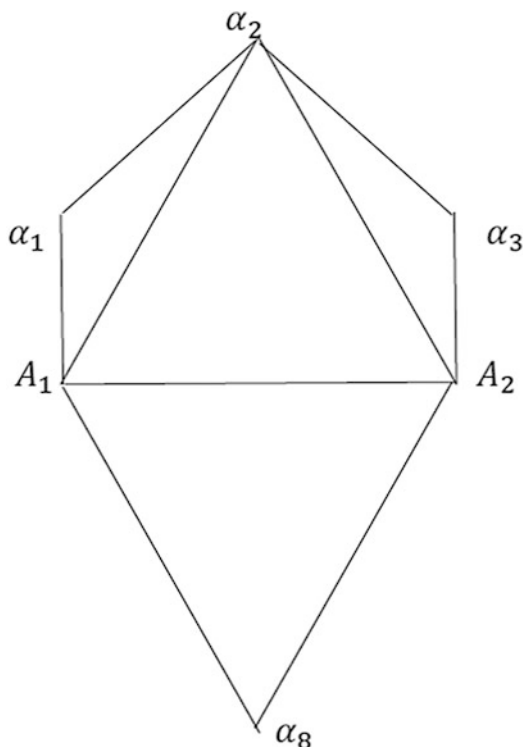
Thus, adamantane is a convex polytope of dimension 4. From each vertex this
polytope outlets 6 rays as in the 16-cell convex regular 4D polytope (Grunbaum
1967; Zhizhin 2014a). All two-dimensional faces of adamantane are simulta-
neously faces of two 3D shapes, indicating the isolation of adamantane as a
polytope. The outer boundary of adamantane consisting of two-dimensional faces
of the polytope is the projection of the polytope on the 3D space, just as the outer
boundary of any closed polytope on 2D plane is a closed circuit composed of
one-dimensional segments.

12.4 Connection Ways of Adamantane Molecules

In view of the established geometric properties of adamantane molecules, they can
join to each other by three ways: (1) at the vertices located at the centers of cube
faces; (2) at the wrong parallel triangle; and (3) at the broken hexagonal contours
formed by the right triangle and its surrounding irregular triangle constituting the
dihedral angles with the right triangle.

12.4.1 The First Way of Joining Adamantane Molecules

It leads to the standard model of translational diamond with the *fcc* unit cell. The coordinates of the adamantane vertices are calculated as integers. Indeed, if we shall take the unit cell edge length equal to 4, the coordinates x, y, and z of vertices in the initial position (denoted by the subscript 0, $\alpha_{i,\,0}(x_{i,\,0}, y_{i,\,0}, z_{i,\,0})$) in Fig. 12.3 are $\alpha_{1,0}(1, 1, 3)$, $\alpha_{2,0}(2, 2, 4)$, $\alpha_{3,0}(2, 0, 2)$, $\alpha_{4,0}(0, 2, 2)$, $\alpha_{5,\,0}(3, 3, 3)$, $\alpha_{6,\,0}(4, 2, 2)$, $\alpha_{7,\,0}(3, 1, 1)$, $\alpha_{8,\,0}(2, 2, 0)$, $\alpha_{9,\,0}(2, 4, 2)$, $\alpha_{10,\,0}(1, 3, 1)$. Then, to translate the cube on $k(k_x, k_y, k_z)$ steps toward x, y, and z coordinates, formula for computing these new vertex positions is

$$\alpha_{i,\,k}\left(x_{i,\,k},\ y_{i,\,k},\ z_{i,\,k}\right) = \alpha_{i,k}\left(x_{i,\,0} + 4k_x,\ y_{i,0} + 4k_y,\ z_{i,\,0} + 4k_z\right);\quad i = 1, 2, \ldots, 10;$$

k_x, k_y, k_z being integers (positive and negative). As it was shown above, for determining the coordinates of adamantane in integers, it is not necessary to use the theory of numbers, as was done in the work of (Balaban 2013).

On the set of cubic cells of adamantane molecules, one can establish the existence of a scaling process, diamond scaling, i.e., formation of large-scale geometric shapes of the same figures as in the smaller scale. For the first time, the process of scaling was detected at the phase transitions of the second kind (Kadanoff 1966). Also it was detected on the grid of hyperrombohedron vertices in quasicrystals (Zhizhin 2014a, b).

Figure 12.5 shows the scaling with an octahedron based on eight cubes, each containing 8 times smaller octahedron. This explains the existence of diamond crystals of macroscopic dimensions with the same form as the microscopic unit cell of diamond. The increase in scale occurs in a discrete manner. Scale crystal diamond increases at n^3 ($n = 1, 2, \ldots$) strokes.

12.5 The Second Way of Joining Adamantane Molecules

As shown in Sect. 12.3, the planes of irregular triangles are perpendicular to the plane of the square section of octahedron. Therefore, adamantane molecules can attach to each other, within an irregular triangle, in two mutually perpendicular directions. Thus, they form a layer of infinite adamantane polyhedra contacting by the free vertices of the octahedron. In such a case, two adamantane molecules adopt a dihedral angle, equal to the dihedral angle between irregular triangles in the adamantane polyhedron. Therefore, in the space of three adamantane polyhedra, contacting the wrong triangles, another adamantane polyhedron can be tightly nested. These form an infinite layer filled by adamantane polyhedra and regular tetrahedra, with a fundamental domain consisting of an adamantane polyhedron and a regular tetrahedron.

Fig. 12.5 Scaling in
diamond
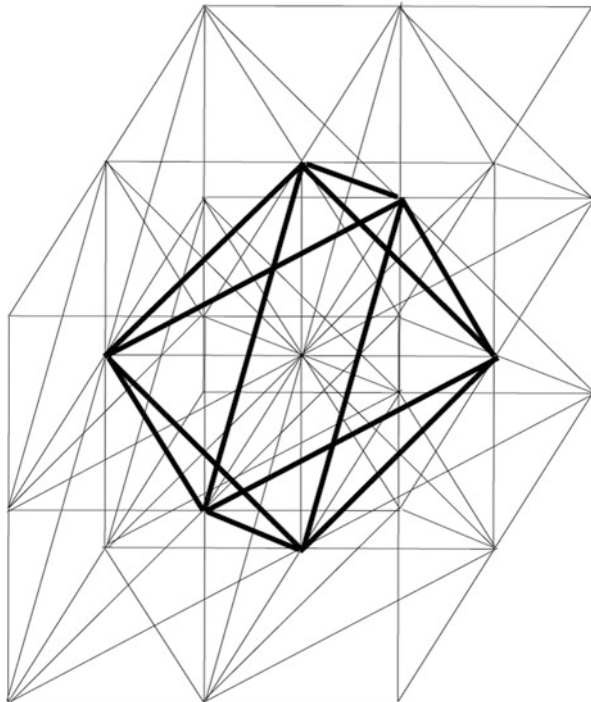
These layers, contacted to each other, completely fill the space. At top view such
a layer is shown in Fig. 12.6 (thick lines designate valence bonds). One can see that
the condition of four valence carbon atoms in all the vertices was fulfilled, as in the
four valence bond carbon atoms, directed from layer to layer (vertically). The
distribution of carbon atoms, as shown in Fig. 12.6, describes the oblique coordi-
nate system. The density of this carbon atom arrangement must be higher than the
density of the *fcc* diamond fundamental domain.

12.5.1 The Third Way of Connecting Adamantane Molecules

The adamantane polyhedra can communicate with each other besides the tops and
irregular triangles also by the broken hexagonal spatial contours whose edges
correspond to the valence bonds. The boundary of each adamantane consists of
four of these circuits. Combining the two adamantane on such a contour, we obtain
the diamantane. A next connection leads to triamantane and so on. Based on this
mechanism, a general formula for diamondoids is available (Bauschlicher
et al. 2007; Dahl et al. 2003): C_nH_{n+6}, $n = 4i + 6$, $i = 1, 2, \ldots.$

Fig. 12.6 Adamantane compound in an oblique lattice
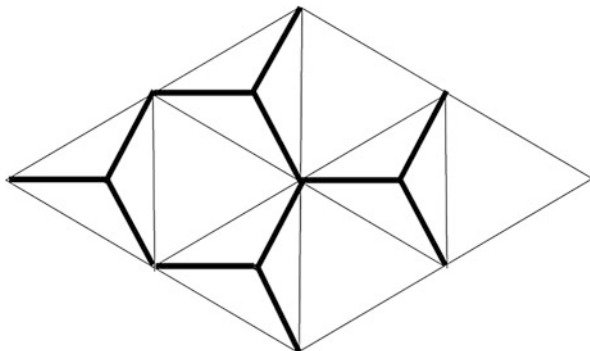
These diamondoids are shells of the hexagonal loops. Significantly, these coatings may be connected to the carbon structures derived by the second method. This may provide even more complex and diverse compounds.

12.6   Structures of Diamond D_5

A diamondoid crystal structure, with pentagon/hexagon rings, of which 90 % pentagons, was called (Diudea and Nagy 2013) diamond D_5; it is also known as the clathrate II, or *mtn*, and is a 3-periodic, 3-nodal net, of point symbol {5^5.6}12 {5^6}5 and 2[5^{12}]; [5^{12}.6^4], a tiling that belongs to the space group Fd-3 m. The clathrate II structure exists in the synthetic zeolite ZSM-39 (Meyer and Olson 1992), in silica (Böhme et al. 2007; Adams et al. 1994) and in germanium allotrope Ge(cF136) (Guloy et al. 2006; Schwarz et al. 2008) as real substances.

Substructures of D_5 are related to the classical D_6 diamond (Diudea et al. 2012; Böhme et al. 2007). An adamantane-like structure D_5_ada can form two diamantane-like D_5_dia forms: anti and syn (Fig. 12.1). Next, D_5_dia_anti substructure will form a 3-periodic *fcc*-crystal network (Benedek and Colombo 1996) (Fig. 12.1, bottom, right), while D_5_dia_syn will self-arrange into a starlike quasi-crystal (Diudea 2013) (Fig. 12.1, bottom, left).

Topology of D_5_*anti* in a triclinic domain (k,k,k) (see Fig. 12.7) is presented in Table 12.1: formulas to calculate the number of atoms and number of rings R and the limits (at infinity) for the ratio R$_5$/all rings are given function of k (i.e., the number of repeating units in the domain) (Diudea et al. 2012).

The hyperdiamond D_5 mainly consists of sp^3 carbon atoms building ada-like repeating units (C$_{20}$ cages including C$_{28}$ as hollows). The ratio $C - sp^3/C$-total trends to 1 in a large-enough network. The content of pentagons R[5] per total rings trends to 90 % (see Table 12.1) and, by this reason, this allotrope was called the diamond D_5. For comparison, in this table, topology of diamond D_6 net is included.

Considering the hexagons as "window faces" to the C$_{28}$ hollows, one can evaluate the genus of D_5 net according to the following.

$D_5\_ada\_158 = C_{28}@((C_{20})_3)_4$ $D_5\_ada\_198 = C_{28}@((C_{20})_4)_4$

$D_5\_dia\_anti\_226$ $D_5\_dia\_syn\_226$

$D_5\_dia\_anti\_306$ $D_5\_dia\_syn\_270$

$D_5\_syn\_531s\_1185$ $D_5\_anti\_333\_860$
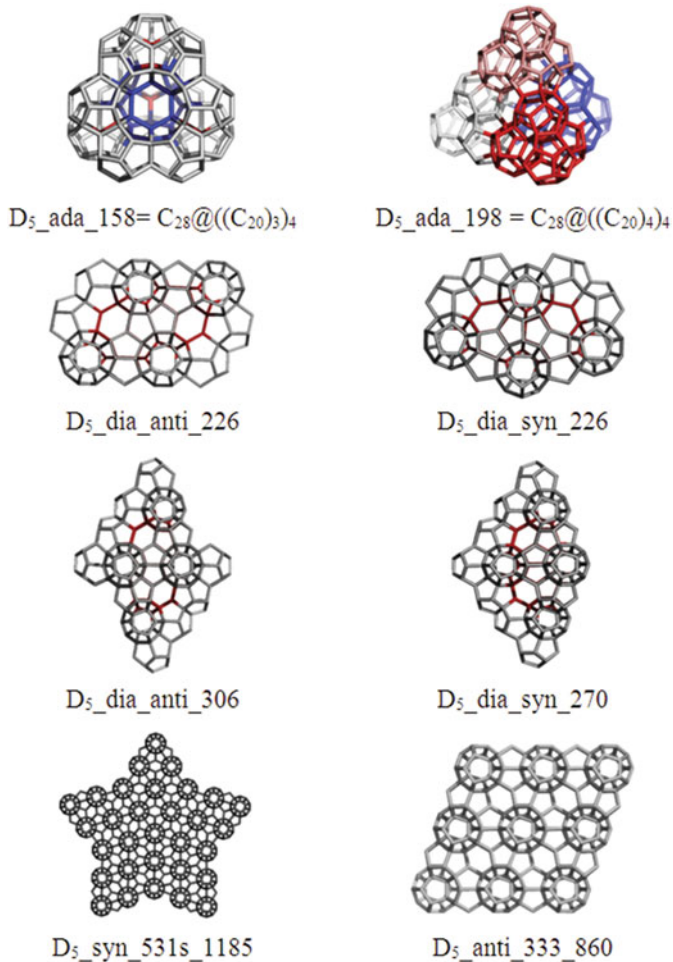
Fig. 12.7 Structures of diamond D_5

Theorem (Diudea and Szefler 2012): In spongy structures built up from u tube junction units, of genus g_u, the genus is calculated as $g = u(g_u - 1) + 1$, irrespective of the unit tessellation.

Data are given in Table 12.2.

Design of the crystal networks herein discussed was performed by using our software programs CVNET (Stefu and Diudea 2005) and NANO-STUDIO (Nagy and Diudea 2009). Topological data were provided by NANO-STUDIO.

Table 12.1 Topology of diamonds D5_anti, and D6, as a function of the number of repeating units k ($k = 1, 2,...$) on the edge of a (k, k, k) triclinical domain

Formulas
$v(D_5\_anti) = -22 - 12k + 34k^3$
$sp^3 atoms = -10 - 36k^2 + 34k^3$
$Ring[5] = -18 - 6k - 18k^2 + 36k^3$
$Ring[6] = -1 + 6k - 9k^2 + 4k^3$
$R[5] + R[6] = -19 - 27k^2 + 40k^3$
$\lim_{k \to \infty} \frac{R[5]}{R[5]+R[6]} = 9/10$
$v(D_6) = 6k + 6k^2 + 2k^3$
$sp^3 atoms = -2 + 6k + 2k^3$
$Ring[6] = 3k^2 + 4k^3$
$\lim_{k \to \infty} \left[\frac{Atoms(sp^3)}{v(G)} = \frac{-2+6k+2k^3}{6k+6k^2+2k^3} \right] = 1$

Table 12.2 Genus calculation in diamond D_5 substructures

D_5	v	e	$g = 1 + u(g_u - 1)$	g_u	u
$(C_{20})_{12}C_{28}\_Ada\_158$	158	274	3	1.5	4
$(C_{20})_{18}(C_{28})_2\_Dia\_syn\_226$	226	398	5	2;1.5	3 + 2
$(C_{20})_{18}(C_{28})_2\_Dia\_anti\_226$	226	398	5	1.5	8

12.7   Omega Polynomial of Diamonds D_5 and D_6

Let $G(V,E)$ be a connected bipartite graph, with the vertex set $V(G)$ and edge set $E(G)$. Two edges $e = (x,y)$ and $f = (u,v)$ of G are called *codistant* (briefly: *e co f*) if $d(x, v) = d(x, u) + 1 = d(y, v) + 1 = d(y, u)$.

For some edges of a connected graph G, the following relations are satisfied (John et al. 2007):

$$e\ co\ e$$
$$e\ co\ f\ \Leftrightarrow\ f\ co\ e$$
$$e\ co\ f\ \&\ f\ co\ h\ \Rightarrow\ e\ co\ h$$

though the last relation is not always valid.

Let $C(e) := \{f \in E(G); f\ co\ e\}$ denote the set of edges in G, codistant to the edge $e \in E(G)$. If relation *co* is an equivalence relation, then G is called a *co-graph*. Consequently, $C(e)$ is called an *orthogonal cut qoc* of G, and $E(G)$ is the union of disjoint orthogonal cuts $C_1 \cup C_2 \cup \ldots \cup C_k$ and $Ci \cap Cj = \emptyset$ for $i \neq j$, $i, j = 1, 2, .., k$.

A *quasi-orthogonal cut qoc* with respect to a given edge is the smallest subset of edges closed undertaking opposite edges on faces. Since the transitivity of the *co* relation is not necessarily obeyed, *qoc* represents a less constrained condition: any

oc strip is a *qoc* strip but the reverse is not always true. More about Omega polynomial, the reader can find in Chap. 2 of this book.

Let $m(G,c)$ denote the number of *qoc* strips of length c (*i.e.*, the number of cutoff edges); for the sake of simplicity, $m(G,c)$ can be written as m. The Omega polynomial is defined on the ground of *qoc* strips (Diudea 2006):

$$\Omega(G,x) = \sum_c m(G,c) \cdot x^c$$

Its first derivative (in $x = 1$) equals the number of edges in the graph:

$$\Omega'(G,1) \;\; = \sum_c m \cdot c = e = |E(G)|$$

On Omega polynomial, the Cluj-Ilmenau index (John et al. 2007), $CI = CI(G)$, was defined (Diudea 2006):

$$CI(G) = \left\{ \left[\Omega'(G,1) \right]^2 - \left[\Omega'(G,1) + \Omega''(G,1) \right] \right\}$$

Topology of diamond D_5, in a cubic (k,k,k) domain, is presented in Table 12.2 (Diudea et al. 2011): formulas to calculate the number of atoms, number of rings, and the limits (to infinity) for the ratio of $sp^3 C$ atoms over total number of atoms and also the ratio $R[5]$ over the total number of rings are given. Tables 12.3 to 12.5 give formulas for calculating Omega polynomial in diamonds D_5 and D_6 and some numerical examples.

12.8   Cluj Polynomial in Diamond D_6

A counting polynomial can be written as

$$P(G,x) = \sum_k m(G,k) \cdot x^k$$

where the exponents of indeterminate x show the extent of partition $p(G)$, $\cup p(G) = P(G)$, of a graph property $P(G)$, while the coefficients $m(G,k)$ are related to the occurrence of partitions of extent k. Quantum chemistry first used the polynomial description of molecular graphs, namely, the *characteristic polynomial* (Diudea et al. 2002; Aihara 1976; Gutman et al. 1977); its roots represent the energies of the Hückel *pi*-molecular graphs. Counting polynomials have been introduced in the Mathematical Chemistry literature by Hosoya (1988, 1990; Hosoya and Yamaguchi 1975).

The Cluj polynomials (Diudea 2009; Diudea et al. 2007, 2010a, b, c; Dorosti et al. 2009; Saheli and Diudea 2013) are defined on the basis of Cluj matrices; they count the vertex proximity of a vertex i with respect to any vertex j in G, joined to

Table 12.3 Omega polynomial in diamonds D_5 and D_6 as a function of the number of repeating units k along the edge of a cubic (k,k,k) domain

	Omega(D_5); R[6]
1	$\Omega(D_5,x) = (32 - 54k + 36k^2 + 44k^3) \cdot x + (-3 + 18k - 27k^2 + 12k^3) \cdot x^2$
2	$\Omega'(1) = e(G) = -38 - 18k - 18k^2 + 68k^3$
3	$CI(G) = 1488 + 1350k + 1764k^2 - 4612k^3 - 2124k^4 - 2448k^5 + 4624k^6$
	Omega(D_6); R[6]
4	$\Omega(D_6-k_{odd},x) = \left(\displaystyle\sum_{i=1}^{k} 2x^{\frac{(i+1)(i+2)}{2}}\right) + \left(\displaystyle\sum_{i=1}^{(k-1)/2} 2x^{\frac{(k+1)(k+2)}{2}+\frac{k\times k-1}{4}-i(i-1)}\right) + 3kx^{(k+1)^2}$
5	$\Omega(D_6-k_{even},x) = \left(\displaystyle\sum_{i=1}^{k} 2x^{\frac{(i+1)(i+2)}{2}}\right) + \left(\displaystyle\sum_{i=1}^{k/2} 2x^{\frac{(k+1)(k+2)}{2}+\frac{k\times k}{4}-(i-1)(i-1)}\right) - x^{\frac{(k+1)(k+2)}{2}+\frac{k\times k}{4}} + 3kx^{(k+1)^2}$
6	$\Omega'(1) = e(G) = -1 + 6k + 9k^2 + 4k^3$
7	$CI(G) = 2 - 187k/10 - k^2/4 + 305k^3/4 + 457k^4/4 + 1369k^5/20 + 16k^6$

Table 12.4 Examples, omega polynomial in diamond D_5

K	Omega(D_5); R[6]	Atoms	sp^{3}Atoms (%)	Bonds	CI	R[5]	R[6]
2	$356\ x^1 + 21\ x^2$	226	118 (52.21)	398	157,964	186	7
3	$1318\ x^1 + 132\ x^2$	860	584 (67.91)	1582	2,500,878	774	44
4	$3144\ x^1 + 405\ x^2$	2106	1590 (75.50)	3954	15,629,352	1974	135
5	$6098\ x^1 + 912\ x^2$	4168	3340 (80.13)	7922	62,748,338	4002	304

Table 12.5 Examples, omega polynomial in diamond D_6

k	Omega(D_6); R[6]	Atoms	sp^{3}Atoms (%)	Bonds	CI(G)	R [6]
2	$2x^3 + 2x^6 + 1x^7 + 6x^9$	52	26 (50.00)	79	5616	44
3	$2x^3 + 2x^6 + 2x^{10} + 2x^{12} + 9x^{16}$	126	70 (55.56)	206	39,554	135
4	$2x^3 + 2x^6 + 2x^{10} + 2x^{15} + 2x^{18} + 1x^{19} + 12x^{25}$	248	150 (60.48)	423	169,680	304
5	$2x^3 + 2x^6 + 2x^{10} + 2x^{15} + 2x^{21} + 2x^{25} + 2x^{27} + 15x^{36}$	430	278 (64.65)	754	544,746	575

i by an edge (the Cluj-edge polynomials CJDI$_e(x)$) or by a path (the Cluj-path polynomials CJDI$_p(x)$). The coefficients $m(k)$can be calculated from the entries of the corresponding UCJDI matrices by the TOPOCLUJ software program (Ursu and Diudea 2005). The summation runs over all $k = |\{p\}|$in G.

In bipartite graphs, the coefficients of CJ polynomial can be calculated by an orthogonal edge-cut procedure (Diudea et al. 2010a, b; Gutman and Klavžar 1995; Klavžar 2008).

To perform an orthogonal cut, take a straight line segment, orthogonal to the edge e, and intersect e and all its parallel edges in the graph. The set of these intersections is called an *orthogonal cut* $c_k(e)$, $k = 1,2,..,k_{max}$. An example is given in Fig. 12.8. To any orthogonal cut c_k, two numbers can be associated: (i) *number of edges* e_k intersected (i.e., cutting cardinality $|c_k|$) and (ii) v_k or the number of points lying to the left hand with respect to c_k (in round brackets, in Fig. 12.8).

Let us define the *partial cube* as a graph embeddable in the hypercube n-cube Q_n, which is a regular graph whose vertices are binary strings of length n, two strings being adjacent if they differ in exactly one position (Harary 1969). The distance function in the n-cube is the Hamming distance. A hypercube can be expressed as the Cartesian product: $Q_n = \Box_{i=1}^{n} K_2$ where K_2 is the complete graph on two vertices.

For any edge $e = (u,v)$ of G, let n_{uv} denote the set of vertices lying closer to u than to v: $n_{uv} = \{w \in V(G) | d(w,u) < d(w,v)\}$.   Then   we   can   write $n_{uv} = \{w \in V(G) | d(w,v) = d(w,u) + 1\}$. The sets (and subgraphs) induced by these vertices, namely, n_{uv} and n_{vu}, are called *semicubes* of G; they are disjoint *opposite semicubes* (Diudea and Klavžar 2010; Diudea et al. 2008).

A graph G is bipartite if and only if, for any edge of G, the opposite semicubes define a partition of G: $n_{uv} + n_{vu} = v = |V(G)|$. These semicubes represent the
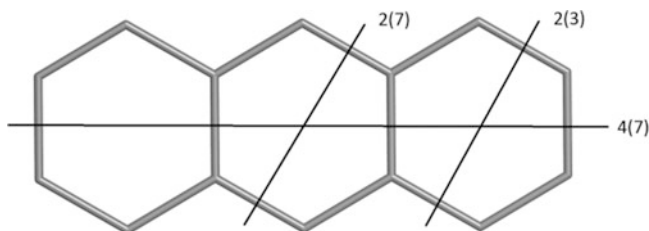
Fig. 12.8 Cutting procedure in Cluj polynomials

$CJS(x) = 4 \times 2(x^3 + x^{(14-3)}) + 4(x^7 + x^{(14-7)}) + 2 \times 2(x^7 + x^{(14-7)}) = 8x^{11} + 16x^7 + 8x^3$

$CJS'(1) = 224 = v \times e = Sum(UCJDI_e)_{i,j}$

$CJP(x) = 4 \times 2(x^{3(14-3)}) + 4(x^{7(14-7)}) + 2 \times 2(x^{7(14-7)}) = 8x^{49} + 8x^{33} CJP'(1) = 656 = 1312/2 = (1/2)Sum(SCJDI_e)_{i,j}$

vertex proximities of the endpoints of edge $e = (u,v)$, on which *CJ* polynomials are defined. In partial cubes, the semicubes can be estimated by an orthogonal cutting-edge procedure. The orthogonal cuts form a partition of the graph edges

$$E(G) = c_1 \cup c_2 \cup \ldots \cup c_k, \quad c_i \cap c_j = \emptyset, \ i \neq j$$

Let $v = v(G) = |V(G)|$ and $e = e(G) = |E(G)|$ be the cardinality of the vertex and edge sets, respectively. The Cluj polynomials are calculated by recomposing the local contributions (as provided by the cutting procedure) to the global graph property, differing only by the arithmetic operation used (Diudea 2010a, b):

(i) *Cluj-Sum* polynomial, CJS(x), is counted by summation of local contributions (Diudea 2009; Diudea et al. 2007, 2010a):

$$CJS(x) = \sum_e (x^{v_k} + x^{v-v_k})$$

(ii) *Cluj-Product* polynomial, CJP(x), is counted by the pair-wise product of the cutting contributions (Diudea 1997a, b). It is identical to the *Szeged* polynomial, $SZ_v(x)$ (Gutman 1994; Ashrafi et al. 2008; Khalifeh et al. 2008; Mansour and Schork 2009):

$$CJP(x) = SZ_v(x) = \sum_e x^{v_k(v-v_k)}$$

The first derivatives (in $x = 1$) provide single numbers, often called topological indices, characterizing the encoded topological property (e.g., the vertex proximities in the graph); thus, $CJS'(1) = Sum(UCJDI_e)_{i,j}$ and $CJP'(1) = (1/2)Sum(SCJDI_e)_{i,j}$, respectively.

In case of CJS(x), the following theorem (Diudea 2009; Diudea et al. 2007) is involved:

Theorem The sum of all edge-counted vertex proximities, p_e, in a bipartite graph, is $p_e = v \times e$, i.e., the product of the number of vertices and edges in G.

Demonstration In a bipartite planar graph, which allows orthogonal edge-cuts, for every edge $e(i,j) \in E(G)$, the vertex proximities $\{p_{e,i}\}$ and $\{p_{e,j}\}$ of its endpoints are clearly separation. Denote the cardinalities of the above sets by $p_{e,i}$ and $p_{e,j}$, then

$$p_{e,i} + p_{e,j} = v$$

and next, by summing the contributions of all the edges in G, one obtains the total of vertex proximities, $p_e = v \times e$.

$$p_e = \sum_c m(G,c) \cdot c \cdot \left(p_{e,i} + p_{e,j}\right) = \sum_c m(G,c) \cdot c \cdot v = e \times v$$
$$= \sum_{i,j} \left[\text{UCJDI}_e(G)\right]_{i,j} = \text{CJS}'(G,1)$$

thus demonstrating the theorem.

Corollary In a bipartite graph, there are no equidistant vertices with respect to the two endpoints of any edge.

This is the main result provided by the Cluj matrix/polynomial (Diudea et al. 2007). It was independently discovered in (Došlić and Vukičević 2007) and proposed as the "bipartite edge-frustration" index, a criterion for checking the bipartivity of a graph.

Formulas for calculating Cluj *CJS* polynomial in diamond D_6 are presented in Table 12.6, while Table 12.7 gives some numerical examples (Saheli and Diudea 2013).

Table 12.6 Cluj *CJS* polynomial in diamond D_6

	Cluj polynomial
1	$CJS(x) = \sum_{i=1}^{k} (i^2 + 3i + 2)\left[x^{\frac{1}{6}i(2i^2+9i+13)} + x^{2k(k^2+3k+3)} - \frac{1}{6}i(2i^2+9i+13)\right]$ $+ \sum_{i=1}^{\lfloor\frac{k}{2}\rfloor}[(k+1)(k+2) + 2i(k-i)]\left[x^{\frac{1}{6}k(2k^2+9k+13)} + ik(3+i+k) + \frac{i}{3}(5-2i^2)\right]$ $+ \sum_{i=1}^{\lfloor\frac{k}{2}\rfloor-1}[(k+1)(k+2) + 2i(k-i)]\left[x^{\frac{1}{6}k(10k^2+27k+23)} - ik(3+i+k) - \frac{i}{3}(5-2i^2)\right]$ $+ \left[\frac{1-(-1)^k}{4}\right](3k^2+6k+3)x^{\left(k^3+\frac{15}{4}k^2+\frac{9}{2}k+\frac{3}{4}\right)} + 6(k+1)^2 \sum_{i=1}^{k} x^{2k(k^2+3k+3)} - 2i(k+1)^2 + 1$
2	$CJS'(1) = 8k^6 + 42k^5 + 90k^4 + 88k^3 + 30k^2 - 6k$

Table 12.7 Examples of Cluj CJS polynomial in diamond D_6 Net

k	Polynomial CJS	CJS'
1	$6x^{10} + 24x^7 + 6x^4$	252
2	$6x^{48} + 12x^{39} + 54x^{35} + 14x^{26} + 54x^{17} + 2x^{13} + 6x^4$	4108
3	$6x^{122} + 12x^{113} + 20x^{97} + 96x^{95} + 24x^{75} + 96x^{63} + 24x^{51} + 96x^{31} + 20x^{29} + 12x^{13} + 6x^4$	25,956
4	$6x^{244} + 12x^{235} + 20x^{219} + 150x^{199} + 30x^{194} + 36x^{161} + 150x^{149} + 38x^{124} + 150x^{99}$ $+ 36x^{87} + 30x^{54} + 150x^{49} + 20x^{29} + 12x^{13} + 6x^4$	104,904

12.9 Conclusions

In this chapter, the possible existence of local spaces of higher dimension (more than 3), of the indissoluble connection of space and matter, of the space as a form of the existence of matter, and of the heterogeneity of this space, was demonstrated. In a previous paper (Zhizhin 2014a, b), it was shown that the experimental electron diffraction patterns of intermetallic compounds (quasi crystals) can be uniquely described by assuming higher dimensions of space for such materials. It was proved here that the dimension of the adamantane molecule (and its derivatives), due to the special distribution of matter (atoms), is equal to 4. From the proven geometric properties of the adamantane, three major ways for the connection of adamantane molecules were proposed. It was shown that the higher-dimension regions can combine with each other to form nanoscale layers. Nevertheless, they are separated in the 3D space. The same mathematical treatment can be applied to diamond D_5, which is basically a type II clathrate.

Design of diamond D_6 and hyperdiamond D_5 crystal networks was performed by using original software programs CVNET and NANO-STUDIO, developed at TOPO GROUP CLUJ. The topology of the networks was described in terms of Omega and Cluj CJS polynomials, respectively, as functions of the net parameter k representing the number of repeating units in a (k,k,k) cuboid.

References

Adams GB, O'Keeffe M, Demkov AA, Sankey OF, Huang Y-M (1994) Wide – band – gap Si in open fourfold – coordinated clathrate structures. Phys Rev B 49:8048–8053

Aihara J (1976) A new definition of Dewar – type resonance energies. J Am Chem Soc 98:2750–2758

Ashrafi A, Ghorbani M, Jalali M (2008) The vertex PI and Szeged indices of an infinite family of fullerenes. J Theor Comput Chem 7:221–231

Ashrafi AR, Koorepazan – Moftakhar F, Diudea MV, Stefu M (2013) Chap. 18: Mathematics of D_5 network. In: Diudea MV, Csaba CL (eds) Diamonds and related nanostructures. Springer, Dordrecht, pp 321–333

Atwood W, Maykeylson P, Ritz S (2008) The window in the extreme universe. In the world of science. Sci Am 3:16–21

Balaban AT (2013) Chap 1: Diamond hydrocarbons and related structures. In: Diudea MV, Csaba CL (eds) Diamonds and related nanostructures. Springer, Dordrecht, pp 1–28

Bauschlicher CW, Liu Y, Ricca A, Mattioda AL, Allamandola LJ (2007) Electronic and vibrational spectroscopy of diamondoids and the interstellar infrared bands between 3.35 and 3.55 μm. Astrophys J 671:458–469

Benedek G, Colombo L (1996) Hollow diamonds from fullerenes. Mater Sci Forum 232:247–274

Böhme B, Guloy A, Tang Z, Schnelle W, Burkhardt U, Baitinger M, Yu G (2007) Oxidation of M_4Si_4 (M = Na, K) to clathrates by HCl or H_2O. J Am Chem Soc 129:5348–5349

Burgess K, Quevedo F (2008) Large space travel on the "roller coaster". In the world of science. Sci Am 3:22–31

Dahl JE, Liu SG, Carlson RMK (2003) Isolation and structures of higher diamondoids, nanometer − sized diamond molecules. Science 229:96–99

Decarli PS, Jamieson JC (1961) Formation of diamond by explosive shock. Science 133:1821–1822

Diudea MV (1997) Cluj matrix invariants. J Chem Inf Comput Sci 37:300–305

Diudea MV (2006) Omega polynomial. Carpath J Math 22:43–47

Diudea MV (2009) Cluj polynomials. J Math Chem 45:295–308

Diudea MV (2010a) Counting polynomials in partial cubes. In: Gutman I, Furtula B (eds) Novel molecular structure descriptors − theory and applications I. University of Kragujevac, Kragujevac, pp 191–215

Diudea MV (2010b) Counting polynomials and related indices by edge cutting procedures. In: Gutman I, Furtula B (eds) Novel molecular structure descriptors − theory and applications II. University of Kragujevac, Kragujevac, pp 57–78

Diudea MV (2013) Hyper − graphenes. Int J Chem Model 5:211–220

Diudea MV, Klavžar S (2010) Omega polynomial revisited. Acta Chim Sloven 57:565–570

Diudea MV, Nagy CL (eds) (2013) Diamond and related nanostructures, vol 6, Carbon materials: chemistry and physics. Springer, Dordrecht

Diudea MV, Szefler B (2012) Nanotube junctions and the genus of multi − tori. Phys Chem Chem Phys 14(22):8111–8115

Diudea MV, Gutman I, Jäntschi L (2002) Molecular topology. Nova, New York

Diudea MV, Vizitiu AE, Janežič D (2007) Cluj and related polynomials applied in correlating studies. J Chem Inf Model 47:864–874

Diudea MV, Cigher S, John PE (2008) Omega and related counting polynomials. MATCH Commun Math Comput Chem 60:237–250

Diudea MV, Ilić A, Ghorbani M, Ashrafi AR (2010a) Cluj and PI_v polynomials. Croat Chem Acta 83:283–289

Diudea MV, Dorosti N, Iranmanesh A (2010b) Cluj Cj polynomial and indices in a dendritic molecular graph. Studia Univ "Babes−Bolyai"Chemia 55(4):247–253

Diudea MV, Nagy CL, Žigert P, Klavžar S (2010c) Cluj and related polynomials in tori. Studia Univ "Babes−Bolyai"Chemia 55(4):113–123

Diudea MV, Ilić A, Medeleanu M (2011) Hyperdiamonds: a topological view. Iranian J Math Chem 2:7–29

Diudea MV, Nagy CL, Bende A (2012) On diamond D_5. Struct Chem 23:981–986

Dorosti N, Iranmanesh A, Diudea MV (2009) Computing the Cluj index of dendrimer nanostars. MATCH Commun Math Comput Chem 62(2):389–395

Došlić T, Vukičević D (2007) Computing the bipartite edge frustration of fullerene graphs. Discret Appl Math 155:1294–1301

Dubrovinskaia N, Dub S, Dubrovinsky L (2006) Superior wear resistance of aggregated diamond nanorods. Nano Lett 6:824–826

Einstein A (1930) The problem of space, fields and ether in physics. Dia Koralle 5:486–487

Euclid (2012) Beginnings. URSS, Moscow

Fischer J, Baumgartner J, Marschner C (2005) Synthesis and structure of sila − adamantane. Science 310:825–830

Fisher ME, Pfeuty P (1972) Critical behavior of the anisotropic n−vector model. Phys Rev B 6:1889–1891

Greene B (2011) Theelegant universe. Superstrings, hidden dimensions and the quest for the ultimate theory. Librokom, Moscow

Grunbaum B (1967) Convexpolytopes. Springer, London

Guloy A, Ramlau R, Tang Z, Schnelle W, Baitinger M, Yu G (2006) A quest – free germanium clathrate. Nature 443:320–323

Gutman I (1994) A formula for the Wiener number of trees and its extension to graphs containing cycles. Graph Theory Notes of NY 27:9–15

Gutman I, Klavžar S (1995) An algorithm for the calculation of the Szeged index of benzenoid hydrocarbons. J Chem Inf Comput Sci 35:1011–1014

Gutman I, Milun M, Trinajstić N (1977) Graph theory and molecular orbitals. 19. Nonparametric resonance energies of arbitrary conjugated systems. J Am Chem Soc 99:1692–1704

Harary F (1969) Graph theory. Addison – Wesley, Reading

Hosoya H (1988) On some counting polynomials in chemistry. Discret Appl Math 19:239–257

Hosoya H (1990) Clar's aromatic sextet and sextet polynomial. Top Curr Chem 153:255–272

Hosoya H, Yamaguchi T (1975) Sextet polynomial. A new enumeration and proof technique for the resonance theory applied to the aromatic hydrocarbons. Tetrahedron Lett 16(52): 4659–4662

Janssen T, Chapuis G, De Boissieu M (2007) Aperiodic crystals. From modulated phases to quasicrystals. Oxford University Press, Oxford

John PE, Vizitiu AE, Cigher S, Diudea MV (2007) CI index in tubular nanostructures. MATCH Commun Math Comput Chem 57:479–484

Kadanoff LP (1966) Scaling laws for Isingmodels near τ_c^* Physics 2:263–272

Khachatryan AK, Aloyan SG, May PW, Sargsyan R, Khachatryan VA, Baghdasaryan VS (2008) Graphite-to-diamond transformation induced by ultrasound cavitation. Diam Relat Mater 17:931–936

Khalaj Z, Ghoranneviss M (2012) Investigation of metallic nanoparticles produced by laser ablation method and their catalytic activity on CVD diamond growth. Studia Univ "Babes−Bolyai"Chemia 57(2):21–28

Khalaj Z, Ghoranneviss M, Vaghri E, Saghaleini A, Diudea MV (2012) Deposition of DLC film on stainless steel substrates coated by Nickel using PECVD method. Acta Chim Slov 59:338–343

Khalifeh M, Yousefi − Azari H, Ashrafi A (2008) A matrix method for computing Szeged and vertex PI indices of join and composition of graphs. Linear Algebra Appl 429:2702–2709

Klavžar S (2008) A bird's eye view of the cut method and a survey of its applications in chemical graph theory. MATCH Commun Math Comput Chem 60:255–274

Landa S, Machacek V (1933) Sur l'adamantane, nouvel hydrocarbure exait du naphte. Collection Czech Commun 5:1–5

Landau LD (1937) On the theory of phase transitions I. J Exp Theor Phys 7:19–38

Lobachevsky NI (1835) Imaginary geometry. Sci Notes Kazan Univ 1:3–88

Lorenz HP (1995) Investigation of TiN as an interlayer for diamond deposition on steel. Diam Relat Mater 4:1088–1092

Mansour T, Schork M (2009) The vertex PI index and Szeged index of bridge graphs. Discret Appl Math 157:1600–1606

Mathematical encyclopedia 4 (1984) Sov encyclopedia, Moscow

Meier WM, Olson DH (1992) Atlas of zeolite structure types, 3rd edn. Butterworth − Heineman, London

Merkle RC, Freitas RA Jr (2003) Theoretical analysis of a carbon-carbon dimer placement tool for diamond mechanosynthesis. J Nanosci Nanotechnol 3(4):319–324

Nagy CL, Diudea MV (2009) NANO–studio software program. Babes–Bolyai University, Cluj

Nagy CL, Diudea MV (2013) Chap 5: Diamond D_5. In: Diudea MV, Csaba CL (eds) Diamonds and related nanostructures. Springer, Dordrecht, pp 91–106

Osawa E (2007) Recent progress and perspectives in single − digit nano diamond. Diam Relat Mater 16:2018–2022

Osawa E (2008) Monodisperse single nano diamond particulates. Pure Appl Chem 80:1365–1379

Poincaré A (1895) Analysis situs. J de Ecole Polyt 1:1–121

Poincaré A (1902) La science et Chypothe'se. Flammarion, Paris

Riemann B (1868) On the hypotheses underlying geometry. Gëtt. Abhandlungen 13

Saheli M, Diudea MV (2013) Chap. 10: Cluj and other polynomials of D_6 and related networks. In: MV Diudea, CL Nagy (eds) Carbon materials: chemistry and physics, 6: Diamond and related nanostructures, Springer, Dordrecht, Heidelberg, New York, London, pp 191–204

Schwarz U, Wosylus A, Böhme B, Baitinger M, Hanfland M, Yu G (2008) A 3D network of four − bonded germanium: a link between open and dense. Angew Chem Int Ed 47:6790–6793

Shafranovsky II (1964) Diamonds. Nauka, Moscow − Leningrad

Sharda T, Rahaman MM, Nukaya Y, Soga T, Jimbo T, Umeno M (2001) Structural and optical properties of diamond and nano–diamond films grown by microwave plasma chemical vapor deposition. Diam Relat Mater 10:561–467

Shevchenko VYA, Zhizhin GV, Mackay A (2013a) On the structure of quasicrystals in the space of higher dimension. News RAS Chem Ser 2:269–274

Shevchenko VYA, Zhizhin GV, Mackay A (2013b) Chapter 17: On the structure of the quasi-crystals in the high dimention space. In: Diamonds and related nanostructures. Springer, Dordrecht, pp 311–320

Sourina O, Korolev N (2005) Design and analysis of a molecular tool for carbon transfer in mechanosynthesis. J Comput Theor Nanosci 2(4):492–498

Stefu M, Diudea MV (2005) CageVersatile_CVNET software program. Babes–Bolyai University, Cluj

Takano Y, Nagao M, Takenouchi T, Umezawa H, Sakaguchi I, Tachiki M, Kawarada H (2005) Superconductivity in polycrystalline diamond thin films. Diam Relat Mater 14:1936–1938

Tarasov D, Izotova E, Alisheva D, Akberova N, Freitas RA Jr (2011) Structural stability of clean, passivated, and partially dehydrogenated cuboid and octahedral nanodiamonds up to 2 nano-meters in size. J Comput Theor Nanosci 8:147–167

Ursu O, Diudea MV (2005) TopoCluj software program. Babes–Bolyai University Cluj, Cluj

Williams OA, Douhéret O, Daenen M, Haenen K, Osawa E, Takahashi M (2007) Enhanced diamond nucleation on monodispersed nanocrystalline diamond. Chem Phys Lett 445:255–258

Wilson RG (1971a) Renormalization group and critical phenomena. I. Renormalization group and the Kadanoff scaling picture. Phys Rev B 4:3174–3183

Wilson RG (1971b) Renormalization group and critical phenomena. II. Phase-space cell analysis of critical behavior. Phys Rev B 4:3184–3205

Yamazaki K, Furuichi K, Tsumura I, Takagi Y (2008) The large–sized diamond single–crystal synthesis by hot filament CVD. J Cryst Growth 310:1019–1022

Zhizhin GV (2014a) World 4D. Polytechnic Service, St. Petersburg

Zhizhin GV (2014b) Disproportionate and fluctuating structure in space earthly reality. Biosphere 3:211–221

Zhizhin GV (2014c) On higher dimension in nature. Biosphere 4:1–10

Zwiebach B (2011) Initial course theory string. URSS, Moscow

Chapter 13
Mathematical Aspects of Omega Polynomial

Modjtaba Ghorbani and Mircea V. Diudea

Abstract Omega polynomial $\Omega(G, x)$ counts the *qoc* strips of all extent in G. The first and second derivatives, in $x = 1$, of this polynomial enable the calculation of the recently proposed *CI* index. In this chapter, we introduce the weighted version of omega polynomial and then we compute them for some class of graphs.

13.1 Introduction

A *graph* is a collection of points and lines connecting them. Let us to call these points and lines by vertices and edges, respectively. Two vertices x and y are adjacent, if $e = uv$ be an edge of graph. A graph whose all pairs of vertices are connected by a path is called a connected graph. A simple graph is a graph without loop and parallel edges. For example, the graph depicted in Fig. 13.1 is not simple.

A *molecular graph* is a simple one whose vertices are corresponded to the atoms and the edges to the bonds between them.

In quantum chemistry, the early Hückel theory calculates the levels of $\pi-$ electron energy of the molecular orbitals, in conjugated hydrocarbons, as roots of the *characteristic polynomial* (Diudea et al. 2002; Harary 1962; Sachs 1964; Trinajstić 1992):

$$P(G, x) = \det[x\mathrm{I} - \mathrm{A}(G)] \tag{13.1}$$

In the above, I is the unit matrix of a pertinent order and A the adjacency matrix of the graph G. The characteristic polynomial is involved in the evaluation of topological resonance energy TRE, the topological effect on molecular orbitals TEMO, the aromatic sextet theory, the Kekulé structure count, etc. (Gutman et al. 1975,

M. Ghorbani (✉)
Department of Mathematics, Faculty of Science, Shahid Rajaee Teacher Training University, Tehran 16785-136, Iran
e-mail: mghorbani@srttu.edu

M.V. Diudea
Department of Chemistry, Faculty of Chemistry and Chemical Engineering, Babes-Bolyai University, Arany Janos Street 11, Cluj-Napoca RO-400028, Romania
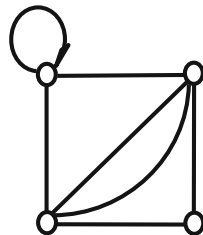
1977; Aihara 1976; Tang 1986). The coefficients $m(G,k)$ in the polynomial expression

$$P(G,x) = \sum_k m(G,k) \cdot x^k \tag{13.2}$$

are calculable from the graph G by a method making use of the *Sachs graphs*, which are subgraphs of G. Relation (13.2) was also found by other scientists. Some numeric methods of linear algebra can eventually be more efficient in large graphs (Dwyes 1951; Fadeev and Sominsky 1965).

Relation (13.1) was generalized by Hosoya (Hosoya et al. 1973) and others (Graham and Lovaśz 1978; Diudea et al. 1997; Ivanciuc et al. 1998, 1999) by changing the adjacency matrix with the distance matrix or any other square topological matrix.

Relation (13.2) is a general expression of a counting polynomial, written as a sequence of numbers, with the exponents showing the extent of partitions $p(G)$, $\cup$ $p(G) = P(G)$ of a graph property $P(G)$, while the coefficients $m(G,k)$ are related to the number of partitions of extent k.

In the mathematical chemistry literature, the counting polynomials have first been introduced by Hosoya (Hosoya 1971, 1988): $Z(G,x)$ counts independent edge sets, while $H(G,x)$ (initially called Wiener and later Hosoya) (Konstantinova and Diudea 2000; Gutman et al. 2001) counts the distances in G. Further, Hosoya proposed the sextet polynomial (Hosoya and Yamaguchi 1975; Ohkami et al. 1981; Ohkami and Hosoya 1983; Hosoya 1990) for counting the resonant rings in a benzenoid molecule (Clar 1964, 1972). Other counting polynomials have later been proposed: *independence*, *king*, *color*, *star*, or *clique polynomials* (Gutman and Hosoya 1990; Gutman 1992; Stevanović 1998; Balasubramanian and Ramaraj 1985; Farrell 1979; Farrell and De Matas 1988a; b).

13.2　Definitions

Let $G(V,E)$ be a connected bipartite graph, with the vertex set $V(G)$ and edge set E (G). Two edges $e = (x,y)$ and $f = (u,v)$ of G are called *co-distant* (briefly: $e\ co\ f$) if

Table 13.1 The number of co-distant edges of e_i, $1 \leq i \leq 10$

No.	Number of co-distant edges	Type of edges
1	1	e_1
9	2	e_2
4	3	e_3
2	4	e_4
$2n-3$	10	e_5
2	$\begin{cases} 2n+1 & 5\|n \\ 4n+3 & 5\|n-1 \\ 2n & 5\|n-4, n-2 \\ 2n+2 & 5\|n-3 \end{cases}$	e_6
$\begin{cases} 2 \\ 4 \\ 4 \end{cases}$	$\begin{cases} 4n-1 & 5\|n-3 \\ 2n & 5\|n, n-2 \\ 2n-2 & 5\|n-1, n-4 \end{cases}$	e_7
$\begin{cases} 4 \\ 4 \\ 2 \end{cases}$	$\begin{cases} 2n-2 & 5\|n-1, n-3 \\ 2n-1 & 5\|n-2, n-4 \\ 4n-1 & 5\|n \end{cases}$	e_8
$\begin{cases} 1 \\ 2 \\ 2 \\ 2 \end{cases}$	$\begin{cases} 8n+6 & 5\|n-4 \\ 4n+2 & 5\|n-3 \\ 4n+4 & 5\|n-1 \\ 4n & 5\|n, n-2 \end{cases}$	e_9
2	$\begin{cases} 4n-1 & 5\|n, n-3 \\ 4n+1 & 5\|n-1 \\ 4n+2 & 5\|n-2 \\ 4n+3 & 5\|n-4 \end{cases}$	e_{10}
2	$\begin{cases} 2n+1 & 5\|n \\ 2n & 5\|n-2, n-4 \\ 2n+2 & 5\|n-3 \end{cases}$	e_{11}

$$d(x,v) = d(x,u) + 1 = d(y,v) + 1 = d(y,u) \qquad (13.3)$$

For some edges of a connected graph G, these are the following relations satisfied (John et al. 2007a, b):

$$e \; co \; e \qquad (13.4)$$

$$e \; co \; f \; \Leftrightarrow \; f \; co \; e \qquad (13.5)$$

$$e \; co \; f \; \& \; f \; co \; h \; \Rightarrow \; e \; co \; h \qquad (13.6)$$

though the relation (13.6) is not always valid (Fig. 13.1 and Table 13.1).

Let $C(e) := \{f \in E(G); \; f \; co \; e\}$ denote the set of edges in G, co-distant to the edge $e \in E(G)$. If relation co is an equivalence relation (i.e., $C(e)$ obeys (4) to (6)), then G is called a *co-graph* . Consequently, $C(e)$ is called an *orthogonal cut oc* of G and $E(G)$ is the union of disjoint orthogonal cuts: $C_1 \cup C_2 \cup \ldots \cup C_k$ and $Ci \cap Cj = \emptyset$ for $i \neq j$, $i,j = 1, 2, .., k$.

Observe co is a Θ relation (Djoković-Winkler) (Djoković 1973; Winkler 1984):

$$d(x, u) + d(y, v) \neq d(x, v) + d(y, u) \tag{13.7}$$

and Θ is a co-relation if and only if G is a partial cube, as Klavžar (Klavžar 2008) correctly stated in a recent paper. Relation Θ is reflexive and symmetric but need not be transitive. Klavžar noted by Θ^* the Θ transitive closure and then Θ^* is an equivalence (see also the co relation). In this respect, recall some other definitions.

Let $G = (V, E)$ be a connected graph and d be its distance function. A subgraph $H \subseteq G$ is called *isometric*, if $d_H(u, v) = d_G(u, v)$, for any $(u, v) \in H$; it is *convex* if any shortest path in G between vertices of H belongs to H. A *partial cube* is an isometric subgraph of a *hypercube* Q_n; this can be obtained as a Cartesian product $Q_n = \prod_{i=1}^{n} K_2$. Examples of partial cubes are even cycles, benzenoid graphs, phenylenes, trees, etc. (Ovchinikov 2007; Diudea et al. 2007).

For any two adjacent vertices $(u, v) \in E(G)$, let denote by W_{uv}, the set of vertices lying closer to u than to b:

$$W_{uv} = \left\{ w \in V \big| d(w, u) < d(w, v) \right\} \tag{13.8}$$

The set W_{uv} and its induced subgraphs $\langle W_{uv} \rangle$ are called *semi-cubes* of G. A graph G is bipartite if and only if its semi-cubes W_{uv} and W_{vu} form a partition of V for any $(u, v) \in E(G)$. The semi-cubes W_{uv} and W_{vu} are called opposite semi-cubes and they are disjoint. Let $w \in W_{uv}$ for some edge $(u, v) \in E(G)$. Then $d(w, v) = d(w, u) + 1$ and consequently $W_{uv} = \left\{ w \in V \big| d(w, v) = d(w, u) + 1 \right\}$. In a partial cube, all semi-cubes are convex and the relation Θ is an equivalence relation on E. The distinct semi-cubes are just the Θ classes and represent the ground for the cut procedure (see below) for the calculation of distance-based indices. Note that Cluj polynomial (Diudea et al. 2006a, b) is based on calculation of opposite semi-cubes (non-equidistant vertices).

In a partial cube, any two opposite edges e and f are in relation Θ. Then an orthogonal cut oc with respect to the edge e of G is the smallest subset of edges closed under this operation and $C(e)$ is precisely a $\Theta -$class. Resuming, a graph G is a co-graph if and only if it is a partial cube.

A *quasi-orthogonal cut qoc* with respect to a given edge is the smallest subset of edges closed under taking opposite edges on faces. Since the transitivity relation (13.6) of the *co* relation is not necessarily obeyed, *qoc* represents a new concept within the cut methods. Any *oc* strip is a *qoc* strip, but the reverse is not always true (Vizitiu et al. 2007; Diudea 2006).

Let $m(G,c)$ be the number of *qoc* strips of length c (i.e., the number of cutoff edges); for the sake of simplicity, $m(G,c)$ can be written as m. The omega polynomial is defined (Diudea et al. 2009) on the ground of *qoc* strips:

$$\Omega(G, x) = \sum_c m(G, c) \cdot x^c \tag{13.9}$$

In a counting polynomial, the *first derivative* (in $x = 1$) defines the type of the counted property:

Fig. 13.2 Omega
polynomial in the graph G_1
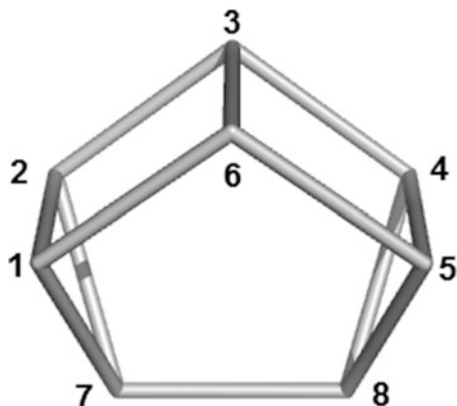
$$\Omega'(G,1) \;=\; \sum_c m \cdot c = e = |E(G)| \qquad\qquad (13.10)$$

On omega polynomial, the Cluj-Ilmenau index, $CI = CI(G)$, is calculable as

$$CI(G) = \left\{ \left[\Omega'(G,1) \right]^2 - \left[\Omega'(G,1) + \Omega''(G,1) \right] \right\} \qquad (13.11)$$

It is easily seen that, for a single *qoc*, one calculates the polynomial: $\Omega(G,x) = 1 \times x^c$ and $CI(G) = c^2 - (c + c(c-1)) = c^2 - c^2 = 0$. Figure 13.2 gives an example of calculation:

$\Omega(G,x) = 5x + 2x^2 + x^3$; $\Omega'(G,1) = e = 12$; $CI = 122$.

There exist graphs for which the above polynomial and index show degenerate values. In any tree, the omega polynomial simply counts the non-opposite edges, being included in the term of exponent $c = 1$. The coefficient of the term of exponent $c = 1$ has found utility as a topological index, called n_p, the number of *pentagon fusions*, appearing in small fullerenes as a destabilizing factor. This index accounts for more than 90 % of the variance in heat of formation *HF* of fullerenes C_{40} and C_{50} (Diudea and Nagy 2007). For more details on omega polynomial, see Refs (Diudea 2002, 2004, 2005a, b; Diudea et al. 2003, 2006a, b; Stefu et al. 2005; Cigher and Diudea 2007; Ashrafi et al. 2008a, b, Ashrafi and Ghorbani 2008c; Ghorbani and Ashrafi 2006; Jalali and Ghorbani 2009).

In graph theory a *fullerene* is a three connected cubic regular graphs with *r*-gonal and hexagonal faces satisfying in Euler's formula where *r* is a positive integer. The first and most stable fullerene, C_{60} fullerene, was discovered by H. Kroto and his team (Kroto et al. 1985, 1993). By this discovery the fullerene era was started. It is not difficult by Euler's theorem to construct fullerenes with hexagonal and *r*-gonal faces where $r \in \{3, 4, 5\}$, see Fig. 13.3.

Denoted by (5,6) fullerenes, we mean a fullerenes whose faces are pentagons and hexagons and so on. By using Euler's theorem, one can easily prove that a (5,6) fullerene on *n* vertices has exactly 12 pentagons and $n/2 - 10$, while *n* is a natural
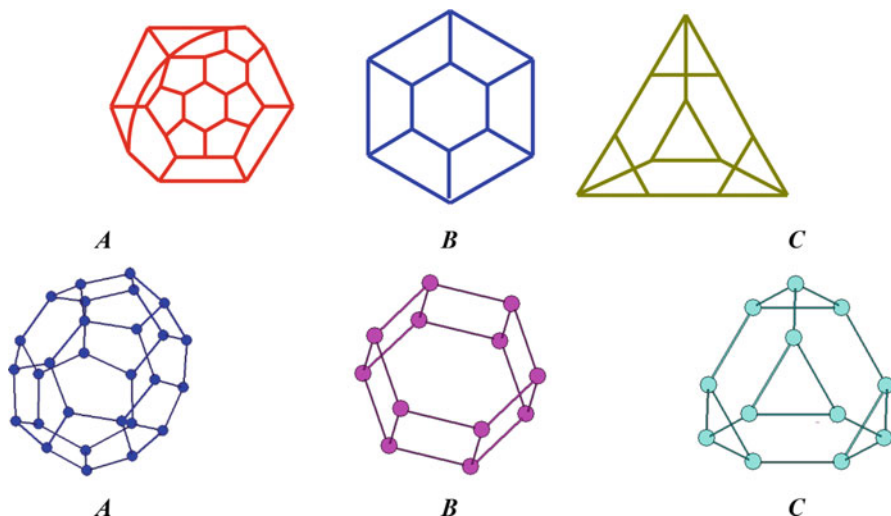
Fig. 13.3 2D and 3D graphs of some (5,6), (4,6), and (3,6) fullerenes

number equal or greater than 20 and $n \neq 22$. By a similar way, we can prove a (3,6) fullerene has exactly four triangles and a (4,6) fullerene has six quadrangles. Throughout this chapter, by a fullerene we mean a (5,6) fullerene and for simplicity, we denote a fullerene by F.

Let F be a fullerene graph on n vertices. A leapfrog transform F^l of G is a graph on $3n$ vertices obtained by truncating the dual of G. Hence, $F^l = Tr(F^*)$, where F^* denotes the dual of F. It is easy to check that F^l itself is a fullerene graph. We say that F^l is a leapfrog fullerene obtained from F and write $F^l = Le(F)$. In other words, for a given fullerene F, put an extra vertex into the center of each face of F and then connect these new vertices with all the vertices surrounding the corresponding face. Then the dual polyhedron is again a fullerene having $3n$ vertices and 12 pentagonal and $(3n/2) - 10$ hexagonal faces. A sequence of stellation-dualization rotates the parent s-gonal faces by π/s. A leapfrog operation is illustrated for a pentagonal face, in Fig. 13.4. In Fig. 13.5 the 3D leapfrog graphs of C_{24} and C_{30} are depicted.

13.3   Mathematics Discussion on Omega Polynomial

In this section, we focus on omega polynomial to derive some mathematics properties of this polynomial. Many classes of graphs can be interpreted with respect to product graphs. Hence, it is natural to ask about omega polynomial of graph products. Here, we compute just the omega polynomial of Cartesian product. By a similar method, one can investigate this polynomial for other classes of graph products.
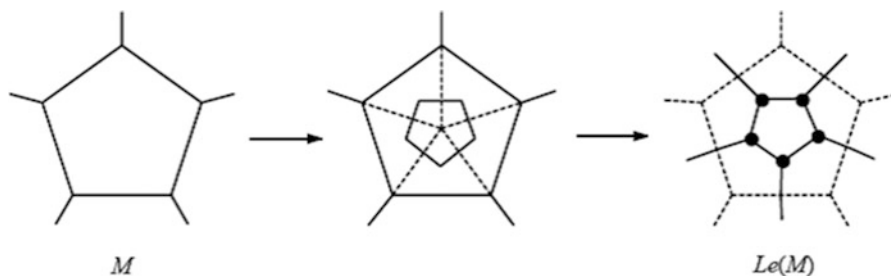
Fig. 13.4 Leapfrog of a pentagonal face
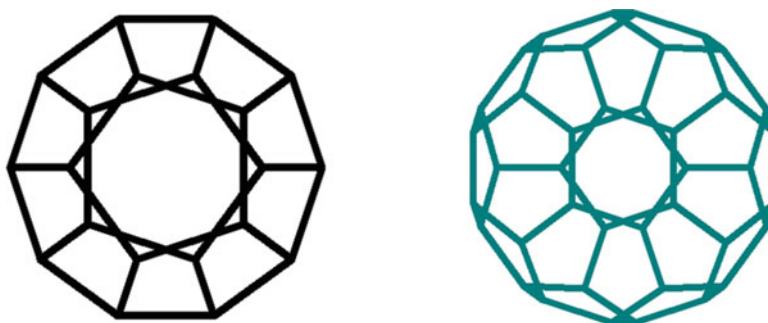
Fig. 13.5 $L(C_{20}) = C_{60}$

The Cartesian product $G \times H$ of graphs G and H is a graph such that $V(G \times H) = V(G) \times V(H)$, and any two vertices (a, b) and (u, v) are adjacent in $G \times H$ if and only if either $a = u$ and b is adjacent with v or $b = v$ and a is adjacent with u. The following properties of the Cartesian product of graphs are crucial:

(a) $|V(G \times H)| = |V(G)| \, |V(H)|$ and $|E(G \times H)| = |E(G)| \, |V(H)| + |V(G)| \, |E(H)|$.
(b) $G \times H$ is connected if and only if G and H are connected.
(c) If (a, x) and (b, y) are vertices of $G \times H$, then $d_{G \times H}((a, x), (b, y)) = d_G(a, b) + d_H(x, y)$.
(d) The Cartesian product is associative.

Theorem 13.2.1 Let G and H be bipartite connected co-graphs. Then

$$\Omega(G \times H, x) = \sum_{c_1} m(G, c_1) . x^{\left| \text{V (H)} \right| \left| c_1 \right.} + \sum_{c_2} m(H, c_2) . x^{\left| \text{V (G)} \right| \left| c_2 \right.}.$$

Proof Suppose that for an edge $e = uv$ of an arbitrary graph L, $N_L(e) = |E| - (n_u(e) + n_v(e))$. Then by definition,

$$N_{G \times H} \left((a, x), (b, y) \right) = \begin{cases} |V(G)| N(f) & for \ a = b \ and \ xy = f \in E(H) \\ |V(H)| N(g) & for \ x = y \ and \ ab = g \in E(G). \end{cases}$$

By the above paragraph and definition of the omega polynomial, we have

$$\Omega(G \times H, x) = \sum_c m(G \times H, c).x^c$$

$$= \sum_{c_1} m(G, c_1).x^{\left| V(H) \right| c_1} + \sum_{c_2} m(H, c_2).x^{\left| V(G) \right| c_2}.$$

which completes the proof.

Corollary 13.2.2 Let $G_1, G_2, \cdots, G_n$ be bipartite connected co-graphs. Then we have

$$\Omega(G_1 \times G_2 \times \quad \times G_n, x) = \sum_{i=1}^{n} \sum_{c_i} m(G_i, c_i).x^{\prod_{\substack{j=1 \\ j \neq i}}^{n} |V(G_j)| c_i}.$$

Proof Use induction on n. By Theorem 13.2.1, the result is valid for $n = 2$. Let $n \geq 3$ and assume the theorem holds for $n - 1$. Set $G = G_1 \times \cdots \times G_{n-1}$. Then we have

$$\Omega(G \times G_n, x) = \sum_c m(G, c).x^{\left| V(G_n) \right| c} + \sum_{c_n} m(G_n, c_n).x^{\left| V(G) \right| c_n}$$

$$= \sum_{i=1}^{n-1} \sum_{c_i} m(G_i, c_i).x^{\prod_{\substack{j=1 \\ j \neq i}}^{n} |V(G_j)| c_i} + \sum_{c_n} m(G_n, c_n).x^{\left| V(G) \right| c_n}$$

$$= \sum_{i=1}^{n} \sum_{c_i} m(G_i, c_i).x^{\prod_{\substack{j=1 \\ j \neq i}}^{n} |V(G_j)| c_i}.$$

An automorphism of the graph $G = (V, E)$ is a bijection σ on V which preserves the edge set e, i. e., if $e = uv$ is an edge, then $\sigma(e) = \sigma(u)\sigma(v)$ is an edge of E. Here the image of vertex u is denoted by $\sigma(u)$. The set of all automorphisms of G under the composition of mappings forms a group which is denoted by $Aut(G)$. $Aut(G)$ acts transitively on V if for any vertices u and v in V, there is $\alpha \in Aut(G)$ such that $\alpha(u) = v$. Similarly $G = (V, E)$ is called edge-transitive graph if for any two edges $e_1 = uv$ and $e_2 = xy$ in E, there is an element $\beta \in Aut(G)$ such that $\beta(e_1) = e_2$ where $\beta(e_1) = \beta(u)\beta(v)$. Furthermore, if F be a fullerene graph, then $Aut(F) = Aut(Le(F))$. Now, let $G = (V, E)$ be a graph. If $Aut(G)$ acts edge-transitively on V, then we have the following Lemma:

Lemma 13.2.3 Let $e \in E(G)$ be an arbitrary edge and $c = |C(e)|$. Then the omega polynomial of graph G is as follows:

$$\Omega(x) = \frac{|E(G)|}{c}x^c.$$

Proof Because $Aut(G)$ acts edge-transitively on E, so we can divide E to some qoc strips of equal size. One can see that each qoc strip is of length c.

As a result of Lemma 13.2.3, we compute the omega polynomial of a hypercube. The vertex set of the hypercube H_n consist of all n-tuples $b_1 b_2 \ldots b_n$ with $b_i \in \{0, 1\}$. Two vertices are adjacent if the corresponding tuples differ in precisely one place. So the hypercube H_n has 2^n vertices and $n.2^{n-1}$ edges. In other words, $H_n \cong K_2 \times K_2 \times \underbrace{\cdots}_{n} \times K_2$. Darafsheh in (Darafsheh 2010) proved H_n is vertex and edge transitive. By using his result, we have the following theorem:

Theorem 13.2.4 $\Omega(H_n) = nx^{2^{n-1}}$.

Proof Let $e = uv$ be an arbitrary edge of H_n. By computing the qoc strips, one can see that $c = |C(e)| = 2^{n-1}$. Furthermore, since $|E(H_n)| = n.2^{n-1}$, the proof is completed.

Fullerenes C_{20} and C_{60} are the only edge-transitive fullerenes. So it is important how to compute the omega polynomial of graphs in which $Aut(G)$ is not edge transitive. One can apply the following theorem for this case:

Theorem 13.2.5 Suppose $Aut(G)$ acts on E and $E_1, E_2, \ldots, E_n$ be its orbits. Then the omega polynomial of G is as $\Omega(G) = \sum_{i=1}^{n} \frac{|E_i|}{c_i}x^{c_i}$, where $e \in E_i$ and $c_i = |C(e_i)|$.

Proof We know $Aut(G)$ acts edge-transitively on its orbits. By using Lemma 13.2.3, the proof is straightforward.

Theorem 13.2.5 implies when the acting $Aut(G)$ is not edge transitive, then $m(G, c)$'s in Eq. 13.1 determine exactly the qoc strips of orbits of $Aut(G)$. In other words, for an arbitrary edge e belong to $E(G)$, when we say $m(G,c) = k$, it means there exist an orbit such that Δ with $c = |C(e)|$ and $m(G,c) = |\Delta| = k$. Thus for a given graph with high order, it is sufficient to compute all of the orbits of $Aut(G)$ acting on E.

Let $G = (V, E)$ be a graph with finite vertex set V and edge set $E \subseteq (V \times V) \setminus \{(v, v) | v \in V\}$. An edge $(v, w) \in E$ is directed if $(w, v) \notin E$ and undirected if $(w, v) \in E$. We denote a directed edge (v, w) by $v \to w$ and write $v - w$ if (v, w) is undirected. If $(v, w) \in E$ then v and w are adjacent. If $v \to w$ then v is a parent of w, and if $v - w$ then v is a neighbor of w, see Fig. 13.6.

A path in G is a sequence of distinct vertices $<v_0, \ldots, v_k>$ such that v_{i-1} and v_i are adjacent for all $1 \leq i \leq k$. A path $<v_0, \ldots, v_k>$ is a semi-directed cycle if $(v_i, v_{i+1}) \in E$ for all $0 \leq i \leq k$ and at least one of the edges is directed as $v_i \to v_{i+1}$. Here, $v_{k+1} \equiv v_0$. A chain graph is a graph without semi-directed cycles.

Let $G = G(G_1, \ldots, G_k, v_1, \ldots, v_k)$ be a simple connected chain graph in Fig. 13.7. Then $|V(G)| = \sum_{i=1}^{k} |V(G_i)|$ and $|E(G)| = (k-1) + \sum_{i=1}^{k} |E(G_i)|$.
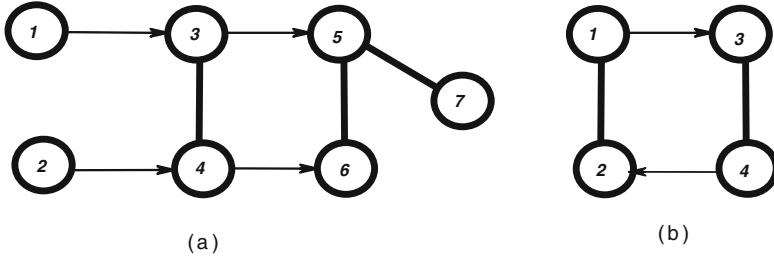
Fig. 13.6 (**a**) Chain graph with chain components $\{1\}$, $\{2\}$, $\{3, 4\}$, and $\{5, 6, 7\}$; (**b**) a graph that is not a chain graph
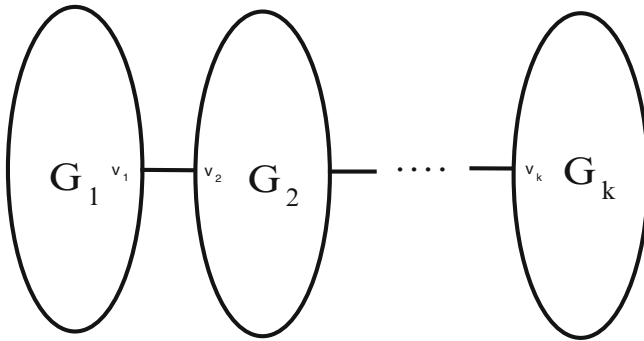
Fig. 13.7 Chain graph $G = G(G_1, \ldots, G_k, v_1, \ldots, v_k)$

Lemma 13.2.6 Let $G = G(G_1, \ldots, G_k, v_1, \ldots, v_k)$ be a simple connected chain graph in which $e \in E(G_1)$ and $f \in (G_2)$. Then the edges e and f do not satisfy in "co-" relation. In other words, $e \not\!\!\!\theta f$.

Proof Let $e = ab \in G_1$ and $f = xy \in G_2$ be arbitrary edges. We consider following cases:

(1) $d(a, v_1) = d(b, v_1) = k_1$ and $d(x, v_2) = d(y, v_2) = k_2$. Then $d(a, y) = d(a, v_1)$
    $+ d(v_1, v_2) + d(v_2, y) = k_1 + k_2 + 1$ and
    $d(a, x) = d(a, v_1) + d(v_1, v_2) + d(v_2, x) = k_1 + k_2 + 1$. This implies that $e \not\!\!\!\theta f$.
(2) $d(a, v_1) = d(b, v_1) = k_1$ and $d(x, v_2) = k_2$, $d(y, v_2) = k_2 + 1$. So, $d(a, x) = d$
    $(a, v_1) + d(v_1, v_2) + d(v_2, x) = k_1 + k_2 + 1$ and
    $d(b, x) = d(b, v_1) + d(v_1, v_2) + d(v_2, x) = k_1 + k_2 + 1$. This implies that $e \not\!\!\!\theta f$.
(3) $d(a, v_1) = k_1$, $d(b, v_1) = k_1 + 1$ and so, $d(x, a) = d(x, v_2) + d(v_2, v_1) + d(v_1, a)$
    $= k_2 + k_1 + 1$ and $d(y, a) = d(y, v_2) + d(v_2, v_1) + d(v_1, a) = k_2 + k_1 + 1$.
    This implies that $e \not\!\!\!\theta f$.

Fig. 13.8 A graph G with a cut-edge uv
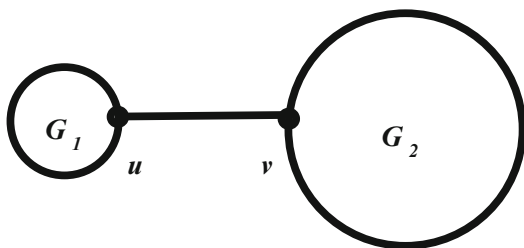
Lemma 13.2.7 Let $G = G(G_1, \ldots, G_k, v_1, \ldots, v_k)$ be a chain graph, $u \in V(G_i)$ and $v \in V(G_j)$ $(1 \leq i,j \leq k, i \neq j)$. So, $d(u,v) = d(u,v_i) + d(v_i, v_j) + d(v_j, v) = d(u,v_i) + d(v_j, v) + 1$.

Proof We know $d(u_i, u_j) = 1$ and this completes the proof.

Theorem 13.2.8 Let G be a simple connected graph with blocks G_1, G_2 and a cut-edge uv (Fig. 13.8).So, we have $\Omega(G,x) = x + \Omega(G_1,x) + \Omega(G_2,x)$.

Proof By using the definition of omega polynomial and Lemma 13.2.7, one can see that
$$\Omega(G,x) = x + \sum_{c_1} m(G_1, c_1)x^{c_1} + \sum_{c_2} m(G_2, c_2)x^{c_2} = x + \Omega(G_1, x) + \Omega(G_2, x).$$

Corollary 13.2.9 If $G = G(G_1, \ldots, G_k, v_1, \ldots, v_k)$ be a simple connected chain graph, then we have $\Omega(G,x) = (k-1)x + \sum_{i=1}^{k} \Omega(G_i, x)$.

Theorem 13.2.10 Let $G = G(G_1, G_2, v_1, v_2)$ be a simple connected chain graph. Then
$$\theta(G,x) = x + \theta(G_1, x) + \theta(G_2, x),$$
and
$$Sd(G,x) = x^{|E(G)|-1} + \sum_{c_1} m(G_1, c_1)x^{|E(G)|-c_1} + \sum_{c_2} m(G_2, c_2)x^{|E(G)|-c_2}.$$

Corollary 13.2.11 Let $G = G(G_1, \ldots, G_k, v_1, \ldots, v_k)$, so:
$$Sd(G,x) = (k-1)x^{|E(G)|-1} + \sum_{i=1}^{k} \sum_{c_i} m(G_i, c_i)x^{|E(G)|-c_i} \quad \text{and} \quad \theta(G,x) =$$
$$(k-1)x + \sum_{i=1}^{k} \theta(G_i, x).$$

Corollary   13.2.12 Let T be   a   tree   with n vertices   and $T = T_n = T(T_{n-1}, T_1, v_{n-1}, v_1)$. Thus we have $\Omega(T_n, x) = (n-1)x$.

Proof Let T_{n-1} be a tree with n-1 vertices constructed by cutting a vertex of degree 1   of T_n.   It   is   easy   to   see   that $\Omega(T_n, x) - \Omega(T_{n-1}, x) = x$, $\Omega(T_{n-1}, x) - \Omega(T_{n-2}, x) = x, \ldots$ and $\Omega(T_2, x) - \Omega(T_1, x) = x$.   So, $\Omega(T_n, x) = (n-1)x$.

Theorem 13.2.13 Let F be a fullerene. Then $\Omega'(0) = 0$ if and only if F be an IPR fullerene.

Proof Let $\Omega'(0) = 0$; this implies that the multiplicity of x in the definition of omega polynomial is zero. Since every hexagonal face has three strips of length 2, thus none of the pentagons make contact with each other. Conversely, if F be an IPR fullerene, then the length of every strip is greater than 2. Hence, $\Omega'(0) = \lambda_1 x + \lambda_2 x^2 + \ldots|_{x=0} = 0$.

Lemma 13.2.14 Let G be a graph on n vertices, m edges, and α be number of its *qoc* strips. Then

$$\alpha = \frac{Sd(G)}{m} + 1.$$

Proof By using the definition of Sadhana index, we have

$$Sd(G) = \sum_s m_s\big(|E(G)| - s\big) = \sum_s m_s|E(G)| - \sum_s m_s \cdot s = (\alpha - 1)m.$$

Corollary 13.2.15 Let F_1 and F_2 be fullerenes of order n. Then
$Sd(F_1) \le Sd(F_2) \Leftrightarrow \alpha(F_1) \le \alpha(F_2)$.

Proof Since $Sd(G) = (\alpha - 1)m$, the proof is straightforward.

Theorem 13.2.16 Suppose F be an IPR fullerene, then

$$Sd(G) \le m(m - 2)/2.$$

Proof For every *qoc* strip C of F, $|C| \ge 2$. Since $2\alpha \le m$, thus $\frac{Sd(G)}{m} + 1 \le m/2$ and so $Sd(G) \le m(m - 2)/2$.

Theorem 13.2.17 Let F be a fullerene graph, then

$$Sd(F) \ge (2 + \Omega'(0))m.$$

Proof Let r and s be the number of *qoc* strips of length 1 and 2, respectively. Clearly $r = \Omega'(0)$ and since every hexagonal face has at least three *qoc* strips of length 2, thus $\alpha \ge 3 + \Omega'(0)$. By using equation (1), the proof is completed.

Conjecture Among all of fullerenes F on n vertices, the *IPR* fullerene has the minimum value of $Sd(F)$.

13.4 Weighted Version of Omega Polynomial

Let $e = uv$ be an edge of G and v be an arbitrary vertex. Denote by $w_G(e)$ and $w_G(v)$ the weights of edge e and vertex v, respectively. For each strip s of G, the weight of s can be defined as

$$w_{G,e}(s) = \sum_{e \in s} w_G(e),$$

$$w_{G,v}(S) = \sum_{v \in V(G[s])} w_G(v) = \sum_{uv \in s} (w_G(u) + w_G(v)).$$

where $G[s]$ is the induced subgraph in G by s. One can see that if G is a co-graph, then

$$w_e(G) = \sum_{e \in E(G)} w_G(e) = \sum_{s \in S} \sum_{e \in s} w_G(e).$$

By using the concept of weighted graph, we define three new versions of omega polynomial: the edge-weighted, vertex-weighted, and edge-vertex-weighted omega polynomial. These new polynomials are defined as follows:

$$\Omega_e(G, x) = \sum_{s \in S} \left\lfloor \frac{w_{G,e}(s)}{|s|} \right\rfloor m(G, s) x^{|s|},$$

$$\Omega_v(G, x) = \sum_{s \in S} m(G, s) x^{\left\lfloor \frac{w_{G,v}(s)}{2} \right\rfloor},$$

$$\Omega_{ev}(G, x) = \sum_{s \in S} \left\lfloor \frac{w_{G,e}(s)}{|s|} \right\rfloor m(G, s) x^{\left\lfloor \frac{w_{G,v}(s)}{2} \right\rfloor}.$$

Obviously, if the weight of each edge and vertex is 1, then

$$\Omega_e(G, x) = \Omega_v(G, x) = \Omega_{ev}(G, x) = \Omega(G, x).$$

Analogously, for theta and Sadhana polynomials, we have

$$\Theta_e(G, x) = \sum_{c \in C} w_{G,e}(c) m(G, c) x^{|c|},$$

$$\Theta_v(G, x) = \sum_{c \in C} m(G, c) |c| x^{\left\lfloor \frac{w_{G,v}(c)}{2} \right\rfloor},$$

$$\Theta_{ev}(G, x) = \sum_{c \in C} w_{G,e}(c) m(G, c) x^{\left\lfloor \frac{w_{G,v}(c)}{2} \right\rfloor},$$

$$Sd_e(G, x) = \sum_{c \in C} m(G, c) x^{w_e(G) - w_{G,e}(c)},$$

$$Sd_v(G, x) = \sum_{c \in C} \left\lfloor \frac{w_{G,v}(c)}{2|c|} \right\rfloor m(G, c) x^{|E| - |c|},$$

$$Sd_{ev}(G, x) = \sum_{c \in C} \left\lfloor \frac{w_{G,v}(c)}{2|c|} \right\rfloor m(G, c) x^{w_e(G) - w_{G,e}(c)}.$$

One can see again, if the weight of each edge and vertex be 1, then $\Theta_e(G, x) = \Theta_v(G, x) = \Theta_{ev}(G, x) = \Theta(G, x)$ and $Sd_e(G, x) = Sd_v(G, x) = Sd_{ev}(G, x) = Sd(G, x)$, respectively. Note that, in co-graphs, $|c_k| = |s_k|$, and the symbols c/s interchanges.

Let G and H be two edge-weighted graphs. The Cartesian product graph of G and H is a graph with vertex set $V(G \times H) = V(G) \times V(H)$ and edge set:

$$E(G \times H) = \{((a, b), (c, d)) : a = c, \ bd \in E(H) \ or \ b = d, \ ac \in E(G)\}.$$

Then, the weight of an edge $((a, b), (c, d))$ is as follows:

- If $a = c$, then $w_{G \times H}(((a, b),(c, d))) = w_H(bd)$.
- If $b = d$, then $w_{G \times H}(((a, b),(c, d))) = w_G(ac)$.

In this section, we compute the weighted omega polynomial of Cartesian product of two weighted graphs.

Lemma 13.3.1 Let G and H be graphs. Then we have:

(a) $|V(G \times H)| = |V(G)| \, |V(H)|,$
$|E(G \times H)| = |E(G)| \, |V(H)| + |V(G)| \, |E(H)|;$
(b) $G \times H$ is connected if and only if G and H are connected.
(c) If (a, x) and (b, y) are vertices of $G \times H$, then $d_{G \times H}((a, x), (b, y)) = d_G(a, b) + d_H(x, y)$.
(d) The Cartesian product is associative.

We recall that for a graph G and $e \in E(G)$, $N(e) = |E| - (n_e u(e|G) + n_e v(e|G))$.

The following result is a direct consequence of Lemma 1.

Lemma 13.3.2 Suppose (a, x) and (b, y) are adjacent vertices of $G \times H$, where G and H are co-graphs. Then

$$N_{G \times H}((a, x)(b, y)) = \begin{cases} |V(G)| \, N(f) & for \ a = b \ and \ x \, y = f \in E(H) \\ |V(H)| \, N(g) & for \ x = y \ and \ ab = g \in E(G) \end{cases},$$

$$w_{G \times H, e}(c) = \begin{cases} |V(G)| \, w_{H, e}(c) & for \ c = |V(G)| c_H \\ |V(H)| \, w_{G, e}(c) & for \ c = |V(H)| c_G \end{cases}.$$

Theorem 13.3.3 Let G and H be connected co-graphs. Then

Proof By using Lemmas 1 and 2 and the definition of omega polynomial of a graph, we have

$$\Omega_e(G \times H, x) = \sum_{c_1} \left\lfloor \frac{w_{G,e}(c_1)}{|c_1|} \right\rfloor m_1 . x^{\left| V(H) \right| \left| c_1 \right|} + \sum_{c_2} \left\lfloor \frac{w_{H,e}(c_2)}{|c_2|} \right\rfloor m_2 . x^{\left| V(G) \right| \left| c_2 \right|}$$

and

$$\Omega_e(G \times H, x) = \sum_c m(G \times H, c).x^c$$
$$= \sum_{c_1} \left\lfloor \frac{w_{G,e}(c_1)}{|c_1|} \right\rfloor m_1.x^{\left| V(H) \right| c_1}$$
$$+ \sum_{c_2} \left\lfloor \frac{w_{H,e}(c_2)}{|c_2|} \right\rfloor m_2.x^{\left| V(G) \right| c_2}$$

where $m_1 = m(G, c_1)$ and $m_2 = m(H, c_2)$, and this completes the proof.

Theorem 13.3.4 Let $G_1, G_2, \cdots, G_n$ be connected co-graphs. Then we have

$$\Omega_e(G_1 \times G_2 \times \quad \times G_n, x) = \sum_{i=1}^{n} \sum_{c_i} \left\lfloor \frac{w_{G_i,e}(c_i)}{|c_i|} \right\rfloor m(G_i, c_i).x^{\prod_{\substack{j=1 \\ j \neq i}}^{n} | V(G_j) | c_i}$$

Proof We use induction on n. By Theorem 13.3.1, the result is valid for $n = 2$. Let $n \geq 3$ and assume the theorem holds for $n - 1$. Set $G = G_1 \times \ldots \times G_{n-1}$. Then we have

$$\Omega_e(G \times G_n, x) = \sum_c \left\lfloor \frac{w_{G,e}(c)}{|c|} \right\rfloor m(G, c).x^{\left| V(G_n) \right| c}$$
$$+ \sum_{c_n} \left\lfloor \frac{w_{G_n,e}(c_n)}{|c_n|} \right\rfloor m(G_n, c_n).x^{\left| V(G) \right| c_n}$$
$$= \sum_{i=1}^{n-1} \sum_{c_i} \left\lfloor \frac{w_{G_i,e}(c_i)}{|c_i|} \right\rfloor m(G_i, c_i).x^{\prod_{\substack{j=1 \\ j \neq i}}^{n} | V(G_j) | c_i}$$
$$+ \sum_{c_n} \left\lfloor \frac{w_{G_n,e}(c_n)}{|c_n|} \right\rfloor m(G_n, c_n).x^{\left| V(G) \right| c_n}$$
$$= \sum_{i=1}^{n} \sum_{c_i} \left\lfloor \frac{w_{G_i,e}(c_i)}{|c_i|} \right\rfloor m(G_i, c_i).x^{\prod_{\substack{j=1 \\ j \neq i}}^{n} | V(G_j) | c_i} \qquad .$$

One can compute the same results for the Sadhana and theta polynomials as previously.

Theorem 13.3.5 The omega polynomial of fullerene graph $G = C_{40n+6}$ is computed as follows:

$$\Omega(G, x) = \begin{cases} a(x) + 4x^{2n} + 4x^{2n+1} + 4x^{4n-1} + 2x^{4n} & 5|n \\ a(x) + 2x^{4n+3} + 8x^{2n-2} + 2x^{4n+4} + 2x^{4n+1} & 5|n-1 \\ a(x) + 8x^{2n} + 4x^{2n-1} + 2x^{4n} + 2x^{4n+2} & 5|n-2 \,, \\ a(x) + 4x^{2n-2} + 4x^{2n+2} + 4x^{4n-1} + 2x^{4n+2} & 5|n-3 \\ a(x) + 4x^{2n-2} + 4x^{2n-1} + 4x^{2n} + 2x^{4n+3} + x^{8n+6} & 5|n-4 \end{cases}$$

where $a(x) = x + 9x^2 + 4x^3 + 2x^4 + (2n-3)x^{10}$.

Proof From Fig. 13.9, one can see that there are ten distinct cases of ops strips in G. We denote the corresponding edges by $e_1, e_2, \ldots, e_{10}$. By using calculations given in Table 13.1 and Fig. 13.10, the proof is completed.

Next, we consider a class of fullerenes with exactly $10n$ vertices, Fig. 13.11. There are six distinct cases of *qoc* strips as shown in Fig. 13.12.

We denote the corresponding edges by $e_1, e_2, \ldots, e_6$. Then $|C(e_1)| = |C(e_2)| = |C(e_3)| = |C(e_6)| = 1$, $|C(e_4)| = 5$ and $|C(e_5)| = n - 1$. On the other hand, there are five similar edges for each of edges e_1, e_2, e_3, and e_6, $n - 2$ edges similar to e_4 and 10 edges similar to e_5. Therefore,

$$\Omega(F_n, x) = 20x + (n - 2)x^5 + 10x^{(n-1)}.$$

In what follows, a new class of fullerenes with $10n$ carbon atoms are considered. In Table 13.2, we list the omega polynomial of F_n for $n \leq 9$.

Theorem 13.3.6 Consider the fullerene graphs C_{10n}, $n \geq 2$. Then the omega polynomial of C_{10n} is computed as follows:
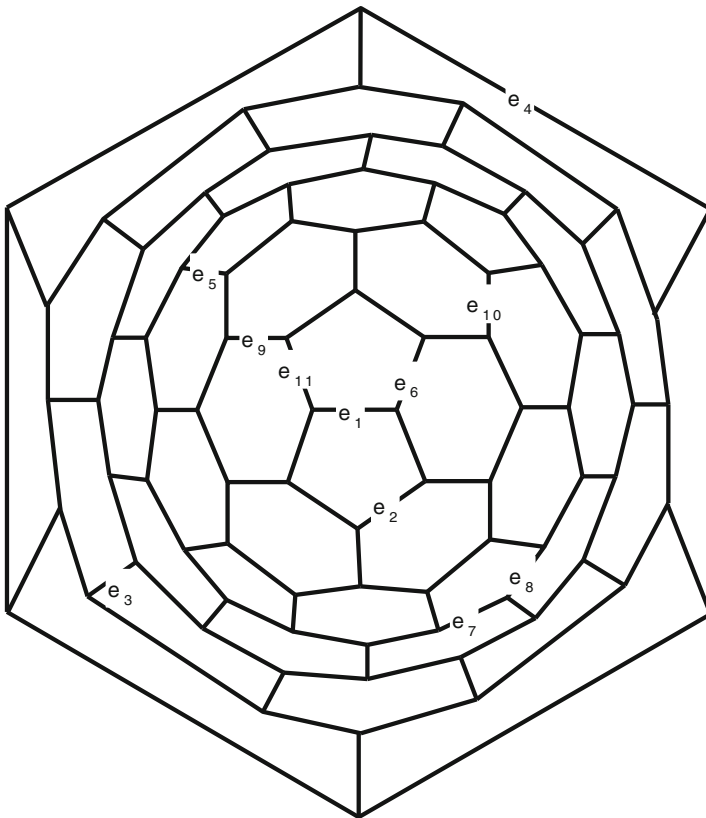
Fig. 13.9 The graph of fullerene C_{40n+6}, when $n = 2$

Graph of fullerene C_{40n+6} Edges co distant to e_1 Edges co distant to e_2

Edges co distant to e_3 Edges co distant to e_4 Edges co distant to e_5

Edges co distant to e_6 Edges co distant to e_7 Edges co distant to e_8

Edges co distant to e_9 Edges co distant to e_{10} Edges co distant to e_{11}
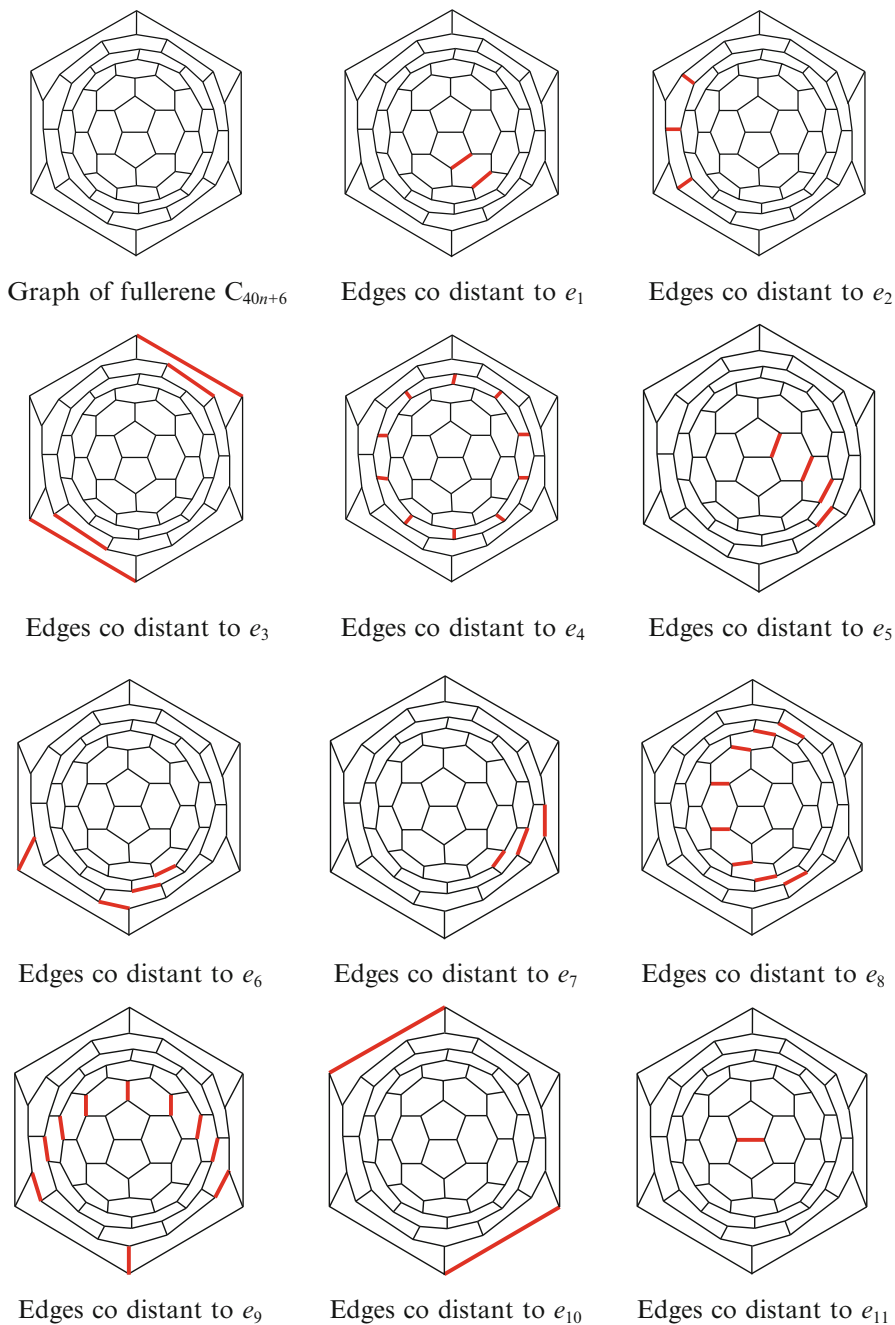
Fig. 13.10 The main cases of C_{40n+6} fullerenes regarding co-distant edges

Fig. 13.11 The fullerene graph F_n, $n = 8$

e_1 $\qquad\qquad\qquad$ e_2 $\qquad\qquad\qquad$ e_3

e_4 $\qquad\qquad\qquad$ e_5 $\qquad\qquad\qquad$ e_6
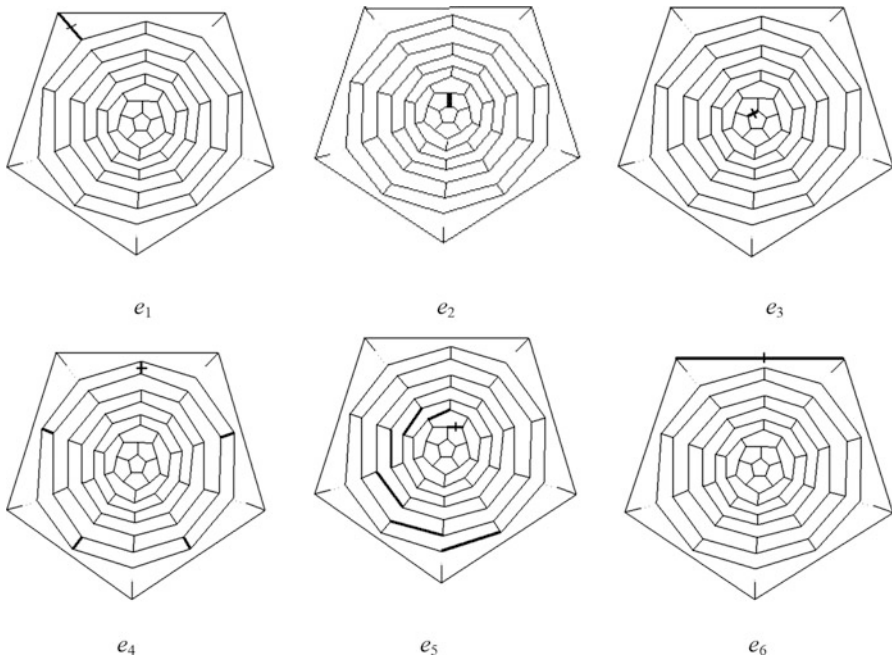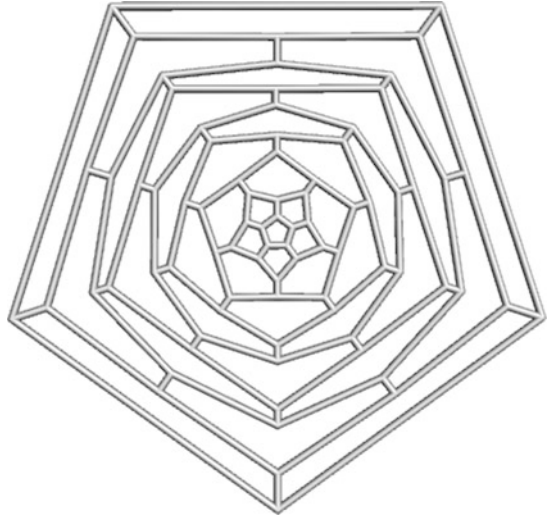
Fig. 13.12 The *qoc* strips of edges $e_1, e_2, \ldots, e_6$ in F_n

$$\Omega(F_{10n}, x) = \begin{cases} 10x^3 + 10x^{\frac{n}{2}} + 10x^{n-3} & 2 \mid n \\ 10x^3 + 5x^{\frac{n-3}{2}} + 5x^{\frac{n+3}{2}} + 10x^{n-3} & 2 \nmid n \end{cases},$$

Table 13.2 The omega polynomial of F_n for $n \leq 9$

Fullerenes	Omega polynomials
C_{20}	$30X^1$
C_{30}	$20X^1 + 1X^5 + 10X^2$
C_{40}	$20X^1 + 2X^5 + 10X^3$
C_{50}	$20X^1 + 3X^5 + 10X^4$
C_{60}	$20X^1 + 4X^5 + 10X^5$
C_{70}	$20X^1 + 5X^5 + 10X^6$
C_{80}	$20X^1 + 6X^5 + 10X^7$
C_{90}	$20X^1 + 7X^5 + 10X^8$

Table 13.3 The number of co-distant edges, when $2|n$

Type of edges	Number of co-distant edges	No.
e_1	3	10
e_2	$n/2$	10
e_3	$n - 3$	10

Table 13.4 The number of co-distant edges, when $2 \nmid n$

Type of edges	Number of co-distant edges	No.
e_1	3	10
e_2	$(n-3)/2$	5
e_3	$(n+3)/2$	5
e_4	$n - 3$	10

Proof To compute the omega polynomial of C_{10n}, it is enough to calculate $C(e)$ for every $e \in E(G)$. In Tables 13.4 and 13.5, the number of co-distant edges of this fullerene is computed.

From calculations given in Tables 13.3 and 13.4 and Figs. 13.13 and 13.14, the equation is obtained which completes the proof.

Theorem 13.3.7 Suppose G is the molecular graph of C_{24n} fullerene. Then the omega polynomial of G is $\Omega(G, x) = 3x^{2n} + 6x^n + 12x^{2n-3} + 12x^3$.

Proof It is easy to see that there are four different type of edges, f_1, f_2, f_3, and f_4, Fig. 13.10. The number of edges co-distant to f_1, f_2, f_3, and f_4 are $2n$, $2n - 3$, 3, and n, respectively. On the other hand, there are 3 edges similar to f_1, 12 edges similar to f_2, 12 edges similar to f_3, and 6 edges similar to f_4, Fig. 13.15. Therefore,

$$\Omega(G, x) = 3x^{2n} + 6x^n + 12x^{2n-3} + 12x^3.$$

Theorem 13.3.8 The omega polynomial of fullerene graph C_{12n+4} is as follows:

$$\Omega(C_{12n+4}, x) = 18x + 4x^2 + (n-2)x^6 + 8x^{n-1} + 4x^n.$$

Fig. 13.13 The fullerene graph C_{10n} (*n* is odd)
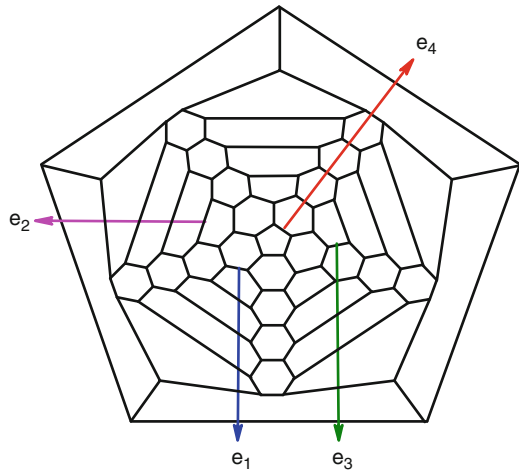
Fig. 13.14 The fullerene graph C_{10n} (*n* is even)
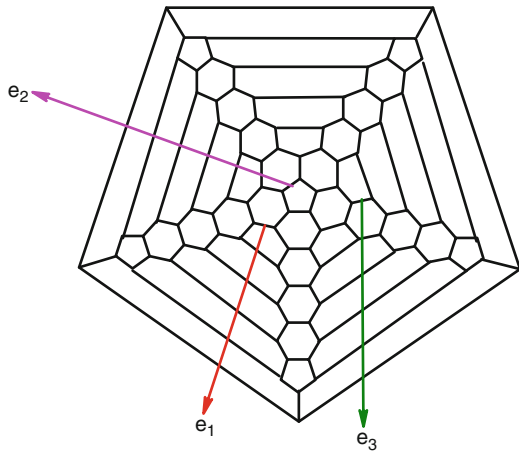
Proof By Fig. 13.16, there are five distinct cases of *qoc* strips. We denote the corresponding edges by $e_1, e_2, \ldots, e_5$. By Table 13.5 one can see that $|C(e_1)| = 2$, $|C(e_2)| = n - 1$, $|C(e_3)| = n$, $|C(e_4)| = 1$, and $|C(e_5)| = 6$. On the other hand, there are 4, 8, 4, 18, and $n-2$ similar edges for each of edges e_1, e_2, e_3, e_4, and e_5, respectively. So, we have

$$\Omega(C_{12n+4}, x) = 18x + 4x^2 + (n - 2)x^6 + 8x^{n-1} + 4x^n.$$

Theorem 13.3.9 The omega polynomial of the fullerene graph $C_{12(2n+1)}$ is as follows:

Fig. 13.15 The Schlegel graph of C_{24n} fullerene
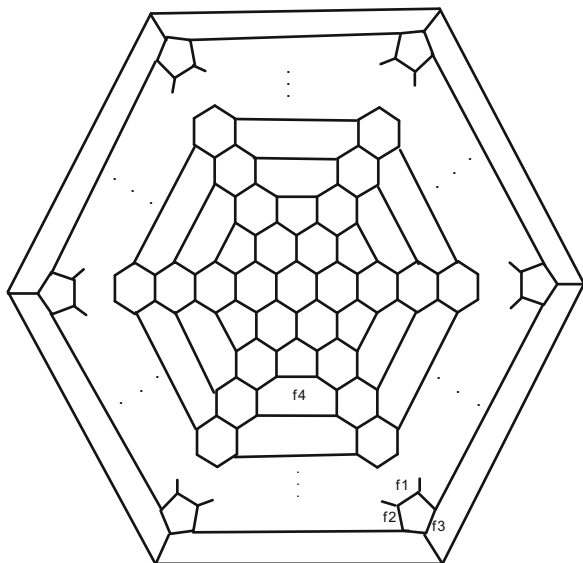
$$\Omega(G,x) = 12x^3 + 12x^{2n-2} + 6x^{n-1} + 3x^{2n+4} , \; n \geq 2$$

Proof By Fig. 13.17, there are four distinct cases of *qoc* strips. We denote the corresponding edges by e_1, e_2, e_3, and e_4. By Table 13.6, one can see that $|C(e_1)| = 3$, $|C(e_2)| = 2n - 2$, $|C(e_3)| = 2n + 4$, and $|C(e_4)| = n - 1$. On the other hand, there are 12, 12, 3, and 6 similar edges for each of edges e_1, e_2, e_3, and e_4, respectively. So, we have $\Omega(G,x) = 12x^3 + 12x^{2n-2} + 6x^{n-1} + 3x^{2n+4} , \; n \geq 2$.

13.5 Examples

In this section, the omega polynomial of some well-known graphs is computed.

Example 13.4.1 Consider the graph of dendrimer D with n vertices depicted in Fig. 13.18. Because this graph is a tree with n vertices, we have $\Omega(D, x) = (n - 1)x$.

Example 13.4.2 Consider the graph of nano-star dendrimer N with n vertices, see Fig. 13.19. It is easy to see that $|V(G_n)| = 19n$ and $|E(G_n)| = 22n - 1$. Now we have

$G_n = G(G_{n-1}, G_1, v_{n-1}, v_1)$ and then the following relations:
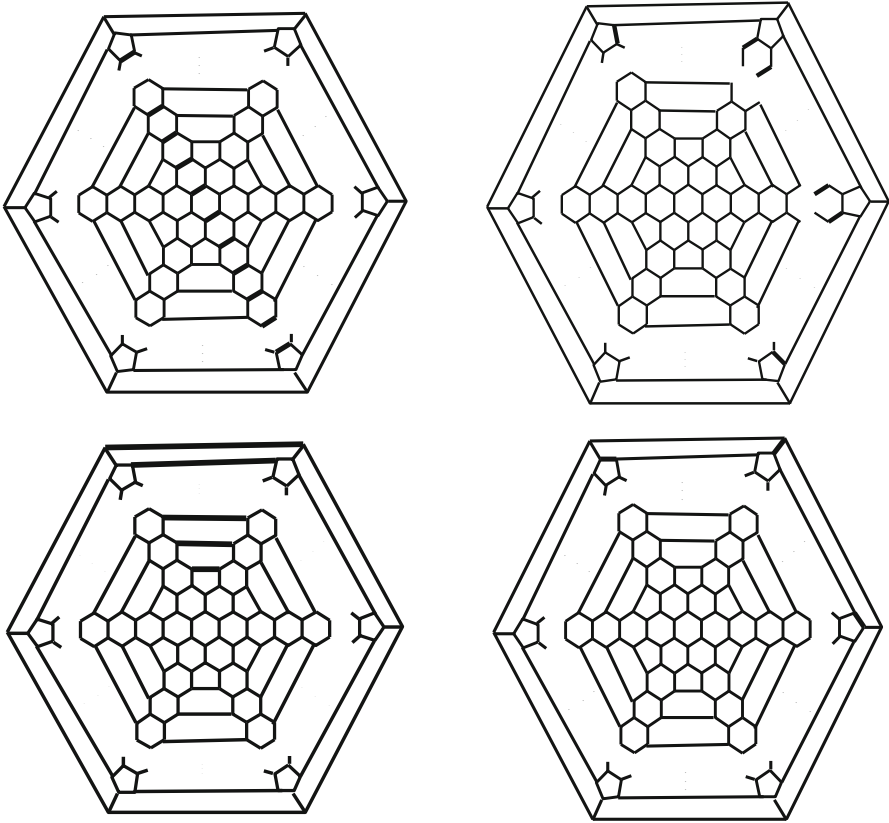
Fig. 13.16 Four different types of edges in C_{24n} fullerene

Table 13.5 The number of co-distant edges of e_i, $1 \leq i \leq 5$

No.	Number of co-distant edges	Type of edges
4	2	e_1
8	$n-1$	e_2
4	n	e_3
18	1	e_4
$n-2$	6	e_5

$$\Omega(G_n, x) = x + \Omega(G_{n-1}, x) + \Omega(G_1, x),$$
$$\Omega(G_n, x) - \Omega(G_{n-1}, x) = x + \Omega(G_1, x),$$
$$\Omega(G_{n-1}, x) - \Omega(G_{n-2}, x) = x + \Omega(G_1, x),$$
$$\Omega(G_2, x) - \Omega(G_1, x) = x + \Omega(G_1, x).$$

Now by summation of these relations, we have
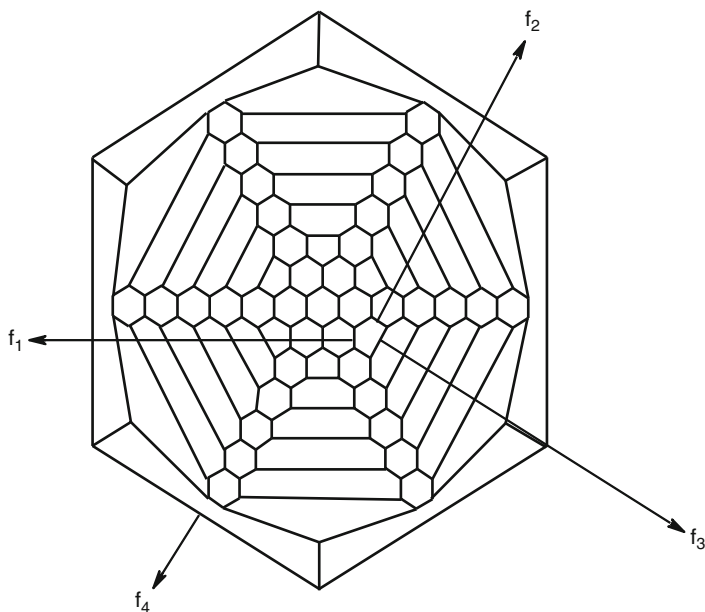
Fig. 13.17 The *qoc* strips of edges in graph of fullerene $C_{12(2n+1)}$

Table 13.6 The number of co-distant edges of e_i, $1 \leq i \leq 4$

Edge	The number of co-distant edges	No.
e_1	3	12
e_2	$2n-2$	12
e_3	$2n+4$	3
e_4	$n-1$	6

$\Omega(G_n, x) - \Omega(G_1, x) = (n-1)x + (n-1)\Omega(G_1, x)$. So $\Omega(G_n, x) = (n-1)x + n\Omega(G_1, x)$. But $\Omega(G_1, x) = 3x + 9x^2$. Thus, $\Omega(G_n, x) = (n-1)x + n(3x + 9x^2) = 9nx^2 + (4n-1)x$, $Sd(G_n, x) = (4n-1)x^{22n-2} + 9nx^{22n-3}$, and $\theta(G_n, x) = 18nx^2 + (4n-1)x$.

Example 13.4.3 Suppose Q_n denotes a hypercube of dimension n. Then

$$\Omega_e(Q_n, x) = \Omega_e\left(K_2^n, x\right) = n. \sum_c \left\lfloor \frac{w_{K_2,e}(c)}{|c|} \right\rfloor m(K_2, c).x^{\left| V(K_2) \right| \left| n-1_c \right|}.$$

$$= n. \lfloor w_e(K_2) \rfloor . x^{2^{n-1}}.$$

Example 13.4.4 Let P_n be a path of length n and C_n an n-cycle. Then

$$\Omega_e(C_n, x) = \begin{cases} \sum_{i=1}^{\frac{n}{2}} \left\lfloor \frac{w_{C_n,e}(c_i)}{2} \right\rfloor x^2 & 2 \mid n \\ \sum_{i=1}^{n} \lfloor w_{C_n,e}(c_i) \rfloor x & 2 \nmid n \end{cases}.$$
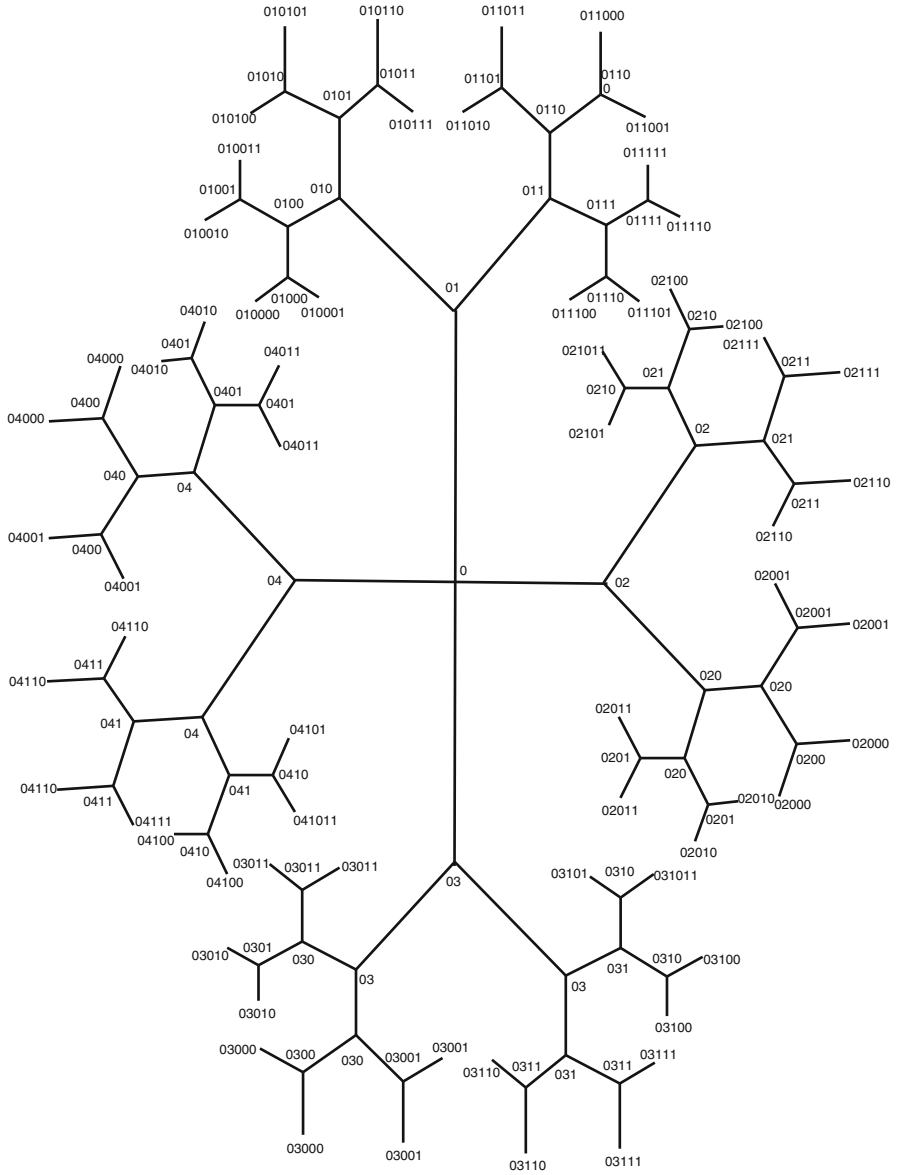
Fig. 13.18 2*D* graphical representation of a dendrimer *D*

Also we have

$$\Omega_e(P_n, x) = \sum_{i=1}^{n-1} \lfloor w_{P_n, e}(c_i) \rfloor x.$$
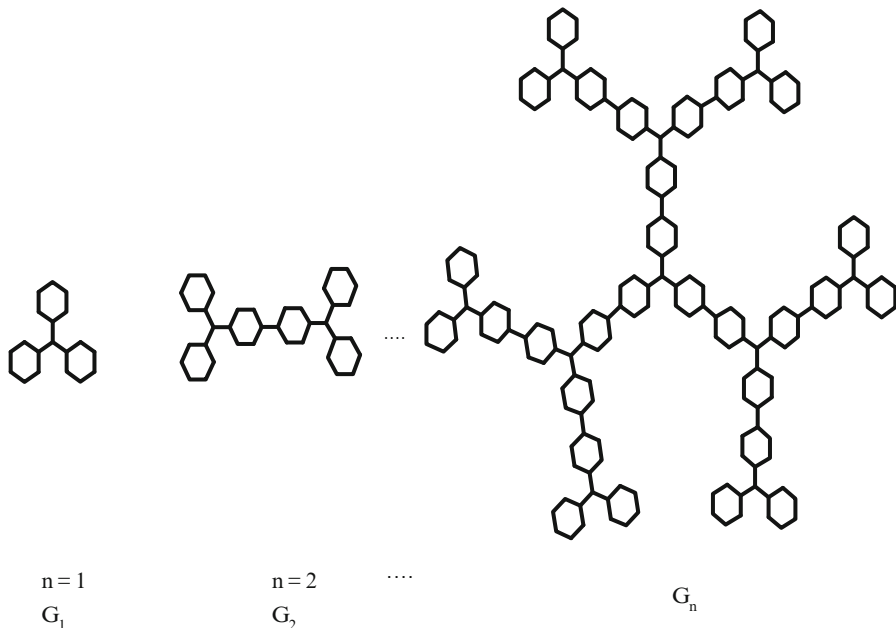
Fig. 13.19 $2D$ graphical representation of a nano-star dendrimer N

So,

$$\Omega_e(P_n \times P_m, x) = \sum_{i=1}^{n-1} \lfloor w_{P_n,e}(c_i) \rfloor x^m + \sum_{j=1}^{m-1} \lfloor w_{P_n,e}(c_j) \rfloor x^n.$$

In other words

$$\Omega_e(P_n \times C_m, x) = \begin{cases} \displaystyle\sum_{i=1}^{n-1} \lfloor w_{P_n,e}(c_i) \rfloor x^m + \sum_{j=1}^{\frac{m}{2}} \left\lfloor \frac{w_{C_m,e}(c_j)}{2} \right\rfloor x^{2n} & 2|m \\[3ex] \displaystyle\sum_{i=1}^{n-1} \lfloor w_{P_n,e}(c_i) \rfloor x^m + \sum_{j=1}^{m} \lfloor w_{C_m,e}(c_j) \rfloor x^n & 2 \nmid m \end{cases},$$

$$\Omega_e(C_n \times C_m, x) = \begin{cases} \displaystyle\sum_{i=1}^{n} \lfloor w_{C_n,e}(c_i) \rfloor x^m + \sum_{j=1}^{m} \lfloor w_{C_m,e}(c_j) \rfloor x^n & 2 \nmid m,\ 2 \nmid n \\[3ex] \displaystyle\sum_{i=1}^{n} \lfloor w_{C_n,e}(c_i) \rfloor x^m + \sum_{j=1}^{\frac{m}{2}} \left\lfloor \frac{w_{C_m,e}(c_j)}{2} \right\rfloor x^{2n} & 2|m,\ 2 \nmid n \\[3ex] \displaystyle\sum_{i=1}^{\frac{n}{2}} \left\lfloor \frac{w_{C_n,e}(c_i)}{2} \right\rfloor x^{2m} + \sum_{j=1}^{m} \lfloor w_{C_m,e}(c_j) \rfloor x^n & 2 \nmid m,\ 2|n \\[3ex] \displaystyle\sum_{i=1}^{\frac{n}{2}} \left\lfloor \frac{w_{C_n,e}(c_i)}{2} \right\rfloor x^{2m} + \sum_{j=1}^{\frac{m}{2}} \left\lfloor \frac{w_{C_m,e}(c_j)}{2} \right\rfloor x^{2n} & 2|m,\ 2|n \end{cases}.$$

Fig. 13.20 The graph F_{24}
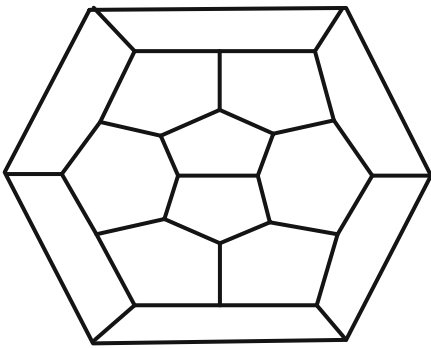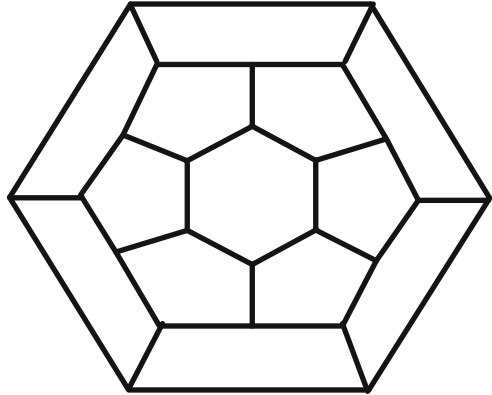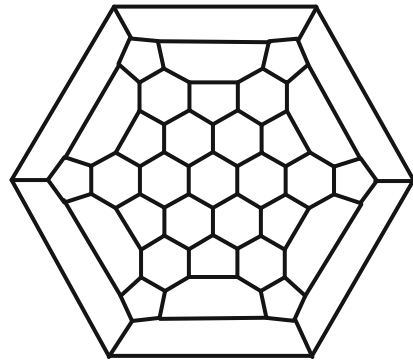
F_{26} $Le(F_{26})$

Fig. 13.21 The leapfrog of graph F_{26}

Example 13.4.5 Consider the fullerene graph F_{24} in Fig. 13.20. This fullerene graph has 36 edges. One can see that $\Omega(x) = 24x + 6x^2$ and so $Sd(x) = 24x^{35} + 6x^{34}$.

Example 13.4.6 Consider the fullerene graph F_{26} depicted in Fig. 13.21. This fullerene graph has 39 edges. Similar to the last example, one can see that $\Omega(F_{26}, x) = 21x + 9x^2$ and so, $Sd(F_{24}, x) = 21x^{38} + 9x^{37}$. By computing these polynomials for the leapfrog fullerene, we have

$$\Omega(x) = 24x^3 + 6x^6 + x^9.$$

References

Aihara J (1976) A new definition of Dewar – type resonance energies. J Am Chem Soc 98:2750–2758

Ashrafi AR, Ghorbani M (2008) A note on markaracter tables of finite groups. MATCH Commun Math Comput Chem 59:595–603

Ashrafi AR, Ghorbani M, Jalali M (2008a) Computing Sadhana polynomial of V – phenylenic nanotubes and nanotori. Ind J Chem 47A:535–537

Ashrafi AR, Jalali M, Ghorbani M, Diudea MV (2008b) Computing PI and omega polynomials of an infinite family of fullerenes. MATCH Commun Math Comput Chem 60:905–916

Balasubramanian K, Ramaraj R (1985) Computer generation of king and color polynomials of graphs and lattices and their applications to statistical mechanics. J Comput Chem 6:447–454

Cigher S, Diudea MV (2007) Omega Polynomial Counter. Babes-Bolyai University

Clar E (1964) Polycyclic hydrocarbons. London, Academic Press

Clar E (1972) The aromatic sextet. Wiley, New York

Darafsheh MR (2010) Computation of topological indices of some graphs. Acta Appl Math 110:1225–1235

Diudea MV (2002) Toroidal graphenes from 4 – valent tori. Bull Chem Soc Jpn 75(3):487–492

Diudea MV (2004) Covering forms in nanostructures. Forma (Tokyo) 19:131–163

Diudea MV (2005a) Nanoporous carbon allotropes by septupling map operations. J Chem Inf Model 45:1002–1009

Diudea MV (ed) (2005a) Nanostructures. novel architecture, Nova, New York

Diudea MV (2006) Omega polynomial. Carpath J Math 22:43–47

Diudea MV, Nagy CSL (2007) Periodic nanostructures. Springer, Dordrecht

Diudea MV, Ivanciuc O, Nikolic' S, Trinajstic N (1997) Matrices of reciprocal distance, polynomials and derived numbers. MATCH Commun Math Comput Chem 35:41–64

Diudea MV, Gutman I, Jäntschi L (2002) Molecular topology. Nova, New York

Diudea MV, John PE, Graovac A, Primorac M, Pisanski T (2003) Leapfrog and related operations on toroidal fullerenes. Croat Chem Acta 76:153–159

Diudea MV, Cigher S, Vizitiu AE, Ursu O, John PE (2006a) Omega polynomial in tubular nanostructures. Croatica Chemica Acta 79(3):445–448

Diudea MV, Stefu M, John PE, Graovac A (2006b) Generalized operations on maps. Croatica Chemica Acta 79(3):355–362

Diudea MV, Vizitiu AE, Janezic D (2007) Cluj and related polynomials applied in correlating studies. J Chem Inf Model 47(3):864–874

Diudea MV, Cigher S, Vizitiu AE, Florescu MS, John PE (2009) Omega polynomial and its use in nanostructure description. J Math Chem 45:316–329

Djoković DŽ (1973) Distance-preserving subgraphs of hypercubes. J Combin Theory Ser B 14:263–267

Dwyes PS (1951) Linear computations. Wiley, New York

Fadeev DK, Sominsky IS (1965) Problems in higher algebra. Freeman, San Francisco

Farrell EJ (1979) An introduction to matching polynomials. J Comb Theory B 27:75–86

Farrell EJ, De Matas CM (1988a) On star polynomials of complements of graphs. Arkiv for matematik 26(1–2):185–190

Farrell EJ, De Matas CM (1988b) Star polynomials of some families of graphs with small cyclomatic numbers. Util Math 33:33–45

Ghorbani M, Ashrafi AR (2006) Counting the number of hetero fullerenes. J Comput Theor Nanosci 3:803–810

Graham RL, Lovaśz L (1978) Distance matrix polynomials of trees. Adv Math 29:60–88

Gutman I (1992) Some analytical properties of the independence and matching polynomials. MATCH Commun Math Comput Chem 28:139–150

Gutman I, Hosoya H (1990) Molecular graphs with equal Z – counting and independence polynomials. Z Naturforsch 45:645–648

Gutman I, Milun M, Trinajstić N (1975) Topological definition of delocalisation energy. MATCH Commun Math Comput Chem 1:171–175

Gutman I, Milun M, Trinajstić N (1977) Graph theory and molecular orbitals 19. Nonparametric resonance energies of arbitrary conjugated systems. J Am Chem Soc 99:1692–1704

Gutman I, Klavžar S, Petkovšek M, Žigert P (2001) On Hosoya polynomials of benzenoid graphs. MATCH Commun Math Comput Chem 43:49–66

Harary F (1962) The determinant of the adjacency matrix of a graph. SIAM Rev 4:202–210

Hosoya H (1971) Topological index. A newly proposed quantity characterizing the topological nature of structural isomers of saturated hydrocarbons. Bull Chem Soc Japan 44:2332–2339

Hosoya H (1988) On some counting polynomials in chemistry. Discrete Appl Math 19:239–257

Hosoya H (1990) Clar's aromatic sextet and sextet polynomial. Top Curr Chem 153:255–272

Hosoya H, Yamaguchi T (1975) Sextet polynomial. A new enumeration and proof technique for the resonance theory applied to the aromatic hydrocarbons. Tetrahedron Lett 16 (52):4659–4662

Hosoya H, Murakami M, Gotoh M (1973) Distance polynomial and characterization of a graph. Natl Sci Rept Ochanomizu Univ 24:27–34

Ivanciuc O, Diudea MV, Khadikar PV (1998) New topological matrices and their polynomials. Indian J Chem − Sect A Inor, Phys, Theor Anal Chem 37(7):574–585

Ivanciuc O, Ivanciuc T, Diudea MV (1999) Polynomials and spectra of molecular graphs. Roum Chem Quart Rev 7:41–67

Jalali M, Ghorbani M (2009) On omega polynomial of C_{40n+6} fullerenes. Studia Universititatis Babes − Bolyai 54:25–32

John PE, Khadikar PV, Singh J (2007a) A method of computing the PI index of benzenoid hydrocarbons using orthogonal cuts. Journal of Mathematical Chemistry 42(1):37–45

John PE, Vizitiu AE, Cigher S, Diudea MV (2007b) CI index in tubular nanostructures. MATCH Commun Math Comput Chem 57:479–484

Klavžar S (2008) Some comments on co graphs and CI index. MATCH Commun Math Comput Chem 59:217–222

Konstantinova EV, Diudea MV (2000) The Wiener polynomial derivatives and other topological indices in chemical research. Croat Chem Acta 73:383–403

Kroto HW, Heath JR, O'Brien SC, Curl RF, Smalley RE (1985) C_{60}: Buckminster fullerene. Nature 318:162–163

Kroto HW, Fichier JE, Cox DE (1993) The fullerene. Pergamon Press, New York

Ohkami N, Hosoya H (1983) Topological dependency of the aromatic sextets in polycyclic benzenoid hydrocarbons, recursive relations of the sextet polynomial. Theor Chim Acta 64:153–170

Ohkami N, Motoyama A, Yamaguchi T, Hosoya H (1981) Mathematical properties of the set of the Kekule patterns and the sextet polynomial for polycyclic aromatic hydrocarbons. Tetrahedron 37:1113–1122

Ovchinikov S (2007) Partial cubes: structures, characterizations and constructions. arXiv: 0704.0010v1 [math CO].

Sachs H (1964) Beziehungen zwischen den in einem graphen enthaltenen Kreisen und seinem charakteristischen polynom. Publ Math (Debrecen) 11:119–134

Stefu M, Diudea MV, John PE (2005) Composite operations on maps. Studia Univ. "Babes − Bolyai" 50:165–174

Stevanovic D (1998) Graphs with palindromic independence polynomial. Graph Theory Notes NY 34:31–36

Tang A, Kiang Y, Yan G, Tai S (1986) Graph theoretical molecular orbitals. Science Press, Beijing

Trinajstić N (1992) Chemical graph theory. IInd Ed CRC Press, Boca Raton

Vizitiu AE, Cigher S, Diudea MV, Florescu MS (2007) Omega polynomial in ((4,8)3) tubular nanostructures. MATCH Commun Math Comput Chem 57(2):457–462

Winkler PM (1984) Isometric embedding in products of complete graphs. Discret Appl Math 7:221–225

Chapter 14
Edge-Wiener Indices of Composite Graphs

Mahdieh Azari and Ali Iranmanesh

Abstract The distance $d(u, v|G)$ between the vertices u and v of a simple connected graph G is the length of any shortest path in G connecting u and v. The Wiener index $W(G)$ of G is defined as the sum of distances between all pairs of vertices of G. The edge-Wiener index of G is conceived in an analogous manner as the sum of distances between all pairs of edges of G. Two possible distances $d_0(e, f|G)$ and $d_4(e, f|G)$ between the edges e and f of G can be considered and according to them, the corresponding edge-Wiener indices $W_{e_0}(G)$ and $W_{e_4}(G)$ are defined. In this chapter, we report our recent results on computing the first and second edge-Wiener indices of some composite graphs. Results are illustrated by some interesting examples.

14.1 Introduction

In this chapter, we consider connected finite graphs without any loops or multiple edges. In theoretical chemistry, the physicochemical properties of chemical compounds are often modeled by means of molecular-graph-based structure descriptors, which are also referred to as topological indices (Gutman and Polansky 1986; Trinajstić 1992; Todeschini and Consonni 2000; Diudea 2001). In the other words, a topological index $\text{Top}(G)$ of a graph G is a real number with the property that for every graph H isomorphic to G, $\text{Top}(H) = \text{Top}(G)$. Among the variety of topological indices which are designed to capture the different aspects of molecular structure, the Wiener index is the best known one. Vertex version of the Wiener index is the first reported distance-based topological index which was introduced by Wiener (1947a, b). Wiener used his index, for the calculation of the boiling points

M. Azari
Department of Mathematics, Kazerun Branch, Islamic Azad University, 73135-168, Kazerun, Iran
e-mail: azari@kau.ac.ir

A. Iranmanesh (✉)
Department of Pure Mathematics, Faculty of Mathematical Sciences, Tarbiat Modares University, 14115-137, Tehran, Iran
e-mail: iranmanesh@modares.ac.ir

of alkanes. Using the language which in theoretical chemistry emerged several decades after Wiener, we may say that the Wiener index was conceived as the sum of distances between all pairs of vertices in the molecular graph of an alkane, with the evident aim to provide a measure of the compactness of the respective hydrocarbon molecule. From graph-theoretical point of view, Wiener index of a graph G is defined as:

$$W(G) = \sum_{\{u,v\} \subseteq V(G)} d(u,v|G),$$

where $d(u,v|G)$ denotes the distance between the vertices u and v of G which is defined as the length of any shortest path in G connecting them. Wiener index happens to be one of the most frequently and most successfully employed structural descriptors that can be deduced from the molecular graph. Since 1976, the Wiener number has found a remarkable variety of chemical applications. Physical and chemical properties of organic substances, which can be expected to depend on the area of the molecular surface and/or on the branching of the molecular carbonatom skeleton, are usually well correlated with the Wiener index. Among them are the heats of formation, vaporization and atomization, density, boiling point, critical pressure, refractive index, surface tension and viscosity of various acyclic and cyclic, saturated and unsaturated as well as aromatic hydrocarbon species, velocity of ultrasound in alkanes and alcohols, rate of electro reduction of chlorobenzenes etc. (Gutman et al. 1993). We refer the reader to Buckley and Harary (1990); Graovac and Pisanski (1991); Gutman (1994); Diudea (1995); Dobrynin et al. (2001); John and Diudea (2004); Ashrafi and Yousefi (2007); and Putz et al. (2013), for more information about the Wiener index.

The Wiener polynomial of a graph G is defined in terms of a parameter q as follows:

$$W(G; q) = \sum_{\{u,v\} \subseteq V(G)} q^{d(u,v|G)}.$$

This coincides with the definition of Hosoya (1988) and Sagan et al. (1996). It is clear that, the first derivative of the Wiener polynomial of G at $q = 1$ is equal to the Wiener index of G, i.e., $W'(G; 1) = W(G)$.

Edge versions of the Wiener index based on distance between all pairs of edges in a graph G were introduced independently by (Dankelman et al. 2009; Iranmanesh et al. 2009; and Khalifeh et al. 2009b). Two possible distances between the edges $e = uv$ and $f = zt$ of a graph G can be considered (Iranmanesh et al. 2009). The first distance is denoted by $d_0(e,f|G)$ and defined as follows:

$$d_0(e,f|G) = \begin{cases} d_1(e,f|G) + 1 & \text{if } e \neq f, \\ 0 & \text{if } e = f, \end{cases}$$

where $d_1(e,f|G) = \min\{d(u,z|G), d(u,t|G), d(v,z|G), d(v,t|G)\}$. It is easy to see that $d_0(e,f|G) = d(e,f|L(G))$, where $L(G)$ is the line graph of G.

The second distance is denoted by $d_4(e,f|G)$ and defined as follows:

$$d_4(e,f|G) = \begin{cases} d_2(e,f|G) & \text{if } e \neq f, \\ 0 & \text{if } e = f, \end{cases}$$

where $d_2(e,f|G) = \max\{d(u,z|G), d(u,t|G), d(v,z|G), d(v,t|G)\}$.

Corresponding to the above distances, two edge versions of the Wiener index can be defined. The first and second edge-Wiener indices of G are denoted by $W_{e_0}(G)$ and $W_{e_4}(G)$, respectively and defined as follows (Iranmanesh et al. 2009):

$$W_{e_i}(G) = \sum_{\{e,f\} \subseteq E(G)} d_i(e,f|G), \ \ i \in \{0,4\}.$$

Obviously, $W_{e_0}(G) = W(L(G))$. Details on the edge $-$ Wiener indices can be found in (Gutman 2010; Yousefi$-$Azari et al. 2011; Nadjafi$-$Arani et al. 2012; Iranmanesh 2013; Azari and Iranmanesh 2014a, b; Iranmanesh and Azari 2015b) and the references quoted therein.

The edge-Wiener polynomials of a graph G are introduced in terms of a parameter q as follows:

$$W_{e_i}(G;q) = \sum_{\{e,f\} \subseteq E(G)} q^{d_i(e,f|G)}, \ \ i \in \{0,4\}.$$

It is clear that, the first derivative of the edge-Wiener polynomials at $q = 1$ is equal to their corresponding edge-Wiener indices, i.e., $W'_{e_i}(G;1) = W_{e_i}(G)$, where $i \in \{0,4\}$.

Vertex-edge versions of the Wiener index based on the distance between vertices and an edge in a graph G were introduced in Khalifeh et al. (2009b); Azari and Iranmanesh (2011b); and Azari et al. (2013b). The distance between the vertex u and the edge $e = ab$ of a graph G can be defined in two ways. The first distance is denoted by $D_1(u,e|G)$ and defined as follows:

$$D_1(u,e|G) = \min\{d(u,a|G), d(u,b|G)\}.$$

The second distance is denoted by $D_2(u,e|G)$ and defined as follows:

$$D_2(u,e|G) = \max\{d(u,a|G), d(u,b|G)\}.$$

Corresponding to these two distances, two vertex-edge versions of the Wiener index can be defined. The first and second vertex-edge Wiener indices of G are denoted by $W_{ve_1}(G)$ and $W_{ve_2}(G)$, respectively and defined as follows (Azari et al. 2013b):

$$W_{ve_i}(G) = \sum_{u \in V(G)} \sum_{e \in E(G)} D_i(u,e|G), \ \ i \in \{1,2\}.$$

One can easily see that, for arbitrary edges $e = uv$ and $f = zt$ of G, the quantities d_i and D_i, $i \in \{1, 2\}$, satisfy in the following relations:

$$d_1(e,f|G) = \min\{D_1(u,f|G), D_1(v,f|G)\} = \min\{D_1(z,e|G), D_1(t,e|G)\},$$
$$d_2(e,f|G) = \max\{D_2(u,f|G), D_2(v,f|G)\} = \max\{D_2(z,e|G), D_2(t,e|G)\}.$$

The above relations explain the relationship between the edge versions and vertex-edge versions of the Wiener index.

The vertex-edge Wiener polynomials of a graph G are introduced in terms of a parameter q as follows (Azari and Iranmanesh 2011b; Azari et al. 2011):

$$W_{ve_i}(G; q) = \sum_{u \in V(G)} \sum_{e \in E(G)} q^{D_i(u, e|G)}, \ \ i \in \{1, 2\}.$$

It is easy to see that the first derivative of the vertex-edge Wiener polynomials at $q = 1$ are equal to their corresponding vertex-edge Wiener indices, i.e., $W'_{ve_i}(G; 1) = W_{ve_i}(G)$, where $i \in \{1, 2\}$. The first and the second vertex-edge Wiener indices and polynomials are also called the minimum and maximum indices and polynomials, respectively.

The Zagreb indices are among the oldest topological indices and were introduced by Gutman and Trinajstić (1972). The first and second Zagreb indices of G are denoted by $M_1(G)$ and $M_2(G)$, respectively, and defined as:

$$M_1(G) = \sum_{u \in V(G)} \deg_G(u)^2 \ \ \text{and} \ \ M_2(G) = \sum_{uv \in E(G)} \deg_G(u)\deg_G(v),$$

where $\deg_G(u)$ denotes the degree of the vertex u in G which is the number of vertices incident to u.

The first Zagreb index can also be expressed as a sum over edges of G:

$$M_1(G) = \sum_{uv \in E(G)} [\deg_G(u) + \deg_G(v)].$$

For details on the theory and applications of Zagreb indices see Gutman et al. (1975); Gutman and Das (2004); Zhou (2004); Zhou and Gutman (2005); Khalifeh et al. (2009a); Azari and Iranmanesh (2011a, 2013); Réti (2012); Azari et al. (2013a); Falahati-Nezhad (2014); and Iranmanesh and Azari (2015a).

Let $N_G(u)$ denote the set of all first neighbors of u in G. Clearly, the cardinality of $N_G(u)$ is equal to $\deg_G(u)$. We define three quantities related to the graph G as follows:

$$N_1(G) = \sum_{uv \in E(G)} |N_G(u) \cap N_G(v)|,$$
$$N_2(G) = \sum_{uv \in E(G)} \sum_{z \in N_G(u) \cap N_G(v)} |N_G(u) \cap N_G(v) \cap N_G(z)|,$$

$$N_3(G) = \sum_{uv \in E(G)} \sum_{z \in V(G) \setminus (N_G(u) \cup N_G(v))} |N_G(z) \setminus (N_G(u) \cup N_G(v))|.$$

It is easy to see that the quantity $N_1(G)$ is equal to three times the number of all triangles in G. Also, by inclusion–exclusion principle, we obtain:

$$
\begin{aligned}
|N_G(z) \setminus (N_G(u) \cup N_G(v))| = {}& \deg_G(z) - |N_G(u) \cap N_G(z)| - |N_G(v) \cap N_G(z)| \\
& + |N_G(u) \cap N_G(v) \cap N_G(z)|.
\end{aligned}
$$

The fact that many interesting graphs are composed of simpler graphs that serve as their basic building blocks prompted interest in the type of relationship between the Wiener index and polynomial of composite graphs and their building blocks (Yeh and Gutman 1994; Sagan et al. 1996; Stevanović 2001; Eliasi et al. 2012; Eliasi and Iranmanesh 2013). This development was followed by some articles (Azari et al. 2010, 2012; Azari and Iranmanesh 2011b, 2014a, b; Alizadeh et al. 2014) that established corresponding relationships for the edge-Wiener indices.

In this chapter, we review our recent results on computing the first and second edge-Wiener indices of some composite graphs. All considered operations are binary. Hence, we will usually deal with two simple connected graphs G_1 and G_2. For a given graph G_i, its vertex and edge sets will be denoted by $V(G_i)$ and $E(G_i)$, respectively, and their cardinalities by n_i and e_i, respectively, where $i \in \{1, 2\}$. The chapter is organized as follows. In Sect. 14.2, the first and second edge-Wiener polynomials and their related indices are computed for the Cartesian product of graphs. In Sects. 14.3 and 14.4, we compute the first edge-Wiener index of the join and corona product of graphs, respectively. Finally, in Sect. 14.5, an exact formula is obtained for the second edge-Wiener index of the composition of graphs.

14.2 Cartesian Product

In this section, we compute the first and second edge-Wiener polynomials and their related indices for the Cartesian product of graphs. We start this section by definition of the Cartesian product of graphs.

The Cartesian product $G_1 \times G_2$ of the graphs G_1 and G_2 is a graph with the vertex set $V(G_1) \times V(G_2)$ and two vertices $u = (u_1, u_2)$ and $v = (v_1, v_2)$ of $G_1 \times G_2$ are adjacent if and only if $[u_1 = v_1 \text{ and } u_2 v_2 \in E(G_2)]$ or $[u_2 = v_2 \text{ and } u_1 v_1 \in E(G_1)]$. Hence, we can consider the edge set of $G_1 \times G_2$ as $E(G_1 \times G_2) = E_1 \cup {}_2$, where E_1 and E_2 are the following disjoint sets:

$$
\begin{aligned}
E_1 &= \{(u_1, u_2)(u_1, v_2) : u_1 \in V(G_1), u_2 v_2 \in E(G_2)\}, \\
E_2 &= \{(u_1, u_2)(v_1, u_2) : u_1 v_1 \in E(G_1), u_2 \in V(G_2)\}.
\end{aligned}
$$

The number of vertices and edges in $G_1 \times G_2$ are given by:

$$|V(G_1 \times G_2)| = n_1 n_2 \text{ and } |E(G_1 \times G_2)| = n_1 e_2 + n_2 e_1.$$

The Cartesian product of two graphs is associative and commutative and it is connected if and only if both components are connected. According to the proof of Theorem 1 in Stevanović (2001), the distance between the vertices $u = (u_1, u_2)$ and $v = (v_1, v_2)$ of $G_1 \times G_2$ is given by:

$$d(u, v|G_1 \times G_2) = d(u_1, v_1|G_1) + d(u_2, v_2|G_2).$$

Lemma 14.2.1

$$\sum_{\{e,f\} \subseteq E_1} q^{d_i(e,f|G_1 \times G_2)} = e_2 q W(G_1; q) + W_{e_i}(G_2; q)[2W(G_1; q) + n_1], \ \ i \in \{0, 4\}.$$

Proof By definition of the set E_1, for $i \in \{0, 4\}$, we have:

$$\sum_{\{e,f\} \subseteq E_1} q^{d_i(e,f|G_1 \times G_2)} = \sum_{\{u_1,a_1\} \subseteq V(G_1)} \sum_{u_2 v_2 \in E(G_2)} q^{d_i((u_1,u_2)(u_1,v_2),(a_1,u_2)(a_1,v_2)|G_1 \times G_2)}$$

$$+ \sum_{u_1 \in V(G_1)} \sum_{a_1 \in V(G_1)} \sum_{\{u_2 v_2, a_2 b_2\} \subseteq E(G_2)} q^{d_i((u_1,u_2)(u_1,v_2),(a_1,a_2)(a_1,b_2)|G_1 \times G_2)}$$

$$= \sum_{\{u_1, a_1\} \subseteq V(G_1)} \sum_{u_2 v_2 \in E(G_2)} q^{d(u_1,a_1|G_1)+1}$$

$$+ \sum_{u_1 \in V(G_1)} \sum_{a_1 \in V(G_1)} \sum_{\{u_2 v_2, a_2 b_2\} \subseteq E(G_2)} q^{d(u_1,a_1|G_1)+d_i(u_2 v_2, a_2 b_2|G_2)}$$

$$= e_2 q W(G_1; q) + W_{e_i}(G_2; q)[2W(G_1; q) + n_1].$$

Lemma 14.2.2

$$\sum_{\{e,f\} \subseteq E_2} q^{d_i(e,f|G_1 \times G_2)} = e_1 q W(G_2; q) + W_{e_i}(G_1; q)[2W(G_2; q) + n_2], \ \ i \in \{0, 4\}.$$

Proof Similar to the proof of Lemma 14.2.1, we can obtain the desired result.

Lemma 14.2.3

1. $\displaystyle\sum_{e \in E_1, f \in E_2} q^{d_0(e,f|G_1 \times G_2)} = q W_{ve_1}(G_1; q) W_{ve_1}(G_2; q),$

2. $\displaystyle\sum_{e \in E_1, f \in E_2} q^{d_4(e, f|G_1 \times G_2)} = W_{ve_2}(G_1; q) W_{ve_2}(G_2; q).$

Proof We compute:

1.
$$\sum_{e \in E_1, f \in E_2} q^{d_0(e,f|G_1 \times G_2)} = \sum_{u_1 \in V(G_1)} \sum_{u_2 v_2 \in E(G_2)} \sum_{a_1 b_1 \in E(G_1)} \sum_{a_2 \in V(G_2)} q^{d_0((u_1,u_2)(u_1,v_2),(a_1,a_2)(b_1,a_2)|G_1 \times G_2)}$$
$$= \sum_{u_1 \in V(G_1)} \sum_{u_2 v_2 \in E(G_2)} \sum_{a_1 b_1 \in E(G_1)} \sum_{a_2 \in V(G_2)} q^{1+D_1(u_1,a_1 b_1|G_1)+D_1(a_2,u_2 v_2|G_2)}$$
$$= q \sum_{u_1 \in V(G_1)} \sum_{a_1 b_1 \in E(G_1)} q^{D_1(u_1,a_1 b_1|G_1)} \sum_{a_2 \in V(G_2)} \sum_{u_2 v_2 \in E(G_2)} q^{D_1(a_2,u_2 v_2|G_2)}$$
$$= q W_{ve_1}(G_1;q) W_{ve_1}(G_2;q).$$

2.
$$\sum_{e \in E_1, f \in E_2} q^{d_4(e,f|G_1 \times G_2)} = \sum_{u_1 \in V(G_1)} \sum_{u_2 v_2 \in E(G_2)} \sum_{a_1 b_1 \in E(G_1)} \sum_{a_2 \in V(G_2)} q^{d_4((u_1,u_2)(u_1,v_2),(a_1,a_2)(b_1,a_2)|G_1 \times G_2)}$$
$$= \sum_{u_1 \in V(G_1)} \sum_{u_2 v_2 \in E(G_2)} \sum_{a_1 b_1 \in E(G_1)} \sum_{a_2 \in V(G_2)} q^{D_2(u_1,a_1 b_1|G_1)+D_2(a_2,u_2 v_2|G_2)}$$
$$= \sum_{u_1 \in V(G_1)} \sum_{a_1 b_1 \in E(G_1)} q^{D_2(u_1,a_1 b_1|G_1)} \sum_{a_2 \in V(G_2)} \sum_{u_2 v_2 \in E(G_2)} q^{D_2(a_2,u_2 v_2|G_2)}$$
$$= W_{ve_2}(G_1;q) W_{ve_2}(G_2;q).$$

Now, we use the previous lemmas to prove the main theorem of this section.

Theorem 14.2.4 *The first and second edge-Wiener polynomials of $G_1 \times G_2$ are given by:*

1. $W_{e_0}(G_1 \times G_2;q) = e_2 q W(G_1;q) + e_1 q W(G_2;q) + n_2 W_{e_0}(G_1;q) + n_1 W_{e_0}(G_2;q)$
   $+2W(G_1;q)W_{e_0}(G_2;q) + 2W(G_2;q)W_{e_0}(G_1;q) + q W_{ve_1}(G_1;q)W_{ve_1}(G_2;q),$
2. $W_{e_4}(G_1 \times G_2;q) = e_2 q W(G_1;q) + e_1 q W(G_2;q) + n_2 W_{e_4}(G_1;q) + n_1 W_{e_4}(G_2;q)$
   $+2W(G_1;q)W_{e_4}(G_2;q) + 2W(G_2;q)W_{e_4}(G_1;q) + W_{ve_2}(G_1;q)W_{ve_2}(G_2;q).$

Proof Since $E(G_1 \times G_2) = E_1 \cup E_2$ and $E_1 \cap E_2 = \phi$, so for $i \in \{0,4\}$, we have:

$$W_{e_i}(G_1 \times G_2;q) = \sum_{\{e,f\} \subseteq E(G_1 \times G_2)} q^{d_i(e,f|G_1 \times G_2)}$$
$$= \sum_{\{e,f\} \subseteq E_1} q^{d_i(e,f|G_1 \times G_2)} + \sum_{\{e,f\} \subseteq E_2} q^{d_i(e,f|G_1 \times G_2)}$$
$$+ \sum_{e \in E_1, f \in E_2} q^{d_i(e,f|G_1 \times G_2)}.$$

Using the previous lemmas, the proof is obvious.

As a direct consequence of the previous theorem, we can compute the first and second edge-Wiener indices of the Cartesian product as given in Azari and Iranmanesh (2011b).

Corollary 14.2.5 *The first and second edge-Wiener indices of $G_1 \times G_2$ are given by:*

1. $W_{e_0}(G_1 \times G_2) = e_2^2 W(G_1) + e_1^2 W(G_2) + n_2^2 W_{e_0}(G_1)$
   $+n_1^2 W_{e_0}(G_2) + \binom{n_1}{2}e_2 + \binom{n_2}{2}e_1 + n_1 n_2 e_1 e_2$
   $+n_2 e_2 W_{ve_1}(G_1) + n_1 e_1 W_{ve_1}(G_2),$

2. $W_{e_4}(G_1 \times G_2) = e_2{}^2 W(G_1) + e_1{}^2 W(G_2) + n_2{}^2 W_{e_4}(G_1)$
$+ n_1{}^2 W_{e_4}(G_2) + \binom{n_1}{2} e_2 + \binom{n_2}{2} e_1 + n_2 e_2 W_{ve_2}(G_1)$
$+ n_1 e_1 W_{ve_2}(G_2).$

Now, we use Corollary 14.2.5 to find the first and second edge-Wiener indices of the rectangular grids, C_4- nanotubes and C_4- nanotori. The Wiener, edge-Wiener and vertex-edge Wiener indices of the n-vertex path P_n and n-vertex cycle C_n were computed in Sagan et al. (1996); Iranmanesh et al. (2009); and Azari and Iranmanesh (2011b), respectively. We list these results in Table 14.1.

Consider the rectangular grid $P_n \times P_m$ shown in Fig. 14.1. Using Corollary 14.2.5 and Table 14.1, we can get the formula for the edge-Wiener indices of $P_n \times P_m$ as given in Azari and Iranmanesh (2011b).

Table 14.1 The wiener, edge $-$ wiener and vertex $-$ edge wiener indices of paths and cycles

Graph (G)	P_n	C_n, n is odd	C_n, n is even
$W(G)$	$\binom{n+1}{3}$	$\frac{n}{8}(n^2 - 1)$	$\frac{n^3}{8}$
$W_{e_0}(G)$	$\binom{n}{3}$	$\frac{n}{8}(n^2 - 1)$	$\frac{n^3}{8}$
$W_{e_4}(G)$	$\binom{n-1}{2}\frac{n+3}{3}$	$\frac{n}{8}(n^2 + 4n - 13)$	$\frac{n}{8}(n^2 + 4n - 8)$
$W_{ve_1}(G)$	$2\binom{n}{3}$	$\frac{n}{4}(n-1)^2$	$\frac{n^2}{4}(n-2)$
$W_{ve_2}(G)$	$2\binom{n+1}{3}$	$\frac{n}{4}(n-1)(n+3)$	$\frac{n^2}{4}(n+2)$
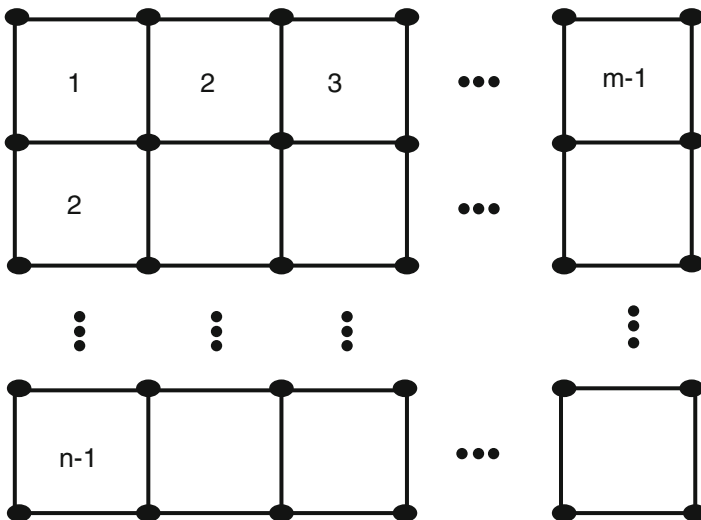
Fig. 14.1 The rectangular grid $P_n \times P_m$

Fig. 14.2 A C_4- Nanotube
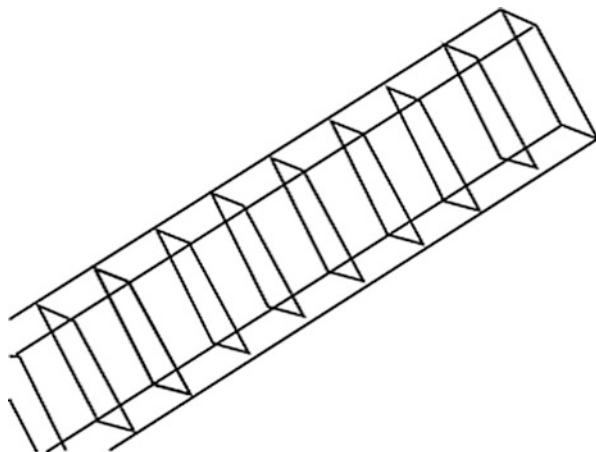
Corollary 14.2.6 *The first and second edge-Wiener indices of $G = P_n \times P_m$ are given by:*

1. $W_{e_0}(G) = \dfrac{m^3}{6}(2n-1)^2 + \dfrac{m^2}{6}\left(4n^3 - 12n^2 + 8n - 3\right)$
$$- \dfrac{m}{3}\left(2n^3 - 4n^2 + 2n - 1\right) + \dfrac{n}{6}\left(n^2 - 3n + 2\right),$$

2. $W_{e_4}(G) = \dfrac{m^3}{6}(2n-1)^2 + \dfrac{m^2}{6}\left(4n^3 - 7n + 3\right)$
$$- \dfrac{m}{6}\left(4n^3 + 7n^2 - 2n - 2\right) + \dfrac{n}{6}\left(n^2 + 3n + 2\right).$$

Let $G = P_n \times C_m$, then $G = TUC_4(m, n)$ is a $C_4 -$nanotube (see Fig. 14.2). Using Corollary 14.2.5 and Table 14.1, we can compute the edge-Wiener indices of C_4- nanotubes as given in Azari and Iranmanesh (2011b).

Corollary 14.2.7 *The first and second edge-Wiener indices of $G = TUC_4(m, n)$ are given by:*

1. $W_{e_0}(G) = \begin{cases} \dfrac{m^3}{8}(2n-1)^2 + \dfrac{m^2}{6}\left(4n^3 - 6n^2 + 5n - 3\right) + \dfrac{m}{8}\left(4n^2 - 8n + 3\right) & \text{if } m \text{ is odd,} \\[2mm] \dfrac{m^3}{8}(2n-1)^2 + \dfrac{m^2}{6}\left(4n^3 - 6n^2 + 5n - 3\right) + \dfrac{m}{2}(n-1)^2 & \text{if } m \text{ is even,} \end{cases}$

2. $W_{e_4}(G) = \begin{cases} \dfrac{m^3}{8}(2n-1)^2 + \dfrac{m^2}{6}\left(4n^3 + 6n^2 - 10n + 3\right) - \dfrac{m}{8}\left(16n^2 - 3\right) & \text{if } m \text{ is odd,} \\[2mm] \dfrac{m^3}{8}(2n-1)^2 + \dfrac{m^2}{6}\left(4n^3 + 6n^2 - 10n + 3\right) - \dfrac{m}{2}(n^2 + 2n - 1) & \text{if } m \text{ is even.} \end{cases}$

Fig. 14.3 A C_4- Nanotorus
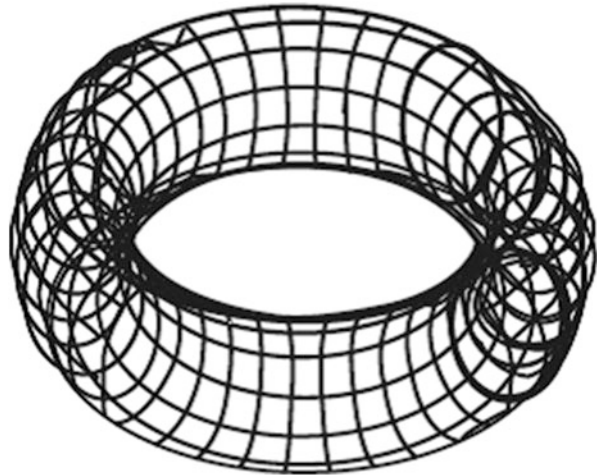
Let $G = C_n \times C_m$, then $G = TC_4(m,n)$ is a C_4- nanotorus (see Fig. 14.3). Using Corollary 14.2.5 and Table 14.1, we can compute the edge-Wiener indices of C_4- nanotori as given in Azari and Iranmanesh (2011b).

Corollary 14.2.8 *The first and second edge-Wiener indices of $G = TC_4(n,m)$ are given by:*

1. $W_{e_0}(G) = \frac{m^3}{2}n^2 + \frac{m^2}{2}n(n^2 + 1) + \frac{m}{2}n(n - 2)$,

2. $W_{e_4}(G) = \begin{cases} \dfrac{m^3}{2}n^2 + \dfrac{m^2}{2}n(n^2 + 4n - 4) - mn(2n + 1) & \text{if } m, n \text{ are odd,} \\[2ex] \dfrac{m^3}{2}n^2 + \dfrac{m^2}{2}n(n^2 + 4n - 1) - \dfrac{m}{2}n(n + 2) & \text{if } m, n \text{ are even,} \\[2ex] \dfrac{m^3}{2}n^2 + \dfrac{m^2}{2}n(n^2 + 4n - 4) - \dfrac{m}{2}n(n + 2) & \text{if } n \text{ is odd, } m \text{ is even.} \end{cases}$

14.3 Join

In this section, we find the first edge-Wiener index of the join of graphs. The results of this section have been reported in Alizadeh et al. (2014). We start this section by definition of the join of graphs.

The join $G_1 \nabla G_2$ of the graphs G_1 and G_2 with disjoint vertex sets $V(G_1)$ and $V(G_2)$ is the graph with the vertex set $V(G_1) \cup V(G_2)$ and the edge set $E(G_1 \nabla G_2) = E(G_1) \cup E(G_2) \cup S$, where $S = \{u_1 u_2 : u_1 \in V(G_1), u_2 \in V(G_2)\}$. Hence, the join of two graphs is obtained by connecting each vertex of one graph to each vertex of the other graph while keeping all edges of both graphs. The join of two graphs is sometimes also called a sum and is denoted by $G_1 + G_2$. Its definition can be extended inductively to more than two graphs in a straightforward manner. It is a commutative operation and hence both its components will appear

symmetrically in any formula including distance-based invariants. The number of vertices and edges in $G_1 \nabla G_2$ are given by:

$$|V(G_1 \nabla G_2)| = n_1 + n_2 \text{ and } |E(G_1 \nabla G_2)| = e_1 + e_2 + n_1 n_2.$$

In the following theorem, the first edge-Wiener index of the join of G_1 and G_2 is computed.

Theorem 14.3.1 *The first edge-Wiener index of $G_1 \nabla G_2$ is given by:*

$$W_{e_0}(G_1 \nabla G_2) = \binom{e_1 + e_2 + n_1 n_2}{2} - (2n_2 - 1)e_1 - (2n_1 - 1)e_2$$
$$- \frac{1}{2}n_1 n_2(n_1 + n_2 - 2) - \frac{1}{2}(M_1(G_1) + M_1(G_2))$$
$$+ \frac{1}{4}(N_3(G_1) + N_3(G_2)).$$

Proof Let Q be the set of all pairs of edges of $G_1 \nabla G_2$. We partition Q into six disjoint sets as follows:

$$Q_1 = \{\{e,f\} : e,f \in E(G_1)\},$$
$$Q_2 = \{\{e,f\} : e,f \in E(G_2)\},$$
$$Q_3 = \{\{e,f\} : e \in E(G_1), f \in E(G_2)\},$$
$$Q_4 = \{\{e,f\} : e \in E(G_1), f \in S\},$$
$$Q_5 = \{\{e,f\} : e \in E(G_2), f \in S\},$$
$$Q_6 = \{\{e,f\} : e,f \in S\}.$$

The first edge-Wiener index of $G_1 \nabla G_2$ is obtained by summing the contributions of all pairs of edges over those six sets. We proceed to evaluate their contributions in order of decreasing complexity.

The case of Q_3 is the simplest. There are $e_1 e_2$ such pairs and each of them contributes 2 to the first edge-Wiener index. Hence, the total contribution of pairs from Q_3 is equal to $2e_1 e_2$.

The set Q_6 contains pairs of edges from S. The total number of such pairs is equal to $\binom{n_1 n_2}{2}$. Among them there are $n_1 \binom{n_2}{2} + n_2 \binom{n_1}{2}$ pairs sharing a vertex. Such pairs contribute 1, and all other pairs contribute 2. Hence the total contribution of pairs from Q_6 is equal to $\binom{n_1 n_2}{2} - n_1 \binom{n_2}{2} - n_2 \binom{n_1}{2}$.

The total number of pairs from Q_4 is equal to $e_1 n_1 n_2$. All of them are either at distance 1 or at distance 2. The adjacent pairs share a vertex in G_1; hence there are $2e_1 n_2$ such pairs, and their contribution is given by $2e_1 n_2$. All other pairs from Q_4 contribute 2, and the total contribution of Q_4 is equal to $2e_1 n_2(n_1 - 1)$.

By symmetry, the total contribution of pairs from Q_5 is equal to $2e_2 n_1(n_2 - 1)$.

It remains to compute the contributions of Q_1 and Q_2. The total number of pairs in Q_1 is equal to $\binom{e_1}{2}$. Clearly, no pair of edges from Q_1 is at a distance greater than 3. Hence, we partition Q_1 into three sets Q_1', Q_1'', and Q_1''', made of the pairs of edges at distance 1, 2, and 3, respectively. Then the total contribution of pairs from Q_1 to the first edge-Wiener index of $G_1 \nabla G_2$ is given by $|Q_1'| + 2|Q_1''| + 3|Q_1'''|$. We have already mentioned that $|Q_1'''| = \frac{1}{4}N_3(G_1)$. Further,

$$|Q_1'| = \sum_{u \in V(G_1)} \binom{\deg_{G_1}(u)}{2} = \frac{1}{2}M_1(G_1) - e_1.$$

From here it immediately follows that the total contribution of Q_1 is given by:

$$e_1^2 - \frac{1}{2}M_1(G_1) + \frac{1}{4}N_3(G_1).$$

Again, the total contribution of Q_2 follows by the symmetry, and the formula from the theorem follows by adding the contributions of $Q_1, \ldots, Q_6$ and simplifying the resulting expression.

As expected, G_1 and G_2 appear symmetrically in the formula of the first edge-Wiener index. It is interesting to note that the formula does not depend on the connectivity of G_1 and G_2. That allows us to compute the first edge-Wiener index of joins of graphs that are not themselves connected.

Now, we can obtain explicit formulae for the first edge-Wiener index of some classes of graphs by specializing components in joins. We start by computing the first edge-Wiener index of a suspension of a graph G.

For a given graph G, we call the graph $K_1 \nabla G$ the suspension of G, where K_1 denotes the single vertex graph.

Corollary 14.3.2 *Let* G *be a graph with* n *vertices and* e *edges. Then*

$$W_{e_0}(K_1 \nabla G) = 2\binom{n+e}{2} - \binom{n}{2} - \frac{1}{2}M_1(G) + \frac{1}{4}N_3(G) - e.$$

The star graph S_{n+1} on $n + 1$ vertices is the suspension of the empty graph on n vertices which is commonly denoted by $\overline{K}_n$. The fan graph F_{n+1} and wheel graph W_{n+1} on $n + 1$ vertices are also suspensions of n-vertex path P_n and n-vertex cycle C_n, respectively (see Fig. 14.4).

The windmill graph $D_n^{(m)}$ is the graph obtained by taking m copies of the complete graph K_n with a vertex in common. The case $n = 3$ therefore corresponds to the Dutch windmill graph (see Fig. 14.5). One can easily see that the windmill graph $D_n^{(m)}$ is the suspension of m copies of K_{n-1}.
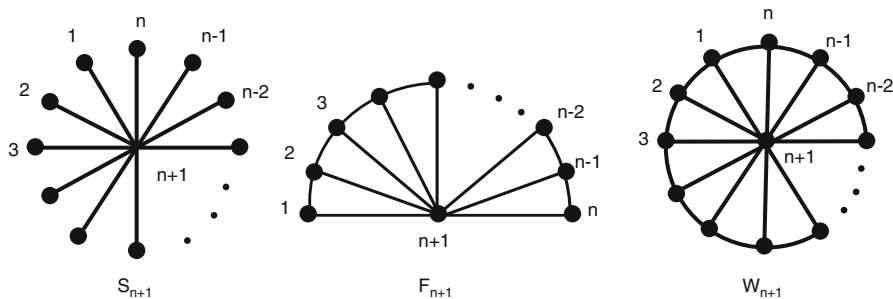
Fig. 14.4 Star, Fan and wheel graphs on $n + 1$ vertices

Fig. 14.5 Dutch windmill graph $D_3^{(m)}$
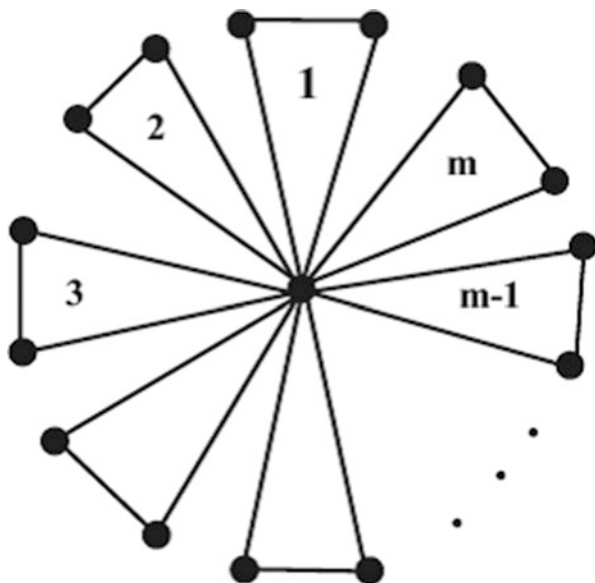
It can be verified by direct calculation that $N_3(P_n) = N_3(C_n) = 0$ for $n < 5$, $N_3(P_n) = 4\binom{n-3}{2}$, $N_3(C_n) = 2n(n-5)$ for $n \geq 5$, and $N_3(K_n) = 0$ for $n \geq 3$. Also, it is easy to see that, $M_1(P_n) = 4n - 6$, $M_1(C_n) = 4n$, and $M_1(K_n) = n(n-1)^2$. So, by Corollary 14.3.2, the first edge-Wiener index of these graphs is obtained, at once.

Corollary 14.3.3 *The first edge-Wiener index of the star, fan, wheel and windmill graphs is given by:*

1. $W_{e_0}(S_{n+1}) = \binom{n}{2}$,

2. $W_{e_0}(F_{n+1}) = \begin{cases} 3 & \text{if } n = 2, \\ \frac{1}{2}(7n^2 - 17n + 12) & \text{if } n = 3, 4, \\ 4(n^2 - 3n + 3) & \text{if } n \geq 5, \end{cases}$

3. $W_{e_0}(W_{n+1}) = \begin{cases} \frac{1}{2}(7n^2 - 9n) & \text{if } 3 \leq n \leq 5, \\ 4n^2 - 7n & \text{if } n \geq 6, \end{cases}$

4. $W_{e_0}\left(D_n^{(m)}\right) = \frac{1}{4}m(n-1)^2\left[m(n^2 - 2) - 2(n-1)\right].$

Now, consider the complete bipartite graph on $m_1 + m_2$ vertices, K_{m_1,m_2}. This graph can be represented as the join of the empty graphs $\overline{K}_{m_1}$ and $\overline{K}_{m_2}$. So, application of Theorem 14.3.1 yields:

Corollary 14.3.4 *The first edge-Wiener index of the complete bipartite graph on $m_1 + m_2$ vertices is given by:*

$$W_{e_0}(K_{m_1,m_2}) = \frac{1}{2}m_1 m_2 (2m_1 m_2 - m_1 - m_2).$$

14.4 Corona Product

In this section, we find the first edge-Wiener index of the corona product of graphs. The results of this section have been reported in Alizadeh et al. (2014). We start this section by definition of the corona product of graphs.

The corona product $G_1 \circ G_2$ of the graphs G_1 and G_2 is the graph obtained by taking one copy of G_1 and $|V(G_1)| = n_1$ copies of G_2 and joining all vertices of the i-th copy of G_2 to the i-th vertex of G_1 for $i = 1, 2, \ldots, n_1$. Obviously, $|V(G_1 \circ G_2)| = n_1(n_2 + 1)$ and $|E(G_1 \circ G_2)| = e_1 + n_1(n_2 + e_2)$. Unlike join and Cartesian product, corona is a noncommutative operation, and its component graphs appear in markedly asymmetric roles.

In the following theorem, the first edge-Wiener index of the corona product of G_1 and G_2 is computed.

Theorem 14.4.1 *The first edge-Wiener index of $G_1 \circ G_2$ is given by:*

$$\begin{aligned} W_{e_0}(G_1 \circ G_2) = {} & W_{e_0}(G_1) + (n_2 + e_2)^2 W(G_1) + (n_2 + e_2)W_{ve_1}(G_1) \\ & - \frac{n_1}{2}M_1(G_2) + \frac{n_1}{4}N_3(G_2) + e_2{}^2\left[3\binom{n_1}{2} + n_1\right] + n_1\binom{n_2}{2} \\ & + n_2{}^2\binom{n_1}{2} + n_1 e_1(n_2 + 2e_2) + 2n_1 e_2(n_2 - 1) \\ & + 2n_1 n_2 e_2(n_1 - 1). \end{aligned}$$

Proof We partition the edge set of $G_1 \circ G_2$ into three sets. The first one is the edge set of G_1, $S_1 = E(G_1)$, the second one contains all edges in all copies of G_2, and the third one contains all edges with one end in G_1 and the other end in some copies of G_2. We denote the copy of G_2 related to the vertex $x \in V(G_1)$ by $G_{2,x}$ and the edge

set of G_2,x by S_2,x. Now set $S_2 = \bigcup\limits_{x \in V(G_1)} S_{2,x}$. Similarly, for a vertex $x \in V(G_1)$, we

set $S_{3,x} = \{e : e = ux, u \in V(G_{2,x})\}$ and then $S_3 = \bigcup\limits_{x \in V(G_1)} S_{3,x}$.

Now, we start to compute the distances between the edges of these three sets. There are six cases:

Case 1 $\{g,f\} \subseteq S_1$.

It is obvious that, $d_0(g,f|G_1 \circ G_2) = d_0(g,f|G_1)$. So,

$$W_1 = \sum_{\{g,f\} \subseteq S_1} d_0(g,f|G_1 \circ G_2) = W_{e_0}(G_1).$$

Case 2 $\{g,f\} \subseteq S_2$, $g \in S_{2,x}$ and $f \in S_{2,y}$.

If $x = y$ then $d_0(g,f|G_1 \circ G_2) = 1$, 2 or 3. By the same reasoning as in the proof of Theorem 14.3.1, we obtain:

$$\sum_{\{g,f\} \subseteq S_{2,x}} d_0(g,f|G_1 \circ G_2) = 2\binom{e_2}{2} - \frac{1}{2}(M_1(G_2) - e_2) = e_2{}^2 - \frac{1}{2}M_1(G_2) + \frac{1}{4}N_3(G_2).$$

If $x \neq y$ then $d_0(g,f|G_1 \circ G_2) = 3 + d(x,y|G_1)$. Now,

$$\begin{aligned}
W_2 &= \sum_{\{g,f\} \subseteq S_2} d_0(g,f|G_1 \circ G_2) \\
&= \sum_{x \in V(G_1)} \sum_{\{g,f\} \subseteq S_{2,x}} d_0(g,f|G_1 \circ G_2) + \sum_{\{x,y\} \subseteq V(G_1)} \sum_{g \in S_{2,x}} \sum_{f \in S_{2,y}} d_0(g,f|G_1 \circ G_2) \\
&= n_1\left[e_2{}^2 - \frac{1}{2}M_1(G_2) + \frac{1}{4}N_3(G_2)\right] + \sum_{\{x,y\} \subseteq V(G_1)} (3 + d(x,y|G_1))e_2{}^2 \\
&= n_1\left[e_2{}^2 - \frac{1}{2}M_1(G_2) + \frac{1}{4}N_3(G_2)\right] + e_2{}^2\left[3\binom{n_1}{2} + W(G_1)\right]
\end{aligned}$$

Case 3 $\{g,f\} \subseteq S_3$.

In this case, we have:

$$\begin{aligned}
W_3 &= \sum_{\{g,f\} \subseteq S_3} d_0(g,f|G_1 \circ G_2) \\
&= \sum_{x \in V(G_1)} \sum_{\{g,f\} \subseteq S_{3,x}} d_0(g,f|G_1 \circ G_2) + \sum_{\{x,y\} \subseteq V(G_1)} \sum_{g \in S_{3,x}} \sum_{f \in S_{3,y}} d_0(g,f|G_1 \circ G_2) \\
&= \sum_{x \in V(G_1)} \sum_{\{g,f\} \subseteq S_{3,x}} 1 + \sum_{\{x,y\} \subseteq V(G_1)} \sum_{g \in S_{3,x}} \sum_{f \in S_{3,y}} (d(x,y|G_1) + 1) \\
&= \sum_{x \in V(G_1)} \frac{1}{2}n_2(n_2 - 1) + \sum_{\{x,y\} \subseteq V(G_1)} \sum_{g \in S_{3,x}} n_2(d(x,y|G_1) + 1) \\
&= \frac{1}{2}n_1 n_2(n_2 - 1) + n_2{}^2 W(G_1) + \frac{1}{2}n_2{}^2 n_1(n_1 - 1)
\end{aligned}$$

Case 4 $g \in S_1, f \in S_2$.

In this case, $g \in S_1, f \in S_{2,x}, d_0(g,f|G_1 \circ G_2) = 2 + D_1(x,g|G_1)$. Now,

$$
\begin{aligned}
W_4 &= \sum_{x \in V(G_1)} \sum_{g \in S_1} \sum_{f \in S_{2,x}} d_0(g,f|G_1 \circ G_2) = \sum_{x \in V(G_1)} \sum_{f \in S_{2,x}} \sum_{g \in S_1} (2 + D_1(x,g|G_1)) \\
&= \sum_{x \in V(G_1)} 2e_1 e_2 + e_2 \sum_{x \in V(G_1)} \sum_{g \in S_1} D_1(x,g|G_1) = e_2(2n_1 e_1 + W_{ve_1}(G_1)).
\end{aligned}
$$

Case 5 $g \in S_1, f \in S_3$.

Similarly to the above case, $g \in S_1, f \in S_{3,x}, d_0(g,f|G_1 \circ G_2) = 1 + D_1(x,g|G_1)$. Now,

$$
\begin{aligned}
W_5 &= \sum_{x \in V(G_1)} \sum_{g \in S_1} \sum_{f \in S_{3,x}} d_0(g,f|G_1 \circ G_2) = \sum_{x \in V(G_1)} \sum_{g \in S_1} \sum_{f \in S_{3,x}} (1 + D_1(x,g|G_1)) \\
&= \sum_{x \in V(G_1)} e_1 n_2 + n_2 \sum_{x \in V(G_1)} \sum_{g \in S_1} D_1(x,g|G_1) = n_2(n_1 e_1 + W_{ve_1}(G_1)).
\end{aligned}
$$

Case 6 $g \in S_2, f \in S_3$.

If $g \in S_{2,x}, f \in S_{3,x}$, then $d_0(g,f|G_1 \circ G_2) = 1$ or 2. The edge g is adjacent to two edges of $S_{3,x}$ and its distance to other edges is 2. So,

$$
\sum_{x \in V(G_1)} \sum_{g \in S_{2,x}} \sum_{f \in S_{3,x}} d_0(g,f|G_1 \circ G_2) = \sum_{x \in V(G_1)} \sum_{g \in S_{2,x}} (2 + 2(n_2 - 2)) = 2(n_2 - 1)e_2 n_1.
$$

If $g \in S_{2,x}, f \in S_{3,y}, x \neq y$ then $d_0(g,f|G_1 \circ G_2) = 2 + d(x,y|G_1)$. Now,

$$
\begin{aligned}
W_6 &= \sum_{x,y \in V(G_1)} \sum_{g \in S_{2,x}} \sum_{f \in S_{3,y}} d_0(g,f|G_1 \circ G_2) \\
&= \sum_{x \in V(G_1)} \sum_{g \in S_{2,x}} \sum_{f \in S_{3,x}} d_0(g,f|G_1 \circ G_2) + \sum_{x \neq y \in V(G_1)} \sum_{g \in S_{2,x}} \sum_{f \in S_{3,x}} d_0(g,f|G_1 \circ G_2) \\
&= (2n_2 - 2)n_1 e_2 + \sum_{x \neq y \in V(G_1)} (2 + d(x,y|G_1))n_2 e_2 \\
&= 2(n_2 - 1)n_1 e_2 + \Big[2n_1(n_1 - 1) + \sum_{x \neq y \in V(G_1)} d(x,y|G_1) \Big] n_2 e_2 \\
&= 2(n_2 - 1)n_1 e_2 + 2[n_1(n_1 - 1) + W(G_1)]n_2 e_2.
\end{aligned}
$$

Now, the formula for the first edge-Wiener index of $G_1 \circ G_2$ follows by adding all six contributions and simplifying the resulting expression.

It is interesting to note that the formula of Theorem 14.4.1 does not include any invariants of G_2 that depend on its connectivity. It is, hence, possible to apply Theorem 14.4.1 to the cases of $G_1 \circ G_2$ with disconnected G_2. Such cases arise in transitions from kenographs to plerographs, where G_2 is given as an empty graph, i.e., as $\overline{K}_n$ for some positive integer n.
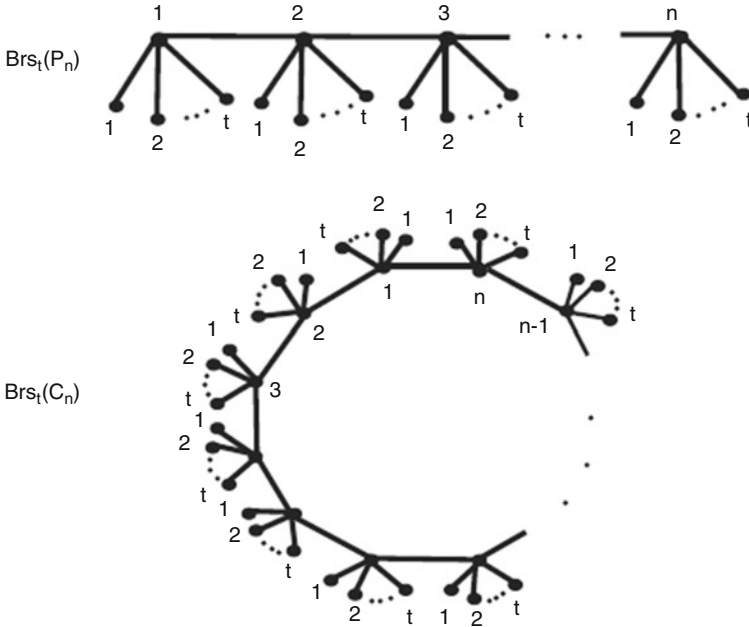
Fig. 14.6   The t − fold bristled graphs of P_n and C_n

For a given graph G, its t-fold bristled graph $Brs_t(G)$ is obtained by attaching t vertices of degree one to each vertex of G. This graph can be represented as the corona product of G and the empty graph on t vertices $\overline{K}_t$. The t-fold bristled graph of a given graph is also known as its t-thorny graph. The t-fold bristled graphs of P_n and C_n are shown in Fig. 14.6.

Using Theorem 14.4.1, the first edge-Wiener index of the t-fold bristled graph of a given graph G is obtained at once.

Corollary 14.4.2 *Let G be a graph with* n *vertices and* e *edges. Then*

$$W_{e_0}(Brs_t(G)) = W_{e_0}(G) + tW_{ve_1}(G) + t^2 W(G) + n\binom{t}{2} + t^2\binom{n}{2} + net.$$

Using Corollary 14.4.2 and Table 14.1, the first edge-Wiener index of $Brs_t(P_n)$ and $Brs_t(C_n)$ can easily be computed.

Corollary 14.4.3 *The first edge-Wiener index of the* t-*fold bristled graphs of* P_n *and* C_n *are given by:*

1. $W_{e_0}(Brs_t(P_n)) = \frac{n}{6}\left[n^2(t+1)^2 + 3n(t^2 - 1) - t(t+5) + 2\right],$

2. $W_{e_0}\left(Brs_t(C_n)\right) = \begin{cases} \dfrac{n(t+1)}{8}[n^2 + nt(n+4) - (t+1)] & \text{if } n \text{ is odd,} \\ \dfrac{n}{8}[n^2(t+1)^2 + 4nt(t+1) - 4t] & \text{if } n \text{ is even.} \end{cases}$

Interesting classes of graphs can also be obtained by specializing the first component in the corona product. For example, for a graph G, the graph $K_2 \circ G$ is called its bottleneck graph. So, using Theorem 14.4.1, we easily arrive at:

Corollary 14.4.4 *Let* G *be a graph with* n *vertices and* e *edges. Then*

$$W_{e_0}(K_2 \circ G) = 6e^2 + 10ne + 3n^2 + n - M_1(G) + \frac{1}{2}N_3(G).$$

Remark 14.4.5 Note that for a given graph G, $K_1 \nabla G = K_1 \circ G$. So, the formulae of the first edge-Wiener index of the suspension of G and its t-fold bristled graph computed in Corollaries 14.3.2 and 14.3.3 can also be obtained from Theorem 14.4.1.

14.5 Composition

In this section, we find the second edge-Wiener index of the composition of graphs. The results of this section have been published in Azari et al. (2012). We start this section by definition of the composition of graphs.

The composition $G_1[G_2]$ of graphs G_1 and G_2 with disjoint vertex sets and edge sets is a graph on vertex set $V(G_1) \times V(G_2)$ in which $u = (u_1, u_2)$ is adjacent with $v = (v_1, v_2)$ whenever $u_1 v_1 \in E(G_1)$ or [$u_1 = v_1$ and $u_2 v_2 \in E(G_2)$]. The composition is not commutative. The easiest way to visualize the composition $G_1[G_2]$ is to expand each vertex of G_1 into a copy of G_2, with each edge of G_1 replaced by the set of all possible edges between the corresponding copies of G_2. Hence, we can define the edge set of $G_1[G_2]$ as $E(G_1[G_2]) = E_1 \cup E_2$, where E_1 and E_2 are the following disjoint sets:

$$E_1 = \{(u_1, u_2)(u_1, v_2) : u_1 \in V(G_1), u_2 v_2 \in E(G_2)\},$$
$$E_2 = \{(u_1, u_2)(v_1, v_2) : u_1 v_1 \in E(G_1), u_2, v_2 \in V(G_2)\}.$$

The number of vertices and edges in $G_1[G_2]$ are given by:

$$|V(G_1[G_2])| = n_1 n_2 \text{ and } |E(G_1[G_2])| = n_1 e_2 + e_1 n_2{}^2.$$

By definition of the composition, the distance between two distinct vertices $u = (u_1, u_2)$ and $v = (v_1, v_2)$ of $G_1[G_2]$ is given by:

$$d(u, v | G_1[G_2]) = \begin{cases} d(u_1, v_1 | G_1) & \text{if } u_1 \neq v_1, \\ 1 & \text{if } u_1 = v_1, u_2 v_2 \in E(G_2), \\ 2 & \text{if } u_1 = v_1, v_2 \notin N_{G_2}(u_2). \end{cases}$$

In Fig. 14.7, you can see the composition of a 3-vertex path P_3 and 2-vertex path P_2.
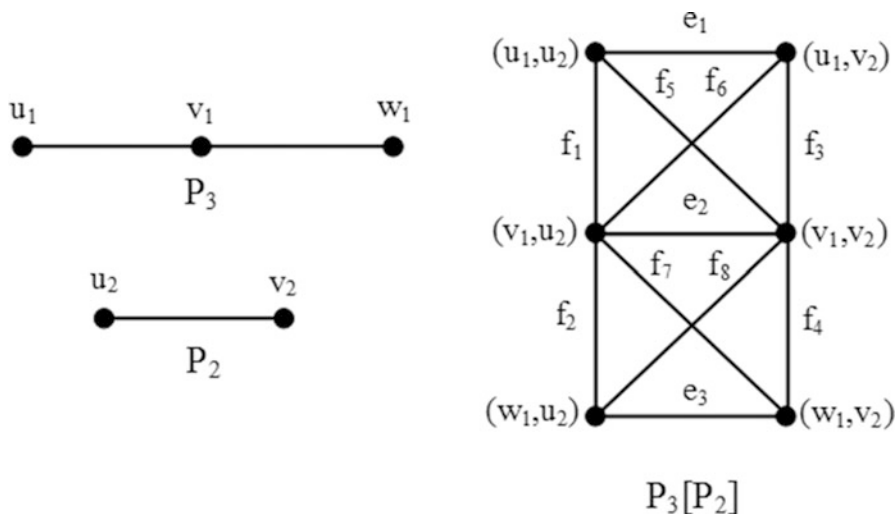
Fig. 14.7 The composition of P_3 and P_2

Here and in the rest of this section, let $G = G_1[G_2]$. Suppose K is the set of all two element subsets of $E(G)$. We partition the set K into the following disjoint sets:

$$A = \{\{e,f\} \in K : e,f \in E_1\},$$
$$B = \{\{e,f\} \in K : e,f \in E_2\},$$
$$C = \{\{e,f\} \in K : e \in E_1, f \in E_2\}.$$

It is easy to see that $|A| = \binom{n_1 e_2}{2}$, $|B| = \binom{n_2^2 e_1}{2}$ and $|C| = n_1 n_2^2 e_1 e_2$. We start to find $W_{e_4}(G)$, by introducing several subsets of the set A as follows:

$$A_1^* = \{\{e,f\} \in A : e = (u_1, u_2)(u_1, v_2), f = (u_1, u_2)(u_1, z_2), u_1 \in V(G_1),$$
$$u_2 \in V(G_2), v_2 z_2 \in E(G_2)\},$$
$$A_2^* = \{\{e,f\} \in A : e = (u_1, u_2)(u_1, v_2), f = (u_1, u_2)(u_1, z_2), u_1 \in V(G_1),$$
$$u_2, v_2, z_2 \in V(G_2), z_2 \notin N_{G_2}(v_2)\},$$
$$A_3^* = \{\{e,f\} \in A : e = (u_1, u_2)(u_1, v_2), f = (u_1, z_2)(u_1, t_2), u_1 \in V(G_1),$$
$$u_2 z_2, u_2 t_2, v_2 z_2, v_2 t_2 \in E(G_2)\},$$
$$A_4^* = \{\{e,f\} \in A : e = (u_1, u_2)(u_1, v_2), f = (u_1, z_2)(u_1, t_2), u_1 \in V(G_1),$$
$$u_2, v_2, z_2, t_2 \in V(G_2), z_2, t_2 \notin \{u_2, v_2\}\} \backslash A_3^*,$$

$$A_5{}^* = \{\{e,f\} \in A : e = (u_1,u_2)(u_1,v_2), f = (v_1,z_2)(v_1,t_2), u_1, v_1 \in V(G_1),$$
$$v_1 \neq u_1, u_2, v_2, z_2, t_2 \in V(G_2)\}.$$

Clearly, every pair of the above sets is disjoint and $A = \overset{5}{\underset{i=1}{\cup}} A_i{}^*$. In the following lemma, we characterize $d_4(e,f|G)$ for all $\{e,f\} \in A$.

Lemma 14.5.1 *Let* $\{e,f\} \in A$.

1. If $\{e,f\} \in A_1{}^* \cup A_3^*$, then $d_4(e,f|G) = 1$.
2. If $\{e,f\} \in A_2{}^* \cup A_4^*$, then $d_4(e,f|G) = 2$.
3. If $\{e,f\} \in A_5{}^*$, then $d_4(e,f|G) = d(u_1,v_1|G_1)$, where $e = (u_1,u_2)(u_1,v_2)$ and $f = (v_1,z_2)(v_1,t_2)$.

Proof Let $\{e,f\} \in A_1^* \cup A_2^*$ and $e = (u_1,u_2)(u_1,v_2)$, $f = (u_1,u_2)(u_1,z_2)$. Since $e \neq f$, $d\big((u_1,v_2),(u_1,z_2)|G\big) \geq 1$. Hence,

$$d_4(e,f|G) = \max\big\{d((u_1,u_2),(u_1,u_2)|G), d((u_1,u_2),(u_1,z_2)|G), d\big((u_1,v_2),$$
$$(u_1,u_2)\big|G\big), d((u_1,v_2),(u_1,z_2)|G)\big\}$$
$$= \max\big\{0,1,1,d\big((u_1,v_2),(u_1,z_2)\big|G\big)\big\} = d\big((u_1,v_2),(u_1,z_2)\big|G\big).$$

If $\{e,f\} \in A_1{}^*$, then $v_2 z_2 \in E(G_2)^2$. So, $d_4(e,f|G) = 1$ and if $\{e,f\} \in A_2{}^*$, then z_2 is not adjacent to v_2 in G_2. So, $d_4(e,f|G) = 2$. Now, let $\{e,f\} \in A_3^* \cup A_4^*$ and $e = (u_1,u_2)(u_1,v_2), f = (u_1,z_2)(u_1,t_2)$. Then

$$d_4(e,f|G) = \max\{d((u_1,u_2),(u_1,z_2)|G), d((u_1,u_2),(u_1,t_2)|G), d((u_1,v_2),$$
$$(u_1,z_2)|G), d((u_1,v_2),(u_1,t_2)|G)\}, d((u_1,v_2),(u_1,t_2)|G)\}.$$

If $\{e,f\} \in A_3{}^*$, then $d_4(e,f|G) = \max\{1,1,1,1\} = 1$ and if $\{e,f\} \in A_4{}^*$, then at least one of the $d((u_1,u_2),(u_1,z_2)\,|\,G)$, $d((u_1,u_2),(u_1,t_2)\,|\,G)$, $d((u_1,v_2),(u_1,z_2)\,|\,G)$ and $d((u_1,v_2),(u_1,t_2)\,|\,G)$ is equal to 2. Therefore, $d_4(e,f|G) = 2$. So, (1) and (2) hold.

In order to prove (3), let $\{e,f\} \in A_5{}^*$ and $e = (u_1,u_2)(u_1,v_2), f = (v_1,z_2)(v_1,t_2)$. Then $v_1 \neq u_1$ and

$$d_4(e,f|G) = \max\big\{d((u_1,u_2),(v_1,z_2)|G), d((u_1,u_2),(v_1,t_2)|G), d\big((u_1,v_2),$$
$$(v_1,z_2)\big|G\big), d((u_1,v_2),(v_1,t_2)|G)\big\} = \max\{d(u_1,v_1|G_1),$$
$$d(u_1,v_1|G_1), d(u_1,v_1|G_1), d(u_1,v_1|G_1)\} = d(u_1,v_1|G_1).$$

So, (3) holds.

Now, we define several subsets of the set B as follows:

$$B_1{}^* = \{\{e,f\} \in B : e = (u_1, u_2)(v_1, v_2), f = (u_1, u_2)(v_1, z_2), u_1, v_1 \in V(G_1),$$
$$u_2 \in V(G_2), v_2z_2 \in E(G_2)\},$$

$$B_2{}^* = \{\{e,f\} \in B : e = (u_1, u_2)(v_1, v_2), f = (u_1, u_2)(v_1, z_2), u_1, v_1 \in V(G_1),$$
$$u_2, v_2, z_2 \in V(G_2), z_2 \notin N_{G_2}(v_2)\},$$

$$B_3{}^* = \{\{e,f\} \in B : e = (u_1, u_2)(v_1, v_2), f = (u_1, z_2)(v_1, t_2), u_1, v_1 \in V(G_1),$$
$$u_2z_2, v_2t_2 \in E(G_2)\},$$

$$B_4{}^* = \{\{e,f\} \in B : e = (u_1, u_2)(v_1, v_2), f = (u_1, z_2)(v_1, t_2), u_1, v_1 \in V(G_1),$$
$$u_2, v_2, z_2, t_2 \in V(G_2), z_2 \neq u_2, t_2 \neq v_2\} \backslash B_3{}^*,$$

$$B_5{}^* = \{\{e,f\} \in B : e = (u_1, u_2)(v_1, v_2), f = (u_1, u_2)(z_1, z_2), u_1, v_1, z_1 \in V(G_1),$$
$$z_1 \neq v_1, u_2, v_2, z_2 \in V(G_2)\},$$

$$B_6{}^* = \{\{e,f\} \in B : e = (u_1, u_2)(v_1, v_2), f = (u_1, t_2)(z_1, z_2), u_1, v_1, z_1 \in V(G_1),$$
$$z_1 \neq v_1, u_2t_2 \in E(G_2), v_2, z_2 \in V(G_2)\},$$

$$B_7{}^* = \{\{e,f\} \in B : e = (u_1, u_2)(v_1, v_2), f = (u_1, t_2)(z_1, z_2), u_1, v_1, z_1 \in V(G_1),$$
$$z_1 \neq v_1, u_2, v_2, t_2, z_2 \in V(G_2), t_2 \neq u_2, t_2 \notin N_{G_2}(u_2)\},$$

$$B_8{}^* = \{\{e,f\} \in B : e = (u_1, u_2)(v_1, v_2), f = (z_1, z_2)(t_1, t_2), u_1, v_1, z_1, t_1 \in V(G_1),$$
$$z_1, t_1 \notin \{u_1, v_1\}, u_2, v_2, z_2, t_2 \in V(G_2)\}.$$

It is clear that, each pair of the above sets is disjoint and $B = \overset{8}{\underset{i=1}{\cup}} B_i{}^*$. In the next lemma, we characterize $d_4(e, f|G)$ for all $\{e, f\} \in B$.

Lemma 14.5.2 *Let* $\{e, f\} \in B$.

1. If $\{e, f\} \in B_1{}^* \cup B_3^*$, then $d_4(e, f|G) = 1$.
2. If $\{e, f\} \in B_2{}^* \cup B_4^* \cup B_7^*$, then $d_4(e, f|G) = 2$.
3. If $\{e, f\} \in B_5{}^*$, then $d_4(e, f|G) = d_4(u_1v_1, u_1z_1|G_1)$, where $e = (u_1, u_2)(v_1, v_2)$, $f = (u_1, u_2)(z_1, z_2)$.
4. If $\{e, f\} \in B_6{}^*$, then $d_4(e, f|G) = d_4(u_1v_1, u_1z_1|G_1)$, where $e = (u_1, u_2)(v_1, v_2)$, $f = (u_1, t_2)(z_1, z_2)$.
5. If $\{e, f\} \in B_8{}^*$, then $d_4(e, f|G) = d_4(u_1v_1, z_1t_1|G_1)$, where $e = (u_1, u_2)(v_1, v_2)$, $f = (z_1, z_2)(t_1, t_2)$.

Proof The proof is similar to the proof of Lemma 14.5.1.

Consider four subsets of the set C as follows:

$$C_1{}^* = \{\{e,f\} \in C : e = (u_1,u_2)(u_1,v_2), f = (u_1,u_2)(z_1,z_2), u_1,z_1 \in V(G_1),$$

$$u_2,v_2,z_2 \in V(G_2)\},$$

$$C_2{}^* = \{\{e,f\} \in C : e = (u_1,u_2)(u_1,v_2), f = (u_1,t_2)(z_1,z_2), u_1,z_1 \in V(G_1),$$

$$z_2 \in V(G_2), u_2 t_2, v_2 t_2 \in E(G_2)\}$$

$$C_3{}^* = \{\{e,f\} \in C : e = (u_1,u_2)(u_1,v_2), f = (u_1,t_2)(z_1,z_2), u_1,z_1 \in V(G_1),$$

$$u_2,v_2,t_2,z_2 \in V(G_2), t_2 \neq u_2, t_2 \neq v_2\}\backslash C_2{}^*,$$

$$C_4{}^* = \{\{e,f\} \in C : e = (u_1,u_2)(u_1,t_2), f = (v_1,v_2)(z_1,z_2), u_1,v_1,z_1 \in V(G_1),$$

$$v_1 \neq u_1, z_1 \neq u_1, u_2,t_2,v_2,z_2 \in V(G_2)\}.$$

Clearly, each pair of the above sets is disjoint and $C = \overset{4}{\underset{i=1}{\cup}} C_i{}^*$. In the following lemma, we find $d_4(e,f|G)$ for all $\{e,f\} \in C$.

Lemma 14.5.3 *Let* $\{e,f\} \in C$.

1. If $\{e,f\} \in C_1{}^* \cup C_2{}^*$, then $d_4(e,f|G) = 1$.
2. If $\{e,f\} \in C_3{}^*$, then $d_4(e,f|G) = 2$.
3. If $\{e,f\} \in C_4{}^*$, then $d_4(e,f|G) = D_2(u_1,v_1z_1|G_1)$, where $e = (u_1,u_2)(u_1,t_2)$, $f = (v_1,v_2)(z_1,z_2)$.

Proof The proof is straightforward.

In order to clarify the definition of the sets $A_1{}^*, A_2{}^*, \ldots, A_5{}^*, B_1{}^*, B_2{}^*, \ldots, B_8{}^*$, $C_1{}^*, \ldots, C_4{}^*$, we give an example.

Example 14.5.4 Let $G = P_3[P_2]$ be the graph of Fig. 14.7. Then

$$A_i{}^* = B_j{}^* = C_k{}^* = \phi \text{ and}$$

$$A_5{}^* = A = \{\{e_1,e_2\}, \{e_1,e_3\}, \{e_2,e_3\}\},$$

$$B_1{}^* = \{\{f_1,f_5\}, \{f_1,f_6\}, \{f_2,f_7\}, \{f_2,f_8\}, \{f_3,f_5\}, \{f_3,f_6\}, \{f_4,f_7\}, \{f_4,f_8\}\},$$

$$B_3{}^* = \{\{f_1,f_3\}, \{f_2,f_4\}, \{f_5,f_6\}, \{f_7,f_8\}\},$$

$$B_5{}^* = \{\{f_1,f_2\}, \{f_1,f_7\}, \{f_2,f_6\}, \{f_3,f_4\}, \{f_3,f_8\}, \{f_4,f_5\}, \{f_5,f_8\}, \{f_6,f_7\}\},$$

$$B_6{}^* = \{\{f_1,f_4\}, \{f_1,f_8\}, \{f_2,f_3\}, \{f_2,f_5\}, \{f_3,f_7\}, \{f_4,f_6\}, \{f_5,f_7\}, \{f_6,f_8\}\},$$

$$C_1{}^* = \{\{e_1,f_1\},\{e_1,f_3\},\{e_1,f_5\},\{e_1,f_6\},\{e_2,f_1\},\{e_2,f_2\},\{e_2,f_3\},\{e_2,f_4\},$$

$$\{e_2,f_5\},\{e_2,f_6\},\{e_2,f_7\},\{e_2,f_8\},\{e_3,f_2\},\{e_3,f_4\},\{e_3,f_7\},\{e_3,f_8\}\},$$

$$C_4{}^* = \{\{e_1,f_2\},\{e_1,f_4\},\{e_1,f_7\},\{e_1,f_8\},\{e_3,f_1\},\{e_3,f_3\},\{e_3,f_5\},\{e_3,f_6\}\}.$$

Lemma 14.5.5

$$\sum_{\{e,f\}\in A} d_4(e,f|G) = n_1\left(2\binom{e_2}{2} - N_1(G_2) - \frac{1}{4}N_2(G_2)\right) + e_2{}^2 W(G_1).$$

Proof One can easily see that $|A_1{}^*| = n_1 N_1(G_2)$, $|A_3{}^*| = \frac{1}{4}n_1 N_2(G_2)$ and $|A_5{}^*| = \binom{n_1}{2} e_2{}^2$. Now, by Lemma 14.5.1, we obtain:

$$\sum_{\{e,f\}\in A} d_4(e,f|G) = \sum_{i=1}^{5}\sum_{\{e,f\}\in A_i{}^*} d_4(e,f|G) = |A_1{}^*| + 2|A_2{}^*| + |A_3{}^*| + 2|A_4{}^*|$$

$$+ \sum \{d(u_1,v_1|G_1) : \{e,f\}\in A_5{}^*, e = (u_1,u_2)(u_1,v_2),$$

$$f = (v_1,z_2)(v_1,t_2)\} = 2\sum_{i=1}^{5}|A_i{}^*| - |A_1{}^*| - |A_3{}^*| - 2|A_5{}^*|$$

$$+ e_2{}^2 \sum_{\{u_1,v_1\}\subseteq V(G_1)} d(u_1,v_1|G_1) = 2|A| - |A_1{}^*| - |A_3{}^*|$$

$$- 2|A_5{}^*| + e_2{}^2 W(G_1) = 2\binom{n_1 e_2}{2} - n_1 N_1(G_2) - \frac{1}{4}n_1 N_2(G_2)$$

$$- 2\binom{n_1}{2} e_2{}^2 + e_2{}^2 W(G_1) = n_1\left(2\binom{e_2}{2} - N_1(G_2)\right.$$

$$\left. - \frac{1}{4}N_2(G_2)\right) + e_2{}^2 W(G_1). \blacksquare$$

Lemma 14.5.6 *Let* H *be a graph with the vertex set* V(H) *and edge set* E(H) *and let* $|E(H)| = e$. *Then*

$$\sum_{u\in V(H)}\sum_{\{uv,uz\}\subseteq E(H)} d_4(uv,uz|H) = M_1(H) - N_1(H) - 2e.$$

Proof Consider the sets F_1 and F_2 as follows:

$$F_1 = \{\{uv, uz\} \subseteq E(H) : u, v, z \in V(H), vz \in E(H)\},$$
$$F_2 = \{\{uv, uz\} \subseteq E(H) : u, v, z \in V(H), v \neq z, z \notin N_H(v)\}.$$

Clearly, $F_1 \cap F_2 = \phi$, $F_1 \cup F_2 = \{\{e, f\} \subseteq E(H) : e, f \text{ share a vertex}\}$, $|F_1| = N_1(H)$ and $|F_2| = \frac{1}{2}[M_1(H) - 2e - 2N_1(H)]$. Let $\{uv, uz\} \in F_1 \cup F_2$. If $\{uv, uz\} \in F_1$, then $vz \in E(H)$. So,

$$d_4(uv, uz|H) = \max\{d(u, u|H), d(u, z|H), d(v, u|H), d(v, z|H)\} = \max\{0, 1, 1, 1\}$$
$$= 1.$$

Now, if $\{uv, uz\} \in F_2$, then $v \neq z$ and z is not adjacent with v in H. So, $d(v, z|H) = 2$ and

$$d_4(uv, uz|H) = \max\{0, 1, 1, 2\} = 2.$$

Consequently,

$$\sum_{u \in V(H)} \sum_{\{uv, uz\} \subseteq E(H)} d_4(uv, uz|H) = \sum_{u \in V(H)} \sum_{\{uv, uz\} \in F_1 \cup F_2} d_4(uv, uz|H)$$
$$= \sum_{u \in V(H)} \sum_{\{uv, uz\} \in F_1} 1 + \sum_{u \in V(H)} \sum_{\{uv, uz\} \in F_2} 2 = (|F_1| + 2|F_2|)$$
$$= M_1(H) - N_1(H) - 2e. \qquad \blacksquare$$

Lemma 14.5.7

$$\sum_{\{e, f\} \in B} d_4(e, f|G) = 2e_1 \binom{n_2^2}{2} - 2e_1 e_2(n_2 + e_2) + n_2^4 W_{e_4}(G_1)$$
$$+ 2n_2^2 (n_2^2 - n_2 - 2e_2) N_1(G_1).$$

Proof It is easy to see that $|B_1^*| = 2e_1 e_2 n_2$, $|B_3^*| = 2e_1 e_2^2$, $|B_5^*| = \frac{1}{2} n_2^3 (M_1(G_1) - 2e_1)$, $|B_6^*| = n_2^2 e_2(M_1(G_1) - 2e_1)$ and $|B_8^*| = \frac{1}{2} n_2^4$ $(e_1^2 + e_1 - M_1(G_1))$. Now, we find $\displaystyle\sum_{\{e, f\} \in B_5^* \cup B_6^* \cup B_8^*} d_4(e, f|G)$.

By Lemma 14.5.2, we have:

$$\sum_{\{e, f\} \in B_5^*} d_4(e, f|G) = \sum \{d_4(u_1 v_1, u_1 z_1|G_1) : \{e, f\} \in B_5^*, e = (u_1, u_2)(v_1, v_2),$$
$$f = (u_1, u_2) \times (z_1, z_2)\}$$
$$= n_2^3 \sum_{u_1 \in V(G_1)} \sum_{\{u_1 v_1, u_1 z_1\} \subseteq E(G_1)} d_4(u_1 v_1, u_1 z_1|G_1).$$

Similarly,

$$
\sum_{\{e,f\}\in B_6^*} d_4(e,f|G) = \sum \left\{ d_4(u_1v_1, u_1z_1|G_1) : \{e,f\} \in B_6^*, e = (u_1,u_2)(v_1,v_2), \right.
$$
$$
\left. f = (u_1,t_2)(z_1,z_2) \right\}
$$
$$
= 2n_2^2 e_2 \sum_{u_1 \in V(G_1)} \sum_{\{u_1v_1, u_1z_1\}\subseteq E(G_1)} d_4(u_1v_1, u_1z_1|G_1),
$$

and

$$
\sum_{\{e,f\}\in B_8^*} d_4(e,f|G) = \sum \left\{ d_4(u_1v_1, z_1t_1|G_1) : \{e,f\} \in B_8^*, e = (u_1,u_2)(v_1,v_2), \right.
$$
$$
\left. f = (z_1,z_2)(t_1,t_2) \right\}
$$
$$
= \frac{1}{2} n_2^4 \sum_{u_1v_1 \in E(G_1)} \sum_{z_1t_1 \in E(G_1),\, z_1,\, t_1 \notin \{u_1,v_1\}} d_4(u_1v_1, z_1t_1|G_1).
$$

Consequently,

$$
\sum_{\{e,f\}\in B_5^*\cup B_6^*\cup B_8^*} d_4(e,f|G) = 2n_2^2 e_2 \sum_{u_1 \in V(G_1)} \sum_{\{u_1v_1, u_1z_1\}\subseteq E(G_1)} d_4(u_1v_1, u_1z_1|G_1)
$$
$$
+ \frac{1}{2} n_2^4 \sum_{u_1v_1 \in E(G_1)} \sum_{z_1t_1 \in E(G_1),\, z_1,\, t_1 \notin \{u_1,v_1\}} d_4(u_1v_1, z_1t_1|G_1)
$$
$$
= \left(n_2^3 + 2n_2^2 e_2 \right) \sum_{u_1 \in V(G_1)} \sum_{\{u_1v_1, u_1z_1\}\subseteq E(G_1)}
$$
$$
\times d_4(u_1v_1, u_1z_1|G_1) + \frac{1}{2} n_2^4 (2W_{e_4}(G_1)
$$
$$
- 2 \sum_{u_1 \in V(G_1)} \sum_{\{u_1v_1, u_1z_1\}\subseteq E(G_1)} d_4(u_1v_1, u_1z_1|G_1))
$$
$$
= n_2^4 W_{e_4}(G_1) + n_2^2 \left(n_2 + 2e_2 - n_2^2 \right)
$$
$$
\times \sum_{u_1 \in V(G_1)} \sum_{\{u_1v_1, u_1z_1\}\subseteq E(G_1)} d_4(u_1v_1, z_1t_1|G_1).
$$

Now, using Lemma 14.5.6, we obtain:

$$\sum_{\{e,f\}\in B_5{}^*\cup B_6{}^*\cup B_8{}^*} d_4(e,f|G) = n_2{}^4 W_{e_4}(G_1) + n_2{}^2\left(n_2 + 2e_2 - n_2{}^2\right)$$
$$\times (M_1(G_1) - 2N_1(G_1) - 2e_1).$$

Therefore,

$$\sum_{\{e,f\}\in B} d_4(e,f|G) = \sum_{i=1}^{4} \sum_{\{e,f\}\in B_i{}^*} d_4(e,f|G) + \sum_{\{e,f\}\in B_7{}^*} d_4(e,f|G)$$
$$+ \sum_{\{e,f\}\in B_5{}^*\cup B_6{}^*\cup B_8{}^*} d_4(e,f|G)$$
$$= \left|B_1{}^*\right| + 2\left|B_2{}^*\right| + \left|B_3{}^*\right| + 2\left|B_4{}^*\right| + 2\left|B_7{}^*\right|$$
$$+ \sum_{\{e,f\}\in B_5{}^*\cup B_6{}^*\cup B_8{}^*} d_4(e,f|G)$$
$$= 2|B| - \left|B_1{}^*\right| - \left|B_3{}^*\right| - 2\left|B_5{}^*\right| - 2\left|B_6{}^*\right| - 2\left|B_8{}^*\right|$$
$$+ \sum_{\{e,f\}\in B_5{}^*\cup B_6{}^*\cup B_8{}^*} d_4\left(e,f|G\right)$$
$$= 2e_1\binom{n_2{}^2}{2} - 2e_1 e_2(n_2 + e_2) + n_2{}^4 W_{e_4}(G_1)$$
$$+ 2n_2{}^2\left(n_2{}^2 - n_2 - 2e_2\right)N_1(G_1). \ \blacksquare$$

Lemma 14.5.8

$$\sum_{\{e,f\}\in C} d_4(e,f|G) = 2e_1 e_2 n_2(n_2 - 2) - 2e_1 n_2 N_1(G_2) + n_2{}^2 e_2 W_{ve_2}(G_1).$$

Proof One can easily see that, $\left|C_1{}^*\right| = 4e_1 e_2 n_2$, $\left|C_2{}^*\right| = 2e_1 n_2 N_1(G_2)$ and $\left|C_2{}^*\cup C_3{}^*\right| = 2e_1 e_2 n_2(n_2 - 2)$. By Lemma 14.5.3, we obtain:

$$\sum_{\{e,f\}\in C_4^*} d_4(e,f|G) = \sum \left\{ D_2(u_1,v_1z_1|G_1) : \{e,f\}\in C_4^*, e=(u_1,u_2),(u_1,t_2), \right.$$

$$f=(v_1,v_2),(z_1,z_2)\big\}$$

$$= n_2{}^2 e_2 \sum_{u_1\in V(G_1)} \sum_{v_1z_1\in E(G_1),\,v_1\neq u_1,\,z_1\neq u_1} D_2(u_1,v_1z_1|G_1)$$

$$= n_2{}^2 e_2 \sum_{u_1\in V(G_1)} \sum_{v_1z_1\in E(G_1)} D_2(u_1,v_1z_1|G_1)$$

$$- n_2{}^2 e_2 \sum_{u_1\in V(G_1)} \sum_{u_1v_1\in E(G_1)} D_2(u_1,u_1v_1|G_1)$$

$$= n_2{}^2 e_2 \left(W_{ve_2}(G_1) - \sum_{u_1\in V(G_1)} \sum_{u_1v_1\in E(G_1)} 1 \right)$$

$$= n_2{}^2 e_2 \left(W_{ve_2}(G_1) - \sum_{u_1\in V(G_1)} \deg_{G_1}(u) \right)$$

$$= n_2{}^2 e_2 (W_{ve_2}(G_1) - 2e_1).$$

Hence,

$$\sum_{\{e,f\}\in C} d_4(e,f|G) = \sum_{i=1}^{4} \sum_{\{e,f\}\in C_i^*} d_4(e,f|G) = |C_1^*| + |C_2^*| + 2|C_3^*|$$

$$+ \sum_{\{e,f\}\in C_4^*} d_4(e,f|G) = |C_1^*| + 2|C_2^*\cup C_3^*| - |C_2^*|$$

$$+ \sum_{\{e,f\}\in C_4^*} d_4(e,f|G) = 2e_1e_2n_2(n_2-2)$$

$$- 2e_1n_2N_1(G_2) + n_2{}^2 e_2 W_{ve_2}(G_1).$$

Now, we express the main theorem of this section.

Theorem 14.5.9 *The second edge-Wiener index of* $G_1[G_2]$ *is given by:*

$$W_{e_4}(G_1[G_2]) = 2n_1 \binom{e_2}{2} + 2e_1 \binom{n_2{}^2}{2} + 2e_1e_2(n_2{}^2 - 3n_2 - e_2)$$

$$+ e_2{}^2 W(G_1) + n_2{}^4 W_{e_4}(G_1)$$

$$+ n_2{}^2 e_2 W_{ve_2}(G_1) + 2n_2{}^2 (n_2{}^2 - n_2 - 2e_2)N_1(G_1) - (n_1 + 2e_1n_2)$$

$$\times N_1(G_2) - \frac{1}{4} n_1 N_2(G_2).$$
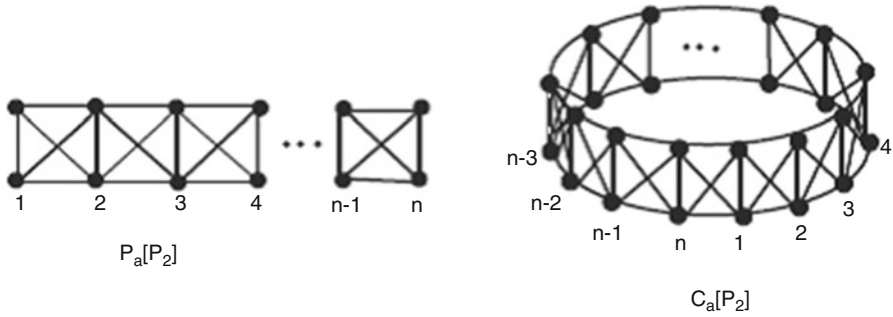
Fig. 14.8 Fence and closed − fence graphs on $2n$ vertices

Proof Since $\{A, B, C\}$ is a partition of the set K, so by definition of $W_{e_4}(G)$, we have:

$$W_{e_4}(G) = \sum_{\{e,f\} \in K} d_4(e, f | G)$$

$$= \sum_{\{e,f\} \in A} d_4(e, f | G) + \sum_{\{e,f\} \in B} d_4(e, f | G) + \sum_{\{e,f\} \in C} d_4(e, f | G).$$

Now, using Lemmas 14.5.5, 14.5.7 and 14.5.8, the proof is obvious.

Now, we can use Theorem 14.5.9 to obtain explicit formulae for the second edge-Wiener index of some classes of graphs by specializing components in compositions. Because P_n and C_m, $m \geq 4$ are triangle–free graphs, so by definition of the quantity N_1, $N_1(P_n) = N_1(C_m) = 0$ and $N_1(C_3) = 3$. Also, by definition of the quantity N_2, it is easy to see that for $n \geq 2$ and $m \geq 3$, $N_2(P_n) = N_2(C_m) = 0$. Now, using Theorem 14.5.9 and Table 14.1, we can easily get the formulae for the second edge-Wiener index of fence graph $P_n[P_2]$ and closed fence graph $C_n[P_2]$; see Fig. 14.8.

Corollary 14.5.10 *The second edge-Wiener index of the fence graph and closed fence graph are given by:*

1. $W_{e_4}(P_n[P_2]) = \dfrac{25}{6}n^3 - \dfrac{85}{6}n + 10,$

2. $W_{e_4}(C_n[P_2]) = \begin{cases} \dfrac{25}{8}n^3 + 10n^2 - \dfrac{185}{8}n, & \text{if } n \text{ is odd,} \\ \dfrac{25}{8}n^3 + 10n^2 - 10n, & \text{if } n \text{ is even.} \end{cases}$

Our next example is about the composition of arbitrary paths and cycles. Application of Theorem 14.5.9 and Table 14.1 yields:

Corollary 14.5.11 *For $n \geq 2$ and $m \geq 3$,*

1. $W_{e_4}(P_n[C_m]) = \begin{cases} 24n^3 - 66n + 45 & \text{if } m = 3 \\ \dfrac{m^4}{6}\, n(n^2 - 1) + \dfrac{m^3}{3}\, (n^3 + 5n - 6) + \dfrac{m^2}{6}\, (n^3 - 49n + 54) - mn & \text{if } m \geq 4 \end{cases}$,

2. $W_{e_4}(C_m[P_n]) = \begin{cases} 15n^4 - 3n^3 - 24n^2 + 15n + 3, & \text{if } m = 3 \\ \dfrac{m^3}{8}(n^4 + 2n^3 - n^2 - 2n + 1) + \dfrac{m^2}{2}n^2(n^2 + n - 1) & \text{if } m \text{ is odd}, m \neq 3 \\ -\dfrac{m}{8}(5n^4 - 10n^3 + 75n^2 - 58n + 1), & \\ \dfrac{m^3}{8}(n^4 + 2n^3 - n^2 - 2n + 1) + \dfrac{m^2}{2}n^2(n^2 + n - 1) & \text{if } m \text{ is even} \\ +mn(2n^2 - 10n + 7) \end{cases}$.

References

Alizadeh Y, Iranmanesh A, Došlić T, Azari M (2014) The edge Wiener index of suspensions, bottlenecks, and thorny graphs. Glas Mat Ser III 49(69):1–12

Ashrafi AR, Yousefi S (2007) A new algorithm for computing distance matrix and Wiener index of zig − zag polyhex nanotubes. Nanoscale Res Lett 2:202–206

Azari M, Iranmanesh A (2011a) Generalized Zagreb index of graphs. Studia Univ Babes − Bolyai Chem 56(3):59–70

Azari M, Iranmanesh A (2011b) Computation of the edge Wiener indices of the sum of graphs. Ars Combin 100:113–128

Azari M, Iranmanesh A (2013) Chemical graphs constructed from rooted product and their Zagreb indices. MATCH Commun Math Comput Chem 70:901–919

Azari M, Iranmanesh A (2014a) The second edge-Wiener index of some composite graphs. Miskolc Math Notes 15(2):305–316

Azari M, Iranmanesh A (2014b) Computing Wiener − like topological invariants for some composite graphs and some nanotubes and nanotori. In: Gutman I (ed) Topics in chemical graph theory. Univ Kragujevac, Kragujevac, pp 69–90

Azari M, Iranmanesh A, Tehranian A (2010) Computation of the first edge Wiener index of a composition of graphs. Studia Univ Babes − Bolyai Chem 55(4):183–196

Azari M, Iranmanesh A, Tehranian A (2011) Maximum and minimum polynomials of a composite graph. Austral J Basic Appl Sci 5(9):825–830

Azari M, Iranmanesh A, Tehranian A (2012) A method for calculating an edge version of the Wiener number of a graph operation. Util Math 87:151–164

Azari M, Iranmanesh A, Gutman I (2013a) Zagreb indices of bridge and chain graphs. MATCH Commun Math Comput Chem 70:921–938

Azari M, Iranmanesh A, Tehranian A (2013b) Two topological indices of three chemical structures. MATCH Commun Math Comput Chem 69:69–86

Buckley F, Harary F (1990) Distance in graphs. Addison − Wesley, Redwood

Dankelman P, Gutman I, Mukwembi S, Swart HC (2009) The edge Wiener index of a graph. Discrete Math 309:3452–3457

Diudea MV (1995) Wiener index of dendrimers. MATCH Commun Math Comput Chem 32:71–83

Diudea MV (2001) QSPR/QSAR studies by molecular descriptors. Nova, New York

Dobrynin AA, Entringer R, Gutman I (2001) Wiener index for trees: theory and applications. Acta Appl Math 66(3):211–249

Eliasi M, Iranmanesh A (2013) Hosoya polynomial of hierarchical product of graphs. MATCH Commun Math Comput Chem 69(1):111–119

Eliasi M, Raeisi GH, Taeri B (2012) Wiener index of some graph operations. Discrete Appl Math 160(9):1333–1344

Falahati-Nezhad F, Iranmanesh A, Tehranian A, Azari M (2014) Strict lower bounds on the multiplicative Zagreb indices of graph operations. Ars Combin 117:399–409

Graovac A, Pisanski T (1991) On the Wiener index of a graph. J Math Chem 8:53–62

Gutman I (1994) A formula for the Wiener number of trees and its extension to graphs containing cycles. Graph Theory Notes NY 27:9–15

Gutman I (2010) Edge versions of topological indices. In: Gutman I, Furtula B (eds) Novel molecular structure descriptors-theory and applications II. Univ Kragujevac, Kragujevac, pp 3–20

Gutman I, Das KC (2004) The first Zagreb index 30 years after. MATCH Commun Math Comput Chem 50:83–92

Gutman I, Polansky OE (1986) Mathematical concepts in organic chemistry. Springer, Berlin

Gutman I, Trinajstić N (1972) Graph theory and molecular orbitals, total $\pi-$electron energy of alternant hydrocarbons. Chem Phys Lett 17:535–538

Gutman I, Ruscić B, Trinajstić N, Wilcox CF (1975) Graph theory and molecular orbitals. XII Acyclic polyenes J Chem Phys 62(9):3399–3405

Gutman I, Yeh YN, Lee SL, Luo YL (1993) Some new results in the theory of the Wiener number. Indian J Chem 32A:651–661

Hosoya H (1988) On some counting polynomials in chemistry. Discrete Appl Math 19:239–257

Iranmanesh A (2013) (Chapter 13): The edge-wiener index and its computation for some nanostructures. In: Ashrafi AR, Cataldo F, Iranmanesh A, Ori O (eds) Topological modelling of nanostructures and extended systems. Springer, Netherlands, pp 425–471

Iranmanesh A, Azari M (2015a) (Chapter 7): The first and second Zagreb indices of several interesting classes of chemical graphs and nanostructures. In: Putz MV, Ori O (eds) Exotic properties of carbon nanomatter, vol 8. Springer, Netherlands, pp 153–183

Iranmanesh A, Azari M (2015b) Edge-Wiener descriptors in chemical graph theory: a survey. Curr Org Chem 19(3):219–239

Iranmanesh A, Gutman I, Khormali O, Mahmiani A (2009) The edge versions of the Wiener index. MATCH Commun Math Comput Chem 61:663–672

John PE, Diudea MV (2004) Wiener index of zig−zag polyhex nanotubes. Croat Chem Acta 77:127–132

Khalifeh MH, Yousefi−Azari H, Ashrafi AR (2009a) The first and second Zagreb indices of some graph operations. Discrete Appl Math 157:804–811

Khalifeh MH, Yousefi−Azari H, Ashrafi AR, Wagner SG (2009b) Some new results on distance−based graph invariants. Eur J Combin 30:1149–1163

Nadjafi-Arani MJ, Khodashenas H, Ashrafi AR (2012) Relationship between edge Szeged and edge Wiener indices of graphs. Glas Mat Ser III 47:21–29

Putz MV, Ori O, Cataldo F, Putz AM (2013) Parabolic reactivity "coloring" molecular topology: application to carcinogenic PAHs. Curr Org Chem 17(23):2816–2830

Réti T (2012) On the relationships between the first and second Zagreb indices. MATCH Commun Math Comput Chem 68:169–188

Sagan BE, Yeh YN, Zhang P (1996) The Wiener polynomial of a graph. Inter J Quantum Chem 60 (5):959–969

Stevanović D (2001) Hosoya polynomials of composite graphs. Discrete Math 235:237–244

Todeschini R, Consonni V (2000) Handbook of molecular descriptors. Wiley-VCH, Weinheim

Trinajstić N (1992) Chemical graph theory. CRC Press, Boca Raton

Wiener H (1947a) Structural determination of paraffin boiling points. J Am Chem Soc 69(1):17–20

Wiener H (1947b) Correlation of heats of isomerization and differences in heats of vaporization of isomers among the paraffin hydrocarbons. J Am Chem Soc 69:2636–2638

Yeh YN, Gutman I (1994) On the sum of all distances in composite graphs. Discrete Math 135:359–365

Yousefi-Azari H, Khalifeh MH, Ashrafi AR (2011) Calculating the edge Wiener and edge Szeged indices of graphs. J Comput Appl Math 235(16):4866–4870

Zhou B (2004) Zagreb indices. MATCH Commun Math Comput Chem 52:113–118

Zhou B, Gutman I (2005) Further properties of Zagreb indices. MATCH Commun Math Comput Chem 54:233–239

Chapter 15
Study of the Bipartite Edge Frustration of Graphs

Zahra Yarahmadi

Abstract The smallest number of edges that have to be deleted from a graph to obtain a bipartite spanning subgraph is called the bipartite edge frustration of G and denoted by $\varphi(G)$. This topological index is related to the well-known $\mathrm{Max-cut}$ problem, and has important applications in computing stability of fullerenes. In this paper we determine the bipartite edge frustration of some classes of composite graphs. Moreover, this quantity for four classes of graphs arising from a given graph under different types of edge subdivisions is investigated.

15.1 Introduction

The problem of finding large bipartite spanning subgraphs of a given non-bipartite graph has a long and rich history. The first results were obtained by Erdös (Erdös 1965) and Edwards (Edwards 1973), who showed that every graph G on $|V(G)|$ vertices and $|E(G)|$ edges contains a bipartite subgraph with at least $|E(G)|/2 + (|V(G)| - 1)/4$ edges. Those bounds were further improved for various classes of graphs; for example, the lower bound of $(4/5)|E(G)|$ was established for cubic triangle-free graphs (Hopkins and Staton 1982) and also for sub-cubic triangle-free graphs (Bondy and Locke 1986). The best currently known (Cui and Wang 2009) lower bound for cubic, planar, and triangle-free graphs is

$$\frac{39}{539} \left| V(G) \right| - \frac{9}{16} \ .$$

Instead of looking for large bipartite subgraphs of a given graph G, it is sometimes more convenient to look at the equivalent problem of finding a smallest

Z. Yarahmadi (✉)

Department of Mathematics, Faculty of Sciences, Khorramabad Branch, Islamic Azad University, Khorramabad, Iran

e-mail: Z.yarahmadi@khoiau.ac.ir; Z.yarahmadi@gmail.com

set of edges that must be deleted from G in order to make the remaining graph bipartite. Borrowing from the terminology of the antiferromagnetic Ising model, the cardinality of any such set is then called the bipartite edge frustration of a graph. More formally, let G be a graph with the vertex and edge sets $|V(G)|$ and $|E(G)|$, respectively. The bipartite edge frustration of G is then defined as the minimum number of edges that have to be deleted from G to obtain a bipartite spanning subgraph. We denote it by $\varphi(G)$. Clearly, if G is bipartite, then $\varphi(G) = 0$ and $\varphi(G)$ is a topological index. It can be easily shown that $\varphi(G) \leq \frac{|E(G)|}{2}$ and that the complete graph on n vertices has the maximum possible bipartite edge frustration among all graphs on n vertices. Hence, the bipartite edge frustration has properties that make it useful as a measure of non-bipartivity of a given graph.

Schmalz et al. (1986) observed that the isolated pentagon fullerenes have the best stability. Because of this success, it is natural to study its vertex version. The bipartite vertex frustration of G, $\varphi(G)$, is defined as the minimum number of vertices that have to be deleted from G to obtain a bipartite subgraph H of G (Yarahmadi and Ashrafi 2011a). Obviously, if G is not bipartite, then $\underline{H}$ is not a spanning subgraph of G and so, H is not in general a large bipartite subgraph of G. The quantity $\varphi(G)$ is, in general, difficult to compute; it is NP-hard for general graphs. Hence, it makes sense to search for classes of graphs that allow its efficient computation. Some results in this direction are reported in (Došlić and Vukičević 2007) for fullerenes and other polyhedral graphs and in (Ghojavand and Ashrafi 2008) for some classes of nanotubes. For mathematical properties of this new topological index, we refer to (Yarahmadi and Ashrafi 2011b, 2013; Yarahmadi et al. 2010; Yarahmadi 2010; Ashrafi et al. 2013).

In this chapter, we will present explicit formulas for the bipartite edge frustration for the Cartesian product, chain, bridge, extended bridge graphs, splice, link, hierarchical product and its generalization. Also, some inequalities of the Nordhaus-Gaddum type will be presented. Moreover, four types of graphs resulting from edge subdivision will be introduced. Two of them, the subdivision graph and the total graph, belong to the folklore, while the other two were introduced in (Cvetković et al 1980) and further investigated in (Yan et al. 2007).

15.2 Definitions and Preliminaries

A *graph* is a pair $G = (V,E)$ of *points* and *lines*. The points and lines of G are also called *vertices* and *edges* of the graph, respectively. If e is an edge of G, connecting the vertices u and v, then we write $e = uv$ and say "u and v are adjacent."

Suppose G is a connected graph and $x, y \in V(G)$. The length of a minimal path connecting x and y is denoted by $d_G(x, y)$. It is easy to see that $(V(G), d_G(x, y))$ is a metric space.

It is well known that the bipartite edge frustration is a measure of stability for the fullerene molecules; see (Došlić 2005a, b; Fajtlowicz and Larson 2003). Here, a fullerene is a planar, 3-regular, and 3-connected molecular graph, 12 of whose faces

are pentagons, and any remaining faces are hexagons. Such molecules are entirely constructed from carbon atoms. A fullerene is called an isolated pentagon (IP for short) if its pentagons do not have a common edge.The citation Fajtlowicz (2003) have been changed to Fajtlowicz and Larson (2003) as per the reference list. Please check if okay.It is okay.

In this section we introduce the composite graphs that will be considered here and recall their basic properties relevant for our goal. We start by composite graphs that arise by splicing, i.e., by identifying certain vertices.

Following Imrich and Klavžar ([2000](#)), the *Cartesian product* $G \times H$ of two graphs G and H is defined on the Cartesian product $V(G) \times V(H)$ of the vertex sets of the factors. The edge set $E(G \times H)$ is the set of all edges $(u,v)(x,y)$ for which either $u = x$ and $vy \in E(H)$ or $ux \in E(G)$ and $v = y$. Thus, the vertex and edge sets of $G \times H$ are the following sets: $V(G \times H) = V(G) \times V(H)$ and $E(G \times H) = \{(u,v)(x,y) \mid u = x, \, vy \in E(H), \, \text{or}, \, ux \in E(G), \, v = y\}$.

For a sequence $G_1, G_2, \ldots, G_n$ of graphs, we denote $G_1 \times \cdots \times G_n$ by $\prod_{i=1}^{n} G_i$. In the case that $G_1 = G = \cdots = G_n = G$, we denote $\prod_{i=1}^{n} G_i$ by G^n.

The *join*, $G + H$ of graphs G and H with disjoint vertex sets $V(G)$ and $V(H)$ and edge sets $E(G)$ and $E(H)$, is the graph union $G \cup H$ together with all the edges joining $V(G)$ and $V(H)$. If $G = H + \cdots + H$, then we denote G by nH. The graph ∇G is obtained from G by adding a new vertex and making it adjacent to all vertices of G. The graph ∇G is called suspension of G. Obviously $\nabla G = G + K_1$. A join of two graphs is bipartite if and only if both graphs are empty, i.e., without edges. Hence, $\varphi(G + H) > 0$ if at least one of components contains an edge.

Both Cartesian product and join are standard graph operations. We refer the reader to monograph of Imrich (2000) for more information on those products.

The *complement* G of graph $\overline{G}$ has $V(G)$ as its vertex set, and two vertices are adjacent in $\overline{G}$ if and only if they are not adjacent in G.

Let $\{G_i\}_{i=1}^{n}$ be a set of finite pair wise disjoint graphs with $v_i \in V(G_i)$. The *bridge graph* $B = B(G_1, G_2, \ldots, G_n, v_1, v_2, \ldots, v_n)$ is the graph obtained from the graphs $G_1, G_2, \ldots, G_n$ by connecting the vertices v_i and v_{i+1} by an edge, for all $i = 1, 2, \ldots, n$, as shown in Fig. [15.1](#). We abbreviate the notation to $B(G_1, G_2, \ldots, G_n)$ when the vertices v_i are clear from context.

The *extended bridge graph* $EB(G, H_1, H_2, \ldots, H_n; v_1, \ldots, v_n)$ of G and $\{H_i\}_{i=1}^{n}$ with respect to $\{v_i\}_{i=1}^{n}$ is constructed by identifying the vertex v_i in G and H_i, for all $i = 1, 2, \cdots, n$. An example is shown in Fig. [15.2](#).

Let $\{G_i\}_{i=1}^{n}$ be a set of finite pairwise disjoint graphs with $v_i, w_i \in V(G_i)$. The *chain graph* $C = C(G_1, G_2, \ldots, G_n, v_1, w_1, \ldots, v_n, w_n)$ of $\{G_i\}_{i=1}^{n}$ with respect to the vertices $\{v_i, w_i\}_{i=1}^{n}$ is the graph obtained from graphs $G_1, G_2, \ldots, G_n$ by identifying the vertex w_i with v_{i+1}, for all $i = 1, 2, \ldots, n$, as shown in Fig. [15.3](#).

Again, the dependence on $v_1, v_2, \ldots, v_n$ and $w_1, w_2, \ldots, w_n$ will be often omitted in notation. The above classes of graphs were considered in Mansour and Schork ([2009](#)).
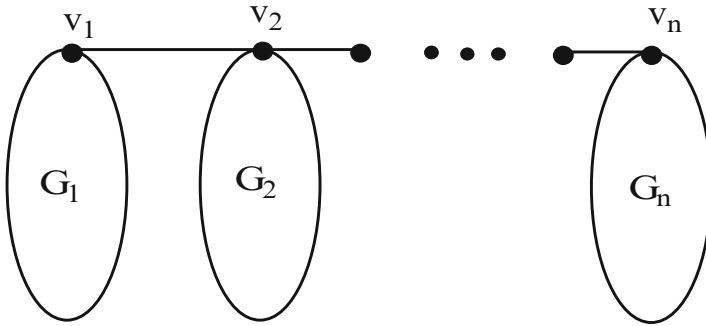
Fig. 15.1 The bridge graph
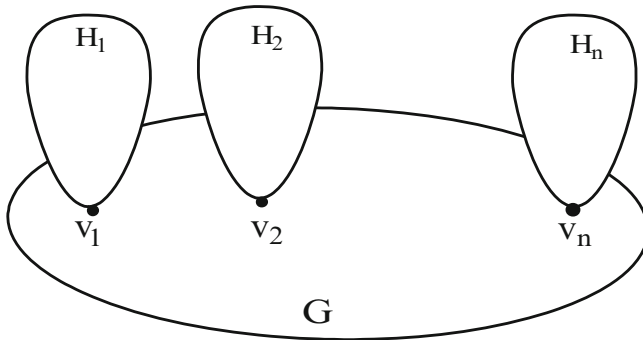
Fig. 15.2 The extended bridge graph
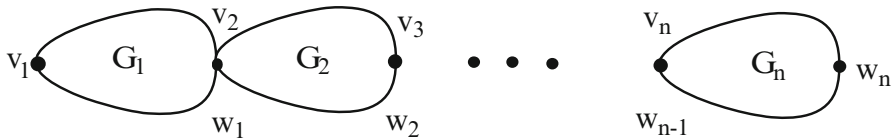
Fig. 15.3 The chain graph

Let G and H be two simple and connected graphs with disjoint vertex sets. For given vertices $a \in V(G)$ and $b \in V(H)$, a *splice* of G and H is defined as the graph, $(G.H)(a, b)$ obtained by identifying the vertices a and b. Similarly, a *link* of G and H is defined as the graph $(G \sim H)(a, b)$ obtained by joining a and b by an edge. The splices and links considered in (Došlić 2005a, b) could be viewed as their special cases.

The following theorem immediately concludes.

Theorem 15.2.1 *Let G and H be two simple and connected graphs with disjoint vertex sets. For each $a \in V(G)$ and $b \in V(H)$, the bipartite edge frustration of splice and link of G and H are obtained as follows:*
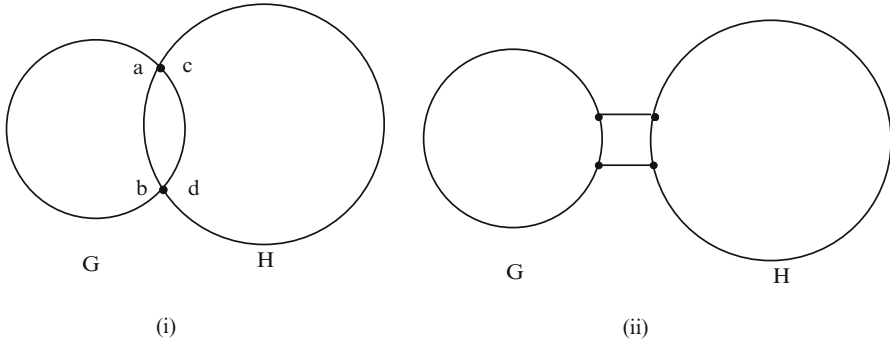
Fig. 15.4 The double splice and double link

1. $\varphi((G.H)(a, b)) = \varphi(G) + \varphi(H),$
2. $\varphi((G \sim H)(a, b)) = \varphi(G) + \varphi(H).$

Now we extend the above operations, for splice of G *and* H *by identifying two vertices and for link* G *and* H *by joining two vertices as the following definition.*

Definition 15.2.2 Let G and H be two simple and connected graphs with disjoint vertex sets. For given vertices $a, b \in V(G)$ and $c, d \in V(H)$, a *double splice* of G and H is defined as the graph $(G:H)(a, b:c, d)$ obtained by identifying the vertices a and c and vertices b and d. Similarly, a *double link* of G and H is defined as the graph $(G \approx H)(a, b : c, d)$ obtained by joining a and c by an edge and b and d by another edge. A double splice and double link of two graphs are shown schematically in Fig. 15.4.

A new operation on graphs is *hierarchical product*, because of the strong (connectedness) hierarchy of the vertices in the resulting graphs, see Barriére et al. (2009a). In fact, the obtained graphs turn out to be subgraphs of the Cartesian product of the corresponding factors. Some well-known properties of the Cartesian product, such as reduced mean distance and diameter, simple routing algorithms and some optimal communication protocols are inherited by the hierarchical product. Let $G_i = (V_i, E_i)$ be N graphs with each vertex set Vi, $1 \leq i \leq N$, having a distinguished or root vertex, labeled 0. The hierarchical product $H = G_N \Pi \ldots \Pi G_2 \Pi G_1$ is the graph with vertices the $N-$tuples $x_N \ldots x_2 x_1$, $x_i \in V_i$, and edges defined by the adjacencies:

$$x_N \ldots x_2 x_1 \approx \begin{cases} x_N \ldots x_3 x_2 y_1 & \text{if } y_1 \approx x_1 \text{ in } G_1 \\ x_N \ldots x_3 y_2 x_1 & \text{if } y_2 \approx x_2 \text{ in } G_2 \text{ and } x_1 = 0, \\ x_N \ldots y_3 x_2 x_1 & \text{if } y_3 \approx x_3 \text{ in } G_3 \text{ and } x_1 = x_2 = 0, \\ \vdots & \vdots \\ y_N \ldots x_3 x_2 x_1 & \text{if } y_N \approx x_N \text{ in } G_N \text{ and } x_1 = x_2 = \cdots = x_{N-1} = 0 \end{cases}$$

Notice that the structure of the obtained product graph H heavily depends on the root vertices of the factors G_i for $1 \leq i \leq N$. Also, if $|V_i| = n_i$ and $|E_i| = m_i$, the

number of vertices of H is $n_N \ldots n_2 n_1$ and the number of edges is equal to $m_N + \sum_{i=1}^{N-1} \prod_{j=i+1}^{N} n_j m_i$.

Note also that the hierarchical $H = G_N \Pi \ldots \Pi G_2 \Pi G_1$ is simply subgraph of classical Cartesian product $G_N \times \cdots \times G_2 \times G_1$. Although the Cartesian product is both commutative and associative, the hierarchical product has only the second property, provided that the root vertices are conveniently chosen (in the natural way).

A natural generalization of the hierarchical product, proposed in Barriére et al. (2009b), is as follows: Given N graphs $G_i = (V_i, E_i)$ and (nonempty) vertex subsets $U_i \subseteq V_i$, for $1 \le i \le N - 1$, the *generalized hierarchical* product $H_g = G_N \Pi \ldots \Pi G_2 (U_2) \Pi G_1 (U_1)$ is the graph with vertex set $V_N \times \cdots \times V_2 \times V_1$ and adjacencies:

$$x_N \ldots x_2 x_1 \approx \begin{cases} x_N \ldots x_3 x_2 y_1 & \text{if } y_1 \approx x_1 \text{ in } G_1, \\ x_N \ldots x_3 y_2 x_1 & \text{if } y_2 \approx x_2 \text{ in } G_2 \text{ and } x_1 \in U_1, \\ x_N \ldots y_3 x_2 x_1 & \text{if } y_3 \approx x_3 \text{ in } G_3 \text{ and } x_i \in U_i \text{ for } i = 1, 2, \\ \vdots & \vdots \\ y_N \ldots x_3 x_2 x_1 & \text{if } y_N \approx x_N \text{ in } G_N \text{ and } x_i \in U_i \text{ for } i = 1, 2, \ldots, N. \end{cases}$$

Now, we define four related graphs, for a connected graph G, as follows:

1. $S(G)$ is the graph obtained by inserting an additional vertex in each edge of G. Equivalently, each edge of G is replaced by a path of length 2.
2. $R(G)$ is obtained from G by adding a new vertex corresponding to each edge of G and then joining each new vertex to the end vertices of the corresponding edge. Another way to describe $R(G)$ is to replace each edge of G by a triangle.
3. $Q(G)$ is obtained from G by inserting a new vertex into each edge of G and then joining with edges those pairs of new vertices on adjacent edges of G.
4. $T(G)$ has as its vertices, the edges and vertices of G. Adjacency in $T(G)$ is defined as adjacency or incidence for the corresponding elements of G.

The graphs $S(G)$ and $T(G)$ are called the *subdivision* and *total* graphs of G, respectively; see Fig. 15.5.

Let F be one of the symbols S, R, Q, or T. The $F-$ sum $G +_F H$ is a graph with the set of vertices $V(G +_F H) = (V(G) \cup E(H)) \times V(H)$, and two vertices (u_1, u_2) and (v_1, v_2) of $G +_F H$ are adjacent if and only if $[u_1 = v_1 \in V(G)$ and $(u_2, v_2) \in E(H)]$ or $[u_2 = v_2$ and $(u_1, v_1) \in E(F(G))]$. In an exact phrase,

$E(G +_F H) = \{((u_1, u_2), (v_1, v_2)) | [u_1 = v_1 \in V(G) \text{ and } (u_2, v_2) \in E(H)] \text{ or } [u_2 = v_2$ and $(u_1, v_1) \in E(F(G))]\}$.

Note that $G +_F H$ has $|V(H)|$ copies of the graph $F(G)$, and we may label these copies by vertices of H. The vertices in each copy have two situations: the vertices in $V(H)$ (we refer to these vertices as black vertices) and the vertices in $E(G)$ (we refer to these vertices as white vertices). Now we join only black vertices with the same name in $F(G)$ in which their corresponding labels are adjacent in H. We

A graph G   The graph S(G)   The graph R(G)

The graph Q(G)   The graph T(G)
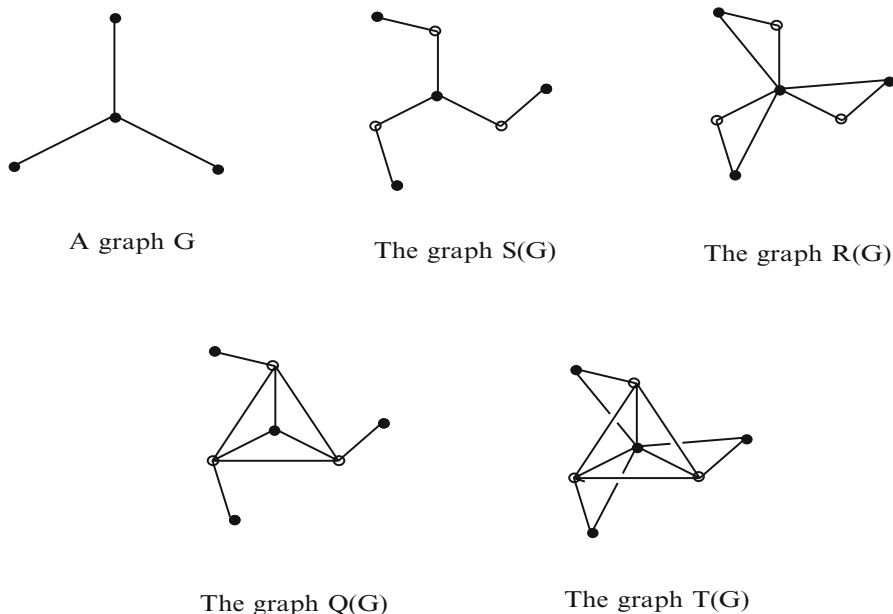
Fig. 15.5 The graph G together with its subdivision $S(G)$, total graph $T(G)$ and the related graphs $R(G)$ and $Q(G)$

illustrate this definition in Fig. 15.6. For more details on these operations we refer the reader to Eliasi and Taeri (2009).

It is obvious from the definition that the bipartite edge frustration of a disconnected graph is equal to the sum of bipartite edge frustration of its components. Hence, it suffices to consider connected graphs. The following observation shows that this type of additive behavior extends also to the graphs with cut-vertices. We will find it useful when dealing with some classes of composite graph introduced above.

Lemma 15.2.3 *Let $v \in V(G)$ be a cut-vertex of a graph G and G_i, $i = 1, \ldots, s$ be the components of $G - \{v\}$. Then $\varphi(G) = \sum_{i=1}^{s} \varphi(G[G_i \cup \{v\}])$. Here $G[G_i \cup \{v\}]$ denotes the graph induced in G by $V(G_i) \cup \{v\}$.*

The notation we used for a graph induced by a certain set of vertices should not be confused with a similar notation used for composition; here in the square brackets is a set of vertices, while in the composition case there is a whole graph. We close the section by formulas for the bipartite edge frustration of cycles and complete graphs.

$$\varphi(C_n) = \frac{1 - (-1)^n}{2} \text{ and } \varphi(K_n) = \left\lfloor \frac{n-1}{2} \right\rfloor \left\lceil \frac{n-1}{2} \right\rceil$$
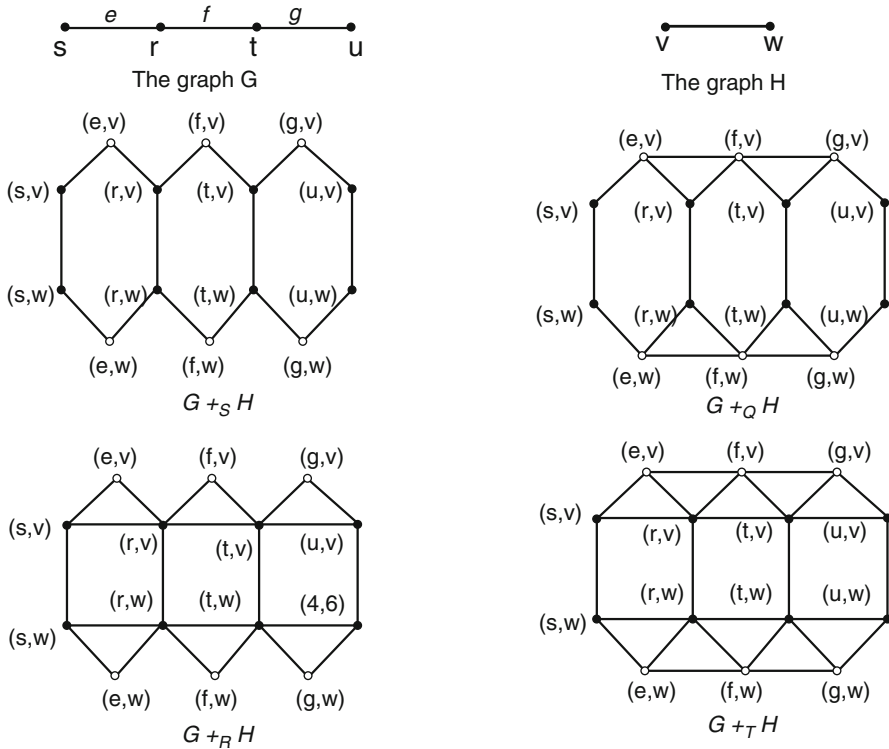
Fig. 15.6 The graphs G, H and $G +_F H$

15.3 The Bipartite Edge Frustration of Some Composite Graphs

The three classes of graphs considered in this section share a certain number of similarities that enable their synoptic treatment. In both chain and bridge graphs their building blocks are so well isolated from each other that their bipartite edge frustrations can be computed separately and then added in order to obtain the bipartite edge frustration of the whole graph. All interaction between components of a bridge graph is via its path backbone, which is itself bipartite. If the backbone is replaced by a non−bipartite scaffold, as in the case of extended bridges, the only additional complication is to compute the bipartite edge frustration of the scaffold graph. This results in (at most) one additional term in the formula for the total bipartite edge frustration.

Theorem 15.3.1

1. Let $G = C(G_1, G_2, \ldots, G_n)$ be a chain graph. Then $\varphi(G) = \sum_{i=1}^{n} \varphi(G_i)$.
2. Let $G = B(G_1, G_2, \ldots, G_n)$ be a bridge graph. Then $\varphi(G) = \sum_{i=1}^{n} \varphi(G_i)$

3. Let $K = EB(G, H_1, H_2, \ldots, H_n)$ be an extended bridge graph. Then $\varphi(K) = \varphi(G) + \sum_{i=1}^{n} \varphi(H_i)$.

The results of this subsection can be specialized in a straightforward way to the cases where all building blocks are identical, yielding the explicit formulas for the bipartite edge frustrations of rooted products of two graphs. Similarly, the results for chain graphs remain valid without any modifications also for splices of two or more graphs and for generalized cactus graphs. The results and proofs follow directly from Lemma 15.2.3, and we leave their formulation and proofs to the reader.

The Cartesian product gives rise to many interesting classes of graphs, such as lattices, tubes, tori, Hamming graphs, and hypercubes, to mention just a few examples.

Theorem 15.3.2. *Let $G_1, G_2, \ldots, G_s$ be connected graphs and $G = \prod_{i=1}^{s} G_i$. Then*

$$\varphi(G) = \prod_{i=1}^{s} |V(G_i)| \sum_{j=1}^{s} \frac{\varphi(G_j)}{|V(G_j)|}.$$

In special case, let B be a bipartite graph on n vertices. Then for any graph G, we have $\varphi(B \times G) = n\varphi(G)$. This case covers the linear polymers $P_n \times G$ induced by an arbitrary graph G. Also, for a non-bipartite graph G on n vertices, $\phi(G^s) = n^{s-1}\phi(G)$.

We present explicit formulas for the bipartite edge frustration of C_4 nanotubes and nanotori in the following example.

Example

(a) $\varphi(P_n \times C_{2m+1}) = n$,
(b) $\varphi(C_{2n} \times C_{2m+1}) = 2n$,
(c) $\varphi(C_{2n+1} \times C_{2m+1}) = 2(m + n + 1)$.

We have already mentioned that $G_1 + G_2$ is non-bipartite as soon as any of its components contains an edge. It is intuitively clear that joins are "very much" non-bipartite, and our findings confirm this feeling.

Theorem 15.3.3 *Let G_1 and G_2 be two connected bipartite graphs with bipartitions (A_1, B_1) and (A_2, B_2), respectively. Let us denote $a_i = |A_i|$ and $b_i = |B_i|$, $i = 1, 2$ and let $a_i \leq b_i$ for $i = 1, 2$, Fig. 15.7. Then*

$$\varphi(G_1 + G_2) \leq \min\{a_1 a_2 + b_1 b_2, a_1 b_2 + b_1 a_2, a_1 |V(G_2)| + |E(G_2)|, a_2 |V(G_1)| + |E(G_1)|, |E(G_1)| + |E(G_2)|\}.$$

Now, the logical thing to do would be to proceed and show that the above upper bound is always achieved. The next example shows that this cannot be done in all

Fig. 15.7 A join of two
bipartite graphs.
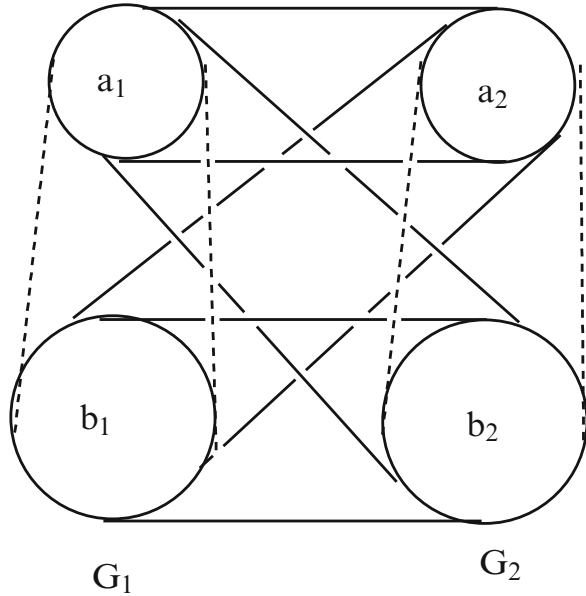
cases. Take $K_{5,50}$ and attach a path of length 4 to its smaller class by identifying one
of its end-vertices with any vertex of the smaller class. Denote the obtained bipartite
graph by G_1, and its bipartition by (A_1, B_1). Obviously, $a_1 = 7$, $b_1 = 52$, and
$|E(G_1)| = 254$. Call the vertices from the path exceptional. Take $K_{8,9}$ and call it
G_2. Now consider $G = G_1 + G_2$ as shown in Fig. 15.8. By computing all terms of
the right-hand side of the inequality of Theorem 15.3.3 it follows that the minimum
is achieved

For $a_1 |V(G_2)| + |E(G_2)| = 191$. Hence G can be made bipartite by deleting
119 edge between A_1 and G_2 and 72 edges of G_2. Let us denote so obtained bipartite
graph by G_0. Now take any two vertices of A_2 and connect them to the two
exceptional vertices of A_1 by all four possible edges. The new edges are shown
by dashed lines in Fig. 15.8. The resulting graph is not bipartite, but it can be made
bipartite by removing the three edges connecting the exceptional vertices of A_1 with
the exceptional vertices in B_1. The total result is a bipartite spanning subgraph of
$G_1 + G_2$ obtained by deleting 190 edges, a strictly smaller number than the
minimum of the right-hand side of the inequality of Theorem 15.3.3. With some
care the number of vertices in the example could be made smaller, but this is not
essential for our conclusion. The inequality of Theorem 15.3.3 can be converted to
equality when the minimum of the right-hand side is equal to $|E(G_1)| + |E(G_2)|$.

Theorem 15.3.4 *Let G be a connected bipartite graph on n vertices. Then*

$$\varphi(\nabla S_n) \leq \varphi(\nabla G) \leq \varphi(\nabla P_n).$$
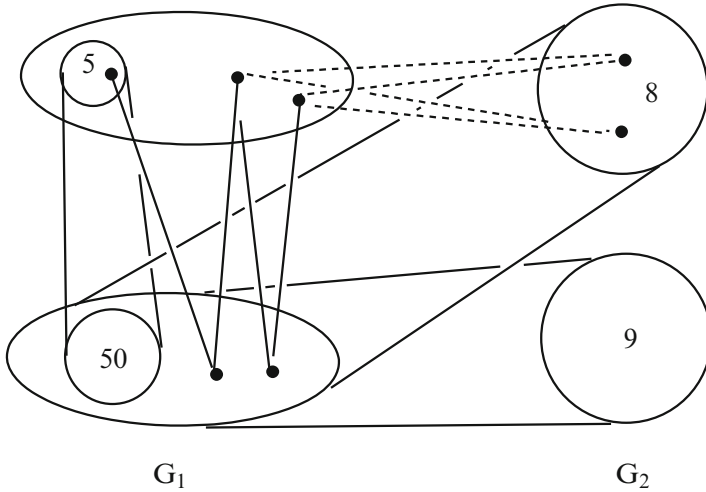
Fig. 15.8   A graph for which the inequality of Theorem 15.3.3 remains strict

The bipartite edge frustration of corona products can be neatly expressed when the non − scaffold graph is bipartite. Again, the result crucially depends on the formula for the bipartite edge frustration of a suspension.

Let us mention to the bipartite edge frustration of double splice and double link of graphs. At first we define a concept that is used for proving the next theorems.

Definition 15.3.5 Let G be a graph. For $a, b \in V(G)$, $\varphi_{a,b}(G)$ is the smallest number of edges that have to be deleted from a graph G to obtain a bipartite spanning subgraph such that a and b are occurred in the same partition. Similarly, we define $\varphi'_{a,b}(G)$, for each $a, b \in V(G)$, as the smallest number of edges that have to be deleted from a graph G to obtain a bipartite spanning subgraph such that a and b are occurred in the different partitions. It is easy to show that $\varphi(G) = \min \{ \varphi_{a,b}(G), \varphi'_{a,b}(G) \}$.

Example

1. $\varphi_{a,b}(P_n) = \begin{cases} 0 & 2 | d(a,b) \\ 1 & 2 | d(a,b) \end{cases}$, $\varphi'_{a,b}(P_n) = \begin{cases} 1 & 2 | d(a,b) \\ 0 & 2 | d(a,b) \end{cases}$,

2. $\varphi_{a,b}(C_{2n}) = \begin{cases} 0 & 2 | d(a,b) \\ 1 & 2 | d(a,b) \end{cases}$, $\varphi'_{a,b}(C_{2n}) = \begin{cases} 1 & 2 | d(a,b) \\ 0 & 2 | d(a,b) \end{cases}$,

3. $\varphi_{a,b}(C_{2n+1}) = \varphi'_{a,b}(C_{2n+1}) = \varphi(C_{2n+1})$, for each $a, b \in V(C_{2n+1})$,

4. $\varphi_{a,b}(K_n) = \varphi'_{a,b}(K_n) = \varphi(K_n)$, for each $a, b \in V(K_n)$.

Remark Let G and H be two graphs. If $ab \in E(G)$ and $cd \in E(H)$, then these edges are identified in double splice graph $(G:H)(a,b:c,d)$. In this case, the number of edges of $(G:H)(a,b:c,d)$ is equal to $|E((G:H)(a, b : c,d))| = |E(G)| + |E(H)| - 1$.

Otherwise, $|E((G:H)(a, b : c, d))|\$\$ = |E(G)| + |E(H)|$. In double splice graph when the vertices a and c are identified, we can certainly assume that $u = a = b$, by similar argument we assume $v = c = d$. Indeed we can assume that, $u, v \in V(G) \cap V(H)$. We abbreviate the notation to $(G:H)$ when the vertices u, v $\in V(G) \cap V(H)$ are clear from context.

In the following theorems formulas for the bipartite edge frustration of double splice and double link of two graphs are computed.

Theorem 15.3.6 *Let G and H be two graphs. For each u, $v \in V(G) \cap V(H)$ such that $|E((G : H)(a, b : c, d))| = |E(G)| + |E(H)|$, we have*

$$\varphi((G : H)) = \min\left\{ \varphi_{u,v}(G) + \varphi_{u,v}(H),\ \varphi'_{u,v}(G) + \varphi'_{u,v}(H) \right\}.$$

Theorem 15.3.7 *Let G and H be two graphs. For each u, $v \in V(G) \cap V(H)$ such that $|E((G : H)(a, b : c, d))| = |E(G)| + |E(H)| - 1$, we have*

$$\varphi((G : H)) = \min\left\{ \varphi_{u,v}(G) + \varphi_{u,v}(H) - 1,\ \varphi'_{u,v}(G) + \varphi'_{u,v}(H) \right\}.$$

Lemma 15.3.8 *Let G be a connected graph. If G_0 be a bipartite subgraph of G by deleting $\varphi(G)$ edges, then G_0 is connected.*

In the following we obtain formulas for the bipartite edge frustration of double link of graphs.

Theorem 15.3.9 *Let G and H be two graphs. If a, $b \in V(G)$ and c, $d \in V(H)$, then*

1. If $\left(\varphi_{a,b}(G) = \varphi(G),\ \varphi_{c,d}(H) = \varphi(H)\right)$ or $\left(\varphi'_{a,b}(G) = \varphi(G),\ \varphi'_{c,d}(H) = \varphi(H)\right)$, then $\varphi((G \approx H)(a, b : c, d)) = \varphi(G) + \varphi(H)$.
2. If $\left(\varphi_{a,b}(G) = \varphi(G),\ \varphi'_{c,d}(H) = \varphi(H)\right)$ or $\left(\varphi'_{a,b}(G) = \varphi(G),\ \varphi_{c,d}(H) = \varphi(H)\right)$, then $\varphi((G \approx H)(a, b : c, d)) = \varphi(G) + \varphi(H) + 1$.

For the sake of completeness, we mention here a theorem of Došlić and Vukičević as follows:

Definition 15.3.10 Let G and H be two connected graphs on disjoint vertex sets, and let $a \in V(G)$ and $b \in V(H)$ An n-link of G and H is a graph obtained by connecting the vertices a and b by a path of length n so that each of these vertices is identified with one of the terminal vertices of P_n. We denote n-link of G and H by $(G\tilde{\ }_nH)(a, b)$.

Theorem 15.3.11 *Let G and H be two connected graphs with disjoint vertex sets. For each $a \in V(G)$ and $b \in V(H)$, the bipartite edge frustration of n-link of G and H is obtained as follows:*

$$\varphi((G\tilde{\ }_nH)(a, b)) = \varphi(G) + \varphi(H).$$

Definition 15.3.12 Let G and H be two simple and connected graphs with disjoint vertex sets. For given vertices a, $b \in V(G)$ and c, $d \in V(H)$, a $(m, n)-$ link of G and H is defined as the graph $(G\approx_{m,n}H)(a, b : c, d)$ obtained by joining a and c by a path of length m and b and d by another path of length n; see Fig. 15.9.

The following theorem can be proved in much the same way as Theorem 15.3.9.

Theorem 15.3.13 *Let G and H be two graphs and a, $b \in V(G)$ and c, $d \in V(H)$. Then*

1. If $\left(\varphi_{a,b}(G) = \varphi(G), \varphi_{c,d}(H) = \varphi(H)\right)$ or $\left(\varphi'_{a,b}(G) = \varphi(G), \varphi'_{c,d}(H) = \varphi(H)\right)$ and $m + n$ be an even number, then $\varphi((G\approx_{m,n}H)(a, b : c, d)) = \varphi(G) + \varphi(H)$.
2. If $\left(\varphi_{a,b}(G) = \varphi(G), \varphi_{c,d}(H) = \varphi(H)\right)$ or $\left(\varphi'_{a,b}(G) = \varphi(G), \varphi'_{c,d}(H) = \varphi(H)\right)$ and $m + n$ be   an   odd   number,   then $\varphi((G\approx_{m,n}H)(a, b : c, d)) = \varphi(G) + \varphi(H) + 1$.
3. If $\left(\varphi_{a,b}(G) = \varphi(G), \varphi'_{c,d}(H) = \varphi(H)\right)$ or $\left(\varphi'_{a,b}(G) = \varphi(G), \varphi_{c,d}(H) = \varphi(H)\right)$ and $m + n$ be   an   even   number,   then $\varphi((G\approx_{m,n}H)(a, b : c, d)) = \varphi(G) + \varphi(H) + 1$.
4. If $\left(\varphi_{a,b}(G) = \varphi(G), \varphi'_{c,d}(H) = \varphi(H)\right)$ or $\left(\varphi'_{a,b}(G) = \varphi(G), \varphi_{c,d}(H) = \varphi(H)\right)$ and $m + n$ be an odd number, then $\varphi((G\approx_{m,n}H)(a, b : c, d)) = \varphi(G) + \varphi(H)$.

Finally, we address the study bipartite edge frustration of the hierarchical product of two or more graphs. Some natural generalizations of the hierarchic product are proposed and we consider the bipartite edge frustration of this generalization.

Theorem 15.3.14 *Let $G_i = (V_i, E_i)$ be N graphs with each vertex set V_i, $i = 1$, $2, \ldots, N$, and $H = G_N \Pi \cdots \Pi G_2 \Pi G_1$. Then the bipartite edge frustration of H is obtained as follows:*

$$\varphi(H) = \varphi(G_N) + \sum_{i=1}^{N-1}\left(\prod_{j=i+1}^{N}|V_j|\right)\varphi(G_i).$$
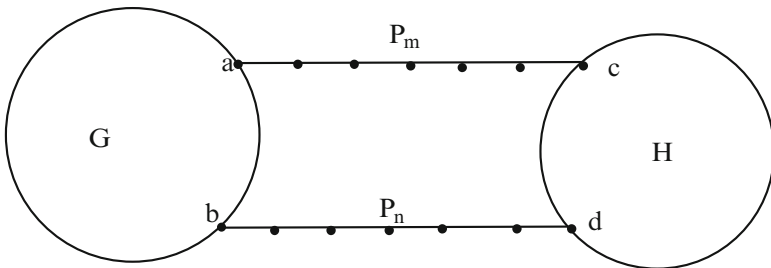
Fig. 15.9 The $(m, n)-$link

Theorem 15.3.15 *Let $f \upharpoonright$ or $i = 1, 2, \ldots, N$, G_i be a graph and for $i = 1, 2, \ldots, N-1$, $U_i \subseteq V_i$ and $H_g = G_N \Pi \ldots \Pi G_2 (U_2) \Pi G_1 (U_1)$. The bipartite edge frustration of H_g is computed as follows:*

$$\varphi\left(H_g\right) = \sum_{i=2}^{N-1} \varphi\left(G_i\right) \left(\prod_{k=1}^{i-1} |U_k| \prod_{j=i+1}^{N} |V_j| \right) + \prod_{s=2}^{N} |V_s| \varphi\left(G_1\right) + \prod_{s=1}^{N-1} |U_s| \varphi\left(G_N\right).$$

Corollary 15.3.16 Let $G_i = (V_i, E_i)$ be N graphs and (nonempty) vertex subsets $U_i \subseteq V_i$, for $1 \leq i \leq N-1$. Then the following statements are equivalent:

1. For each $i = 1, 2, \ldots, N$, G_i is bipartite.
2. The graph $H = G_N \Pi \ldots \Pi G_2 \Pi G_1$ is bipartite.
3. The graph $H_g = G_N \Pi \ldots \Pi G_2 (U_2) \Pi G_1 (U_1)$ is bipartite.

15.4 The Bipartite Edge Frustration of Graphs Under Subdivided Edges and Their Related Sums

In this section, the bipartite edge frustration of two related graphs $S(G)$ and $R(G)$ are computed generally. We also investigate the $\varphi(Q(G))$ in the case that G is a tree or graph with disjoint cycles. A lot of sharp inequalitiesfor $\varphi(Q(G))$ together with a simple inequality for $\varphi(T(G))$ are also proved.

Lemma 15.4.1 *Let G be a graph, then*

1. $\varphi(S(G)) = 0$,
2. $\varphi(R(G)) = |E(G)|$.

Corollary 15.4.2 Let G be a connected graphs on n vertices, then

$$\varphi(R(T_n)) \leq \varphi(R(G)) \leq \varphi(R(K_n)),$$

where T_n is an arbitrary n-vertex tree.

Lemma 15.4.3 *Let G be a graph, then $\varphi(Q(G)) \geq \sum_{v \in V(G)} \varphi\left(K_{\delta(v)+1}\right)$.*

One can show that if G be a tree or a graph with disjoint cycles, then $\varphi(Q(G)) = \sum_{v \in V(G)} \varphi\left(K_{\delta(v)+1}\right)$..

A transformation of type A for a tree is defined as follows. Let T be a tree with n vertices. Choose a maximum path P_{m+1} in T of length, say m. Remove an end vertex of T (which is not in P_{m+1}) and connect a new vertex to one of the end vertices of P_{m+1} to obtain P_{m+2}. This new tree is denoted by T_1. In Fig. 15.10, this
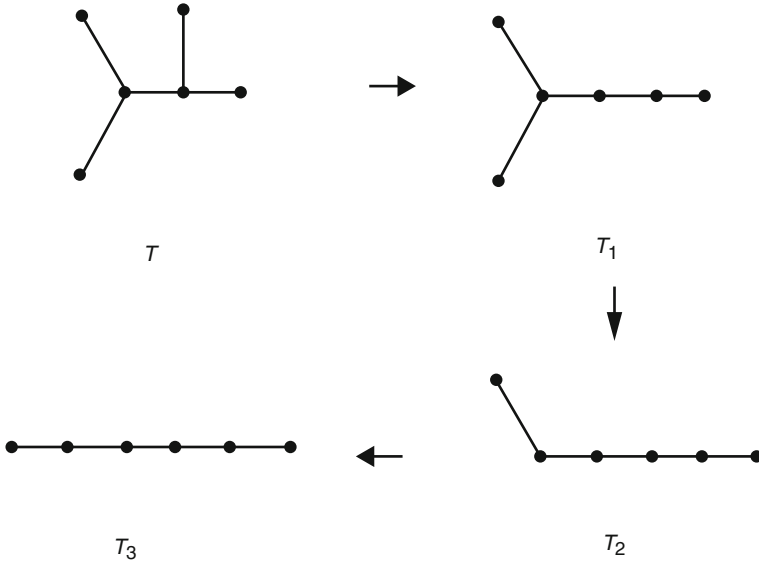
Fig. 15.10 Three transformations of type A for tree T

process is applied on T (three times) to obtain T_1, T_2 and T_3. Clearly, if T is a path then T_1 is equal to T. Notice that T_i's are not uniquely constructed.

We now define a transformation of type B for trees. To do this, we assume that T is a tree with n vertices. Suppose v is a vertex of maximum degree and $\delta_T(v) = \Delta(T)$. Omit an end vertex of T which is not adjacent to v and add a new vertex adjacent to this vertex. This new tree is denoted by T^1. It is obvious that $\delta_{T^1}(v) = \Delta(T) + 1$. Clearly, if T is a star then T^1 is isomorphic to T. In Fig. 15.11, this process is applied on T (three times) to obtain T^1, T^2 and T^3. Notice that T^i's are not uniquely constructed, but after finishing the process we will find a star of size $|V(T)|$.

By using these transformations, it is easy to show that, for a tree T,

$$\varphi(Q(T_1)) \leq \varphi(Q(T)) \leq \varphi\big(Q(T^1)\big),$$

where T_1 is a tree constructed from T transformation of type A and T^1 is a tree constructed from T transformation of type B. By using this result, one can see that

$$\cdots \leq \varphi(Q(T_i)) \leq \cdots \leq \varphi(Q(T_2)) \leq \varphi(Q(T_1)) \leq \varphi(Q(T))$$

and

$$\varphi(Q(T)) \leq \varphi\big(Q(T^1)\big) \leq \varphi\big(Q(T^2)\big) \leq \cdots \leq \varphi\big(Q(T^i)\big) \leq \cdots$$

By an inductive argument, one can see that there exists a positive integer m such that $T_m = P_n$ and there exists a positive integer k such that $T^k = S_n$. Therefore, this argument proved the following theorem.
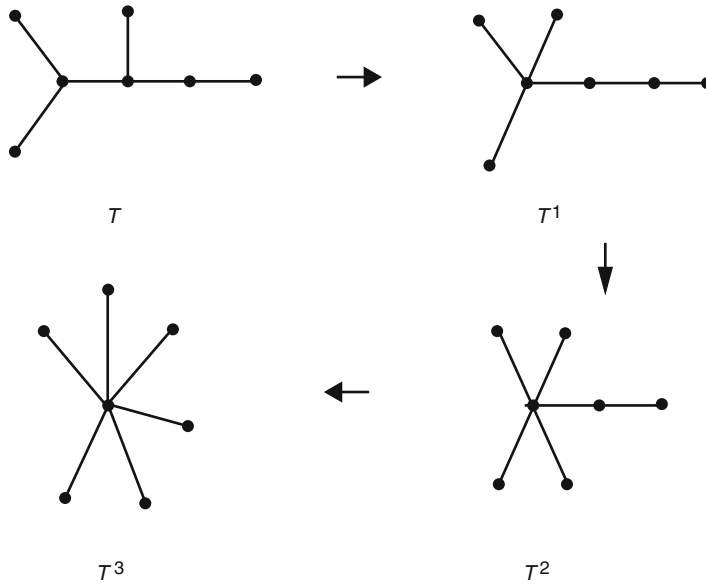
Fig. 15.11 Three transformations of type **B** for tree T

Theorem 15.4.4 *Let T be a tree on n vertices, then*

$$\varphi\left(Q(P_n)\right) \leq \varphi\left(Q(T)\right) \leq \varphi\left(Q(S_n)\right).$$

Hence it is clear that $\varphi(Q(P_n)) \leq \varphi(Q(T)) \leq \varphi(Q(K_n))$, and it is straightforward to prove that $\varphi(Q(G)) \leq \varphi(Q(T)) \leq \varphi(Q(G)) + |E(G)|$.

Theorem 15.4.5 *Let G and H be two graphs then*

$$\varphi(G + {}_F H) = |V(G)|\varphi(H) + |V(H)|\varphi(F(G)).$$

15.5 Results of the Nordhaus-Gaddum Type

A *Nordhaus-Gaddum*-type result is a lower or upper bound on the sum or product of an invariant of a graph and its complement. It is named after a paper (Nordhaus and Gaddum 1956) in which Nordhaus and Gaddum gave sharp bounds on the sum and product of the chromatic numbers of a graph and its complement. Since then such results were obtained for many other invariants. A trivial lower bound $\varphi(G) + \varphi(\overline{G}) \geq 1$ is valid for all graphs on more than five vertices. It follows from Ramsey's theorem, since at least one of G and $\overline{G}$ contains a triangle if G has at least six vertices.

We start with the following simple observation: Let G be a graph and e an edge not in $E(G)$. Then $\varphi(G + e) \le \varphi(G) + 1$. In other words, adding an edge to a graph cannot increase its bipartite edge frustration by more than one. By the same reasoning, one can establish that $\varphi(G + e_1 + \cdots + e_k) \le \varphi(G) + k$ for any choice $e_1, \ldots, e_k$ of edges not in $E(G)$.

Now we tackle the reverse problem: what happens to $\varphi(G)$ if we delete edges from G? It is intuitively clear that the answer depends on the density of edges in G; for graphs rich in edges, each edge removal will affect the value of $\varphi(G)$, while for graphs with few edges, the removal is less likely to have an effect.

Theorem 15.5.1 *Let $G = K_n - \{e_1, \ldots, e_l\}$.*

1. *If $l \le \left\lfloor \frac{n+1}{4} \right\rfloor$, then $\varphi(G) = \varphi(K_n) - l$.*
2. *If $l > \left\lfloor \frac{n+1}{4} \right\rfloor$, then $\varphi(K_n) - l \le \varphi(G) \le \varphi(K_n) - \left\lfloor \frac{n+1}{4} \right\rfloor$.*

Let   us   now   consider $G = K_n - \{e_1, \ldots, e_l\}$.   *Then*

$$\overline{G} = K_n - \left\{ e_{l+1}, \ldots, e_{\binom{n}{2}} \right\}.$$ *We can relabel the edges of $\overline{G}$ by subtracting*

1 from their labels, so that G can be written as $\overline{G} = K_n - \{e_1, \ldots, e_s\}.$, where

$s = \binom{n}{2} - l$. It is easy to see that at least one of the numbers l and s must exceed

the critical value $\left\lfloor \frac{n+1}{4} \right\rfloor$. Depending on whether the other one also exceeds it or not, we have three different situations. Two of them are symmetric, hence it suffices to consider only one of them. We look at the case $l \le \left\lfloor \frac{n+1}{4} \right\rfloor$ and $s > \left\lfloor \frac{n+1}{4} \right\rfloor$ first. By Theorem 10 it immediately follows that

$$\varphi(G) + \varphi(\overline{G}) \le 2\varphi(K_n) - \left\lfloor \frac{n+1}{4} \right\rfloor - |E(\overline{G})|.$$

Finally, when both $l, s > \left\lfloor \frac{n+1}{4} \right\rfloor$, we obtain

$$\varphi(G) + \varphi(\overline{G}) \le 2\varphi(K_n) - 2\left\lfloor \frac{n+1}{4} \right\rfloor.$$

In general case, when nothing is known on the value of $E(G)$, we have an upper bound equal to the worst case, i.e., to the maximum of the above three expressions. By plugging in the formula for $\varphi(K_n)$ and rearranging the terms, we obtain an upper bound valid for all graphs.

Theorem 15.5.2
$$\varphi(G) + \varphi(\overline{G}) \le 2\left\lfloor \frac{n-1}{2} \right\rfloor \left\lceil \frac{n-1}{2} \right\rceil - \left\lfloor \frac{n+1}{4} \right\rfloor$$
$$- \min\left\{ |E(G)|, |E(\overline{G})|, \left\lfloor \frac{n+1}{4} \right\rfloor \right\}.$$

For a bipartite graph $\varphi(G) + \varphi(\overline{G}) = \varphi(\overline{G})$. By combining this fact with the above results, we can determine the bipartite edge frustration of complements of some graphs with (relatively) few edges.

Example

1. Let T_n be a tree $n \geq 7$ vertices. Then $\varphi(\overline{T_n}) = \left\lfloor \frac{n-1}{2} \right\rfloor \left\lceil \frac{n-1}{2} \right\rceil - (n-1)$.
2. Let C_n be a tree $n \geq 10$ vertices. Then $\varphi(\overline{C_n}) = \left\lfloor \frac{n-1}{2} \right\rfloor \left\lceil \frac{n-1}{2} \right\rceil - n$.

It is tempting to think of $\varphi(\overline{G})$ as of a measure of bipartivity of a given bipartite graph G: the more frustration a bipartite graph leaves to its complement, the more bipartite it is. Based on this idea, we could say that the trees are the "most bipartite" among all connected graphs on the same number of vertices.

References

Ashrafi AR, Iranmanesh MA, Yarahmadi Z (2013) Topological modelling of nanostructures and extended systems. Springer, Dortrecht

Barriére L, Comellas F, Dafló C, Fiol MA (2009a) The hierarchical product of graphs. Discret Appl Math 157:36–48

Barriére L, Dafló C, Fiol MA, Mitjana M (2009b) The generalized hierarchical product of graphs. Discret Math 309:3871–3881

Bondy JA, Locke SC (1986) Largest bipartite subgraphs in triangle-free graphs with maximum degree three. J Graph Theory 10:477–504

Cui Q, Wang J (2009) Maximum bipartite subgraphs of cubic triangle-free planar graphs. Discret Math 309:1091–1111

Cvetković DM, Doob M, Sachs H (1980) Spectra of graphs– theory and application. Academic, New York

Došlić T (2005a) Bipartivity of fullerene graphs and fullerene stability. Chem Phys Lett 412:336–340

Došlić T (2005b) Splices, links, and their valence-weighted Wiener polynomials. Graph Theory Notes NY 48:47–55

Došlić T, Vukičević D (2007) Computing the bipartite edge frustration of fullerene graphs. Discrete Appl Math 155:1294–1301

Edwards CS (1973) Some extremal properties of bipartite subgraphs. Canad J Math 25:475–485

Eliasi M, Taeri B (2009) Four new sums of graphs and their Wiener indices. Discret Appl Math 157:794–803

Erdös P (1965) On some extremal problems in graph theory. Israel J Math 3:113–116

Fajtlowicz S, Larson CE (2003) Graph theoric independence as a predictor of fullerene stability. Chem Phys Lett 377:485–494

Ghojavand M, Ashrafi AR (2008) Computing the bipartite edge frustration of some nanotubes. Digest J Nanomater Bios 3:209–2014

Hopkins G, Staton W (1982) Extremal bipartite subgraphs of cubic triangle-free graphs. J Graph Theory 6:115–121

Imrich W, Klavžar S (2000) Product graphs, structure and recognition. Wiley, New York

Mansour T, Schork M (2009) The vertex PI and Szeged index of bridge and chain graphs. Discret Appl Math 157:1600–1606

Nordhaus EA, Gaddum JW (1956) On complementary graphs. Am Math Monthly 63:175–177

West DB (1996) Introduction to graph theory. Prentice-Hall, Upper Saddle River

Yan W, Yang B-Y, Yeh Y-N (2007) The behavior of Wiener indices and polynomials of graphs under five graph decorations. Appl Math Lett 20:290–295

Yarahmadi Z (2010) The bipartite edge frustration of extension of splice and link of graphs. Appl Math Lett 23:1077–1081

Yarahmadi Z, Ashrafi AR (2011a) Extremal graphs with respect to the bipartite vertex frustration. Appl Math Lett 24:1774–1777

Yarahmadi Z, Ashrafi AR (2011b) The bipartite edge frustration of graphs under subdivided edges and their related sums. Comput Math Appl 62:319–325

Yarahmadi Z, Ashrafi AR (2013) The bipartite vertex frustration of some infinite families of fullerenes. Fullerene Nanotube Carbon Nanostruct 21:129–133

Yarahmadi Z, Došlić T, Ashrafi AR (2010) The bipartite edge frustration of composite graphs. Discret Appl Math 158:1551–1558

Chapter 16
The Hosoya Index and the Merrifield–Simmons Index of Some Nanostructures

**Asma Hamzeh, Ali Iranmanesh, Samaneh Hossein–Zadeh,
and Mohammad Ali Hosseinzadeh**

Abstract The Hosoya index and the Merrifield–Simmons index are two types of graph invariants used in mathematical chemistry. In this chapter, we give ex act formulas for the Hosoya index and the Merrifield–Simmons index of bridge graph and as an application of these formulas, we obtain these indices for some nano structures.

16.1 Introduction

Let $G = (V, E)$ be a simple connected graph of order n and size m. Two distinct edges in a graph G are independent if they are not incident with a common vertex in G. A set of pairwise independent edges in G is called a matching. A $k-$matching of G is a set of k mutually independent edges. In theoretical chemistry molecular structure descriptors are used for modeling physico-chemical, phar-macologic, toxicologic, biological and other properties of chemical compounds. For detailed information on the chemical applications, we refer to (Bondy and Murty 1976; Chan et al. 1998; Gutman 1987; Gutman and Polansky 1986; Trinajstić 1992). The Hosoya index also known as the Z-index of a graph which is the total number of matchings in it and denoted by $Z(G)$. This graph invariant was introduced by Haruo Hosoya (Hosoya 1971). Let $m(G, k)$ be the number of its k-matchings and $m(G, 0) = 1$ for any graph G. Then $Z(G)$ is defined as follows:

A. Hamzeh • S. Hossein–Zadeh • M.A. Hosseinzadeh
Department of Mathematics, Faculty of Mathematical Sciences, Tarbiat Modares University, 14115–137, Tehran, Iran

A. Iranmanesh (✉)
Department of Pure Mathematics, Faculty of Mathematical Sciences, Tarbiat Modares University, 14115-137, Tehran, Iran
e-mail: iranmanesh@modares.ac.ir

$$Z(G) = \sum_{k=0}^{\lfloor \frac{n}{2} \rfloor} m(G, k).$$

Some papers related to this index can be found in (Hua 2008; Li and Zhu 2009; Wagner 2007; Xu 2010).

Two vertices of G are said to be independent if they are not adjacent in G. The Merrifield–Simmons index of G, denoted by $i(G)$, is defined as the number of subsets of the vertex set, in which any two vertices are non-adjacent, that is the number of independent vertex set of G (Prodinger and Tichy 1982). The Merrifield-Simmons index is one of the most popular topological indices in chemistry, which was extensively studied in a monograph (Merrifield and Simmons 1989). There have been many papers studied the Merrifield–Simmons index, for example see (Li et al. 2005; Lv and Yu 2006; Yu and Tian 2006; Yu and Lv 2007).

Fibonacci numbers are terms of the sequence defined in a quite simple recursive fashion. The Fibonacci numbers are defined as follows: $F_0 = 0$, $F_1 = 1$, and for $n \geq 2$, $F_n = F_{n-1} + F_{n-2}$.

Suppose G and H are two graphs with disjoint vertex sets. For given vertices $y \in V(G)$ and $z \in V(H)$ a link of G and H by vertices y and z is defined as the graph $(G \sim H)(y, z)$ obtained by joining y and z by an edge in the union of these graphs (Došlić 2005).

Let G_i, $1 \leq i \leq k$, be some graphs and $v_i \in V(G_i)$. A bridge graph denoted by $B = B(G_1, \ldots, G_k, v_1, \ldots, v_k)$ is obtained from the union of the graphs G_i, $i = 1, \ldots, k$, by adding the edges $v_i v_{i+1}$ $1 \leq i \leq k - 1$, see Fig. 16.1. Then

$$|V(G)| = \sum_{i=1}^{k} |V(G_i)| \text{ and } |E(G)| = (k - 1) + \sum_{i=1}^{k} |E(G_i)|.$$

It is obvious that $B(G_1, G_2, v_1, v_2) \cong (G_1 \sim G_2)(v_1, v_2)$.

It is worth noting that the above-specified class of bridge graph embraces, as special cases, all trees (among which are the molecular graphs of alkanes) and all unicyclic graphs (among which are the molecular graphs of monocycloalkanes). Also the molecular graphs of many polymers and dendrimers are bridge graph. Further, when all G_i are equal to G, the bridge graph becomes a rooted product of
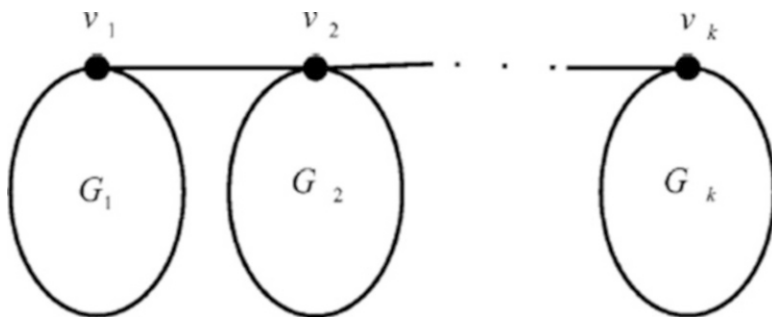
Fig. 16.1 The bridge graph $B = B(G_1, \ldots, G_k, v_1, \ldots, v_k)$

the path on k vertices and G, and if, in addition, all v_i are equal to v, we have the crown of P_k and G that is denoted by $G_k(G, v)$. Clearly, $G_1(G, v) = G$ for any vertex v of G (Hosseinzadeh et al. 2013). The notation we use is mostly standard and taken from standard graph theory textbooks such as (Bondy and Murty 1976).

Mansour and Schork (2009a, b, 2010), Xing and Zhou (2011) and Zhan and Qiao (2013) obtained formulas for Wiener, hyper–Wiener, detour, hyper–detour, vertex PI and Szeged indices of the bridge graph. In this chapter, we continue the above results about the obtaining exact formula of Hosoya and the Merrifield–Simmons indices of bridge graph, and as an application of these formulas, we obtain these indices for some nano structures.

16.1.1   The Hosoya Index of Bridge Graph

In this section, we give exact formulas for Hosoya index of bridge graph. At first, we state the following Lemma:

Lemma 16.2.1 (Gutman and Polansky 1986) Let $G = (V(G), E(G))$ be a graph. Then

1. If $G_1, G_2, \ldots, G_m$ are the components of the graph G, then $Z(G) = \prod_{i=1}^{m} Z(G_i)$.
2. If $e = xy \in E(G)$, then $Z(G) = Z(G - e) + Z(G - \{x, y\})$.
3. If $x \in V(G)$, then $Z(G) = Z(G - \{x\}) + \sum_{y \in N_G(x)} Z(G - \{x, y\})$.
4. $Z(P_n) = F_{n+1}$ for any $n > 0$; $Z(C_n) = F_{n-1} + F_{n+1}$ for any $n \geq 3$.

Theorem 16.2.2 Let $B = B(G_1, \ldots, G_k, v_1, \ldots, v_k)$ be a bridge graph. If k is an even number, then

(a) $$Z(B) = \sum_{0 \leq x_1 + x_2 + \cdots + x_k \leq k} \left[\frac{\prod_{i=1}^{k} Z(G_i)}{\prod_{1 \leq j \leq k} z(x_j) Z(G_j)} \prod_{r=1}^{k} z'(x_r) Z(G_r - v_r) \right],$$

and if k is an odd number, then

(b) $$Z(B) = \sum_{0 \leq x_1 + x_2 + \cdots + x_k \leq k-1} \left[\frac{\prod_{i=1}^{k} Z(G_i)}{\prod_{1 \leq j \leq k} z(x_j) Z(G_j)} \prod_{r=1}^{k} z'(x_r) Z(G_r - v_r) \right],$$

where x_i s can only have values 0 or 1 and should be established following conditions:

If k is an even(odd) number, then

(i) The number of elements x_i in this equation which are zero must be an even (odd) number.
(ii) If $x_i = 0$ is the last zero, then i should be even(odd).

(iii) If $x_i = 0$ and the first zero element after x_i is x_j, then i and j are not both odd or both even.

And also

$$z(x_j) = \begin{cases} 1 & x_j = 1 \\ \dfrac{1}{Z(G_j)} & x_j = 0 \end{cases},$$

$$z'(x_r) = \begin{cases} 1 & x_r = 1 \\ \dfrac{1}{Z(G_r - v_r)} & x_r = 0 \end{cases}.$$

Proof Use induction on k. By Lemma 16.2.1(ii), the result is valid for $k = 2$. Assume the theorem holds for numbers less than k. Let k be an even number. By Lemma 16.2.1(ii) and induction hypothesis, we have:

$$
\begin{aligned}
Z(B) &= Z(B - v_{k-1}v_k) + Z(B - \{v_{k-1}, v_k\}) \\
&= Z\Big(B(G_1, \ldots, G_{k-1}, v_1, \ldots, v_{k-1})\Big)Z(G_k) \\
&\quad + Z(G_k - v_k)Z(G_{k-1} - v_{k-1})Z\Big(B(G_1, \ldots, G_{k-2}, v_1, \ldots, v_{k-2})\Big) \\
&= \sum_{0 \le x_1 + x_2 + \cdots + x_{k-1} \le k-1} \left[\dfrac{\prod_{i=1}^{k-1} Z(G_i)}{\prod_{1 \le j \le k-1} z(x_j)Z(G_j)} \prod_{r=1}^{k-1} z'(x_r)Z(G_r - v_r) \right] \times Z(G_k) \\
&\quad + \sum_{0 \le x_1 + x_2 + \cdots + x_{k-2} \le k-2} \left[\dfrac{\prod_{i=1}^{k-2} Z(G_i)}{\prod_{1 \le j \le k-2} z(x_j)Z(G_j)} \prod_{r=1}^{k-2} z'(x_r)Z(G_r - v_r) \right] \\
&\quad \times Z(G_k - v_k)Z(G_{k-1} - v_{k-1}) \\
&= \sum_{0 \le x_1 + x_2 + \cdots + x_k \le k} \left[\dfrac{\prod_{i=1}^{k} Z(G_i)}{\prod_{1 \le j \le k} z(x_j)Z(G_j)} \prod_{r=1}^{k} z'(x_r)Z(G_r - v_r) \right].
\end{aligned}
$$

Proof of the odd case is similar.

Assume that in graph B, all G_i are equal to G.

Corollary 16.2.3 Let H be the rooted product of the path on k vertices and G. Then using the above symbols, the Hosoya index of H is as follows:

If k is an even number, then

$$Z(H) = \sum_{0 \le x_1 + x_2 + \cdots + x_k \le k} \left[\dfrac{Z(G)^k}{\prod_{1 \le j \le k} z(x_j)Z(G)} \prod_{r=1}^{k} z'(x_r)Z(G - v_r) \right],$$

and if k is an odd number, then

$$Z(H) = \sum_{0 \le x_1 + x_2 + \cdots + x_k \le k-1} \left[\frac{Z(G)^k}{\prod_{1 \le j \le k} z(x_j) Z(G)} \prod_{r=1}^{k} z'(x_r) Z(G - v_r) \right].$$

With the same conditions for x_i as above theorem.

Corollary 16.2.4 The Hosoya index of $G_k(G, v)$ is as follows:

$$Z\Big(G_k(G, v)\Big) = \begin{cases} \sum_{j=0}^{k} h_j Z(G - v)^{k-j} Z(G)^j & k \text{ and } j \text{ are even} \\ \sum_{j=1}^{k} h_j Z(G - v)^{k-j} Z(G)^j & k \text{ and } j \text{ are odd.} \end{cases}$$

where in equation $x_1 + x_2 + \cdots + x_k = k - j$, x_i s can only have values 0 or 1 and h_j is the number of solutions of the above equation by considering the following conditions:

If k is an even(odd) number, then

1. The number of elements x_i in this equation which are zero must be an even(odd) number.
2. If $x_i = 0$ is the last zero, then i should be even(odd).
3. If $x_i = 0$ and the first zero element after x_i is x_j, then i and j are not both odd or both even.

Above corollary was also given in (Gutman et al. 1989a)

Let P_n be the path graph on n vertices $v_1, \ldots, v_n$ and $A_{k,n} = G_k(P_n, v_1)$, see Fig. 16.2 for $n = 3$. Clearly, $A_{k,1} = P_k$ as well as $A_{1,n} = P_n$.
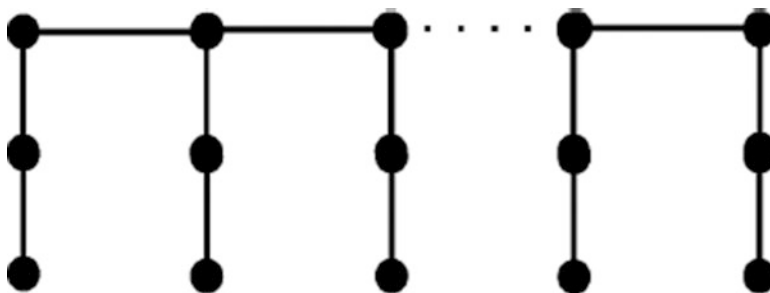
Fig. 16.2 The graph $A_{k,3}$

Corollary 16.2.5 By Lemmas 16.2.1 and Corollary 16.2.4, we have:

$$Z(A_{k,n}) = \begin{cases} \displaystyle\sum_{j=0}^{k} h_j F_n^{k-j} F_{n+1}^{j} & k \text{ and } j \text{ are even} \\ \displaystyle\sum_{j=1}^{k} h_j F_n^{k-j} F_{n+1}^{j} & k \text{ and } j \text{ are odd,} \end{cases}$$

where h_j is defined in the Corollary 16.2.4.

Above corollary was also given in (Gutman et al. 1989a)

By above corollary, we have $Z(A_{1,n}) = Z(P_n) = F_{n+1}$.

As another example, let us consider a graph which is not a tree. Let C_n be the cycle with n vertices and define $T_{k,n} = G_k(C_n, v_1)$, see Fig. 16.3 when $n = 6$.

Corollary 16.2.6 The Hosoya index of $T_{k,n}$ is given by

$$Z(T_{k,n}) = \begin{cases} \displaystyle\sum_{j=0}^{k} h_j F_n^{k-j} (F_{n-1} + F_{n+1})^{j} & k \text{ and } j \text{ are even} \\ \displaystyle\sum_{j=1}^{k} h_j F_n^{k-j} (F_{n-1} + F_{n+1})^{j} & k \text{ and } j \text{ are odd,} \end{cases}$$

where h_j is defined in the Corollary 16.2.4.

Example 16.2.7 The Hosoya index of $T_{n,6}$ is given by

$$Z(T_{n,6}) = \begin{cases} \displaystyle\sum_{j=0}^{k} h_j F_6^{n-j} (F_5 + F_7)^{j} & k \text{ and } j \text{ are even} \\ \displaystyle\sum_{j=1}^{k} h_j F_6^{n-j} (F_5 + F_7)^{j} & k \text{ and } j \text{ are odd.} \end{cases}$$

By above corollary, we have $Z(T_{1,n}) = Z(C_n) = F_{n-1} + F_{n+1}$.

Relations for the Hosoya index of the benzenoid systems from Fig 16.4. is computed in (Gutman et al. 1989b).

Example 16.2.8 (Gutman et al. 1989b)

$Z(L_n) = 9\,Z(L_{n-1}) - 7\,Z(L_{n-2}) + Z(L_{n-3})$;	$n \geq 3$
$Z(A_n) = 9\,Z(A_{n-1}) - 5\,Z(A_{n-2}) - 5\,Z(A_{n-3}) + Z(A_{n-4})$;	$n \geq 4$
$Z(H_n) = 6\,Z(H_{n-1}) + 19\,Z(H_{n-2}) + 2\,Z(H_{n-3}) - Z(H_{n-4})$;	$n \geq 4$
$Z(Q_n) = 226\,Z(Q_{n-1}) - 892\,Z(Q_{n-2}) + 104\,Z(Q_{n-3})$;	$n \geq 3$ where $Q = R$ or P
$Z(B_n) = 34\,Z(B_{n-1}) - 165\,Z(B_{n-2}) + 190\,Z(B_{n-3}) + 153\,Z(B_{n-4}) - 278\,Z(B_{n-5})$	$n \geq 8$
$-11\,Z(B_{n-6}) + 72\,Z(B_{n-7}) - 10\,Z(B_{n-8})$	
$Z(C_n) = 29\,Z(C_{n-1}) - 54\,Z(C_{n-2}) + 242\,Z(C_{n-3}) + 436\,Z(C_{n-4}) - 98\,Z(C_{n-5}) -$	$n \geq 8$
$54\,Z(C_{n-6}) + 17\,Z(C_{n-7}) - Z(C_{n-8})$	
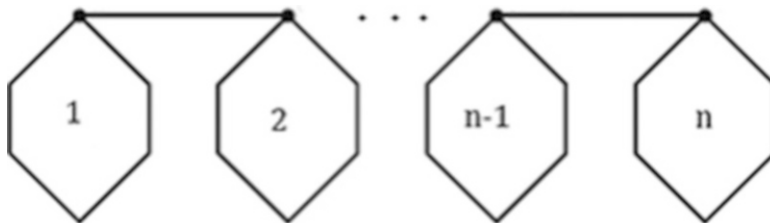
Fig. 16.3 The graph $T_{n,6}$
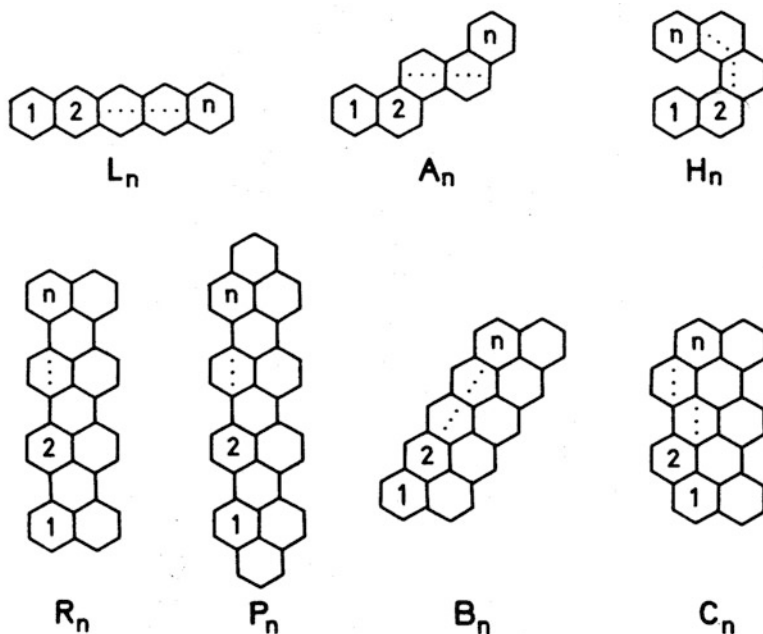
Fig. 16.4 Benzenoid systems

Relation for computing Hosoya index of an infinite family of dendrimers is computed in (Xu 2011).

They have shown structure of dendrimer $D[n]$ in Fig. 16.5, for $n = 1,2,3$, where n denotes the step of growth in this type of dendrimer.

Let T_n be the binary tree whose step of growth is equal to n (see Fig. 16.6).

Theorem 16.2.9 (Xu 2011) $Z(T_n) = Z(T_{n-1})^2 + 2Z(T_{n-2}) \, Z(T_{n-1})$, where $Z(T_0) = 1$ and $Z(T_1) = 3$.

Theorem 16.2.10 (Xu 2011) $Z(D[n]) = Z(T_{n-1})^4 + 4Z(T_{n-2})^2 Z(T_{n-1})^3$, where $Z(D[1]) = 5$.
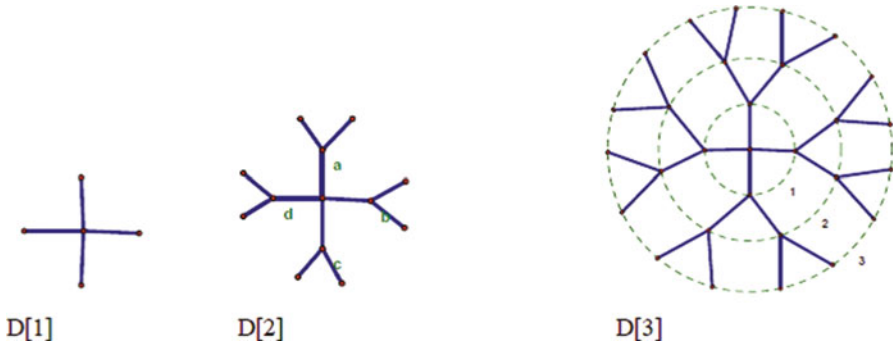
Fig. 16.5 Dendrimer $D[n]$ for $n = 1,2,3$
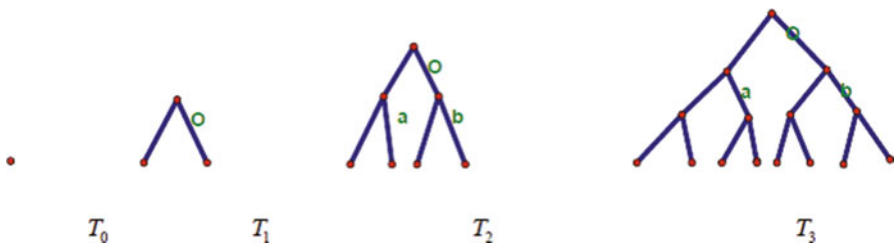
Fig. 16.6 The tree T_n

16.1.2 The Merrifield–Simmons Index of Bridge Graph

In order to compute the Merrifield–Simmons index of bridge graph, we need the following lemma:

Lemma 16.3.1 (Gutman and Polansky 1986) Let $G = (V(G), E(G))$ be a graph. Then

1. If $G_1, G_2, \ldots, G_m$ are the components of the graph G, then $i(G) = \prod_{k=1}^{m} i(G_k)$.
2. If $e = xy \in E(G)$, then $i(G) = i(G - e) - i(G - \{N_G[x] \cup N_G[y]\})$.
3. If $x \in V(G)$, then $i(G) = i(G - \{x\}) + i(G - N_G[x])$.
4. $i(P_n) = F_{n+2}$ for any $n > 0$; $i(C_n) = F_{n-1} + F_{n+1}$ for any $n \geq 3$.

The following theorem can be proved as the similar of proof of the Theorem 16.2.2.

Theorem 16.3.2 Let $B = B(G_1, \ldots, G_k, v_1, \ldots, v_k)$ be a bridge graph. If k is an even number, then

(a) $i(B) = \displaystyle\sum_{0 \leq x_1 + x_2 + \cdots + x_k \leq k} (-1)^{\frac{n}{2}} \left[\dfrac{\prod_{i=1}^{k} i(G_i)}{\prod_{1 \leq j \leq k} I(x_j) i(G_j)} \prod_{r=1}^{k} I'(x_r) \times i(G_r - N_{G_r}[v_r]) \right],$

and if k is an odd number, then

$$(b)\ i(B) = \sum_{0 \le x_1+x_2+\cdots+x_k \le k-1} (-1)^{\frac{n}{2}} \left[\frac{\prod_{i=1}^{k} i(G_i)}{\prod_{1 \le j \le k} I(x_j)i(G_j)} \prod_{r=1}^{k} I'(x_r) \times i(G_r - N_{G_r}[v_r]) \right],$$

where x_i s can only have values 0 or 1 and n is the number of $x_i = 1$ in equations $0 \le x_1 + x_2 + \cdots + x_k \le k$ and $0 \le x_1 + x_2 + \cdots + x_k \le k - 1$, and

$$I(x_j) = \begin{cases} 1 & x_j = 1 \\ \dfrac{1}{i(G_j)} & x_j = 0 \end{cases},$$

$$I'(x_r) = \begin{cases} 1 & x_r = 1 \\ \dfrac{1}{i(G_r - N_{G_r}[v_r])} & x_r = 0 \end{cases}.$$

Also in equations $0 \le x_1 + x_2 + \cdots + x_k \le k$ and $0 \le x_1 + x_2 + \cdots + x_k \le k - 1$, should be established Theorem 16.2.2 conditions.

Corollary 16.3.3 Let H be the rooted product of the path on k vertices and G. Then using the above theorem symbols, the Merrifield–Simmons index of H is as follows:
If k is an even number, then

$$i(H) = \sum_{0 \le x_1+x_2+\cdots+x_k \le k} (-1)^{\frac{n}{2}} \left[\frac{i(G)^k}{\prod_{1 \le j \le k} \left(I(x_j)i(G) \right)} \prod_{r=1}^{k} I'(x_r) \times i(G - N_G[v_r]) \right],$$

and if k is an odd number, then

$$i(H) = \sum_{0 \le x_1+x_2+\cdots+x_k \le k-1} (-1)^{\frac{n}{2}} \left[\frac{i(G)^k}{\prod_{1 \le j \le k} \left(I(x_j)i(G) \right)} \prod_{r=1}^{k} I'(x_r) \times i(G - N_G[v_r]) \right],$$

where x_i s can only have values 0 or 1 and n is the number of $x_i = 1$ in equations $0 \le x_1 + x_2 + \cdots + x_k \le k$ and $0 \le x_1 + x_2 + \cdots + x_k \le k - 1$, and in these equations, should be established Theorem 16.3.2 conditions.

Corollary 16.3.4 The Merrifield–Simmons index of $G_k(G, v)$ is as follows:

$$i\left(G_k(G, v) \right) = \begin{cases} \sum_{j=0}^{k} (-1)^{\frac{k-j}{2}} h_j i(G - N_G[v])^{k-j} i(G)^j & k \text{ and } j \text{ are even} \\[2mm] \sum_{j=1}^{k} (-1)^{\frac{k-j}{2}} h_j i(G - N_G[v])^{k-j} i(G)^j & k \text{ and } j \text{ are odd}. \end{cases}$$

where x_i s can only have values 0 or 1 in equation $x_1 + x_2 + \cdots + x_k = k - j$, and h_j is the number of solutions of the above equation by considering the following conditions:

If k is an even(odd) number, then

1. The number of elements x_i in this equation which are zero must be an even(odd) number.
2. If $x_i = 0$ is the last zero, then i should be even(odd).
3. If $x_i = 0$ and the first zero element after x_i is x_j, then i and j are not both odd or both even.

Corollary 16.3.5 By Lemmas 16.3.1 and Corollary 16.3.4, we have:

$$
i(A_{k,n}) = \begin{cases}
\displaystyle\sum_{j=0}^{k} (-1)^{\frac{k-j}{2}} h_j F_{n+1}^{k-j} F_{n+2}^{j} & k \text{ and } j \text{ are even} \\[3mm]
\displaystyle\sum_{j=1}^{k} (-1)^{\frac{k-j}{2}} h_j F_{n+1}^{k-j} F_{n+2}^{j} & k \text{ and } j \text{ are odd,}
\end{cases}
$$

where h_j is defined in the Corollary 16.3.4.

By above corollary, we have $i(A_{1,n}) = i(P_n) = F_{n+2}$.

Corollary 16.3.6 The Merrifield–Simmons index of $T_{k,n}$ is given by

$$
i(T_{k,n}) = \begin{cases}
\displaystyle\sum_{j=0}^{k} (-1)^{\frac{k-j}{2}} h_j F_{n+1}^{k-j} (F_{n-1} + F_{n+1})^{j} & k \text{ and } j \text{ are even} \\[3mm]
\displaystyle\sum_{j=1}^{k} (-1)^{\frac{k-j}{2}} h_j F_{n+1}^{k-j} (F_{n-1} + F_{n+1})^{j} & k \text{ and } j \text{ are odd,}
\end{cases}
$$

where h_j is defined in the Corollary 16.3.4.

Example 16.3.7 The Hosoya index of $T_{n,6}$ is given by

$$
i(T_{n,6}) = \begin{cases}
\displaystyle\sum_{j=0}^{k} (-1)^{\frac{n-j}{2}} h_j F_{6}^{n-j} (F_5 + F_7)^{j} & n \text{ and } j \text{ are even} \\[3mm]
\displaystyle\sum_{j=1}^{k} (-1)^{\frac{n-j}{2}} h_j F_{6}^{n-j} (F_5 + F_7)^{j} & n \text{ and } j \text{ are odd.}
\end{cases}
$$

By above corollary, we have $i(T_{1,n}) = i(C_n) = F_{n-1} + F_{n+1}$.

Theorem 16.3.8 (Ahmadi and Seif 2010) The Merrifield–Simmons index of T_n, is $i(T_n) = i(T_{n-1})^2 + i(T_{n-2})^4$, for $n \geq 2$ where $i(T_0) = 2$ and $i(T_1) = 5$.

Theorem 16.3.9 (Ahmadi and Seif 2010) For $n = 1$, $i(D[n]) = 17$ and for $n \geq 2$, $i(D[n]) = i(T_{n-1})^4 + i(T_{n-2})^8$.

References

Ahmadi MB, Seif M (2010) The Merrifield–Simmons index of an infinite class of dendrimers. Digest J Nano mater Bios 5:335–338

Bondy JA, Murty USR (1976) Graph theory with applications. Macmillan Press, New York

Chan O, Gutman I, Lam TK, Merris R (1998) Algebraic connections between topological indices. J Chem Inform Comput Sci 38:62–65

Došlić T (2005) Splices, links, and their degree–weighted Wiener polynomials. Graph Theory Notes NY 48:47–55

Gutman I (1987) Acyclic conjugated molecules, trees and their energies. J Math Chem 29:123–143

Gutman I, Polansky OE (1986) Mathematical concepts in organic chemistry. Springer, Berlin

Gutman I, Kolavi N, Cyvin SJ (1989a) Hosoya index of some polymers. MATCH Commun Math Comput Chem 24:105–117

Gutman I, Kolaković N, Graovac A, Babić D (1989b) A method for calculation of the Hosoya index of polymers. In: Graovac A (ed) MATH/CHEM/COMP 1988, vol 63. Elsevier, Amesterdam, The Netherlands, p 141–154

Hosoya H (1971) Topological index, a newly proposed quantity characterizing the topological nature of structural isomers of saturated hydrocarbons. Bull Chem Soc Jpn 44:2332–2339

Hosseinzadeh MA, Iranmanesh A, Došlić T (2013) On the Narumi–Katayama index of composite graphs. Croat Chem Acta 86:503–508

Hua H (2008) Hosoya index of unicyclic graphs with prescribed pendent vertices. J Math Chem 43:831–844

Li S, Zhu Z (2009) The number of independent sets in unicyclic graphs with a given diameter. Discret Appl Math 157:1387–1395

Li X, Zhao H, Gutman I (2005) On the Merrifield–Simmons index of trees. MATCH Commun Math Comput Chem 54:389–402

Lv X, Yu A (2006) The Merrifield–Simmons indices and Hosoya indices of trees with a given maximum degree. MATCH Commun Math Comput Chem 56:605–616

Mansour T, Schork M (2009a) The vertex PI index and Szeged index of bridge graphs. Discret Appl Math 157:1600–1606

Mansour T, Schork M (2009b) The PI index of bridge and chain graphs. MATCH Commun Math Comput Chem 61:723–734

Mansour T, Schork M (2010) Wiener, hyper–Wiener, detour and hyper–detour indices of bridge and chain graphs. J Math Chem 47:72–98

Merrifield RE, Simmons HE (1989) Topological methods in chemistry. Wiley, New York

Prodinger H, Tichy RF (1982) Fibonacci numbers of graphs. Fibonacci Quart 20:16–21

Trinajstić N (1992) Chemical graph theory. CRC press, Boca Raton

Wagner SG (2007) Extremal trees with respect to Hosoya index and Merrifield–Simmons index. MATCH Commun Math Comput Chem 57:221–233

Xing R, Zhou B (2011) On the edge Szeged index of bridge graphs. Comptes Rendus Mathematique 349:489–492

Xu K (2010) On the Hosoya index and the Merrifield–Simmons index of graphs with a given clique number. Appl Math Lett 23:395–398

Xu K (2011) Computin the Hosoya index and the Wiener index of an infinite class of dendrimers. Digest J Nanomater Bios 6:265–270

Yu A, Lv X (2007) The Merrifield–Simmons indices and Hosoya indices of trees with k pendent vertices. J Math Chem 41:33–43

Yu A, Tian F (2006) A kind of graphs with minimal Hosoya indices and maximal Merrifield–Simmons indices. MATCH Commun Math Comput Chem 55:103–118

Zhan F, QiaoY (2013) On edge Szeged index of bridge graphs. Inf Manag Sci III Lect Notes Electri Eng 206:167–172

Chapter 17
Topological Indices of 3-Generalized Fullerenes

Z. Mehranian and A.R. Ashrafi

Abstract A molecular graph G is said to be three connected if there does not exist a two-element set of vertices whose removal disconnects the graph. A three-connected cubic planar graph $G = (V;E)$ is called m-generalized fullerene if it has two m-gons and all other faces are pentagons and hexagons. The aim of this chapter is to compute some distance topology of eight infinite sequences of 3-generalized fullerene.

17.1 Introduction

A *molecular graph* is a pair of a nonempty sets V and a set E, not necessarily nonempty, in which V is the set of all atoms of a molecule M and E is a subset of all two-element subsets of V such that the atoms x and y are adjacent if and only if there exists a chemical bond between them. We know that a given molecule M can be constituted from the same atoms. For example, some molecules are constructed entirely from carbon atoms, but in its molecular graphs, they are assumed to be different. In mathematics, it is usual to call V and E as the set of vertices and edges, respectively. Balaban, the pioneer of *Chemical Graph Theory*, discovered several applications of this concept in solving some problems in chemistry (Balaban 1973, 1980, 1982).

Suppose F is a *3D* picture. A function $\beta: R^3 \longrightarrow R^3$ is called a *symmetry* for F, if $\beta(F) = F$. In chemistry, symmetry elements are usually assumed to be *isometry*.

Z. Mehranian
Department of Mathematics, University of Qom, Qom, Iran

A.R. Ashrafi (✉)
Department of Nanocomputing, Institute of Nanoscience and Nanotechnology, University of Kashan, Kashan 87317-53153, Iran

Department of Pure Mathematics, Faculty of Mathematical Sciences, University of Kashan, Kashan 87317-53153, Iran
e-mail: ashrafi@kashanu.ac.ir

This means that $d(x,y) = d(\beta(x), \beta(y))$, for all atoms x and y. It is well known that the set of all symmetries of a molecule is a *group* under composition of functions. Here, a group is a nonempty set G equipped with an operation $\square: G \times G \to G$ such that:

  (i) For every element a, b, and c of G, $a \square (b \square c) = (a \square b) \square c$
 (ii) There exists an element $e \in G$ such that for all $a \in G$, $a \square e = e \square a = a$
(iii) For every element $a \in G$, there exists an element b such that $a \square b = b \square a = e$

A subset S in a group G is called a generating set for G, if each element $g \in G$ can be written as a product of some elements in $S \cup S^{-1}$, where $S^{-1} = \{x^{-1} \mid x \in G\}$. Suppose Γ is the molecular graph of a molecule M. A one-to-one mapping β from Γ onto Γ is called a topological symmetry of M, if β and β^{-1} preserve the adjacencies. The set of all such mapping is denoted by $Sym(\Gamma)$ or $Sym(M)$. One can see that $Sym(M)$ has a group structure under composition. This group is called the topological symmetry group (symmetry group for short) of the molecule M.

A molecular graph G is said to be three connected if there does not exist a two-element set of vertices whose removal disconnects the graph. Fullerenes are polyhedral carbon molecules that can be modeled by planar three-connected cubic graphs whose faces are pentagons and hexagons. The molecular graph of a fullerene molecule is called a *fullerene graph*. In (Kroto et al. 1985), Kroto and his team discovered the existence of buckminsterfullerene C_{60}. After this discovery that resulted in the Nobel Prize for Kroto in 1996, several researchers devoted their time to study the mathematical behavior of this new form of matter. We encourage the interested readers to consult *Atlas of Fullerenes*, the famous book of Fowler and Manolopoulos (Fowler and Manolopoulos 1995), for more information on this topic.

Behmaram in his PhD thesis (Behmaram 2013) extended the definition of fullerene graph to m-generalized fullerene graphs. Following his work, a three-connected cubic planar graph G is called an *m-generalized fullerene* if its faces are two m-gons and all other pentagons and hexagons. Note that if $m = 5$ or 6, then an m-generalized fullerene graph will be ordinary fullerenes. Similar to fullerene graphs, by applying Euler formula, one can easily prove that the number of pentagons in m-generalized fullerene is $2m$, while the number of hexagons is not determined. The smallest m-generalized fullerene has $4m$ vertices. So, for $m \neq 6$, an m-generalized fullerene has exactly two m-gons and $2m$ pentagons. It is easy to construct an m-generalized fullerene with mk hexagons, when $k \geq 0$ is an integer. He also conjectured that there exists K such that for each $k \geq K$, there exists an m-generalized fullerene. Finally, Behmaram gave lower and upper bounds for the number of perfect matchings in m-generalized fullerenes. We refer to (Deza et al. 2004) for some other generalization of fullerenes. In the mentioned paper, Deza and his coworkers established some deep results on connections between fullerene structures and alternating knots.

Suppose G and H are graphs and Y is the class of all graphs. A mapping η: $G \longrightarrow H$ is called an *isomorphism* if η and its inverse preserve adjacency of vertices. If $G = H$ then η is said to be *automorphism*. A function f: $Y \longrightarrow R^{\geq 0}$ is called a *graph invariant*, if isomorphism $H \cong G$ implies that $f(H) = f(G)$. A *topological index* is a graph invariant applicable in chemistry. The number of edges and vertices of a graph G are simplest topological indices of G.

Many topological indices based on distances in a graph have been used to estimate molecular structure properties. The Wiener, *PI*, vertex *PI*, Szeged, edge Szeged, revised Szeged, and edge revised Szeged indices are the most important distance-based graph invariants with several applications in correlating some physicochemical properties of alkanes, cycloalkanes, and benzenoid systems. To define these topological indices, we need some notation. Suppose x and y are vertices and $e = uv$ and $f = ab$ are edges of a graph G. The length of a shortest path connecting x and y is denoted by $d_G(x,y)$. By definition, the function d_G is a meter on $V(G)$ and the pair $(V(G), d_G)$ is a metric space. We also define $D_G(x,e)$ to be the minimum values of $d_G(x,u)$ and $d_G(x,v)$. The number of vertices and edges closer to u than v are denoted by $n_e(e)$ and $m_u(e)$, respectively. The quantities $n_v(e)$ and $m_v(e)$ can be defined in a similar way. The number of edges that are equidistant from end vertices of e is denoted by $m_0(e)$.

The Wiener index is the first distance-based topological index that was introduced by American chemist Harold Wiener in 1947 (Wiener 1947). He observed that there is a direct relationship between the boiling point and a quantity that he named *path number* for paraffins. The path number (or nowadays *Wiener index*) of a graph G is defined as the sum of all distances between pair of vertices of the graph G. The *vertex Szeged index* of G, $Sz_v(G)$, was introduced by Ivan Gutman in 1994 as a generalization of the Wiener index to cyclic graphs (Gutman 1994). It was defined as $Sz_v(G) = \Sigma_{e=uv}[n_u(e) \times n_v(e)]$. The *edge Padmakar-Ivan index* (PI_e index for short) is a Szeged-like topological index that was introduced by Padmakar Khadikar in Khadikar et al. (2001). It is defined as $PI_e(G) = \Sigma_{e=uv}[m_u(e) + m_v(e)]$. The *edge Szeged index* and *vertex PI index* are edge and vertex variants of these topological indices, respectively. These are defined as:

$$Sz_e(G) = \Sigma_{e=uv}[m_u(e) \times m_v(e)] \text{ and } PI_v(G) = \Sigma_{e=uv}[n_u(e) + n_v(e)].$$

These topological indices were introduced in (Gutman and Ashrafi 2008) and (Khalifeh et al. 2008), respectively. The revised Szeged index, Sz^*, was introduced by Milan Randić as summation of all quantities in the form

$$[n_u(e) + n_0(e)/2] \times [n_v(e) + n_0(e)/2],$$

overall edges of the graph (Randić 2011). Finally, the edge revised Szeged index, Sz_e^*, was introduced by one of the present authors (ARA) as an edge variant of the revised Szeged and in a similar way (Faghani and Ashrafi 2014).

Throughout this chapter our notation is standard and can be taken from the standard book on graph theory. We encourage the interested readers to consult two books (Cataldo et al. 2011; Ashrafi et al. 2013) for more information on mathematical properties of fullerene graphs. In the papers (Myrvold et al. 2007; Schwerdtfeger et al. 2013) two important packages for working by fullerenes are presented which are important in our calculations. Finally, we continue our works on fullerenes presented in (Ashrafi et al. 2008, 2009; Ashrafi and Sabaghian−Bidgoli 2009; Koorepazan−Moftakhar and Ashrafi 2013; Koorepazan−Moftakhar et al. 2014; Ashrafi and Mehranian 2013).

17.2   Topology of *3*-Generalized Fullerenes

In this section, the exact values of some topological indices for eight infinite sequences $H_1[n] = C_{6n+6}$, $H_2[n] = C_{12n+12}$, $H_3[n] = C_{16n+18}$, $H_4[n] = C_{12n+40}$, $H_5[n] = C_{16n+14}$, $H_6[n] = C_{12n+20}$, $H_7[n] = C_{12n+26}$, and $H_8[n] = C_{10n+40}$ are computed. By our discussion given Sect. 17.1, these fullerenes have exactly two triangles, six pentagons, and $n/2 - 6$ hexagons Figs 17.1 and 17.2.

We note that in the process of computing a topological index T of generalized fullerenes, there are usually some exceptional cases and for large n, it is possible to find a polynomial of small degree to evaluate T. We start by three generalized fullerene $H_1[n]$. Clearly $H_1[n]$ has exactly $3n - 3$ hexagons. In Table 17.1, three exceptional cases in computing *PI*, edge Szeged, and revised edge Szeged indices of H_1 are recorded. So, it is enough to assume that $n \geq 4$. We first draw the molecular graph of $H_1[n]$, for some values of n, by HyperChem

Fig. 17.1 The *2D* perception of the three generalized fullerene $H_1[n]$
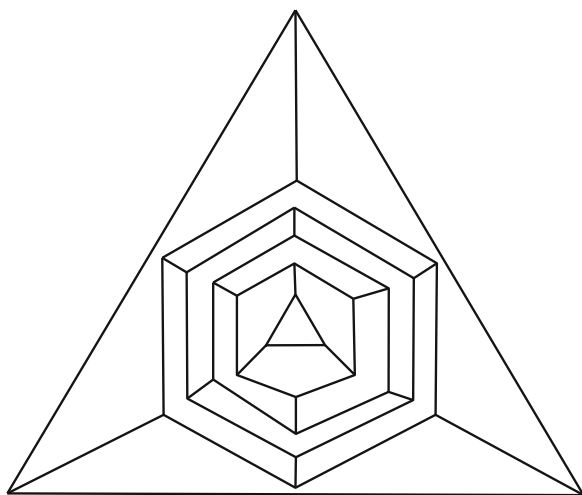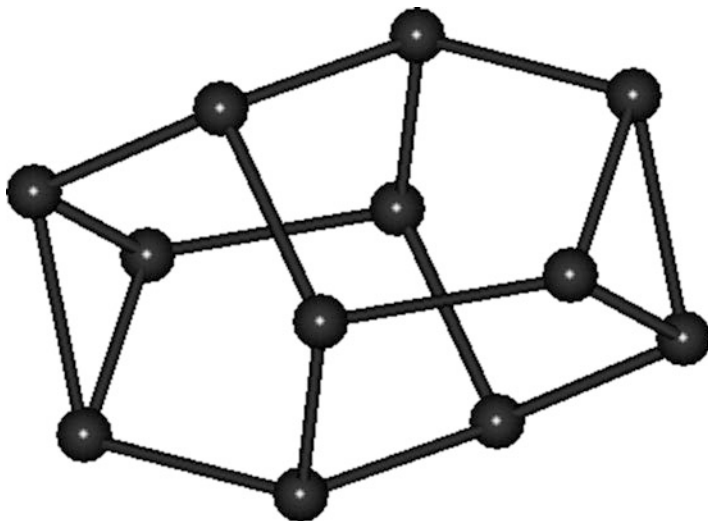
Fig. 17.2 The *3D* perception of $H_1[1]$

Table 17.1 The *PI*, edge Szeged, and revised edge Szeged indices of $H_1[n]$, $1 \leq n \leq 3$

N	1	2	3
$PI(H_1[n])$	228	–	–
$Sz_e(H_1[n])$	714	2670	6126
$Sz_e*(H_1[n])$	1434	18477/4	20907/2

(HyperChem package Release 7.5 for Windows 2002). Then we apply TopoCluj package (Diudea et al. 2002) to compute the adjacency and distance matrices of the constructed molecular graphs. Finally, by some GAP programs (The GAP Team 1995) and MAGMA codes (Bosma et al. 1997), these topological indices are computed.

In Fig. 17.3, six different types for edges of the generalized fullerene $H_1[4] = C_{30}$ are depicted, and in Table 17.2, our observations on quantities $m_u(e)$, $m_v(e)$, and $m_0(e)$ are recorded. These values are examined by some computer programs in GAP and MAGMA. These calculations suggest the following conjecture:

Conjecture 17.1 $PI(H_1[n]) = 81n^2 + 39n + 156$ $(n \geq 2)$; $Sz_e(H_1[n]) = (243/2)n^3 + 54n^2 + (1947/2)n - 585$ $(n \geq 4)$; and $Sz_e^*(H_1[n]) = (243/2)n^3 + 486n^2 + (4671/4)n - (2865/4)$ $(n \geq 4)$.

We now consider our second series of three generalized fullerenes, $H_2[n]$; see Figs. 17.3, 17.4 and 17.5. The general term of this series of three generalized fullerenes has exactly $12n + 12$ carbon atoms. In Table 17.3, the quantities PI_v, PI_e, Sz_v, Sz_e, Sz^*, and Sz_e^* for $H_2[n]$, $1 \leq n \leq 10$, are recorded. These are
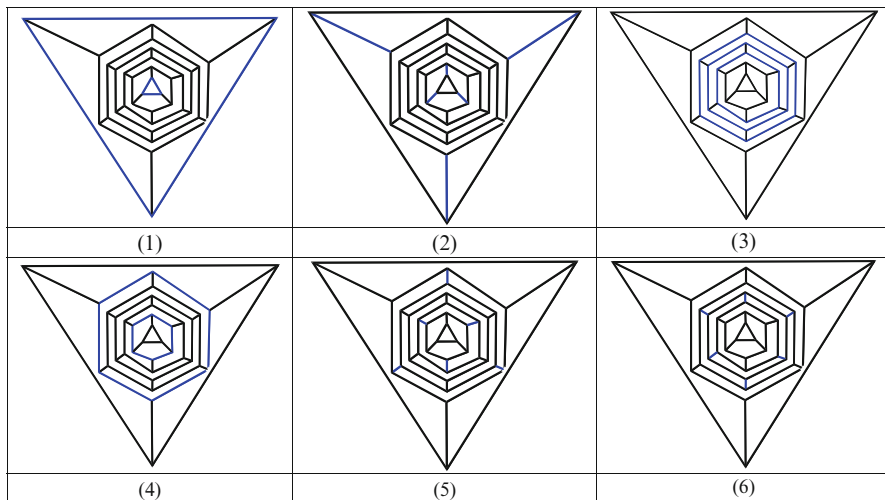
Fig. 17.3 Six types of edges in $H_1[4]$

Table 17.2 The quantities $m_u(e)$, $m_v(e)$, and $m_0(e)$ for different types of edges of $H_1[n]$, $n \geq 4$

$m_u(e)$, $m_v(e)$, and $m_0(e)$	Number of edges
$7, 7, 9n - 5$	6
$5, 9n, 4$	6
$9, 9n - 7, 7$	12
$12, 9n - 6, 3$	6
$15, 9n - 14, 8$	12
$21, 9n - 15, 3, n \geq 5$	6
$22, 9n - 23, 10, n \geq 6$	12
$30, 9n - 24, 3, n \geq 7$	6
$31, 9n - 32, 10, n \geq 8$	12
$\vdots$	$\vdots$
$\begin{cases} \frac{9}{2}n + 3, \frac{9}{2}n + 3, 3 & n \text{ is even} \\ \frac{9}{2}n - \frac{1}{2}, \frac{9}{2}n - \frac{1}{2}, 10 & n \text{ is odd} \end{cases}$	$\begin{cases} 3 \\ 6 \end{cases}$

exceptional cases that usually arise in computing by cubic molecular graphs. By computing these quantities for $H_2[k]$, $11 \leq k \leq 50$, and the fact that there are polynomial of degrees ≤ 6 fitted these parameters, we obtain calculations given Table 17.4.

The types of edges for $n = 6$ are depicted in Fig. 17.6. We are now ready to state our second conjecture-based calculations given in Table 17.4.
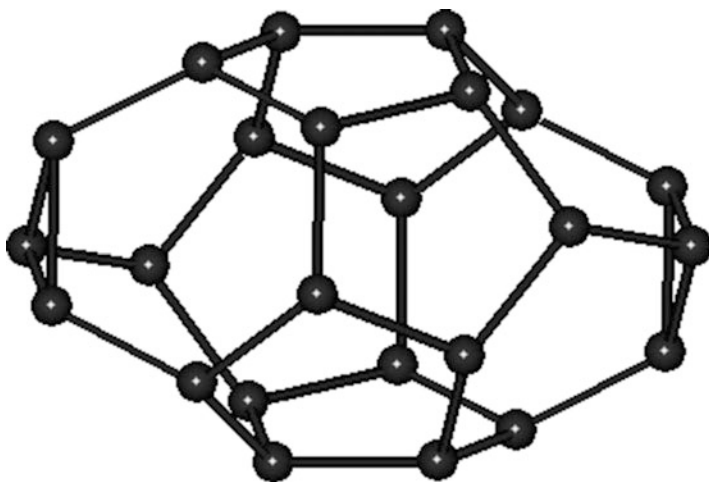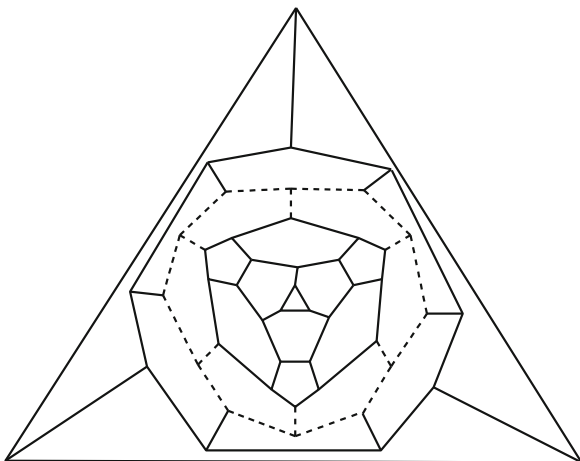
Fig. 17.5 The *3D* perception of $H_2[1]$

Conjecture 17.2 $PI_v(G) = 216n^2 + 288n + 12$ $(n \geq 6)$; $Sz_v(G) = 432n^3 + 1296n^2 + 9144n - 35598$ $(n \geq 11)$; $Sz^*(G) = 432n^3 + 1728n^2 + 12960n - 37275$ $(n \geq 11)$; $PI_e(G) = 324n^2 + 132n + 1086$ $(n \geq 6)$; $Sz_e(G) = 972n^3 + 216n^2 + 28182n - 75084$ $(n \geq 11)$; and $Sz_e^*(G) = 972n^3 + 3888n^2 + 28998n - (168141/2)$ $(n \geq 11)$.

We are now ready to present our third series of three generalized fullerenes with exactly *16n + 18* carbon atoms, $H_3[n]$; see Figs. 17.7 and 17.8.

Similar to other series, there are some exceptional cases that are recorded in Table 17.5.

Table 17.3 The quantities PI_v, PI_e, Sz_v, Sz_e, Sz^*, and Sz_e^* for $H_2[n]$, $1 \leq n \leq 10$

n	1	2	3	4	5	6	7	8	9	10
$PI_v(H_2[n])$	678	1596	3012	4722	6888	–	–	–	–	–
$Sz_v(H_2[n])$	3132	11448	30174	58164	100614	160554	240654	341880	466662	617454
$Sz^*(H_2[n])$	10197/2	16998	39609	151443/2	127578	197217	286761	398331	534297	697131
$PI_e(H_2[n])$	972	2316	4194	6696	9822	–	–	–	–	–
$Sz_e(H_2[n])$	6420	24030	57642	114042	198648	314811	467418	662271	904734	1200348
$Sz_e^*(H_2[n])$	11466	38340	178401/2	169953	572217/2	442659	1287831/2	894741	2400987/2	3133431/2

Table 17.4 The types of vertices and edges in $H_2[n]$, $n \geq 11$

Edges	$n_u(e)$, $n_v(e)$, and $n_0(e)$	No	$m_u(e)$, $m_v(e)$, and $m_0(e)$	No
1	$16,16,12n-20$	6	$26,26,18n-34$	6
2	$12n+1,11,0$	6	$13,18n-2,7$	6
3	$12n-11,19,4$	12	$26,18n-21,13$	12
4	$20,20,12n-28$	6	$34,34,18n-50$	6
5	$12n-18,13,17$	12	$19,18n-23,22$	12
6	$12n-21,28,5$	12	$36,18n-37,19$	12
7	$12n-18,29,1$	12	$37,18n-34,15$	12
8	$12n-12,24,0$	12	$33,18n-21,6$	12
9	$12n-25,37,0$	12	$47,18n-46,17$	12
10	$12n-28,36,4$	12	$47,18n-48,19$	12
11	$12n-24,36,0$	12	$51,18n-39,6$	12
12	$12n-34,46,0$	12	$60,18n-60,18$	12
13	$12n-36,44,4$	12	$60,18n-61,19$	12
14	$12n-36,48,0$	12	$69,18n-57,6$	12
15	$12n-44,55,1$	12	$74,18n-75,19$	12
16	$12n-45,54,3$	12	$74,18n-76,20$	12
17	$12n-48,60,0$	12	$87,18n-75,6$	12
18	$12n-55,66,1$	24	$89,18n-92,21$	24
19	$12n-6i+12,6i,0,\ 12 \leq i \leq n,2/i$	12	$9i-3,18n-9i+15,6,\ 12 \leq i \leq n,2/i$	12
20	$12n-6i+12,6i,0,\ 13 \leq i \leq n,2 \nmid i$	24	$9i-11,18n-9i+7,22,\ 13 \leq i \leq n,2 \nmid i$	24
21	$6n+6,6n+6,0,\ 2/n$	12	$9n-2,9n-2,22,\ 2/n$	12
	$6n+6,6n+6,0,\ 2 \nmid n$	6	$9n+6,9n+6,6,\ 2 \nmid n$	6

Our calculations by GAP and MAGMA suggest the following conjecture:

Conjecture 17.3 $PI_v(G) = 384n^2 + 684n + 270$ $(n \geq 2)$; $Sz_v(G) = (3584/3)n^3 + 3856n^2 + (18166/3)n - 4641$ $(n \geq 4)$; $Sz^*(G) = (3584/3)n^3 + 5056n^2 + (28168/3)n - 3102$ $(n \geq 4)$; $PI_e(G) = 560n^2 + 822n + 740$ $(n \geq 2)$ $Sz_e(G) = 2504n^3 + 5847n^2 + 16124n - 6941$ $(n \geq 4)$; and $Sz_e^*(G) = 2688n^3 + 11260n^2 + 21355n - (27079/4)$ $(n \geq 4)$.

The general term of our fourth series of three generalized fullerenes has exactly $12n + 40$ carbon atoms (Figs. 17.9 and 17.10).

Again some exceptional cases are recorded in Table 17.5 and our calculations by computer algebra systems GAP and MAGMA suggest the following conjecture:

Conjecture 17.4 $PI_v(G) = 216n^2 + 1308n + 1868$ $(n \geq 4)$; $Sz_v(G) = 432n^3 + 4320n^2 + 22476n - 2282$ $(n \geq 9)$; $Sz^*(G) = 432n^3 + 4716n^2 + 28152n + (14159/2)$ $(n \geq 9)$; $PI_e(G) = 324n^2 + 1662n + 3165$ $(n \geq 4)$; $Sz_e(G) = 972n^3 + 7020n^2 + 45678n + 3114$ $(n \geq 9)$; and $Sz_e^*(G) = 972n^3 + 10611n^2 + 63135n + (62485/4)$ $(n \geq 9)$.

Our fifth series of three generalized fullerenes is a sequence $\{H_5[n]\}_{n \geq 1}$ in which the general term has exactly $16n + 14$ carbon atoms; see Figs. 17.11 and 17.12.
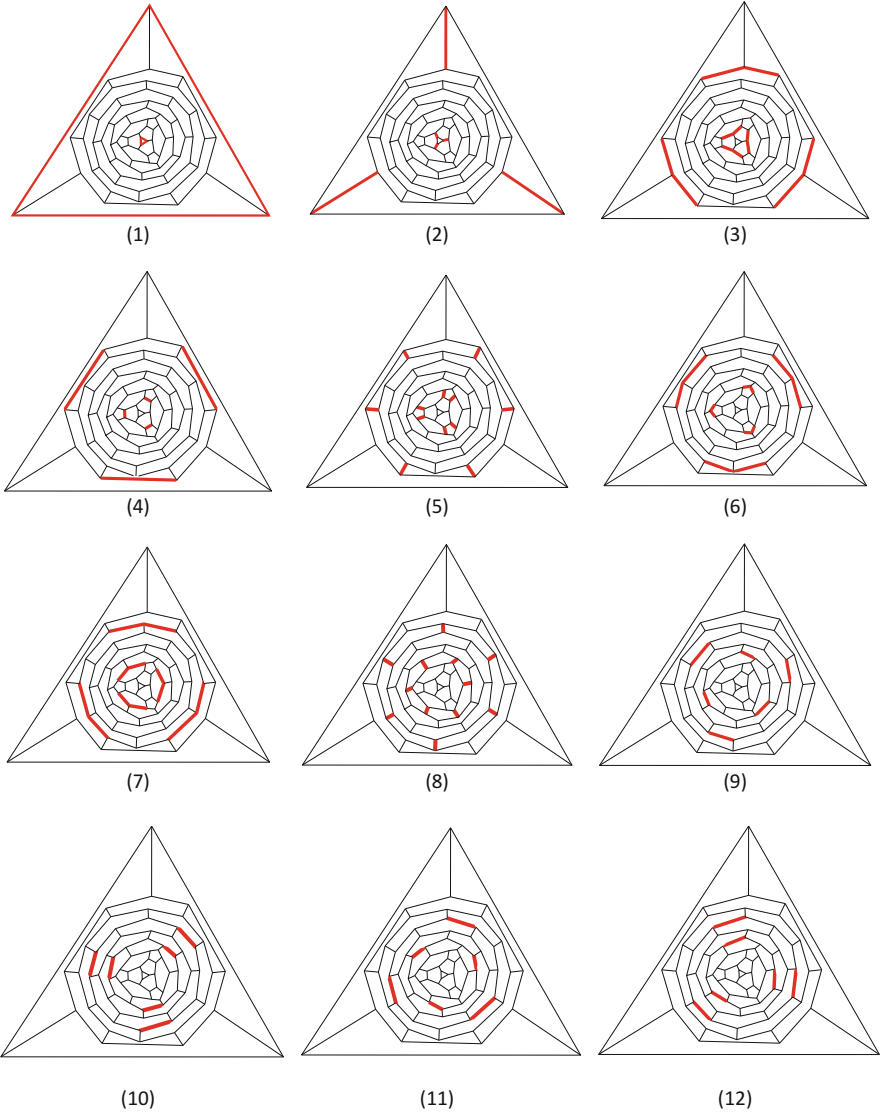
Fig. 17.6 Sixteen types of edges in $H_2[6]$

(13)   (14)   (15)

(16)
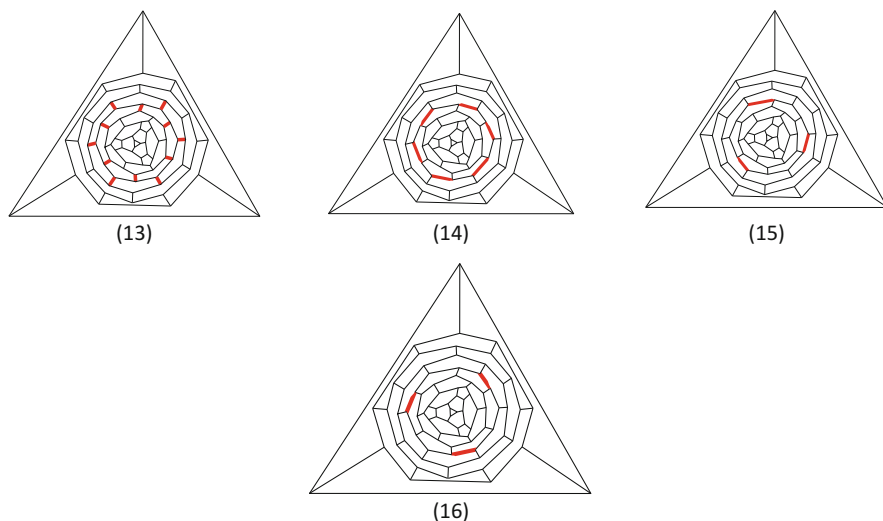
Fig. 17.6 (continued)
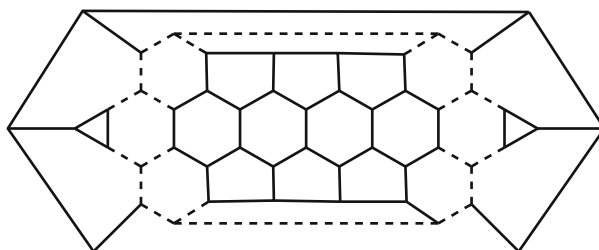
Fig. 17.7 The *2D* perception of the three generalized fullerene $H_3[n]$

Our calculations with this series of three generalized fullerenes suggest the following conjecture:

Conjecture 17.5 $PI_v(G) = 384n^2 + 528n - 314 \ (n \geq 7)$; $Sz(G) = 1024n^3 + 2688n^2 + 47776n - 235661 \quad (n \geq 14)$; $\quad Sz^*(G) = 1024n^3 + 3264n^2 + 57200n - 240930$ $(n \geq 14)$; $\quad PI_e(G) = 576n^2 + 248n + 1816 \quad (n \geq 7)$; $\quad Sz_e(G) = 2304n^3 - 480n^2 + 130832n - 515216 \quad (n \geq 14)$; and $\quad Sz_e^*(G) = 2304n^3 + 7344n^2 + 127308n - (2140107/4) \ (n \geq 14)$. Tables 17.6 and 17.7

The general two-dimensional form of our sixth series of *3*-generalized fullerenes is depicted in Fig. 17.13 and the three-dimensional perception of the first member of this series is shown in Fig. 17.14. Notice that the general term of this series has exactly *12n + 20* carbon atoms.
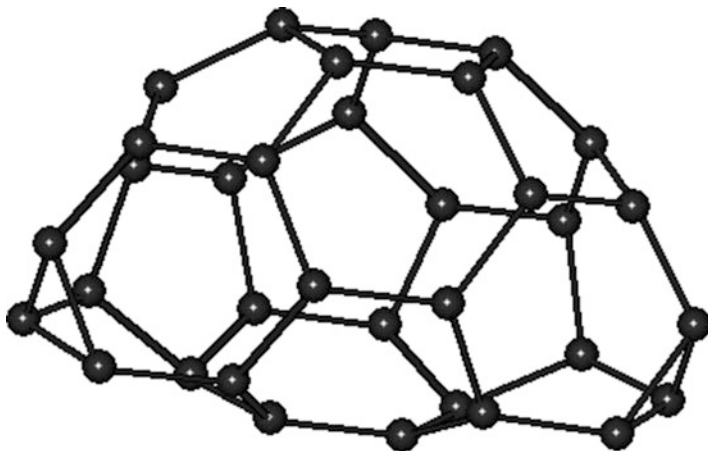
Fig. 17.8 The *3D* perception of $H_3[1]$

Table 17.5 The quantities $PI_v, PI_e, Sz_v, Sz_e, Sz^*$, and Sz_e^* for $H_3[n]$, $1 \leq n \leq 3$

n	1	2	3
PI_v	1434	–	–
Sz_v	9717	32755	80493
Sz^*	14276	45686	102830
PI_e	2042	–	–
Sz_e	19622	69187	161670
Sz_e^*	128813/4	411689/4	924869/4

Fig. 17.9 The *2D* perception of the three generalized fullerene $H_4[n]$
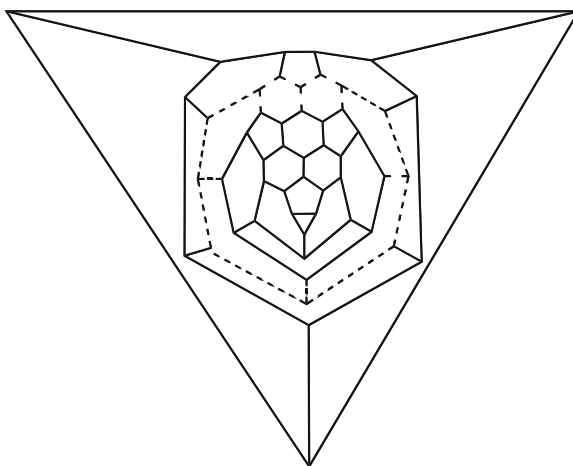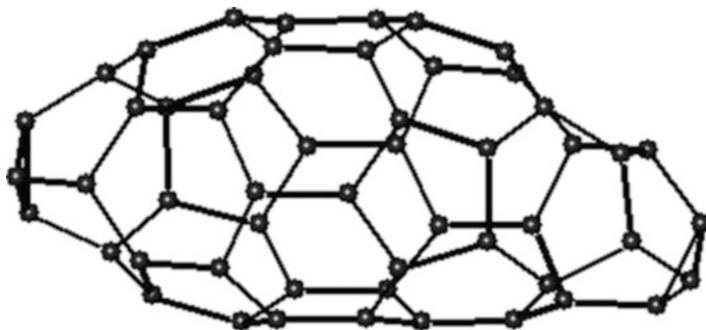
Fig. 17.10 The *3D* perception of $H_4[1]$

Fig. 17.11 The *2D* perception of the three generalized fullerene $H_5[n]$
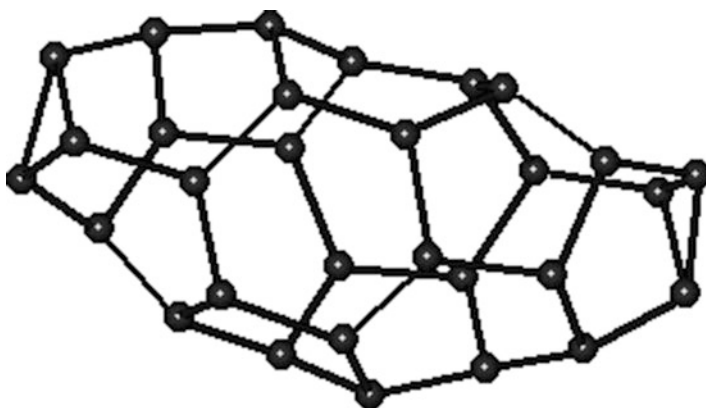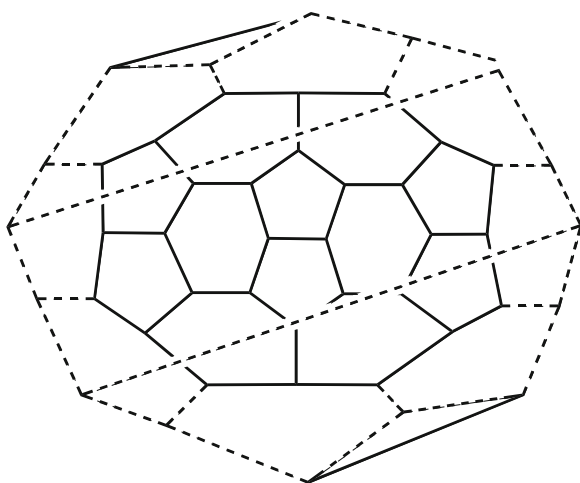
Fig. 17.12 The *3D* perception of $H_5[1]$

Table 17.6 The quantities PI_v, PI_e, Sz_v, Sz_e, Sz^*, and Sz_e^* for $H_4[n]$, $1 \leq n \leq 8$

n	1	2	3	4	5	6	7	8
PI_v	3568	5426	7760	–	–	–	–	–
Sz	38585	70815	118946	185480	272558	381562	514950	675198
Sz^*	49712	1812 97/2	295977/2	447547/2	640215/2	878387/2	1166859/2	1510615/2
PI_e	5007	7720	11051	–	–	–	–	–
Sz_e	74364	139758	234500	362791	529448	740145	1000300	1315490
Sz_e^*	446657/4	406775/2	1328185/4	2009495/4	2875569/4	3946459/4	5243785/4	6789893/4

Table 17.7 The quantities PI_v, PI_e, Sz_v, Sz_e, Sz^*, and Sz_e^* for $H_5[n]$, $1 \leq n \leq 13$

n	1	2	3	4	5	6	7
PI_v	1114	2668	4986	8118	12050	16722	–
Sz	6517	25126	65257	136489	245329	395571	595285
Sz^*	9612	35478	86774	171521	295616	464835	683912
PI_e	1608	3910	7316	11766	17306	23986	–
Sz_e	13315	53589	139282	283946	499812	801644	1197976
Sz_e^*	86275/4	319685/4	780601/4	1542675/4	2657227/4	4175427/4	6142193/4
n	8	9	10	11	12	13	
PI_v	–	–	–	–	–	–	
Sz	850063	1162055	1536405	1978621	2494351	3089451	
Sz^*	956884	1288155	1682917	2146671	2685093	3304032	
PI_e	–	–	–	–	–	–	
Sz_e	1696792	2311020	3052550	3933712	4967292	6166416	
Sz_e^*	8594473/4	11570677/4	15118317/4	19286741/4	24127141/4	29692133/4	

Fig. 17.13 The *2D* perception of the three generalized fullerene $H_6[n]$
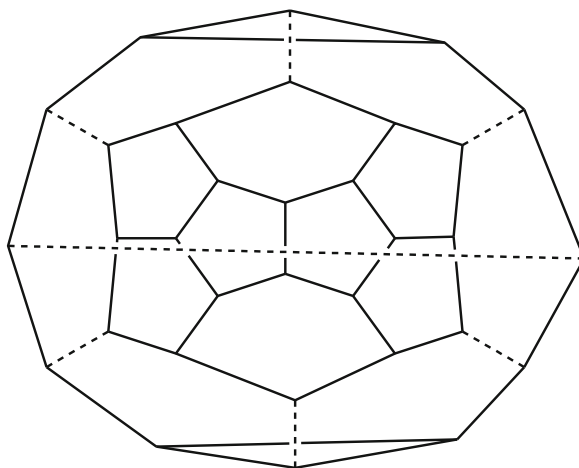
There are eight exceptional cases for $H_6[n]$, that are recorded in Table 17.8. If $n \geq 9$ then the distance-based topological indices of vertex Padmakar-Ivan, edge Padmakar-Ivan, vertex Szeged, edge Szeged, revised Szeged, and edge revised Szeged indices are obeyed from polynomials given the following observation:

Conjecture 17.6 $PI_v(G) = 216n^2 + 624n + 288$ $(n \geq 4)$; $Sz(G) = 432n^3 + 2160n^2 + 13128n - 28798$ $(n \geq 9)$; $Sz^*(G) = 432n^3 + 2448n^2 + 16680n - 27063$ $(n \geq 9)$; $PI_e(G) = 324n^2 + 636n + 1150$ $(n \geq 4)$; $Sz_e(G) = 972n^3 + 2160n^2 + 32106n - 56492$ $(n \geq 9)$; and $Sz_e^*(G) = 972n^3 + 5508n^2 + 37026n - (119341/2)$ $(n \geq 9)$.
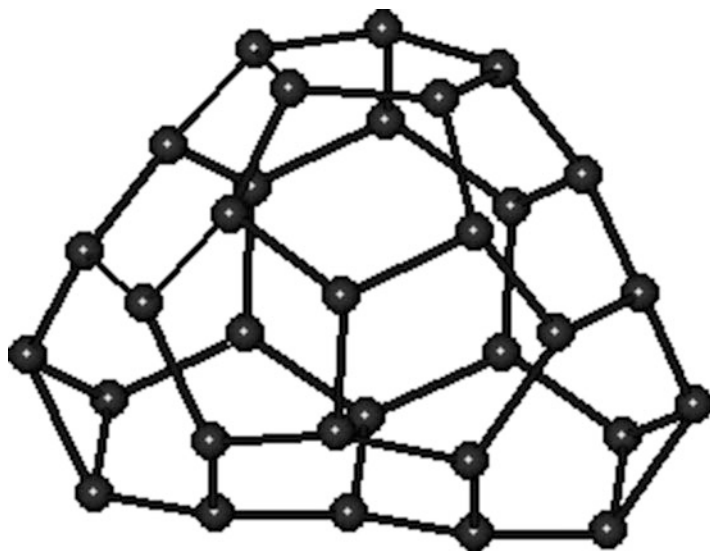
Fig. 17.14 The *3D* perception of $H_6[1]$

Table 17.8 The quantities PI_v, PI_e, Sz_v, Sz_e, $Sz*$, and Sz_e* for $H_6[n]$, $1 \leq n \leq 8$

n	1	2	3	4	5	6	7	8
PI_v	1252	2484	4148	—	—	—	—	—
Sz	8034	22807	48942	88804	146058	221494	317246	435674
Sz^*	12042	61975/2	62627	109234	172703	254879	357939	484251
PI_e	1848	3568	5920	—	—	—	—	—
Sz_e	17445	46556	97796	175280	282422	424934	607798	836308
Sz_e^*	54321/2	69732	140542	489751/2	774511/2	1143311/2	1606095/2	2173491/2

The nth term of our seventh series of three generalized fullerenes, $H_7[n]$, has exactly $12n + 26$ carbon atoms. The two- and three-dimensional perceptions of this molecule are depicted in Figs. 17.15 and 17.16, respectively.

In Table 17.9, nine exceptional cases for our six distance-based topological indices are recorded.

Again, we apply our mentioned method to find good polynomials for fitting PI_v, PI_e, Sz_v, Sz_e, $Sz*$, and Sz_e* for $H_7[n]$, $n \geq 10$. We have the following conjecture:

Conjecture 17.7 $PI_v(G) = 216n^2 + 828n + 646$ $(n \geq 5)$; $Sz(G) = 432n^3 + 2808n^2 + 14880n - 23034$ $(n \geq 10)$; $Sz^*(G) = 432n^3 + 3132n^2 + 19080n - (39359/2)$ $(n \geq 10)$; $PI_e(G) = 324n^2 + 942n + 1576$ $(n \geq 5)$; $Sz_e(G) = 972n^3 + 3618n^2 + 34068n - 43349$ $(n \geq 10)$; and $Sz_e^*(G) = 972n^3 + 7047n^2 + 42777n - (176961/4)$ $(n \geq 10)$.

Fig. 17.15 The *2D* perception of the three generalized fullerene $H_7[n]$
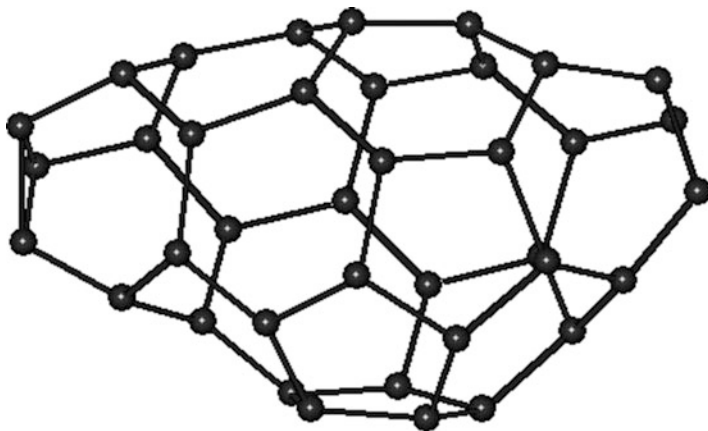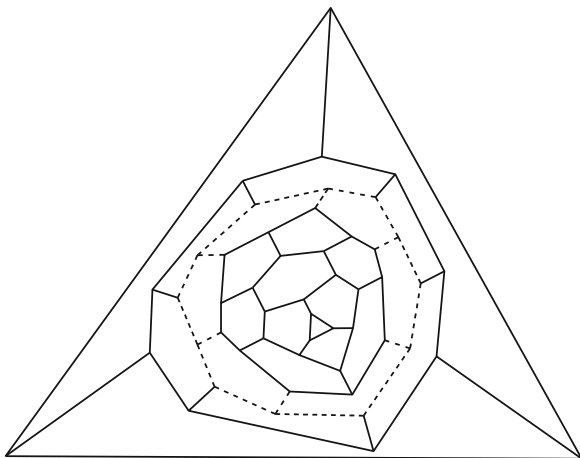
Fig. 17.16 The *3D* perception of $H_7[1]$

We end this section by introducing our eighth series of three generalized fullerenes containing $10n + 40$ carbon atoms. The *2D* and *3D* perceptions of the three generalized fullerene $H_8[n]$ are depicted in Figs. 17.17 and 17.18, respectively.

There are six exceptional cases for this series that are recorded in Table 17.10.

We end this section by a conjecture on our distance-based topological indices for three generalized fullerene series $H_8[n]$.

Conjecture 17.8 $PI_v(G) = 150n^2 + 1100n + 1904$ $(n \geq 3)$; $Sz(G) = 250n^3 + 3000n^2 + 14435n + 10270$ $(n \geq 7)$; $Sz^*(G) = 250n^3 + 3250n^2 + 18165n + 19034$ $(n \geq 7)$; $PI_e(G) = 225n^2 + 1445n + 3030$ $(n \geq 3)$; $Sz_e(G) = (1125/2)n^3 + (10425/2)n^2 + 28025n + 27286$ $(n \geq 7)$; and $Sz_e^*(G) = (1125/2)n^3 + (14625/2)n^2 + (162915/4)n + 42823$ $(n \geq 7)$.

Table 17.9 The quantities PI_v, PI_e, Sz_v, Sz_e, Sz^*, and Sz_e^* for $H_7[n]$, $1 \leq n \leq 9$

n	1	2	3	4	5	6	7	8	9
PI_v	1822	3272	5134	7432	–	–	–	–	–
Sz	14051	33897	65698	112269	176694	261088	367040	496941	653268
Sz^*	19791	44373	82668	136889	418141/2	602515/2	831285/2	1109237/2	1441327/2
PI_e	2616	4615	7262	10512	–	–	–	–	–
Sz_e	28498	66008	128131	218300	341511	502245	706107	958477	1264917
Sz_e^*	177961/4	99706	742513/4	1229601/4	1878699/4	2707719/4	3736575/4	4987754/4	6480607/4

Fig. 17.17 The *2D* perception of the three generalized fullerene $H_8[n]$
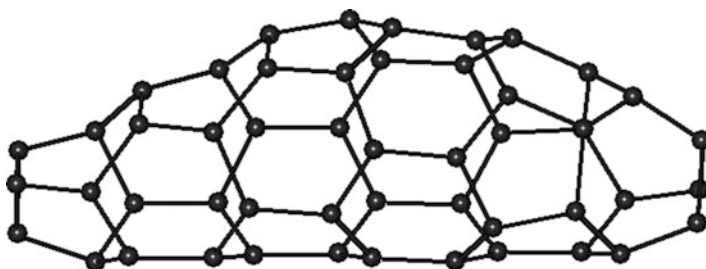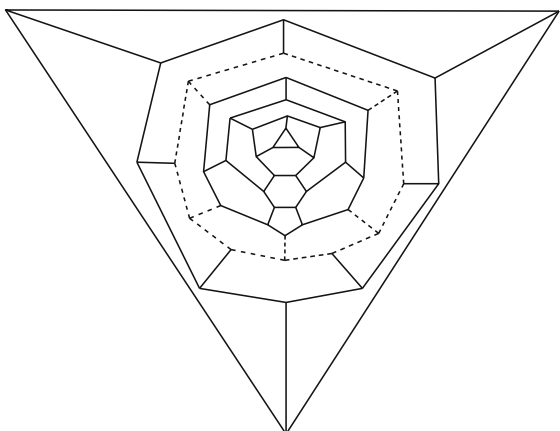
Fig. 17.18 The *3D* perception of $H_8[1]$

Table 17.10 The quantities PI_v, PI_e, Sz_v, Sz_e, Sz^*, and Sz_e^* for $H_8[n]$, $1 \leq n \leq 6$

n	1	2	3	4	5	6
PI_v	3198	4716	—	—	—	—
Sz	30491	54178	87561	132090	188719	258882
Sz^*	42080	70950	109716	159748	222373	299025
PI_e	4684	6812	—	—	—	—
Sz_e	64043	109823	173941	258910	368068	504588
Sz_e^*	377997/4	159292	985657/4	358843	1998459/4	1343893/4

17.3 Concluding Remarks

In this chapter eight infinite classes of three generalized fullerenes are constructed for the first time. We examined these series on a set of six distance-based topological indices containing vertex Padmakar-Ivan, edge Padmakar-Ivan, vertex Szeged, edge Szeged, revised Szeged, and edge revised Szeged indices. Our calculations show that the vertex and edge PI indices are polynomials of degree two, and vertex

Szeged, edge Szeged, revised Szeged, and edge revised Szeged indices of these series are polynomials of degree three. We conjecture that the three generalized fullerenes, in general, obey these facts.

References

Ashrafi AR, Mehranian Z (2013) Topological study of $(3,6)-$ and $(4,6)-$ fullerenes. In: Ashrafi AR et al (eds) Topological modeling of nanostructures and extended systems, vol 7, Carbon materials: chemistry and physics., pp 487–510

Ashrafi AR, Sabaghian $-$ Bidgoli H (2009) A numerical method for computing PI index of fullerene molecules containing carbon atoms. J Comput Theor Nanosci 6:1706–1708

Ashrafi AR, Ghorbani M, Jalali M (2008) The vertex PI and Szeged indices of an infinite family of fullerenes. J Theor Comput Chem 7:221–231

Ashrafi AR, Ghorbani M, Jalali M (2009) Study of IPR fullerenes by counting polynomials. J Theor Comput Chem 8:451–457

Ashrafi AR, Cataldo F, Iranmanesh A, Ori O (eds) (2013) Topological modelling of nanostructures and extended systems, vol 7, Carbon materials: chemistry and physics. Springer Science + Business Media, Dordrecht

Balaban AT (1973) Trivalent graphs of girth nine and eleven, and relationships among cages. Rev Roumaine Math Pures Appl 18:1033–1043

Balaban AT (1980) Chemical graphs. XXXVIII. Synthon graphs. MATCH Commun Math Comput Chem 8:159–192

Balaban AT (1982) Highly discriminating distance $-$ based topological index. Chem Phys Lett 89:399–404

Behmaram A (2013) Matching in fullerene and molecular graphs. PhD thesis, University of Tehran

Bosma W, Cannon J, Playoust C (1997) The magma algebra system. I. The user language. J Symb Comput 24:235–265

Cataldo F, Graovac A, Ori O (eds) (2011) The mathematics and topology of fullerenes, vol 4, Carbon materials: chemistry and physics. Springer Science + Business Media B.V, Dordrecht

Deza M, Dutour Sikiric M, Fowler PW (2004) Zigzags, railroads, and knots in fullerenes. J Chem Inf Comput Sci 44:1282–1293

Diudea MV, Ursu O, Nagy LCS (2002) Topocluj. Babes $-$ Bolyai University, Cluj

Faghani M, Ashrafi AR (2014) Revised and edge revised Szeged indices of graphs. Ars Math Contemp 7:153–160

Fowler PW, Manolopoulos DE (1995) An atlas of fullerenes. Oxford University Press, Oxford

Gutman I (1994) A formula for the Wiener number of trees and its extension to graphs containing cycles. Graph Theory Notes New York 27:9–15

Gutman I, Ashrafi AR (2008) The edge version of the Szeged index. Croat Chem Acta 81:263–266

HyperChem package Release 7.5 for Windows (2002) Hypercube Inc., Florida, USA

Khadikar PV, Karmarkar S, Agrawal VK (2001) A novel PI index and its applications to QSPR/QSAR studies. J Chem Inf Comput Sci 41:934–949

Khalifeh MH, Yousefi $-$ Azari H, Ashrafi AR (2008) Vertex and edge PI indices of Cartesian product graphs. Discrete Appl Math 156:1780–1789

Koorepazan-Moftakhar F, Ashrafi AR (2013) Symmetry and PI index of C_{60+12n} fullerenes. J Comput Theor Nanosci 10:2484–2486

Koorepazan-Moftakhar F, Ashrafi AR, Mehranian Z (2014) Symmetry and PI polynomials of C_{50+10n} fullerenes. MATCH Commun Math Comput Chem 71:425–436

Kroto HW, Heath JR, O'Brien SC, Curl RF, Smalley RE (1985) C_{60}: Buckminsterfullerene. Nature 318:162–163

Myrvold W, Bultena B, Daugherty S, Debroni B, Girn S, Minchenko M, Woodcock J, Fowler PW (2007) FuiGui: a graphical user interface for investigating conjectures about fullerenes. MATCH Commun Math Comput Chem 58:403–422

Randić M (2011) On generalization of Wiener index for cyclic structures. Acta Chim Slovenica 49:483–496

Schwerdtfeger P, Wirz L, Avery J (2013) Program fullerene: a software package for constructing and analyzing structures of regular fullerenes. J Comput Chem 34:1508–1526

The GAP Team (1995) GAP, groups, algorithms and programming. Lehrstuhl De für Mathematik. RWTH, Aachen

Wiener HJ (1947) Structural determination of paraffin boiling points. J Am Chem Soc 69:17–20

Chapter 18
Study of the Matching Interdiction Problem in Some Molecular Graphs of Dendrimers

G.H. Shirdel and N. Kahkeshani

Abstract The purpose of the matching interdiction problem in a weighted graph G is to remove a subset R^* of vertices such that the weight of the maximum matching in the graph $G - R^*$ is minimized. The ratio between the difference of the optimal and approximate solutions of this problem from the weight of maximum matching in the graph G, where is denoted by e_G, is bounded from above. In this paper, we consider some special classes of molecular graphs. It is shown that the value of e_G in these graphs is equal to the maximum value.

18.1 Introduction

There are two opposite forces in the network interdiction problems, the follower and interdictor. The follower tries to optimize the objective of the problem, but the interdictor attempts to restrict the action of the follower. The interdictor does this activity by changing the conditions of the problem such as removing vertices or edges or varying the parameters of the problem. The topic of interdiction has been entered in majority of the optimization problems such as the maximum flow network (Altner et al. 2010), shortest path (Israeli and Wood 2002), and multiterminal maximum flow network (Akgun et al. 2011). The interdiction problems are used in many of real-world problems such as coordinating the tactical air strikes (McMasters and Mustin 1970), controlling the floods (Ratliff et al. 1975), controlling the infections in a hospital (Assimakopoulos 1987), and so on.

In the maximum flow network interdiction problem, the interdictor removes a subset of edges to decrease the maximum flow in the network. The interdictor needs budget for destroying the edges of the network. The first integer linear programming model for this problem was presented by Kevin Wood (Wood 1993). He tightens the relaxation of this model by the valid inequalities. In Altner et al. (2010),

G.H. Shirdel (✉) • N. Kahkeshani
Department of Mathematics, Faculty of Sciences, University of Qom, Qom, Iran
e-mail: Shirdel_math@yahoo.com; nasrinkahkeshani@yahoo.com

the authors proved that the integrality gap of this model is not bounded from below by a constant. The maximum flow network interdiction problem is strongly NP-complete when the interdiction cost of each edge is one. In Akgun et al. (2011), the authors used an idea similar to Wood's idea and presented a linear programming model for the multiterminal maximum flow network interdiction problem. An upper bound for optimal value of this problem was obtained. The goal of the interdictor in the shortest path interdiction problem is to maximize the length of the shortest path between two specific vertices in a network by deleting vertices or edges or increasing the length of some edges in the network. An algorithm was presented for this problem when the vertices or edges of the network were removed by the interdictor (Corley and Sha 1982). This problem was formulated as a linear programming problem, and the algorithms such as the Benders decomposition and covering decomposition were presented for solving it (Israeli and Wood 2002). In recent years, the researchers have considered the topic of interdiction on some combinatorial problems such as the matching (Zenklusen 2010), independent set (Bazgan et al. 2011), and connectivity (Shen et al. 2012). The matching and independent set interdiction problems are defined on a weighted graph G. The purpose of these problems is to find a subset R^* of vertices such that the weight of the maximum matching and independent set in graph $G - R^*$ is minimized. These two problems can be solved in polynomial time on the bipartite graphs with unit weights. The ratio between difference of the optimal and approximate solutions of this problem from the weight of maximum matching in the graph G, where is denoted by e_G, is bounded from above.

According to the structure of some molecules such as dendrimers, fullerenes, and so on, they can be considered as graphs. Therefore, some mathematical problems are expressed on them (Yousefi-Azari and Ashrafi 2012; Diudea et al. 2012; Behmaram et al. 2013).

In this paper, we consider some molecular graphs and their subgraphs (Newkome et al. 2001; Ashrafi et al. 2013). The recurrence relations for the weight of the maximum matching in the subgraphs are obtained. These relations help us to obtain the weight of the maximum matching in these molecular graphs. Then, it is shown that the value of e_G in the molecular graphs G is equal to two.

18.2 Basic Definitions

Let $G = (V_G, E_G)$ be an undirected connected graph such that V_G and E_G are the sets of vertices and edges, respectively. An edge in G is denoted by (i, j), where $i, j \in V_G$. Each edge $e \in E_G$ has a weight $w(e) > 0$. Let $V' \subseteq V_G$. $G - V'$ is a subgraph of G with the vertex set $V_G - V'$ and edge set $\{(i, j) \in E_G \mid i, j \in V_G - V'\}$. The edge e is incident with the vertices i and j if $e = (i, j)$. Two edges are adjacent if they have a common vertex. The set $M' \subseteq E_G$ is called a matching in G if no two edges in M' are adjacent. The weight of the

matching M' is equal to $w\big(M'\big) = \sum_{e \in M'} w(e)$. The matching M is a maximum matching in G if for every matching M' in G, $w(M) \geq w\big(M'\big)$. The weight of the maximum matching M in G is denoted by $v(G)$. The mathematical model of the matching interdiction problem is defined as follows:

$$v\big(G - R^*\big) = \mathrm{Min}\Big\{ v\big(G - R'\big) \big| R' \subseteq V_G, \big|R'\big| = B \Big\},$$

where $B \in N$. R^* is the solution of the matching interdiction problem and is called the optimal interdiction set in G. In this paper, we suppose that $B = 2$. Now, an approximate solution for the matching interdiction problem is presented. Let $M = \{e_1, \ldots, e_k\}$ be the maximum matching in G such that $w(e_1) \geq \cdots \geq w(e_k)$. If $e_1 = (i_1, j_1)$, the set $R = \{i_1, j_1\}$ is the approximate solution of the matching interdiction problem and is called the approximate interdiction set in G. $M \backslash \{e_1\}$ is the maximum matching in the graph $G - R$. Therefore, the following relation holds:

$$v(G - R) = v(G) - w(e_1) \tag{18.1}$$

e_G is defined as follows:

$$e_G = \frac{v(G) - v\big(G - R^*\big)}{v(G) - v(G - R)} \tag{18.2}$$

It has been showed that $e_G \leq 2$ (Zenklusen 2010). In this paper, we obtain the value of e_G for some special classes of molecular graphs.

18.3 Main Results

Suppose that $\{G_n\}_{n=1}^{\infty}$ (or $\{G_n\}$) is a sequence of graphs. The weight of edges in the graph G_n, where $n \geq 1$, is defined as follows. The weight of each edge in G_1 is equal to w_1. The weight of each edge in $E_{G_i} \backslash E_{G_{i-1}}$ is equal to w_i, where $i \geq 2$. We suppose that $w_1 < w_2 < \cdots < w_n < \cdots$. Consider some sequences of graphs depicted in Fig. 18.1a–e. The weights of edges in these sequences of graphs are defined as above. The elements of sets R^* and M in these graphs are denoted by the black vertices and red edges, respectively. Let $\{G_n\}_{n=1}^{\infty}$ be an arbitrary sequence in Fig. 18.1. We obtain the value of $v(G_n)$, where $n \geq 1$, for them. These results are presented in Table 18.1. It is obvious that

$$v(G_n - R) = v(G_n) - w_n \qquad \forall n \geq 1$$
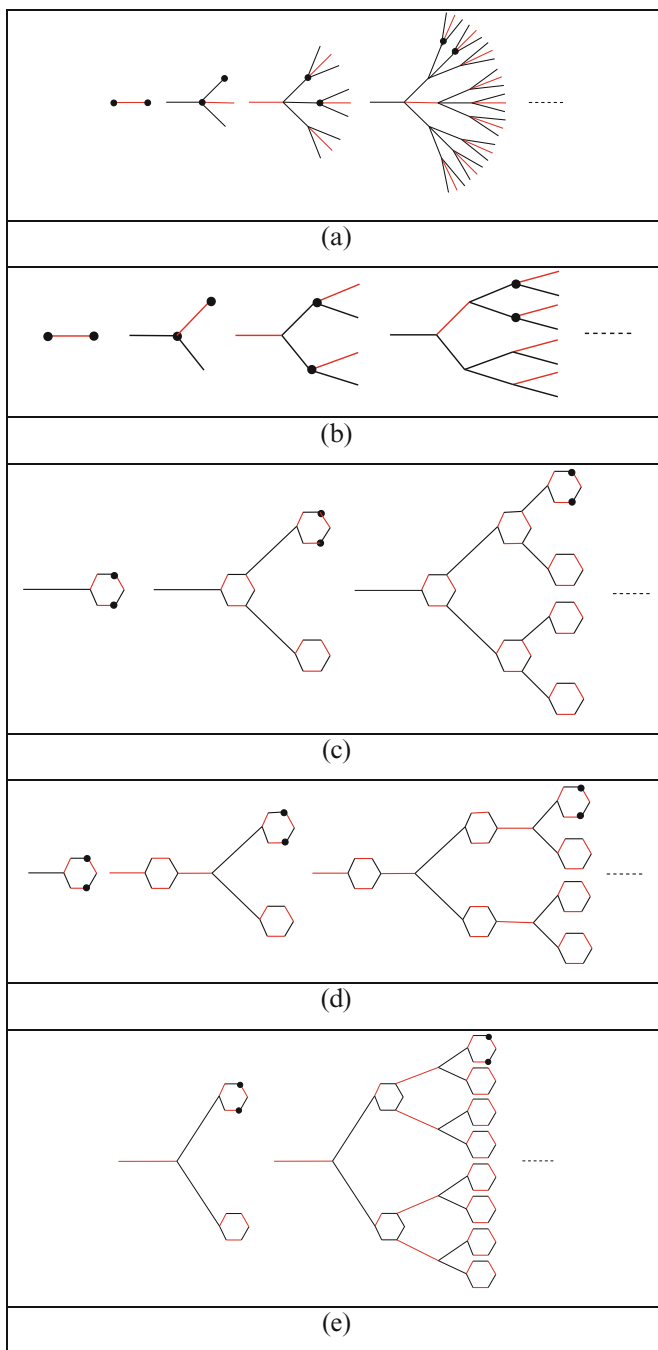
Fig. 18.1 The sequences of graphs: (**a**) $\{A_n\}_{n=1}^{\infty}$; (**b**) $\{B_n\}_{n=1}^{\infty}$; (**c**) $\{C_n\}_{n=1}^{\infty}$; (**d**) $\{D_n\}_{n=}^{\infty}$ (**e**) $\{E_n\}_{n=1}^{\infty}$

Table 18.1 The recurrence relations for the weight of maximum matching in the sequences of graphs

$\{G_n\}_{n=1}^{\infty}$	$v(G_n)$
$\{A_n\}_{n=1}^{\infty}$	$v(A_1) = w_1,\ v(A_2) = w_2,\ v(A_n) = 3^{n-2}w_n + v(A_{n-2}) \quad \forall n \geq 3$
$\{B_n\}_{n=1}^{\infty}$	$v(B_1) = w_1,\ v(B_2) = w_2,\ v(B_n) = 2^{n-2}w_n + v(B_{n-2}) \quad \forall n \geq 3$
$\{C_n\}_{n=1}^{\infty}$	$v(C_1) = 3w_1,\ v(C_n) = 3 \times 2^{n-1}w_n + v(C_{n-1}) \quad\quad \forall n \geq 2$
$\{D_n\}_{n=1}^{\infty}$	$v(D_1) = 3w_1,\ v(D_2) = 3w_1 + 7w_2,\ v(D_n) = 7 \times 2^{n-2}w_n - 2^{n-2}w_{n-1} + v(D_{n-1}) \forall n \geq 3$
$\{E_n\}_{n=1}^{\infty}$	$v(E_1) = 7w_1,\ v(E_n) = 7 \times 4^{n-1}w_n - 4^{n-1}w_{n-1} + v(E_{n-1}) \quad \forall n \geq 2$

If $\{G_n\}_{n=1}^{\infty}$ is $\{A_n\}_{n=1}^{\infty}$ or $\{B_n\}_{n=1}^{\infty}$, the value of $v(G_n - R^*)$ and e_{G_n} are as follows:

$$v(G_n - R^*) = \begin{cases} 0 & n = 1, 2 \\ v(G_n) - 2w_n & \forall n \geq 3 \end{cases}$$

$$e_{G_n} = \begin{cases} 1 & n = 1, 2 \\ 2 & n \geq 3 \end{cases}$$

Else, $v(G_n - R^*) = v(G_n) - 2w_n$ and $e_{G_n} = 2$, for each $n \geq 1$.

For example, we explain how to compute the value of e_{A_n} for $n \geq 1$. By Fig. 18.1a and the weights of edges, we have

$$v(A_1) = w_1$$
$$v(A_2) = w_2$$
$$v(A_3) = w_1 + 3w_3$$
$$v(A_4) = w_2 + 9w_4$$
$$v(A_5) = w_1 + 3w_3 + 27w_5$$
$$v(A_6) = w_2 + 9w_4 + 81w_6$$
$$\vdots$$

The above relations can be summarized as follows:

$$v(A_1) = w_1$$
$$v(A_2) = w_2$$
$$v(A_n) = 3^{n-2}w_n + v(A_{n-2}) \quad \forall n \geq 3$$

This result has been presented in Table 1. Also, we can express $v(A_n)$ as follows. If n is even, we have

$$v(A_n) = \sum_{i=0}^{(n-2)/2} 3^{n-2(i+1)} w_{n-2i}$$

Else,

$$
v(A_n) =
\begin{cases}
w_1 & n = 1 \\
w_1 + \displaystyle\sum_{i=0}^{(n-3)/2} 3^{n-2(i+1)} w_{n-2i} & n \geq 3
\end{cases}
$$

Notice that the edge e_1 in A_n is an edge with weight w_n. According to Rel. (18.1), we have

$$
v(A_n - R) = v(A_n) - w_n \qquad \forall n \geq 1 \tag{18.3}
$$

We call two black vertices in Fig. 18.1a as u and v. We show that $R^* = \{u, v\}$. This claim is obvious in the graphs A_1 and A_2. Now, let $n \geq 3$. Suppose that u' and v' are two arbitrary vertices in A_n. Let

$$
A = \{e \in M \,|\, e \text{ is incident with } u' \text{ or } v'\}
$$

Notice that $|A| \leq 2$. Since $M \setminus A$ is a matching in $A_n - \{u', v'\}$ and $\sum_{e \in A} w(e) \leq 2w_n$, we have

$$
v(A_n) - 2w_n \leq v(A_n) - \sum_{e \in A} w(e) \leq v(A_n - \{u', v'\})
$$

$v(A_n) - 2w_n$ is the weight of maximum matching in the graph $A_n - \{u, v\}$. Therefore,

$$
v(A_n - \{u, v\}) \leq v(A_n - \{u', v'\})
$$

So it follows:

$$
R^* = \{u, v\}
$$

Then, $v(A_n - R^*) = v(A_n) - 2w_n$ for   each $n \geq 3$ and $v(A_1 - R^*) = v(A_2 - R^*) = 0$. By Rel. (18.2), e_{A_n} is obtained as follows:

$$
e_{A_n} =
\begin{cases}
1 & n = 1, 2 \\
2 & n \geq 3
\end{cases}
$$

Similar to the above method for the graph A_n, we can obtain $v(G_n)$ and e_{G_n} for each sequence of graphs in Fig. 18.1.

We consider some molecular graphs which are depicted in Figs. 18.2a–f and 18.3a–e. Notice that the graphs in Fig. 18.1 are the subgraphs of these molecular graphs. For example, the graph F_n, for each $n \geq 1$, is obtained by joining four graph A_n in the red vertex. Hence, each graph in Figs. 18.2 and 18.3 is as sequences of
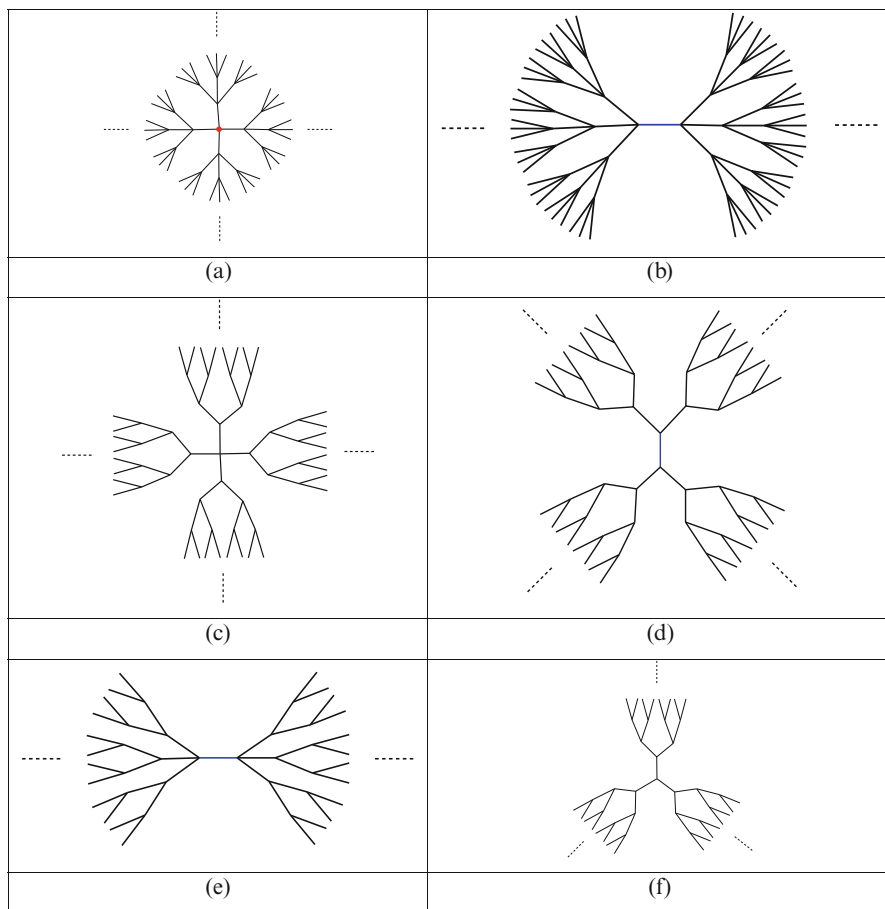
Fig. 18.2 The molecular graphs: (**a**) $\{F_n\}_{n=1}^{\infty}$; (**b**) $\{Q_n\}_{n=0}^{\infty}$; (**c**) $\{H_n\}_{n=1}^{\infty}$; (**d**) $\{I_n\}_{n=0}^{\infty}$; (**e**) $\{J_n\}_{n=0}^{\infty}$; (**f**) $\{K_n\}_{n=1}^{\infty}$

graphs. The sets R^* and M in these graphs are similar to their subgraphs which were denoted in Fig. 18.1. The weight of blue edges in Figs. 18.2 and 18.3 is equal to w_0, but the weight of black edges in each molecular graph is similar to the weight of edges in its subgraph. Also, let $w_0 < w_1 < \cdots < w_n < \cdots$. The presented results in Table 18.1 help us to obtain the value of e_G in the molecular graph G. The weight of maximum matching in these graphs is presented in Table 18.2. These relations are according to the weight of maximum matching in their subgraphs. The values of $v(G - R^*)$ and $v(G - R)$ are presented in Tables 18.3 and 18.4, respectively. $v(G - R^*)$ and $v(G - R)$ are called the optimal and approximate values of the matching interdiction problem, respectively. Now, we can obtain the value of e_G (see Table 18.5).
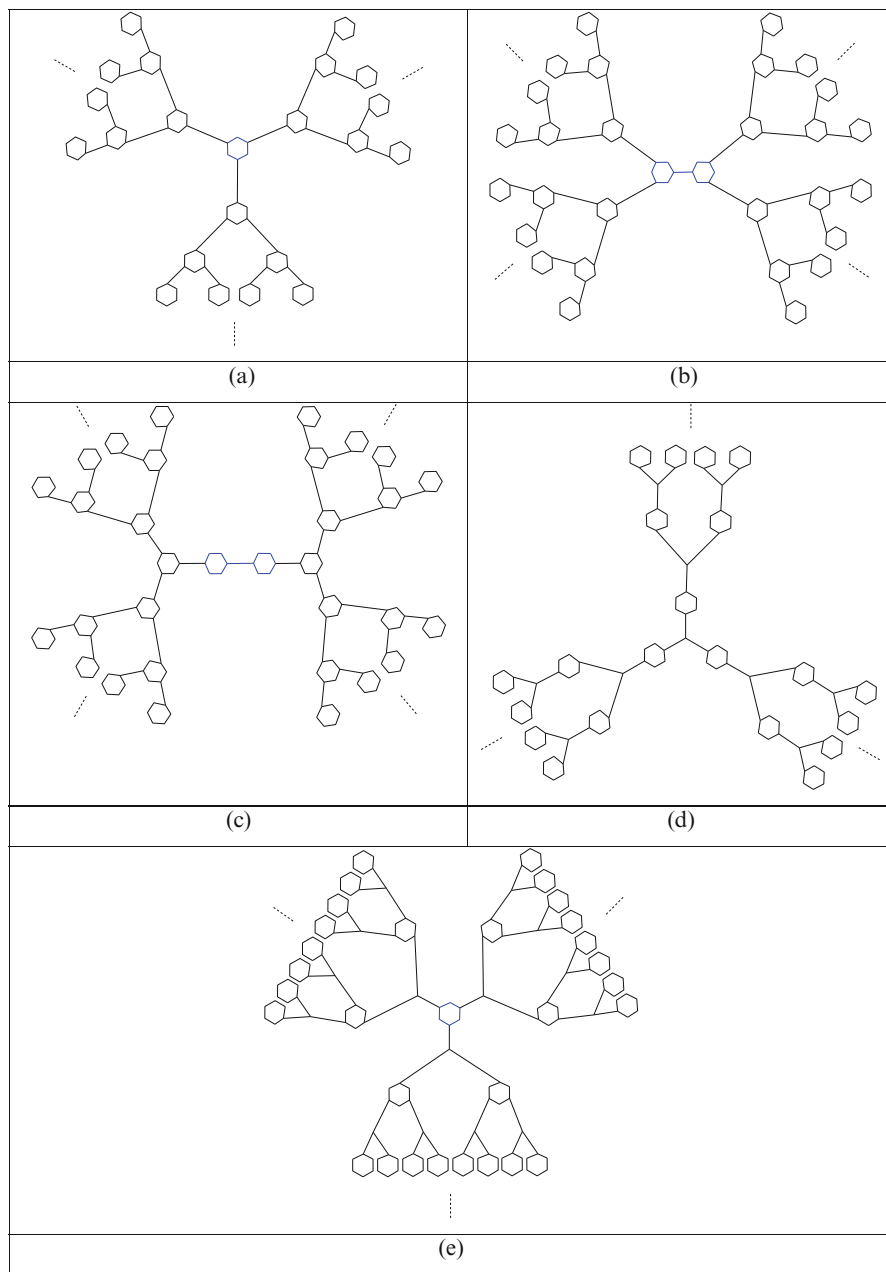
Fig. 18.3 The molecular graphs: (**a**) $\{L_n\}_{n=0}^{\infty}$; (**b**) $\{M_n\}_{n=0}^{\infty}$; (**c**) $\{N_n\}_{n=0}^{\infty}$; (**d**) $\{O_n\}_{n=1}^{\infty}$; (**e**) $\{P_n\}_{n=0}^{\infty}$

Table 18.2 The recurrence relations for the weight of maximum matching in the molecular graphs

$\{G_n\}$	$v(G_n)$
$\{F_n\}_{n=1}^{\infty}$	$v(F_n) = \begin{cases} 4v(A_n) & \text{if } n \text{ be even} \\ 4v(A_n) - 3w_1 & \text{if } n \text{ be odd} \end{cases} \quad \forall n \in N$
$\{Q_n\}_{n=0}^{\infty}$	$v(G_0) = w_0, \; v(G_n) = \begin{cases} 6v(A_n) + w_0 & \text{if } n \text{ be even} \\ 6v(A_n) - 4w_1 & \text{if } n \text{ be odd} \end{cases} \quad \forall n \in N$
$\{H_n\}_{n=1}^{\infty}$	$v(H_n) = \begin{cases} 4v(B_n) & \text{if } n \text{ be even} \\ 4v(B_n) - 3w_1 & \text{if } n \text{ be odd} \end{cases} \quad \forall n \in N$
$\{I_n\}_{n=0}^{\infty}$	$v(I_0) = w_0, \; v(I_n) = \begin{cases} 4v(B_n) + w_0 & \text{if } n \text{ be even} \\ 4v(B_n) - 2w_1 & \text{if } n \text{ be odd} \end{cases} \quad \forall n \in N$
$\{J_n\}_{n=0}^{\infty}$	$v(J_0) = w_0, \; v(J_n) = \begin{cases} 6v(B_n) + w_0 & \text{if } n \text{ be even} \\ 6v(B_n) - 4w_1 & \text{if } n \text{ be odd} \end{cases} \quad \forall n \in N$
$\{K_n\}_{n=1}^{\infty}$	$v(K_n) = \begin{cases} 3v(B_n) & \text{if } n \text{ be even} \\ 3v(B_n) - 2w_1 & \text{if } n \text{ be odd} \end{cases} \quad \forall n \in N$
$\{L_n\}_{n=0}^{\infty}$	$v(L_0) = 3w_0, \; v(L_n) = 3v(C_n) + 3w_0 \quad \forall n \geq 1$
$\{M_n\}_{n=0}^{\infty}$	$v(M_0) = 6w_0, \; v(M_n) = 4v(C_n) + 6w_0 \quad \forall n \geq 1$
$\{N_n\}_{n=0}^{\infty}$	$v(N_0) = 6w_0, \; v(N_n) = 2v(C_n) + 6w_0 \quad \forall n \geq 1$
$\{O_n\}_{n=1}^{\infty}$	$v(O_1) = 9w_1, \; v(O_n) = 3v(D_n) - 2w_1 \quad \forall n \geq 2$
$\{P_n\}_{n=0}^{\infty}$	$v(P_0) = 3w_0, \; v(P_n) = 3v(E_n) \quad \forall n \geq 1$

Table 18.3 The recurrence relations for the optimal value of matching interdiction problem in the molecular graphs

$\{G_n\}$	$v(G_n - R^*)$
$\{F_n\}_{n=1}^{\infty}$	$v(F_1 - R^*) = 0, \; v(F_2 - R^*) = 2w_2$ $v(F_n - R^*) = \begin{cases} 3v(A_n) + v(A_n - R^*) & \text{if } n \text{ be even} \\ 3v(A_n) - 3w_1 + v(A_n - R^*) & \text{if } n \text{ be odd} \end{cases} \quad \forall n \geq 3$
$\{Q_n\}_{n=0}^{\infty}$	$v(G_0 - R^*) = 0, \; v(G_1 - R^*) = 0, \; v(G_2 - R^*) = 4w_2 + w_0$ $v(G_n - R^*) = \begin{cases} 5v(A_n) + v(A_n - R^*) + w_0 & \text{if } n \text{ be even} \\ 5v(A_n) + v(A_n - R^*) - 4w_1 & \text{if } n \text{ be odd} \end{cases} \quad \forall n \geq 3$
$\{H_n\}_{n=1}^{\infty}$	$v(H_2 - R^*) = 2w_2$ $v(H_n - R^*) = \begin{cases} 3v(B_n) + v(B_n - R^*) & \text{if } n \text{ be even} \\ 3v(B_n) - 3w_1 + v(B_n - R^*) & \text{if } n \text{ be odd} \end{cases} \quad \forall n \in N\backslash\{2\}$
$\{I_n\}_{n=0}^{\infty}$	$v(I_0 - R^*) = 0, \; v(I_1 - R^*) = 0, \; v(I_2 - R^*) = 2w_2 + w_0$ $v(I_n - R^*) = \begin{cases} 3v(B_n) + v(B_n - R^*) + w_0 & \text{if } n \text{ be even} \\ 3v(B_n) + v(B_n - R^*) - 2w_1 & \text{if } n \text{ be odd} \end{cases} \quad \forall n \geq 3$
$\{J_n\}_{n=0}^{\infty}$	$v(J_0 - R^*) = 0, \; v(J_1 - R^*) = 0, \; v(J_2 - R^*) = 4w_2 + w_0$ $v(J_n - R^*) = \begin{cases} 5v(B_n) + v(B_n - R^*) + w_0 & \text{if } n \text{ be even} \\ 5v(B_n) + v(B_n - R^*) - 4w_1 & \text{if } n \text{ be odd} \end{cases} \quad \forall n \geq 3$
$\{K_n\}_{n=1}^{\infty}$	$v(K_2 - R^*) = w_2$ $v(K_n - R^*) = \begin{cases} 2v(B_n) + v(B_n - R^*) & \text{if } n \text{ be even} \\ 2v(B_n) + v(B_n - R^*) - 2w_1 & \text{if } n \text{ be odd} \end{cases} \quad \forall n \in N\backslash\{2\}$
$\{L_n\}_{n=0}^{\infty}$	$v(L_0 - R^*) = w_0, \; v(L_n - R^*) = 2v(C_n) + v(C_n - R^*) + 3w_0 \quad \forall n \geq 1$

(continued)

Table 18.3 (continued)

$\{G_n\}$	$v(G_n - R^*)$
$\{M_n\}_{n=0}^{\infty}$	$v(M_0 - R^*) = 4w_0$, $v(M_n - R^*) = 3v(C_n) + v(C_n - R^*) + 6w_0$ $\forall n \geq 1$
$\{N_n\}_{n=0}^{\infty}$	$v(N_0 - R^*) = 4w_0$, $v(N_n - R^*) = v(C_n) + v(C_n - R^*) + 6w_0$ $\forall n \geq 1$
$\{O_n\}_{n=1}^{\infty}$	$v(O_1 - R^*) = 7w_1$, $v(O_n - R^*) = 2v(D_n) + v(D_n - R^*) - 2w_1$ $\forall n \geq 2$
$\{P_n\}_{n=0}^{\infty}$	$v(P_0 - R^*) = w_0$, $v(P_n - R^*) = 2v(E_n) + v(E_n - R^*)$ $\forall n \geq 1$

Table 18.4 The recurrence relations for the approximate value of matching interdiction problem in the molecular graphs

$\{G_n\}$	$v(G_n - R)$
$\{F_n\}_{n=1}^{\infty}$	$v(F_1 - R) = 0$, $v(F_2 - R) = 3w_2$ $v(F_n - R) = \begin{cases} 3v(A_n) + v(A_n - R) & \text{if } n \text{ be even} \\ 3v(A_n) - 3w_1 + v(A_n - R) & \text{if } n \text{ be odd} \end{cases}$ $\forall n \geq 3$
$\{Q_n\}_{n=0}^{\infty}$	$v(G_0 - R) = 0$ $v(G_n - R) = \begin{cases} 5v(A_n) + v(A_n - R) + w_0 & \text{if } n \text{ be even} \\ 5v(A_n) + v(A_n - R) - 4w_1 & \text{if } n \text{ be odd} \end{cases}$ $\forall n \in N$
$\{H_n\}_{n=1}^{\infty}$	$v(H_n - R) = \begin{cases} 3v(B_n) + v(B_n - R) & \text{if } n \text{ be even} \\ 3v(B_n) - 3w_1 + v(B_n - R) & \text{if } n \text{ be odd} \end{cases}$ $\forall n \in N$
$\{I_n\}_{n=0}^{\infty}$	$v(I_0 - R) = 0$ $v(I_n - R) = \begin{cases} 3v(B_n) + v(B_n - R) + w_0 & \text{if } n \text{ be even} \\ 3v(B_n) + v(B_n - R) - 2w_1 & \text{if } n \text{ be odd} \end{cases}$ $\forall n \in N$
$\{J_n\}_{n=0}^{\infty}$	$v(J_0 - R) = 0$ $v(J_n - R) = \begin{cases} 5v(B_n) + v(B_n - R) + w_0 & \text{if } n \text{ be even} \\ 5v(B_n) + v(B_n - R) - 4w_1 & \text{if } n \text{ be odd} \end{cases}$ $\forall n \in N$
$\{K_n\}_{n=1}^{\infty}$	$v(K_n - R) = \begin{cases} 2v(B_n) + v(B_n - R) & \text{if } n \text{ be even} \\ 2v(B_n) + v(B_n - R) - 2w_1 & \text{if } n \text{ be odd} \end{cases}$ $\forall n \in N$
$\{L_n\}_{n=0}^{\infty}$	$v(L_0 - R) = 2w_0$, $v(L_n - R) = 2v(C_n) + v(C_n - R) + 3w_0$ $\forall n \geq 1$
$\{M_n\}_{n=0}^{\infty}$	$v(M_0 - R) = 5w_0$, $v(M_n - R) = 3v(C_n) + v(C_n - R) + 6w_0$ $\forall n \geq 1$
$\{N_n\}_{n=0}^{\infty}$	$v(N_0 - R]) = 5w_0$, $v(N_n - R) = v(C_n) + v(C_n - R) + 6w_0$ $\forall n \geq 1$
$\{O_n\}_{n=1}^{\infty}$	$v(O_1 - R]) = 8w_1$, $v(O_n - R) = 2v(D_n) + v(D_n - R) - 2w_1$ $\forall n \geq 2$
$\{P_n\}_{n=0}^{\infty}$	$v(P_0 - R) = 2w_0$, $v(P_n - R) = 2v(E_n) + v(E_n - R)$ $\forall n \geq 1$

Table 18.5 The value of e_G in the molecular graphs

$\{G_n\}$	e_{G_n}	$\{G_n\}$	e_{G_n}
$\{F_n\}_{n=1}^{\infty}$	$e_{F_n} = \begin{cases} 1 & n = 1 \\ 2 & n \geq 2 \end{cases}$	$\{Q_n\}_{n=0}^{\infty}$	$e_{G_n} = \begin{cases} 1 & n = 0 \\ 2 & n \geq 1 \end{cases}$
$\{H_n\}_{n=1}^{\infty}$	$e_{H_n} = \begin{cases} 1 & n = 1 \\ 2 & n \geq 2 \end{cases}$	$\{I_n\}_{n=0}^{\infty}$	$e_{I_n} = \begin{cases} 1 & n = 0 \\ 2 & n \geq 1 \end{cases}$
$\{J_n\}_{n=0}^{\infty}$	$e_{J_n} = \begin{cases} 1 & n = 0 \\ 2 & n \geq 1 \end{cases}$	$\{K_n\}_{n=1}^{\infty}$	$e_{K_n} = \begin{cases} 1 & n = 1 \\ 2 & n \geq 2 \end{cases}$
$\{L_n\}_{n=0}^{\infty}$	$e_{L_n} = 2$ $\forall n \geq 0$	$\{M_n\}_{n=0}^{\infty}$	$e_{M_n} = 2$ $\forall n \geq 0$
$\{N_n\}_{n=0}^{\infty}$	$e_{N_n} = 2$ $\forall n \geq 0$	$\{O_n\}_{n=1}^{\infty}$	$e_{O_n} = 2$ $\forall n \geq 1$
$\{P_n\}_{n=0}^{\infty}$	$e_{P_n} = 2$ $\forall n \geq 0$		
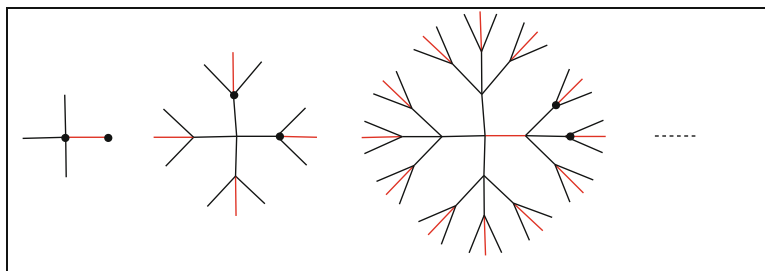
Fig. 18.4 The sequence of graphs $\{F_n\}_{n=1}^{\infty}$

For example, we explain how to compute the value of e_{F_n} for $n \geq 1$. The molecular graph F_n, where $n \geq 1$, is a sequence of graphs which is depicted in Fig. 18.4. By the weights of edges, we have

$$
\begin{aligned}
v(F_1) &= w_1 \\
v(F_2) &= 4w_2 \\
v(F_3) &= w_1 + 12w_3 \\
v(F_4) &= 4w_2 + 36w_4 \\
v(F_5) &= w_1 + 12w_3 + 108w_5 \\
&\vdots
\end{aligned}
$$

According to the weight of maximum matching in A_n (i.e., $v(A_n)$), it results

$$
\begin{aligned}
v(F_1) &= v(A_1) \\
v(F_2) &= 4v(A_2) \\
v(F_3) &= 4v(A_3) - 3w_1 \\
v(F_4) &= 4v(A_4) \\
v(F_5) &= 4v(A_5) - 3w_1 \\
&\vdots
\end{aligned}
$$

Hence, for each $n \in N$, we have

$$
v(F_n) = \begin{cases} 4v(A_n) & \text{if } n \text{ be even} \\ 4v(A_n) - 3w_1 & \text{if } n \text{ be odd} \end{cases} \tag{18.4}
$$

By Rel. (18.1), we have

$$
v(F_n - R) = v(F_n) - w_n \tag{18.5}
$$

Using Rels. (18.3), (18.4), and (18.5), it follows:

$$v(F_1 - R) = 0, \ v(F_2 - R) = 3w_2$$
$$v(F_n - R) = \begin{cases} 3v(A_n) + v(A_n - R) & \text{if } n \text{ be even} \\ 3v(A_n) - 3w_1 + v(A_n - R) & \text{if } n \text{ be odd} \end{cases} \quad \forall n \geq 3$$

It is obvious that $v(F_1 - R^*) = 0$ and $v(F_2 - R^*) = 2w_2$. For each $n \geq 3$, the set R^* in F_n is similar to the set R^* in A_n. Then, for each $n \geq 3$, we have

$$v(F_n - R^*) = \begin{cases} 3v(A_n) + v(A_n - R^*) & \text{if } n \text{ be even} \\ 3v(A_n) - 3w_1 + v(A_n - R^*) & \text{if } n \text{ be odd} \end{cases}$$

The relations related to the graphs A_n and F_n help us to obtain the following relation:

$$e_{F_n} = \begin{cases} 1 & n = 1 \\ 2 & n \geq 2 \end{cases}$$

Similar to the above method for the graph F_n, we can obtain $v(G_n)$ and e_{G_n} for each molecular graph G_n in Figs. 18.2 and 18.3.

Therefore, we can conclude that the value of e_{G_n} in each molecular graph of Figs. 18.2 and 18.3 is equal to two when $n \geq 2$.

References

Akgun I, Tansel BC, Wood RK (2011) The multi-terminal maximum-flow network-interdiction problem. Eur J Oper Res 211:241–251

Altner DS, Ergun O, Uhan NA (2010) The maximum flow network interdiction problem: valid inequalities, integrality gaps, and approximability. Oper Res Lett 38:33–38

Ashrafi AR, Cataldo F, Iranmanesh A, Ori O (eds) (2013) Topological modelling of nanostructures and extended systems, Carbon material: chemistry and physics 7. Springer, Dordrecht/New York

Assimakopoulos N (1987) A network interdiction model for hospital infection control. Comput Biol Med 17:413–422

Bazgan C, Toubaline S, Tuza Z (2011) The most vital nodes with respect to independent set and vertex cover. Discret Appl Math 159:1915–2204

Behmaram A, Yousefi-Azari H, Ashrafi AR (2013) On the number of matchings and independent sets in (3,6)-fullerenes. MATCH Commun Math Comput Chem 70:525–532

Corley HW, Sha DY (1982) Most vital links and nodes in weighted network. Oper Res Lett 1:157–160

Diudea MV, Nagy CL, Bende A (2012) On diamond D_5. Struct Chem 23:981–986

Israeli E, Wood RK (2002) Shortest path network interdiction. Networks 40:97–111

McMasters AW, Mustin TM (1970) Optimal interdiction of a supply network. Naval Res Log Q 17:261–268

Newkome GR, Moorefield CN, Vögtle F (2001) Dendrimers and dendrons: concepts, syntheses, applications. Wiley-VCH, Weinheim

Ratliff HD, Sicilia GT, Lubore SH (1975) Finding the n most vital links in flow networks. Manag Sci 21:531–539

Shen S, Smith JC, Goli R (2012) Exact interdiction models and algorithms for disconnecting networks via node deletions. Discret Optim 9:172–188

Wood RK (1993) Deterministic network interdiction. Math Comput Modell 17:1–18

Yousefi-Azari H, Ashrafi AR (2012) Computing PI index of micelle-like chiral dendrimers. Bulg Chem Commun 44:307–309

Zenklusen R (2010) Matching interdiction. Discret Appl Math 158:1676–1690

Chapter 19
Nullity of Graphs

Modjtaba Ghorbani and Mahin Songhori

Abstract The nullity of a graph is defined as the multiplicity of the eigenvalue zero of graph G which is named the nullity of G denoted by $\eta(G)$. In this chapter we investigate the nullity of some family of graphs.

19.1 Introduction

Let $G = (V, E)$ be a graph and $e \in E(G)$. Then denoted by $G \backslash e$ is the subgraph of G obtained by removing the edge e from G. Denoted by $G \backslash \{v_1, \ldots, v_k\}$ means a graph obtained by removing the vertices $v_1, \ldots, v_k$ from G and all edges incident to any of them.

The adjacency matrix $A(G)$ of graph G with vertex set $V(G) = \{v_1, v_2, \ldots, v_n\}$ is the $n \times n$ symmetric matrix $[a_{ij}]$ such that $a_{ij} = 1$ if v_i and v_j are adjacent and 0, otherwise. The characteristic polynomial of graph G is

$$\chi_G(\lambda) = \chi_\lambda(G) = \det(A(G) - \lambda I),$$

The roots of the characteristic polynomial are the eigenvalues of graph G and form the spectrum of this graph. The number of zero eigenvalues in the spectrum of the graph G is called the nullity of G which is denoted by $\eta(G)$. Suppose $r(A(G))$ is the rank of $A(G)$; it is a well-known fact that $\eta(G) = n - r(A(G))$.

A null graph is a graph in which all vertices are isolated. In other words, a graph has no edges, only vertices called the null graph. It is clear that $\eta(G) = n$ if and only if G is a null graph; see Cvetković et al. (1980).

M. Ghorbani (✉) • M. Songhori
Department of Mathematics, Faculty of Science, Shahid Rajaee Teacher Training University, Tehran 16785-136, Iran
e-mail: mghorbani@srttu.edu

19.2   Main Results

In this section, we study the properties of graph nullity with applications in chemistry. Throughout this chapter, all notations are standard and mainly taken from Biggs (1993) and Cvetković and Gutman (2009). Throughout this chapter, all notations are standard and mainly taken from Cvetković et al. (1975), Godsil and McKay (1978), Biggs (1993), Li and Shiu (2007) and Cvetković and Gutman (2009).

Theorem 19.2.1 Suppose that G is a simple graph on n vertices and $n \geq 2$. Then $\eta(G) = n - 2$ if and only if $A(G)$ is permutation similar to matrix $O_{n1;n1} \bigoplus O_{n2;n2} \bigoplus O_{k;k}$, where $n_1 + n_2 + k = n$, $n_1; n_2 > 0$, and $k \geq 0$.

Theorem 19.2.2 (Cheng and Liu 2007) Suppose that G is a simple graph on n vertices. Then $\eta(G) = n - 3$ if and only if $A(G)$ is permutation similar to matrix $O_{n1;n1} \bigoplus O_{n2;n2} \bigoplus O_{n3;n3} \bigoplus O_{k;k}$, where $n_1 + n_2 + n_3 + k = n$, $n_1; n_2; n_3 > 0$ and $k \geq 0$.

Lemma 19.2.3 (Cvetković et al. 1980)

(i) The adjacency matrix of the complete graph K_n, $A(K_n)$ has 2 distinct eigenvalues $n - 1$, -1 with multiplicities 1, $n - 1$, respectively, where $n > 1$.
(ii) The eigenvalues of C_n are $\lambda_r = \frac{2\cos 2r}{n}$, where $r = 0, \ldots, n - 1$.
(iii) The eigenvalues of P_n are $\lambda_r = \frac{2\cos 2r}{n+1}$, where $r = 1, 2, \ldots, n$.

Lemma 19.2.4

(i) Let H be an induced subgraph of G. Then $r(H) \leq r(G)$.
(ii) Let $G = G_1 + G_2$, then $r(G) = r(G_1) + r(G_2)$, i.e., $\eta(G) = \eta(G_1) + \eta(G_2)$.

Proposition 19.2.5 Let $= G_1 \cup G_2 \cup \ldots \cup G_t$, where $G_1, G_2, \ldots, G_t$ are connectedcomponents of G. Then

$$\eta(G) = \sum_{i=1}^{t} \eta(G_i).$$

Proposition 19.2.6 (Cheng and Liu 2007) Let G be a simple graph on n vertices and K_p be a subgraphof G, where $2 \leq p \leq n$. Then $\eta(G) \leq n - p$.

A clique of a simple graph G is a subset S of $V(G)$ such that $G[S]$ is complete. A clique S is maximum if G has no clique S' with $|S'| > |S|$. The number of vertices in a maximum clique of G is called the clique number of G and is denoted by $\omega(G)$. The following inequality is resulted from Proposition 19.2.6.

Corollary 19.2.7 (Cheng and Liu 2007)

(i) Let G be a simple graph on n vertices and G is not isomorphic to nK_1. Then $\eta(G) + \omega(G) \leq n$.

(ii) Let G be a simple graph on n vertices and let C_p be an induced subgraph of G, where $3 \leq p \leq n$. Then

$$\eta(G) \leq \begin{cases} n - p + 2; & \text{if } p \equiv 0 \pmod 4 \\ n - p; & \text{otherwise} \end{cases}.$$

The length of the shortest cycle in a graph G is the girth of G. denoted by $\text{gir}(G)$. A relation between $\text{gir}(G)$ and $\eta(G)$ is as follows:

If G is simple graph on n vertices and G has at least one cycle, then

$$\eta(G) \leq \begin{cases} n - \text{gir}(G) + 2; & \text{if } p \equiv 0 \pmod 4 \\ n - \text{gir}(G) & \text{otherwise} \end{cases}.$$

Corollary 19.2.8 (Cheng and Liu 2007) Suppose x and y are two vertices in G and there exists an $(x; y)$- path in G. Then

$$\eta(G) \leq \begin{cases} n - d(x; y) & \text{if } d(x; y) \text{ is even;} \\ n - d(x; y) - 1; & \text{otherwise.} \end{cases}$$

Corollary 19.2.9 (Cheng and Liu 2007) Suppose G is simple connected graph on n vertices. Then

$$\eta(G) \leq \begin{cases} n - \text{diam}(G) & \text{if } \text{diam}(G) \text{ is even;} \\ n - \text{diam}(G) - 1; & \text{otherwise.} \end{cases}$$

Proposition 19.2.10 Denote by $\chi_G(\lambda)$ the characteristic polynomial of G. Let $\chi_G(\lambda) = |\lambda I - A| = \lambda_n + a_1\lambda_{n-1} + \ldots + a_n$. Then

$$a_i = \sum_U (-1)^{p(U)} 2^{c(U)} \ (i = 1, 2, \ldots, n), \tag{19.1}$$

where the sum is over all subgraphs U of G consisting of disjoint edges and cycles and having exactly i vertices (called "basic figures"). If U is such a subgraph, then $p(U)$ is the number of its components, of which $c(U)$ components are cycles.

Example 19.2.11 In Fig. 19.1, the graph G and its basic figures H_1, H_2, and H_3 are shown.
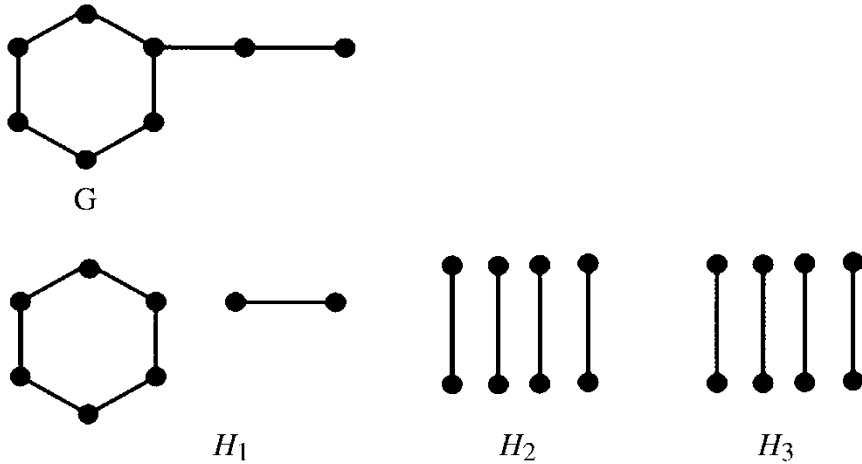
Fig. 19.1 Graph G and its basic figures H_1, H_2, and H_3

For some special classes of bipartite graphs, it is possible to find easily the relation between the structure of G and $\eta(G)$. The problem is solved for trees by the following theorem.

Theorem 19.2.12 (Cvetković and Gutman 1972; Li et al. 2007) Let T be a tree on $n \geq 1$ vertices and let m be the size of its maximum matching. Then its nullity is equal to $\eta(T) = n - 2m$.

This theorem is an immediate consequence of the statement concerning with the coefficients of the characteristic polynomial of the adjacency matrix of a tree (which can be easily deduced from Eq. (19.1)). Theorem 19.2.12 is a special case of one more general theorem that will be formulated in the following.

Recall that a set M of edges of G is a matching if every vertex of G is incident with at most one edge in M; it is a perfect matching if every vertex of G is incident with exactly one edge in M. Maximum matching is a matching with the maximum possible number of edges. The size of a maximum matching of G, i.e., the maximum number of independent edges of G, is denoted by $m = m(G)$.

Theorem 19.2.13 (Cvetković et al. 1972) If a bipartite graph G with $n \geq 1$ vertices does not contain any cycle of length $4s$ $(s = 1, 2, \ldots)$, then $\eta(G) = n - 2m$, where m is the size of its maximum matching.

Theorem 19.2.14 (Longuet−Higgins 1950) For the bipartite graph G with n vertices and incidence matrix, $\eta(G) = n - 2r(B)$, where $r(B)$ is the rank of B.

Since for $G = (X, Y, U)$, we have $r(B) \leq \min(|X|, |Y|)$ and Theorem 19.2.14 yields the following:

Corollary 19.2.15 (Cvetković and Gutman 1972) $\eta(G) \geq \max(|X|, |Y|) - \min(|X|, |Y|)$.

If the number of vertices is odd, then $|X| \neq |Y|$ and $\eta(G) > 0$. Thus a necessary condition to have no zeros in the spectrum of a bipartite graph is that the number of

vertices is even. The following three theorems enable, in special cases, the reduction of the problem of determining $\eta(G)$ for some graphs to the same problem for simpler graphs.

Theorem 19.2.16 (Cvetković and Gutman 1972) Let $G_1 = (X_1, Y_1, U_1)$ and $G_2 = (X_2, Y_2, U_2)$, where $|X_1| = n_1, |Y_1| = n_2, n_1 \leq n_2$, and $\eta(G_1) = n_2 - n_1$. If the graph G is obtained from G_1 and G_2 by joining (any) vertices from X_1 to vertices in Y_2 (or X_2), then the relation $\eta(G) = \eta(G_1) + \eta(G_2)$ holds.

Corollary 19.2.17 (Cvetković et al. 1972) If the bipartite graph G contains a pendent vertex, and if the induced subgraph H of G is obtained by deleting this vertex together with the vertex adjacent to it, then

$$\eta(G) = \eta(H)$$

Corollary 19.2.18 Let G_1 and G_2 be bipartite graphs. If $\eta(G_1) = 0$, and if the graph G is obtained by joining an arbitrary vertex of G_1 by an edge to an arbitrary vertex of G_2, then $\eta(G) = \eta(G_2)$.

Theorem 19.2.19 (Cvetković et al. 1972)

 (i) A path with four vertices of degree 2 in a bipartite graph G can be replaced by an edge without changing the value of $\eta(G)$.
(ii) Two vertices and the four edges of a cycle of length 4, which are positioned in a bipartite graph G, can be removed without changing the value of $\eta(G)$.

Theorem 19.2.20 (Gutman and Sciriha 2001) If T is a tree, then $L(T)$ is either nonsingular or has nullity one.

Proposition 19.2.21 Let $H = K_{p,q}$ be a complete bipartite graph on $p + q = n$ vertices. Then

$$\chi_\lambda(H) = \frac{n\lambda + 2pq}{\lambda^2 - pq}.$$

Definition 19.2.22 Let H be a labeled graph on n vertices. Let G be a sequence of n rooted graphs $G, G_1, \ldots, G_n$. Then by $H(G)$ we denote the graph obtained by identifying the root of G_i with the i-th vertex of H. We call $H(G)$ the *rooted product* of H by G.

Figure 19.2 illustrates this construction with H the path on three vertices and G consisting of three copies of the rooted path on two vertices.

Definition 19.2.23 Given a labeled graph H on n vertices and a sequence G of n rooted graphs, we define the matrix $A_\lambda(H, G)$ as follows:

Fig. 19.2 Rooted product P_3 with P_2

$$A_\lambda(H, G) = (a_{ij})$$

Where

$$a_{ij} = \begin{cases} G_i(\lambda) , & i = j \\ -h_{ij}G_i{}'(\lambda) , & i \neq j \end{cases}.$$

and $A(H) = (h_{ij})$ is the adjacency matrix of H.

If, for example, H and G are represented in Fig. 19.2, then $A_\lambda(H, G) = (a_{ij})$ is the matrix

$$\begin{pmatrix} \lambda^2 - 1 & -\lambda & 0 \\ -\lambda & \lambda^2 - 1 & -\lambda \\ 0 & -\lambda & \lambda^2 - 1 \end{pmatrix}.$$

Lemma 19.2.24 (Ghorbani 2014) Let K and L be rooted graphs, and let $K \bullet L$ denote the graph obtained by identifying the roots of K and L. Then

$$\chi_{K \bullet L}(\lambda) = \chi_K(\lambda)\chi_{L'}(\lambda) + \chi_{K'}(\lambda)\chi_L(\lambda) - \lambda\chi_{K'}(\lambda)\chi_{L'}(\lambda).$$

Proposition 19.2.25 (Guo et al. 2009) Let v be any vertex (which does not need to be a cut point) of a graph G with order at least 2. Then

$$\eta(G) - 1 \leq \eta(G - v) \leq \eta(G) + 1.$$

Theorem 19.2.26 (Guo et al. 2009) Let v be a cut point of a graph G of order n and $G_1, G_2, \ldots, G_s$ be all components of $G - v$. If there exists a component, say G_1, among $G_1, G_2, \ldots, G_s$ such that $\eta(G_1) = \eta(G_1 + v) + 1$, then

$$\eta(G) = \eta(G - v) - 1 = \sum_{i=1}^{s} \eta(G_i) - 1.$$

Theorem 19.2.27 (Guo et al. 2009) Let v be a cut$-$point of a graph G of order n and G_1 be a component of $G - v$. If $\eta(G_1) = \eta(G_1 + v) - 1$, then

$$\eta(G) = \eta(G_1) + \eta(G - G_1).$$

Theorem 19.2.28 (Guo et al. 2009) Suppose G and H are two graphs with eigenvalues $\lambda_i \, (1 \leq i \leq n)$ and $\mu_j \, (1 \leq j \leq m)$. Then the eigenvalues of Cartesian product $G \times H$ are $\lambda_i + \mu_j$.

As a corollary of Theorem 19.2.28, we compute the nullity of the hypercube $H_n = K_2 \times \underbrace{\ldots}_{n \, \text{times}} \times K_2$. It is a well-known fact that the spectrum of K_n is as follows:

$$\text{Spec}(K_n) = \begin{pmatrix} -1 & n-1 \\ n-1 & 1 \end{pmatrix}.$$

So, the eigenvalues of H are ± 1 with multiplicity 1. According to Theorem 19.2.28,

$$\text{Spec}(K_2 \times K_2) = \begin{pmatrix} -2 & 0 & 2 \\ 1 & 2 & 1 \end{pmatrix}.$$

By continuing this method, one can see that the spectrum of $K_2 \times \cdots \times K_2$ is:

$$
\begin{aligned}
&\text{Spec}(K_2 \times \cdots \times K_2) \\
&= \begin{cases}
\begin{pmatrix} -n & \cdots & -2 & 0 & 2 & \cdots & n \\ 1 & \cdots & \binom{n}{(n-2)/2} & \binom{n}{n/2} & \binom{n}{(n+2)/2} & \cdots & 1 \end{pmatrix} & 2 \mid n \\
\begin{pmatrix} -n & 2-n & \cdots & -1 & 1 & \cdots & n-2 & n \\ 1 & \binom{n}{1} & \cdots & \binom{n}{(n-2)/2} & \binom{n}{n/2} & \cdots & \binom{n}{n-1} & 1 \end{pmatrix} & 2 \nmid n
\end{cases}.
\end{aligned}
$$

This implies the nullity of K_n is as follows:

$$\eta(K_n) = \begin{cases} \binom{n}{n/2} & 2 \mid n \\ 0 & 2 \nmid n \end{cases}.$$

Example 19.2.29 Consider graph G_r, with r hexagons depicted in Fig. 19.3a. By using Theorem 19.2.19, it is easy to see that $\eta(G_r) = \eta(G_{r-1}) \, (r = 1, 2, \ldots)$. By induction on r, it is clear that $\eta(G_r) = 0$. Now consider graph H_r (Fig. 19.3b). Since this graph has a pendent vertex, so by Corollary 19.2.15, $\eta(H_r) = \eta(T_{r-1})$. Again
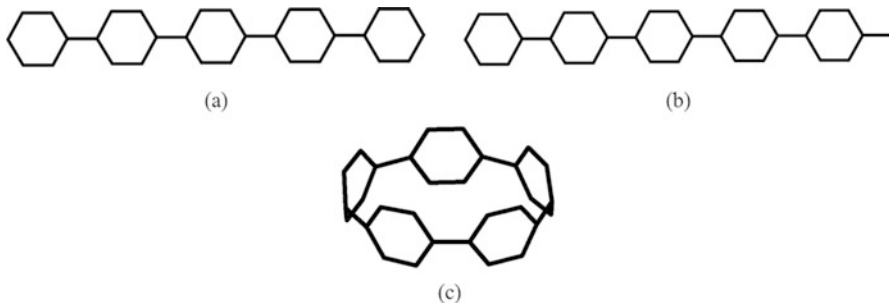
Fig. 19.3 (**a**) Graph G_r, (**b**). Graph H_r, (**c**). Graph T_{r-1}

use Theorem 19.2.27 and then we have $\eta(T_{r-1}) = \eta(H_{r-1})$. By continuing this method we see that $\eta(H_r) = \eta(H_1).H_1$, has a pendent vertex joined to a hexagon. Theorem 19.2.28 implies that $\eta(H_1) = \eta(P_5)$. Corollary 19.2.18 results that $\eta(H_r) = \eta(P_5) = 1$.

Here, by using Theorem 19.2.13, we compute the nullity of triangular benzenoid graph $G[n]$, depicted in Fig. 19.4. The maximum matching of $G[n]$ is depicted in Fig. 19.5. In other words, to obtain the maximum matching at first we color the boundary edges, they are exactly $3 \times n$ edges. The number of colored vertical edges in the $k-$th row is $k - 1$. Hence, the number of colored vertical edges is $1 + 2 + \ldots + n - 2 = (n - 1)(n - 2)/2$. By summation of these values, one can see that the number of colored edges are $3n + (n - 1)(n - 2)/2 = (n^2 + 3n + 2)/2$ which is equal to the size of maximum matching. This graph has $n^2 + 4n + 1$ vertex, $3(n^2 + 3n)/2$ edges and by using Theorem 19.2.13, $\eta(G[n]) = n^2 + 4n + 1 - (n^2 + 3n + 2) = n - 1$, thus we proved the following Theorem.

Theorem 19.2.30 $\eta(G[n]) = n - 1$.

Definition 19.2.31 Let G_1 be a graph containing a vertex u, and let G_2 be a graph of order n that is disjoint from G_1. For $1 \le k \le n$, the k-joining graph of G_1 and G_2 with respect to u, denoted by $G_1(u) \bigotimes^k G_2$, is obtained from $G_1 \cup G_2$ by joining u and arbitrary k vertices of G_2. Note that in above definition, the graph $G_1(u) \bigotimes^k G_2$ is indefinite in some extent, and there are $\binom{n}{k}$ such graphs. In addition, if G_1 is a tree, then G_1 is called a pendant tree of $\ldots G_1(u) \bigotimes^k G_2$ and $G_1(u) \bigotimes^k G_2$ is said a graph with pendant tree. Let $= G_1 \bigoplus G_2 \bigoplus \ldots \bigoplus G_t$. Then $\eta(G) = \sum_{i=1}^{n} \eta(G_i)$.

Lemma 19.2.32 (Guo et al. 2009) Let T be a tree containing a vertex v. The following are equivalent:

1. v is mismatched in T.
2. $\mu(T - v) = \mu(T)$;.
3. $\eta(T - v) = \eta(T) - 1$.

Fig. 19.4 Graph of
triangular benzenoid $G[n]$
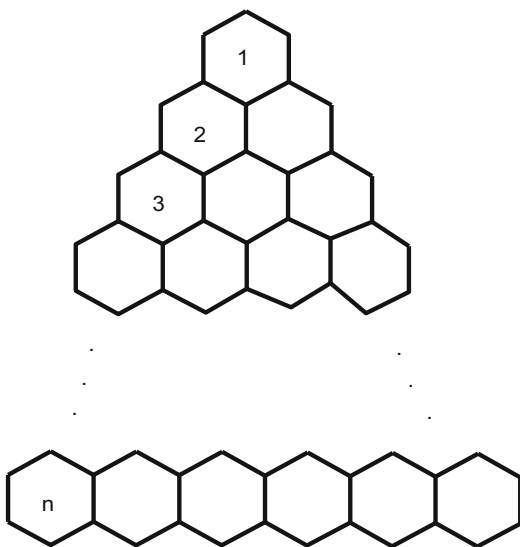
Fig. 19.5 Graph of
triangular benzenoid $G[n]$
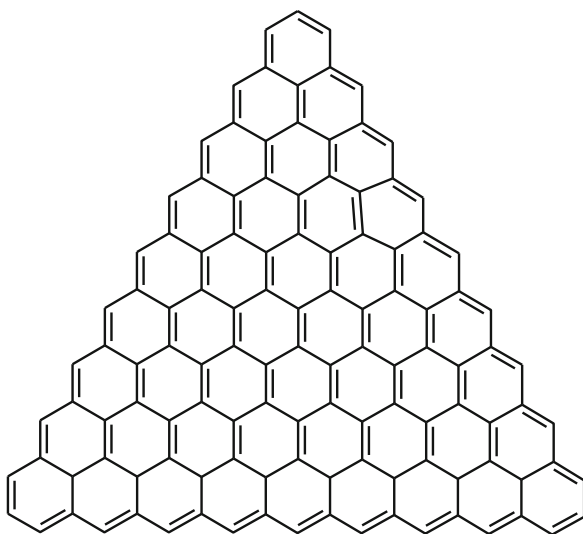
Lemma 19.2.33 (Guo et al. 2009) If v is a quasi-pendant vertex of a tree T, then v is matched in T.

Lemma 19.2.34 (Guo et al. 2009) If v is a mismatched vertex of a tree T, then for any neighbor u of v, u is matched in T and is also matched in the component of $T - v$ that contains u.

19.2.1   Nullity of Graphs with Pendant Trees

Theorem 19.2.1.1 (Guo et al. 2009) Let T be a tree with a matched vertex u and let G be a graph of order n. Then for each integer $k(1 \leq k \leq n)$,

$$\eta\left(T(u) \bigotimes G\right) = \eta(T) + \eta(G).$$

Corollary 19.2.1.2 (Guo et al. 2009) Let T be a PM-tree and G be a graph of order n. Then for each integer k ($1 \leq k \leq n$) and for every vertex $u \in T$, $\eta\left(T(u) \bigotimes^k G\right) = \eta(G)$.

Theorem 19.2.1.3 Let T be a tree with a mismatched vertex u and let G be a graph of order n. Then for each integer $k(1 \leq k \leq n)$,

$$\eta\left(T(u) \overset{k}{\bigotimes} G\right) = \eta(T - u) + \eta(G + u) = \eta(T) + \eta(G + u) - 1.$$

In the following Theorem denoted by H means a reduced form of bicyclic graphs. In other words, in H all paths of length 4 are replaced by an edge.

Theorem 19.2.1.4 Let G be a bicyclic graph as depicted in Fig. 19.6, then
$$\eta(G) = \begin{cases} \|T\| - 2\mu(T) + \alpha & v \text{ is matched} \\ \|T\| - 2\mu(T) - 1 + \beta & v \text{ is mismatched} \end{cases} "$$
where

$$\alpha = \begin{cases} 0 & 2|n, m \\ 1 & 2|n, 2|m \\ 2 & 2|n, m \end{cases} \quad \text{and} \quad \beta = \begin{cases} 0 & H \cong G_1, G_8 \\ 3 & H \cong G_2 \\ 1 & H \cong G_3, G_4, G_5, G_6, G_7, G_9 \end{cases},$$

and the number of vertices of graph G is denoted by $\|G\|$.

Proof According to Lemma 19.2.32, we should to consider two cases:

- *Case 1*: v is matched and

$$\alpha = \begin{cases} 0 & 2|n, m \\ 1 & 2 \nmid n, 2|m \\ 2 & 2|n, 2 \nmid m \end{cases}.$$

In this case one can see that $G \cong T(v) \bigodot^4 P_n \cup P_m$ and so,

$$\eta(G) = \eta(T) + \eta(P_n) + \eta(P_m) = \|T\| - 2\mu(T) + \alpha.$$

Fig. 19.6 Two cycles coincide in a vertex
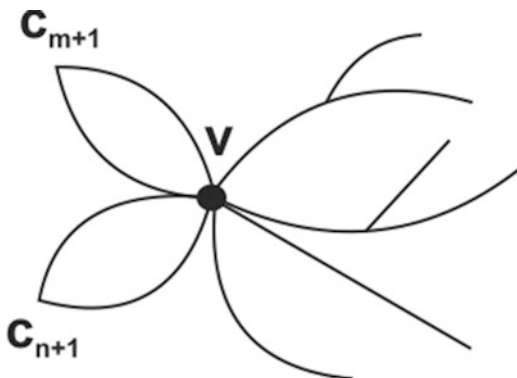
- *Case 2*: v is mismatched:

  In this case one can see that

  $$
  \begin{aligned}
  \eta(T(v)\odot^4 P_n \cup P_m) &= \eta(T - v) + \eta(P_n \cup P_m + v) \\
  &= ||T|| - 2\mu(T) + \eta(P_n \cup P_m + v) - 1 \\
  &= ||T|| - 2\mu(T) + \eta(H) - 1 \\
  &= ||T|| - 2\mu(T) + \eta(H) - 1.
  \end{aligned}
  $$

Let $\beta = \eta(H)$. By Corollary 19.2.17 we have to compute just the nullity of graphs $G_1, \ldots, G_6$ reported in Table 19.1 and this completes the proof.

Suppose G is a unicyclic graph with n vertices and the length of this cycle be l. If G is a cycle C_l or a cycle C_l with pendent edges at some or all vertices of C_l, we call G a canonical unicyclic graph. If G is not canonical, G contains at least one pendent star H_1 such that $G_1^* = G - H_1$ is also a unicyclic graph. We call the procedure of obtaining $G - H_1$ from G a "deleting operator." With repeated applications of the "deleting operators," then a canonical unicyclic graph, denoted by G^*, is obtained from G.

Lemma 19.2.1.5 (Guo et al. 2009) Suppose G is a unicyclic graph with n vertices and the length of the cycle in G is l. Let G^* be the graph defined above. Then $\eta(G) = n - 2v(G) - 1$ if $G^* = C_l$ and l is odd, $\eta(G) = n - 2v(G) + 2$ if $G^* = C_l$ and $l = 0 \pmod 4$, and $\eta(G) = n - 2v(G)$ otherwise.

Denoted by $C_{n,l,k}$ means a cycle graph with n vertices, k pendent stars, and l pendent vertices. We have the following Theorem.

Theorem 19.2.1.6

$$
\eta(C_{n,l,k}) = ||C_{n,l,k}|| - 2k - 2\omega +
\begin{cases}
-1 & 2|n \\
2 & 4|n \\
0 & \text{otherwise}
\end{cases},
$$

where $\omega = \max\{[n/2], l\}$.

Table 19.1 The nullity of graphs $G_1, \ldots, G_9$

G_1	G_2	G_3
$\eta = 0$	$\eta = 1$	$\eta = 0$
G_4	G_5	G_6
$\eta = 1$	$\eta = 1$	$\eta = 3$
G_7	G_8	G_9
$\eta = 1$	$\eta = 0$	$\eta = 1$

Proof By Corollary 19.2.17, one can remove the pendent vertices from G without changing in nullity of G. In other words, $\eta(G) = \eta(C_{l,n,k})$. According to Lemma 19.2.33, it is easy to see that

$$\eta(G) = (n_1 - 2) + \cdots + (n_k - 2) + \eta(C_{n,l}).$$

Let $\omega = \max\left\{ \left[\frac{n}{2}\right], l \right\}$, then $\eta(C_{n,l}) = n + l - 2\omega + \begin{cases} -1 & 2 \mid n \\ 2 & 4 \mid n \\ 0 & \text{otherwise} \end{cases}$.

This implies that

$$\eta(G) = \sum_{i=1}^{k} n_i - 2k + n + l - 2\omega + \begin{cases} -1 & 2 \mid n \\ 2 & 4 \mid n \\ 0 & \text{otherwise} \end{cases}$$

$$= \|G\| - 2k - 2\omega + \begin{cases} -1 & 2 \mid n \\ 2 & 4 \mid n \\ 0 & \text{otherwise} \end{cases}.$$

Suppose C_i is a cycle and put $C_i^* = C_i + u_i$ (a vertex u_i is added to cycle C_i). Now join to k vertices of a star graph on n vertices the graph C_i^*. We denote this graph by $S_{n,k,l}$ in which $l = n - k$ (as depicted in Fig. 19.7). We also recall a cycle whose length is an odd number by odd cycle. In the following Theorem we can obtain a bound for the nullity of $S_{n,k,l}$.

Fig. 19.7 The graph $S_{n,k,l}$
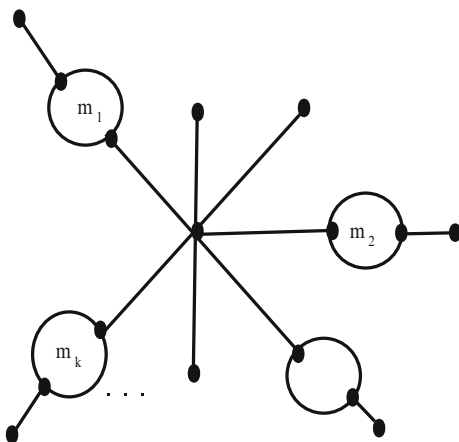
Theorem 19.2.1.7 Let r be the number of odd cycles in $S_{n,k,l}$. Then

$$1 + l + 2r \leq \eta(S_{n,k,l}) \leq 1 + l + 4r.$$

Proof Let n_i be the number of vertices of C_i^*. Remove the pendent vertices attached to r odd cycles. By Corollary 19.2.17 the nullity of resulted graph is the same as G. On the other hand, the resulted graph is bipartite and so by using Theorem 19.2.13, it is enough to compute its maximum matching as follows:

$$\mu(G) = \sum_{i=1}^{r} [n_i/2] + \sum_{i=r+1}^{k} \left([n_i/2] - 1 \right).$$

Since for every integer number x, $x - 1 \leq [x] \leq x$ and $\sum_{i=1}^{k} n_i + l + 1 = n$, then

$$\frac{1}{2}\sum_{i=1}^{k} n_i - \sum_{i=1}^{r} 2 \leq \mu(G) \leq \frac{1}{2}\sum_{i=1}^{k} n_i - \sum_{i=1}^{r} 1$$
$$\Rightarrow \frac{1}{2}(n - l - 1) - r \leq \mu(G) \leq \frac{1}{2}(n - l - 1) - r$$
$$\Rightarrow 1 + l + 2r \leq \eta(G) \leq 1 + l + 4r.$$

Let C_n be a cycle on n vertices, we recall that $\eta(C_n) = 0$ if $n \not\equiv 0 \pmod 4$ and $\eta(C_n) = 2$ otherwise. Consider the graph G depicted in Fig. 19.8. If the central cycle has n vertices and the number of cycles of length $4s$ ($s = 1, 2, \ldots$) of G is m, then we show this graph by $C_{n,m}$ and the nullity of this graph is as follows.

Fig. 19.8 The graph
$G = C_{n,\,k}$
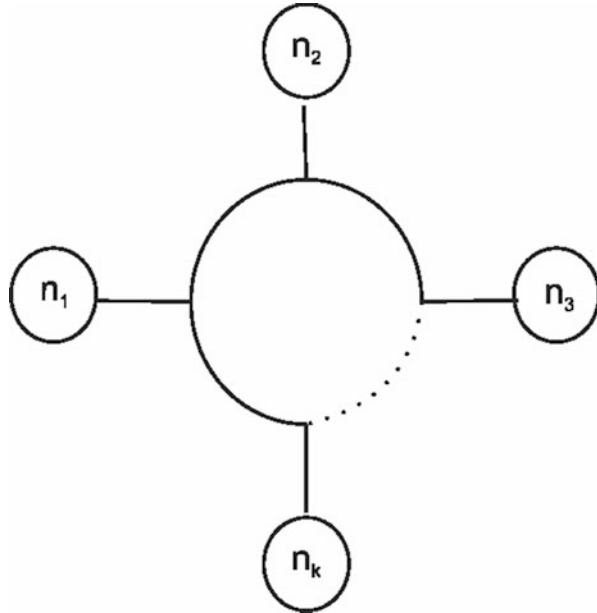
Theorem 19.2.1.8 Let n is an even number, then

$$\eta\big(C_{m,\,n}\big) = n + 2m - 1 + \alpha,$$

where,

$$\alpha = \begin{cases} 2 & 4\,|\,n \\ 0 & \text{otherwise} \end{cases}.$$

Proof By Theorem 19.2.13 one can remove all cycles of length s, $s \not\equiv 0 \pmod 4$ and by Theorem 19.2.13, one can replace all $4s$ ($s = 1, 2, \ldots$) with C_4. Thus the resulted graph is composed of a central cycle with n vertices together m cycles C_4 attached to it. Again using Lemma 19.2.3 (*vii*) results a canonical cycle graph $C_{n,m}$ together with m isolated vertices. Since the final graph is bipartite, apply Lemma 19.2.4 and the proof is completed.

19.2.2 Unicyclic Graphs with a Given Nullity

In this section, we deal with connected unicyclic graphs. Let G be a unicyclic graph and let C be the unique cycle of G. For each vertex $v \in C$, denote by $G\{v\}$ an induced

connected subgraph of G with maximum possible of vertices, which contains the vertex v and contains no other vertices of C. One can find that $G\{v\}$ is a tree and G is obtained by identifying the vertex v of $G\{v\}$ with the vertex v on C for all vertices $v \in C$. The unicyclic graph G is said to be of *Type I* if there exists a vertex v on the cycle such that v is matched in $G\{v\}$; otherwise, G is said to be of *Type II*.

Theorem 19.2.2.1 (Guo et al. 2009) Let G be a unicyclic graph and let C be the cycle of G. If G is of *Type I* and let $v \in C$ be matched in $G\{v\}$, then $\eta(G) = \eta(G\{v\})$ $+\eta(G - G\{v\})$. If G is of *Type II*, then $\eta(G) = \eta(G - C) + \eta(C)$.

Corollary 19.2.2.2 (Guo et al. 2009) Let G be a unicyclic graph with $\eta(G) = k$, and let C_l be the cycle of G. If G is of *Type I* and let $v \in C_l$ be matched in $G\{v\}$, then $\eta(G\{v\}) + \eta(G - G\{v\}) = k$. If G is of *Type II* and $l = 0 \pmod 4$, then $\eta(G - C_l)$ $= k - 2$; otherwise, $\eta(G - C_l) = k$.

Lemma 19.2.2.3 (Guo et al. 2009) Suppose G is a unicyclic graph with n vertices and the length l of the cycle C_l in G is odd. Then $\eta(G) = n - 2\mu(G) - 1$ *if* $\mu(G)$ $= \frac{l-1}{2} + \mu(G - C_l)$ and $\eta(G) = n - 2\mu(G)$ otherwise.

Lemma 19.2.2.4 (Guo et al. 2009) Suppose G is a unicyclic graph with n vertices and the length l of the cycle C_l in G is even. If $\mu(G) \neq \frac{l}{2} + \mu(G - C_l)$ or $\mu(G)$ $= \frac{l}{2} + \mu(G - C_l)$ and $l = 2 \pmod 4$, then $\eta(G) = n - 2\mu(G)$.

Lemma 19.2.2.5 (Guo et al. 2009) Suppose G is a unicyclic graph with n vertices and cycle C_l of length $l = 0 \pmod 4$, and $\mu(G) = \frac{l}{2} + \mu(G - C_l)$. Let E_1 be the set of edges of G between C_l and $G - C_l$ and E_2 be a matching of G with $\mu(G)$ edges. Then $\eta(G) = n - 2\mu(G) + 2$ if $E_1 \cap M = \varnothing$ for all $M \in E_2$, and $\eta(G) = n - 2\mu(G)$ otherwise.

Theorem 19.2.2.6 Suppose G is a unicyclic graph with n vertices and the cycle in G is C_l. Let E_1 be the set of edges of G between C_l and $G - C_l$ and E_2 the set of matchings of G with $\mu(G)$ edges. Then

1. $\eta(G) = n - 2\mu(G) - 1$ if $\mu(G) = \frac{l-1}{2} + \mu(G - C_l)$.
2. $\eta(G) = n - 2\mu(G) + 2$ if G satisfies properties: $\mu(G) = \frac{l}{2} + \mu(G - C_l)$ 2, $l = 0 \pmod 4$, and $E_1 \cap M = \varnothing$ for all $M \in E_2$.
3. $\eta(G) = n - 2\mu(G)$ otherwise.

Lemma 19.2.2.7 (Guo et al. 2009) Suppose H is a pendant star of a graph G. Then $\mu(G) = \mu(G_0) + 1$, where $G_0 = G - H$; see Fig. 19.9.

Suppose G is a unicyclic graph with n vertices. Let the length of the cycle in G be l. If G is a cycle C_l or a cycle C_l with pendant edges at some or all vertices of C_l, we call G a canonical unicyclic graph. If G is not canonical, G contains at least one pendant star H_1 such that $G_1^* = G - H_1$ is also a unicyclic graph. We call the procedure of obtaining $G - H_1$ from G a "deleting operator." With repeated
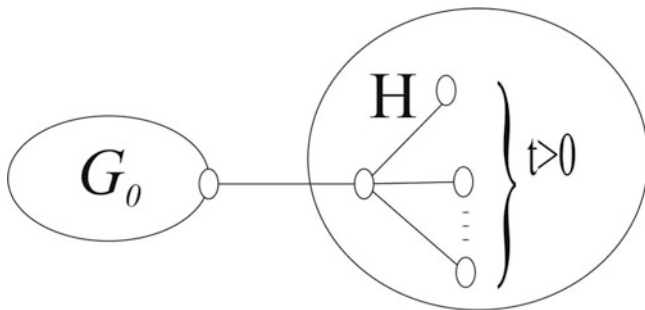
Fig. 19.9 A graph G and a pendant star H of G, where $G_0 = G - H$

applications of the "deleting operators," then a canonical unicyclic graph, denoted by G^*, is obtained from G.

Theorem 19.2.2.8 Suppose G is a unicyclic graph with n vertices and G^* is the graph defined above. Then $\eta(G) = n - 2\mu(G) - 1$ if and only if $\left|\eta(G^*)\right| = \left|V(G^*)\right| - 2\mu(G) - 1$; $\eta(G) = n - 2\mu(G)$ if and only if $\left|\eta(G^*)\right| = \left|V(G^*)\right| - 2\mu(G^*)$; and $\eta(G) = n - 2\mu(G) + 2$ if and only if $\left|\eta(G^*)\right| = \left|V(G^*)\right| - 2\mu(G) + 2$.

Corollary 19.2.2.9 (Guo et al. 2009) Suppose G is a unicyclic graph with n vertices and the length of the cycle in G is l. Let G^* be the graph defined above. Then $(G) = n - 2\mu(G) - 1$ if $G^* = C_l$ and l is odd, $\eta(G) = n - 2\mu(G) + 2$ if $G^* = C_l$, and $l = 0 \pmod 4$ and $\eta(G) = n - 2\mu(G)$ otherwise.

19.2.3 The Unicyclic Graphs with Extremal Nullity

In this section, we use some results in the past section to characterize the unicyclic graphs G with $\eta(G) = 0$ and $n - 5$, respectively.

Theorem 19.2.3.1 (Guo et al. 2009) Let G be a unicyclic graph with n vertices ($n \geq 5$) and with $\eta(G) = n - 5$. Then G must have the form of U_4^* illustrated in Fig. 19.7 or $G = C_5$, where $r > 0$.

Lemma 19.2.3.2 (Guo et al. 2009) Let G be a unicyclic graph with n vertices and the length l of the cycle C_l in G be odd. Then G is nonsingular if and only if G has a perfect matching or $G - C_l$ has a perfect matching (Fig. 19.10).

Lemma 19.2.3.3 (Guo et al. 2009) Let G be a unicyclic graph with n vertices and the length l of the cycle C_l in G be even. Then G is nonsingular if and only if G contains a unique perfect matching or $l \neq 0 \pmod 4$ and G has two perfect matching.
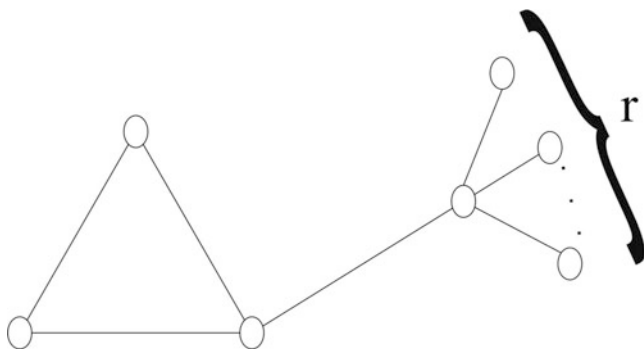
Fig. 19.10 The graph U_4^* in Lemma 19.2.3.2

Theorem 19.2.3.4 (Guo et al. 2009) Suppose G is a unicyclic graph and the cycle in G is denoted by C_l. Then G is nonsingular if and only if G satisfies one of the following properties:

1. l is odd and $G - C_l$ contains a perfect matching.
2. G contains a unique perfect matching.
3. $l \neq 0 \pmod 4$ and G contains two perfect matching.

19.2.4 On the Nullity of Bicyclic Graphs

Call a graph $\theta(p, l, q)$ (or $\infty(p, l, q)$) the base of the corresponding bicyclic graph B which contain it. Denote the base of B by ρ_B. Let $P = B - V(\rho_B)$. P is said to be the periphery of B (Fig. 19.11).

Lemma 19.2.4.1 (Cheng and Liu 2007) Let G be a connected graph of order n. Then $r(G) = 2$ if and only if $G = K_{r,n-r}$; $r(G) = 3$ if and only if $G = K_{a,b,c}$ where $a + b + c = n$.

Lemma 19.2.4.2 (Tan and Liu 2005) Let B be a bicyclic graph of order n. Then $r(B) = 2$ if and only if $B = K_{2,3}$; $r(B) = 3$ if and only if $B = K4 - e$, $e \in E(K_4)$.

Corollary 19.2.4.3 (Hu et al. 2008; Li 2008) Let $B \in B_n$ and $B \notin \{K_{2,3}, K_4 - e\}$. Then $\eta(B) \leq n - 4$.

Lemma 19.2.4.4 (Tan and Liu 2005) The bicyclic graphs with rank 4 are $\theta(1, 2, 3)$ or $\infty(4, 1, 4)$.

Theorem 19.2.4.5 (Tan and Liu 2005) Let $B \in B_n$.

1. $\eta(B) = n - 2$ if and only if $B = K_{2,3}$;
2. $\eta(B) = n - 3$ if and only if $B = K_{4-e}$;
3. $\eta(B) = n - 4$ if and only if $B = B_i$ $(1 \leq i \leq 7)$ (Fig. 19.12).
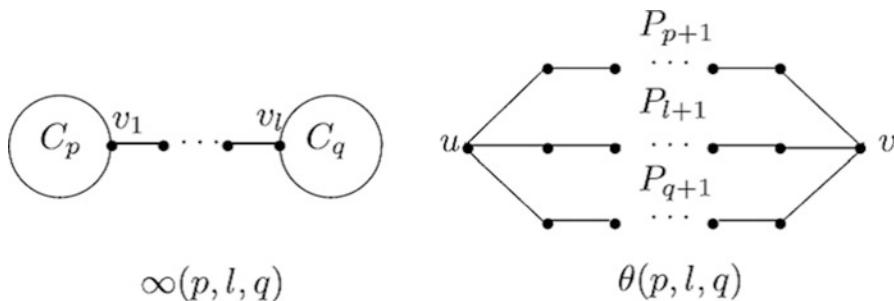
Fig. 19.11 Two bicyclic graphs

Theorem 19.2.4.6 (Hu et al. 2008; Li 2008) The nullity set of B_n is $[0, n-2]$.

Theorem 19.2.4.7 (Hu et al. 2008; Li 2008) Let B be a bicyclic graph satisfying the following conditions:

(i) $\eta(\rho_B) = 0$;
(ii) $\mathcal{P}$ is the union of *PM*-trees.

   Then B is a nonsingular bicyclic graph.

Theorem 19.2.4.8 (Tan and Liu 2005) Let G be a connected n-vertex graph with pendent vertices. Then $\eta(G) = n - 4$ if and only if G is isomorphic to the graph G_1^* or G_2^*, where G_1^* is depicted in Fig. 19.13, G_2^* is a connected spanning subgraph of G_2 (see, e.g., Fig. 19.13) and contains $K_{l,m}$ as its subgraph.

Theorem 19.2.4.9 (Tan and Liu 2005) Let G be a connected graph on n vertices and G has no isolated vertex. Then $\eta(G) = n - 5$ if and only if G is isomorphic to the graph G_3^*, or G_4^*, where G_3^* is depicted in Fig. 19.14; G_4^* is a connected spanning subgraph of G_4(see, e.g., Fig. 19.14) and contains $K_{1,m,p}$ as its subgraph.

Theorem 19.2.4.10 (Tan and Liu 2005) Let $\mathcal{T}_n$ denote the set of all n-vertex trees.

(i) Let $T \in \mathcal{T}_n$, then $\eta(T) \leq n - 2$; the equality holds if and only if $T \cong S_n$.
(ii) Let $T \in \mathcal{T}_n - S_n$, then $\eta(T) \leq n - 4$, the equality holds if and only if $T \cong T_1$ or $T \cong T_2$,where T_1 and T_2 are depicted in Fig. 19.15.
(iii) Let $T \in \mathcal{T}_n - \{S_n, T_1, T_2\}$, then $\eta(T) \leq n - 6$; the equality holds if and only if $T \cong T_3$ or $T \cong T_4$ or $T \cong T_5$,where T_3, T_4, T_5 are shown in Fig. 19.15.

Corollary 19.2.4.11 (Tan and Liu 2005) The nullity set of $\mathcal{T}_n$ is $\{0, 2, 4, \ldots, n-4, n-2\}$ if n is even, otherwise is$\{1, 3, 5, \ldots, n-4, n-2\}$.
   Let $\mathcal{U}_n$ denote the set of all n-vertex unicyclic graphs.
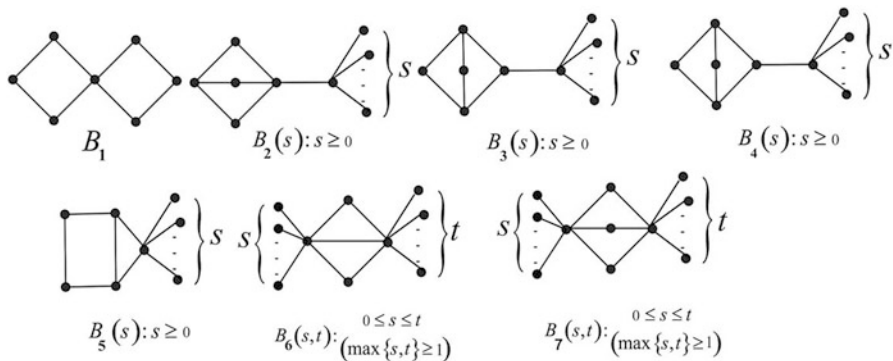
Fig. 19.12 Graphs B1–B7 in Theorem 19.2.4.5
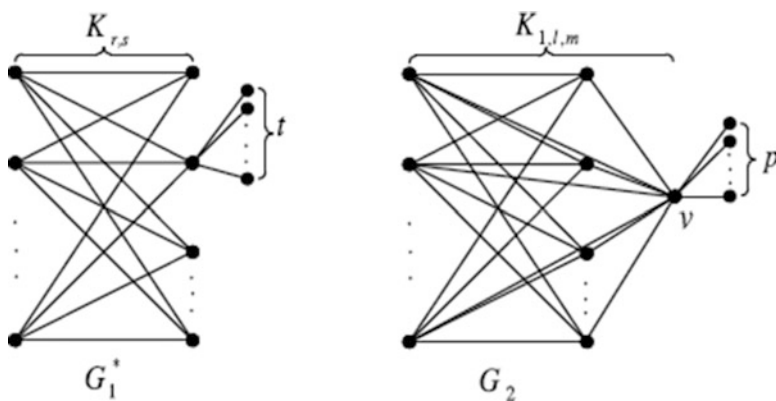
Fig. 19.13 Graphs G_1^* and G_2
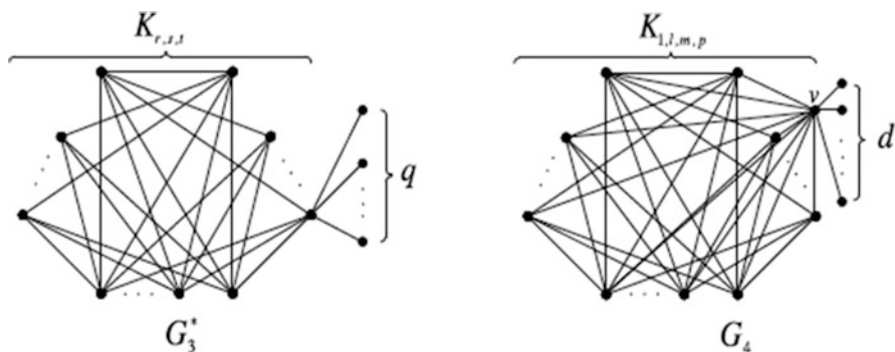
Fig. 19.14 Graphs G_3^* and G_4
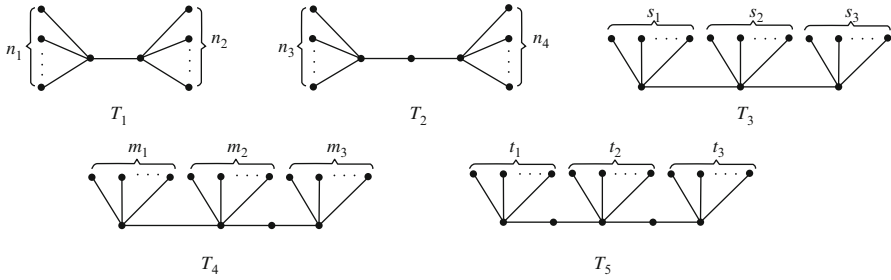
Fig. 19.15 Graphs T_1, T_2, T_3, T_4 and T_5
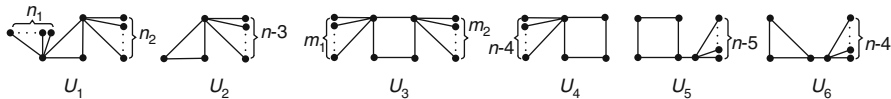
Fig. 19.16 Graphs U_1, U_2, U_3, U_4, U_5 and U_6

Theorem 19.2.4.12 Let $U_n(n-5)$ be the set of unicyclic graphs on n vertices. Let $U \in \mathcal{U}_n$, then $\eta(U) \le n-4$; the equality holds if and only if

$$G \cong U_1 \text{ or} G \cong U_2 \text{ or } G \cong U_3 \text{ or } G \cong U_4 \text{ or } G \cong U_5,$$

where U_1, U_2, U_3, U_4, and U_5 are depicted in Fig. 19.16.

Corollary 19.2.4.13 (Tan and Liu 2005) The nullity set of $\mathcal{U}_n(n \le 5)$ is $\{0, 1, 2, \ldots, n-4\}$.

Here, we compute the eigenvalues of a bridge graph. To do this, let G and H be two connected graphs, $u \in V(G)$ and $v \in V(H)$, respectively. By connecting the vertices u and v, we obtain a bridge graph denoted by $GuvH$

Theorem 19.2.4.14

$$\eta(GuvH) = \min\{\eta(G), \eta(G-u)\} + \min\{\eta(H), \eta(H-v)\}.$$

Proof It is easy to see that the characteristic polynomial of G can be written as follows:

$$\chi_x(G) = x^{\eta(G)} f(x),$$

where $f(x)$ is a polynomial of degree of rank(G). It follows that

$$\chi_x(H) = x^{\eta(H)} g(x), \ \chi_x(G-u) = x^{\eta(G-u)} h(x) \text{ and } \chi_x(H-v) = x^{\eta(H-v)} k(x)$$

for some polynomials $g(x)$, $h(x)$, and $k(x)$, respectively. On the other hand, by Lemma 19.2.3.4, we have

$$\chi_x(GuvH) = \chi_x(G)\chi_x(H) - \chi_x(G-u)\chi_x(H-v).$$

This leads us to conclude that

$$\chi_x(GuvH) = x^{\eta(G)+\eta(H)}f_1(x) + x^{\eta(G-u)+\eta(H-v)}f_2(x)$$

for some polynomials $f_1(x)$ and $f_2(x)$ and this completes the proof.

Corollary 19.2.4.15 In Theorem 19.2.4.13, suppose u and v are cut vertices, G_1, G_2, …, G_k and H_1, H_2, …, H_k be respectively the components of G-u and H-v in which

$$\eta(G_1) = \eta(G_1 + u) + 1 \text{ and } \eta(H_2) = \eta(H_2 + v) + 1$$

Then

$$\eta(GuvH) = \eta(G) + \eta(H).$$

Let $G \bullet H$ be a graph obtained by coinciding vertex u of G by vertex v of H. Then we have:

Corollary 19.2.4.16 $$\eta(G \bullet H) = \eta(G) + \eta(H) + 1.$$

Proof By Lemma 19.2.3.4, it is easy to see that

$$\begin{aligned}
\chi_x(G \cdot H) &= \chi_x(G)\chi_x(H-v) + \chi_x(G-u)\chi_x(H) \\
&\quad - x\chi_x(G-u)\chi_x(H-v) = x^{\eta(G)+\eta(H-v)}p_1(x) \\
&\quad + x^{\eta(G-u)+\eta(H)}p_2(x) - x^{\eta(G-u)+\eta(H-v)+1}p_3(x),
\end{aligned}$$

where $p_1(x)$, $p_2(x)$, and $p_3(x)$ are some polynomials. Clearly we have

$$\begin{aligned}
\eta(G \cdot H) &= \min\{\eta(G) + \eta(H-v), \eta(G-u) + \eta(H), \eta(G-u) + \eta(H-v) + 1\} \\
&= \min\{\eta(G) + \eta(H) + 1, \eta(G) + \eta(H) + 3\} \\
&= \eta(G) + \eta(H) + 1.
\end{aligned}$$

19.2.5   Some Bounds of Nullity of Graphs

Suppose $\chi(G)$, $\alpha(G)$, and $\omega(G)$ are the chromatic number, independence number, and clique number of graph G, respectively. Let K_p be an induced subgraph of G.

Clearly, rank$(G) \geq p$, and so $\eta(G) \leq n - \omega(G)$. In Theorem 19.2.5.1, we compute an upper bound for the nullity of graph G with respect to its chromatic number.

Lemma 19.2.5.1 (Chartrand and Zhang 2008)

$$\omega(G) \geq 2\chi(G) + \alpha(G) - n - 1.$$

Theorem 19.2.5.2
$$\eta(G) \leq 2n - 2\chi(G) - \alpha(G) + 1.$$

Proof Since $\eta(G) \leq n - \omega(G)$, by using Lemma 19.2.5.1 the proof is completed.

It is easy to see that the edge set $E(G)$ of G can be partitioned to disjoint independent sets. Let $E(G) = \cup_{i=1}^{s} E_i$ be a partition of disjoint elements of $E(G)$, where r_i is the number of parts of size $e_i = |E_i|$, $i = 1, 2, \ldots, s$.

Lemma 19.2.5.3 Let G be a bipartite graph with $n \geq 1$ vertices and m edges without any cycle of length $4\, s(s= 1, 2, \ldots)$, then

$$n - 2\frac{m - (s - 1)r_1 e_1}{r_s} \leq \eta(G) \leq n - 2\frac{m + (s - 1)r_1}{r_s + (s - 1)r}.$$

Proof Since e_s is the size of maximum matching of G, $e_s = \mu(G)$ and then

$$m = |E(G)| = r_1 e_1 + r_2 e_2 + \cdots + r_s \mu(G)$$
$$\leq r_s \mu(G) + \sum_{i=1}^{s-1} r_i(\mu(G) - 1) \leq r_s \mu(G) + (\mu(G) - 1)(s - 1)r_1.$$

This implies that

$$\mu(G) \geq \frac{m + (s - 1)r_1}{r_s + (s - 1)r}.$$

For computing the lower bound, it follows that

$$m = \sum_{i=1}^{s} r_i e_i \geq (s - 1)r_1 e_1 + r_s \mu(G).$$

Hence,

$$\mu(G) \leq \frac{m - (s - 1)r_1 e_1}{r_s}$$

and the proof is completed.

Recall that a vertex in graph G is well connected if it is adjacent with other vertices of G.

Lemma 19.2.5.4 Let v be a well-connected vertex so that $G - \{v\}$ is a connected regular graph on n vertices. Then

$$\eta(G) = \eta(G - \{v\}).$$

Proof It is easy to see that $G = G - \{v\} + K_1$. Since $G–\{v\}$ is regular, so by Cvetković et al. (1980), $\mathrm{rank}(G) = \mathrm{rank}(G - \{v\}) + \mathrm{rank}(K_1)$. This implies that

$$\eta(G) = n + 1 - \mathrm{rank}(G) = n + 1 - [\mathrm{rank}(G - \{v\}) + 1] = \eta(G - \{v\}).$$

Corollary 19.2.5.5 If G satisfies in conditions of Lemma 19.2.5.4, then

$$\eta(\overline{G}) = 1 + \eta(G - \{v\}).$$

Theorem 19.2.5.6 Let G be connected graph and w be a vertex of G in which $N(w) = N(u) \cup N(v)$ and $N(u) \cap N(v) = \phi$ for some vertices u and v. Then

$$\eta(G) = \eta(G - \{w\}).$$

Proof Let G satisfy in the above conditions and A be adjacency matrix of G. Clearly, the sum of u-th and v-th rows is equal with w-th row of A, and this completes the proof.

Corollary 19.2.5.7 Let G be connected graph and w be a vertex of G in which $N(w) = \cup_{i=1}^{n} N(u_i)$ so that $N(u_i) \cap N(u_j) = \phi$ ($1 \le i, j \le n$). Then

$$\eta(G) = \eta(G - \{w\}).$$

19.3   Some Classes of Dendrimers

The aim of this section is computing the nullity of some bipartite graphs. Polymer chemistry and technology have traditionally focused on linear polymers, which are widely in use. Linear macromolecules only occasionally

contain some smaller or longer branches. In the recent past, it has been found that the properties of highly branched macromolecules can be very different from conventional polymers. The structure of these materials has also a great impact on their applications. First discovered in the early 1980s by Donald Tomalia and coworkers, these hyperbranched molecules were called dendrimers. The term originates from "dendron," meaning a tree in Greek. At the same time, Newkome's group independently reported synthesis of similar macromolecules. They called them arborols from the Latin word "arbor" also meaning a tree. The term cascade molecule is also used, but "dendrimer" is the best established one.

Example 19.3.1 (Ghorbani and Songhori 2011) Consider the graph C depicted in Fig. 19.17. By using Corollary 19.2.18, $\eta(C) = \eta(C_1)$, and by Corollary 19.2.17 $\eta(C_1) = \eta(C_2)$. By continuing this method, one can see that $\eta(C) = \eta(C_5) = 1$.

By using above method we can prove the following Theorem.
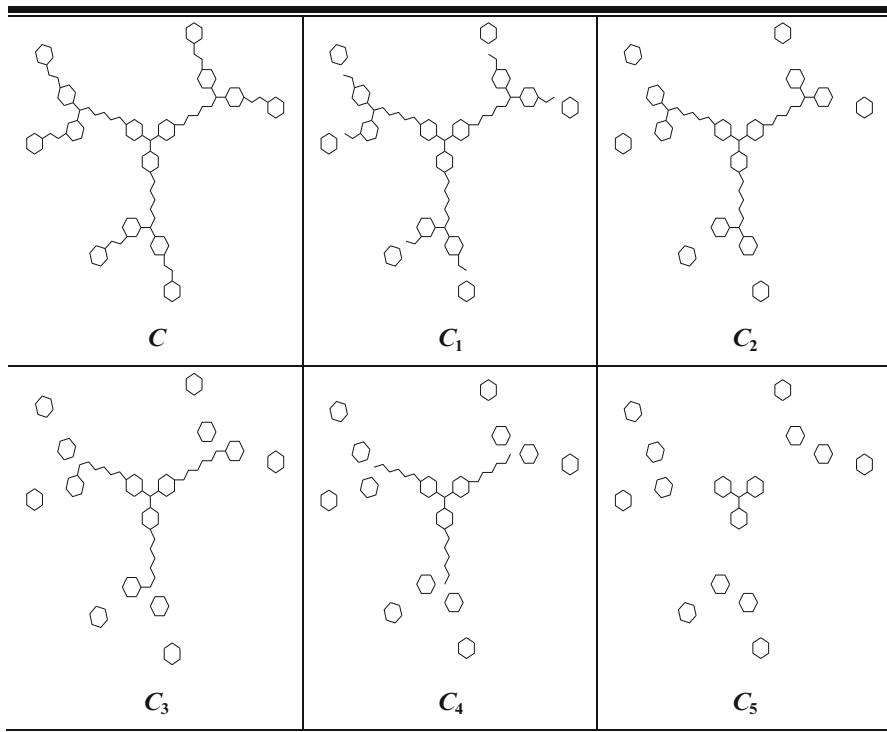
Fig. 19.17 2-D graph of dendrimer C

Fig. 19.18 $2-D$ Graph of S $[n]$
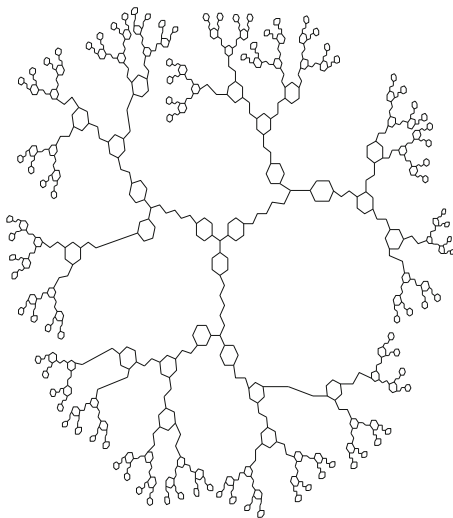
Fig. 19.19 $2-D$ Graph of $D[n]$, for $n = 3$
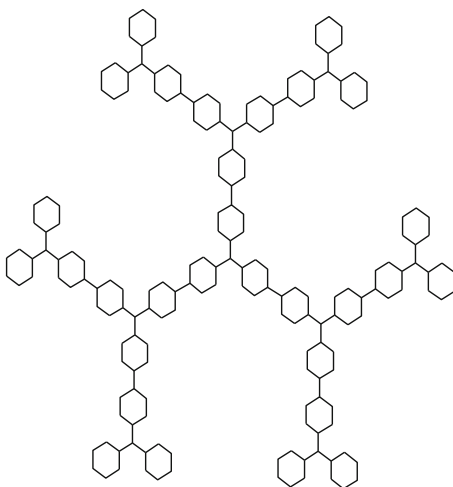
Theorem 19.3.2 (Ghorbani and Songhori 2011) Consider dendrimer graph $S[n]$ depicted in Fig. 19.18. Then $\eta(S[n]) = 1$.

Theorem 19.3.3 (Ghorbani 2014) Consider nanostar dendrimer $D[n]$, then (Figs. 19.19 and 19.20) $\eta(D[n]) = 2^{n-1}, n = 1, 2, \ldots$
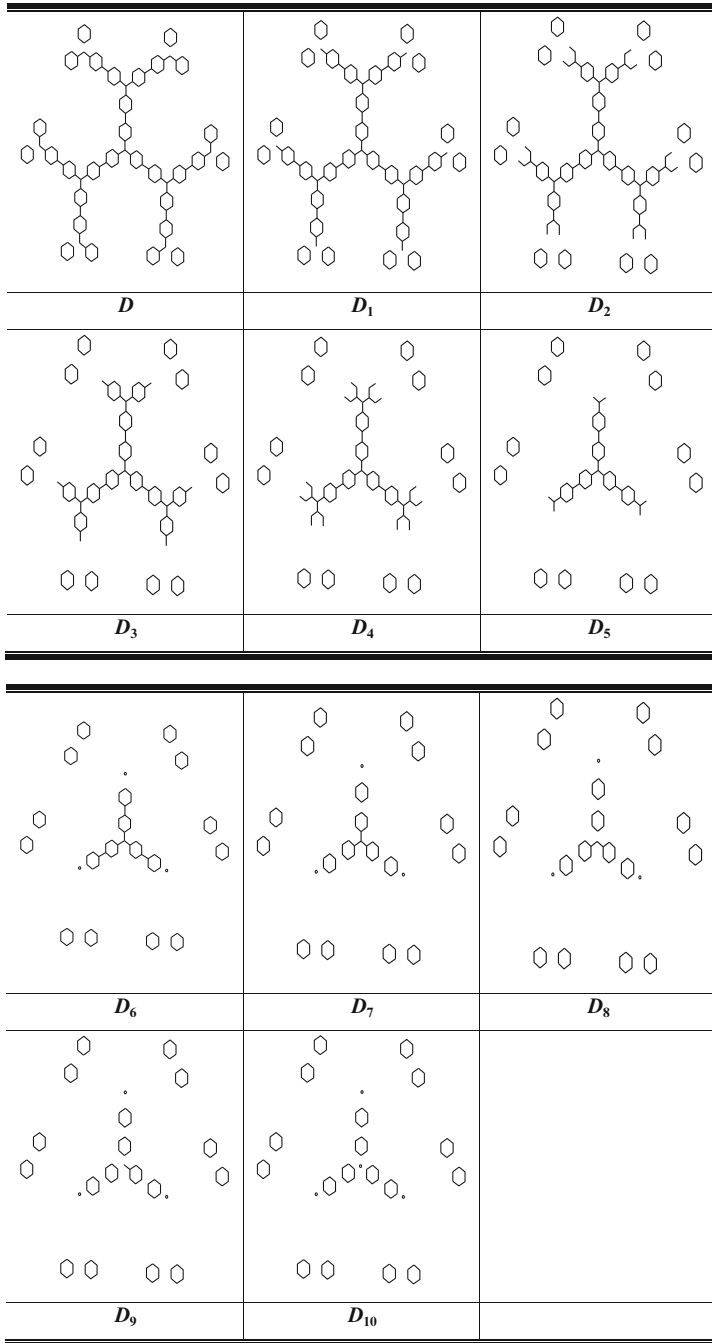
Fig. 19.20 Computing nullity of $D[n]$, for $n = 3$

References

Biggs N (1993) Algebraic graph theory, 2nd edn. Cambridge University Press, Cambridge

Chartrand G, Zhang P (2008) Chromatic graph theory, 1st edn. Chapman and Hall/CRC, Boca Raton

Cheng B, Liu B (2007) On the nullity of graphs. EI J Lin Algebra 16:60–67

Cvetković D, Gutman I (1972) The algebraic multiplicity of the number zero in the spectrum of a bipartite graph. Matematički Vesnik (Beograd) 9:141–150

Cvetković D, Gutman I (2009) Application of graph spectra. Zbornik Radova 13(21):33–63

Cvetković D, Gutman I, Trinajstić N (1972) Graph theory and molecular orbitals II. Croat Chem Acta 44:365–374

Cvetković D, Gutman I, Trinajstić N (1975) Graphical studies on the relations between the structure and the reactivity of conjugated systems: the role of non−bonding molecular orbitals. J Mol Struct 28:289–303

Cvetković D, Doob M, Sach H (1980) Spectra of graph. Academic, New York

Ghorbani M (2014) Some new results on the nullity of molecular graphs. Studia Univ Babes−Bolyai 59(3):127–138

Ghorbani M, Songhori M (2011) A note on nullity of graphs. Studia Univ Babes−Bolyai 56(2):75–84

Godsil CD, McKay BD (1978) A new graph product and its spectrum. Bull Austral Math Soc 18:21–28

Guo J, Yan MW, Yeh YN (2009) On the nullity and the matching number of unicyclic graphs. Lin Algebra Appl 431:1293–1301

Gutman I, Sciriha I (2001) On the nullity of line graphs of trees. Discret Math 232:35–45

Hu S, Liu B, Tan X (2008) On the nullity of bicyclic graphs. Lin Algebra Appl 429:1387–1391

Li S (2008) On the nullity of graphs with pendent vertices. Lin Algebra Appl 429:1619–1628

Li J, Chang A, Shiu WC (2007) On the nullity of bicyclic graphs. MATCH Commun Math Comput Chem 60:21–36

Longuet−Higgins HC (1950) Resonance structures and MO in unsaturated hydrocarbons. J Chem Phys 18:265–274

Tan X, Liu B (2005) On the nullity of unicyclic graphs. Lin Algebra Appl 408:212–220

Chapter 20
Bondonic Chemistry: Spontaneous Symmetry Breaking of the Topo-reactivity on Graphene

Mihai V. Putz, Ottorino Ori, Mircea V. Diudea, Beata Szefler, and Raluca Pop

Abstract Bondonic chemistry promotes the modeling of chemical transformations by quantum particles of the chemical field, the so-called bondons, rather than by molecular wave function. Being a particle of chemical interaction, the bondon is necessarily a boson, here emerging from the chemical field by spontaneous symmetry breaking mechanism, following the Goldstone mechanism yet featuring the

M.V. Putz (✉)
Laboratory of Computational and Structural Physical-Chemistry for Nanosciences and QSAR, Department of Biology-Chemistry, Faculty of Chemistry, Biology, Geography, West University of Timişoara, Pestalozzi Str. No. 16, RO-300115 Timişoara, Romania

Laboratory of Renewable Energies-Photovoltaics, R&D National Institute for Electrochemistry and Condensed Matter, Dr. A. Paunescu Podeanu Str. No. 144, RO-300569 Timişoara, Romania
e-mail: mv_putz@yahoo.com

O. Ori (✉)
Actinium Chemical Research, Via Casilina 1626/A, 00133 Rome, Italy

Laboratory of Computational and Structural Physical-Chemistry for Nanosciences and QSAR, Department of Biology-Chemistry, Faculty of Chemistry, Biology, Geography, West University of Timişoara, Pestalozzi Str. No. 16, 300115 Timişoara, Romania
e-mail: ottorino.ori@gmail.com

M.V. Diudea (✉)
Department of Chemistry, Faculty of Chemistry and Chemical Engineering, Babes-Bolyai University, Arany Janos Street 11, Cluj-Napoca RO-400028, Romania
e-mail: diudea@chem.ubbcluj.ro; diudea@gmail.com

B. Szefler
Department of Physical Chemistry, Faculty of Pharmacy, Collegium Medicum, Nicolaus Copernicus University, Kurpińskiego 5, 85-096 Bydgoszcz, Poland
e-mail: beatas@cm.umk.pl

R. Pop
Faculty of Pharmacy, University of Medicine and Pharmacy "Victor Babes" Timişoara, E. Murgu Square 2, 300041 Timişoara, Romania
e-mail: ralucapop24@gmail.com

345

Higgs bosonic mass rising caring the electronic pair information by a bondon–ant–bondon (Feynman) coupling, eventually corresponding to the bonding–antibonding chemical realms of a given bonding. The present mechanism of bondonic mass is applied for describing the Stone–Wales topological defects on graphene, a 2D carbon material allowing electrons to unidirectionally interact in bosonic–bondonic formation; in this framework, the molecular topology and combined molecular topology–chemical reactivity approaches are unfolded showing that bondons fulfill quantum entangled behavior, according to which (1) their masses increase when chemical reactivity information combines the topological information and (2) their masses increase with increasing the distance of their electronic pairing Feynman interaction.

20.1 Introduction: From Emergence Concept to Entanglement on Graphene

According to the philosopher John Stuart Mill, "...To whatever degree we might imagine our knowledge of the properties of several ingredients of a living body to be extended and perfected, it is certain that no mere summing up of the separate actions of those elements will ever amount to the action of the living body itself" (Mill 1952[1843]), from where *the concept of emergence* is established over a century as: "to characterize certain phenomena as 'novel', and this not merely in the psychological sense of being unexpected, but in the theoretical sense of being unexplainable, or unpredictable, on the basis of information concerning the spatial parts or other constituents of the systems in which the phenomena occur, and which in this context are often referred to as 'wholes'" (Hempel and Oppenheim 2008). It is therefore merely an epistemological concept (thus relating with new discoveries) rather than with the ontological reduction to the vitalism of some fundamental forces and phenomena (either in physics, chemistry, or biochemistry). Accordingly, two different kinds of emergence can be distinguished (Norton 2012):

- Reduction of a composite system (a whole) to its parts
- The reduction of a "higher-level" theory (H-theory) to a lower-level one (L-theory), corresponding to the phenomenological and fundamental theories, respectively

Most interesting is the fact that the H-theory is the phenomenological one and associates with the "infinite whole" in the fist of above emergence manifestations; in physical terms it corresponds either to the classical thermodynamics as a macroscopic manifestation of global observable or to the infinite volume quantum statistical mechanics as a manifestation of the local observables (Landsman 2013). For a system with N-particles at the temperature β ($=1/K_B T$), the H/L scenario may be proposed, also beyond of the notable authorities (Batterman 2002, 2011; Rueger 2000, 2006):

- H = classical mechanics, as the asymptotic limit $\hbar \to 0$ of the L = quantum mechanics
- H = thermodynamics, as the asymptotic limit $N \to \infty$ of the L = quantum statistical mechanics
- H = local quantum statistical mechanics in infinite volume seen as the asymptotic limit $\beta \to 0$ of the L = quantum statistical mechanics

All this framework allows for formalization of the emergence in natural science as a natural passage from fundamental to phenomenological theories (L to H and H to L), among which the emergence by symmetry breaking is the preeminent example if not the example (Anderson 1952, 1972, 1984). In this respect quantum theory affirms its paradoxical nature since the self-consistent L-to-H-to-L circle of determinism, as timely observed by the Landau and Lifshitz emergentists (Landau and Lifshitz 1977): "Thus quantum mechanics occupies a very unusual place among physical theories: it contains classical mechanics as a limiting case, yet at the same time it requires this limiting case for its own formulation." In other words, the Schrödinger cat pure/ quantum (L-) states converge to mixed/classical (H-) states (Landsman and Reuvers 2013), from where the paradox of living/death, paradox of a cat in a box, survives! The solution of solving such paradox was solved by raising another formalization problem in quantum–classical epistemology by the so-called Earman and Butterfield principles relating the symmetry breaking/emergence in physical sciences:

- Earman principle: "While idealizations are useful and, perhaps, even essential to progress in physics, a sound principle of interpretation would seem to be that no effect can be counted as a genuine physical effect if it disappears when the idealizations are removed" (Earman 2003).
- Butterfield principle: "There is a weaker, yet still vivid, novel and robust behaviour that occurs before we get to the limit, i.e., for "finite" N. And it is this weaker behaviour which is physically real" (Butterfield 2011).

Therefore we arrived at the solution of considering the idealized system as the asymptotic behavior of the finite physical systems claimed to be real, being this dichotomy transposed to the local–global observable relationships between the finite yet arbitrarily large subsystems on one hand and the macroscopic thermodynamically averages on the other hand, respectively (Landsman 2007). The connection in between the local and global lays the spontaneous symmetry breaking phenomenology; it featured the consecrated double-well model for the quantum Hamiltonian (Z_2-invariance), the quantum Ising chain for coupling with a transverse magnetic field, and the quantum Curie–Weiss model of finite spin–spin interaction in the macroscopic averaged spin operators while being mathematically supported by the continuous fields of C^* algebras, the continuous fields of states (viz., Schrödinger cat paradox, solved in principle by the unstable lower theory states convergent to a stable pure ground state of the high-level theory), and the continuity of the time evolution (allowing the Wick theorem being applied by switching in between time, energy, and temperature so time unifying the H- and L-theories, i.e., $\hbar\beta \to t \to \hbar/E$). Such treatment leaves also with the ground-excited stated shift to a macroscopic linkage by the exponential decay in the leading term (mean-field approximation), $\hbar \to 0$, and by the quantum-to-classic dynamics (on valence states in physical chemistry terms).

With such a wisdom, the phenomenon of symmetry breaking may be naturally understood as the occurrence/emergence of stable state of the system lower than the symmetry of the interaction potential of the system (Ruckenstein and Berim 2010; Monin and Voloshin 2010). Such definition was successfully applied in the already consecrated disciplines of physics (Goldstone 1961; Nambu and Jona-Lasinio

1961; Goldstone et al. 1962; Higgs 1964a, b; Dirac 1978; Anderson 1963; Elitzur 1975; Englert and Brout 1964; Fradkin and Shenker 1979; Guralnik et al. 1964; Kibble 1967; Weinberg 1996; Frauendorf 2001), chemistry (Mikami and Yamanaka 2003; Terenziani et al. 2006; Sorkin et al. 2008; Putz 2016; Putz and Ori 2015a), and biology (Palmer 2004; Kuhn 2008).

However, with the last decade, the rise of graphene as the new cross-disciplinary material is worthy to be studied for its intrinsic properties as for emergence of both the new physical and chemical phenomena (Novoselov et al. 2012; Sheka 2012). This is because the graphene brings to date the following unique properties for a nanomaterial (Sheka 2014): (1) the lightest material under the environmental conditions, (2) the 2D perfect packing of the benzenoid units assuring the sp^2 configuration, and (3) the mechanical strength due to the C–C high strength (1.41–1.47 Å). Nevertheless, the so-called "Flagship graphene" program of realizations of "low-performance" and "high-performance" applications relies just on the degree in which the physical properties allow for chemical realizations (e.g., touch screens, rollable e-paper, foldable organic light-emitting diode (OLED), tunable sensors, solar cells, etc.), while just the chemistry of graphene resists to physical applications (electronic devices like semimetals–semiconductors) on the other side, respectively. The explications are based on the peculiar chemical features of the above structural properties, namely:

- *The topochemical character* of graphene mechanics (Bissett et al. 2013), rendering – for instance – the mechanical shocks by molecular anisotropic propagation (Long et al. 2015) according to the topological defect anisotropy induced by Stone–Wales waves (Ori et al. 2011).
- *The radical character* of the graphene relates with the so-called edge problem for the carbon skeleton of the fixed structure at the level of odd electrons originating in the number of atoms in the structure added to those from its edge; moreover, toward obtaining graphenic nanoribbons (perfect 2D planar single-layer structures) by cutting graphenic sheets, additional dangling bonds are generated and thus the unpaired electrons, all of these enhancing the graphenic radical properties, with the consequence of the chemical reaction proportion on the ribbon circumference with possible reorganization of the pristine graphene structure; this also relates with the atomic chemical susceptibility thus in relation with graphene magnetism (Sheka 2013) and conductivity (Sheka 2007).
- *The collective behavior character* of the graphene is a direct consequence of the above "odd electrons," as well as due to external actions of electric/magnetic fields along any chemical modification, e.g., hydrogenations (Elias et al. 2009), photoexcitation, or mechanical loading; it is manifested by the $sp^2 \rightarrow sp^3$ transformation of the carbon valence electrons, destroying the 2D planar geometry. This effect is naturally accompanied by the C–C bond length redistribution, so preventing the knowledge about the atom/region (or quantum dot) caring the highest reactivity of the graphene sheet and calling for the next deposition/interaction target; actually with C–C bonding growing up to 1.8–2 Å, the densely packed sp^2 honeycomb crystal changes due to the correlating electrons, due to the occurred radicalization so that the collective excited behavior is manifested

(Staroverov and Davidson 2000); actually the benzenoid carcass of pristine graphene changed to cyclohexanoid units with high heteromorphic configuration – as observed with the high-resolution transmission electron microscopy (HRTEM) providing more natural pictures than the recently proposed artificial "gigantic pseudomagnetic field" (Levy et al. 2010); nevertheless, such electronic π-correlation may be inhibited by deposition of monolayer graphene on substrates such as silicon carbide, boron nitride, and quartz surfaces (Hwang et al. 2012), or by using the rarely yet regularly distributed nanoparticles' grid (Wu et al. 2013), or even by designing the extreme case of graphene–substrate composites by adsorbed carbon monolayers of hexagon patterning (Hoffmann 2013), assuring the free standing of graphene by seeking the best surface science partners so inhibiting the carbon atom radicalization and preserving the hexagonal packed monolayers (Agnoli and Granozzi 2013).

Returning now to spontaneous symmetry breaking (SSB) with special focus on nanosciences, including graphene, one may briefly yet essentially quote the following spectacular advances:

- The macroscopic superconducting islands provided the basis for the development of the Josephson junction (JJ) arrays as phase qubits for quantum computation (Nakamura et al. 1999); due to the macroscopic quantum coherence, JJ poses a *finite* number of order parameters subject to lack in the symmetry restoration (from where the SSB by a Goldstone massless quasiparticle mode) (Chung 2006), thus behaving like an atom or molecule in the 2D-XY framework, in preventing the violation of the custom SSB infinite system conditions as the critical parameter $\beta = E_J/T$ significantly increases with the system size (E_J the Josephson energy); see also the above discussion on finite vs. infinite systems in the emergence concept of SSB.
- Highly correlated molecular states by electron–electron interactions (Egger et al. 1999; Reimann et al. 2000; Ghosal et al. 2006; Kalliakos et al. 2008) are offering the *finite-size* analogue to the Wigner crystals (Wigner 1934) in order to study the SSB on the quantum dots (Reimann and Manninen 2002); in a computational respect, the Hartree–Fock method offers successive levels of allowed symmetry breaking as (Fukutome 1981; Hammes-Schiffer and Andersen 1993) (a) spatially restricted HF (spatially RHF) breaks the total spin symmetry and (b) spatially unrestricted HF (spatially UHF) breaks both the total space and spin symmetries, which supports also the additional constraint for breaking the spin z-component symmetry; they were recently applied on the numerical study of the planar dots with $N = 3$ and six electrons in the presence of a transversal magnetic field so improving the energy estimates for correlation energies of the ground state, fundamental for further designing the equilibrium and transport properties of a given material (e.g., GaAs quantum dot) (Cavaliere and De Giovannini 2010).
- The SSB on graphene substance was computationally predicted with density functional theory Gaussian 03 package macroscopically from the Li double-sided adsorption on aromatic hydrocarbons packed as *finite* graphene nanoflakes (spanning rings from 6 to 20 cardinal), so creating new perspectives in mesoscopics by the appropriate interplay between charge and size dependence

driving the moving nano-devices (Jalbout et al. 2013); on the other side, the so-called chiral symmetry breaking in monolayer graphene was studied by employing the U(1) lattice gauge theory on the above described collective excitations so providing the exciton condensate in the strong coupling limit while identifying the lattice *finite* spacing relating the pristine honeycomb lattice of graphene allowing the fermionic–bosonic π vs. σ excitations so controlling the on-site hopes and the allied transport properties such as the electric conductivity and the Hall effect (Araki 2011).

- Finally but not lastly, the entanglement support of the graphene was just revealed (Tan et al. 2015) by combining many of the above ideas: 2D quantum dots (200 × 150 nm) were carved on a layer of graphene deposited on a silicon dioxide substrate; Cooper pair of two electrons was created by adjusting the quantum dots' electronic level by their *finite* size and then guided to different resonant energies (so inducing the SSB) and separated; they eventually display the elastic co-tunneling effect as the symmetrical or anti-symmetrical energy levels are adjusted by a monitored gate voltage and currently observed with 10 % efficiency; however, such entanglement phenomena of splitting were timely predicted and accordingly accompanied by the electronic restoring symmetry of chemical bonding within the quasiparticle *bondon* (Putz 2010a; see Fig. 20.1), through the chemical bonding teleportation phenomenology on graphene (Putz and Ori 2015b).

It is the last issue that is continued in the present work through combining the bondonic description with the spontaneous symmetry breaking with its propagation in the graphenic nanoribbon so quantifying the Stone–Wales waves. Accordingly, the organization of this chapter is as follows: Sect. 20.2 exposes how the bondonic mass arrives by a modified Goldstone mechanism in a double-well potential – appropriated for mimicking the neighboring hops in graphenic mono-directional layer in agreement with Schrödinger evolution theory; Sects. 20.3 and 20.4 apply the fundamental result from Sect. 20.2 to Stone–Wales defect propagation on
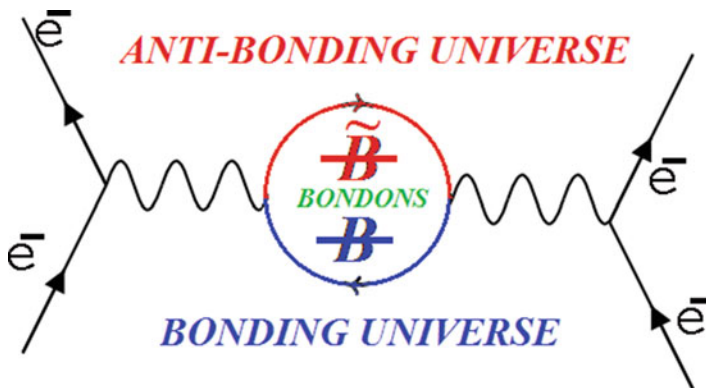
Fig. 20.1 The Feynman diagram of bonding–antibonding complementary universes in chemical bonding involving the bondon and antibondon, respectively (Putz 2016; Putz and Ori 2015b)

graphene by the topological sequential approach of successive dynamic frames on graphene and by topo-reactivity modeling (in terms of electronegativity and chemical hardness and reactivity indices), respectively. The unfolded results and discussions are then resumed in Conclusions section.

The present study, while emphasizing on the pure topological vs. topo-reactivity efficiency in modeling the quantum quasiparticle propagation on graphene, may serve also as a benchmarking computational guide for further designed experiments toward observing the chemical bonding teleportation and quantum computing by graphenic nano-support.

20.2 Bondonic Mass by Spontaneous Symmetry Breaking

One starts with the working field potential under double-well form, adapted from graphenic or quantum dot layers' configurations:

$$V(\phi) = v_1\phi^2 + \frac{1}{2}v_2\phi^4 \qquad (20.1)$$

to generate bonding fields and its particles – the *bondons* – by changing from the upper (positive potential) branch to lower (negative potential) branch of the first-order particle ($\sim \phi^2$) potential.

Figure 20.2 represents graphically the parabolic dependence with $v_1 > 0$ and $v_2 > 0$ (see the upper dashed curve) presenting the minimum zero potential for the vanishing field $\phi = 0$ (so for fermions when v_1 is identified with a positive chemical potential of the system). Instead, a completely different picture is obtained if the same potential is considered with $v_1 < 0$ (or $-v_1 > 0$) and $v_2 > 0$ (so for *bosons* when v_1 is identified with a negative chemical potential) when two distinct nonzero minimum potential values appear in its negative (vacuum) region for the chemical field acquiring the respective values:

$$\frac{\partial V}{\partial \phi} = 0 \Rightarrow \phi_{a,b} = \pm\sqrt{\frac{-v_1}{v_2}} \qquad (20.2)$$

Solutions of Eq. (20.2) thus largely justify the *bosonic* appearance for the activation of the spontaneous symmetry breaking.

Yet, it is worth being noted that going from the fermionic potential driven by $+v_1$ (or the chemical potential $+\mu$) to the bosonic potential for $-v_1$ (actually driven by electronegativity $-\mu = \chi$), the chemical field naturally identifies with the chemical bonding field by shifting the minimum zero potential to its minimum negative range, in quantum vacuum region from where the quantum particles are spontaneously created, namely, the bondon and antibondon (in accordance with the Feynman one-loop diagram of Fig. 20.1) as the quantum particles of the chemical bonding fields.
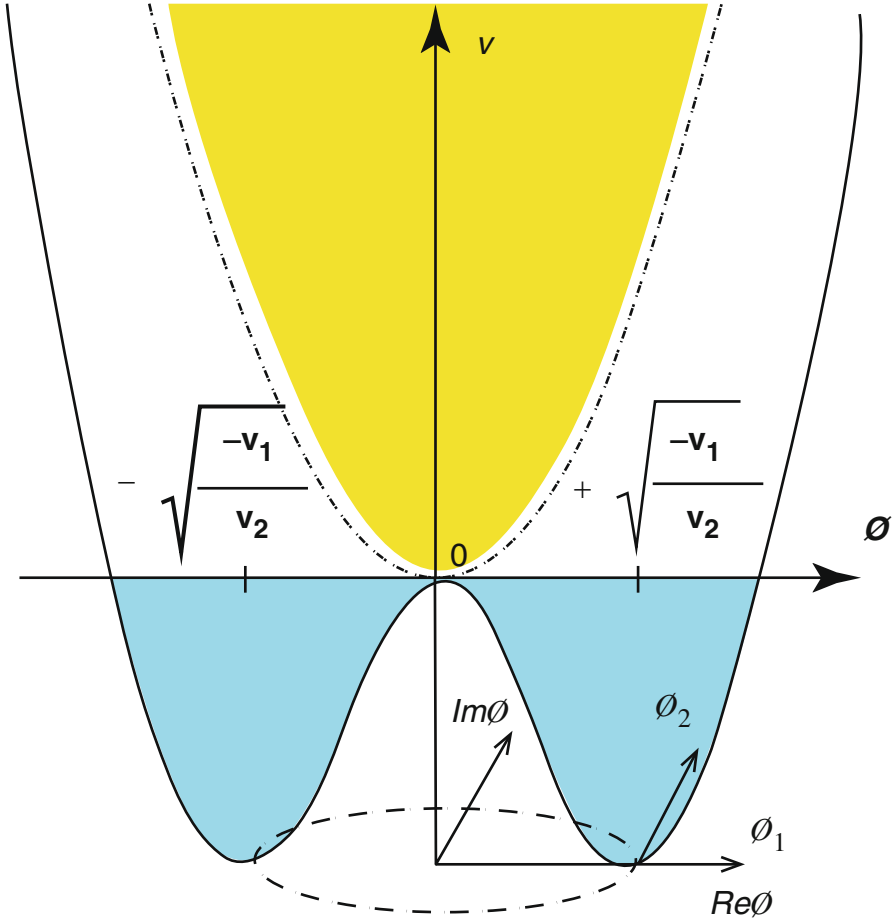
Fig. 20.2 The potential of Eq. (20.1) with $+v_1$ (aka fermionic state for v_1 identification with positive chemical potential) in dashed curve and with $-v_1$ (aka bosonic states for v_1 identification with negative potential) in continuous curve, illustrating the symmetry breaking of the parabolic (*upper curve*) to double-well potential (*lower curve*) that includes also the negative (vacuum, yet more stable) quantum states (Putz 2008a, 2016); see the text for details

Next, one likes employing this phenomenological analysis to analytically determine the bondonic mass through the quantum creation by symmetry breaking mechanism (Putz 2008a). To this aim, one considers the Lagrangian of the Schrödinger field (ϕ) (Putz 2016):

$$\mathscr{L} = i\hbar\phi^*\dot{\phi} - \frac{\hbar^2}{2m_0}\left(\nabla\phi^*\right)(\nabla\phi) - V\phi^*\phi \qquad (20.3)$$

produced by the actual potential V

$$V(\phi) = -v_1\phi^2 + \frac{1}{2}v_2\phi^4 \tag{20.4}$$

by connecting the chemical field (ϕ) with the parabolic expansion of the chemical reactive/valence energy (Parr and Yang 1989; Putz 2011a). Accordingly, the stationary solutions of Eq. (20.2) become for the bondonic fields as

$$\phi_{a,b} = \pm\sqrt{\frac{v_1}{v_2}} \tag{20.5}$$

The positive solution of Eq. (20.5) is used in the gauge shift creating *the bosonic-bondon* field as a broken symmetry effect along the "real axis" of the chemical field:

$$\phi \rightarrow \tilde{\phi} = \phi + \sqrt{\frac{v_1}{v_2}} \tag{20.6}$$

while the negative solution would correspond to the antibondonic evolution (not to be here considered, although not without interest for further development of the *chemical field theory*).

Now it is clear that the working Lagrangian, with Eq. (20.4) in (20.3),

$$\mathscr{L} = \mathscr{L}_0 = i\hbar\phi^*\dot{\phi} - \frac{\hbar^2}{2m_0}(\nabla\phi^*)(\nabla\phi) + \rho\phi^4 - \frac{1}{2}\rho^E\phi^6 \tag{20.7}$$

further transforms under the implementation of gauge local shift of Eq. (20.6) to look like

$$\tilde{\mathscr{L}} = \mathscr{L}_0 + \overline{\mathscr{L}} \tag{20.8}$$

with the newly created chemical field bosonic–bondonic sector unfolded as

$$\begin{aligned}\overline{\mathscr{L}} = {}& i\hbar\sqrt{\frac{v_1}{v_2}}\dot{\phi} - 3\rho^E\sqrt{\frac{v_1}{v_2}}\phi^5 - \frac{15}{2}v_1\phi^4 \\ & - 6v_1\sqrt{\frac{v_1}{v_2}}\phi^3 - \frac{3v_1{}^2}{2v_2}\phi^2 + \frac{v_1{}^2}{v_2}\sqrt{\frac{v_1}{v_2}}\phi + \frac{v_1{}^3}{2v_2{}^2}\end{aligned} \tag{20.9}$$

The invariant condition of the Lagrangian requires that the corrective Lagrangian of Eq. (20.9) should vanish and provides the high-order differential equation:

$$\begin{aligned}i\hbar\dot{\phi} = {}& 3\rho^E\phi^5 + \frac{15}{2}v_1\sqrt{\frac{v_2}{v_1}}\phi^4 + 6v_1\phi^3 \\ & + \frac{3v_1{}^2}{2v_2}\sqrt{\frac{v_2}{v_1}}\phi^2 - \frac{v_1{}^2}{v_2}\phi - \frac{v_1{}^3}{2v_2{}^2}\sqrt{\frac{v_2}{v_1}}\end{aligned} \tag{20.10}$$

whose solutions will give the chemical bonding fields (ϕ). However, one should consider a more specialized equation derived from Eq. (20.10) and then employ the solution to a meaningfully physical–chemical picture especially related with the chemical reactivity phenomenology. Such framework can be achieved when recognizing that the above field transformation leaves invariant the working Lagrangian of Eq. (20.7) under the constraint in Eq. (20.6), namely, when

$$v_1 \rightarrow 0 \tag{20.11}$$

The condition (20.11) allows neglecting all terms a part from the chemical field leading the order in Eq. (20.10). Note that this framework is consistent with the chemical principle stating that the minimum electronegativity (at the limit canceling) will stabilize the system on one side or the zero chemical potential is the turning chemical point where the particles can arise in the system without any supplementary energetic effort, a consistent picture with the spontaneous creation of the bosonic bondons.

When considering the invariant reactivity condition (20.11) in the bondonic field Eq. (20.10), the resulting new equation still preserves its highest order under the form

$$i\hbar\dot{\phi} = 3v_2\phi^5 \tag{20.12}$$

By integrating Eq. (20.12) under the asymptotic limit (ϕ_∞) – to – bonding (ϕ_B), one gets the imaginary relationship:

$$\frac{1}{\phi_\infty^4} - \frac{1}{\phi_B^4} = \frac{12v_2i\Delta t}{\hbar} \tag{20.13}$$

However, the time-to-temperature Wick transformation can be employed (Putz 2009a):

$$i\Delta t = \hbar\beta, \ \beta = \frac{1}{k_BT} \tag{20.14}$$

with Boltzmann constant k_B, so that the spontaneous breaking symmetry chemical bonding field assumes, to the first order, the expanded form

$$\phi_B = \phi_\infty\left[1 + 6\beta\left(\frac{1}{2}v_2\phi_\infty^4\right)\right] \tag{20.15}$$

Relation (20.15) has remarkable features, namely:

- It prescribes the chemical bonding field directly depending on the hopping amplitude v_2 only (in the double-well potential, graphene, or periodic quantum dot grid).

- It models the stage in the high-temperature regime ($\beta \to 0$) aka ultrashort time bondonic creation, in accordance with the regime where the chemical bond is manifested.
- It generally depends on the fifth power of asymptotic bonding field, so appropriately for a phase-transition analysis too.

On the other side, practical implementation requires the asymptotic chemical field to be defined. As suggested by conceptual DFT (Geerlings et al. 2003; Putz and Chattaraj 2013), a suitable choice may be derived from the asymptotic electronic density form determined by the ionization potential (IP), proportional to "inertia" in chemical hopping (IP $\approx v_2$):

$$\phi_\infty(r, v_2) = \exp\left(-\frac{r}{a_0}\sqrt{2v_2/Ha}\right) \tag{20.16}$$

where v_2 is energetically normalized by appropriate Hartree's atomic unit of energy $Ha = 27.11$ eV. Note that the field normalization condition is not a compulsory quantum constraint when particles are created by the quantum field as it is the present case with Eq. (20.16).

With expression (20.16), the bondonic field (20.15) becomes

$$\phi_B = e^{-\frac{r}{a_0}\sqrt{2v_2/Ha}}\left[1 + 3\beta v_2 e^{-4\frac{r}{a_0}\sqrt{2v_2/Ha}}\right] \tag{20.17}$$

so depending only on hopping potential (or chemical inertia potential) and the radius of chemical field action and having the temperature (the inverse of β) as an intensive physical parameter.

Finally, the bondonic mass will result from spatially integrating the squares of Eq. (20.17) appropriately scaled on the electronic bare mass (m_0) and on the first Bohr radius (a_0):

$$
\begin{aligned}
m_B &= \frac{m_0}{a_0}\int_0^\xi e^{-2\frac{r}{a_0}\sqrt{2v_2/Ha}}\left[1 + 3\beta v_2 e^{-4\frac{r}{a_0}\sqrt{2v_2/Ha}}\right]^2 dr \\
&= \frac{m_0}{10\sqrt{2v_2/Ha}}\left[\begin{array}{l} 5\left(1 - e^{-2\frac{\xi}{a_0}\sqrt{2v_2/Ha}}\right) \\ +10\beta v_2\left(1 - e^{-6\frac{\xi}{a_0}\sqrt{2v_2/Ha}}\right) \\ +9\beta^2 v_2{}^2\left(1 - e^{-10\frac{\xi}{a_0}\sqrt{2v_2/Ha}}\right)\end{array}\right]
\end{aligned}
\tag{20.18}
$$

The equation displays the interesting dependence on what we can safely call the bondonic "eccentricity" (ξ) viewed as the action radii over the entire structure it characterizes or evolves, including the teleportation or entangled phenomena – see

the Introduction section and Putz and Ori (2015a); it fortunately identifies with the eccentricity topological index as defined by the molecular topology theory – see the next section.

In practical cases, one should consider the result of Eq. (20.18) only in the asymptotical region of temperature $\beta \to 0$, where the above asymptotic chemical field (ϕ_∞) is active (see the comments of the above Eq. (20.15)), so arriving to the bondon-to-electron working mass ratio:

$$\left(\frac{m_B}{m_0}\right)_{\beta \to 0} = \frac{1}{2\sqrt{2v_2/Ha}}\left(1 - e^{-2\frac{\xi}{a_0}\sqrt{2v_2/Ha}}\right) \qquad (20.19)$$

Remarkably, for the unitary hopping amplitude (i.e., equal with one atomic unit taken as the elementary energetic in nanoworld regime)

$$v_2/Ha \to 1 \qquad (20.20)$$

one may evaluate the general bondonic behavior for extended (infinite) structures in the limit of large eccentricity values, viz., the ideal conditions of the symmetry breaking manifestation from higher-to-lower theory (see the Introduction section); Eq. (20.19) has the analytical limit

$$\left(\frac{m_B}{m_0}\right)_{\substack{\beta \to 0 \\ T \to \infty \\ v_2/Ha \to 1}} = \frac{1}{2\sqrt{2}}\left(1 - e^{-2\frac{\xi}{a_0}\sqrt{2}}\right) \xrightarrow{\xi \to \infty} \frac{1}{2\sqrt{2}} = 0.353553 \qquad (20.21)$$

The result of Eq. (20.21) recalls of the so-called quark chemistry/quark electronegativity (Lackner and Zweig 1983) now at the level of bondonic quasiparticle describing and driving the chemical bonding in molecules and/or complex systems.

The present formalism will be in the next two sections specialized for topological and topo-reactivity modeling of chemical bond by bondons with systematic illustration on graphene structures with successive topological defect/wave propagation.

20.3 Topo-bondons on Graphenic Nanoribbons

The role of topology in influencing the chemical properties of molecules made by similar units (e.g., molecules formed by hexagonal rings only) is conveniently described by the distance-based Wiener index $W(N)$ characterizing the hydrogen-depleted molecular graphs (Putz et al. 2013a; Putz and Ori 2015a). For a chemical graph $G(N)$ with N atoms, the integer number $W(N)$ represents an invariant of the

graph (Wiener 1947) corresponding to the sum of the minimum topological distances d_{ij} of $G(N)$:

$$W(N) = \frac{1}{2} \sum_{ij} d_{ij}, \ d_{ii} = 0, \ i,j = 1, 2, \ldots, N-1, N \tag{20.22}$$

Entries d_{ij} in Eq. (20.22) constitute the $N \times N$ distance matrix of the graph $\widehat{D} = [d_{ij}]$. Matrix $\widehat{D}$ is symmetric by definition and $d_{ij} = d_{ji}$. The Wiener index of Eq. (20.22) measures the average *topological compactness* of the molecular graphs, and, when a minimum principle is superimposed on it, $W(N)$ promptly selects stable systems among the possible candidates, as demonstrated by recent studies (Vukicevic et al. 2011) on C_{66} fullerene cages and defective graphenic planes with nanocones (Cataldo et al. 2010,2011). Various applications of topological modeling (TM) methods are summarized in a recent report (Iranmanesh et al. 2012). In the following relation, $M(N)$ is the graph *diameter* (e.g., the largest distance in the graph), b_{ik} is the number of k-neighbors of the i-atom, and the contribution w_i to Eq. (22) due to i-atom is

$$w_i = \frac{1}{2} \sum_k k b_{ik}, \ k = 1, 2, \ldots, M-1, M \tag{20.23}$$

with

$$W(N) = \sum_i w_i \tag{20.24}$$

and

$$1 - N = \sum_k b_{ik} \tag{20.25}$$

for each graph vertex v_i. From Eq. (20.23), both minimal $\underline{w}$ and maximal $\underline{\underline{w}}$ contributions to $W(N)$ are calculated:

$$\underline{w} = \min\{w_i\}, \ i = 1, 2, \ldots, N-1, N \tag{20.26}$$
$$\underline{\underline{w}} = \max\{w_i\}, \ i = 1, 2, \ldots, N-1, N \tag{20.27}$$

There are two new important invariants, namely, the *topological efficiency (sphericity) index* ρ

$$\rho = \frac{W}{N\underline{w}}, \ \rho \geq 1 \tag{20.28}$$

and the *extreme topological efficiency (E-sphericity) index* ρ^E:

$$\rho^E = \frac{\underline{\underline{w}}}{\underline{w}}, \ \rho^E \geq 1 \tag{20.29}$$

The descriptor ρ was first introduced to investigate graphenic lattices (Cataldo et al. 2010), whereas ρ^E has recently been proposed (Schwerdtfeger et al. 2014) and successfully applied to classify the topological stability of schwarzitic infinite lattices (De Corato et al. 2012). Along the E-sphericity, by definition, the sphericity invariants will show a preference for chemical structures growing in the most compact manner around their minimal sites; for instance, for benzene or $C_{60} - I_h$ buckminsterfullerene, these indices reach the lower limits $\rho = \rho^E = 1$, the topological signature of a chemical structure made by symmetry-equivalent atoms. Only few exceptions have been discovered so far to this rule, e.g., the $C_{240} - I_h$ cage, the smallest icosahedral fullerene with non-transitive atoms and maximal sphericality (Ori et al. 2014).

Such considerations inspire the guiding criterion for stable systems, i.e., *the smallest is the topological efficiency index, and the highest is the stability of the chemical structure under focus*. In this line of analysis, it is worth observing that the stability peculiar property allows the conceptual correspondence with the chemical reactivity descriptors of chemical reactivity such as the electronegativity and chemical hardness (Pearson 1997):

$$\begin{cases} \rho \leftrightarrow -\chi \\ \rho^E \leftrightarrow \eta \end{cases} \tag{20.30}$$

The correspondence (20.30) is supported by the min–max definitions (20.28) and (20.29) of topological efficiency invariants with the min–max variational principles specific to electronegativity and chemical hardness (see the next section), all linked to the molecular stability from where also is the justification of the "sphericity" name.

Going now to further explore the topological distances in a chemical compound by counting the chemical bondings in the associated chemical graph (G), for a given vertex v_i of G, one calls the *eccentricity* ε_i as the largest distance between v_i and any other vertex of G, with the graph diameter M being the maximum possible eccentricity, $M = \max\{\varepsilon_i\}$. Therefore, the *eccentric connectivity index* $\xi(N)$ of a graph G is analytically defined as (Sharma et al. 1997)

$$\xi(N) = \frac{1}{2} \sum_i b_{i1} \varepsilon_i \tag{20.31}$$

where b_{i1} is the number of bonds of atom v_i; clearly, $b_{ik} = 0$ for $\varepsilon_i < k \leq M$. However, recent studies (Dureja and Madan 2007; Kumar et al. 2004; Ashrafi et al. 2011; Doslic et al. 2010, 2011) have shown various applications of the molecular descriptor (20.31) to the study of chemical–physical properties of molecules and crystals, while in this work ξ will have the original role of measuring the range of action of the bosonic chemical field spread around a given chemical structure by the collective movements of its *bondons*, which is collectively behaving as the *delocalized quanta of the chemical field* (Putz and Ori 2012, 2014a); see also the discussion for graphene in the Introduction section.

Recently, Putz and Ori (2014b) proposed a new version of this topological index, named *Timişoara eccentricity* (EC^{TM}) *index*. This topological index can be defined as the shell summation of $b(v)\varepsilon(v)\tau(v)$ over all vertices v, where $\tau(v)$ is the number of atoms at the shell distance $\varepsilon(v)$ from atom v:

$$\xi^{TM}(N) = \frac{1}{2}\sum_{i=1}^{i=N} b_{i1}\varepsilon_i\tau_i \tag{20.32}$$

This index (yet without the prefactor 1/2) was employed along the ordinary eccentricity as in Eq. (20.31) to find closed formulas for sphericality index of four infinite series of fullerenes (Koorepazan-Moftakhar et al. 2014) while being further devoted to study of nanocones and fullerenes so proving that EC^{TM} index of a fullerene can be bounded by a polynomial of degree 2, for 12 infinite series of fullerenes. In the last case, it was also shown that in one pentagonal carbon nanocone with exactly $5N^2 + 10N + 5$ carbon atoms, one has $\rho \approx 1.24$ and $EC^{TM} = 280N^3 + 385N^2 + 195N + 40$, while the dual of this nanocone still preserves the sphericity $\rho \approx 1.24$ but not the eccentricity $EC^{TM} = 70N^3 + 20N^2 - 5N$ (Koorepazan-Moftakhar et al. 2015). In connection with the shell distance distribution, the reader is invited to consult Diudea's papers (Diudea 1994, 2010; Diudea and Ursu 2003; Diudea et al. 1994).

Overall, topological methods have applications in various chemical sectors, from small molecule to biological systems, in studying, for example, enzyme-catalyzed reactions and protein folding kinetics till the DNA sequence characterization (Randić, et al. 2011). Topological descriptors are also tools for QSAR/QSPR modeling and, furthermore, are able to individuate the regions which are stabilized (or, vice versa, made reactive) by certain topological interactions. The Wiener indices above and other distance-based invariants, constrained by the minimum principle, oppose any unfavorable topological variation in the molecular structure (e.g., chemical transformations) so driving/modeling the chemical stability dynamics, being suitable as parameters for the spontaneous symmetry breaking topological analysis. Yet, although topological models characterize chemical structures with astonishing details by the carried topological information (eventually complemented by quantum chemical methods by geometrical information content), they are able to predict novel chemical mechanisms. Besides, the recently reported topological methods were employed for simulating complex chemical mechanism and interesting chemical structures while preserving the computational simplicity, an evident alliance between chemistry and mathematics in explaining how the nanoworld works (Putz et al. 2015).

Returning to the bondonic existence/movement on hexagonal systems like graphene layers, graphenic nanoribbons (GNRs), and carbon nanotubes (CNTs), it is noticeable that the isolated pentagon–heptagon *single* pair arises from the celebrated Stone–Wales (SW) transformation or SW rotation (Stone and Wales 1986); they are important topological structural defects largely influencing chemical, mechanical, and electronic properties (Terrones et al. 2010); see Fig. 20.3.
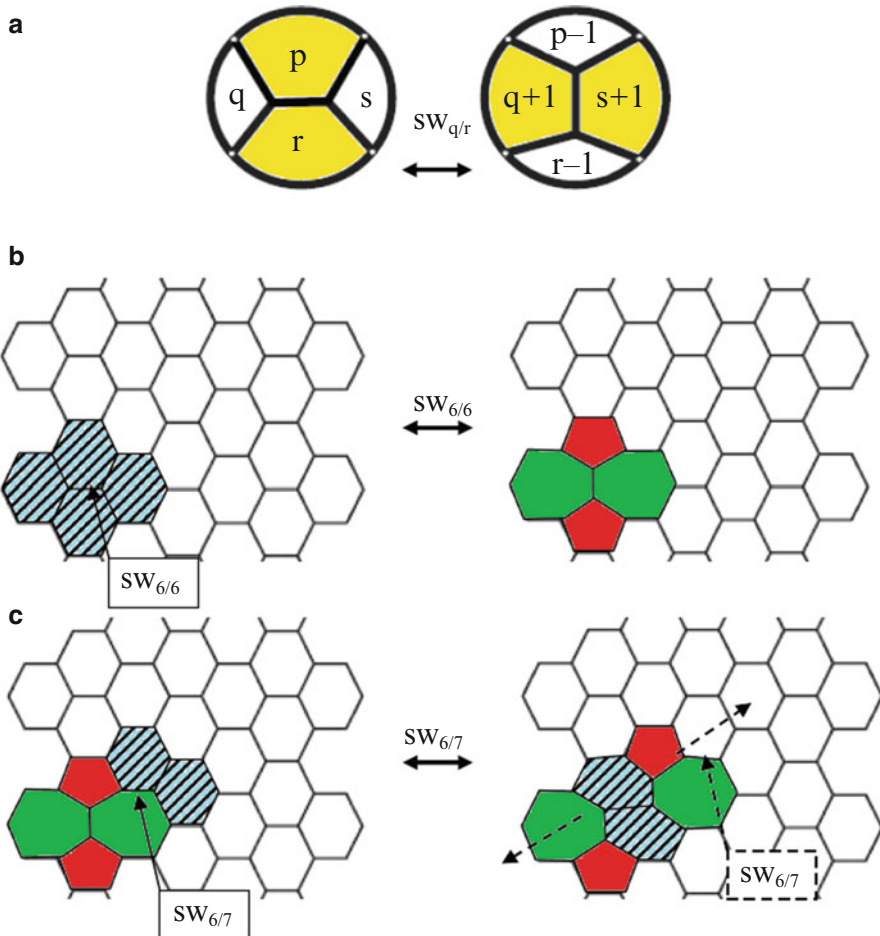
Fig. 20.3 (**a**) Local transformation $SW_{q/r}$ changes in a group of four proximal faces with p, q, r, and s atoms in four new rings with $p-1$, $q+1$, $r-1$, and $s+1$ atoms; (**b**) $SW_{6/6}$ (shaded) originates two 5|7 pairs; (**c**) $SW_{6/7}$ splits the pairs by swapping one of them with two nearby hexagons (shaded). Dotted $SW_{6/7}$ pushes the SW wave in the dashed direction, after Ori et al. (2011)

Moreover, the diffusion of a 6|7 pair in the hexagonal network appears as a consequence of iterated SW rotations; this topology-based mechanism *that produces a linear rearrangement of the hexagonal mesh* is called here the *SW wave*. SW waves allow 5|7 dislocations also to be annealed by just involving surrounding 6|6 pairs and moving *backward*, being all transformations in Fig. 20.3 completely *reversible*, so appropriately to support bondons–antibondons alike, according to the quantum mechanism described in Fig. 20.1.

On the computational side, e.g., by using the extended Hückel method, once enlarging the relaxation region around the SW defect, viewed as a *dislocation dipole*, one can found that the formation energy of such SW defect considerably decreases to 6.02 eV in a flat graphene fragment case. This result has been verified by using *ab initio* pseudopotential (Zhoua and Shib 2003). On the experimental side, accurate high-resolution TEM studies made on single-walled carbon nanotubes (Hashimoto et al. 2004) or electron-irradiated pristine graphene (Kotakoski et al. 2011) document *in situ* formation of SW dislocation dipoles. TEM measured also the evidence for stable grain boundaries with alternating sequence of pentagons and heptagons that show the relevance of wavelike defects during graphene edge reconstruction (Chuvilin et al. 2009).

This choice limits the $SW_{p/r}$ rotations that reside just to the operators $SW_{6/6}$ and $SW_{6/7}$; see Fig. 20.3. In spite of the apparent simplicity of our model, *SW waves present* an evident and *marked topological anisotropy* immediately signaled by the Wiener index (Todeschini and Consonni 2000) and the above allied stability or spherical topo-descriptors. Accordingly, the passage to the actual bondonic mass information can be acquired through the one-to-one correspondences between the potential amplitudes of Eq. (20.4) and the topological indices (20.28) and (20.29):

$$\begin{cases} v_1 \leftrightarrow (Ha)\rho \\ v_2 \leftrightarrow (Ha)\rho^E \end{cases} \tag{20.33}$$

The rules (20.33) transform the potential (20.4) into the actual one:

$$V(\phi) = -(Ha)\rho\phi^2 + \frac{1}{2}(Ha)\rho^E\phi^4 \tag{20.34}$$

Equation (20.34) leads with the respective dimensional transformation of the relation (20.19) into the actual topological bondonic mass formulation:

$$\left(\frac{m_B}{m_0}\right)_{\beta \to 0} = \frac{1}{2\sqrt{2\rho^E}}\left(1 - e^{-2\frac{\xi^{TM}}{<a_0>}\sqrt{2\rho^E}}\right) \tag{20.35}$$

with two amendments regarding the eccentricity: one regards the fact that it is worth exploring both the direct and TM forms of it according to Eqs. (20.31) and (20.32), respectively, and the second the remaining of the normalization of the eccentricity exponential factor to the nominal value of the Bohr radius, taken without dimension ($< a_0 >= 0.529$), yet at the atomic scale (angstroms) so preserving the physical nano-bonding information inside the purely topological approach. The topological bondon is now explored and characterized by the allied mass (20.35) for a successive series of SW wave propagation on a graphenic nanoribbon cell, as in Table 20.1.

The structures in step 0–step 6 of Table 20.1 were computed within two-layer ONIOM (Our own N-layered Integrated molecular Orbital and molecular Mechanics) Gaussian algorithm for large systems by using HF/6-31G(d) for the high-level layer (Dapprich et al. 1999), while for the low-level layer, the molecular mechanics, AMBER (as Assisted Model Building with Energy Refinement) methodology

Table 20.1 The topological information of Eqs. (20.22), (20.23), (20.24), (20.25), (20.26), and (20.27) for $N = 238$ carbon graphenic nanoribbons then turned into sphericity ρ and E-sphericity ρ^E and eccentricity ξ and Timişoara eccentricity ξ^{TM} indices of Eqs. (20.28) and (20.29) and (20.31) and (20.32), respectively, along the computed associated bondonic-to-electronic masses ratio (20.35) for the Stone–Wales topological defect/wave propagation on a supercell nanoribbon in high-temperature/ultrashort time dynamics regime; see text for details

Step structure	W E_ONIOM [a.u.]	Wmin Wmax	ρ	ρ^E	$\xi(N)$ $\xi^{TM}(N)$	m_Φ/m_0 $(m_\Phi/m_0)^{TM}$
Step 0:	334628	1024.5	1.372377	1.882382	7562	0.257692
	−611.502	1928.5			18679.5	0.257692
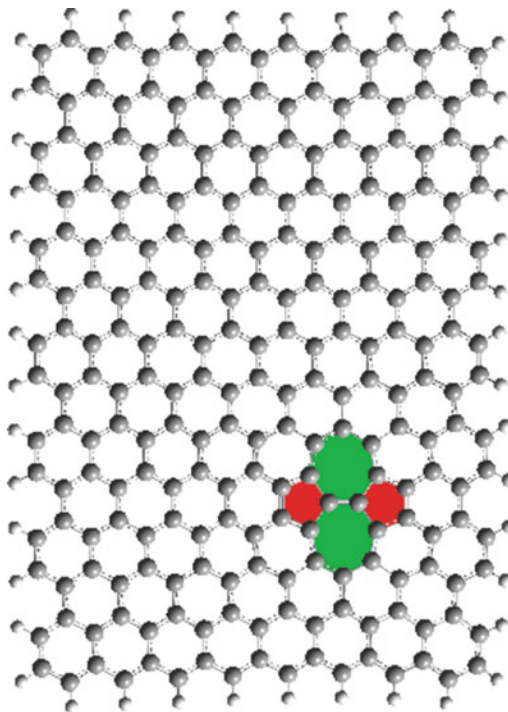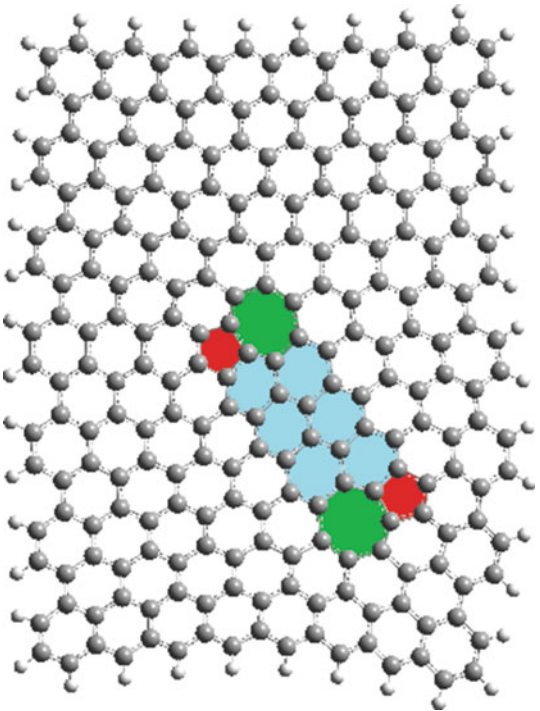
| Step 3: | | 330972 | 1005.5 | 1.383032 | 1.917951 | 7482 | 0.255291 |
| | | −1296.760 | 1928.5 | | | 12414.5 | 0.255291 |

(continued)

Table 20.1 (continued)
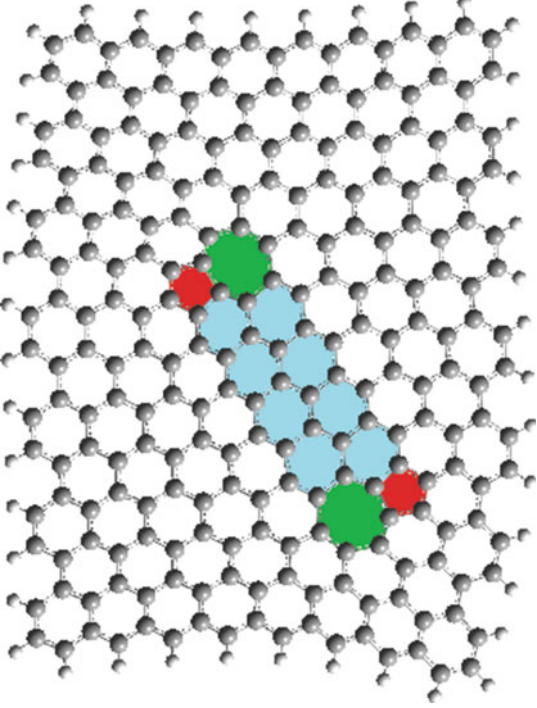
Step structure	W E_ONIOM [a.u.]	Wmin Wmax	ρ	ρ^{E}	$\xi(N)$ $\xi^{TM}(N)$	m_e/m_0 $(m_e/m_0)^{TM}$
Step 4:	330483	1009	1.376198	1.911298	7482	0.255735
	−1525.211	1928.5			10471	0.255735
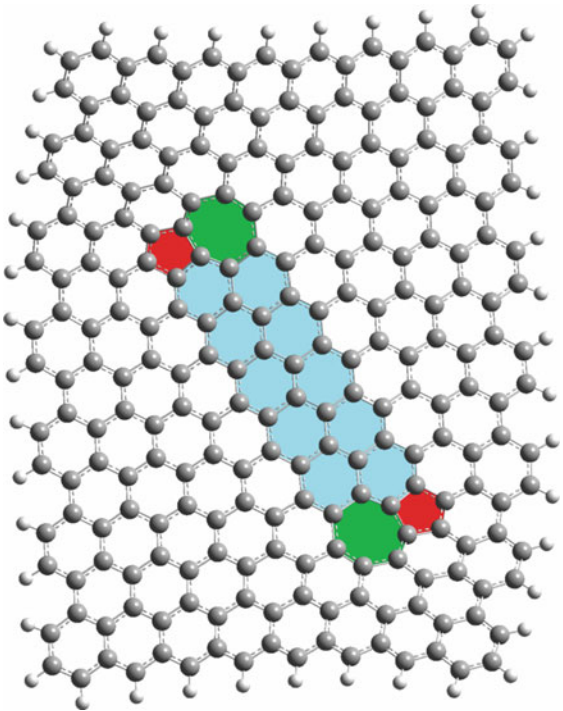
| Step 5: | 330397 | 1012 | 1.371762 | 1.905632 | 7482 | 0.256115 |
| | −1753.549 | 1928.5 | | | 10471 | 0.256115 |

Table 20.1 (continued)

Step structure	W E_ONIOM [a.u.]	Wmin Wmax	ρ	ρ^{E}	$\xi(N)$ / $\xi^{TM}(N)$	m_e/m_0 / $(m_e/m_0)^{TM}$
Step 6:	330655	1014.5	1.36945	1.900936	7482	0.256431
	−1981.695	1928.5			10471	0.256431
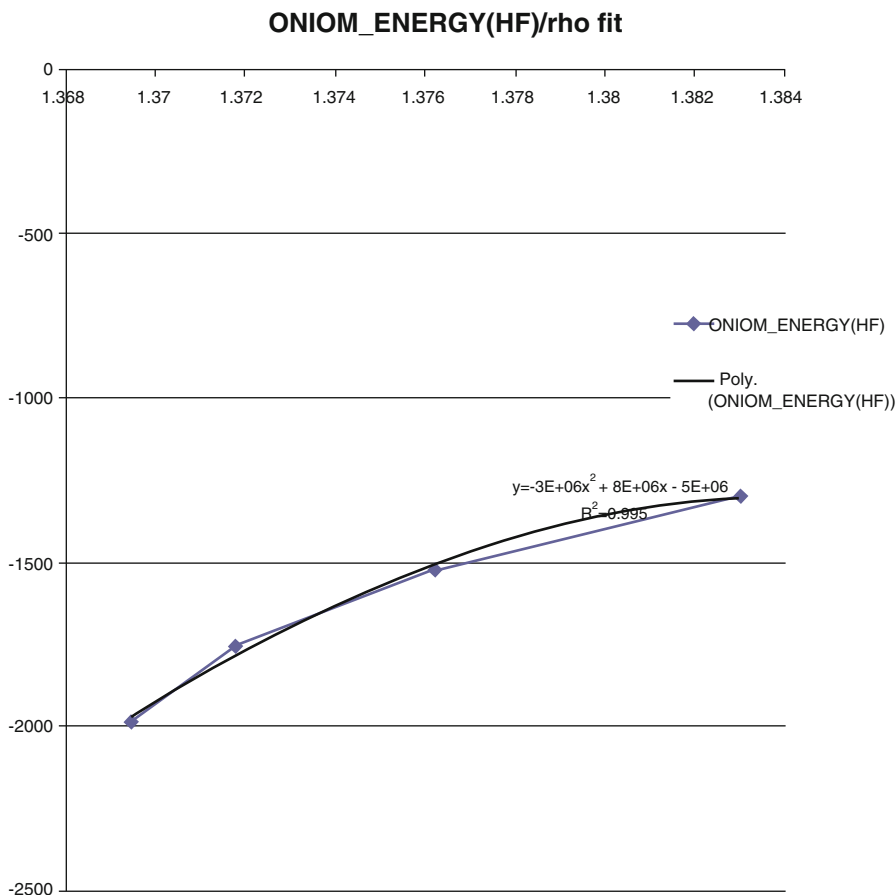
Fig. 20.4 The joined ONIOM energy points as well as their polynomial fit respecting the sphericity ρ parameter for the steps reported in Table 20.1

(Cornell et al. 1995), was used for the universal force field (UFF) – a general algorithm with parameters for the full periodic table up to and including the actinoids; see Rappe et al. (1992).

The main features of the results of Table 20.1 are:

- The main dependence of the bondonic mass to the sphericity (so related to the stability of the graphenic/chemical systems), especially extreme sphericity dependence, since entering both the pre-exponential and exponential factors according to Eq. (20.35).
- The stability nature of the (E-)sphericity concept is here tested (and confirmed) by the parabolic best fit of structural (ONIOM) energy respecting both sphericity ρ and E-sphericity ρ^E, as illustrated in Figs. 20.4 and 20.5, respectively – being

ONIOM_ENERGY(HF)/Erho fit
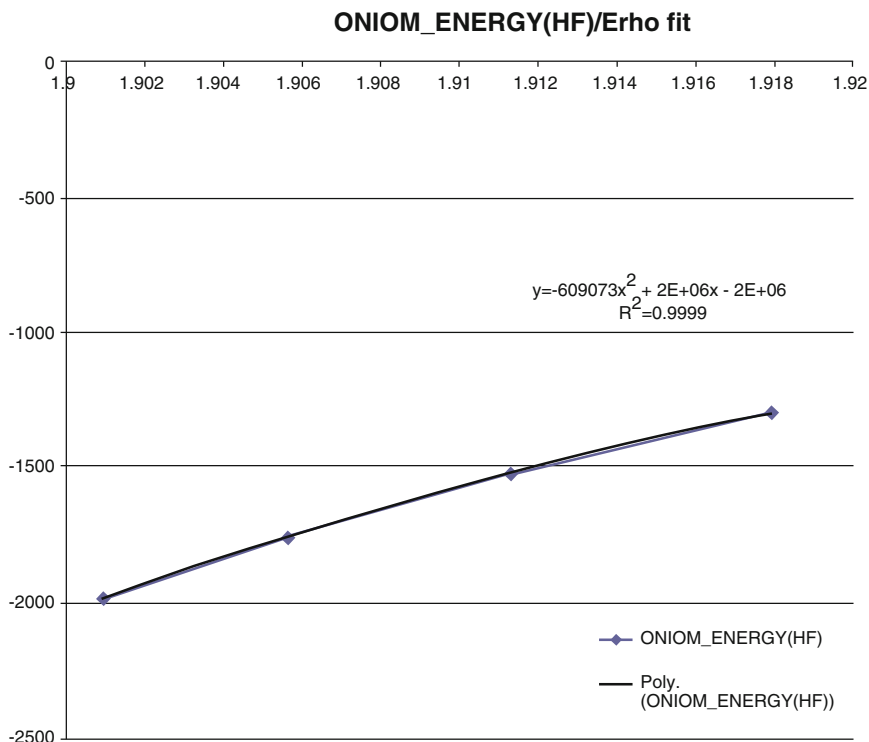
Fig. 20.5 The same kind of representation as in Fig. 20.4 yet for E-sphericity ρ^E for the Stone–Wales defective steps of Table 20.1

this in accordance with the second-order energy–chemical hardness dependence (see Eq. (20.41) in Sect. 20.4, as well as the discussion thereof).

- The bondonic mass seems not to be influenced by the type of eccentricity used, since the genuine and Timişoara (EC-TM) versions give the same results.
- However, Timişoara eccentricity offers more sensitivity to various topological defects on graphene, since panning more defective steps with different values than the genuine eccentricity.
- The bondonic mass itself resulted under the topological limit of Eq. (20.21), $m_B/m_0 < 0.353553$, in all treated topological Stone–Wales cases on graphene, thus suggesting the bosonic "condensation" of electronic pairing is "dissolved" in the entire nanoribbon structure/supercell considered so corresponding to the π-bondons as representing the collective π-electrons on the graphene (see the discussion on graphene in Sect. 20.1), so being "more chemical."
- These π-bondons on graphene behave more at the wave function nature of quantum representation of chemical bonding, so merely corresponding to the massless bosons typical for Goldstone mechanisms of spontaneous symmetry breaking.

- These π-bondons on graphene are of the same nature as the predicted bondons on the basic benzenoids as stable nano-precursors like polycyclic aromatic hydrocarbons (PAHs) in high-temperature regime; see Putz and Ori (2015a).

However, eccentricity remains as the topological ingredient accounting for the action radii of the bondonic emergence, as anticipated from Eq. (19); this way, the Timişoara eccentricity data of Table 20.1 is employed to provide working fit equations respecting the bondon steps on graphenic topological defects' dynamics as well as respecting the (ONIOM) energies, as revealed in Fig. 20.6. It will be further used in the next section employing the topo-reactivity realization of spontaneous emerging of bondons on graphenic nanoribbons.

20.4 Topo-reactivity Bondons on Graphenic Nanoribbons

We constantly made reference throughout this chapter to chemical reactivity and to its descriptors as electronegativity (χ) and chemical hardness (η). It is now the time to unfold more about them within the so-called *chemical orthogonal space* (COS) of chemical bonding (Putz 2012, 2013; Putz and Dudaş 2013) of which definition is based on the phenomenological orthogonality relationship between the indices and the principles, of electronegativity and chemical hardness ($\chi \perp \eta$), as will be cleared below.

Electronegativity is viewed as an instantaneous variation of total (or valence) energy of a neutral or charged system with N-electrons (Parr and Yang 1989):

$$\chi \equiv -\left(\frac{\partial E_N}{\partial N}\right)_{V(r)} \tag{20.36}$$

It may also be related to frontier electronic behavior by performing the central finite difference upon Eq. (20.36) in terms of ionization potential (IP) and electronic affinity (EA), thus facilitating further connection with the highest occupied and lowest unoccupied molecular orbitals (HOMO and LUMO), respectively, according to Koopmans' frozen spin orbitals' theorem (Koopmans 1934):

$$\chi_{FD} \cong \frac{(E_{N_0-1} - E_{N_0}) + (E_{N_0} - E_{N_0+1})}{2}$$
$$\equiv \frac{IP + EA}{2} \cong -\frac{\varepsilon_{\text{LUMO}} + \varepsilon_{\text{HOMO}}}{2} \tag{20.37}$$

As such, in the course of a chemical reaction or in chemical reactivity in general, electronegativity basically assures the energetic stabilization through equalization of middle HOMO–LUMO levels among the adducts which identifies it with the negativity of the chemical potential of a system according to Parr et al. (1978); this feature is supported by natural thermodynamic law of two fluids in contact, since
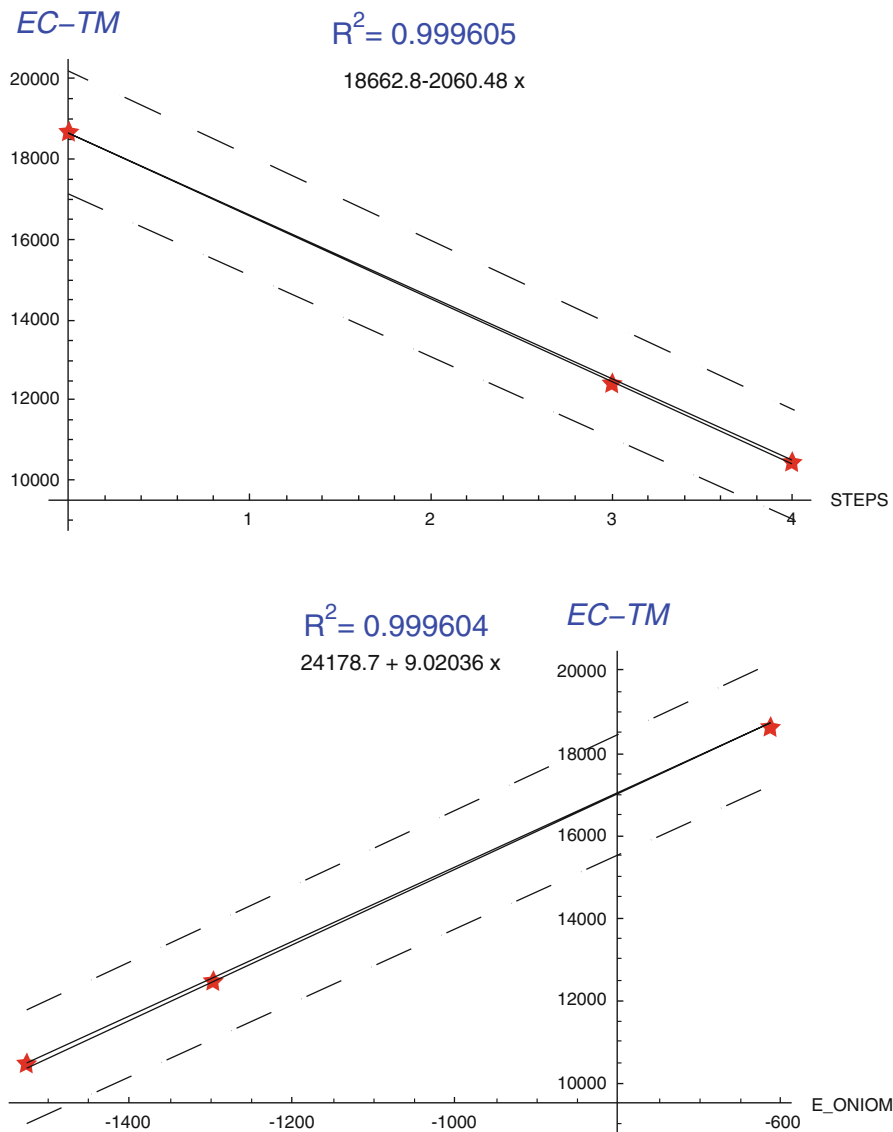
Fig. 20.6 The Timișoara eccentricity (EC-TM, ξ^{TM}) fit for topological defective steps (upper representation) and for ONIOM energy (lower representation) by employing the first three nanoribbon configurations of graphene with Stone–Wales defects' propagation in Table 20.1

they evolve toward equalization of the individual chemical potentials into a global one, being this principle already consecrated in the solid-state physics (Mortier et al. 1985); in chemistry it was coined to represent the so-called *electronegativity equalization (EE) principle*:

$$\Delta\chi = 0 \qquad (20.38)$$

as originally stated by Sanderson under the assumption according to which "for molecules in their fundamental state, the electronegativities of different electronic regions in the molecule—are equal" (Sanderson 1988); however, its variational form was recently clarified within the context of the double-variational procedure (Putz 2011b), specific to chemical systems:

$$\delta\chi \leq 0 \qquad (20.39)$$

under the minimum electronegativity principle stating that "a chemical reaction is promoted so as to minimize further charge transfer between atoms-in-molecules or between molecular fragments within a complex" (Tachibana 1987; Tachibana and Parr 1992; Tachibana et al. 1999). Nevertheless the minimum electronegativity principle for stability ("inert" chemical systems) was firstly formulated by Parr and Yang (1984) understanding it as contrary to its maximum form favoring chemical reactivity (Parr and Yang 1984; Yang et al. 1984): "given two different sites with generally similar disposition for reacting with a given reagent, the reagent prefers the one which on the reagent's approach is associated with the maximum response of the system's electronegativity. In short, $\Delta\chi \geq 0$ is good for reactivity (n. a.)." Yet, for assessing the chemical stability, the reverse form of the latter idea will be considered, from the above minimum electronegativity principle (Eq. 20.39). However, in order to not conflict with the equality of electronegativity, this principle should be seen as quantum fluctuation remnant effects in the system upon which the electronegativity equalization was consumed, *i.e.*, it needs to be further optimized in order that the system maintains its stable equilibrium (Putz 2003).

From such further optimization of electronegativity, the chemical hardness appeared as the instantaneous electronegativity change with charge (Pearson 1997):

$$\eta \equiv -\frac{1}{2}\left(\frac{\partial\chi}{\partial N}\right)_{V(r)} \qquad (10.40)$$

Also chemical hardness finite difference expansion benefits from the Koopmans' frozen spin orbital reformulation at the level of molecular frontier, *i.e.*, where chemical reactivity takes place, through the expression (Putz 2011a)

$$\eta_{FD} = \frac{1}{2}\left(\frac{\partial^2 E_N}{\partial N^2}\right)_{V(r)} \cong \frac{E_{N_0+1} - 2E_{N_0} + E_{N_0-1}}{2} = \frac{IP - EA}{2} \cong \frac{\varepsilon_{LUMO} - \varepsilon_{HOMO}}{2}$$

$$(20.41)$$

At this point, while comparing Eqs. (20.37) and (20.41), it is clear that the electronegativity and chemical hardness may be viewed as the basis for an orthogonal space $\{\chi, \eta | \chi \perp \eta\}$ for chemical reactivity analysis since the conceptual and practical differences noted between the energetic level characterizing the "observed" electronegativity and the energetic gap characterizing the "observed" chemical hardness, respectively (Putz 2009b, 2010b).

Likewise electronegativity, chemical hardness also supports two types of variational equations accompanying the chemical reactions and transformations. The first one promoting equalization of chemical hardness of the atoms in a molecule or between molecular fragments in a complex or between adducts in a chemical bond refers to the so-called the hard and soft acids and bases (HSAB) principle (Chattaraj and Schleyer 1994; Chattaraj and Maiti 2003; Putz et al. 2004):

$$\Delta\eta = 0 \qquad (20.42)$$

It was initially formulated by Pearson affirming that "the species with a high chemical hardness prefer the coordination with species that are high in their chemical hardness, and the species with low softness (the inverse of the chemical hardness) will prefer reactions with species that are low in their softness, respectively" (Pearson 1990). It therefore leads to numerous applications in both inorganic and organic chemistry, since it practically reshapes the basic Lewis and Brönsted qualitative theories of acids and bases into a rigorous orbital-based rule of chemical reactivity and bonding quantification (Pearson 1985). Nevertheless, being of a quantum nature, chemical hardness inherently contains fluctuations leading to the inequality or variational form of its evolution toward bonding stabilization; as such, within the abovementioned double-variational formalism, the actual *maximum hardness principle* was advanced (Chattaraj et al. 1991, 1995; Putz 2008b):

$$\delta\eta \geq 0 \qquad (20.43)$$

stating that the charge transfer during a chemical reaction or binding continues until the resulted bonded complex acquires maximum stability through hardness, *i.e.*, maximizing the HOMO–LUMO energetic gap thus impeding further electronic transitions (Ayers and Parr 2000). It is supported by the Pearson observation according to which "there seems to be a rule of nature that molecules (or the many-electronic systems in general; n. a.) arrange themselves (in their ground or valence states; n. a.) to be as hard as possible" (Pearson 1985); it nevertheless leads to the practical application merely through its inverse formulation, chemical softness; the chemical softness is in turn related with the polarizability features of a system, *i.e.*, as an observable quantity rooted in the quantum structure of the system; accordingly, the resulted minimum polarization principle to be fulfilled for stable systems was successfully tested for various chemical systems (Mineva et al. 1998), including also the symmetry breaking-related phenomena such as

tunneling the rotational barriers accounting for conformational properties and thus for the steric effects (Torrent-Sucarrat and Solà 2006).

It is therefore natural to combine the correspondences (20.30) and (20.33) to produce the actual chemical reactivity basis (with preserving the appropriate energetic bijection scales):

$$\begin{cases} v_1 \leftrightarrow -\chi \\ v_2 \leftrightarrow \eta \end{cases} \tag{20.44}$$

so ruling out the working chemical reactivity potential (20.4) under the form

$$V(\phi) = \chi\phi^2 + \frac{1}{2}\eta\phi^4 \tag{20.45}$$

yielding the respective topo-reactivity bondon-to-electron mass ratio abstracted from Eq. (20.19):

$$\left(\frac{m_B}{m_0}\right)_{\beta \to 0} = \frac{1}{2\sqrt{2\eta/Ha}}\left(1 - e^{-2\frac{\xi}{<a_0>}\sqrt{2\eta/Ha}}\right) \tag{20.46}$$

under correct dimensionalities at the nanoworld scale, as also earlier stressed.

Worth noting that Eq. (20.46) is a mix of chemical reactivity (by the chemical hardness η presence) with the topological information (since the eccentricity dependence was maintained) so justifying the actual topo-reactivity framework for the bondon modeling.

The analysis on the graphenic SW wave propagation is made by completing the previous section nanoribbon topologies of Table 20.1 with all steps, yet along employing the interpolated eccentricity information combined with two computational environments, AMBER and Gaussian, as reported in Table 20.2; for computations, again, the geometry optimization of the investigated structures step 0–step 6 in Table 20.2 has been performed using a two-layer ONIOM algorithm: HF/6-31G(d) was used for the high-level layer; however, for the low-level layer, the molecular mechanics force field, UFF, has been employed – with the alternative AMBER and Gaussian 09 for Windows software used for the HOMO–LUMO (chemical hardness) evaluations.

The results of Table 20.2 display the following bondonic features:

- The bondonic mass analysis benefits from the complete step 0–step 6 instances of graphenic Stone–Wales topological defects' propagation, also due the actual enriched topological with chemical reactivity information.
- The bondonic mass depends now mainly on the chemical hardness (see Eq. (20.46)), accounting for the stability of the systems with defects, as it was previously the case with E-sphericity (see Eq. (20.35)).

Table 20.2 The quantum chemical frontier information as the highest occupied and lowest unoccupied molecular orbitals' energies, ε_{HOMO} and ε_{LUMO}, providing the chemical hardness (η) of Eq. (20.41), for the complete sequence of bondonic propagation on the nanoribbon sheets of Table 20.1, while employing the Timişoara eccentricity topological information under the defective step fits of Fig. 20.6 and completing the missing chemical/HOMO information (*) for the AMBER/step 1 record by proceeding with the appropriate fit by the rest of entries in Fig. 20.7, so providing the associated bondonic-to-electronic masses ratio (20.46) in AMBER and Gaussian 09 W frameworks, respectively; see text for details

Step structure	E_ONIOM [a.u.]	HOMO [a.u.] (AMBER) (Gaussian)	LUMO [a.u.] (AMBER) (Gaussian)	η [eV] (AMBER) (Gaussian)	ξ^{TM} (Steps) ξ^{TM} (E_ONIOM)	$(m_{\text{B}}/m_0)^{TM}$ (AMBER) $(m_{\text{B}}/m_0)^{TM}$ (Gaussian)
Step 0:	−642.61678	(−0.239) (−0.59917)	(0.047) (−0.33286)	(3.87673) (3.60983)	18662.8 18382.1	0.934947 0.968894

Step 1:

−871.13501	(—)	(—)	(3.43607)*	16602.3	0.99309
	(−0.53528)	(−0.26869)	(3.61363)	16320.8	0.968385

(continued)

Table 20.2 (continued)

Step structure	E_ONIOM [a.u.]	HOMO [a.u.] (AMBER) (Gaussian)	LUMO [a.u.] (AMBER) (Gaussian)	η [eV] (AMBER) (Gaussian)	ξ^{TM} (Steps) ξ^{TM} (E_ONIOM)	$(m_B/m_0)^{TM}$ (AMBER) $(m_B/m_0)^{TM}$ (Gaussian)
Step 2:	−1099.55121	(−0.199) (−0.48851)	(0.020) (−0.24258)	2.96854 3.33358	14541.8 14260.4	1.06844 1.00824

Step 3:	−1327.89011	(−0.183)	(0.021)	2.76522	12481.3	1.10702
		(−0.45365)	(−0.23714)	2.93479	12200.7	1.07456

Table 20.2 (continued)

Step structure	E_ONIOM [a.u.]	HOMO [a.u.] (AMBER) (Gaussian)	LUMO [a.u.] (AMBER) (Gaussian)	η [eV] (AMBER) (Gaussian)	ξ^{TM} (Steps) ξ^{TM} (E_ONIOM)	$(m_{\text{H}}/m_0)^{TM}$ (AMBER) $(m_{\text{H}}/m_0)^{TM}$ (Gaussian)
Step 4:	−1556.36495	(−0.174) (−0.42604)	(0.015) (−0.22887)	2.5619 2.67264	10420.9 10139.7	1.15011 1.12603
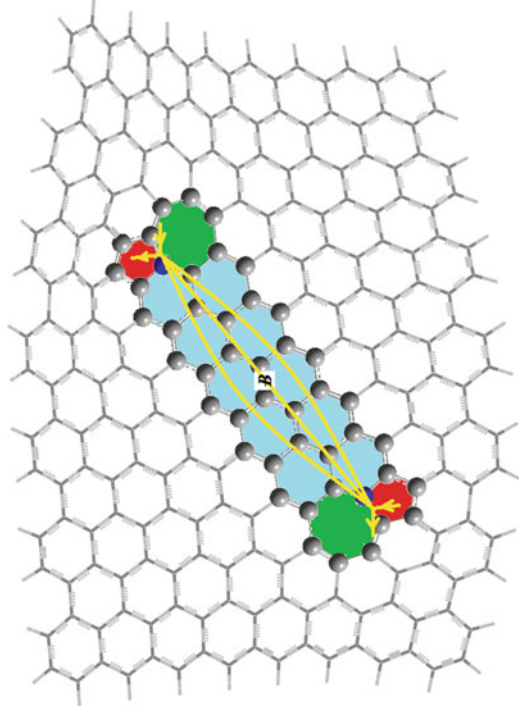
Step 5:	−1784.84185	(−0.167)	(−0.002)	2.23658	8360.38	1.23091
		(−0.40217)	(−0.22014)	2.46742	8078.8	1.17192

Table 20.2 (continued)

Step structure	E_ONIOM [a.u.]	HOMO [a.u.] (AMBER) (Gaussian)	LUMO [a.u.] (AMBER) (Gaussian)	η [eV] (AMBER) (Gaussian)	ξ^{TM} (Steps) ξ^{TM} (E_ONIOM)	$(m_e/m_0)^{TM}$ (AMBER) $(m_e/m_0)^{TM}$ (Gaussian)
Step 6:	−2013.20276	(−0.170) (−0.38227)	(−0.031) (−0.21403)	1.88415 2.28049	6299.9 6018.91	1.3411 1.21901
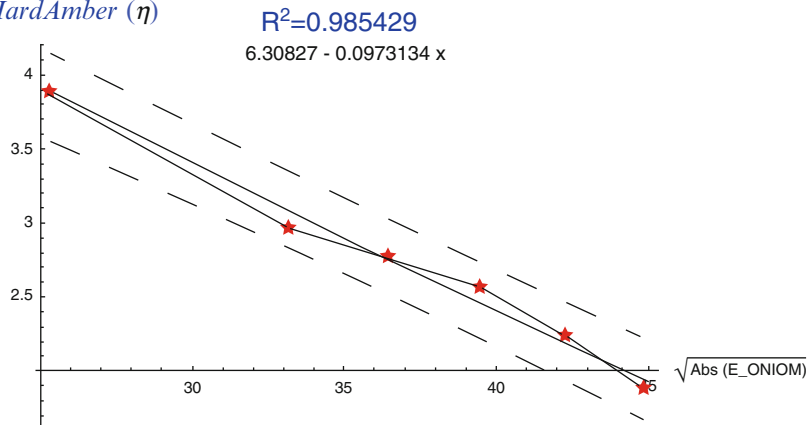
Fig. 20.7 The AMBER chemical hardness fit versus the square root of the ONIOM energies for the bondonic instances associated with the Stone–Wales topological defective waves in Table 20.2

- Chemical hardness dependence appears in both pre-exponential and exponential factors, and, accordingly, it takes over the eccentricity influence, either for graphenic defective steps or (ONIOM) energies.
- Chemical hardness itself is computed following the HOMO–LUMO finite difference receipt of Eq. (20.41), at their turn computed within AMBER or Gaussian computational frameworks (see above); the one single miss in AMBER chemical information for step 1 of defective graphenic nanoribbons is completed by considering the interpolation procedure, graphically illustrated in Fig. 20.7, as based on the rest of entries in Table 20.2, and then accordingly implemented in bondonic topo-reactivity evaluations.
- The bondonic mass results appear in a drastic difference respecting the previous pure topological approach, with the systematic values greatly above the topological limit of Eq. (20.21), $m_B/m_0 > 0.353553$ (see Fig. 20.8); this strongly suggests of heavy mass bosonic–bondonic formation, which continues to grow as the chemical bonding of the topological defect is enlarged.
- These bondons may correspond therefore with the Higgs-like mechanism of emerging of heavy bosons, eventually being "called" as σ-bondons, in opposition to the previously Goldstone-based π-bondons (delocalized, with lower/ dissipative mass).
- These σ-bondons seem to be more massive as the defect is spreading more on the graphenic realm, surpassing the single electronic mass in absolute value, so acquiring the entangled information of the localized paring electrons, despite their spatial long-range separation (see the graphical illustration of bonding– antibonding Feynman connection on the structures of Table 20.2 adapting the bondonic Feynman diagram of Fig. 20.1).
- It is worth noting that the eventually connections between the attractive–repulsive interactions in the bondonic structure associated with the cyclopentane/
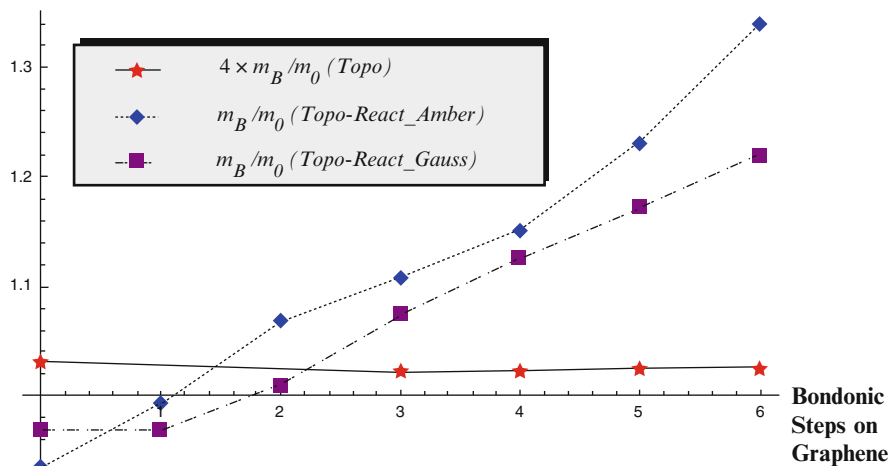
Fig. 20.8 Representation, on a common scale, for the bondon-to-electron mass ratio dynamics along the topological Stone–Wales defects' propagation on a graphenic nanoribbon, for purely topological as well as for topo-reactivity (AMBER and Gaussian) records, as abstracted from Tables 20.1 and 20.2, respectively

heptane connection for the structures of Table 20.2 are still intriguing in the view of Stone–Wales rotation of Fig. 20.3 and deserve a separate study in the near future.

- Such σ-bondonic behavior is nevertheless in accordance with the earlier quantum mechanical bondonic mass determinations, according to which the dependence runs with the inverse of the square of the chemical bonding action radii (Putz 2010a):

$$m \begin{pmatrix} B \\ \widetilde{B} \end{pmatrix} = \frac{\hbar^2}{2} \frac{(2\pi n \pm 1)^2}{E_{\text{bond}} X_{\text{bond}}^2}, \quad n = 0, 1, 2 \dots, \tag{20.47}$$

It is therefore apparent that the chemical reactivity added values to the purely topological approach that brings the bondonic mass, by the spontaneous symmetry breaking, to the level predicted by the Schrödinger–Dirac quantum equations. This finding is in the recent line of topo-reactivity research on carbon-based nanosystems, especially PAHS, where it was proved that always the chemical reactivity information enriches the physicochemical contents of chemical topology approach and improves the concerned structural–chemical property/biological activity correlations (Putz 2011c; Putz et al. 2013a, b, 2016; Tudoran and Putz 2015). Accordingly, this way of topo-reactivity treatment of chemical systems should continue in general and by bondonic chemistry in special.

20.5   Conclusions

Entangled chemistry on graphene seems to be the next frontier in nanosciences: it was nowadays predicted (Putz and Ori 2015b), and the first steps in experimental side were also independently just reported (Tan et al. 2015). When successful it practically will allow the chemical bonding teleportation, control, and/or the molecular design and synthesis on the graphenic pattern; this nevertheless implies the control of the fermionic–bosonic transformation in general and of the wave–particle quantum symmetry breaking at the level of chemical bonding in special. In this context the *bondonic chemistry* appears to be the most adequate conceptual framework in which the delocalization, condensation, and long-range phenomena are unitarily described according to quantum mechanical principles. The bosonic bondon reveals therefore intriguing yet highly versatile properties: it appears either by Schrödinger or Dirac theories (Putz 2010a), yet it can be modeled as emerging from spontaneous symmetry breaking of the chemical field, with mass and dynamics manifestation, according to the high–low epistemology–ontology binomial in the emergence theory in science, respectively. The present chapter contribution follows this line and succeeds in distinguishing among the topo-bondons and topo-reactivity bondons in a systematic way (Putz and Tudoran 2014a,b), here employing the spontaneous symmetry breaking at both analytical and applicative (numerical) levels, so revealing the π-bondonic and σ-bondonic behavior, paralleling the quasi-massless Goldstone-like (mainly depending on the topologically extreme sphericity) and massive Higgs-like (mainly depending on chemical hardness) bondons, respectively. They may be further employed to develop further chemistry at long-range interaction, in an ultrashort time regime, as the next level of quantum matter manifestation: the physics will unify chemistry by bosonization of fermions on bondons, at high electronic velocity on 2D carbon matter, manifesting mass at the short-distance interaction and dissipating into delocalized topology of defects on the other side. A new awaken paradigm of nanoworld matter transformation is at the horizon waiting to be discovered!

References

Agnoli S, Granozzi G (2013) Second generation graphene: opportunities and challenges for surface science. Surf Sci 609:1–5

Anderson PW (1952) An approximate quantum theory of the antiferromagnetic ground state. Phys Rev 86:694–701

Anderson PW (1963) Plasmons, gauge invariance, and mass. Phys Rev 130:439–442

Anderson PW (1972) more is difference. Science 177(4047):393–396

Anderson PW (1984) Basic notions of condensed matter physics. Westview Press, Boulder

Araki Y (2011) Chiral symmetry breaking in monolayer graphene by strong coupling expansion of compact and non-compact U(l) lattice gauge theories. Ann Phys 326:1408–1424

Ashrafi AR, Doslic T, Saheli M (2011) The eccentric connectivity index of TUC4C8 (R) nanotubes. MATCH Commun Math Comput Chem 65:221–230

Ayers PW, Parr RG (2000) Variational principles for describing chemical reactions: the Fukui function and chemical hardness revisited. J Am Chem Soc 122:2010–2018

Batterman R (2002) The devil in the details: asymptotic reasoning in explanation, reduction, and emergence. Oxford University Press, Oxford

Batterman R (2011) Emergence, singularities, and symmetry breaking. Found Phys 41:1031–1050

Bissett MA, Konabe S, Okada S, Tsuji M, Ago H (2013) Enhanced chemical reactivity of graphene induced by mechanical strain. ACS Nano 7:10335–10343

Butterfield J (2011) Less is different: emergence and reduction reconciled. Found Phys 41:1065–1135

Cataldo F, Ori O, Iglesias-Groth S (2010) Topological lattice descriptors of graphene. Mol Simul 36:341–353

Cataldo F, Ori O, Graovac A (2011) Topological efficiency of C66 fullerene. Int J Chem Model 3:45–63

Cavaliere F, De Giovannini U (2010) General Hartree-Fock method and symmetry breaking in quantum dots. Phys E 42:606–609

Chattaraj PK, Maiti B (2003) HSAB principle applied to the time evolution of chemical reactions. J Am Chem Soc 125:2705–2710

Chattaraj PK, Schleyer PVR (1994) An ab initio study resulting in a greater understanding of the HSAB principle. J Am Chem Soc 116:1067–1071

Chattaraj PK, Lee H, Parr RG (1991) Principle of maximum hardness. J Am Chem Soc 113:1854–1855

Chattaraj PK, Liu GH, Parr RG (1995) The maximum hardness principle in the Gyftpoulos-Hatsopoulos three-level model for an atomic or molecular species and its positive and negative ions. Chem Phys Lett 237:171–176

Chung SG (2006) Spontaneous symmetry breaking in Josephson junction arrays. Phys Lett A 355:394–398

Chuvilin A, Meyer JC, Algara-Siller G, Kaiser U (2009) From graphene constrictions to single carbon chains. New J Phys 11:083019

Cornell WD, Cieplak P, Bayly CI, Gould IR, Merz KM Jr., Ferguson DM, Spellmeyer DC, Fox T, Caldwell JW, Kollman PA (1995) Nucleic acids, and organic molecules. J Am Chem Soc 117:5179–5197. http://en.wikipedia.org/wiki/Digital_object_identifier

Dapprich S, Komáromi I, Byun KS, Morokuma K, Frisch MJ (1999) A new ONIOM implementation in GAUSSIAN98: Part 1. The calculation of energies, gradient, vibrational frequencies and electric field derivatives. J Mol Struct (Theochem) 462:1–21

De Corato M, Benedek G, Ori O, Putz MV (2012) Topological study of schwarzitic junctions. in 1D lattices. Int J Chem Model 4:105–113

Dirac PAM (1978) In: Marlow A (ed) Mathematical foundations of quantum theory. Academic, New York

Diudea MV (1994) Molecular topology. 16. Layer matrices in molecular graphs. J Chem Inf Comput Sci 34(5):1064–1071

Diudea MV (2010) Nanomolecules and nanostructures – polynomials and indices, MCM, No. 10. University Kragujevac, Kragujevac

Diudea MV, Ursu O (2003) Layer matrices and distance property descriptors. Indian J Chem A 42 (6):1283–1294

Diudea MV, Topan M, Graovac A (1994) Molecular topology. 17. Layer matrices of walk degrees. J Chem Inf Comput Sci 34(5):1072–1078

Doslic T, Saheli M, Vukicevic D (2010) Eccentric connectivity index: extremal graphs and values. Iranian J Math Chem 1:45–55

Doslic T, Graovac A, Ori O (2011) Eccentric connectivity index of hexagonal belts and chains. Commun Math Comput Chem 65:745–752

Dureja H, Madan AK (2007) Superaugmented eccentric connectivity indices: new-generation highly discriminating topological descriptors for QSAR/QSPR modeling. Med Chem Res 16:331–341

Earman J (2003) In: Brading K, Castellani E (eds) Symmetries in physics. Cambridge University Press, Cambridge, pp 335–346

Egger R, Hausler W, Mak CH, Grabert H (1999) Crossover from Fermi liquid to Wigner molecule behavior in quantum dots. Phys Rev Lett 82:3320–3323

Elias DC, Nair RR, Mohiuddin TMG, Morozov SV, Blake P, Halsall MP, Ferrari AC, Boukhvalov DW, Katsnelson MI, Geim AK, Novoselov KS (2009) Control of graphene's properties by reversible hydrogenation: evidence for graphene. Science 323:610–613

Elitzur S (1975) Impossibility of spontaneously breaking local symmetries. Phys Rev D 12:3978–3982

Englert F, Brout R (1964) Broken symmetry and the mass of gauge vector mesons. Phys Rev Lett 13:321–323

Fradkin E, Shenker SH (1979) Phase diagrams of lattice gauge theories with Higgs fields. Phys Rev D 19:3682–3697

Frauendorf S (2001) Spontaneous symmetry breaking in rotating nuclei. Rev Mod Phys 73:463–514

Fukutome H (1981) Unrestricted Hartree-Fock theory and its applications to molecules and chemical reactions. Int J Quantum Chem 20:955–1065

Geerlings P, De Proft F, Langenaeker W (2003) Conceptual density functional theory. Chem Rev 103:1793–1874

Ghosal A, Guclu AD, Umrigar CJ, Ullmo D, Baranger HU (2006) Correlation-induced inhomogeneity in circular quantum dots. Nat Phys 2:336–340

Goldstone J (1961) Field theories with superconductor solutions. Nuovo Cimento XIX:154–164

Goldstone J, Salam A, Weinberg S (1962) Symmetry groups in nuclear and particle physics. Phys Rev 127:965–970

Guralnik GS, Hagen CR, Kibble TWB (1964) Global conservation laws and massless particles. Phys Rev Lett 13:585–587

Hammes-Schiffer S, Andersen HC (1993) The advantages of the general Hartree-Fock method for future. J Chem Phys 99:1901–1913

Hashimoto A, Suenaga K, Gloter A, Urita K, Iijima S (2004) Direct evidence for atomic defects in graphene layers. Nature 430:870–873

Hempel C, Oppenheim P (2008) In: Bedau MA, Humphreys P (eds.), Emergence. MIT Press, Cambridge (MA), pp 61–80. Originally published in Hempel C (1965) Aspects of scientific explanation and other essays in the philosophy of science. The Free Press/Collier-Macmillan Ltd, New York/London

Higgs PW (1964a) Broken symmetries, massless particles and gauge fields. Phys Lett 12:132–133

Higgs PW (1964b) Broken symmetries and the masses of gauge bosons. Phys Rev Lett 13:508–509

Hoffmann R (2013) Small but strong lessons from chemistry for nanoscience. Angew Chem Int Ed 52:93–103

Hwang C, Siegel DA, Mo SK, Regan W, Ismach A, Zhang Y, Zettl A, Lanzara A (2012) Fermi velocity engineering in graphene by substrate modification. Sci Rep 2(590):1–4

Iranmanesh A, Ashrafi AR, Graovac A, Cataldo F, Ori O (2012) In: Gutman I, Furtula B (eds) Distance in molecular graphs, vol 13, Mathematical chemistry monographs series. Faculty of Science, Kragujevac, pp 35–155

Jalbout AF, Ortiz YP, Seligman TH (2013) Spontaneous symmetry breaking and strong deforma-
    tions in metal adsorbed graphene sheets. Chem Phys Lett 564:69–72
Kalliakos S, Rontani M, Pellegrini V, Garcia CP, Pinczuk A, Goldoni G, Molinari E, Pfeiffer LN,
    West KW (2008) A molecular state of correlated electrons in a quantum dot. Nat Phys
    4:467–471
Kibble TWB (1967) Symmetry breaking in non-abelian gauge theories. Phys Rev 155:1554–1561
Koopmans T (1934) Chemical bonds and bond energy. Physica 1:104–113
Koorepazan-Moftakhar F, Ashrafi AR, Ori O, Putz MV (2015) Topological invariants of
    nanocones and fullerenes. Curr Org Chem 19(3):240–248
Koorepazan–Moftakhar F, Ashrafi AR, Ori O, Putz MV (2014) In: Ellis SB (ed) Fullerenes:
    chemistry natural sources and technological applications. Nova Science Publishers,
    New York, pp 285–304
Kotakoski J, Krasheninnikov AV, Kaiser U, Meyer JC (2011) From point defects in graphene to
    two-dimensional amorphous carbon. Phys Rev Lett 106(105505):1–4
Kuhn H (2008) Origin of life—symmetry breaking in the universe: emergence of homochirality.
    Curr Opin Colloid Interface Sci 13:3–11
Kumar V, Sardana S, Madan AK (2004) Predicting anti- HIV activity of 2,3-diary
    l-1,3-thiazolidin-4-ones: computational approaches using reformed eccentric connectivity
    index. J Mol Model 10:399–407
Lackner KS, Zweig G (1983) Introduction to the chemistry of fractionally charged atoms:
    electronegativity. Phys Rev D 28:1671–1691
Landau LD, Lifshitz EM (1977) The conservation laws of non-relativistic classical and *quantum
    mechanics* for a system of interacting, 3rd edn. Quantum Mechanics Pergamon Press, Oxford
Landsman NP (2007) In: Butterfield J, Earman J (eds) Handbook of the philosophy of science, vol
    2, Philosophy of physics, Part A. North-Holland, Amsterdam, pp 417–553
Landsman NP (2013) Spontaneous symmetry breaking in quantum systems: Emergence or
    reduction? Stud Hist Philos Mod Phys 44:379–394
Landsman NP, Reuvers R (2013) Real- and imaginary-time field theory at finite temperature and
    density. Found Phys 43:373–407
Levy N, Burke SA, Meaker KL, Panlasigui M, Zettl A, Guinea F, Castro Neto AH, Crommie MF
    (2010) Strain-induced pseudo-magnetic fields greater than. Science 329:544–547
Long X, Zhao F, Liu H, Huang J, Lin Y, Zhu J, Luo S-N (2015) Anisotropic shock response of
    Stone–Wales defects in graphene. J Phys Chem C 119(13):7453–7460
Mikami K, Yamanaka M (2003) Strain-induced pseudo–magnetic fields greater than 300 Tesla in
    graphene nanobubbles. Chem Rev 103:3369–3400
Mill JS (1952[1843]) A system of logic, 8th edn. Longmans, Green, Reader, and Dyer, London
Mineva T, Sicilia E, Russo N (1998) Density functional approach to hardness evaluation and use in
    the study of the maximum hardness principle. J Am Chem Soc 120:9053–9058
Monin A, Voloshin MB (2010) Spontaneous and induced decay of metastable strings and domain
    walls. Ann Phys 325:16–48
Mortier WJ, Genechten KV, Gasteiger J (1985) Electronegativity equalization: application and
    parametrization. J Am Chem Soc 107:829–835
Nakamura Y, Yu P, Tsai JS (1999) Coherent control of macroscopic quantum states in a single-
    Cooper-pair box. Nature 398:786–788
Nambu J, Jona-Lasinio G (1961) Dynamical model of elementary particles based on an analogy
    with superconductivity. Phys Rev 122:345–358
Norton JD (2012) Approximation and idealization: why the difference matters. Philos Sci
    79:207–232
Novoselov KS, Fal'ko VI, Colombo L, Gellert PR, Schwab MG, Kim K (2012) A roadmap for
    graphene. Nature 490:192–200
Ori O, Cataldo F, Putz MV (2011) Topological Anisotropy of Stone-Wales Waves in Graphenic
    Fragments. Int J Mol Sci 12:7934–7949

Ori O, Putz MV, Gutman I, Schwerdtfeger P (2014) In: Gutman I, Pokrić B, Vukičević D (eds) Ante graovac – life and works, vol 16, Mathematical chemistry monographs series. Faculty of Science, Kragujevac, pp 259–272

Palmer AR (2004) Symmetry breaking and the evolution of development. Science 306:828–833

Parr RG, Yang W (1984) Density functional approach to the frontier electron theory of chemical reactivity. J Am Chem Soc 106:4049–4050

Parr RG, Yang W (1989) Density functional theory of atoms and molecules. Oxford University Press, New York

Parr RG, Donnelly RA, Levy M, Palke WE (1978) Electronegativity: the density functional viewpoint. J Chem Phys 68:3801–3808

Pearson RG (1985) Absolute electronegativity and absolute hardness of Lewis acids and bases. J Am Chem Soc 107:6801–6806

Pearson RG (1990) Hard and soft acids and bases-the evolution of a concept. Coord Chem Rev 100:403–425

Pearson RG (1997) Chemical hardness. Wiley, Weinheim

Putz MV (2003) Contributions within density functional theory with applications in chemical reactivity theory and electronegativity. Dissertation.com, Parkland

Putz MV (2008a) The chemical bond: spontaneous symmetry – breaking approach. Symmetr Cult Sci 19(4):249–262

Putz MV (2008b) Maximum hardness index of quantum acid–base bonding. MATCH Commun Math Comput Chem 60:845–868

Putz MV (2009a) Path integrals for electronic densities, reactivity indices, and localization function in quantum systems. Int J Mol Sci 10:4816–4940

Putz MV (2009b) Electronegativity: quantum observable. Int J Quantum Chem 109:733–738

Putz MV (2010a) The bondons: the quantum particles of the chemical bond. Int J Mol Sci 11 (11):4227–4256

Putz MV (2010b) Chemical hardness: quantum observable? Studia Univ Babeş-Bolyai–Ser Chem 55:47–50

Putz MV (2011a) Electronegativity and chemical hardness: different patterns in quantum chemistry. Curr Phys Chem 1:111–139

Putz MV (2011b) Chemical action concept and principle. MATCH Commun Math Comput Chem 66:35–63

Putz MV (2011c) In: Putz MV (ed) Carbon bonding and structures: advances in physics and chemistry, vol. 5. Springer, Dordrecht, Chapter 1, pp 1–32

Putz MV (2012) Chemical orthogonal spaces, vol 14, Mathematical chemistry monographs. Faculty of Science, Kragujevac

Putz MV (2013) Chemical Orthogonal Spaces (COSs): from structure to reactivity to biological activity. Int J Chem Model 5:1–34

Putz MV (2016) Quantum nanochemistry. A fully integrated approach: vol III. Quantum molecules and reactivity. Apple Academic Press/CRC Press, Toronto

Putz MV, Chattaraj PK (2013) Electrophilicity kernel and its hierarchy through softness in conceptual density functional theory. Int J Quantum Chem 113:2163–2171

Putz MV, Dudaş NA (2013) The anti-HIV pyrimidines' bonding mechanism. Molecules 18 (8):9061–9116

Putz MV, Ori O (2012) Bondonic characterization of extended nano systems: application to graphene's nanoribbons. Chem Phys Lett 548:95–100

Putz MV, Ori O (2014a) Bondonic effects in group-IV honeycomb nanoribbons with stone-wales topological defects. Molecules 19:4157–4188

Putz MV, Ori O (2014b) Timişoara eccentricity index (TM-EC). Personal Communication. West University of Timişoara, 2−9 March

Putz MV, Ori O (2015a) Predicting bondons by Goldstone mechanism with chemical topological indices. Int J Quantum Chem 115(3):137–143

Putz MV, Ori O (2015b) In: Putz MV, Ori O (eds) Exotic properties of carbon nanomatter, advances in physics and chemistry series, vol 8. Springer, Dordrecht, Chapter 10, pp 229–260

Putz MV, Tudoran MA (2014a) Bondonic effects on the topo-reactivity of PAHs. Int J Chem Model 6(2–3):311–346

Putz MV, Tudoran MA (2014b) Anti-bondonic effects on the topo-reactivity of PAHs. Int J Chem Model 6(4):475–505

Putz MV, Russo N, Sicilia E (2004) On the application of the HSAB principle through the use of improved computational schemes for chemical hardness evaluation. J Comput Chem 25:994–1003

Putz MV, Ori O, Cataldo F, Putz AM (2013a) Parabolic reactivity "Coloring" molecular topology: application to carcinogenic PAHs. Curr Org Chem 17(23):2816–2830

Putz MV, Tudoran MA, Putz AM (2013b) Structure properties and chemical-bio/ecological of PAH interactions: from synthesis to cosmic spectral lines, nanochemistry, and lipophilicity-driven reactivity. Curr Org Chem 17(23):2845–2871

Putz MV, Tudoran MA, Ori O (2015) Topological organic chemistry: from distance matrix to timisoara eccentricity. Curr Org Chem 19(3):249–273

Putz MV, Ori O, Diudea M (2016) In: Aliofkhazraei M, Ali N, Milne WI, Ozkan CS, Mitura S, Gervasoni JL (eds) Graphene science handbook, vol 3. Electrical and optical properties. CRC Press/Taylor & Francis Group, Boca Raton, Chapter 14

Randić M, Zupan J, Balaban AT, Vikić-Topić D, Plavšić D (2011) Graphical representation for protein. Chem Rev 111(2):790–862

Rappe AK, Casewit CJ, Colwell KS, Goddard WA, Skiff WM (1992) UFF, a full periodic table force field for molecular mechanics and molecular dynamics simulations. J Am Chem Soc 114 (25):10024–10035

Reimann SM, Manninen M (2002) Electronic structure of quantum dots. Rev Mod Phys 74:1283–1342

Reimann SM, Koskinen M, Manninen M (2000) Formation of Wigner molecules in small quantum dots. Phys Rev B 62:8108–8113

Ruckenstein E, Berim GO (2010) Contact angle of a nanodrop on a nanorough solid surface. Adv Colloid Interf Sci 154:56–76

Rueger A (2000) Physical emergence, diachronic and synchronic. Synthese 124:297–322

Rueger A (2006) Functional reduction and emergence in the physical sciences. Synthese 151:335–346

Sanderson RT (1988) Principles of electronegativity. J Chem Educ 65:112–119

Schwerdtfeger P, Wirz L, Avery J (2014) Program FULLERENE – a fortran/C++ program for creating fullerene structures and for performing topological analyses (Version 4.4). Massey University Albany, Auckland. http://ctcp.massey.ac.nz/index.php?group=&page=fullerenes&menu=fullerenes. Accessed 1 May 2014

Sharma V, Goswami R, Madan AK (1997) Eccentric connectivity index: a novel highly discriminating topological descriptor for structure–property and structure-activity studies. J Chem Inf Comput Sci 37:273–282

Sheka EF (2007) Odd electrons in molecular chemistry, surface science, and solid state magnetism. Int J Quantum Chem 107:2935–2955

Sheka EF (2012) Computational strategy for graphene: insight from odd electrons correlation. Int J Quantum Chem 112:3076–3090

Sheka EF (2013) Molecular Theory of Graphene. In: Hetokka M, Brandas E, Maruani J, Delgado-Barrio G (eds) Prog Theor Chem Phys 27:249–284

Sheka EF (2014) The uniqueness of physical and chemical natures of graphene: their coherence and conflicts. Int J Quantum Chem 114:1079–1095

Sorkin A, Iron MA, Truhlar DG (2008) Density functional theory in transition-metal chemistry: relative energies of low-lying states of iron compounds and the effect of spatial symmetry breaking. J Chem Theory Comput 4:307–315

Staroverov VN, Davidson ER (2000) Distribution of effectively unpaired electrons. Chem Phys Lett 330:161–168

Stone AJ, Wales DJ (1986) Theoretical studies of icosahedral C60 and some related species. Chem Phys Lett 128:501–503

Tachibana A (1987) Density functional rationale of chemical reaction coordinate. Int J Quantum Chem 21:181–190

Tachibana A, Parr RG (1992) On the redistribution of electrons for chemical reaction systems. Int J Quantum Chem 41:527–555

Tachibana A, Nakamura K, Sakata K, Morisaki T (1999) Application of the regional density functional theory: the chemical potential inequality in the HeH$^+$ system. Int J Quantum Chem 74:669–679

Tan ZB, Cox D, Nieminen T, Lähteenmäki P, Golubev D, Lesovik GB, Hakonen PJ (2015) Cooper pair splitting by means of graphene quantum dots. Phys Rev Lett 114(096602):1–5

Terenziani F, Painelli A, Katan C, Charlot M, Blanchard-Desce M (2006) Chromophores: symmetry breaking and solvatochromism. J Am Chem Soc 128:15742–15755

Terrones M, Botello-Mendez AR, Campos-Delgado J, Lopez-Urias F, Vega-Cantu YI, Rodriguez-Macias FJ, Elias AL, Munoz-Sandoval E, Cano-Marquez AG, Charlier JC, Terrones H (2010) Graphene and graphite nanoribbons: Morphology, properties, synthesis, defects and applications. Nano Today 5:351–372

Todeschini R, Consonni V (2000) Handbook of molecular descriptors. Wiley, Weinheim

Torrent-Sucarrat M, Solà M (2006) Gas-phase structures, rotational barriers, and conformational properties of hydroxyl and mercapto derivatives of cyclohexa-2,5-dienone and cyclohexa-2,5-dienthione. J Phys Chem A 110:8901–8911

Tudoran MA, Putz MV (2015) Molecular graph theory: from adjacency information to colored topology by chemical reactivity. Curr Org Chem 19(4):359–386

Vukicevic D, Cataldo F, Ori O, Graovac A (2011) Topological efficiency of C66 fullerene. Chem Phys Lett 501:442–445

Weinberg S (1996) The quantum theory of fields, vol II. Modern applications, Cambridge University Press, Cambridge, Chapters 19 and 21

Wiener H (1947) The *Wiener* number of graphs. J Am Chem Soc 69:17–20

Wigner EP (1934) On the interaction of electrons in metals. Phys Rev 46:1002–1011

Wu Q, Wu Y, Hao Y, Geng J, Charlton M, Chen S, Ren Y, Ji H, Li H, Boukhvalov DW, Piner RD, Bielawski CW, Ruoff RS (2013) Selective surface functionalization at regions of high local curvature in graphene. Chem Commun 49:677–679

Yang W, Parr RG, Pucci R (1984) Electron density, Kohn-Sham frontier orbitals, and Fukui functions. J Chem Phys 81:2862–2863

Zhoua LG, Shib SQ (2003) Formation energy of Stone-Wales defects in carbon nanotubes. Appl Phys Lett 83:1222–1224

Chapter 21
Counting Distance and Szeged (on Distance) Polynomials in Dodecahedron Nano-assemblies

Sorana D. Bolboacă and Lorentz Jäntschi

Abstract Six dodecahedron nano-assemblies, complexes with 5-, 6-, 12-, 15-, 24-, and 25-dodecahedron units, were constructed by HyperChem software and investigated. Two polynomials, namely, the counting distance polynomial and counting Szeged (on distance) polynomial, graph invariants encoding important properties of the investigated nano-assemblies, have been calculated; the counting polynomial roots were calculated for each investigated nano-assembly. Distinct patterns of polynomial roots were obtained for each of these polynomials, with similarities among dodecahedron congeners.

S.D. Bolboacă (✉)
University of Agricultural Science and Veterinary Medicine Cluj-Napoca, Calea Mănăştur no. 3-5, RO-400372 Cluj-Napoca, Romania

Department of Medical Informatics and Biostatistics, Iuliu Haţieganu University of Medicine and Pharmacy, 6 Louis Pasteur, 400349 Cluj-Napoca, Romania
e-mail: sbolboaca@umfcluj.ro

L. Jäntschi
Department of Physics and Chemistry, Technical University of Cluj-Napoca, Muncii Blvd. no. 103-105, RO-400641 Cluj-Napoca, Romania

Institute for Doctoral Studies, Babeş-Bolyai University, Kogălniceanu Street no. 1, RO-400084 Cluj-Napoca, Romania

University of Agricultural Science and Veterinary Medicine Cluj-Napoca, Calea Mănăştur no. 3-5, RO-400372 Cluj-Napoca, Romania

Department of Chemistry, University of Oradea, Universităţii Street no. 1, RO-410087 Oradea, Romania
e-mail: lorentz.jantschi@gmail.com

21.1 Dodecahedrane and Its Relatives

Dodecahedrane is a chemical compound with 20 carbon atoms and 20 hydrogen atoms first synthesized in 1982 by Leo Paquette at Ohio State University (Ternansky et al. 1982; Paquette et al. 1983). In this molecule, each vertex is a carbon atom that bonds to three neighboring carbon atoms and one hydrogen atom (Fig. 21.1). Five Platonic bodies are recognized as regular 3D polyhedra (Fig. 21.1): tetrahedron, hexahedron/cube, octahedron, icosahedron, and dodecahedron (Friedlander 1964; MacGillivray and Atwood 1999). Several characteristics of Platonic structures are presented in Table 21.1. Tetra-tert-butyltetrahedrane was the first isolated molecule that contains the tetrahedron skeleton (Maier and Pfriem 1978). Tetrakis(trimethylsilyl)tetrahedrane proved to be a stable molecule just at up to 300 °C (Maier et al. 2002). Removal of one silyl group on tetrakis(trimethylsilyl) tetrahedrane can be seen as a step toward the synthesis of tetrahedrane (Sekiguchi and Tanaka 2003; see also Nemirowski et al. 2006).

Cubane, a solid crystalline substance, has been first synthesized in 1964 by Philip Eaton, a professor of chemistry at the University of Chicago (Eaton and Cole 1964a, b). Several nitrated cubanes, dense and highly energetic compounds predicted to be shock insensitive, were investigated (tetra-, penta-, hexa-, hepta-, and octanitro-cubanes) (Kamlet and Jacobs 1968; Eremenko and Nesterenko 1997; Astakhov et al. 1998; Zhang et al. 2000). Polyisocyanocubanes, a possible new generation of explosives, have been proposed in a theoretical study, with the high heats of formation, values of which increasing linearly with the number of isocyano groups in the molecule (Xiao and Zhang 2002).

Dodecahedron shows the highest point group symmetry; this structure, with unusual esthetic beauty (Hopf 2000), does not occur in nature. The stability of dodecahedrane is given by its high symmetry (I_h). Its bond angles (108°) are close to the bond angles in tetrahedrane (109.5°), while the length of the C–C bond (1.54 Å) is close to that in diamond (Banfalvia 2014).

Fig. 21.1 The five Platonic solids or the regular 3D polyhedra

Table 21.1 Characteristics of Platonic solids

Object	Symmetry	Vertices	Edges	Faces
Tetrahedron	T_d	4	6	4
Hexahedron	O_h	8	12	6
Octahedron	O_h	6	12	8
Icosahedron	I_h	12	30	20
Dodecahedron	I_h	20	30	12

Wahl et al. (2006) explored the substitution of the 20 hydrogen atoms in dodecahedrane ($C_{20}H_{20}$) by OH ($C_{20}(OH)_{20}$), F ($C_{20}F_{20}$, perfluorododecahedranes), Cl ($C_{20}Cl_{20}$), and Br ($C_{20}Br_{20}$); $C_{20}F_{20}$ was obtained only in very low yield, $C_{20}Cl_{20}$ was observed just as a trace component, and $C_{20}(OH)_{20}$ is yet an elusive compound, while $C_{20}Br_{20}$ was not identified. Perfluorododecahedrane ($C_{20}F_{20}$) is relatively unstable, merely produced in mg quantities, and the synthesis of different branched and linear polymer beads on a string seems to be feasible.

21.2   Dodecahedrane-Linked Complexes

Starting with the dodecahedrane cage, a double-cage molecule formed by a dodecahedrane cage and a pentaprismane cage $C_{25}H_{20}$ was investigated by Liu (2004a) who proved that the molecule shows a certain stability. Two $C_{30}H_{20}$ isomers with one dodecahedrane cage and two pentaprismane cages were investigated in a theoretical study regarding structures, energies, and vibrational frequencies (Liu et al. 2005a). Both isomers have shown values on vibrational analysis and heat of formation that recommend these molecules for experimental preparation (Liu et al. 2005a). Liu et al. (2005b) also investigated a tri-cage molecule with two dodecahedrane cages at both ends and one pentaprismane cage in the center ($C_{40}H_{30}$). The complex proved to be a stable structure (Liu et al. 2005b). Liu (2004b) also built a coplanar double-cage dodecahedrane ($C_{35}H_{30}$) and identified it as a potential candidate for experimental study.

Modification of the properties of cage structures was done by encapsulating atoms or small molecules inside the structure. One of the earliest studies with atoms/ions encapsulated into the cage of dodecahedrane was done using H^+, H_2, He, Li^+, Li^-, Be, and Be^{2+} (Dixon and Deerfield 1981). Dixon and Deerfield (1981) have shown that $C_{20}H_{20}$–H^+ complex is weakly bound, while that with Be^{2+} is strongly bound. Cross et al. (1999) shouted helium ions at a film of $C_{20}H_{20}$ and thus encapsulated a helium atom inside of one molecule of dodecahedron ($He@C_{20}H_{20}$) obtaining a quite stable complex. This complex is known as "the world's smallest helium balloon." Jiménez–Vázquez et al. (2001) investigated the Ne inside the dodecahedrane molecule ($Ne@C_{20}H_{20}$) and showed that it has an energy (98.3 kcal/mol) almost 3 times higher compared to $He@C_{20}H_{20}$ (33.8 kcal/mol).

Chen et al. (2003) investigated the relative energies/stabilities of the endohedral ($X@C_{20}H_{20}$) and exohedral ($XC_{20}H_{20}$) dodecahedrane complexes ($X = H^+$, H, N, P, C^-, Si^-, O^+, S^+) and showed that exohedral isomers are energetically more favorable than the endohedral ones. Moran et al. (2002) investigated endohedral dodecahedrane complexes ($X@C_{20}H_{20}$; X = H, He, Ne, Ar, Li, Li^+, Be, Be^+, Be^{2+}, Na, Na^+, Mg, Mg^+, and Mg^{2+}) and showed that their stability can be significantly increased by the removal of dodecahedron hydrogens. An et al. (2009) showed that the hydrogens outside of the molecule are not favorable to the electronic transport, while the electronic conductivity is improved when the Li atom is inserted into the $C_{20}H_{20}$ molecule ($Li@C_{20}H_{20}$).

21.3   Dodecahedron Nano-complexes

21.3.1   Nanostructure Complexes

The first three structures from the total number of congeners that can be constructed as pentagonal and hexagonal hyper-faces were built up and characterized by the counting distance and Szeged (on distance) polynomials.

The congeners made from dodecahedral units are as follows:

- Hyper-pentagonal structures, being assemblies of 5 dodecahedron units (75 C atoms, Fig. 21.2, *left*), 15 units (225 C atoms, Fig. 21.3, *right*), and 25 units (375 C atoms, Fig. 21.5)
- Hyper-hexagonal structures, with 6 dodecahedron units (90 C atoms, Fig. 21.2, *right*), 12 units (180 C atoms, Fig. 21.3, *left*), and 24 units (360 C atoms, Fig. 21.4)

21.3.2   Counting Distance-Based Polynomials

Counting distance polynomials are characteristic polynomials of the graph distance matrix (Devillers and Balaban 2000). The distance matrix (d_{ij}) contains as elements the topological distances (equal to the number of edges) calculated on a graph. Floyd (1962) published an algorithm for computing the distance matrix, as:

Fig. 21.2 Hyper-pentagon (by five-dodecahedron units, *left*) and hyper-hexagon (by six-dodecahedron units, *right*)
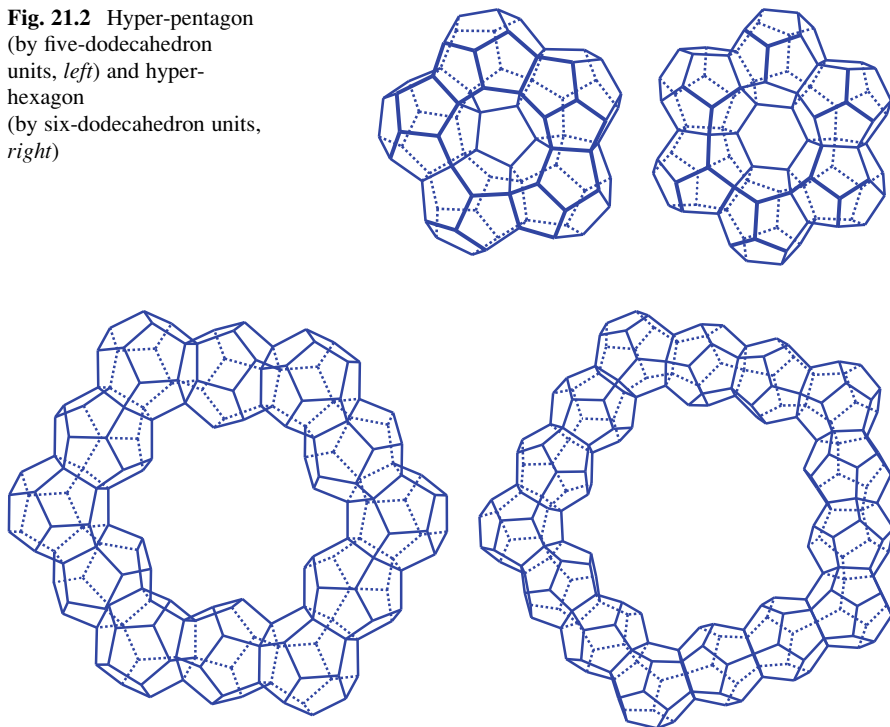
Fig. 21.3 Twelve- (*left*) and 15- (*right*) dodecahedron complexes
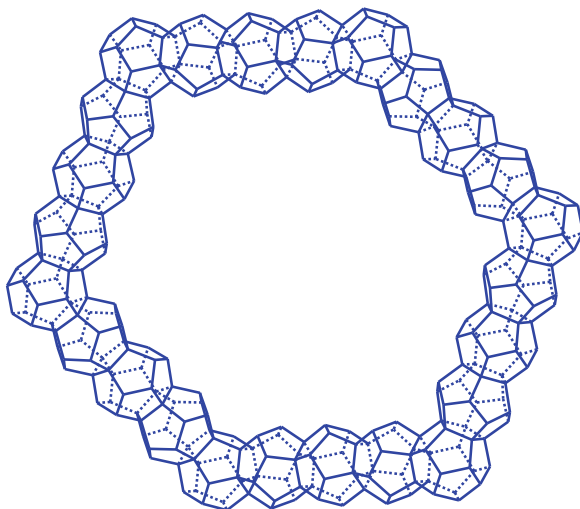
Fig. 21.4 Twenty-four-dodecahedron complex
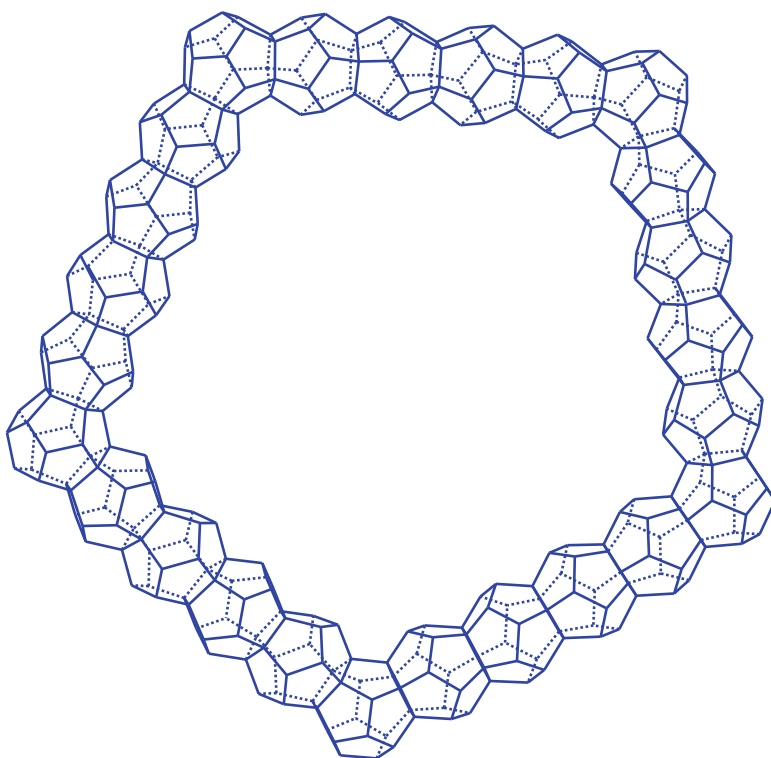
Fig. 21.5 Twenty-five-dodecahedron complex

Table 21.2 Counting distance (*DiM*) and Szeged distance (*SzDM*) counting on path matrices

i\j	1	2	3	4	5	6	7		i\j	1	2	3	4	5	6	7
1	0	1	2	2	2	3	1		1	0	2	3	2	3	4	3
2	1	0	1	1	2	2	2		2	4	0	6	3	3	4	4
3	2	1	0	2	3	3	3		3	1	1	0	1	2	3	2
4	2	1	2	0	1	1	2		4	3	3	4	0	4	6	4
5	2	2	3	1	0	2	1		5	3	2	4	2	0	3	3
6	3	2	3	1	2	0	3		6	2	1	3	1	1	0	2
7	1	2	3	2	1	3	0		7	2	2	3	2	2	3	0

DiM   SzDM

i\j	1	2	3	4		i\j	1	2	3	4
1	0	1	2	2		1	0	1	1	1
2	1	0	1	1		2	3	0	3	3
3	2	1	0	2		3	1	1	0	1
4	2	1	2	0		4	1	1	1	0

DiM   SzDM

i\j	1	2	3	4	5	6	7	8		i\j	1	2	3	4	5	6	7	8
1	0	1	2	2	3	4	5	5		1	0	1	1	1	3	3	4	4
2	1	0	1	1	2	3	4	4		2	7	0	7	3	3	4	4	4
3	2	1	0	2	3	4	5	5		3	1	1	0	1	3	3	4	4
4	2	1	2	0	1	2	3	3		4	5	5	5	0	4	4	5	5
5	3	2	3	1	0	1	2	2		5	5	4	5	4	0	5	5	5
6	4	3	4	2	1	0	1	1		6	4	4	4	3	3	0	7	7
7	5	4	4	3	2	1	0	2		7	4	3	4	3	1	1	0	1
8	5	4	5	3	2	1	2	0		8	4	3	4	3	1	1	1	0

DiM   SzDM

Function: f(*N*,*M*,*A*,*D*)

Arguments: *N* = number of vertices, *M* = number of edges, *A* = adjacency matrix as input data, and *D* = distance matrix as output data

Algorithm:

For each vertex *i* in 1..*N* and for each vertex *j* in 1..*N*:

If $(i \neq j) \& (A[i][j] = 0) \, then \, D[i][j] \leftarrow M + 1 \, else \, D[i][j] \leftarrow A[i][j]$

For each vertex *k* in 1..*N*

For each vertex *i* in 1..*N* and for each vertex *j* in 1..*N*:

If $D[i][j] > D[i][k] + D[k][j] \, then \, D[i][j] \leftarrow D[i][k] + D[k][j]$

Szeged matrix (Diudea et al. 1997) is besides Cluj fragmental matrices (Jäntschi 2000), minimal fragments (Jäntschi and Bolboacă 2009), and maximal fragments (Jäntschi and Diudea 2009), a counting square matrix where the vertices are counted instead of the paths. The formula of unsymmetrical Szeged matrix, defined by paths for distances, as it was used in this study is given by:

$$SzDi_{ij} = \left| \left\{ k \middle| Di_{kj} < Di_{kj} \right\} \right| \tag{21.1}$$

Examples of counting the distance matrix and path Szeged on distance matrix are given in Table 21.2.

The relation with other matrices calculated for molecular graph (connected graph) is shown below:

$$0 \leq Ad_{ij} \leq \mathrm{Min}F_{ij} \leq Di_{ij} \leq De_{ij} \leq \mathrm{Max}F_{ij} \leq N - 1 \leq M$$
$$\mathrm{Min}F_{i,j} \leq SzDi_{i,j} \leq \mathrm{Max}F_{i,j}$$
$$\mathrm{Min}F_{i,j} \leq CfDi_{i,j} \leq \mathrm{Max}F_{i,j}$$
$$\mathrm{Min}F_{i,j} \leq CfDe_{i,j} \leq \mathrm{Max}F_{i,j}$$
$$\mathrm{Min}F_{i,j} \leq SzDe_{i,j} \leq \mathrm{Max}F_{i,j}$$
$$\mathrm{Max}(SzDi_{i,j}, CfDi_{i,j}, CfDe_{i,j}, SzDe_{i,j}, De_{i,j}) \leq \mathrm{Max}F_{i,j} \qquad (21.2)$$

where Ad = adjacency matrix, Di = distance matrix, De = detour matrix, N = number of vertices, M = number of edges, $\mathrm{Min}F$ = minimal fragment matrix, $\mathrm{Max}F$ = maximal fragment matrix, $SzDi$ = Szeged matrix from distances, $CfDi$ = Cluj fragmental matrix from distances, $SzDe$ = Szeged matrix from detours, and $CfDe$ = Cluj fragmental matrix from detours.

The results obtained from layer matrices (i.e., sequence matrices) can be expressed in a polynomial form, and then the polynomials are called counting polynomials. A layer matrix could be derived from a counting square matrix, and thus the general definition of the *counting polynomial* (noted here with $P_{\Sigma M}$) on the matrix M (computed on the graph G) is

$$P_{\Sigma M}(X) = P_{\Sigma}(X, M) = P_{\Sigma}(X, M(G))$$
$$= \Sigma_k a_k X^k, \; a_k = \left| \left\{ M_{i,j} \middle| M_{i,j} = k \right\} \right| \qquad (21.3)$$

The counting polynomials for cycles are defined to count only once each cycle. Distance polynomial (*CDi*) and Szeged polynomial (*CSz*) were used to investigate dodecahedron-based complexes (Figs. 21.2, 21.3, 21.4, and 21.5). These polynomials, besides the characteristic polynomials, proved to be useful in the prediction of nonane isomer properties (Jäntschi 2007; Bolboacă and Jäntschi 2007; Jäntschi et al. 2009).

Free online software hosted by academic direct allows calculation of adjacency, distance, and Szeged matrices whenever the user provides a *.hin file for a molecule:

http://l.academicdirect.ro/Fundamentals/Graphs/polynomials/a_Szeged_Matrices_in.php

© November 22, 2010 Lorentz JÄNTSCHI

Up Please provide as a hin file containing a structure of all non-hydrogen type atoms. Then we will provide to you the following matrices of the structure:

- Adjacency matrix
- Distance matrix
- Szeged matrix

Note: too many vertices (atoms) and/or too many edges (bonds) it will crash the program. A example hin file can be found here.

Browse... No file selected.   Submit Query

Table 21.3 Examples of counting distance and Szeged (on distance) polynomials

Molecule	Matrix	Polynomial
	Distance	$6x^2 + 6x^1 + 4x^0$
	Szeged	$3x^3 + 9x^1 + 4x^0$
	Distance	$8x^5 + 8x^4 + 10x^3 + 16x^2 + 14x^1 + 8x^0$
	Szeged	$4x^7 + 10x^5 + 18x^4 + 12x^3 + 12x^1 + 8x^0$
	Distance	$12x^1 + 4x^0$
	Szeged	$12x^1 + 4x^0$
	Distance	$8x^3 + 24x^2 + 24x^1 + 8x^0$
	Szeged	$32x^4 + 24x^2 + 8x^0$

The main disadvantage of this application is that it allows investigation of a single molecule, while computations are time consuming for large molecules. Note that the matrix is not invariant, if the numbering of atoms in the molecule is changed; contrarily, when the counting polynomials and their roots are calculated, they represent invariants and do not depend on how the atoms are numbered in the molecule.

The counting of distance and Szeged (on distance) polynomials is exemplified in Table 21.3 for C_4, C_8, tetrahedron, and cube. Note that the distance polynomial used in this research is not Hosoya's polynomial (Hosoya 2013).

Several counting polynomials, distance, maximal fragments, complement of maximal fragments, and Szeged and Cluj fragmental matrices, could be computed for any *.hin file using the following online resource:

A look in Table 21.3 provides some information:

- The same degree is observed for both counting distance and Szeged (on distance) polynomials.
- Generally, the degree of Szeged polynomial is higher compared to distance polynomials.

A root of a polynomial $P(z)$ is a number z_i such that $P(z_i) = 0$; a polynomial of degree n has n roots (Pan 1997). The complexity of counting the matrix is directly proportional to the number of atoms in the molecule. In this regard, a PHP program was implemented and used to obtain the distance and Szeged matrices and next to write the polynomials. The collection of all roots for a graph is called the spectrum of the respective molecule and polynomial; in the case of polyhedron complexes herein studied, the roots for both polynomials (either real or imaginary) were investigated for the pattern (if any) of the root values.

21.3.2.1 Counting Distance Polynomial

The counting distance polynomials for the investigated dodecahedron assemblies are listed in Table 21.4. As expected, the degree of polynomial increases as the number of dodecahedron units inside the complex increased.

Several observations can be drawn by analyzing the formulas in Table 21.4:

Table 21.4 Counting distance polynomials (*CDi*) for dodecahedron and its nano-assemblies

Complex	CDi
1-dodeca	$20x^5 + 60x^4 + 120x^3 + 120x^2 + 60x^1 + 20x^0$
5-dodeca	$10x^{10} + 60x^9 + 290x^8 + 580x^7 + 870x^6 + 1000x^5 + 990x^4 + 900x^3 + 600x^2 + 250x^1$ $+ 75x^0$
6-dodeca	$12x^{11} + 72x^{10} + 288x^9 + 684x^8 + 1032x^7 + 1260x^6 + 1320x^5 + 1236x^4 + 1086x^3 + 720x^2$ $+ 300x^1 + 90x^0$
12-dodeca	$48X^{18} + 198X^{17} + 468X^{16} + 1044X^{15} + 1896X^{14} + 2502X^{13} + 2532X^{12} + 2424X^{11}$ $+ 2472X^{10} + 2520X^9 + 2400X^8 + 2304X^7 + 2352X^6 + 2448X^5 + 2400X^4 + 2172X^3$ $+ 1440X^2 + 600X^1 + 180X^0$
15-dodeca	$40X^{22} + 280X^{21} + 1000X^{20} + 2000X^{19} + 2600X^{18} + 2790X^{17} + 2830X^{16} + 2810X^{15}$ $+ 2740X^{14} + 2770X^{13} + 2900X^{12} + 2830X^{11} + 2690X^{10} + 2680X^9 + 2720X^8 + 2760X^7$ $+ 2810X^6 + 2940X^5 + 2950X^4 + 2710X^3 + 1800X^2 + 750X^1 + 225X^0$
24-dodeca	$48X^{34} + 372X^{33} + 1332X^{32} + 3024X^{31} + 4104X^{30} + 4320X^{29} + 4344X^{28} + 4272X^{27}$ $+ 4296X^{26} + 4464X^{25} + 4416X^{24} + 4248X^{23} + 4236X^{22} + 4296X^{21} + 4236X^{20}$ $+ 4284X^{19} + 4284X^{18} + 4224X^{17} + 4248X^{16} + 4368X^{15} + 4248X^{14} + 4116X^{13} +$ $4200X^{12} + 4260X^{11} + 4176X^{10} + 4176X^9 + 4224X^8 + 4332X^7 + 4392X^6 + 4608X^5$ $+ 4680X^4 + 4332X^3 + 2880X^2 + 1200X^1 + 360X^0$
25-dodeca	$370X^{35} + 1590X^{34} + 3420X^{33} + 4330X^{32} + 4450X^{31} + 4360X^{30} + 4260X^{29} + 4290X^{28}$ $+ 4350X^{27} + 4280X^{26} + 4290X^{25} + 4340X^{24} + 4290X^{23} + 4340X^{22} + 4340X^{21}$ $+ 4270X^{20} + 4300X^{19} + 4400X^{18} + 4320X^{17} + 4220X^{16} + 4210X^{15} + 4210X^{14}$ $+ 4170X^{13} + 4300X^{12} + 4350X^{11} + 4280X^{10} + 4280X^9 + 4320X^8 + 4460X^7 + 4510X^6$ $+ 4740X^5 + 4850X^4 + 4510X^3 + 3000X^2 + 1250X^1 + 375X^0$

Table 21.5 Roots summary: counting distance polynomial

Dodecahedrane assembly	Polynomial root	n	m ± stdev	Min	Max
1-dodeca	Real	5	-0.6000 ± 0.3302	-1.0000	-0.2571
	Imaginary		0.0000 ± 1.1441	-1.5291	1.5291
5-dodeca	Real	10	-0.6000 ± 0.7882	-1.8178	0.4253
	Imaginary		0.0000 ± 1.8617	-3.6263	3.6263
6-dodeca	Real	11	-0.5455 ± 0.7113	-1.6720	0.5255
	imaginary		0.0000 ± 1.4259	-2.8149	2.8149
12-dodeca	Real	18	-0.2292 ± 0.7819	-1.7469	0.8874
	Imaginary		0.0000 ± 0.9017	-1.8031	1.8031
15-dodeca	Real	22	-0.3182 ± 0.8537	-1.8036	0.9422
	Imaginary		0.0000 ± 0.9394	-2.1071	2.1071
24-dodeca	Real	34	-0.2279 ± 0.9078	-3.3600	0.9786
	Imaginary		0.0000 ± 0.8599	-2.1498	2.1498
25-dodeca	Real	35	-0.1228 ± 0.7333	-1.2931	0.9823
	Imaginary		0.0000 ± 0.7442	-1.1424	1.1424

n number of roots, m arithmetic mean, *stdev* standard deviation values, *Min* the smallest values, *Max* the highest value

- The degree of polynomial equals the number of dodecahedron units in the assembly.
- The difference in the polynomial degrees equals one, when five- and six-dodecahedron assemblies are compared.
- With two exceptions, the difference in the polynomial degrees is four, when 12- and 15-dodecahedron assemblies are compared. The *CDi* polynomial of 15-dodeca has more four terms, in comparison to that of 12-dodeca.
- A factor of 10 seems to factorize all the polynomial coefficient values associated to multiple of 5-dodecahedron assemblies (5-dodeca, 15-dodeca, and 25-dodeca). The factor of 6 proved to factorize the polynomial for 12-dodeca, while the value of 2*6 can factorize the polynomial for 6-dodeca and 24-dodeca assemblies.

The root pairs (real and imaginary) of *CDi* polynomial, obtained for the investigated dodecahedron complexes (and the associated summary statistics), are provided in Table 21.5.

The patterns of the polynomial roots according to the number of dodecahedron units in the assembly are presented in Fig. 21.6.

The analysis of the above patterns of *CDi* polynomial roots shows the absence of similarity when a small number of dodecahedron units are linked together (5-dodeca and 6-dodeca), but clear similarity appears as the number of linked units increases (see 12- and 15-dodeca in Fig. 21.6). An ellipsoid pattern could be observed starting with 15-dodeca assembly (Fig. 21.6).

The overlap of patterns of polynomial roots in the case of complexes with a similar number of dodecahedron units is presented in Fig. 21.7.
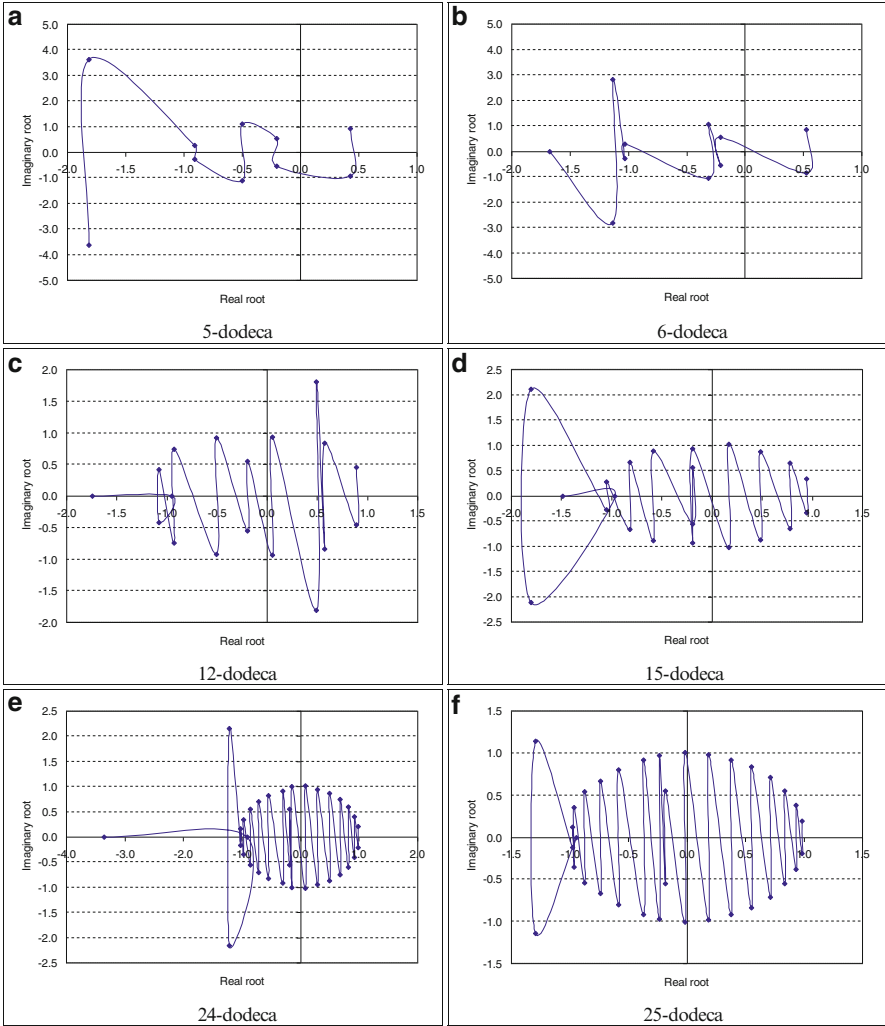
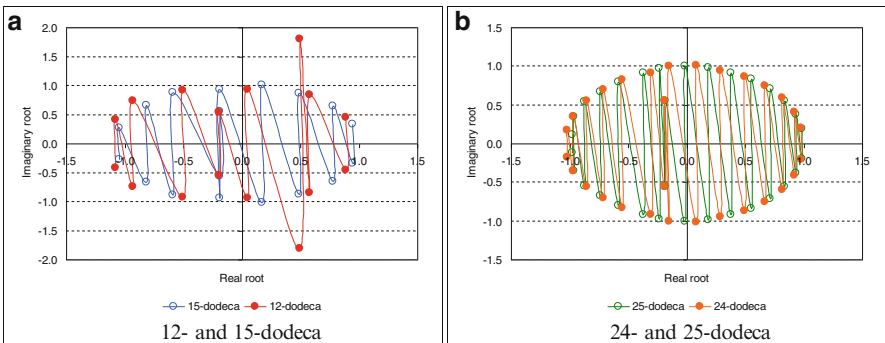**Fig. 21.6** Pattern of polynomial roots: counting distance polynomials

Fig. 21.7 Counting distance polynomial roots: pattern similarity

The similarity of patterns is little envisaged for 12- and 15-dodeca but becomes obvious as the number of linked dodecahedrane increases (see Fig. 21.7b).

21.3.2.2 Counting Szeged (On Distance) Polynomials

The counting Szeged (on distance) polynomials for the investigated dodecahedron-based nano-assemblies are listed in Table 21.6. A behavior similar to that observed in the case of *CDi* polynomial is seen for the counting Szeged (on distance) polynomial, an increase in the polynomial degree, as the number of dodecahedron

Table 21.6 Szeged polynomial for dodecahedron-based complexes

Complex	CSz
1-dodeca	$20x^{10} + 360x^8 + 20x^0$
5-dodeca	$10x^{57} + 10x^{55} + 140x^{54} + 60x^{53} + 10x^{52} + 30x^{51} + 30x^{50} + 60x^{49} + 90x^{48} + 80x^{47}$ $+ 100x^{46} + 100x^{45} + 160x^{44} + 60x^{43} + 70x^{42} + 180x^{41} + 100x^{40} + 240x^{39} + 200x^{38}$ $+ 290x^{37} + 150x^{36} + 190x^{35} + 190x^{34} + 280x^{33} + 290x^{32} + 220x^{31} + 170x^{30} + 100x^{29}$ $+ 160x^{28} + 120x^{27} + 100x^{26} + 200x^{25} + 150x^{24} + 180x^{23} + 100x^{22} + 200x^{21} + 110x^{20}$ $+ 40x^{18} + 120x^{17} + 30x^{16} + 210x^{14} + 100x^{12} + 60x^{11} + 20x^9 + 40x^8 + 75x^0$
6-dodeca	$12x^{72} + 12x^{70} + 168x^{69} + 72x^{68} + 36x^{66} + 12x^{65} + 72x^{63} + 108x^{61} + 84x^{60} + 168x^{59}$ $+ 168x^{57} + 60x^{56} + 24x^{55} + 120x^{54} + 192x^{53} + 48x^{52} + 120x^{51} + 180x^{50} + 156x^{49}$ $+ 252x^{48} + 180x^{47} + 120x^{46} + 516x^{45} + 192x^{44} + 252x^{43} + 180x^{42} + 402x^{41} + 276x^{40}$ $+ 312x^{39} + 312x^{38} + 192x^{37} + 264x^{36} + 72x^{35} + 132x^{34} + 144x^{33} + 96x^{32} + 120x^{31}$ $+ 192x^{30} + 156x^{29} + 240x^{28} + 96x^{27} + 72x^{26} + 216x^{25} + 96x^{24} + 120x^{23} + 48x^{22}$ $+ 168x^{21} + 36x^{20} + 12x^{19} + 72x^{18} + 120x^{17} + 24x^{16} + 252x^{14} + 120x^{12} + 72x^{11} + 24x^9$ $+ 48x^8 + 90x^0$
12-dodeca	$12x^{158} + 12x^{155} + 24x^{154} + 24x^{152} + 60x^{151} + 36x^{150} + 24x^{148} + 36x^{146} + 12x^{145} +$ $12x^{144} + 24x^{143} + 48x^{141} + 66x^{140} + 36x^{139} + 84x^{138} + 24x^{135} + 12x^{134} + 12x^{133} +$ $24x^{132} + 24x^{131} + 12x^{130} + 24x^{129} + 96x^{128} + 12x^{127} + 24x^{126} + 36x^{125} + 24x^{121} +$ $12x^{115} + 6x^{112} + 12x^{111} + 6x^{108} + 24x^{105} + 12x^{104} + 180x^{103} + 120x^{102} + 180x^{101}$ $+ 330x^{100} + 300x^{99} + 552x^{98} + 600x^{97} + 756x^{96} + 816x^{95} + 876x^{94} + 1200x^{93}$ $+ 1176x^{92} + 948x^{91} + 2262x^{90} + 996x^{89} + 1296x^{88} + 1884x^{87} + 2052x^{86} + 1152x^{85}$ $+ 1320x^{84} + 1896x^{83} + 1146x^{82} + 1140x^{81} + 1230x^{80} + 672x^{79} + 984x^{78} + 756x^{77}$ $+ 576x^{76} + 624x^{75} + 336x^{74} + 264x^{73} + 204x^{72} + 204x^{71} + 96x^{70} + 24x^{69} + 36x^{68}$ $+ 12x^{67} + 6x^{60} + 12x^{58} + 12x^{56} + 24x^{55} + 36x^{52} + 36x^{51} + 36x^{50} + 48x^{49} + 12x^{48}$ $+ 24x^{47} + 48x^{46} + 72x^{45} + 24x^{44} + 60x^{42} + 24x^{41} + 24x^{40} + 12x^{39} + 84x^{38} + 12x^{36}$ $+ 48x^{35} + 12x^{33} + 6x^{32} + 24x^{31} + 108x^{30} + 120x^{29} + 18x^{28} + 132x^{27} + 72x^{26} + 108x^{25}$ $+ 24x^{24} + 24x^{22} + 48x^{21} + 156x^{20} + 48x^{19} + 264x^{18} + 48x^{17} + 84x^{15} + 24x^{13} + 72x^{12}$ $+ 24x^9 + 48x^8 + 180x^0$
15-dodeca	$10x^{203} + 20x^{198} + 10x^{196} + 20x^{193} + 60x^{192} + 10x^{189} + 30x^{187} + 50x^{186} + 20x^{178} +$ $10x^{177} + 20x^{176} + 20x^{175} + 60x^{171} + 60x^{168} + 70x^{166} + 40x^{163} + 10x^{161} + 50x^{160} +$ $20x^{159} + 40x^{158} + 30x^{156} + 20x^{152} + 10x^{150} + 20x^{148} + 20x^{147} + 20x^{134} + 40x^{125}$ $+ 140x^{124} + 190x^{123} + 230x^{122} + 400x^{121} + 570x^{120} + 850x^{119} + 1020x^{118} + 1460x^{117}$ $+ 1260x^{116} + 2310x^{115} + 2740x^{114} + 2190x^{113} + 3400x^{112} + 2440x^{111} + 3170x^{110}$ $+ 3110x^{109} + 3940x^{108} + 2390x^{107} + 3160x^{106} + 2700x^{105} + 1680x^{104} + 2410x^{103}$ $+ 1520x^{102} + 1350x^{101} + 730x^{100} + 590x^{99} + 510x^{98} + 390x^{97} + 340x^{96} + 190x^{95}$ $+ 100x^{94} + 40x^{93} + 20x^{91} + 20x^{90} + 20x^{88} + 20x^{73} + 20x^{71} + 20x^{70} + 40x^{67} + 20x^{66}$

Table 21.6 (continued)

Complex	CSz
	$+20x^{63}+40x^{55}+40x^{54}+40x^{53}+80x^{50}+40x^{49}+60x^{44}+50x^{42}+60x^{41}+50x^{40}$ $+40x^{37}+40x^{36}+20x^{35}+40x^{34}+80x^{33}+100x^{32}+20x^{31}+50x^{30}+20x^{29}+40x^{28}$ $+40x^{27}+100x^{26}+20x^{25}+120x^{24}+130x^{22}+140x^{21}+40x^{20}+100x^{19}+20x^{18}+$ $40x^{17}+80x^{16}+10x^{15}+20x^{13}+60x^{12}+20x^{9}+40x^{8}+225x^{0}$
24-dodeca	$12x^{338}+24x^{333}+12x^{330}+24x^{327}+72x^{326}+12x^{323}+24x^{321}+36x^{320}+24x^{311}+$ $12x^{310}+24x^{306}+24x^{305}+96x^{296}+24x^{290}+12x^{288}+12x^{287}+72x^{283}+36x^{282}+$ $36x^{280}+12x^{279}+12x^{278}+36x^{277}+24x^{275}+12x^{198}+12x^{197}+12x^{195}+60x^{194}+$ $24x^{193}+24x^{192}+108x^{191}+108x^{190}+612x^{189}+444x^{188}+1248x^{187}+2280x^{186}$ $+2340x^{185}+3960x^{184}+5064x^{183}+4836x^{182}+5364x^{181}+11928x^{180}+7548x^{179}$ $+9072x^{178}+12024x^{177}+10440x^{176}+8844x^{175}+8340x^{174}+7800x^{173}+5520x^{172}$ $+5052x^{171}+4200x^{170}+2628x^{169}+2004x^{168}+1608x^{167}+720x^{166}+384x^{165}$ $+384x^{164}+204x^{63}+132x^{162}+156x^{161}+132x^{160}+96x^{159}+120x^{158}+24x^{157}+$ $60x^{156}+24x^{155}+12x^{153}+2x^{152}+2x^{132}+12x^{127}+12x^{126}+12x^{87}+12x^{84}+12x^{77}$ $+24x^{76}+36x^{73}+24x^{72}+48x^{67}+12x^{61}+48x^{56}+24x^{55}+72x^{54}+36x^{53}+48x^{52}$ $+24x^{51}+48x^{46}+24x^{45}+24x^{44}+24x^{43}+60x^{42}+24x^{41}+36x^{38}+72x^{36}+48x^{35}$ $+96x^{34}+168x^{33}+24x^{32}+48x^{31}+204x^{30}+24x^{29}+24x^{28}+48x^{27}+48x^{26}+348x^{25}$ $+192x^{22}+24x^{21}+48x^{20}+120x^{19}+24x^{18}+48x^{17}+96x^{16}+12x^{15}+24x^{13}+72x^{12}$ $+24x^{9}+48x^{8}+360x^{0}$
25-dodeca	$10x^{353}+20x^{348}+10x^{345}+20x^{342}+60x^{341}+10x^{338}+20x^{336}+30x^{335}+20x^{326}+$ $10x^{325}+20x^{320}+20x^{319}+20x^{310}+20x^{304}+10x^{299}+20x^{298}+60x^{289}+60x^{286}+$ $30x^{280}+60x^{276}+20x^{205}+20x^{204}+40x^{201}+20x^{200}+40x^{199}+100x^{198}+280x^{197}$ $+440x^{196}+450x^{195}+1840x^{194}+1560x^{193}+3430x^{192}+3540x^{191}+5050x^{190}$ $+6860x^{189}+8960x^{188}+12090x^{187}+11810x^{186}+11630x^{185}+9080x^{184}+$ $14630x^{183}+11070x^{182}+8770x^{181}+6560x^{180}+5880x^{179}+4280x^{178}+2590x^{177}$ $+2350x^{176}+1030x^{175}+790x^{174}+580x^{173}+330x^{172}+220x^{171}+200x^{170}+280x^{169}$ $+210x^{168}+60x^{167}+80x^{166}+120x^{165}+20x^{164}+20x^{163}+50x^{76}+20x^{75}+20x^{74}$ $+20x^{68}+20x^{67}+40x^{56}+40x^{55}+80x^{54}+40x^{52}+20x^{51}+40x^{46}+20x^{45}+50x^{44}$ $+20x^{43}+50x^{42}+20x^{41}+60x^{39}+60x^{36}+40x^{35}+170x^{34}+120x^{33}+20x^{32}+160x^{31}$ $+70x^{30}+20x^{29}+110x^{28}+40x^{27}+220x^{26}+140x^{25}+160x^{22}+20x^{21}+40x^{20}+$ $100x^{19}+20x^{18}+40x^{17}+80x^{16}+10x^{15}+20x^{13}+60x^{12}+20x^{9}+40x^{8}+375x^{0}$

units in the assembly increases. Furthermore, the degree of Szeged polynomial is constantly higher than the degree of counting distance polynomial, for the same dodecahedron nano-assembly, see Table 21.7.

Szeged polynomial for the investigated dodecahedron complexes could be factorized by certain value:

- A factor of 10 is common to all counting Szeged (on distance) polynomial coefficients for 5-dodeca, 15-dodeca, and 25-dodeca.
- A factor of 12 can be applied to all Szeged polynomial coefficients for 6-dodeca and 24-doceca.
- A factor of 6 is appropriate for all the Szeged polynomial coefficients of 12-dodeca.

Table 21.7 Relation between number of dodecahedrane in the assembly and the power of polynomial coefficients: analysis for first 45 coefficients

| n-dodeca (x) | =x*15−a_i | | Pow-1 | a_i | Pow-2 | a_i | Pow-3 | a_i | ... | Pow-10 | a_i | ... | Pow-43 | a_i | Pow-44 | a_i | Pow-45 | a_i |
	Pow	a_i																
5	57	18	55	20	54	21	53	22		46	29		9	66	8	67	0	75
6	72		70	22	69		68			57	33		24		23		22	67
12	158	22	155	25	154	26	152	28		143	37		93	87	92	88	91	89
15	203		198	27	196	29	193	32		176	49		108	117	107	118	106	119
24	338		333		330	30	327	33		306	54		177	183	176	184	175	185
25	353		348		345		342			320	55		180	195	179	196	178	197

Pow = the degree of polynomial;
Pow-X (for $1 \leq X \leq 45$, where 45 = maximum number of coefficients in the polynomial for 5-dodeca)

Table 21.8 Root summary: Szeged on distance polynomials

Dodecahedrane assembly	Polynomial root	n	m ± stdev	Min	Max
5-dodeca	Real	57	$1.05 \cdot 10^{-9} \pm 0.7812$	−2.0822	1.2606
	Imaginary		0.0000 ± 0.8038	−2.1943	2.1943
6-dodeca	Real	72	$1.66 \cdot 10^{-11} \pm 0.7664$	−2.0686	1.2594
	Imaginary		0.0000 ± 0.7845	−2.1982	2.1982
12-dodeca	Real	158	$2.25 \cdot 10^{-16} \pm 0.7248$	−1.0551	1.1408
	Imaginary		0.0000 ± 0.7248	−1.1991	1.1991
15-dodeca	Real	203	$2.38 \cdot 10^{-16} \pm 0.7217$	−1.2755	1.1160
	Imaginary		0.0000 ± 0.7217	−1.1347	1.1347
24-dodeca	Real	338	$1.18 \cdot 10^{-16} \pm 0.7164$	−1.1296	1.1088
	Imaginary		0.0000 ± 0.7164	−1.2166	1.2166
25-dodeca	Real	353	$-3.30 \cdot 10^{-16} \pm 0.7165$	−1.1289	1.1090
	Imaginary		0.0000 ± 0.7165	−1.2164	1.2164

n number of roots, m arithmetic mean, *stdev* standard deviation values, *Min* the smallest values, *Max* the highest value

The pair (real and imaginary) roots of counting Szeged (on distance) polynomials for the investigated dodecahedron nano-complexes and the associated summary statistics are provided in Tables 21.7 and 21.8.

The patterns of the counting polynomial roots according to the number of dodecahedron units in the assembly are presented in Fig. 21.8.

A similarity in the root value patterns of the counting Szeged on distance is observed (see Fig. 21.8), while the ellipsoid model is analogous to the one observed in the case of the counting distance polynomial.

21.4 Conclusions

In this chapter, six dodecahedron-based nano-assemblies have been investigated by the aid of two counting polynomials: counting distance polynomial and counting Szeged (on distance) polynomial. The roots of the investigated polynomials showed similarity just for complexes with more than 12-dodecahedron units inside. The roots of counting Szeged (on distance) polynomials for these complexes mimic an ellipsoidal pattern.
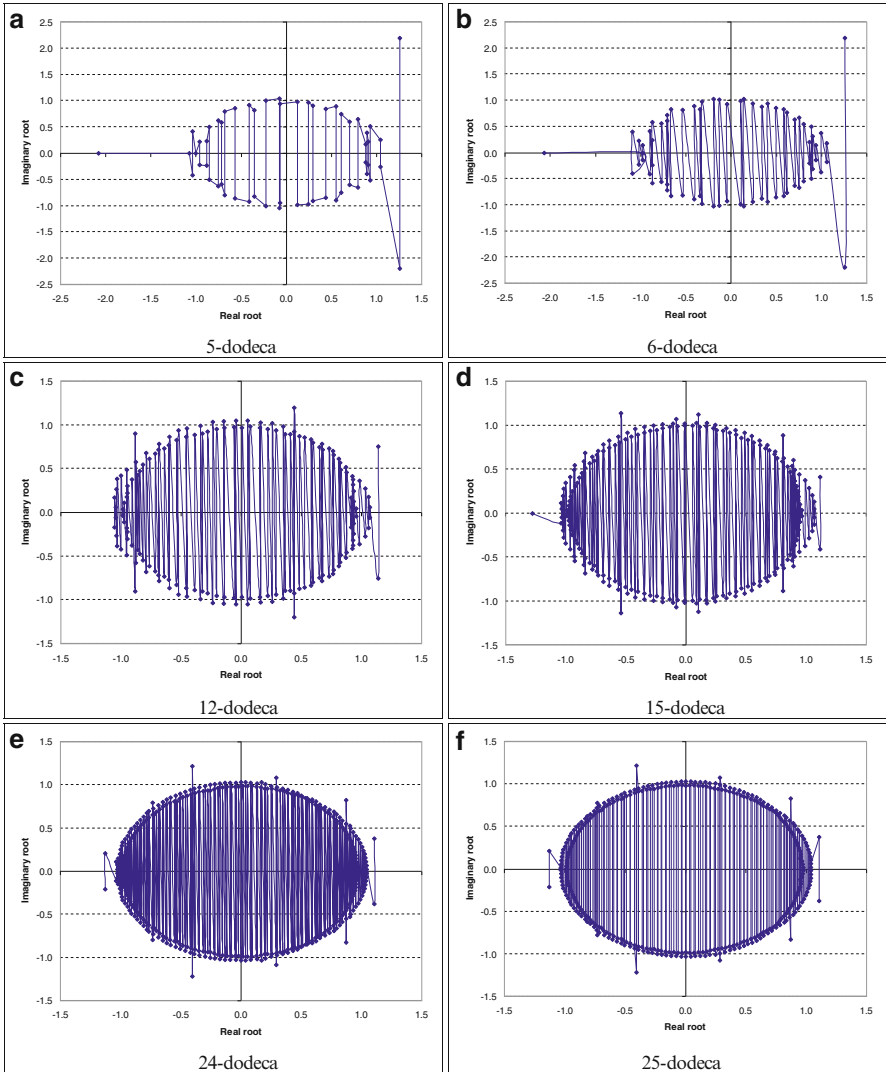
Fig. 21.8 Pattern of polynomial roots: counting Szeged on distance polynomials (**a**) 5-dodeca, (**b**) 6-dodeca, (**c**) 12-dodeca, (**d**) 15-dodeca, (**e**) 24-dodeca, and (**f**) 25-dodeca

References

An Y-P, Yang C-L, Wang M-S, Ma X-G, Wang D-H (2009) First-principles study of electronic transport properties of dodecahedrane $C_{20}H_{20}$ and its endohedral complex Li@$C_{20}H_{20}$. J Phys Chem C 113(35):15756–15760

Astakhov AM, Stepanov RS, Babushkin AY (1998) On the detonation parameters of octanitrocubane. Combust Explo Shock 34(1):85–87

Banfalvia G (2014) Dodecahedrane minibead polymers. RSC Adv 4:3003–3008

Bolboacă S, Jäntschi L (2007) How good the characteristic polynomial can be for correlations? Int J Mol Sci 8(4):335–345

Chen Z, Jiao H, Moran D, Hirsch A, Thiel W, von Ragué SP (2003) Structures and stabilities of endo- and exohedral dodecahedrane complexes ($X^@C_{20}H_{20}$ and $XC_{20}H_{20}$, X = H^+, H, N, P, C^-, Si^-, O^+, S^+). J Phys Chem A 107(12):2075–2079

Cross RJ, Saunders M, Prinzbach H (1999) Putting helium inside dodecahedrane. Org Lett 1 (9):1479–1481

Devillers J, Balaban AT (eds) (2000) Topological indices and related descriptors in QSAR and QSPR. Gordon and Breach, Amsterdam, pp 96–97

Diudea MV, Minailiuc OM, Katona G, Gutman I (1997) Szeged matrices and related numbers. MATCH Commun Math Comput Chem 35:129–143

Dixon DA, Deerfield D (1981) The electronic structure of dodecahedrane and the nature of the central cavity. Chem Phys Lett 78(1):161–164

Eaton PE, Cole TW (1964a) Cubane. J Am Chem Soc 86(15):3157–3158

Eaton PE, Cole TW (1964b) The cubane system. J Am Chem Soc 86(5):962–964

Eremenko LT, Nesterenko DA (1997) Energetics of decomposition of polynitrocubanes (Analytical prediction). Chem Phys Rep 16:1675–1683

Floyd RW (1962) Algorithm 97: shortest path. Commun ACM 5(6):344–345

Friedlander P (1964) Chapter XIV: Platon als Atomphysiker. In: Friedlander P (ed) Platon, Vol I. Walter de Gruyter & Co, Berlin, pp 260–275

Hopf H (2000) Classics in hydrocarbon chemistry. Wiley-VCH, Weinheim

Hosoya H (2013) Distance polynomial and the related counting polynomials. Croat Chem Acta 86 (4):443–451

Jäntschi L (2000) CF matrices (§4.7) In: Jäntschi L (ed) Prediction of physical, chemical and biological properties using mathematical descriptors (in Romanian). PhD Thesis in Chemistry (PhD Advisor: Prof. Dr. Mircea V. DIUDEA). Cluj-Napoca, Babeş-Bolyai University

Jäntschi L (2007) Characteristic and counting polynomials of nonane isomers. Academic Direct Publishing House (eISBN: 978-973-86211-3-8). Available at: http://ph.academicdirect.org/CCPNI_2007.pdf

Jäntschi L, Bolboacă SD (2009) Counting polynomials on regular iterative structures. Appl Med Inform 24(1–2):67–95

Jäntschi L, Diudea MV (2009) Subgraphs of pair vertices. J Math Chem 45(2):364–371

Jäntschi L, Bolboacă SD, Furdui CM (2009) Characteristic and counting polynomials: modelling nonane isomers properties. Mol Simul 35(3):220–227

Jiménez-Vázquez HA, Tamariz J, Cross RJ (2001) Binding energy in and equilibrium constant of formation for the dodecahedrane compounds He@$C_{20}H_{20}$ and Ne@$C_{20}H_{20}$. J Phys Chem A 105(8):1315–1319

Kamlet MJ, Jacobs SJ (1968) Chemistry of detonations I. A simple method for calculating detonation properties of C–H–N–O explosives. J Chem Phys 48:23–35

Liu F-L (2004a) DFT study on a molecule $C_{25}H_{20}$ with a dodecahedrane cage and a pentaprismane cage sharing the same pentagon. J Mol Struct-Theochem 681(1–3):51–55

Liu F-L (2004b) Theoretical study on the coplanar double-cage dodecahedrane $C_{35}H_{30}$. Phys Chem Chem Phys 6:906–909

Liu F-L, Zhao J-X, Xie Y, Dai L-H (2005a) Theoretical study of two $C_{30}H_{20}$ isomers with a dodecahedrane cage and two pentaprismane cages sharing two pentagons. Int J Quantum Chem 102:275–281

Liu F-L, Zhai Y-Q, Feng S, Guo W-L (2005b) DFT study on the molecule $C_{40}H_{30}$: two dodecahedrane cages linked by five carbon–carbon single bonds. J Mol Struct-Theochem 719(1–3):185–189

MacGillivray LR, Atwood JL (1999) Structural classification and general principles for the design of spherical molecular hosts. Angew Chem 38(8):1018–1033

Maier G, Pfriem S (1978) Tetra-tert-butyltetrahedrane. Angew Chem 17(7):520–521

Maier G, Neudert J, Wolf O, Pappusch D, Sekiguchi A, Tanaka M, Matsuo T (2002) Tetrakis (trimethylsilyl) tetrahedrane. J Am Chem Soc 124(46):13819–13826

Moran D, Stahl F, Jemmis ED, Schaefer HF III, von Schleyer PR (2002) Structures, stabilities, and ionization potentials of dodecahedrane endohedral complexes. J Phys Chem A 106 (20):5144–5154

Nemirowski A, Reisenauer HP, Schreiner PR (2006) Tetrahedrane-Dossier of an unknown. Chem Eur J 12:7411–7420

Pan VY (1997) Solving a polynomial equation: some history and recent progress. SIAM Rev 39:187–220

Paquette LA, Ternansky RJ, Balogh DW, Kentgen G (1983) Total synthesis of dodecahedrane. J Am Chem Soc 105(16):5446–5450

Sekiguchi A, Tanaka M (2003) Tetrahedranyllithium: synthesis, characterization, and reactivity. J Am Chem Soc 125(42):12684–12685

Ternansky RJ, Balogh DW, Paquette LA (1982) Dodecahedrane. J Am Chem Soc 104 (16):4503–4504

Wahl F, Weiler A, Landenberger P, Sackers E, Voss T, Haas A, Lieb M, Hunkler D, Wörth J, Knothe L, Prinzbach H (2006) Towards perfunctionalized dodecahedranes-en route to C_{20} fullerene. Chem Eur J 12(24):6255–6267

Xiao H, Zhang J (2002) Theoretical prediction on heats of formation for polyisocyanocubanes. Sci China Ser B 45(1):21–29

Zhang M-X, Eaton PE, Gilardi R (2000) Hepta- and octanitrocubanes. Angew Chem Int Ed 39 (2):401–404

Chapter 22
Tetrahedral Nanoclusters

Csaba L. Nagy, Katalin Nagy, and Mircea V. Diudea

Abstract Conserving the sp^2 hybridization of carbon atoms in tetrahedral arrangements is possible in both closed and opened nanostructures. Between the two classes, a structural relationship exists, and they can be easily transformed into each other to facilitate design of complex highly symmetric clusters. A classification of fullerenes with tetrahedral symmetry is here provided, and the corresponding zigzag and armchair tetrapodal nanotube junctions are discussed in detail.

22.1 Introduction

Shortly after the discovery of multi-walled carbon nanotubes, by Iijima, fullerene analogs with negative Gaussian curvature have been proposed (Scuseria 1992), where the pentagons in fullerenes are replaced with large non-hexagonal rings (e.g., heptagons) (Terrones and Terrones 2003). Highly symmetric nanotube junctions, as tetrahedral or octahedral units, can be assembled into networks resulting into infinite periodic minimal surfaces (Diudea and Nagy 2007). Such junctions could play an important role in the use of nanotubes in microelectronic devices (Terrones et al. 2002a, b, 2003).

There are software programs (Brinkmann et al. 2010; Schwerdtfeger et al. 2013) that can be used for the generation of fullerene cages. However, since a nanotube junction corresponds to a spanned fullerene, a systematic design of multiterminal junctions, with a given number of terminals and molecular symmetry, is required for the appropriate transforming of fullerenes.

C.L. Nagy (✉) • K. Nagy
Department of Chemistry, Faculty of Chemistry and Chemical Engineering, University of Babes-Bolyai, 400028 Cluj-Napoca, Romania
e-mail: nc35@chem.ubbcluj.ro

M.V. Diudea
Department of Chemistry, Faculty of Chemistry and Chemical Engineering, Babes-Bolyai University, Arany Janos Street 11, Cluj-Napoca RO-400028, Romania

Tetrahedral fullerenes with an open-shell electronic configuration should be very reactive; therefore, the ground state will have a lowered symmetry because of the first-order Jahn–Teller distortion (Jahn and Teller 1937). However, the topological symmetry could be achieved in the case of ions, heteroatom-doped analogs, or adducts. For example, the tetrahedral isomer of fullerene C_{40} has only two electrons in the triply degenerated frontier orbitals. The tetra-anion C_{40}^{4-}, the $C_{36}N_4$ nitrogen heteroanalog, and the $C_{40}H_4$ hydrogen adduct have a tetrahedral T_d configuration. It was found that the two electron-rich species are also highly aromatic, with nucleus-independent chemical shift (NICS) (Schleyer et al. 1996) values in the cage center -15.7 and -11.8 for C_{40}^{4-} and $C_{36}N_4$, respectively (Chen et al. 2001b).

Tetrahedral fullerene dication was also found to be highly stable (Diaz-Tendero et al. 2003, 2005). C_{52}^{2+} (T) has six adjacent pentagons and possesses lower energy than the isomers with only five adjacent pentagons, which reveals that the pentagon adjacency penalty rule (PAPR) (Campbell et al. 1996) does not necessarily apply to the charged fullerene cages. It is highly aromatic, as suggested by the -46.2 ppm negative NICS value (GIAO-6-31G*//B3LYP/6-31G*), and also very stable, as a consequence of the closed-shell electronic structure and nearly perfect sphericity.

The smallest tetrahedral fullerene has 28 carbon atoms and follows the $2(N+1)^2$ rule for spherical aromaticity (Hirsch et al. 2000). The ground state has an open-shell configuration with four singly occupied frontier orbitals; therefore, it is considered to be tetravalent with four dangling bonds localized on the triplet-pentagon fusion apices and prefers to encapsulate metal atom inside to form endohedral metallofullerenes $M@C_{28}$, as was observed in the gas-phase experiments (Guo et al. 1992). Upon reduction, the valence shell is completely filled, and the C_{28}^{4-} anion is highly aromatic, as predicted by -35.5 ppm (GIAO–SCF/ 6–31G*//B3LYP/6–31G*) NICS value at the cage center (Chen et al. 2001a). The heteroatom-substituted $C_{24}N_4$ also has a high delocalization of the electrons as indicated by the -27.8 ppm NICS at the cage center (Chen et al. 2001a).

By means of group theory, the formulas for the number of IR and Raman active modes, for all of the tetrahedral fullerenes, have been obtained (Cheng et al. 1999).

22.2   Tetrahedral Carbon Cages

According to the distribution of carbon atoms, the tetrahedral fullerenes can be classified as follows: (a) cages with no atoms along the symmetry axis, (b) fullerenes with four atoms lying on the threefold axis, and (c) cages with each of the threefold axes crossing two carbon atoms.

According to the number of carbon atoms (n), the tetrahedral fullerenes have been divided into three classes. It was found that the electronic structure, evaluated by means of Hückel theory, varies according to (1) $n = 12\,N$ in closed-shell fullerenes, (2) $n = 12N + 4$ in open shell, and (3) $n = 12N + 8$ in open-shell or pseudo-closed-shell electronic configuration, where N represents a nonnegative integer determined by group properties (Tang and Huang 1996).
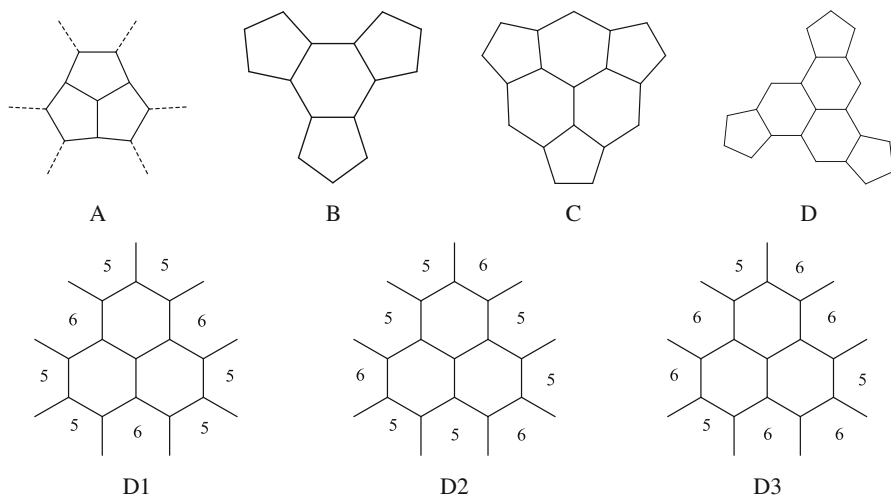
Fig. 22.1 Classification of the structural fragments decorating the tetrahedral carbon cages lying along the threefold symmetry axis. Some of the patterns have a common D fragment

The 12 fivefold rings are divided, by the molecular symmetry, into four equivalent fragments, each lying along one of the four threefold symmetry axis. The four structural patterns that have been identified are shown in Fig. 22.1. Pattern A is a directly fused pentagon triple, and, as a consequence, these fullerenes do not obey the isolated pentagon rule (IPR) (Manolopoulos and Fowler 1992). With the increase of the number of atoms, the geometry of such a structure will become polyhedral, resembling a tetrahedron, as the giant icosahedral fullerenes resemble an icosahedron (Noël et al. 2014). Fragment B, commonly known as the sumanene, has a hexagonal ring core, surrounded by alternating pentagonal and hexagonal faces (with one exception, C_{28}–T_d). All fullerenes with B structural motif on at least 60 carbon atoms obey the IPR, and some of them are leapfrog fullerenes (Dias 1993). The other two classes have a carbon atom core and have isolated pentagons within the fragment.

Notice that tetrahedral fullerenes must have two of these fragments, and accordingly they belong to two classes, e.g., in the case of the C_{40}–T_d fullerene, the C_3 axis crosses both an A and a B motif.

In the systematic built of all tetrahedral armchair [3,3] nanotube junctions by the transformation (spanning) of tetrahedral fullerene cages, it seems that a given junction can be derived from more than one cluster. The structural relationship between the different molecule series is listed in Table 22.1. Some of the fullerenes have icosahedral instead of tetrahedral symmetry (e.g., C_{20}, C_{60}, and C_{80}); however, they arise by applying the structural transformation used in the other cases. Empty cells in the table represent non-fullerene polyhedrons.

Geometry optimization followed by the calculation of harmonic vibrational frequencies was performed at the density functional level of theory (DFT) using the hybrid B3LYP functional and the standard polarized double-zeta 6-31G(d,p) basis set. Single point energy calculation results are summarized in Fig. 22.2, where the

Table 22.1 Classification of the tetrahedral fullerenes with respect to the structural fragment and the structural relationship with the corresponding tetrahedral armchair nanotube junction

#	Tetrahedral armchair [3,3] junction	Tetrahedral fullerenes			
		C_{n-8} (A)	C_{n-24} (B)	C_{n-32} (C)	C_{n-56} (D)
1	$Tj[3,3]_{52}^{4-}–T$	$C_{44}–T$	$C_{28}^{4-}–T_d$	–	–
2	$Tj[3,3]_{64}^{4-}–T_d$	$C_{56}–T_d$	$C_{40}^{4-}–T_d$	–	–
3	$Tj[3,3]_{76}^{4-}–T$	$C_{68}–T$	$C_{52}^{4-}–T$	$C_{44}–T$	$C_{20}^{2+}–I_h$
4	$Tj[3,3]_{84}–T$	$C_{76}^{4-}–T$	$C_{60}–I_h$	$C_{52}^{4-}–T$	$C_{28}^{4-}–T_d$
5	$Tj[3,3]_{100}^{4-}–T_d$	$C_{92}–T_d$	$C_{76}^{4-}–T_d$	$C_{68}^{4-}–T_d$	$C_{44}–T$
6	$Tj[3,3]_{108}–T_d$	$C_{100}^{4-}–T_d$	$C_{84}–T_d$	$C_{76}^{4-}–T_d$	$C_{52}^{4-}–T$
7	$Tj[3,3]_{112}^{4-}–T$	$C_{104}–T$	$C_{88}^{4-}–T$	$C_{80}^{6-}–I_h$	$C_{56}–T_d$
8	$Tj[3,3]_{124}^{4-}–T$	$C_{116a}–T$	$C_{100}^{4-}–T$	$C_{92}–T$	$C_{68}^{4-/0}–T_d/T$
9	$Tj[3,3]_{144}–T_d$	$C_{136}^{4-}–T_d$	$C_{120}–T_d$	$C_{112}^{4-}–T_d$	$C_{88}^{4-}–T$

For open-shell clusters, the ionic form is mentioned

total energy per atom and the HOMO–LUMO energy gap are plotted as a function of the number of carbon atoms. It can be observed that within series A, the charged fullerenes have very high energy gap values. The total energy per atom decreases with the cluster size. Within series B, the neutral structures show the highest stability according to the gap values, as these fullerenes have leapfrog structures.

22.2.1 C_{57} Multi-cage

The assembly of four C_{20} (I_h) fullerene cages results in a tetrahedral multi-cage with 57 carbon atoms having exclusively five-membered rings (Diudea and Nagy 2012, 2013). Each cage shares the core vertex, such as C_{57} can be considered as a tetrahedral sp^3 carbon hyper-atom, where the cages correspond to the hybrid orbitals. The framework of the structure consists of a centrohexaquinane core (shaded rings in Fig. 22.3 left), with all tetravalent atoms, enclosed by four acepentalene (triple fused pentagon) fragments. The unit can assemble into hyperstructures, including the classical network of the diamond and lonsdaleite. Because of the high percentage of pentagons, these structures were generically called diamond D_5 (Diudea et al. 2011, 2012).

C$_{57}$ has an open-shell electronic configuration, and the neutral structure lowers the symmetry to D_{2d}. The reduced form achieves maximal symmetry, and all fivefold rings belonging to the acepentalene fragment are equivalent. The electron-rich multi-cage has aromatic pentagons with NICS values comparable to the ones predicted for the acepentalene dianion $C_{10}H_6^{2-}$, −9.34 and −9.53 ppm, respectively. Strain relief by partial or total hydrogenation of the sp^2 carbon atoms was theoretically evaluated (Diudea and Nagy 2012).

The core of the adamantane hyperstructure C_{158} (Fig. 22.3 right) is the tetrahedral C_{28} (T_d) carbon cage. In a larger network, the hexagons are shared between two C_{28} fullerenes.
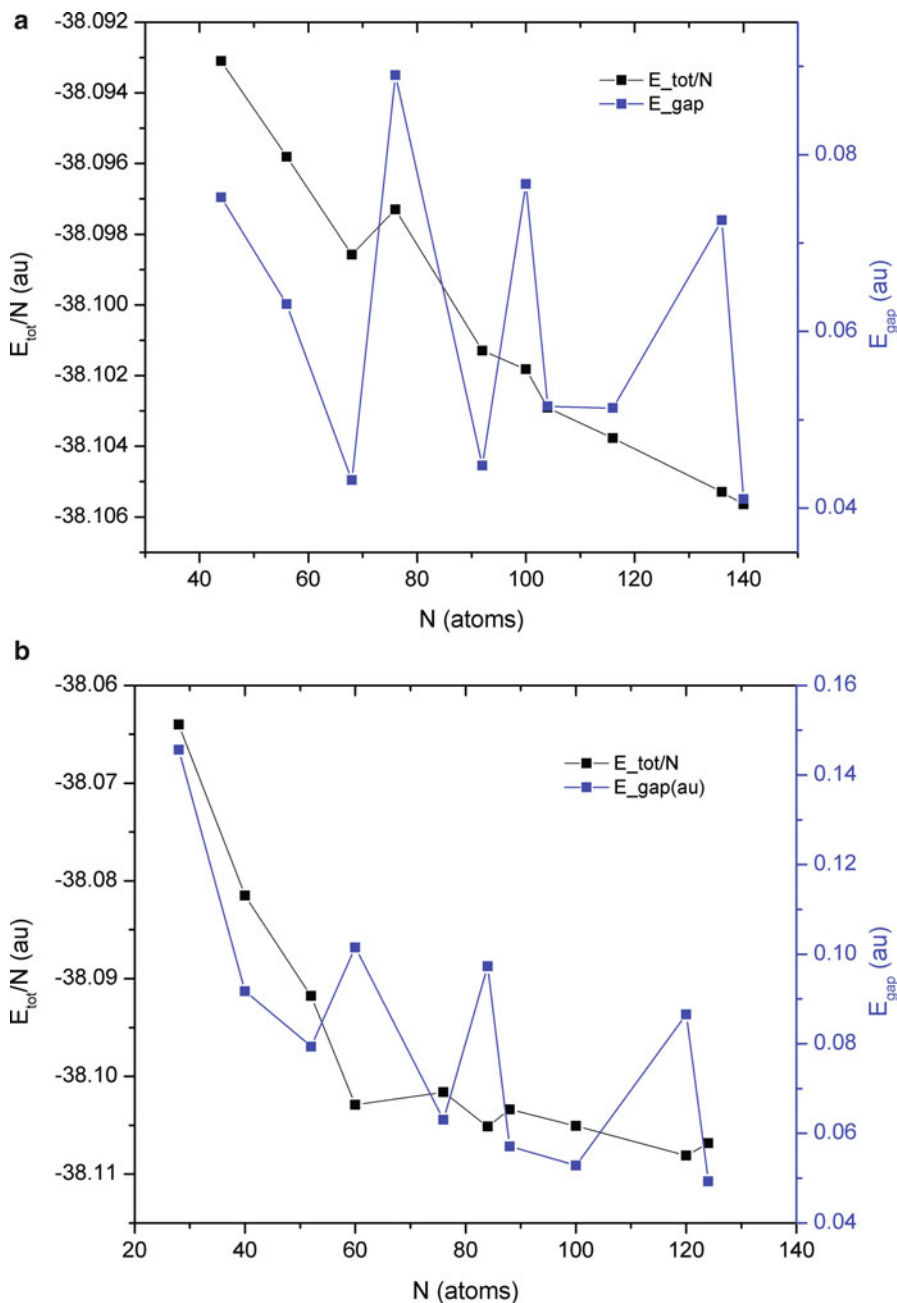
Fig. 22.2 Plot of the variation of the total energy per atom (E_{tot}/N in a.u.) and the HOMO–LUMO energy gap (E_{gap} in a.u.) as a function of the cluster size for the set of fullerenes in class A (*top*) and class B (*bottom*)
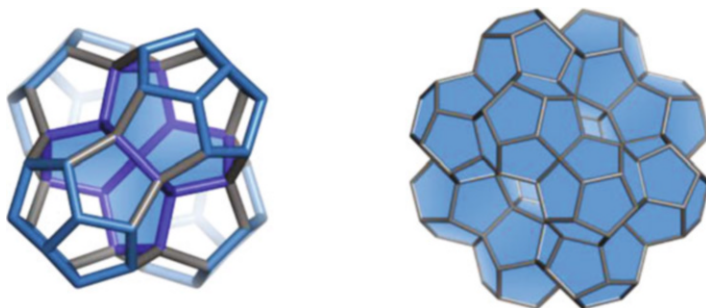
Fig. 22.3 Fragments of D_5 network: the C_{57} (T_d) multi-cage (*left*) and the corresponding hyper-adamantane C_{158} structure (*right*) (B3LYP/6-31G(d) optimized geometries)

22.3 Four-Terminal Nanotube Junctions

Multiterminal carbon nanotube junctions require, from a topological point of view, the insertion of structural defects in the hexagonal network of single-walled nanotubes. These defects are rings larger than hexagons which enables the assembly of individual nanotubes into a periodic network while preserving the sp^2 hybridization of the carbon atoms. In the following, tetrahedral zigzag and armchair nanotube junctions derived from fullerenes are presented, containing only heptagonal rings as defects.

22.3.1 Zigzag [3,0] Tetrahedral Junctions

The structure and stability of two tetrahedral three-terminal zigzag junctions consisting only of sp^2 covalent carbon atoms, Tj[3,0]$_{40}$ and Tj[3,0]$_{52}$, were investigated (Nagy et al. 2013) at the Hartree–Fock level of theory using the 6–31G(d,p) basis set as implemented in the Gaussian 09 software (Frisch et al. 2009). The structures were proven to be stable and possible to self-assemble in building diamond-like networks and hyper-dodecahedral architectures. Each opening of the junction fits a [3,0] zigzag single-walled carbon nanotube, found to be narrow-gap semiconductors (Borštnik et al. 2005). The junctions have been derived from the corresponding tetrahedral non-IPR fullerenes C_{44} (T) and C_{56} (T_d) by the removal of the core carbon atom from each of the triple directly fused pentagons. Both tetrapodal junctions incorporate only hexagonal rings; however, in a network, three octagonal rings are necessary at each connection to give a periodic surface with negative curvature (Romo-Herrera et al. 2007). The optimized geometries of the junctions are shown in Fig. 22.4.

The fullerenes C_{44} (T) and C_{56} (T_d) both have, according to the simple Hückel theory, pseudo-closed electron configuration, while the corresponding junctions are pseudo-open. As a consequence, the highest topological symmetry can be achieved
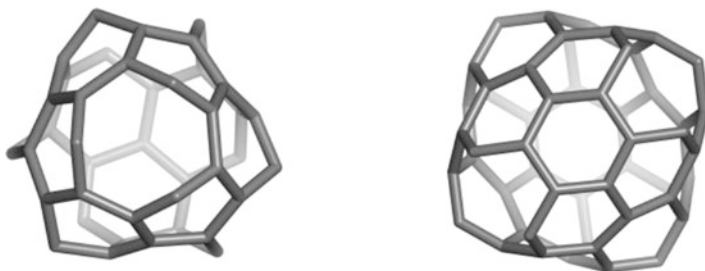
Fig. 22.4 HF/6-31G(d,p) optimized geometries of tetrahedral zigzag nanotube junctions: Tj[3,0] 40–T (*left*) and Tj[3,0]$_{52}$–T_d (*right*)

Table 22.2 Energetic data for fullerenes and the corresponding tetrahedral junctions, at HF/6-31G(d,p) level of theory

Structure	E_{tot}/C atom (eV)	E_{gap} (eV)	SE (kcal/mol)
C$_{44}$–T	−37.852	6.595	12.73
Tj[3,0]$_{40}$–D_2	−38.021	6.681	5.80
Tj[3,0]$_{40}^{4-}$–T	−38.006	7.414	6.70
C$_{52}$–T_d	−37.854	5.505	10.65
Tj[3,0]$_{52}$–D_{2d}	−37.986	6.144	5.44
C$_{60}$–I_h	−37.864	7.418	8.256

by addition of some negative charges. The hexagonal framework of both junctions consists of four phenalene fragments. These motifs share one bond with each neighbor, in the case of the Tj[3,0]$_{40}$ junction, while in the case of Tj[3,0]$_{52}$, the fragments are disjointly separated by one bond. The 13-carbon phenalene cation and anion motif has a diatropic perimeter ring current, as in case of coronene (Balaban et al. 2010), predicted by the ipsocentric model (Cyrański et al. 2007).

Computational data, obtained using HF/6-31G(d,p) method, are listed in Table 22.2 (Nagy et al. 2013). The strain energy, evaluated according to POAV theory (Haddon 1990, 2001) is also included. It can be observed that the closed fullerenes show a higher strain in comparison to the opened junctions. The higher symmetry of the charged Tj[3,0]$_{40}^{4-}$ results in a higher strain when compared to the neutral lower symmetry structure.

As a consequence of the difference in the symmetry, the two tetrahedral junctions enable the building of two different networks by the assembly of the necessary number of units. In the case of the Tj[3,0]$_{40}$ dimer, the openings (terminals) are oriented in a staggered conformation, which leads to the assembly of a hyper-hexagon (chair conformation). Furthermore, a hyper-adamantane and hyper-diamantane can be obtained, as shown in Fig. 22.5. In contrast to this, from the Tj[3,0]$_{52}$ junction, a hyper-dodecahedron can be derived using 20 units, as a result of the occurrence of eclipsed terminals in the dimer (Fig. 22.6).

Details on the stability of some small structures built from the tetrapodal units can be found in Table 22.3, obtained at the HF/3–21G* level of theory
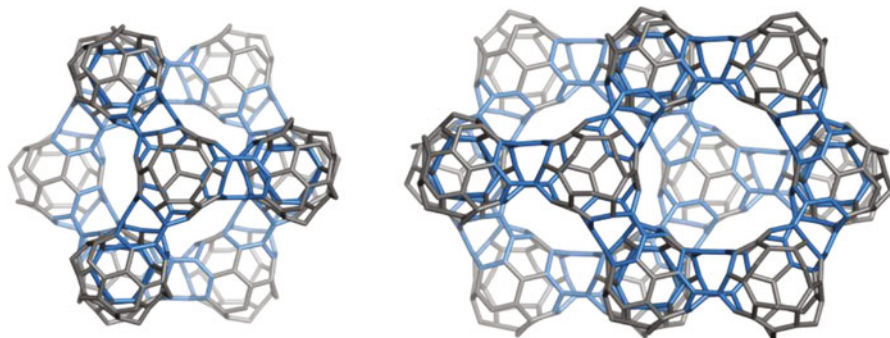
Fig. 22.5 The hyper-diamond substructures designed by Tj[3,0]$_{40}$ unit: hyper-adamantane Tj [3,0]$_{40}$_ada (*left*) and hyper-diamantane Tj[3,0]$_{40}$_dia (*right*)
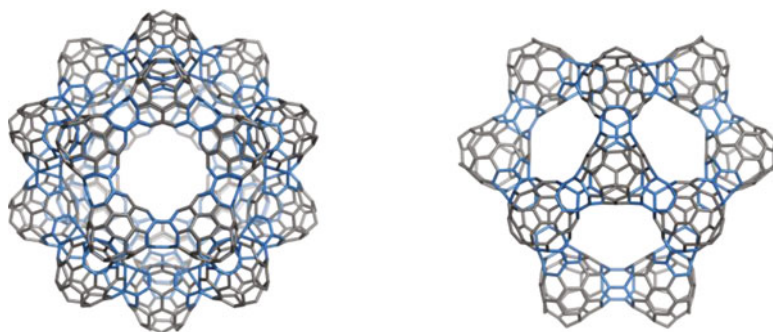

Fig. 22.6 The junction Tj[3,0]$_{52}$ enables the design of a hyper-dodecahedral architecture by joining 20 units (*left*). On the right side, a directly fused hyper-pentagon triple can be seen

Table 22.3 Computational data (HF/3–21G*) for smaller structures obtained by the assembly of tetrahedral nanotube junctions

Structure	E_{tot}/C atom (eV)	E_{gap} (eV)	SE (kcal/mol)
T$_{j40}$–dimer–C_3	−37.768	1.698	5.31
T$_{j40}$–trimer–C_2	−37.755	0.927	5.03
T$_{j40}$–hexagon–D_3	−37.728	7.382	4.57
T$_{j52}$–dimer–D_{3h}	−37.741	1.247	4.90
T$_{j52}$–trimer–C_{2v}	−37.731	0.891	4.67
T$_{j52}$–pentagon–D_{5h}	−37.711	6.755	4.25

(Nagy et al. 2013). Notice the overall structural relaxation increment observed in the strain energy with the increase in the number of joined units. According to HOMO–LUMO gap values, both hyper-ring structures have high kinetic stability.

In open multi-tori built up from u tetrapodal junction units, the genus of structure is calculated as $g = u + 1$, irrespective of the unit tessellation (Diudea and Szefler 2012). In closed unit multi-tori, the genus can be calculated by formula

Table 22.4 Calculation of the genus in opened and closed adamantane- and diamantane-like hyperstructures (multi-tori) by the Euler polyhedral formula and the number of repeat units

	v	e	f_6	f_8	f	$v-e+f$	g	u
Tj_{40}–ada	400	576	120	36	156	−20	11	10
Tj_{40}–dia	560	810	168	54	222	−28	15	14
Tj_{52}–hypDo	1040	1530	360	90	450	−40	21	20
	v	e	f_6	f_8	f_5	f	$v-e+f$	g
Tj_{52}–hypDo-closed	1060	1590	360	90	60	510	−20	11
Tj_{40}–ada-closed	416	624	120	36	48	204	−4	3
Tj_{40}–dia-closed	580	870	168	54	60	282	−8	5

$g = u - \sum_c (u_c \times c/2) + 1$ where c represents the number of closures per unit, while u_c is the number of units with c closures. Table 22.4 lists examples representing the proof of the above theorem (in agreement with the Euler formula) in both open and closed structures built up by the assembly of tetrapodal nanotube junctions (Nagy et al. 2013).

22.3.2 Armchair [3,3] Tetrahedral Junctions

Armchair nanotube junctions were systematically designed starting from the corresponding tetrahedral fullerenes; the structural relationship is listed in Table 22.1. The structural transformation involves removal and/or addition of atoms, also modification of the connectivity. The first nine elements of the [3,3] tetrahedral nanotube junctions are shown in Fig. 22.7, where the position of the heptagonal rings is marked in blue (B3LYP/6–31G(d,p) optimized geometries). According to the Euler formula, it is necessary to introduce 12 heptagons to obtain a genus 2 structure.

The orientation of the openings enables the construction of dimers in staggered conformation, resulting a hyper-diamond network. The hydrogenated units were studied using DFT method; the single point results are plotted in Fig 22.8. All structures were geometry optimized in the highest symmetry configuration; therefore, negative charges were included as necessary in the case of open-shell structures. Notice that the electronic shell of the junctions corresponds to that of the class B tetrahedral fullerenes.

The smallest junction includes only heptagonal rings and can be derived from fullerene C_{28} by replacing the pentagons with sevenfold rings. The junction having the hexagonal framework of C_{60} fullerene is $Tj[3,3]_{84}$ (T), which is the smallest leapfrog structure with isolated heptagonal rings.

In Fig. 22.8, one can observe that the stability ordering of the junctions is almost identical to the one observed in the case of class A fullerenes. The neutral tetrahedral junction $Tj[3,3]_{84}$ (T) showed the highest gap value indicating that the cluster has a high molecular stability.
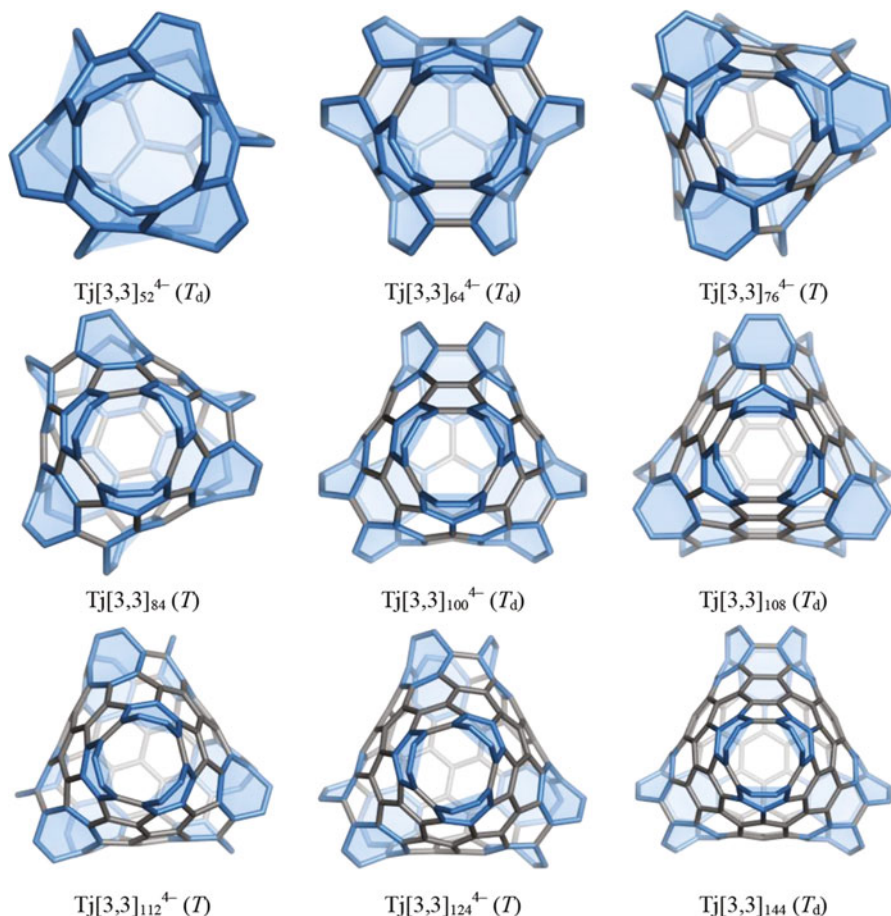
Fig. 22.7 DFT B3LYP/6–31G(d,p) optimized geometries of the armchair [3,3] carbon nanotube junctions. Position of the heptagonal rings is highlighted in *blue*

22.4   Conclusions

Tetrahedral fullerene cages have been classified according to the structural pattern found along the threefold symmetry axis and by the structural relationship with the corresponding nanotube junction. Armchair nanotube junctions having only heptagons and hexagons in the framework were built in a systematic way by spanning of the fullerenes. The supplied DFT results give an insight into the stability of tetrahedral nanoclusters. Diamond-like and dodecahedral hyperstructures were described from a topological point of view.
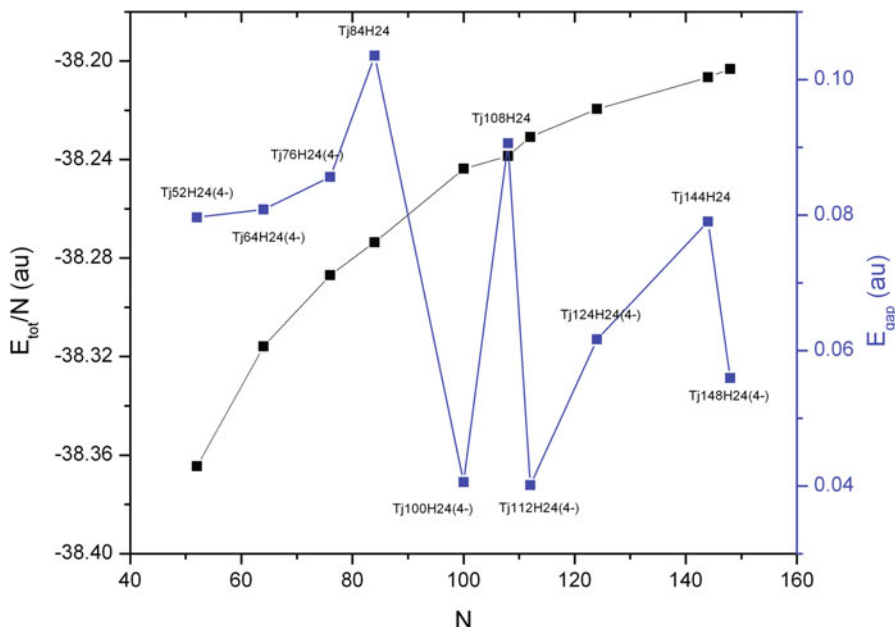
Fig. 22.8 Plot of the variation of the total energy per atom (E_{tot}/N in a.u.) and the HOMO–LUMO energy gap (E_{gap} in a.u.) as a function of the tetrahedral junction size

References

Balaban AT, Bean DE, Fowler PW (2010) Patterns of ring current in coronene isomers. Acta Chim Slov 57:507–512

Borštnik U, Hodošček M, Janežič D, Lukovits I (2005) Electronic structure properties of carbon nanotubes obtained by density functional calculations. Chem Phys Lett 411:384–388

Brinkmann G, Delgado Friedrichs O, Lisken S, Peeters A, Van Cleemput N (2010) CaGe – a virtual environment for studying some special classes of plane graphs – an update. MATCH Commun Math Comput Chem 63:533–552

Campbell EEB, Fowler PW, Mitchell D, Zerbetto F (1996) Increasing cost of pentagon adjacency for larger fullerenes. Chem Phys Lett 250:544–548

Chen Z, Jiao H, Buhl M, Hirsch A, Thiel W (2001a) The $2(N + 1)^2$ rule for spherical aromaticity: further validation. J Mol Model 7:161–163

Chen Z, Jiao H, Buhl M, Hirsch A, Thiel W (2001b) Theoretical investigation into structures and magnetic properties of smaller fullerenes and their heteroanalogues. Theor Chem Accounts 106:352–363

Cheng W, Li QS, Tang AC (1999) Vibrational spectra of tetrahedral fullerenes. J Mol Spectrosc 193:1–6

Cyrański MK, Havenith RWA, Dobrowolski MA, Gray BR, Krygowski TM, Fowler PW, Jenneskens LW (2007) The phenalenyl motif: a magnetic chameleon. Chem Eur J 13:2201–2207

Diaz-Tendero S, Alcami M, Martin F (2003) Theoretical study of ionization potentials and dissociation energies of C_n^{q+} fullerenes (n = 50–60, q = 0, 1 and 2). J Chem Phys 119:5545–5557

Diaz-Tendero S, Martin F, Alcami M (2005) Structure and electronic properties of fullerenes C_{52}^{q+}: is C_{52}^{2+} an exception to the pentagon adjacency penalty rule? ChemPhysChem 6:92–100

Diudea MV, Nagy CL (2007) Periodic nanostructures. Springer, Dordrecht

Diudea MV, Nagy CL (2012) C_{20}-related structures: diamond D_5. Diam Relat Mater 23:105–108

Diudea MV, Nagy CL (2013) Diamond D_5. In: Diudea MV, Nagy CL (eds) Diamond and related nanostructures, vol 6, Carbon materials: chemistry and physics. Springer, Dordrecht, pp 91–106

Diudea MV, Szefler B (2012) Nanotube junctions and the genus of multi-tori. Phys Chem Chem Phys 14:8111–8115

Diudea MV, Nagy CL, Ilic A (2011) Diamond D_5, a novel class of carbon allotropes. In: Putz MV (ed) Carbon bonding and structures, vol 5, Carbon materials: chemistry and physics. Springer, Dordrecht, pp 273–289

Diudea MV, Nagy CL, Bende A (2012) On diamond D_5. Struct Chem 23:981–986

Frisch MJ, Trucks GW, Schlegel HB, Scuseria GE, Robb MA, Cheeseman JR, Scalmani G, Barone V, Mennucci B, Petersson GA, Nakatsuji H, Caricato M, Li X, Hratchian HP, Izmaylov AF, Bloino J, Zheng G, Sonnenberg JL, Hada M, Ehara M, Toyota K, Fukuda R, Hasegawa J, Ishida M, Nakajima T, Honda Y, Kitao O, Nakai H, Vreven T, Montgomery JA, Peralta JE, Ogliaro F, Bearpark M, Heyd JJ, Brothers E, Kudin KN, Staroverov VN, Kobayashi R, Normand J, Raghavachari K, Rendell A, Burant JC, Iyengar SS, Tomasi J, Cossi M, Rega N, Millam NJ, Klene M, Knox JE, Cross JB, Bakken V, Adamo C, Jaramillo J, Gomperts R, Stratmann RE, Yazyev O, Austin AJ, Cammi R, Pomelli C, Ochterski JW, Martin RL, Morokuma K, Zakrzewski VG, Voth GA, Salvador P, Dannenberg JJ, Dapprich S, Daniels AD, Farkas Ö, Foresman JB, Ortiz JV, Cioslowski J, Fox DJ (2009) Gaussian 09, revision A.1. Gaussian Inc, Wallingford

Guo T, Diener MD, Chai Y, Alford MJ, Haufler RE, McClure SM, Ohno T, Weaver JH, Scuseria GE, Smalley RE (1992) Uranium stabilization of C_{28}: a tetravalent fullerene. Science 257:1661–1664

Haddon RC (1990) Measure of nonplanarity in conjugated organic molecules: which structurally characterized molecule displays the highest degree of pyramidalization? J Am Chem Soc 112:3385–3389

Haddon RC (2001) Comment on the relationship of the pyramidalization angle at a conjugated carbon atom to the σ bond angles. J Phys Chem A 105:4164–4165

Hirsch A, Chen Z, Jiao H (2000) Spherical aromaticity in I_h symmetrical fullerenes: the $2(N+1)^2$ rule. Angew Chem Int Ed 39:3915–3917

Jahn H, Teller E (1937) Stability of polyatomic molecules in degenerate electronic states. I. Orbital degeneracy. Proc R Soc A 161:220–235

Manolopoulos DE, Fowler PW (1992) Molecular graphs, point groups, and fullerenes. J Chem Phys 96:7603–7614

Nagy K, Nagy CL, Tasnadi E, Katona G, Diudea MV (2013) Hyper-diamonds and dodecahedral architectures by tetrapodal carbon nanotube junctions. Acta Chim Slov 60:1–4

Noël Y, De La Pierre M, Zicovich-Wilson CM, Orlando R, Dovesi R (2014) Structural, electronic and energetic properties of giant icosahedral fullerenes up to C6000: Insights from an ab initio hybrid DFT study. Phys Chem Chem Phys 16:13390–13401

Ray Dias J (1993) Fullerenes to benzenoids and the leapfrog algorithm. Chem Phys Lett 204:486–490

Romo-Herrera JM, Terrones M, Terrones H, Dag S, Meunier V (2007) Covalent 2D and 3D networks from 1D nanostructures: designing new materials. Nano Lett 7:570–576

Schleyer PVR, Maerker C, Dransfeld A, Jiao H, Van Eikema Hommes NJR (1996) Nucleus-independent chemical shifts: a simple and efficient aromaticity probe. J Am Chem Soc 118:6317–6318

Schwerdtfeger P, Wirz L, Avery J (2013) Program fullerene – a software package for constructing and analyzing structures of regular fullerenes, version 4.4. J Comput Chem 34:1508–1526

Scuseria GE (1992) Negative curvature and hyperfullerenes. Chem Phys Lett 195:534–536

Tang AC, Huang FQ (1996) Electronic structures and stability rules of tetrahedral fullerenes. Chem Phys Lett 258:562–573

Terrones H, Terrones M (2003) Curved nanostructured materials. New J Phys 5:126.1–126.37

Terrones M, Banhart F, Grobert N, Charlier JC, Terrones H, Ajayan PM (2002a) Molecular junctions by joining single-walled carbon nanotubes. Phys Rev Lett 89:075505/1–075505/4

Terrones M, Charlier JC, Banhart F, Grobert N, Terrones H, Ajayan PM (2002b) Towards nanodevice fabrication: joining and connecting single-walled carbon nanotubes. New Diamond Front Carbon Technol 12:315–323

Terrones M, Banhart F, Hernández E, Grobert N, Charlier JC, Terrones H, Ajayan PM (2003) In-situ welding of single-walled carbon nanotubes and melting of encapsulated metal clusters in carbon shells: theory and experiment. Microsc Microanal 9:320–321

Chapter 23
Cyclic Carbon Polyynes

Lorentz Jäntschi, Sorana D. Bolboacă, and Dusanka Janezic

Abstract Monocyclic rings with even carbon atoms, from 6 to 24, were studied using five restricted Hartree–Fock computational refinements (STO-3G, 3-21G, 6-31G*, RI-MP2/6-31G*, and RI-MP2/6-311G*) in order to identify stable polyyne rings. Polyyne rings with 24 carbon atoms were revealed to be stable, and a crossed cyclic polyyne, with 4 such rings, was designed in order to evaluate its condensed state stability. Density functional theory calculation was performed on this nano-structure. The study predicted stable monocyclic polyyne for a number of C atoms equal or higher than 16. The distance between carbon atoms followed an exponential decay to a limit value very near to the distance in C_{24} polyyne, sustaining its stability. The condensed $4C_{24}$ polyyne seemed to be stable, with a sum of bond order per atom of 3.78. The total energy value calculation leads to the conclusion that condensation by crossing the rings failed to provide supplementary stabilization, but also did not induce destabilization. The theoretical IR spectrum as well as

L. Jäntschi
Department of Physics and Chemistry, Technical University of Cluj-Napoca, Muncii Blvd. no. 103-105, RO-400641 Cluj-Napoca, Romania

Institute for Doctoral Studies, Babeş-Bolyai University, Kogălniceanu Street no. 1, RO-400084 Cluj-Napoca, Romania

University of Agricultural Science and Veterinary Medicine Cluj-Napoca, Calea Mănăştur no. 3-5, RO-400372 Cluj-Napoca, Romania

Department of Chemistry, University of Oradea, Universităţii Street no. 1, RO-410087 Oradea, Romania
e-mail: lorentz.jantschi@gmail.com

S.D. Bolboacă (✉)
University of Agricultural Science and Veterinary Medicine Cluj-Napoca, Calea Mănăştur no. 3-5, RO-400372 Cluj-Napoca, Romania

Department of Medical Informatics and Biostatistics, Iuliu Haţieganu University of Medicine and Pharmacy, 6 Louis Pasteur, 400349 Cluj-Napoca, Romania
e-mail: sbolboaca@umfcluj.ro

D. Janezic
Natural Sciences and Information Technologies, Faculty of Mathematics, University of Primorska, SI-6000 Koper, Slovenia
e-mail: dusanka.janezic@gmail.com

the thermodynamic parameters of $4C_{24}$ polyyne was rationalized from a molecular dynamics study.

23.1 Background Information on Polyyne

Polyynes are the oligomeric cousins of carbine, having linear chains of sp-hybridized carbon atoms (Smith and Buseck 1982) that are of scientific interest either as linear or cyclic complexes (McCarthy et al. 2000). Carbon, a chemical element with three naturally occurring isotopes (12C and 13C, stable, and 14C, radioactive), is part of several compounds, such as those summarized in Fig. 23.1.

Polyynes, organic compounds with alternating single and triple bonds $(-C \equiv C-)_n$ (where $n > 1$), have been reported in the scientific literature since 1951 (Bohlmann 1951a, b, c; 1955). Significant contributions to the chemistry of naturally occurring acetylenes are attributed to Bohlmann (1951a, b, c, 1953, 1955; Bohlmann et al. 1955, 1962) and Jones (2003). Synthetic routes to hydrogen terminated linear polyynes have been reported since 1972 (Eastmond et al. 1972).

Polyynes have been the focus of much study because of their unique feature, the carbon–carbon triple bonds (Cataldo 2006). A chain with over 300 carbons and alternating triple and single bonds was reported in 1995 by Lagow et al. (1995). Such linear alternating chain has been demonstrated to possess the properties of both metals and semiconductors (Gorjizadeh et al. 2011) and behave like electronic materials with very high mobility (Zhang et al. 2011).
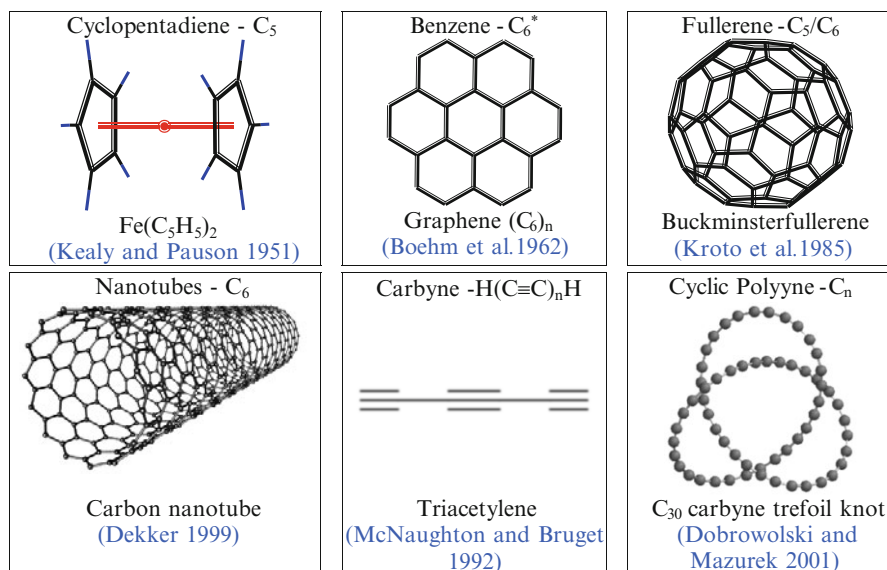
Fig. 23.1 Carbon-based compounds

Cyclic polyynes, in particular the acetylene-based polymers, have also been investigated. Examples of these include the cyclic C_{10}, C_{14}, and C_{18} polyynes (Anderson 2012) or the C_6–C_{26} clusters (Li 2012), which are all-carbon structures. Information regarding the stability of polyyne rings is essential in identification of new materials with interesting properties.

The present study reports a computational chemistry study of cyclic polyynes at the post-Hartree–Fock (HF) level of theory in order to rationalize the stabilization of polyyne rings in a condensed arrangement.

23.2 Monocyclic Polyynes

The cyclic polyynes with an even number of carbon atoms, from 6 to 24, were investigated. The following approach has been applied in characterization of monocyclic ring polyynes:

- Geometry optimization: The structural optimization of the investigated structures was performed by Spartan (v. 10, http://www.wavefun.com) ab initio package at the restricted (post)-HF (Hartree–Fock) (Hartree 1928a, b; Fock 1930a, b; Hartree and Hartree 1935) level of theory. Five computational refinements were explored: STO-3G (slater-type orbitals – Gaussian approximated with $5 \cdot n$ basis functions (Hehre et al. 1969)), 3-21G (with $9 \cdot n$ basis functions (Moller and Plesset 1934)), 6-31G* (split-valence basis sets with $15 \cdot n$ basis functions (Ditchfield et al. 1971)), RI-MP2/6-31G* (with $15 \cdot n$ basis functions, MP = Møller–Plesset perturbation method (Moller and Plesset 1934), 2 = second order, RI = resolution of the identity), and RI-MP2/6-311G* (with $18 \cdot n$ basis functions). In all cases, n is the number of carbon atoms.
- Rationalization: To characterize the monocyclic ring polyynes, the average energy per atom and distances between C atoms have been calculated under the investigated refinements of theory levels.

23.2.1 Energy Assessment

Stable monocyclic ring of polyynes was calculated beginning with six carbon atoms – the first even number investigated. The energy values obtained for monocyclic polyynes are listed in Table 23.1.

As can be observed from Table 23.1, the energy values decrease as the number of C atoms in the monocyclic ring increases. This decrease is steep until $n = 14$, and

Table 23.1 Average energy per atom (E(kcal/mol)) for a single monocyclic ring polyyne, calculated at different theory levels

n	STO-3G	3-21G	6-31G*	RI-MP2/6-31G*	RI-MP2/6-311G*
6	$-37.308 \cdot n$	$-37.577 \cdot n$	[a]		
8	$-37.329 \cdot n$	$-37.593 \cdot n$	[a]		
10	$-37.346 \cdot n$	$-37.610 \cdot n$	[a]		
12	$-37.352 \cdot n$	$-37.614 \cdot n$	[a]		
14	$-37.358 \cdot n$	$-37.619 \cdot n$	$-37.829 \cdot n$	[b]	
16	$-37.361 \cdot n$	$-37.621 \cdot n$	$-37.831 \cdot n$	$-37.958 \cdot n$	$-37.970 \cdot n$
18	$-37.363 \cdot n$	$-37.624 \cdot n$	$-37.833 \cdot n$	[c]	
20	$-37.364 \cdot n$	$-37.625 \cdot n$	$-37.835 \cdot n$	$-37.961 \cdot n$	$-37.973 \cdot n$
22	$-37.365 \cdot n$	$-37.626 \cdot n$	$-37.836 \cdot n$	[c]	
24	$-37.366 \cdot n$	$-37.627 \cdot n$	$-37.836 \cdot n$	$-37.962 \cdot n$	$-37.974 \cdot n$

n, number of carbon atoms (only the coefficients were included in the exponential fit)
[a]symmetry broken at 6-31G* level of theory
[b]planarity broken at RI-MP2/6-31G* level of theory
[c]optimization oscillated between equilibrium states

then it becomes and remains very slight. The exponential fit reveals a decay that supports the stabilization of the monocyclic rings at C_{23}. For STO-3G level of theory, the fit is

$$\hat{Y} = -37.3664 + 0.2482 \cdot \exp(-n/4.1462)$$
$$R^2 = 0.9977; \; R^2_{adj} = 0.9970; \; F = 1494$$

where $\hat{Y}$ = energy per atom estimated by the exponential function, n = number of C atoms in the monocyclic ring, R^2 = determination coefficient, R^2_{adj} = adjusted determination coefficient, and F = Fisher's statistics associated with the regression model.

The minimum energy values were in every case related to the STO-3G basis set, while the maximum values were provided by RI-MP2/6-311G* whenever it could be calculated, depending upon the stability of the monocyclic ring polyynes (see Table 23.1). The following interesting observation about the stability of monocyclic ring polyynes could be made: stabilization of the polyynes occurs when the number of carbon atoms is a multiple of 4 and no less than 16. As can be concluded from the exponential decay of the average energy per C atom, starting with $n = 16$, the cyclic polyynes quickly approach the minimum energy state. The difference due to RI-MP2/6-311G* in the average energy values per atom for polyynes between C_{20} and C_{24} is less than $1\% \cdot n$.

23.2.2 Bond Length

The stability of a monocyclic ring can be assessed by inspection of the C–C and $C\equiv C$ interatomic separation, i.e., the bond lengths (Table 23.2). Analysis of the results presented in Table 23.2 shows:

- In general, there is a decrease in $C\equiv C$ length, when n increases, for STO-G, 3-21G, and 6-31G* levels of theory; there are two exceptions (at C_{14} and C_{18}) for 3-21G and one exception (at C_{18}) for 6-31G*.
- The general trend is a smooth increase in the $C\equiv C$ bond length and a smooth decrease of C–C length for the RI-MP2/6-31G* and RI-MP2/6-311G* levels of theory; the C–C length increases systematically in the monocyclic rings, and those differing by four C atoms are clustered with a smooth decrease at C_{22} and C_{24} for STO-G level of theory; the C–C distance systematically increases in the monocyclic rings, and those differing by four C atoms are clustered with a plateau as the difference between C_{18} and C_{22} is concerned for 3-21G level of theory.

The plot of $C\equiv C$ bond lengths, provided by STO-3G (column 2, STO-3G/d_1 in Table 23.2), vs. the number of atoms (n) also shows an exponential decay which fits well with the observed values while ($C\equiv C;C_{24}$) is near to the estimated optimal value of 118.63 pm:

$$\hat{d}_{\text{STO}-3G}(C\equiv C; C_n) = 118.63(\pm0.27) + 152(\pm54)\cdot e^{-n/2.3(\pm0.3)}$$

The above equation estimates a value of 119.6 pm for $n=12$ while the calculated value is of 119.0 pm, a value of 118.7 pm for $n=18$ while the calculated value is of 118.6 pm, and a value of 118.6 pm for $n=24$ while the calculated value is of 118.6 pm.

Table 23.2 $C\equiv C$ and C–C bond length in monocyclic rings at different theory levels

|	STO-3G		3-21G		6-31G*		RI-MP2/6-31G*		RI-MP2/6-311G*	
n	$C\equiv C$	C–C	$C\equiv C$	C–C	$C\equiv C$	C–C	$C\equiv C$	C–C	$C\equiv C$	C–C
6	129.8	129.8	129.5	129.6	[a]					
8	123.7	142.1	123.3	139.5	[a]					
10	120.4	138.9	122.1	133.8	[a]					
12	119.0	141.4	119.7	138.3	[a]					
14	119.2	139.9	120.3	135.9	121.7	136.0	[b]			
16	118.8	140.3	119.7	137.0	119.7	138.5	125.2	135.7	125.0	135.4
18	118.8	139.9	119.9	136.2	119.8	138.0	[c]			
20	118.7	139.9	119.7	136.5	119.6	138.1	125.5	134.6	125.3	134.3
22	118.7	139.8	119.7	136.2	119.6	137.9	[c]			
24	118.6	139.8	119.6	136.2	119.6	138.0	125.7	133.9	125.6	133.6

n, number of C atoms in monocyclic polyyne ring, bond length in pm
[a] symmetry broken at 6-31G* level of theory
[b] planarity broken at RI-MP2/6-31G* level of theory
[c] optimization oscillated between equilibrium states

Fig. 23.2 C_{24} standard
chemical structure
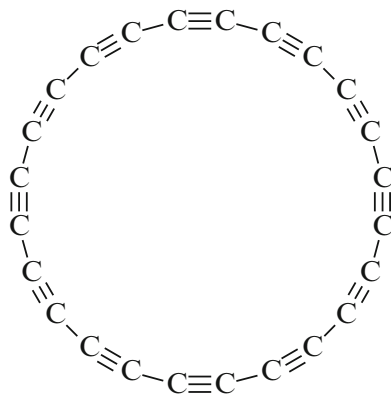
23.2.3 Stable Monocyclic Polyyne

The monocyclic ring with 24 atoms appeared to be a stable complex, and subsequent work was performed on the polycyclic C_{24} polyyne (Fig. 23.2).

The crossed arrangement of the polyynes was of interest in this study and was driven at 6-31G* level of refinement for geometry optimization. A stable C_{24} cyclic polyyne in a form of crossed cycles was searched.

23.2.4 Characteristic Polynomials of C_{24} Polyyne

The characteristic polynomial (noted here with P_φ), calculated by the determinant of the matrix obtained as a difference between unity matrix $I_{|V|}$ multiplied with a symbolic variable (X, for instance) and the adjacency matrix (Ad),

$$P_\varphi(X) \ = \ P_\varphi(X, G) \ = \ \left| X \cdot I_{|V|} - Ad(G) \right|$$

has been evaluated for C_{24} polyyne.

Characteristic polynomial, as other polynomials, encodes the topological information of a chemical structure and can be seen as a source of structural descriptors used in structure–property/activity modeling (Ivanciuc et al. 1999; Balasubramanian and Randi 1982; Jäntschi et al. 2009; Bolboacă and Jäntschi 2007).

The characteristic polynomial was computed in two different ways: the classical characteristic polynomial (ChP) and a weighted polynomial. For this, the adjacency matrix ("0/1," Table 23.3) was replaced by the bond order matrix ("0/1/3"; see Table 23.4).

The characteristic polynomial ChP of C_{24} polyyne is

Table 23.3 C$_{24}$ polyyne: negative signed adjacency matrix

[Ch]	1	2	3	4	5	6	7	8	9	10	11	12	13	14	15	16	17	18	19	20	21	22	23	24
1		-1	0	0	0	-1	0	0	0	0	0	0	0	0	0	0	0	0	0	0	0	0	0	0
2	-1		0	0	0	0	0	0	-1	0	0	0	0	0	0	0	0	0	0	0	0	0	0	0
3	0	0		-1	0	0	0	-1	0	0	0	0	0	0	0	0	0	0	0	0	0	0	0	0
4	0	0	-1		-1	0	0	0	0	0	0	0	0	0	0	0	0	0	0	0	0	0	0	0
5	0	0	0	-1		-1	0	0	0	0	0	0	0	0	0	0	0	0	0	0	0	0	0	0
6	-1	0	0	0	-1		0	0	0	0	0	0	0	0	0	0	0	0	0	0	0	0	0	0
7	0	0	0	0	0	0		-1	0	0	0	-1	0	0	0	0	0	0	0	0	0	0	0	0
8	0	0	-1	0	0	0	-1		0	0	0	0	0	0	0	0	0	0	0	0	0	0	0	0
9	0	-1	0	0	0	0	0	0		-1	0	0	0	0	0	0	0	0	0	0	0	0	0	0
10	0	0	0	0	0	0	0	0	-1		0	0	-1	0	0	0	0	0	0	0	0	0	0	0
11	0	0	0	0	0	0	0	0	0	0		-1	0	0	0	-1	0	0	0	0	0	0	0	0
12	0	0	0	0	0	0	-1	0	0	0	-1		0	0	0	0	0	0	0	0	0	0	0	0
13	0	0	0	0	0	0	0	0	0	0	-1	0	0		-1	0	0	0	0	0	0	0	0	0
14	0	0	0	0	0	0	0	0	0	0	0	0	-1		0	0	-1	0	0	0	0	0	0	0
15	0	0	0	0	0	0	0	0	0	0	0	0	0	0		-1	0	0	0	-1	0	0	0	0
16	0	0	0	0	0	0	0	0	0	0	-1	0	0	0	-1		0	0	0	0	0	0	0	0
17	0	0	0	0	0	0	0	0	0	0	0	0	0	-1	0	0		-1	0	0	0	0	0	0
18	0	0	0	0	0	0	0	0	0	0	0	0	0	0	-1	0	0		0	0	-1	0	0	0
19	0	0	0	0	0	0	0	0	0	0	0	0	0	0	0	0	0	0		-1	0	0	0	-1
20	0	0	0	0	0	0	0	0	0	0	0	0	0	0	-1	0	0	0	-1		0	0	0	0
21	0	0	0	0	0	0	0	0	0	0	0	0	0	0	0	0	0	-1	0	0		-1	0	0
22	0	0	0	0	0	0	0	0	0	0	0	0	0	0	0	0	0	0	0	0	-1		-1	0
23	0	0	0	0	0	0	0	0	0	0	0	0	0	0	0	0	0	0	0	0	0	-1		-1
24	0	0	0	0	0	0	0	0	0	0	0	0	0	0	0	0	0	0	-1	0	0	0	-1	

Table 23.4 C$_{24}$ polyyne: negative signed bond order matrix

[Ch]	1	2	3	4	5	6	7	8	9	10	11	12	13	14	15	16	17	18	19	20	21	22	23	24
1		-3	0	0	0	-1	0	0	0	0	0	0	0	0	0	0	0	0	0	0	0	0	0	0
2	-3		0	0	0	0	0	0	-1	0	0	0	0	0	0	0	0	0	0	0	0	0	0	0
3	0	0		-3	0	0	0	-1	0	0	0	0	0	0	0	0	0	0	0	0	0	0	0	0
4	0	0	-3		-1	0	0	0	0	0	0	0	0	0	0	0	0	0	0	0	0	0	0	0
5	0	0	0	-1		-3	0	0	0	0	0	0	0	0	0	0	0	0	0	0	0	0	0	0
6	-1	0	0	0	-3		0	0	0	0	0	0	0	0	0	0	0	0	0	0	0	0	0	0
7	0	0	0	0	0	0		-3	0	0	0	-1	0	0	0	0	0	0	0	0	0	0	0	0
8	0	0	-1	0	0	0	-3		0	0	0	0	0	0	0	0	0	0	0	0	0	0	0	0
9	0	-1	0	0	0	0	0	0		-3	0	0	0	0	0	0	0	0	0	0	0	0	0	0
10	0	0	0	0	0	0	0	0	-3		0	0	-1	0	0	0	0	0	0	0	0	0	0	0
11	0	0	0	0	0	0	0	0	0	0		-3	0	0	0	-1	0	0	0	0	0	0	0	0
12	0	0	0	0	0	0	-1	0	0	0	-3		0	0	0	0	0	0	0	0	0	0	0	0
13	0	0	0	0	0	0	0	0	0	-1	0	0		-3	0	0	0	0	0	0	0	0	0	0
14	0	0	0	0	0	0	0	0	0	0	0	0	-3		0	0	-1	0	0	0	0	0	0	0
15	0	0	0	0	0	0	0	0	0	0	0	0	0	0		-3	0	0	0	-1	0	0	0	0
16	0	0	0	0	0	0	0	0	0	0	-1	0	0	0	-3		0	0	0	0	0	0	0	0
17	0	0	0	0	0	0	0	0	0	0	0	0	0	-1	0	0		-3	0	0	0	0	0	0
18	0	0	0	0	0	0	0	0	0	0	0	0	0	0	-3	0	0		0	0	-1	0	0	0
19	0	0	0	0	0	0	0	0	0	0	0	0	0	0	0	0	0	0		-3	0	0	0	-1
20	0	0	0	0	0	0	0	0	0	0	0	0	0	0	-1	0	0	0	-3		0	0	0	0
21	0	0	0	0	0	0	0	0	0	0	0	0	0	0	0	0	0	-1	0	0		-3	0	0
22	0	0	0	0	0	0	0	0	0	0	0	0	0	0	0	0	0	0	0	0	-3		-1	0
23	0	0	0	0	0	0	0	0	0	0	0	0	0	0	0	0	0	0	0	0	0	-1		-3
24	0	0	0	0	0	0	0	0	0	0	0	0	0	0	0	0	0	0	-1	0	0	0	-3	

$$
\begin{aligned}
ChP(C_{24}polyyne) = \ & +1 \cdot x^{24} - 24 \cdot x^{22} + 252 \cdot x^{20} \\
& - 1520 \cdot x^{18} + 5814 \cdot x^{16} - 14688 \cdot x^{14} + 24752 \cdot x^{12} \\
& - 27456 \cdot x^{10} + 19305 \cdot x^{8} - 8008 \cdot x^{6} + 1716 \cdot x^{4} \\
& - 144x^{2}
\end{aligned}
$$

The roots of characteristic polynomial varied from -2 to 2, with an average of 0 and a standard deviation of 1.44. The value of Anderson–Darling statistics is equal to 0.7456 ($p = 0.4795$ (Jäntschi 2014)) saying that the values of roots are normally distributed.

The orbital energies and the Hessian eigenvalues were furthermore calculated for monocyclic C_{24} polyyne. The C_{24} polyyne has eighty-two orbitals, ten being unoccupied molecular orbitals (the last ten in the right upper corner of the graph in Fig. 23.3).

The pattern distribution of the characteristic polynomial roots is shown in Fig. 23.4.
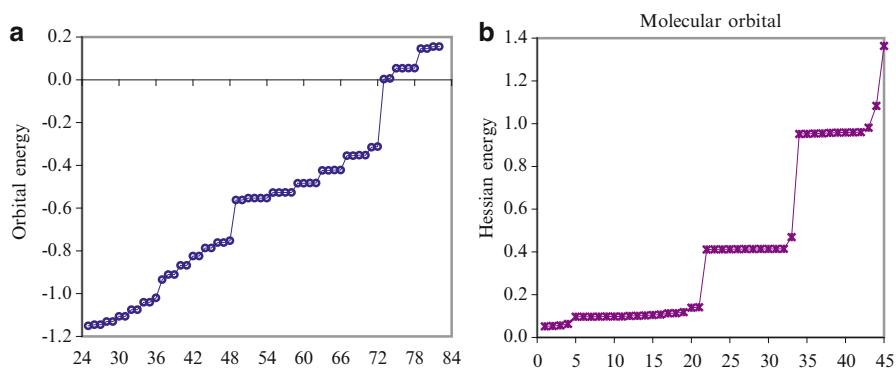
Fig. 23.3 Pattern distribution for monocyclic C_{24} polyyne: (**a**) orbital energy, (**b**) Hessian energy
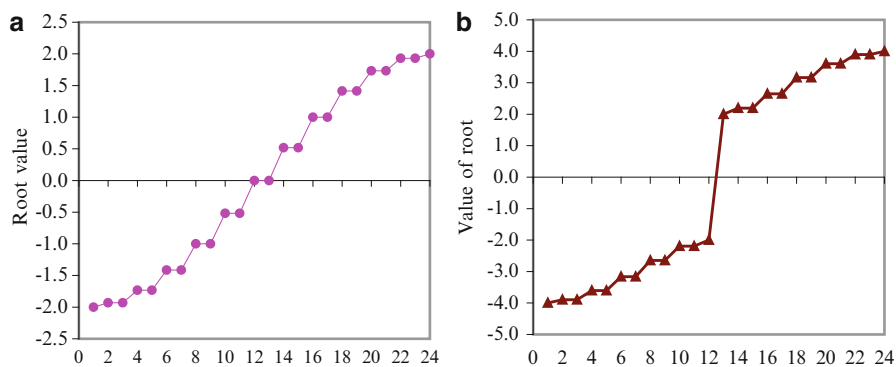
Fig. 23.4 Pattern distribution for monocyclic C_{24} polyyne: (**a**) roots of the characteristic polynomial, (**b**) roots of the characteristic polynomial on bond order

The coefficient of similarity (Myers 1986) between the root values and values of orbital energy is 43.19 % when 24 roots are compared to 48 orbital energies (the first 24 and the last 10 values not included) and increases to 47.78 % when 24 roots are linked with 24 values of orbital energies. A similar value is found when the similarity of roots and Hessian energy is investigated (42.48 %).

The bond order matrix for monocyclic C_{24} polyyne is presented in Table 23.4. The pattern distribution of the values of roots of the characteristic polynomial on bond order is presented in Fig. 23.4b.

The coefficient of similarity [29] between values of roots and values of orbital energy is 39.41 % when 24 roots are compared to 48 orbital energies (not included the first 24 and the last 10 values) and increase to 43.59 % when 24 roots are linked with 24 values of orbital energies. A similar value is found when the similarity of roots of the characteristic polynomial on bond order matrix and Hessian energy is investigated (40.74 %).

The characteristic polynomial on bond order (ChP_{bo}) of C_{24} polyyne is

$$
\begin{aligned}
ChP_{bo}(C_{24}\text{polyyne}) = {} & +1 \cdot x^{24} - 120 \cdot x^{22} + 6492 \cdot x^{20} \\
& - 209200 \cdot x^{18} + 4468374 \cdot x^{16} - 66589920 \cdot x^{14} \\
& + 709365552 \cdot x^{12} - 5438445120 \cdot x^{10} + 29760016905 \cdot x^{8} \\
& - 113288996200 \cdot x^{6} + 284636017236 \cdot x^{4} \\
& - 423644304720 \cdot x^{2} + 282428473600 \cdot x^{0}
\end{aligned}
$$

The value of characteristic polynomial on bond order matrix roots varied from -4 to 4, with an average of 0 and a standard deviation of 3.23. The value of Anderson–Darling statistics equal to 1.8896 ($p = 0.8936$) sustains that the values of roots of characteristic polynomial on bond order matrix are also normally distributed.

23.3 Assembly of C_{24} Polyyne

Identification and characterization of condensed cyclic polyynes was done following the next steps:

- Crossing the structures: A trial has been conducted to identify how many monocyclic ring polyyne could be crossed to form a stable crossed structure.
- Geometry optimization: The geometry optimization was conducted on the crossed cyclic polyynes identified at the previous step with the Spartan ab initio package at the restricted (post)-HF level of theory, with 6-31G* computational refinement. The reason of using 6-31G* level of refinement could be found in the *Supplementary Material* which shows that for the elements of first period, it is the best choice in estimating the geometry.
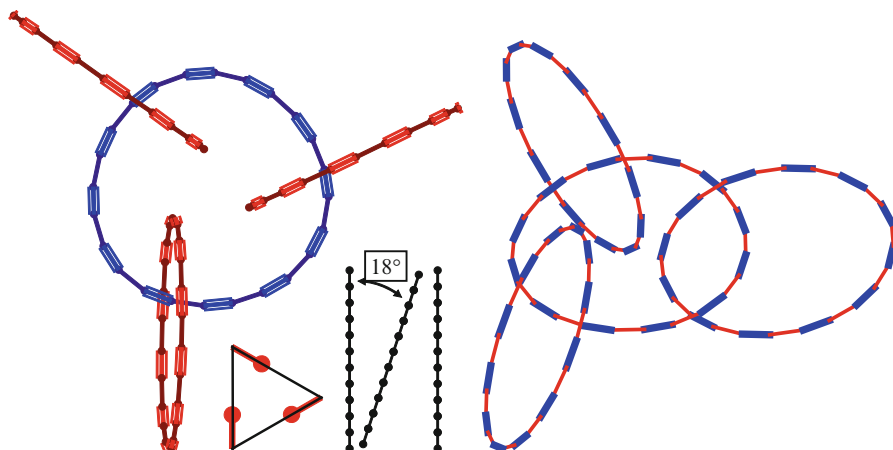
Fig. 23.5 $4C_{24}$ optimized structure of even-C-atom polycyclic cluster at 6-31G*

- Molecular dynamics study: It has been performed by Spartan using DFT (density functional theory (Pierre and Kohn 1964; Kohn and Sham 1965)) method using M06 functionals (Zhao and Truhlar 2008) at the 6-31G* basis set.

Geometry optimization revealed that in both the isolated polyyne-24 and the 4-condensed-polyyne-24, the distance between carbon atoms (i.e., the bond length) is optimal (Fig. 23.5):

$$d(C\equiv C) \ = \ 120 \text{ pm}, \ d(C-C) \ = \ 136 \text{ pm}$$

The following values were calculated for the $4C_{24}$ complex (6-31G* level of refinement): molecular weight = 1153.056 amu, energy = 11785.29 kJ/mol, E-HOMO (energy of highest occupied molecular orbital) = −9.36 eV, E-LUMO (energy of lowest unoccupied molecular orbital) = −2.03 eV, and dipole moment = 0.07 debye.

The molecular dynamics study performed on $4C_{24}$ using DFT-M06 led to the following reasonable values of thermodynamic parameters: ZPE (zero-point energy) = 1383.93 kJ/mol, S (entropy) = 1377.75 J/mol, H (enthalpy) = 5.0861 au (atomic units, 1 au = 2625 kJ/mol), G (free enthalpy) = 4.9296 au, and C_v (heat capacity at constant volume) = 1325.31 J/mol.

The total energy of the four-cyclic ring structure ($4C_{24}$) was calculated as −3587.1360 kcal/mol, leading to an energy per atom of −37.3660 kcal/at · mol, while the total energy for monocyclic ring C_{24} was of −896.783 kcal/mol with energy per atom equal to −37.3662 kcal/at · mol. In consequence, condensation of $4C_{24}$ provided neither supplementary stabilization nor destabilization.

The bond lengths in $4C_{24}$ optimized structure and the estimated bond orders are listed in Table 23.5.

Table 23.5 Bond length in $4C_{24}$ polyyne complex

Ring	Bond	Distance $k \cdot$ distance (pm)	Averaged distance (pm)	Lowden	Mulliken
Belt ring	C≡C	$11 \cdot 118.8$, $1 \cdot 118.7$	≈ 118.8	1.16	1.16
Exterior ring #1	C≡C	$11 \cdot 118.6$, $1 \cdot 118.7$	≈ 118.6		
Exterior rings #2 and #3	C≡C	$12 \cdot 118.6$	118.6		
Belt ring	C–C	6 (140.2, 140.3)	140.25	2.69	2.70
Exterior rings #1, #2, and #3	C–C	$11 \cdot 139.8$, $1 \cdot 139.9$	≈ 139.8		

k number of bonds

Fig. 23.6 Electrostatic potential of $4C_{24}$ polycyclic polyyne
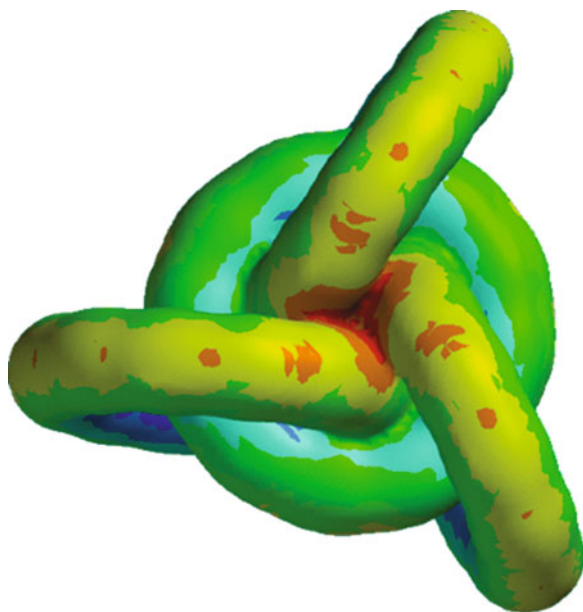
The sum of bond order per atom was of 3.78 (either Lowden or Mulliken) and is near to the ideal value of 4. The average distance between carbon atoms in organic compounds found in literature (Jäntschi 2013) is 154 pm for the C–C bond, 134 pm for the C=C bond, and 120 pm for the C≡C bond, while in the proposed polycyclic polyyne, the values were 139.91 pm on average for the C–C bond and 118.65 pm on average for the C≡C bond. These results obtained on the $4C_{24}$ condensed cyclic polyyne suggest a high hardness in the solid state.

The electrostatic potential for the proposed polycyclic polyyne is illustrated in Fig. 23.6 and was obtained from the model at DFT-M06 level of theory.

Similar IR spectra were obtained from the molecular dynamics study performed at DFT-M06 theory level on both one monocyclic polyyne (Fig. 23.7) and $4C_{24}$polycyclic polyyne (Fig. 23.8). Several similarities could be observed in the
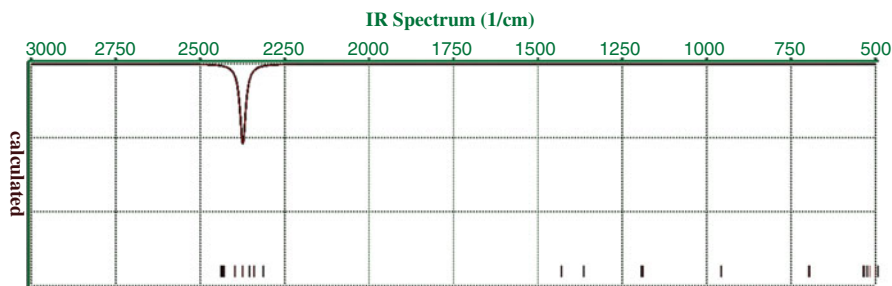
Fig. 23.7 IR spectrum (1/cm) of C_{24} monocyclic polyyne (at DFT-M06/6-31G* level of theory)
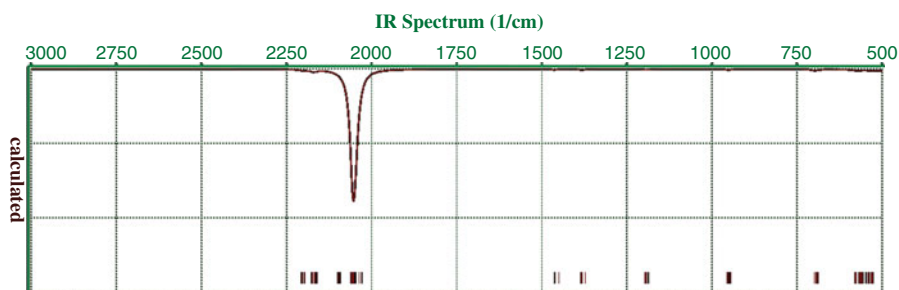
Fig. 23.8 IR spectrum (1/cm) of $4C_{24}$ polycyclic polyyne (at DFT-M06/6-31G* level of theory)

obtained IR spectra: there is only one broad band corresponding to the energy absorption/emission for the vibration/rotation/translation of one C atom from the chain (Figs. 23.7 and 23.8). Furthermore, there are several signals of smaller intensity (compared to the broad band) which correspond to the fine interactions (resonance) between chains, the condensed structure of polyyne being not a rigid one. The IR spectrum of $4C_{24}$ polycyclic polyyne shows the stability of the condensed structure, the energy absorbed by atoms being higher than the energy absorbed by the assemblies of atoms.

Searching for new improved materials with various applications among molecules containing carbon atoms has been a subject of research in recent years (Wang et al. 2004, 2014; Trogadas et al. 2014). Cyclic polyynes theoretically studied by have previously predicted heaving optical and electronic properties that could be useful in advanced materials (Ditchfield et al. 1971; Bunz et al. 1999).

23.4 Conclusions

In this chapter, we presented a computational chemistry study of cyclic polyynes with an even number of carbon atoms. Our results show that C_n cyclic polyynes are more likely to be stable when $n \geq 16$ since starting at this point of energy value, at

STO-3G and 3-21G levels, reaches a plateau. Exponential decay of energy per atom sustains the stability of monocyclic rings at C_{24}, and a complex of four crossed C_{24} cycles was identified as a stable and reliable new entity. According to the calculations, it is expected for the identified $4C_{24}$ complex to have the best hardness among its homologues, being thus a very good candidate for experimental synthesis. Further research will be needed to characterize this new complex.

References

Anderson BD (2012) Cyclic polyynes as examples of the quantum mechanical particle on a ring. J Chem Educ 89:724–727

Balasubramanian K, Randi M (1982) The characteristic polynomials of structures with pending bond. Theor Chim Acta (Berl) 61:307–323

Boehm HP, Clauss A, Fischer GO, Hofmann U (1962) Das Adsorptionsverhalten sehr dünner Kohlenstofffolien. Z Anorg Allg Chem 316:119–127

Bohlmann F (1951a) Polyacetylenverbindungen I. Darstellung von Triacetylen-Verbindungen. Angew Chem 63:218

Bohlmann F (1951b) Konstitution und Lichtabsorption II. Diacetylen-Verbindungen. Chem Ber 84:545–546

Bohlmann F (1951c) Konstitution und Lichtabsorption III. Polyacetylenverbindungen. Chem Ber 84:785–794

Bohlmann F (1953) Polyacetylenverbindungen IV. Darstellung von Di-tert.-butyl-polyacetylenen. Chem Ber 86:657–667

Bohlmann F (1955) The naturally occurring polyacetylene compounds. Angew Chem 67:389–394

Bohlmann F, Mannhardt H-J, Viehe H-G (1955) Polyacetylenverbindungen VII. Synthese des Polyinketons aus Artemisia vulgaris. Chem Ber 88:361–370

Bohlmann F, Bornowski H, Arndt C (1962) Natürlich vorkommende Acetylenverbindungen. Fortschr Chem Forsch 4:138–272

Bolboacă S, Jäntschi L (2007) How good the characteristic polynomial can be for correlations? Int J Mol Sci 8(4):335–345

Bunz UHF, Rubin Y, Tobe Y (1999) Polyethynylated cyclic π-systems: scaffoldings for novel two and three-dimensional carbon networks. Chem Soc Rev 28:107–119

Cataldo F (ed) (2006) Polyynes: synthesis, properties and applications. CRC Press, Boca Raton

Dekker C (1999) Carbon nanotubes as molecular quantum wires. Phys Today 52:22–28

Ditchfield R, Hehre WJ, Pople JA (1971) Self-consistent molecular-orbital methods IX. An extended gaussian-type basis for molecular-orbital studies of organic molecules. J Chem Phys 54:724–728

Dobrowolski JC, Mazurek AP (2001) On the qualitative theoretical NMR chemical shifts of model carbyne catenanes and knots. Chem Phys Lett 348:60–66

Eastmond R, Johnson TR, Walton DRM (1972) Silylation as a protective method for terminal alkynes in oxidative couplings: a general synthesis of the parent polyynes $H(C≡C)nH$ (n = 4–10, 12). Tetrahedron 28:4601–4616

Fock VA (1930a) Approximation method for solving the quantum mechanical many-body problem. Z Phys 61:126–148

Fock VA (1930b) Self consistent field with exchange for sodium. Z Phys 62:795–805

Gorjizadeh N, Farajian AA, Kawazoe Y (2011) Non-coherent transport in carbon chains. J Phys Condens Matter 23:75301

Hartree DR (1928a) The wave mechanics of an atom with a non-coulomb central field. Part I. Theory and methods. Math Proc Camb 24:89–110

Hartree DR (1928b) The wave mechanics of an atom with a non-coulomb central field. Part II. Some results and discussion. Math Proc Camb 24:111–132

Hartree DR, Hartree W (1935) Self-consistent field, with exchange, for beryllium. Proc R Soc London 150:9–33

Hehre WJ, Stewart RF, Pople JA (1969) Self-consistent molecular-orbital methods I. Use of gaussian expansions of slater-type atomic orbitals. J Chem Phys 51:2657–2664

Ivanciuc O, Ivanciuc T, Diudea MV (1999) Polynomials and spectra of molecular graphs. Rom Chem Q Rev 7(1):41–67

Jäntschi L (2013) General chemistry course. AcademicDirect, Cluj-Napoca

Jäntschi L (2014) Anderson darling statistics online calculator. http://l.academicdirect.org/Statistics/tests/AD/?n=24&a=0.7456&p=1.0E-11

Jäntschi L, Bolboacă SD, Furdui CM (2009) Characteristic and counting polynomials: modelling nonane isomers properties. Mol Simul 35(3):220–227

Jones JH (2003) Sir Ewart Ray Herbert Jones 16 March 1911–7 May 2002 Elected FRS 1950. Biogr Mems Fell R Soc 49:263–282

Kealy TJ, Pauson PL (1951) A new type of organo-iron compound. Nature 168:1039–1040

Kohn W, Sham LJ (1965) Self-consistent equations including exchange and correlation effects. Phys Rev 140:A1133–A1138

Kroto HW, Heath JR, O'Brien SC, Curl RF, Smalley RE (1985) Buckminsterfullerene. Nature 318:162–163

Lagow RJ, Kampa JJ, Han-Chao W, Battle SL, Genge JW, Laude DA, Harper CJ, Bau R, Stevens RC, Haw JF, Munson E (1995) Synthesis of linear acetylenic carbon: the "sp" carbon allotrope. Science 267:362–367

Li P (2012) DFT studies on configurations, stabilities, and IR spectra of neutral carbon clusters. J At Mol Sci 3:308–322

McCarthy MC, Chen W, Travers MJ, Thaddeus P (2000) Microwave spectra of 11 polyyne carbon chains. Astrophys J 129:611–623

McNaughton D, Bruget DN (1992) The high-resolution infrared spectrum of diacetylene and structures of diacetylene, triacetylene and dicyanoacetylene. J Mol Struct 273:11–25

Moller C, Plesset MS (1934) Note on an approximation treatment for many-electron systems. Phys Rev 46:618–622

Myers EW (1986) An O(ND) Difference algorithm and its variations [online]. Accessed 8 Mar 2015. Available from: http://www.xmailserver.org/diff2.pdf

Pierre H, Kohn W (1964) Inhomogeneous electron gas. Phys Rev 136:B864–B871

Smith PPK, Buseck PR (1982) Carbyne forms of carbon: do they exist? Science 216:984–986

Trogadas P, Fuller TF, Strasser P (2014) Carbon as catalyst and support for electrochemical energy conversion. Carbon 75:5–42

Wang C, Guo ZX, Fu S, Wu W, Zhu D (2004) Polymers containing fullerene or carbon nanotube structures. Prog Polym Sci 29:1079–1141

Wang A, Li L, Wang X, Bu H, Zhao M (2014) Graphyne-based carbon allotropes with tunable properties: from dirac fermion to semiconductor. Diam Relat Mater 41:65–72

Zhang Y, Su Y, Wang L, Kong ESW, Chen X, Zhang Y (2011) A one-dimensional extremely covalent material: monatomic carbon linear chain. Nanoscale Res Lett 6:1–4

Zhao Y, Truhlar DG (2008) The M06 suite of density functionals for main group thermochemistry, thermochemical kinetics, noncovalent interactions, excited states, and transition elements: two new functionals and systematic testing of four M06-class functionals and 12 other functionals. Theor Chem Accounts 120:215–241

Chapter 24
Tiling Fullerene Surfaces

Ali Asghar Rezaei

Abstract A tiling of a surface is a decomposition of the surface into pieces, i.e., tiles, which cover it without gaps or overlaps. Sphere, ellipsoid, cylinder, and torus are the most abundant shapes for fullerenes, nanotubes, and carbon nanostructures. In this chapter the polygonal tiling of these surfaces is investigated.

24.1 Introduction

Tilings are all around us. In general, a tiling is just a way of decomposing some space into lots of little pieces (tiles) that fit together without gaps or overlaps. Re-tiling surfaces by regular geodesic polygons has been widely used since antiquity and has applications in the modern world and many branches of science.

The study of tiling in some surfaces like sphere, cylinder, and torus is important in nanoscience, because they are the most abundant shapes of fullerenes. Our study involves every other shape which is topologically homeomorphic to one of the mentioned three surfaces.

Fullerenes and nanotubes are two important carbon allotropes which are composed entirely of carbon atom, in the form of a sphere, ellipsoid, cylinder, or tube. The structure of ordinary fullerenes is composed of hexagonal and pentagonal faces but in general form heptagonal and octagonal rings can also be considered, see for example Fujimori et al. (2010), Jeong et al. (2008), Sánchez-Bernabe et al. (2013), Tchoffo et al. (2014). Other geometric shapes such as squares and triangles may be found in the structure of fullerenes. We investigated the number of polygons with k-sides in the structure of a fullerene, for $k = 3,4,5,6,7$, and 8. In recent years several mathematicians studied the structure of fullerene by graph theory we refer to Ashrafi et al. (2013), Balasubramanian (1993), Cataldo et al. (2011), and Ori et al. (2009).

A.A. Rezaei (✉)
Department of Pure Mathematics, Faculty of Mathematical Sciences, University of Kashan, Kashan 87317-53153, Iran
e-mail: a_rezaei@kashanu.ac.ir

We consider the fullerene as a polyhedron whose vertices, edges, and faces are atoms, chemical bond, and the rings, respectively. In our study, the Euler characteristic plays an important role.

Euler characteristic is an important topological invariant for surfaces, polyhedrons, polygons, and CW complexes. We recall that A polyhedron is simply three-dimensional solid flat faces which consist of a collection of polygons. For example, pyramids and prisms are polyhedrons. The *Euler characteristic* of a polyhedron M is defined as $\chi = V - E + F$, where V, E, and F are the number of vertices, edges, and faces in M, respectively. Two homeomorphic topological spaces have the same Euler characteristic. Recall that two objects are homeomorphic if they can be deformed into each other by a continuous, invertible mapping in both directions. For example, one can deform a sphere into a cube and vice versa. So in order to compute the Euler characteristic of a given surface, it is enough to compute the Euler characteristic of some polyhedron homeomorphic to it. It is easy to see that the Euler characteristic of our desire surfaces, sphere, and ellipsoid is two and of cylinder and torus is zero. To do this, consider the following tetrahedron which is homeomorphic to sphere.
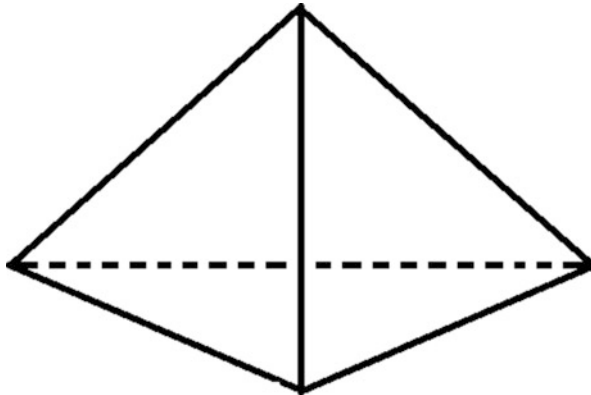
In this case, we have $V = 4$, $E = 6$, and $F = 4$. Thus the Euler characteristic for tetrahedron (and hence for sphere or ellipsoid) is two. Same calculation for cylinder and torus is down by considering suitable polyhedrons.

24.1.1 Definitions and Notations

In this section we introduce some notions which will be used in the rest of this chapter. For more details see (Rezaei 2014, 2015).

An *edge-to-edge polygonal tiling* of a surface is a covering of the entire surface by geodesic polygons, with no gaps or overlaps, such that the edge of a tile coincides entirely with the edge of a bordering tile. A tiling is said to be *d-regular*, if its corresponding graph is d-regular. We denote by
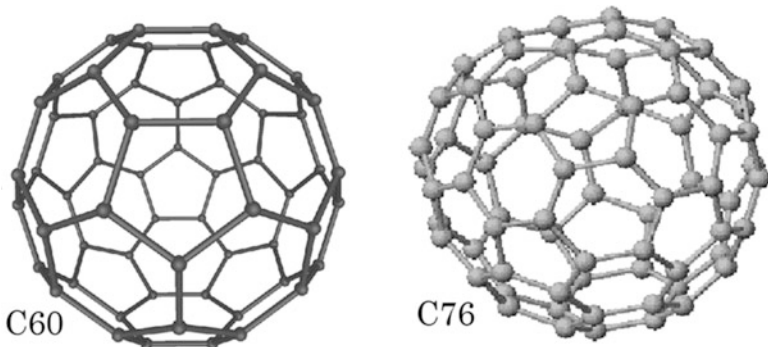
Fig. 24.1 2-Tilings with same class for sphere

$[(k_1, k_2, \ldots, k_r), (n_{k_1}, n_{k_2}, \ldots, n_{k_r})]$ a tiling in which there is n_{k_i} numbers of k_i -gons. Two d-regular edge-to-edge tilings $[(k_1, k_2, \ldots, k_r), (n_{k_1}, n_{k_2}, \ldots, n_{k_r})]$ and $[(k_1', k_2', \ldots, k_r'), (n_{k_{1'}}, n_{k_{2'}}, \ldots, n_{k_{r'}})]$ for the surface M are said to be *polygonal similar* if $k_i = k_i'$ for $i = 1, \ldots, r$.

It is clear that polygonal similarity is an equivalence relation on the set of all tilings for a surface. The equivalence class of $[(k_1, k_2, \ldots, k_r), (n_{k_1}, n_{k_2}, \ldots, n_{k_r})]$ is denoted by $T(k_1, k_2, \ldots, k_r)$.

Example 24.1 The fullerene C_{60} is a 3-regular edge-to-edge tilling for sphere containing 12 pentagons and 20 hexagons. The representation of this tiling is $[(5,6), (12, 20)]$ and the corresponding equivalence class is $T(5,6)$. As an another example consider the fullerene C_{76}. The representation of this tiling is $[(5,6), (12, 28)]$, while its equivalence class is $T(5,6)$. In our notations C_{60} and C_{76} are polygonal similar (see Fig. 24.1).

Theorem 24.2 Let $[(k_1, k_2, \ldots, k_r), (n_{k_1}, n_{k_2}, \ldots, n_{k_r})]$ be a d-regular, edge-to-edge tiling for a surface with Euler characteristic χ. Then

$$\sum_{i=1}^{r} \Big((2 - d)k_i + 2d\Big)n_{k_i} = 2\chi d. \tag{24.1}$$

In the rest of this chapter, all tilings are supposed to be 3-regular and edge to edge as the fullerenes.

Corollary 24.3 For every spherical fullerene with tiling $[(k_1, k_2, \ldots, k_r), (n_{k_1}, n_{k_2}, \ldots, n_{k_r})]$, we have

$$\sum_{i=1}^{r} (6 - k_i)n_{k_i} = 12.$$

The same result for cylinder and torus is

$$\sum_{i=1}^{r} (6 - k_i)n_{k_i} = 0.$$

According to Eq. (24.1), we cannot state anything about the number of hexagons in a fullerene. For example, C_{60} and C_{76} are models for $T(5, 6)$, while the number of hexagons in these models is different and the number of pentagons in all of them is 12, and it is easy to show that the number of pentagons in every model $T(5, 6)$ is 12.

Since fullerene and nanotube molecules have hexagonal rings in their structure, we study tilings of classes $T(k_1, k_2)$, $T(k_1, k_2, k_3)$, $T(k_1, k_2, k_3, k_4)$, $T(k_1, k_2, k_3, k_4, k_5)$, $T(k_1, k_2, k_3, k_4, k_5, k_6)$ for $k_i \in \{3, 4, 5, 6, 7, 8\}$ which contain at least one hexagon. The possible such tilings have been presented in the following table. However as we see later, some of these tilings don't exist for our desire surfaces.

2-Tiling	3-Tiling	4-Tiling	5-Tiling	6-Tiling
$T(3,6)$	$T(3,4,6)$	$T(3,4,5,6)$	$T(3,4,5,6,7)$	$T(3,4,5,6,7,8)$
$T(4,6)$	$T(3,5,6)$	$T(3,4,6,7)$	$T(3,4,5,6,8)$	
$T(5,6)$	$T(3,6,7)$	$T(3,4,6,8)$	$T(3,5,6,7,8)$	
$T(6,7)$	$T(3,6,8)$	$T(3,5,6,7)$	$T(4,5,6,7,8)$	
$T(6,8)$	$T(4,5,6)$	$T(3,5,6,8)$		
	$T(4,6,7)$	$T(3,6,7,8)$		
	$T(4,6,8)$	$T(4,5,6,7)$		
	$T(5,6,7)$	$T(4,5,6,8)$		
	$T(5,6,8)$	$T(4,6,7,8)$		
	$T(6,7,8)$	$T(5,6,7,8)$		

The following statements hold for tilings of sphere, cylinder, and torus.

Theorem 24.4

(a) For every tiling $T(4, 6, k)$, $T(k, 6, 8)$, and $T(4, , 6, k, 8)$, n_k is even, where $k = 3, 5, 7$.
(b) In every tiling $T(3, 6, k)$ for $k = 4$, 5, and 7, n_k is divisible by 3.
(c) In every tiling of class $T(3,4,6,7)$, $n_3 - n_7$ is even.
(d) In every tiling of class $T(3,4,6,8)$, n_3 is even and $3 | n_4 - n_8$.
(e) In every tiling of class $T(3,5,6,7)$, $3 | n_5 - n_7$.
(f) In every tiling of class $T(3,5,6,8)$, $n_3 + n_5$ is even and $3 | n_5 + n_8$.
(g) In every tiling of class $T(3,6,7,8)$, $n_3 - n_7$ is even and $3 | n_8 - n_7$.
(h) In every tiling of classes $T(4,5,6,7)$, $T(5,6,7,8)$, and $T(4,5,6,7,8)$, $n_5 - n_7$ is even.
(i) In every tiling of classes $T(5,6,8)$ and $T(4,5,6,8)$, n_5 is even.
(j) In every tiling of classes $T(4,6,7)$ and $T(4,6,7,8)$, n_7 is even.
(k) In every tiling of class $T(5,6,7,8)$, $n_5 - n_7$ is even.

By simple calculation one can show more results for other tilings. We will list some results in following two sections.

Tiling	Equation	Properties
$T(3,6)$	$3n_3 = 12$	$n_3 = 4$
$T(4,6)$	$2n_4 = 12$	$n_4 = 6$
$T(5,6)$	$n_5 = 12$	$n_5 = 12$

Table 24.1 2-Tilings for sphere and ellipsoid

24.1.2 Tilings for Sphere and Ellipsoid

The Euler characteristic of sphere and ellipsoid is two, so Eq. (24.1) for a general tiling $[(3, 4, 5, 6, 7, 8), (n_3, n_4, n_5, n_6, n_7, n_8)]$ is of the form

$$3n_3 + 2n_4 + n_5 + 0n_6 - n_7 - 2n_8 = 12.$$

Considering this equation we study the properties of tilings for sphere and ellipsoid.

24.1.3 2-Tilings for Sphere and Ellipsoid

There are only three classes of 2-tiling for sphere and ellipsoid.
Some properties of 2-tilings:

(a) There is no tiling of classes, $T(6, 7)$ and $T(6, 8)$, for sphere and ellipsoid.
(b) In every tiling $T(3,6)$ for sphere or ellipsoid, the number of triangles is four.
(c) In every tiling $T(4,6)$ for sphere or ellipsoid, the number of squares is six.
(d) In every tiling $T(5,6)$ for sphere or ellipsoid, the number of pentagons is 12.

All 2-Tilings for sphere and ellipsoid with their properties have been presented in Table 24.1.

24.1.4 3-Tilings for Sphere and Ellipsoid

There are nine classes of 3-tilings for sphere and ellipsoid.
Some properties of 3-tilings:

(a) There is no tiling of class $T(6, 7, 8)$ for sphere and ellipsoid.
(b) Every tiling of class $T(3,4,6)$ for sphere or ellipsoid has exactly two triangles and three squares.
(c) Every tiling of classes $T(4,6,7)$ and $T(4,6,8)$ for sphere or ellipsoid contain at least seven squares.
(d) Every tiling of class $T(5,6,7)$ for sphere or ellipsoid contains at least 13 pentagons.
(e) Every tiling of class $T(5,6,8)$ for sphere or ellipsoid contains at least 14 pentagons.

Table 24.2 shows the 3-tiling with their properties.

Table 24.2 3-Tilings for sphere and ellipsoid

Tiling	Equation	Properties
$T(3,4,6)$	$3n_3 + 2n_4 = 12$	$n_3 = 2,\ n_4 = 3$
$T(3,5,6)$	$3n_3 + n_5 = 12$	$n_5 = 3, 6, 9$
$T(3,6,7)$	$3n_3 - n_7 = 12$	$3\|n_7,\ n_3 \geq 5$
$T(3,6,8)$	$3n_3 - 2n_8 = 12$	$3\|n_8,\ 2\|n_3,\ n_3 \geq 6$
$T(4,5,6)$	$2n_4 + n_5 = 12$	$n_5 = 2, 4, 6, 8, 10$
$T(4,6,7)$	$2n_4 - n_7 = 12$	$2\|n_7,\ n_4 \geq 7$
$T(4,6,8)$	$2n_4 - 2n_8 = 12$	$n_4 \geq 7$
$T(5,6,7)$	$n_5 - n_7 = 12$	$n_5 \geq 13$
$T(5,6,8)$	$n_5 - 2n_8 = 12$	$2\|n_5,\ n_5 \geq 14$

Table 24.3 4-Tilings for sphere and ellipsoid

Tiling	Equation	Properties
$T(3,4,5,6)$	$3n_3 + 2n_4 + n_5 = 12$	$n_3 \leq 3, n_4 \leq 4, n_5 \leq 7$
$T(3,4,6,7)$	$3n_3 + 2n_4 - n_7 = 12$	$2\|n_3 - n_7$
$T(3,4,6,8)$	$3n_3 + 2n_4 - 2n_8 = 12$	$3\|n_4 - n_8,\ 2\|n_3$
$T(3,5,6,7)$	$3n_3 + n_5 - n_7 = 12$	$3\|n_5 - n_7$
$T(3,5,6,8)$	$3n_3 + n_5 - 2n_8 = 12$	$2\|n_3 + n_5,\ 3\|n_5 + n_8$
$T(3,6,7,8)$	$3n_3 - n_7 - 2n_8 = 12$	$2\|n_3 - n_7,\ 3\|n_8 - n_7,\ n_3 \geq 5$
$T(4,5,6,7)$	$2n_4 + n_5 - n_7 = 12$	$2\|n_5 - n_7$
$T(4,5,6,8)$	$2n_4 + n_5 - 2n_8 = 12$	$2\|n_5$
$T(4,6,7,8)$	$2n_4 - n_7 - 2n_8 = 12$	$2\|n_7,\ n_4 \geq 8$
$T(5,6,7,8)$	$n_5 - n_7 - 2n_8 = 12$	$2\|n_5 - n_7,\ n_5 \geq 15$

24.1.5 4-Tilings for Sphere and Ellipsoid

The number of classes of 4-tilings for sphere and ellipsoid is ten.

Some properties of 4-tilings:

(a) Every tiling of class $T(3,4,5,6)$ for sphere or ellipsoid contains at most three triangles, at most four squares, and at most seven pentagons.

(b) Every tiling of class $T(3,6,7,8)$ for sphere or ellipsoid contains at least five triangles.

(c) Every tiling of class $T(4,6,7,8)$ for sphere or ellipsoid contains at least eight squares.

(d) Every tiling of class $T(5,6,7,8)$ for sphere or ellipsoid contains at least 15 pentagons (Table 24.3).

24.1.6 5-Tilings for Sphere and Ellipsoid

There are four classes of 5-tilings for sphere and ellipsoid. These classes are shown in Table 24.4.

Table 24.4 5-Tilings for sphere and ellipsoid

Tiling	Equation	Properties
$T(3,4,5,6,7)$	$3n_3 + 2n_4 + n_5 - n_7 = 12$	$2\big|n_3 + n_5 - n_7$
$T(3,4,5,6,8)$	$3n_3 + 2n_4 + n_5 - 2n_8 = 12$	$2\big|n_3 + n_5$
$T(3,5,6,7,8)$	$3n_3 + n_5 - n_7 - 2n_8 = 12$	$2\big|n_3 + n_5 - n_7$
$T(4,5,6,7,8)$	$2n_4 + n_5 - n_7 - 2n_8 = 12$	$2\big|n_5 - n_7$

Table 24.5 The only 6-tiling for sphere and ellipsoid

Tiling	Equation	Properties
$T(3,4,5,6,7,8)$	$3\boldsymbol{n}_3 + 2\boldsymbol{n}_4 + \boldsymbol{n}_5 - \boldsymbol{n}_7 - 2\boldsymbol{n}_8 = 12$	$2\big|\boldsymbol{n}_3 + \boldsymbol{n}_5 - \boldsymbol{n}_7$

24.1.7 6-Tilings for Sphere and Ellipsoid

The only 6-tilings for sphere and ellipsoid are $T(3,4,5,6,7,8)$ which have been presented in Table 24.5.

24.1.8 Tilings for Torus and Cylinder

The Euler characteristic of torus and cylinder is zero, so the Eq. (24.1) for a general tiling $[(3, 4, 5, 6, 7, 8), (n_3, n_4, n_5, n_6, n_7, n_8)]$ is of the form

$$3n_3 + 2n_4 + n_5 + 0n_6 - n_7 - 2n_8 = 0.$$

Similar to previous section, we can investigate the tilings for these surfaces.

Theorem 24.5 Torus and cylinder have no 2-tiling. More precisely there is no tiling of class $T(6,k)$ for $k = 3,4,5,7$, and 8. So we continue with 3-tilings.

24.1.9 3-Tilings for Torus and Cylinder

There exist six classes of 3-tilings for torus and cylinder.
    Some properties of 3-tilings:

(a) There is no tiling of classes $T(3,4,6)$, $T(3,5,6)$, $T(4,5,6)$, and $T(6, 7, 8)$ for torus and cylinder.
(b) In every tiling of classes $T(3,6,7)$, the number of heptagons is three times of the number of triangles.
(c) In every tiling of classes $T(4,6,8)$, the number of squares is equal to the number of octagons.

Table 24.6 3-Tilings for torus and cylinder

Tiling	Equation	Properties
$T(3,6,7)$	$3n_3 - n_7 = 0$	$3\|n_7,\ n_7 = 3n_3$
$T(3,6,8)$	$3n_3 - 2n_8 = 0$	$3\|n_8,\ 2\|n_3,\ 3n_3 = 2n_8$
$T(4,6,7)$	$2n_4 - n_7 = 0$	$2\|n_7,\ n_7 = 2n_4$
$T(4,6,8)$	$2n_4 - 2n_8 = 0$	$n_4 = n_8$
$T(5,6,7)$	$n_5 - n_7 = 0$	$n_5 = n_7$
$T(5,6,8)$	$n_5 - 2n_8 = 0$	$2\|n_5,\ n_5 = 2n_8$

Table 24.7 4-Tilings for torus and cylinder

Tiling	Equation	Properties
$T(3,4,6,7)$	$3n_3 + 2n_4 - n_7 = 0$	$2\|n_3 - n_7,\ n_7 \geq 5$
$T(3,4,6,8)$	$3n_3 + 2n_4 - 2n_8 = 0$	$3\|n_4 - n_8,\ 2\|n_3, n_8 \geq 4$
$T(3,5,6,7)$	$3n_3 + n_5 - n_7 = 0$	$3\|n_5 - n_7,\ n_7 \geq 4$
$T(3,5,6,8)$	$3n_3 + n_5 - 2n_8 = 0$	$2\|n_3 + n_5,\ 3\|n_5 + n_8, n_8 \geq 2$
$T(3,6,7,8)$	$3n_3 - n_7 - 2n_8 = 0$	$2\|n_3 - n_7,\ 3\|n_8 - n_7$
$T(4,5,6,7)$	$2n_4 + n_5 - n_7 = 0$	$2\|n_5 - n_7,\ n_7 \geq 3$
$T(4,5,6,8)$	$2n_4 + n_5 - 2n_8 = 0$	$2\|n_5,\ n_8 \geq 2$
$T(4,6,7,8)$	$2n_4 - n_7 - 2n_8 = 0$	$2\|n_7,\ n_4 \geq 2$
$T(5,6,7,8)$	$n_5 - n_7 - 2n_8 = 0$	$2\|n_5 - n_7,\ n_5 \geq 3$

(d) In every tiling of classes $T(4,6,7)$, the number of octagons is double of the number of squares.

(e) In every tiling $T(5,6,7)$, the number of pentagons is equal to the number of heptagons.

Table 24.6 shows 3-Tilings for torus and cylinder.

24.1.10 4-Tilings for Torus and Cylinder

Some Properties of 4-tilings:

(a) There is no tiling of classes $T(3,4,5,6)$ for torus and cylinder.

(b) Every tiling of class $T(3,4,6,7)$ for torus or cylinder contains at least five heptagons.

(c) Every tiling of class $T(3,4,6,8)$ for torus or cylinder contains at least four octagons.

(d) Every tiling of class $T(3,5,6,7)$ for torus or cylinder contains at least four heptagons.

(e) Every tiling of classes $T(3,5,6,8)$ and $T(4,5,6,8)$ for torus or cylinder contains at least two octagons.

Table 24.8 5-Tilings for torus and cylinder

Tiling	Equation	Properties
$T(3,4,5,6,7)$	$3n_3 + 2n_4 + n_5 - n_7 = 0$	$2\mid n_3 + n_5 - n_7,\ n_7 \geq 6$
$T(3,4,5,6,8)$	$3n_3 + 2n_4 + n_5 - 2n_8 = 0$	$2\mid n_3 + n_5,\ n_8 \geq 3$
$T(3,5,6,7,8)$	$3n_3 + n_5 - n_7 - 2n_8 = 0$	$2\mid n_3 + n_5 - n_7$
$T(4,5,6,7,8)$	$2n_4 + n_5 - n_7 - 2n_8 = 0$	$2\mid n_5 - n_7$

Table 24.9 The only 6-tiling for torus and cylinder

Tiling	Equation	Properties
$T(3,4,5,6,7,8)$	$3\mathbf{n}_3 + 2\mathbf{n}_4 + \mathbf{n}_5 - \mathbf{n}_7 - 2\mathbf{n}_8 = 0$	$2\mid \boldsymbol{n}_3 + \mathbf{n}_5 - \boldsymbol{n}_7$

(f) Every tiling of class $T(4,5,6,7)$ for torus or cylinder contains at least three heptagons.

(g) Every tiling of class $T(4,6,7,8)$ for torus or cylinder contains at least two squares.

(h) Every tiling of class $T(5,6,7,8)$ for torus or cylinder contains at least three pentagons (Table 24.7).

24.1.11 5-Tilings for Torus and Cylinder

Some Properties of 5-tilings:

(a) Every tiling of class $T(3,4,5,6,7)$ for torus or cylinder contains at least six heptagons.

(b) Every tiling of class $T(3,4,5,6,7)$ for torus or cylinder contains at least three octagons (Table 24.8).

24.1.12 6-Tilings for Torus and Cylinder

Same as sphere and ellipsoid, the only 6-tiling for torus and cylinder is $T(3,4,5,6,7,8)$, which is presented below (Table 24.9).

24.1.13 More Comments and Remarks

Our argument about the number of polygons in the tiling fullerene surfaces is a mathematical declaration which asserts that if there exist such fullerenes, their tiling must hold in our results. But whether these tilings exist or not is another problem. From a practical standpoint, there is no guarantee that the obtained

structures are constructible. Indeed it is a challenge to make a stable structure in the nature. In the mathematical point of view, we only investigate which constructions are qualified to make.

Although the Eq. (24.1) holds for every d-regular, edge-to-edge tiling of an arbitrary surface, we only considered the 3-regular one, because the structure of carbon atom and fullerene molecule leads to 3-regular tilings. However same arguments can be down for every d-regular tiling in some area that tiling plays a mathematical and geometrical role.

References

Ashrafi AR, Cataldo F, Iranmanesh A, Ori O (2013) Topological modelling of nanostructures and extended systems. Springer, Berlin

Balasubramanian K (1993) Graph-theoretical characterization of fullerene cages. Polycycl Aromat Compd 3:247–259

Cataldo F, Graovac A, Ori O (2011) The mathematics and topology of fullerenes. Springer, Berlin

Fujimori T, Urita K, Ohba T, Kanoh H, Kaneko K (2010) Evidence of dynamic pentagon-heptagon pairs in single-wall carbon nanotubes using surface-enhanced raman scattering. J Am Chem Soc 132(19):6764–6767

Jeong BW, Ihm J, Lee GD (2008) Stability of dislocation defect with two pentagon-heptagon pairs in graphene. Phys Rev B 78:165403:1–165403:5

Ori O, Cataldo F, Graovac A (2009) Topological ranking of C28 fullerenes reactivity. Fullerenes Nanotubes Carbon Nanostruct 17(3):308–323

Rezaei AA (2014) Polygonal tiling of some surfaces containing fullerene molecules. Iranian J Math Chem 5(2):99–105

Rezaei AA (2015) Tiling fullerene surface with heptagon and octagon. Fullerenes Nanotubes Carbon Nanostruct 23(12):1033–1036

Sánchez-Bernabe FJ, Salcedo B, Salcedo J (2013) On some examples of fullerenes with heptagonal rings. IJRRAS 14(3):498–505

Tchoffo F, Zekeng S, Ndjaka JM (2014) New nonclassical fullerene with mixed square and octagonal faces. IJRRAS 18(3):231–235

Chapter 25
Enhancing Gauge Symmetries Via the Symplectic Embedding Approach

Salman Abarghouei Nejad and Majid Monemzadeh

Abstract One of the best ways to increase the fundamental symmetries of the physical systems with singular Lagrangian is the gauging of those models with the help of symplectic formalism of constrained systems. The main idea of this approach is based on the embedding of the model in an extended phase-space. After the gauging process had done, we can obtain generators of gauge transformations of the model.

25.1 Introduction

Every high energy physicist is aware of the importance of gauge theories. As a matter of fact, gauge invariance is the most significant and practical concept in high energy physics. The standard model of elementary particles is founded on this concept. Gauge invariance occurred due to the presence of the physical variables which are called gauge-invariant variables, and they are independent of local reference frames (Henneaux and Teiltelboim 1992).

It is very important to know that the quantization of gauge theories is as simple as it is thought to be due to the presence of internal symmetries which are called gauge symmetries. These symmetries exist some nonphysical degrees of freedom, that must be wiped out before and after the quantization is applied (Abreu et al. 2012).

On the other hand, in gauge theory, using the equations of motion, the dynamics of the system cannot be determined completely at every moment. Hence, one of the features of gauge theory is the advent of arbitrary time-dependent functions in general solutions of the equations of motion. The emergence of such functions forms some relations between phase-space coordinates, called constraints (Bergmann and Goldberg 1955).

To quantize such systems, Dirac classified the identities between phase-space coordinates into two main groups (Dirac 1967). The first group is identities that

S.A. Nejad • M. Monemzadeh (✉)
Department of Particle Physics and Gravity, Faculty of Physics, University of Kashan, Kashan 87317-53153, Iran
e-mail: monem@kashanu.ac.ir

present in the phase-space, like coordinates or momentum variables, which transform the physical system without any changes in the phase-space. These identities are called first-class constraints. Dirac, as the pioneer of constrained systems, named them as generators of the gauge transformations in the phase-space. The second group is not related to any degrees of freedom and must be eliminated. Presence of such identities indicates the absence of the gauge symmetry in the system. These identities are called second-class constraints. Therefore, to gauge a system which contains second-class constraints, we must convert them to first-class ones (Dirac 1950; Shirzad and Monemzadeh 2004).

To achieve this aim, there have been invented some approaches like BFT method (Batalin and Fradkin 1987; Batalin et al. 1989; Batalin and Tyutin 1991; Shirzad and Monemzadeh 2005; Ebrahimi and Monemzadeh 2014) and F-J approach or its newer version the symplectic formalism (Abreu et al. 2012; Faddeev and Jackiw 1988; Woodhouse 1992; Neto et al. 2001). The main strategy which these methods are based on is embedding a non-invariant system in an extended phase-space (Becchi et al. 1976; Batalin and Vilkovisky 1981; Monemzadeh and Ebrahimi 2012).

25.2 The Symplectic Formalism

The F-J formalism which was formulated first by Faddeev and Jackiw (Faddeev and Jackiw 1988) existed to prevent us from the consistency problems which deviate Poisson brackets algebra from common one, which consequently spoils all quantization techniques in constrained systems (Abreu et al. 2013; Monemzadeh et al. 2014). This method is mathematically founded on the symplectic structure of phase-space. Thus, it is different from approaches with similar usage. Moreover, the interpretation and classification of constraints which are presented by this formalism are different from other congener ones. As we mentioned before, in order to solve the quantization problems of any system, Dirac presented a theory and classified constraints into primary and secondary and first- and second-class constraints (Dirac 1967), whereas in symplectic formalism, all constraints are presumed to be equal and there is no dissimilarity between first- and second-class constraints. However, both formalisms are verified to be equivalent (Govaerts 1990; Montani 1993).

To use the symplectic method, we should start using the first-order Lagrangian, whose corresponding equation of motion does not imbue any acceleration. Thus, one can obtain the Hamiltonian equation of motion from the variational principle (Abreu et al. 2013; Jackiw 1994). So, we must start with first-order Lagrangian, and any other second-order Lagrangian should be transformed into a first-order one by expanding the configuration space, including conjugate momentum and coordinate variables. Also, one can use the Legendre transform to pass from Lagrangian to Hamiltonian (Paschalis and Porfyriadis 1996). We consider a non-invariant

mechanical model with the dynamics which are described by the Lagrangian L $(q_\mu, \dot{q}_\mu, t)$ with $\mu = 1, \ldots, N$ and its corresponding spatial variables q_μ and velocities $\dot{q}_\mu$.

The singularity nature of the Lagrangian due to its configuration constraint $\phi_i(q_\mu)$ can be imposed by a new dynamical variable (say undetermined Lagrange multiplier) λ_i in such a way that adds the constraints to free Lagrangian:

$$L^{(0)} = \dot{q}_\mu p^\mu - H_c - \lambda_i \phi^i(q_\mu). \tag{25.1}$$

Mutually we can calculate H_c as

$$H_c = \frac{\partial L}{\partial \dot{q}^\mu} \dot{q}_\mu - L^{(0)}. \tag{25.2}$$

The symplectic variables and symplectic one-form can be read off from the model straightforwardly:

$$\xi_\alpha^{(0)} = (q_\mu, p_\mu, \lambda_i).$$
$$\mathcal{A}_\alpha^{(0)} = (p_\nu, 0_\nu, 0_j). \tag{25.3}$$

Then, the symplectic two-form, $f_{\alpha\beta}^{(0)} = \partial_\alpha \mathcal{A}_\beta^{(0)} - \partial_\beta \mathcal{A}_\alpha^{(0)}$, will be obtained in the form of the following matrix:

$$f_{\alpha\beta}^{(0)} = \begin{pmatrix} 0_{\mu\nu} & -\delta_{\mu\nu} & 0_{\mu j} \\ \delta_{\mu\nu} & 0_{\mu\nu} & 0_{\mu j} \\ 0_{i\nu} & 0_{i\nu} & 0_{ij} \end{pmatrix}. \tag{25.4}$$

This matrix is apparently singular, and so, it has some zero-modes which are defined by $n_\alpha^{i(0)}$. As a matter of fact, because of our knowledge from linear algebra, we know that the linear combination of these null vectors is also a zero-mode.

Using the zero iterative potential,

$$\mathcal{V}^{(0)} = H_c + \lambda_i \phi^i. \tag{25.5}$$

Primary constraints will be obtained from the following relation:

$$\phi^i = n_\alpha^{i(0)} \partial^\alpha \mathcal{V}^{(0)}, \tag{25.6}$$

where ∂^α is the derivation with respect to the symplectic variables.

We can put the constraint into the kinetic part of the Lagrangian by substituting these constraints, obtained from (25.6) into the original Lagrangian. It means that we make primary constraints ϕ_i, as momenta conjugate to the variables λ_i. In other words, we convert strongly nonlinear constraints, ϕ_i, into the momenta (linear

constraint) of the phase-space. Hence, the first iterative Lagrangian will be obtained as

$$L^{(1)} = \dot{q}_\mu p^\mu - \dot{\lambda}_i \phi^i - H_c, \tag{25.7}$$

and the first iterative potential we have

$$\mathcal{V}^{(1)} = H_c. \tag{25.8}$$

New symplectic variables and one-form are defined as follows:

$$\xi_\alpha^{(1)} = \left(q_\mu, p_\mu, \lambda_i\right).$$
$$\mathcal{A}_\alpha^{(1)} = \left(p_\nu, 0_\nu, \phi_j\right). \tag{25.9}$$

The corresponding symplectic two-form is

$$f_{\alpha\beta}^{(1)} = \begin{pmatrix} 0_{\mu\nu} & -\delta_{\mu\nu} & u_{i\nu}^T \\ \delta_{\mu\nu} & 0_{\mu\nu} & 0_{\mu j} \\ -u_{i\nu} & 0_{i\nu} & 0_{ij} \end{pmatrix}, \tag{25.10}$$

where

$$u_{i\mu} = \frac{\partial \phi_i}{\partial q_\mu}. \tag{25.11}$$

This matrix (25.10) is a singular matrix, and it has some null vectors $n_\alpha^{i(1)}$. Using (25.6), we obtain secondary constraints as

$$\phi_{i'} = \mathcal{A}_\alpha^{(0)} \partial^\alpha \phi_i. \tag{25.12}$$

We can write the second iterative Lagrangian as

$$L^{(2)} = \dot{q}_\mu p^\mu - \dot{\lambda}_i \phi^i - \dot{\lambda}_{i'} \phi^{i'} - H_c. \tag{25.13}$$

New symplectic variables and one-form are as follows:

$$\xi_\alpha^{(2)} = \left(q_\mu, p_\mu, \lambda_i, \lambda_{i'}\right).$$
$$\mathcal{A}_\alpha^{(2)} = \left(p_\nu, 0_\nu, \phi_j, \phi_{j'}\right). \tag{25.14}$$

The corresponding two-form symplectic matrix is non-singular. Thus, it does not have any null vector, and consequently, there is no other constraint:

$$
f^{(2)}_{\alpha\beta} = \begin{pmatrix}
0_{\mu\nu} & -\delta_{\mu\nu} & u^T_{i\nu} & v^T_{i'\nu} \\
\delta_{\mu\nu} & 0_{\mu\nu} & 0_{i\nu} & w^T_{i'\nu} \\
-u_{i\nu} & 0_{\mu j} & 0_{ij} & 0_{ij'} \\
-v_{i'\nu} & -w_{i'\nu} & 0_{i'j} & 0_{i'j'}
\end{pmatrix},
\tag{25.15}
$$

where v_α and w_α are defined as follows:

$$
v_{i'\mu} = \frac{\partial \overline{\phi}_{i'}}{\partial q^\mu}.
$$

$$
w_{i'\mu} = \frac{\partial \overline{\phi}_{i'}}{\partial p^\mu}.
\tag{25.16}
$$

25.3 Symplectic Embedding Formalism

The corresponding symplectic two-form is non-singular. Thus, it does not have any null vector and consequently, the iterative process stops and no other constraint will be obtained.

Now, we start the symplectic embedding procedure to convert second-class constraints to first ones. The main idea of this procedure is to adjoin the Wess-Zumino variables to the original phase-space (Wess and Zumino 1971). In order to do that, we expand the original phase-space by introduction of a function G as WZ Lagrangian, depending on the original phase-space variables and the WZ variable θ, as the expansion in terms of the WZ variables, defined by

$$
G(q_\mu, p_\mu, \lambda_i, \theta) = \sum_{n=0}^{\infty} \mathcal{G}^{(n)}.
\tag{25.17}
$$

This function is gauging potential and satisfies the following boundary condition by vanishing $\mathcal{G}^{(0)}$:

$$
G(q_\mu, p_\mu, \lambda_i, \theta = 0) = 0.
\tag{25.18}
$$

Introducing the new term G into the Lagrangian (7),

$$
\begin{aligned}
\widetilde{L}^{(1)} &= L^{(1)} + L_{WZ} \\
&= L^{(1)} + G(q_\mu, p_\mu, \lambda_i, \theta).
\end{aligned}
\tag{25.19}
$$

With the corresponding symplectic variables and one-form,

$$\widetilde{\xi}_{\overline{\alpha}}^{(0)} = \left(q_{\mu}, p_{\mu}, \lambda_i, \theta\right),$$
$$\widetilde{\mathcal{A}}_{\overline{\alpha}}^{(0)} = \left(p_{\nu}, 0_{\nu}, \phi_j, 0\right), \tag{25.20}$$

the two-form symplectic matrix will be

$$\widetilde{f}_{\overline{\alpha}\overline{\beta}}^{(1)} = \begin{pmatrix} f_{\alpha\beta}^{(1)} & 0_{\alpha 1} \\ 0_{1\beta} & 0_{1\times 1} \end{pmatrix}, \tag{25.21}$$

which has the following null vectors $\widetilde{n}_{\overline{\alpha}}^{i(1)}$:

$$\widetilde{n}_{\overline{\alpha}}^{1(1)} = \begin{pmatrix} 0_{\alpha} & 1 \end{pmatrix}.$$
$$\widetilde{n}_{\overline{\alpha}}^{2(1)} = \begin{pmatrix} n_{\alpha}^{i(1)} & 0 \end{pmatrix}. \tag{25.22}$$

We define $\widetilde{n}_{\overline{\alpha}}$ as the linear combination of the corresponding null vectors:

$$\widetilde{n}_{\overline{\alpha}} = \sum_i \widetilde{n}_{\overline{\alpha}}^{i(1)} = \begin{pmatrix} n_{\alpha}^{i(1)} & a \end{pmatrix}. \tag{25.23}$$

Using the following relation,

$$\widetilde{n}_{\overline{\alpha}} \frac{\partial \mathcal{V}^{(1)}}{\partial \widetilde{\xi}^{(0)\overline{\alpha}}} = \frac{\partial \mathcal{G}^{(n)}}{\partial \theta}. \tag{25.24}$$

To start the iterative process, we substitute (25.8) into (25.24), using the zero-mode (25.23) to obtain $\mathcal{G}^{(1)}$ as

$$\mathcal{G}^{(1)} = \theta \phi_{i'}. \tag{25.25}$$

Putting $\mathcal{G}^{(1)}$ into (25.19), the potential will be

$$\widetilde{\mathcal{V}}^{(1)} = H_c - \mathcal{G}^{(1)}. \tag{25.26}$$

Using (25.24) for the second time with respect to the modified first iterative potential (25.26), one can obtain $\mathcal{G}^{(2)}$. Also, with the help of (25.24), one can find the explicit relation which gives $\mathcal{G}^{(n)}$ for $n \geq 2$, as

$$n_{\alpha}^{i(1)} \left[\frac{\partial \mathcal{G}^{(n-1)}}{\partial \widetilde{\xi}^{(0)\alpha}} \right] + a \frac{\partial \mathcal{G}^{(n)}}{\partial \theta} + b \frac{\partial \mathcal{G}^{(n)}}{\partial p_{\theta}} = 0. \tag{25.27}$$

Substituting $\mathcal{G}^{(2)}$ into the first iterative Lagrangian, we will obtain the second iterative Lagrangian. Thus,

$$\widetilde{\mathcal{V}}^{(1)} = H_c - \mathcal{G}^{(1)} - \mathcal{G}^{(2)}. \tag{25.28}$$

Again, using (25.24) to obtain, considering the (25.28) as the modified potential, we obtain $\mathcal{G}^{(3)}$. This process should be continued so far forth that $\frac{\partial \mathcal{G}^{(n)}}{\partial \theta}$ become null. Therefore, the zero-mode $\widetilde{n}_{\widetilde{\alpha}}$ does not make a new constraint. Thus, the gauged symplectic potential will be obtained as $\widetilde{\mathcal{V}}$

$$\widetilde{\mathcal{V}}^{(1)}\big(q_\mu, p_\mu, \lambda_i\big) = \widetilde{\mathcal{V}}^{(0)}\big(q_\mu, p_\mu\big) - \mathcal{G}^{(1)} - \mathcal{G}^{(2)} - \cdots - \mathcal{G}^{(n-1)}, \tag{25.29}$$

and for the canonical Hamiltonian, we have

$$\widetilde{H}_c = H_c + \lambda_i \phi^i - G\big(q_\mu, p_\mu, \lambda_i\big). \tag{25.30}$$

The gauged Lagrangian is obtained as

$$\widetilde{L}^{(1)} = L^{(1)} + G\big(q_\mu, p_\mu, \lambda_i\big). \tag{25.31}$$

25.4   Gauged Lagrangian

As we mentioned before about the relation (25.19), the gauged Lagrangian of an ungauged system, i.e., $\widetilde{L}^{(1)}$, will be obtained by adding a Lagrangian-like term to the first-order Lagrangian. This term depends on a new dynamical variable, which is called a WZ variable.

As we have shown in the previous section, an iterative differential equation with the help of zero -modes of the symplectic two-form and the potential of the model in (25.27) (Abreu et al. 2012) has been driven to obtain this added term. As a matter of fact, for most cases, and particularly for the studied model in this chapter, that iteration will not go more than two levels. Thus, a shortcut formula to make the WZ Lagrangian con be introduced here (Abarghouei Nejad et al. 2014).

To start with, let's imagine that our model has some primary constraints which are introduced by ϕ_i. First, we should find the constraint which is first class in comparison to other primary constraints. We call this primary first-class constraint as $\overline{\phi}_j$:

$$\big\{\phi_i, \overline{\phi}_j\big\} = 0. \tag{25.32}$$

Applying the symplectic approach will give us some secondary constraints, denoted by ϕ_i'. We construct the WZ Lagrangian by adding two generators $G^{(1)}$ and $G^{(2)}$, as

$$L_{WZ} = G^{(1)} + G^{(2)}, \tag{25.33}$$

where

$$G^{(1)} = \theta \phi_i' \quad ,$$
$$G^{(2)} = -\theta^2 \left\{ \phi_i', \overline{\phi}_j \right\}. \tag{25.34}$$

Also, θ is the WZ variable, and its conjugate momentum, p_θ, which will not appear in the gauged model is a first-class constraint. According to Dirac's guess, the presence of the first-class constraint guarantees the presence of a gauge symmetry in the model.

25.5   Constraint Structure of the Gauged Lagrangian

Using the symplectic method, we enhance the gauge symmetry of the primary model. In the following, we derive constraints and phase-space structure of the gauged Lagrangian (25.31). In this gauged model, new dynamical variables λ_i and θ appear first orderly in the Lagrangian. So, their momenta are primary constraints in the phase-space. Thus,

$$\frac{\partial \widetilde{L}^{(0)}}{\partial \dot{\lambda}^i} = 0 :\rightarrow \rho_{1_i} = p_{\lambda_i}, \tag{25.35}$$

$$\frac{\partial \widetilde{L}^{(0)}}{\partial \dot{\theta}} = 0 :\rightarrow \rho_2 = p_\theta. \tag{25.36}$$

So, for the total Hamiltonian, corresponding to Lagrangian (25.31) and redefining the constraints $\rho_s = \left(\rho_{1_i}, \rho_2 \right)$, we can write

$$\widetilde{H}_T = \widetilde{H}_c + \omega^s \rho_s. \tag{25.37}$$

In the chain-by-chain method (Shirzad and Mojiri 2001), the consistency of each individual constraint starts a chain and gives the next element of that chain. Also, the consistency of second-class constraints determines some of the Lagrange multipliers, ω^s, while the consistency of first-class ones leads to constraints of the next level:

$$0 = \left\{ \rho_s, \widetilde{H}_T \right\}.$$

$$0 = \left\{ \rho_s, \widetilde{H}_c \right\} + \omega^r \{\rho_s, \rho_r\}. \tag{25.38}$$

We see that primary constraints are Abelian, i.e., $\{\rho_r, \rho_s\} = 0$. So, we arrive to secondary constraints $\psi_s = \left\{ \rho_s, \widetilde{H}_c \right\}$.

The consistency of second level of constraints may give us new constraints, like

$$\left\{ \psi_s, \widetilde{H}_c \right\} = \Lambda_s, \tag{25.39}$$

or may determine a Lagrange multiplier due to the fact that $\{\psi_2, \rho_2\} \neq 0$, as

$$\left\{ \psi_s, \widetilde{H}_c \right\} \neq 0. \tag{25.40}$$

The relation (25.39) is identically true on the constrained surface. We should check the consistency condition (25.38) for Λ_s to see whether there exists any new constraint in the model or the chain is truncated.

Calculating all Poisson brackets, one can find first-class constraints. As we mentioned before, the first-class constraint, Φ_{FC_i}, is one whose Poisson bracket with other constraints vanishes:

$$\left\{ \Phi_{FC_i}, \phi_j \right\} = 0. \tag{25.41}$$

Also, the Poisson bracket matrix of all second-class constraints, Δ_{ij}, must be non-singular.

In order to determine all Dirac brackets of the original and gauged model, we put the inverse of Δ_{ij} in the following formula:

$$\left\{ \xi_{\overline{\alpha}}, \xi_{\overline{\beta}} \right\}^* = \left\{ \xi_{\overline{\alpha}}, \xi_{\overline{\beta}} \right\} - \{\xi_{\overline{\alpha}}, \Phi_{SC_i}\} \Delta_{ij}^{-1} \left\{ \Phi_{SC_j}, \xi_{\overline{\beta}} \right\}, \tag{25.42}$$

where Φ_{SC_i} is the set of all second-class constraints.

Also, by characterizing first-class constraints and Dirac brackets of a classical system, its quantized model, say Hilbert space of the quantum states, is fully available at tree level, according to Dirac prescription:

$$\{A, B\}^* \rightarrow \frac{1}{i\hbar} [A, B], \tag{25.43}$$

$$\hat{\Phi}_{FC_i} |phys>= 0, \tag{25.44}$$

where $\hat{\Phi}_{FC_i}$ is the quantized version of first-class constraints.

25.6 Gauge Invariance of the Extended Lagrangian

We can obtain all gauge symmetries of the Lagrangian (25.19), using the Poisson brackets of the first-class constraints, Φ_{FC_i}, and symplectic variables (Shirzad and Shabani Moghadam 1999; Henneaux et al. 1990):

$$\delta\widetilde{\xi}_{\overline{\alpha}}^{(0)} = \left\{\widetilde{\xi}_{\overline{\alpha}}^{(0)}, \Phi_{FC_j}\right\}\varepsilon^j \tag{25.45}$$

Also, the generators of infinitesimal gauge transformations can be obtained with the help of zero-modes of the symplectic two-form (25.23), using $\delta\widetilde{\xi}_{\overline{\alpha}}^{(1)} = \varepsilon_i\widetilde{n}_{\overline{\alpha}}$:

$$\delta x_i = 0,$$
$$\delta p_i = u_i\varepsilon_1,$$
$$\delta\lambda = \varepsilon_2,$$
$$\delta\theta = \varepsilon_1, \tag{25.46}$$

where ε_i is the infinitesimal time-dependent parameter (Abreu et al. 2013; Kim et al. 2004). Thus, the gauge symmetry of the model is determined via these transformations. In other words, the gained model is invariant under these transformations.

Apparently the results obtained from (25.45) are the same as the infinitesimal gauge transformations (25.46). Considering constrained analysis of the Lagrangian (25.31) and detaching its corresponding constraints in the following section, we study the gauge symmetry of the following model easily.

25.7 Particle Model on Hyperplane as a Toy Model

We consider a nonrelativistic particle with unit mass, which is confined on a hyperplane. We try to gauge the model using the symplectic formalism and extract its corresponding generators of infinitesimal gauge transformations.

The Hamiltonian of such a particle is defined as

$$H = \frac{1}{2}p_\mu p^\mu + \lambda_1\phi^1, \tag{25.47}$$

where ϕ_1 is the constraint which is imposed by the condition of the presence of the particle on the hyperplane. This model has been studied via the Skyrme model (Neto et al. 2001):

$$\phi_1 = q_\mu q^\mu - 1 \tag{25.48}$$

As we mentioned before, we start with the zeroth-iterated first-order Lagrangian as

$$L^{(0)} = \dot{q}_\mu p^\mu - \frac{1}{2} p_\mu p^\mu + \lambda_1 \left(q_\mu q^\mu - 1 \right). \tag{25.49}$$

Symplectic variables and one-form can be read off from the Lagrangian (25.49) as

$$\xi_\alpha^{(0)} = \left(q_\mu, p_\mu, \lambda_1 \right),$$
$$\mathcal{A}_\alpha^{(0)} = (p_\nu, 0_\nu, 0). \tag{25.50}$$

Then, the symplectic two-form will be obtained in the form of the following matrix:

$$f_{\alpha\beta}^{(0)} = \begin{pmatrix} 0_{\mu\nu} & -\delta_{\mu\nu} & 0_{\mu 1} \\ \delta_{\mu\nu} & 0_{\mu\nu} & 0_{\mu 1} \\ 0_{1\nu} & 0_{1\nu} & 0_{1\times 1} \end{pmatrix}, \tag{25.51}$$

which is apparently singular.

The corresponding some zero-mode is defined as

$$n_\alpha^{(0)} = \begin{pmatrix} 0_\mu & 0_\mu & 0 \end{pmatrix}. \tag{25.52}$$

Using the relation (25.6), one can again find the primary constraint of the model as

$$\phi_1 = q_\mu q^\mu - 1. \tag{25.53}$$

Now, we redefine the zeroth iterative potential as

$$\mathcal{V}^{(0)} = \frac{1}{2} p_\mu p^\mu - \lambda_1 \left(q_\mu q^\mu - 1 \right). \tag{25.54}$$

The first iterative Lagrangian is

$$L^{(1)} = q_\mu p^\mu + \dot{\lambda}_1 \phi^1 - \frac{1}{2} p_\mu p^\mu. \tag{25.55}$$

Then the symplectic variables and one-form are as follows:

$$\xi_\alpha^{(1)} = \left(q_\mu, p_\mu, \lambda_1 \right).$$
$$\mathcal{A}_\alpha^{(1)} = (p_\nu, 0_\nu, \phi_1). \tag{25.56}$$

Therefore, the corresponding symplectic two-form tensor is obtained as

$$f^{(1)}_{\alpha\beta} = \begin{pmatrix} 0_{\mu\nu} & -\delta_{\mu\nu} & 2q_{\mu 1} \\ \delta_{\mu\nu} & 0_{\mu\nu} & 0_{\mu 1} \\ -2q_{1\nu} & 0_{1\nu} & 0_{1\times 1} \end{pmatrix}. \tag{25.57}$$

Since the above tensor is singular, one can find its associated zero-mode as

$$n^{(1)}_{\alpha} = \begin{pmatrix} 0_\mu & q_\mu & \dfrac{1}{2} \end{pmatrix}, \tag{25.58}$$

which is the generator of the following secondary constraint; with the help of (25.6), we have

$$\phi_2 = q_\mu p^\mu. \tag{25.59}$$

Updating our potential, the first iterative potential will be

$$\mathcal{V}^{(1)} = \frac{1}{2} p_\mu p^\mu. \tag{25.60}$$

Now, the second iterative potential can be read off as

$$L^{(1)} = q_\mu p^\mu + \dot{\lambda}_1 \phi^1 + \dot{\lambda}_2 \phi^2 + -\frac{1}{2} p_\mu p^\mu. \tag{25.61}$$

Looking for symplectic variables and one-form, we will have

$$\xi^{(2)}_\alpha = \left(q_\mu, p_\mu, \lambda_1, \lambda_2 \right).$$
$$\mathcal{A}^{(2)}_\alpha = \left(p_\nu, 0_\nu, \phi_1, \phi_2 \right). \tag{25.62}$$

The second-iterated symplectic two-form can be obtained as

$$f^{(2)}_{\alpha\beta} = \begin{pmatrix} 0_{\mu\nu} & -\delta_{\mu\nu} & 2q_{\mu 1} & p_{\mu 1} \\ \delta_{\mu\nu} & 0_{\mu\nu} & 0_{i\nu} & q_{\mu 1} \\ -2q_{1\nu}u_{i\nu} & 0_{\mu j} & 0_{ij} & 0_{ij'} \\ -p_{1\nu} & -q_{1\nu} & 0_{i'j} & 0_{i'j'} \end{pmatrix}. \tag{25.63}$$

This tensor is non-singular. So, it does not have any null vector to generate new constraint. Therefore, the constraint-making process truncates. As we mentioned before, the inverse of (25.63) gives the usual Dirac brackets, using the relation (25.42).

Now, this is the time to start the embedding process. First, we should find the Wess-Zumino Lagrangian as the relation (25.17) with the corresponding boundary condition (25.18).

Introducing this Lagrangian into the first iterative Lagrangian (25.55), we will obtain

$$\widetilde{L}^{(1)} = \dot{q}_\mu p^\mu + \dot{\lambda}_1 \phi^1 - \frac{1}{2} p_\mu p^\mu + G(q_\mu, p_\mu, \theta). \tag{25.64}$$

We can read off extended symplectic variable and one-form as follows:

$$\widetilde{\xi}_\alpha^{(1)} = (q_\mu, p_\mu, \lambda_1, \theta).$$
$$\widetilde{\mathcal{A}}_\alpha^{(1)} = (p_\nu, 0_\nu, \phi_1, 0). \tag{25.65}$$

Computing the symplectic tensor, $\widetilde{f}_{\alpha\beta}^{(1)}$, as

$$\widetilde{f}_{\alpha\beta}^{(1)} = \begin{pmatrix} 0_{\mu\nu} & -\delta_{\mu\nu} & 2q_{\mu 1} & 0_{\mu 1} \\ \delta_{\mu\nu} & 0_{\mu\nu} & 0_{\mu 1} & 0_{\mu 1} \\ -2q_{1\nu} & 0_{1\nu} & 0_{1\times 1} & 0_{1\times 1} \\ 0_{1\nu} & 0_{1\nu} & 0_{1\times 1} & 0_{1\times 1} \end{pmatrix}. \tag{25.66}$$

which is exactly in the form of (25.21). This tensor is apparently singular and has the following zero-modes:

$$\widetilde{n}_{\overline{\alpha}}^{1(1)} = \begin{pmatrix} 0_\alpha & 1 \end{pmatrix}.$$
$$\widetilde{n}_{\overline{\alpha}}^{2(1)} = \begin{pmatrix} n_\alpha^{(1)} & 0 \end{pmatrix}. \tag{25.67}$$

Similar to (25.23), we use the linear combination of these zero-modes to start generating constraints.

Using (25.24) and (25.25), one can obtain the first iterative term, depending on θ as

$$\mathcal{G}^{(1)}(q_\mu, p_\mu, \theta) = (q_\mu p^\mu)\theta. \tag{25.68}$$

Putting this term in the Lagrangian (25.64), we have

$$\widetilde{L}^{(1)} = \dot{q}_\mu p^\mu + \dot{\lambda}_1 \phi^1 - \frac{1}{2} p_\mu p^\mu + (q_\mu p^\mu)\theta. \tag{25.69}$$

While the zero-mode (25.67) generated a new constraint, the Lagrangian is not still a gauge-invariant one:

$$\widetilde{n}_\alpha^{(1)} \frac{\partial \mathcal{V}^{(1)}}{\partial \widetilde{\xi}_\alpha^{(1)}} = q_\mu q^\mu \theta. \tag{25.70}$$

Thus,

$$\mathcal{G}^{(2)} = -\frac{1}{2} q_\mu q^\mu \theta^2. \tag{25.71}$$

So, the first iterative Lagrangian will be

$$\widetilde{L}^{(1)} = \dot{q}_\mu p^\mu + \dot{\lambda}_1 \phi^1 - \frac{1}{2} p_\mu p^\mu + (q_\mu p^\mu)\theta - \frac{1}{2} q_\mu q^\mu \theta^2. \tag{25.72}$$

At this stage, the null vector (25.67) does not produce any new constraint. Thus, correction terms $\mathcal{G}^n$ with $n \geq 3$ vanish. Hence, (25.72) is an invariant Lagrangian. Also, the corresponding canonical Hamiltonian can be obtained as

$$\widetilde{H}_c^{(1)} = \frac{1}{2} p_\mu p^\mu - \lambda_1 \phi^1 - (q_\mu p^\mu)\theta + \frac{1}{2} q_\mu q^\mu \theta^2. \tag{25.73}$$

Now, according to gauge transformation-generating functions (25.46), we can obtain the infinitesimal variations, under which both Hamiltonian (25.73) and (25.72) are invariant:

$$\delta q_\mu = 0.$$
$$\delta p_\mu = \varepsilon_1 q_\mu.$$
$$\delta \lambda = \frac{1}{2} \varepsilon_2.$$
$$\delta \theta = \varepsilon_1. \tag{25.74}$$

References

Abarghouei Nejad S, Dehghani M, Monemzadeh M (2014) Gauging the relativistic particle model on the noncommutative plane. arXiv:hep-th/1507.02329

Abreu EMC, Neto JA, Mendes ACR, Neves C, Oliveira W (2012) Obtaining gauge invariant actions via symplectic embedding formalism. Ann Phys 524(8):434–455

Abreu EMC, Mendes ACR, Neves C, Oliveira W, Silva RCN (2013) QCD gauge symmetries through Faddeev–Jackiw symplectic method. JHEP 6:093, front matter + 10 pp

Batalin IA, Fradkin ES (1987) Operational quantization of dynamical systems subject to second class constraints. Nucl Phys B 279:514–528

Batalin IA, Tyutin IV (1991) Existence theorem for the effective gauge algebra in the generalized canonical formalism with abelian conversion of second-class constraints. Inter J Mod Phys A 6 (18):3255–3282

Batalin IA, Vilkovisky GA (1981) Gauge algebra and quantization. Phys Lett B 102(1):27–31

Batalin IA, Fradkin ES, Fradkina TE (1989) Another version for operatorial quantization of dynamical systems with irreducible constraints. Nucl Phys B 314(1):158–174

Becchi C, Rouet A, Stora R (1976) Renormalization of gauge theories. Ann Phys 98(2):287–321

Bergmann PG, Goldberg I (1955) Dirac bracket transformations in phase space. Phys Rev 98 (2):531–538

Dirac PAM (1950) Generalized Hamiltonian dynamics. Can J Math 2:129–148

Dirac PAM (1967) Lectures on quantum mechanics. Second printing of the 1964 original. Belfer Graduate School of Science monographs series, 2. Belfer Graduate School of Science, New York; produced and distributed by Academic Press, Inc, New York

Ebrahimi AS, Monemzadeh M (2014) Mathematical feature of gauge theory. Inter J Theor Phys 53 (12):4121–4131

Faddeev L, Jackiw R (1988) Hamiltonian reduction of unconstrained and constrained systems. Phys Rev Lett 60(17):1692–1694

Govaerts J (1990) Hamiltonian reduction of first-order actions. Inter J Mod Phys A 5 (18):3625–3640

Henneaux M, Teiltelboim C (1992) Quantization of gauge system. Princeton University Press, Princeton

Henneaux M, Teitelboim C, Zanelli J (1990) Gauge invariance and degree of freedom count. Nucl Phys B 332(1):169–188

Jackiw R (1994) (Constrained) Quantization without tears. Constraint theory and quantization methods (Montepulciano, 1993). World Sci Publ, River Edge, pp 163–175

Kim YW, Lee CY, Kim SK (2004) Symplectic embedding of amassive vector–tensor theory with topological coupling. Eur Phys J C 34:383–392

Monemzadeh M, Ebrahimi AS (2012) Embedding of noncommutative massive QED. Mod Phys Lett A 27(14):5163–5176

Monemzadeh M, Ebrahimi AS, Sramadi S, Dehghani M (2014) Gauging of non–abelian Chern–Simons model. Mod Phys Lett A 29(5):1450028, 9 pp

Montani H (1993) Symplectic analysis of constrained systems. Inter J Mod Phys A 8 (24):4319–4337

Neto JA, Neves C, Oliveira W (2001) Gauging the SU(2) Skyrme model. Phys Rev D 63 (8):5018–5027

Paschalis JE, Porfyriadis PI (1996) BFV analysis of the U-em(1) Gauged SU(3) WZW model and the Faddeev-Jackiw approach. THES-TP 96/07

Shirzad A, Mojiri M (2001) Constraint structure in modified Faddeev-Jackiw method. Mod Phys Lett A 16(38):2439–2448

Shirzad A, Monemzadeh M (2004) The BFT method with chain structure. Phys Lett B 584 (1–2):220–224

Shirzad A, Monemzadeh M (2005) BFT method for mixed constrained systems and Chern-Simons theory. Phys Rev D 72:045004

Shirzad A, Shabani Moghadam M (1999) Explicit form of the gauge transformation generator in terms of constraints. J Phys A 32(46):8185–8195

Wess J, Zumino B (1971) Consequences of anomalous ward identities. Phys Lett 37B:95–97

Woodhouse NMJ (1992) Geometric quantization, 2nd edn, Oxford mathematical monographs. Oxford Science Publications/The Clarendon Press/Oxford University Press, New York

Chapter 26
A Lower Bound for Graph Energy of Fullerenes

Morteza Faghani, Gyula Y. Katona, Ali Reza Ashrafi, and Fatemeh Koorepazan-Moftakhar

Abstract A molecular graph is a graph in which vertices are atoms and edges are molecular bonds. These graphs are good mathematical models for molecules. Suppose G is a molecular graph with adjacency matrix A. The graph energy G is defined as the sum of the absolute values of the eigenvalues of A. The aim of this chapter is to describe a method for computing energy of fullerenes. We apply this method for computing a lower bound for energy of an infinite class of fullerene graphs with exactly $12n$ vertices. Our method is general and can be extended to other class of fullerene graphs.

26.1 Introduction

All graphs in this chapter are finite, simple, and connected. Suppose G is such a graph with vertex and edge sets $V(G)$ and $E(G)$, respectively. The *eigenvalues* of G are defined as the eigenvalues of its adjacency matrix and the set of all eigenvalues is called the *spectrum*, $Spec(G)$, of G. Set $Spec(G) = \{\lambda_1, \lambda_2,\ldots, \lambda_n\}$. The *graph energy*

M. Faghani
Department of Mathematics, Payam-e Noor University, Tehran, Iran

G.Y. Katona
Department of Computer Science and Information Theory, Budapest University of Technology and Economics, Budapest, Hungary

MTA-ELTE Numerical Analysis and Large Networks, Research Group, Budapest, Hungary

A.R. Ashrafi (✉) • F. Koorepazan-Moftakhar
Department of Nanocomputing, Institute of Nanoscience and Nanotechnology, University of Kashan, Kashan 87317-53153, Iran

Department of Pure Mathematics, Faculty of Mathematical Sciences, University of Kashan, Kashan 87317-53153, Iran
e-mail: ashrafi@kashanu.ac.ir

of G, $\varepsilon(G)$, is defined as $\varepsilon(G) = \sum_{i=1}^{n} |\lambda_i|$ (Gutman 1978, 2012). This graph invariant has some important applications in Hückel theory, and so it has been extensively studied. An extension of this graph invariant was done by Nikiforov (Nikiforov 2007). We refer the interested readers to (Li et al. 2012) for more information on this topic.

Suppose K_n and $K_{n,n}$ denote the complete graph on n vertices and balanced complete bipartite graph on 2n vertices. Define $K(a_n(k))$, $K(b_n(k))$, $K(c_n(k))$, and $K(d_n(k))$ to be graphs obtained from K_n by deleting k edges so that all of them have a common endpoint, by deleting k independent edges, by deleting a complete set of $k(k-1)/2$ mutually incident edges, and by deleting the edges of a k-membered cycle, respectively. In (Gutman and Pavlović 1999), some inequalities among the energies of the above graphs are given, and in Gutman (2001), the connection between the energy and the total electron energy of a class of organic molecules is investigated.

A graph G is called *3-connected*, if there does not exist vertices $x, y \in V(G)$ whose removal disconnects the graph. If all vertices of G have degree 3, then we say G is *cubic*. A *fullerene* graph is a cubic planar and 3-connected graph such that its faces are pentagon and hexagon. Suppose p, h, n, and m are the number of pentagons, hexagons, vertices, and edges of a fullerene graph F, respectively. Then $f = p + h$ and the Euler's theorem implies that $n - m + f = 2$. Since F is cubic, $m = 3n/2$ and since each vertex lies in exactly three faces, $n = (5p + 6h)/3$ and $m = (5p + 6h)/2 = 3/2n$. So $(5p + 6h)/3 - (5p + 6h)/2 + p + h = 2$. Therefore, $p = 12$, $n = 2h + 20$, and $m = 3h + 30$. We encourage the interested readers to consult the famous book (Fowler and Manolopoulos 2006) for the mathematical properties of this important class of molecular graphs and (Djafari et al. 2013; Koorepazan–Moftakhar et al. 2014) for more information on this topic.

26.2   Algebraic Background

Some of the present authors (Katona and Faghani 2014) applied Ky Fan theorem (Fan 1951) to obtain a lower bound for the graph energy of a sequence of fullerenes. To describe this method, we need some algebraic notions. A matrix $A_{n \times n}$ is called centrosymmetric if $a_{ij} = a_{n-i+1,n-j+1}$, $1 \leq i,j \leq n$. The mathematical properties of this special class of matrices can be found in (Liu 2003). In Gutman et al (2007), the authors proved that the energy of any n-vertex regular graph G of degree $r > 0$ is greater than or equal to n with equality if and only if every component of G is isomorphic to the complete bipartite graph $K_{r,r}$. If G is triangle- and quadrangle-free, then $\varepsilon(G) \geq nr / \sqrt{(2r - 1)}$. In particular, every n-vertex fullerene F satisfies $1.34n \leq \varepsilon(F) \leq 1.73n$. In (Katona and Faghani 2014), the authors improved the last inequality. They proved that a particular $10n$-vertex fullerene graph can have a centrosymmetric adjacency matrix. Then by applying the mathematical properties of these matrices and an iterative use of the Key–Fan theorem, a relation between energies of two fullerenes of orders $10 \times 2^k m$ and m, respectively, is provided. They observed that the relation gives a better lower bound to the energy of an n-vertex fullerene than the lower bound $1.34n$, for the special cases that $n = 10 \times 2 \times 5$, $10 \times 2 \times 7$, $10 \times 2 \times 11$, or $10 \times 2 \times 13$. We encourage the interested readers to

consult (Ghorbani et al. 2014) for more information on the energy of this infinite sequence of fullerenes. In this paper, the authors applied the centrosymmetricity of adjacency and PI adjacency matrices to approximate the energy and PI-energy of this class of fullerenes with exactly *10n* vertices. It is noteworthy to mention here that the centrosymmetricity of adjacency matrix of fullerene usually implies the same property for other vertex- or edge-weighted matrices obtained from the adjacency matrix of the fullerene graph under consideration.

Suppose G is a graph and $x, y \in V(G)$. The distance between x and y is defined as the length of a shortest path connecting x and y. The *Wiener index* of G, $W(G)$, is then the sum of all such distances over all pairs of vertices in G. Wiener called this graph invariant, the *path number* (Wiener 1947). It is the oldest distance-based graph invariant applicable in molecular branching. A fullerene graph is said to be *centrosymmetric* if it has a vertex labeling for which its adjacency matrix is centrosymmetric. (Graovac et al. 2011) considered a sequence of centrosymmetric fullerenes and applied this property to obtain exact formula for the Wiener index of the general term of fullerene sequence under consideration. In the mentioned paper, the authors conjectured that all fullerenes are centrosymmetric. In a recent paper (Fowler and Myrvold 2014), this conjecture was disproved; in fact, it proved that most fullerenes are not centrosymmetric. In this paper the necessary and sufficient conditions are stated in terms of the 28 possible fullerene automorphism groups: if the group is C_1 or C_3, the fullerene is not centrosymmetric; for C_{3h}, C_{3v}, or C_s, the fullerene is centrosymmetric unless some vertex is fixed by a mirror plane; for all other groups, the fullerene is centrosymmetric. Briefly, they noticed that most fullerenes have trivial C_1 symmetry group and hence they are not centrosymmetric.

Let J_n be an $n \times n$, $\{0, 1\}$ matrix in which an entry is unit if and only if it lies on counterdiagonal of J_n. It is clear that the matrix A is centrosymmetric if and only if $AJ = JA$. The set of all centrosymmetric matrices is denoted by *Cen*.

Theorem 26.1 (Cantoni and Buter 1976) If $n = 2m$ and $A_{n \times n} \in Cen$, then

$$\mathbf{A} = \begin{pmatrix} B & J_m C J_m \\ C & J_m B J_m \end{pmatrix}$$

where B and C are $m \times m$ matrices. Moreover, we have,

$$\mathbf{Q^T A Q} = \begin{pmatrix} B - J_m C & 0 \\ 0 & B + J_m C \end{pmatrix},$$

where

$$\mathbf{Q} = \frac{\sqrt{2}}{2} \begin{pmatrix} I_m & I_m \\ -J_m & J_m \end{pmatrix}.$$

Let

$$
\mathbf{A} = \begin{pmatrix}
A_{11} & A_{12} & 0 & 0 & 0 & A_{1m} \\
A_{21} & A_{22} & 0 & 0 & 0 & A_{2m} \\
0 & 0 & 0 & 0 & 0 & 0 \\
0 & 0 & 0 & 0 & 0 & 0 \\
0 & 0 & 0 & 0 & 0 & 0 \\
A_{m1} & A_{m2} & 0 & 0 & 0 & A_{mm}
\end{pmatrix}
$$

be the block form of $A = [a_{i,j}]$, $1 \leq i, j \leq n$, and all blocks are $s \times s$ matrices. The following theorem is useful when the adjacency matrix have a block form (Katona and Faghani 2014):

Theorem 26.2 Let

$$
\mathbf{A} = \begin{pmatrix}
A_{11} & 0 & 0 & 0 & A_{1m} \\
0 & 0 & 0 & 0 & A_{2m} \\
0 & 0 & 0 & 0 & 0 \\
0 & 0 & 0 & 0 & 0 \\
0 & 0 & 0 & 0 & 0 \\
A_{m1} & 0 & 0 & 0 & A_{mm}
\end{pmatrix}
$$

be the block form of A. If $m = 2k$ and $A_{i,j}J = JA_{2k-i+1,2k-j+1}$, then A is orthogonally similar to the following block matrix:

$$
\begin{pmatrix}
\amalg + \Psi\cup & o \\
o & \amalg - \Psi\cup
\end{pmatrix}
$$

in which

$$
\amalg = \begin{pmatrix}
A_{1,1} & 0 & 0 & 0 & A_{1,k} \\
0 & 0 & 0 & 0 & 0 \\
0 & 0 & 0 & 0 & 0 \\
0 & 0 & 0 & 0 & 0 \\
A_{k,1} & 0 & 0 & 0 & A_{k,k}
\end{pmatrix}
\quad \text{and} \quad
U = \begin{pmatrix}
A_{k+1,1} & 0 & 0 & 0 & A_{k+1,k} \\
0 & 0 & 0 & 0 & 0 \\
0 & 0 & 0 & 0 & 0 \\
0 & 0 & 0 & 0 & 0 \\
A_{2k,1} & 0 & 0 & 0 & A_{2k,k}
\end{pmatrix}
$$

Proof See (Katona and Faghani 2014) for details.

26.3 A Lower Bound for the Energy of C_{12n}

We are now ready to describe our method for an infinite sequence of fullerenes, C_{12n}, with exactly $12n$ carbon atoms, Fig. 26.1. By tedious calculations, we can find a centrosymmetric labeling for the vertices of C_{12n}. The adjacency matrix of the general term of this fullerene series is as follows:
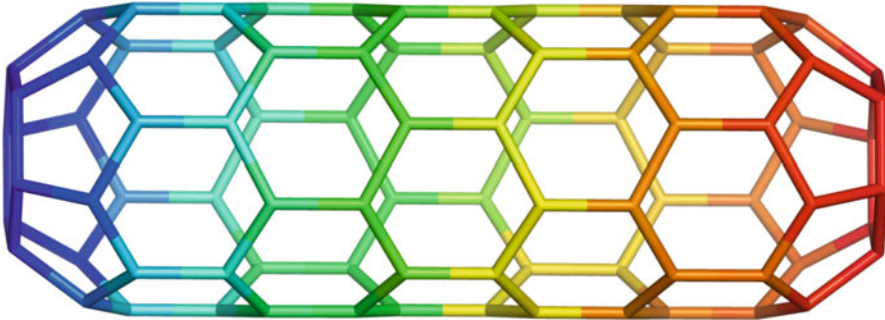
Fig. 26.1 The fullerene C_{12n}, $n = 7$

$$A(C_{12n}) = \begin{pmatrix} X & I & 0 & 0 & 0 & 0 & 0 & 0 & 0 \\ I & 0 & P & 0 & 0 & 0 & 0 & 0 & 0 \\ 0 & Q & 0 & I & 0 & 0 & 0 & 0 & 0 \\ 0 & 0 & 0 & 0 & 0 & 0 & 0 & 0 & 0 \\ 0 & 0 & 0 & 0 & 0 & 0 & 0 & 0 & 0 \\ 0 & 0 & 0 & 0 & 0 & 0 & I & 0 & 0 \\ 0 & . & . & . & 0 & I & 0 & P & 0 \\ 0 & 0 & . & . & . & 0 & Q & 0 & I \\ 0 & 0 & . & . & . & . & 0 & I & X \end{pmatrix},$$

in which $Q = P^t$ and all blocks are 6×6 matrices given by:

$$I = \begin{pmatrix} 1 & 0 & 0 & 0 & 0 & 0 \\ 0 & 1 & 0 & 0 & 0 & 0 \\ 0 & 0 & 1 & 0 & 0 & 0 \\ 0 & 0 & 0 & 1 & 0 & 0 \\ 0 & 0 & 0 & 0 & 1 & 0 \\ 0 & 0 & 0 & 0 & 0 & 1 \end{pmatrix}, \quad \mathbf{p} = \begin{pmatrix} 1 & 1 & 0 & 0 & 0 & 0 \\ 0 & 1 & 1 & 0 & 0 & 0 \\ 0 & 0 & 1 & 1 & 0 & 0 \\ 0 & 0 & 0 & 1 & 1 & 0 \\ 0 & 0 & 0 & 0 & 1 & 1 \\ 1 & 0 & 0 & 0 & 0 & 1 \end{pmatrix},$$

$$X = \begin{pmatrix} 0 & 1 & 0 & 0 & 0 & 1 \\ 1 & 0 & 1 & 0 & 0 & 0 \\ 0 & 1 & 0 & 1 & 0 & 0 \\ 0 & 0 & 1 & 0 & 1 & 0 \\ 0 & 0 & 0 & 1 & 0 & 1 \\ 1 & 0 & 0 & 0 & 1 & 0 \end{pmatrix}.$$

By Theorem 26.2, we can take the adjacency matrix as follows:

$$\begin{pmatrix} A & B \\ C & D \end{pmatrix}$$

in which

$$
\mathbf{A} = \begin{pmatrix}
X & I & 0 & 0 & 0 & 0 & 0 & 0 & 0 \\
I & 0 & P & 0 & 0 & 0 & 0 & 0 & 0 \\
0 & Q & 0 & I & 0 & 0 & 0 & 0 & 0 \\
0 & 0 & 0 & 0 & 0 & 0 & 0 & 0 & 0 \\
0 & 0 & 0 & 0 & 0 & 0 & 0 & 0 & 0 \\
0 & 0 & 0 & 0 & 0 & 0 & I & 0 & 0 \\
0 & . & . & . & 0 & I & 0 & P & 0 \\
0 & 0 & . & . & . & 0 & Q & 0 & I \\
0 & 0 & . & . & . & . & 0 & I & X
\end{pmatrix} \text{ and}
$$

$$
\mathbf{D} = \begin{pmatrix}
0 & I & 0 & 0 & 0 & 0 & 0 & 0 & 0 \\
I & 0 & P & 0 & 0 & 0 & 0 & 0 & 0 \\
0 & Q & 0 & I & 0 & 0 & 0 & 0 & 0 \\
0 & 0 & 0 & 0 & 0 & 0 & 0 & 0 & 0 \\
0 & 0 & 0 & 0 & 0 & 0 & 0 & 0 & 0 \\
0 & 0 & 0 & 0 & 0 & 0 & I & 0 & 0 \\
0 & 0. & . & . & 0 & I & 0 & P & 0 \\
0 & 0 & . & . & . & 0 & Q & 0 & I \\
0 & 0 & . & . & . & . & 0 & I & X
\end{pmatrix} \quad
\mathbf{C} = \begin{pmatrix}
0 & 0 & 0 & 0 & 0 & 0 & 0 & 0 & 0 \\
0 & 0 & 0 & 0 & 0 & 0 & 0 & 0 & 0 \\
0 & 0 & 0 & 0 & 0 & 0 & 0 & 0 & 0 \\
0 & 0 & 0 & 0 & 0 & 0 & 0 & 0 & 0 \\
0 & 0 & 0 & 0 & 0 & 0 & 0 & 0 & 0 \\
0 & 0 & 0 & 0 & 0 & 0 & 0 & 0 & 0 \\
0 & 0. & . & . & 0 & 0 & 0 & 0 & 0 \\
0 & 0 & . & . & . & 0 & 0 & 0 & 0 \\
0 & 0 & . & . & . & . & 0 & 0 & 0
\end{pmatrix}
$$

$$
\mathbf{B} = \begin{pmatrix}
0 & 0 & 0 & 0 & 0 & 0 & 0 & 0 & 0 \\
0 & 0 & 0 & 0 & 0 & 0 & 0 & 0 & 0 \\
0 & Q & 0 & 0 & 0 & 0 & 0 & 0 & 0 \\
0 & 0 & 0 & 0 & 0 & 0 & 0 & 0 & 0 \\
0 & 0 & 0 & 0 & 0 & 0 & 0 & 0 & 0 \\
0 & 0 & 0 & 0 & 0 & 0 & 0 & 0 & 0 \\
0 & . & . & . & 0 & 0 & 0 & 0 & 0 \\
P & 0 & . & . & . & 0 & Q & 0 & I \\
0 & 0 & . & . & . & . & 0 & 0 & 0
\end{pmatrix}.
$$

So, the matrix A (C_{12n}) is similar to the matrix

$$
\begin{pmatrix}
A + \Psi C & 0 \\
0 & A - \Psi C
\end{pmatrix}.
$$

Furthermore,

$$
\mathbf{A} + \Psi\mathbf{C} = \begin{pmatrix}
X & I & 0 & 0 & 0 & 0 & 0 & 0 & 0 \\
I & 0 & P & 0 & 0 & 0 & 0 & 0 & 0 \\
0 & Q & 0 & I & 0 & 0 & 0 & 0 & 0 \\
0 & 0 & 0 & 0 & 0 & 0 & 0 & 0 & 0 \\
0 & 0 & 0 & 0 & 0 & 0 & 0 & 0 & 0 \\
0 & 0 & 0 & 0 & 0 & 0 & I & 0 & 0 \\
0 & . & . & . & 0 & I & 0 & P & 0 \\
0 & 0 & . & . & . & 0 & Q & 0 & I \\
0 & 0 & . & . & . & . & 0 & I & JQ
\end{pmatrix}
$$

and

$$\mathbf{A} - \Psi\mathbf{C} = \begin{pmatrix} X & I & 0 & 0 & 0 & 0 & 0 & 0 & 0 \\ I & 0 & P & 0 & 0 & 0 & 0 & 0 & 0 \\ 0 & Q & 0 & I & 0 & 0 & 0 & 0 & 0 \\ 0 & 0 & 0 & 0 & 0 & 0 & 0 & 0 & 0 \\ 0 & 0 & 0 & 0 & 0 & 0 & 0 & 0 & 0 \\ 0 & 0 & 0 & 0 & 0 & 0 & I & 0 & 0 \\ 0 & . & . & . & 0 & I & 0 & P & 0 \\ 0 & 0 & . & . & . & 0 & Q & 0 & I \\ 0 & 0 & . & . & . & . & 0 & I & -JQ \end{pmatrix}.$$

So, $\varepsilon(A(C_{12n})) = \varepsilon(A + \Psi C) + \varepsilon(A - \Psi C)$. Notice that

$$(A + \Psi C) + \begin{pmatrix} 0 & 0 & 0 & 0 & 0 & 0 & 0 & 0 & 0 \\ 0 & 0 & 0 & 0 & 0 & 0 & 0 & 0 & 0 \\ 0 & 0 & 0 & I & 0 & 0 & 0 & 0 & 0 \\ 0 & 0 & 0 & 0 & 0 & 0 & 0 & 0 & 0 \\ 0 & 0 & 0 & 0 & 0 & 0 & 0 & 0 & 0 \\ 0 & 0 & 0 & 0 & 0 & 0 & 0 & 0 & 0 \\ 0 & . & . & . & 0 & 0 & 0 & 0 & 0 \\ 0 & 0 & . & . & . & 0 & 0 & 0 & 0 \\ 0 & 0 & . & . & . & . & 0 & X & -JQ \end{pmatrix}$$

$$= \begin{pmatrix} X & I & 0 & 0 & 0 & 0 & 0 & 0 & 0 \\ I & 0 & P & 0 & 0 & 0 & 0 & 0 & 0 \\ 0 & Q & 0 & I & 0 & 0 & 0 & 0 & 0 \\ 0 & 0 & 0 & 0 & 0 & 0 & 0 & 0 & 0 \\ 0 & 0 & 0 & 0 & 0 & 0 & 0 & 0 & 0 \\ 0 & 0 & 0 & 0 & 0 & 0 & I & 0 & 0 \\ 0 & . & . & . & 0 & I & 0 & P & 0 \\ 0 & 0 & . & . & . & 0 & Q & 0 & I \\ 0 & 0 & . & . & . & . & 0 & I & X \end{pmatrix}.$$

This means that we can reduce the order of $A(C_{12n})$ into half such that the centrosymmetricity preserves.

Notice that, $\varepsilon(X - JQ) \approx 7.4641$. and $\varepsilon(X + JQ) \approx 11.4641$. By an iterative use of the Key–Fan Theorem, one can prove the following inequality:

Table 26.1 The energy and bounds for some fullerenes

n	k	M	Energy	$2^k \epsilon(A(C_{12m})) - 18.9282(2^k - 1)$.
3	0	3	55.244	55.244
5	0	5	93.174	93.174
6	1	3	112.075	91.5598
7	0	7	130.97	130.97
9	0	9	168.733	168.733
11	0	11	206.481	206.481
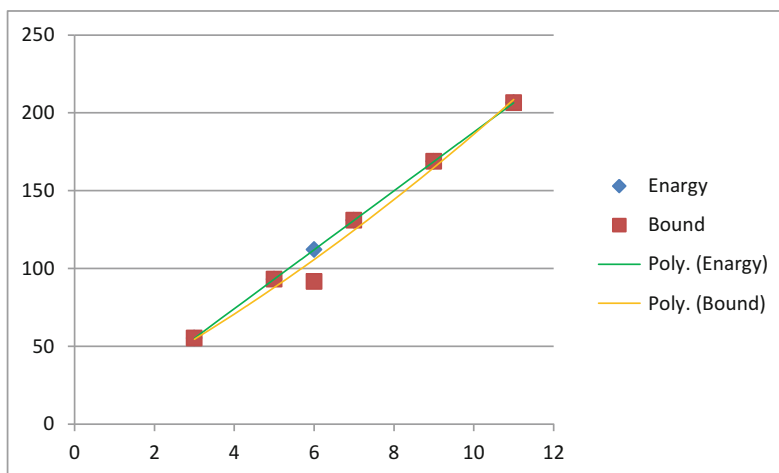
Fig. 26.2 The diagrams for exact and estimated energies

$$\epsilon((A(C_{12n}))) \geq 2\epsilon \left(\left(\begin{pmatrix} X & I & 0 & 0 & 0 & 0 & 0 & 0 & 0 \\ I & 0 & P & 0 & 0 & 0 & 0 & 0 & 0 \\ 0 & Q & 0 & I & 0 & 0 & 0 & 0 & 0 \\ 0 & 0 & 0 & 0 & 0 & 0 & 0 & 0 & 0 \\ 0 & 0 & 0 & 0 & 0 & 0 & 0 & 0 & 0 \\ 0 & 0 & 0 & 0 & 0 & 0 & I & 0 & 0 \\ 0 & . & . & . & 0 & I & 0 & P & 0 \\ 0 & 0 & . & . & . & 0 & Q & 0 & I \\ 0 & 0 & . & . & . & . & 0 & I & X \end{pmatrix}\right)\right) - 18.9282.$$

The right-hand side matrix is again centrosymmetric as its size is half the size of $A(C_{12n})$. So, if n is even, then by repeating the above procedure, we can obtain the following lower bound for the energy of $A(C_{12n})$ as follows:

Theorem 26.3 If $n = 2^k m$ then $\varepsilon(A(C_{12n})) = \varepsilon(A(C_{12(2^k m)})) > 2^k \varepsilon(A(C_{12m})) - 18.9282(2^k - 1)$.

In Table 26.1, the exact values of energy in some cases are compared with our bound. It seems that the bound is good, but it is important to always compare the exact energy with the computed bound. Since the fullerene is a huge molecule, this is an open question that the error is small. In Fig. 26.2, these values are compared in a diagram.

References

Cantoni A, Buter P (1976) Eigenvalues and eigenvectors of symmetric centrosymmetric matrices. Linear Algebra Appl 13:275–288

Djafari S, Koorepazan–Moftakhar F, Ashrafi AR (2013) Eccentric sequences of two infinite classes of fullerenes. J Comput Theor Nanosci 10:2636–2638

Fan K (1951) Maximum properties for the eigenvalues of completely continuous operators. Proc Natl Acad Sci ASA 37:760–766

Fowler P W, Manolopoulos DE (2006) An Atlas of fullerenes. Oxford University Press, Oxford 1995, Dover, New York 2006

Fowler PW, Myrvold W (2014) Most fullerenes have no centrosymmetric labelling. MATCH Commun Math Comput Chem 71:93–97

Ghorbani M, Faghani M, Ashrafi AR, Heidari-Rad S, Graovac A (2014) An upper bound for energy of matrices associated to an infinite class of fullerenes. MATCH Commun Math Comput Chem 71:341–354

Graovac A, Ori O, Faghani M, Ashrafi AR (2011) Distance property of fullerenes. Iran J Math Chem 2:99–107

Gutman I (1978) The energy of a graph. Ber Math Statist Sekt Forschungszentrum (Graz) 103:1–22

Gutman I (2001) The energy of a graph: old and new results. Algebraic combinatorics and applications (Gößweinstein 1999). Springer, Berlin, pp 196–211

Gutman I (2012) Bounds for all graph energies. Chem Phys Lett 528:72–74

Gutman I, Pavlović L (1999) The energy of some graphs with large number of edges. Bull Cl Sci Math Nat Sci Math 24:35–50

Gutman I, Zare Firoozabadi S, de la Peña JA, Rada J (2007) On the energy of regular graphs. MATCH Commun Math Comput Chem 57:435–442

Katona GY, Faghani M (2014) Centrosymmetric graphs and lower bound for graph energy of fullerene. Discuss Math Graph Theory 34:751–768

Koorepazan–Moftakhar F, Ashrafi A R, Ori O and Putz M V (2014) Sphericality of some classes of fullerenes measured by topology. In: Shannon BE (ed) Fullerenes: chemistry, natural sources and technological applications, Nova Science Publishers, Inc, New York, p. 285–304

Li X, Shi Y, Gutman I (2012) Graph energy. Springer, New York

Liu ZY (2003) Some properties of centrosymmetric matrices. Appl Math Comput 141:297–306

Nikiforov V (2007) The energy of graphs and matrices. J Math Anal Appl 326:1472–1475

Wiener H (1947) Structural determination of paraffin boiling points. J Am Chem Soc 69:17–20

Index